

STRUCTURAL MOTION ENGINEERING

Fourth Draft. March 13 2014

Jerome J. Connor & Simon Laflamme

Preface

Conventional structural design procedures are generally based on two requirements namely safety and serviceability. Safety relates to extreme loadings, which have a very low probability of occurring, on the order of 2%, during a structure's life, and is concerned with the collapse of the structure, major damage to the structure and its contents, and loss of life. Serviceability pertains to medium to large loadings, which may occur during the structure's lifetime. For service loadings, the structure should remain operational (i.e., the structure should suffer minimal damage, and furthermore, the motion experienced by the structure should not exceed specified comfort limits for humans and motion-sensitive equipment mounted on the structure). Typical occurrence probabilities for service loads range from 10% to 50%.

Safety concerns are satisfied by requiring the resistance (i.e., strength) of the individual structural elements to be greater than the demand associated with the extreme loading. Once the structure is proportioned, the stiffness properties are derived and used to check the various serviceability constraints such as elastic behavior. Iteration is usually necessary for convergence to an acceptable structural design. This approach is referred to as strength-based design since the elements are proportioned initially according to strength requirements.

Applying a strength-based approach for preliminary design is appropriate when strength is the dominant design requirement. In the past, most structural design problems have fallen in this category. However, the following developments have occurred recently that have limited the effectiveness of the strength-based approach. Firstly, the trend toward more flexible structures such as tall buildings and longer-span horizontal structures has resulted in more structural motion under service loading, thus

shifting the emphasis from safety toward serviceability. Secondly, some of the new types of facilities such as space platforms and semiconductor manufacturing centers have more severe design constraints on motion than the typical civil structure. For example, in the case of micro-device manufacturing, the environment has to be essentially motion free. Thirdly, recent advances in material science and engineering have resulted in significant increases in the strength of traditional civil engineering materials. However, the material stiffness has not increased at the same rate. The lag in material stiffness versus material strength has led to a problem with satisfying the requirements on the various motion parameters. Indeed, for very high-strength materials, the motion requirements control the design. Fourthly, experience with recent earthquakes has shown that the cost of repairing the structural and nonstructural damage due to the motion occurring during a seismic event is considerably greater than anticipated. This finding has resulted in more emphasis placed on limiting the structural response with various types of energy dissipation and absorption mechanisms.

Structural motion engineering is an alternate paradigm that addresses these issues. The approach takes as its primary objective the satisfaction of motion-related design requirements such as restrictions on displacement and acceleration and seeks the optimal deployment of material stiffness and motion control devices to achieve these design targets as well as satisfy the constraints on strength. Structural motion control is the enabling technology for motion engineering. This book presents a systematic treatment of the basic concepts and computational procedures for structural motion control. Numerous examples illustrating the application of motion control to a wide spectrum

of buildings are included. Topics covered include optimal stiffness distributions for building-type structures, the role of damping in controlling motion, tuned mass dampers, base isolation systems, linear control, and nonlinear control. The targeted audience is practicing engineers and graduate students.

This work was motivated by the authors' interest in the design of structures for dynamic excitation and by members of the Structural Engineering Community who have been enthusiastic supporters of this design paradigm.

JEROME J. CONNOR

Massachusetts Institute of Technology

SIMON LAFLAMME

Iowa State University

Acknowledgements

We would like to thank our spouses Barbara Connor and Jill Polson for their patience and moral support over the seemingly endless time required to complete this text. We are most appreciative. We would also like to thank ... We are especially in debt to ...

Acknowledgements

We would like to thank our spouses Barbara Connor and Jill Polson for their patience and moral support over the seemingly endless time required to complete this text. We are most appreciative. We would like to thank our colleagues and students who provided us with many valuable suggestions concerning the content and organization of the text. We are especially indebted to Dr. Pierre Ghisbain his support as the text was evolving.

Contents

1	Introduction	19
1.1	Source of Motion Problems	20
1.2	Structural motion Engineering Methodology . . .	23
1.3	Motion versus Strength Issues - Static Loading . .	23
1.3.1	Building Type Structures	23
1.3.2	Bridge Type Structures	32
1.4	Motion-Induced Problems - Periodic Loading . . .	35
1.4.1	Resonance-Related Problems	35
1.4.2	Response for Periodic Excitation	37
1.5	Motion Control Methodologies	46
1.5.1	Passive and Active Control	46
1.5.2	Desired Response	54
1.6	Scope of Text	55
2	Optimal Stiffness Distribution - Static Loading	63
2.1	Introduction	64
2.2	Governing Equations: Transverse Bending of Planar Beams	65
2.2.1	Planar Deformation-Displacement Relations	66
2.2.2	Optimal Deformation and Displacement Profiles	67
2.2.3	Equilibrium Equations	69
2.2.4	Force-Deformation Relations	71
2.3	Stiffness Distribution for a Continuous Cantilever Beam under Static Loading	77
2.4	Buildings Modeled as Shear Beams	83
2.4.1	Governing Equations for Buildings Modeled as Pseudo Shear Beams	83

CONTENTS

2.4.2	Stiffness Distribution for a Discrete Shear Beam: Static Loading	90
2.5	Stiffness Distribution: Truss under Static Loading	92
2.5.1	An Introductory Example	92
2.5.2	A General Procedure	102
3	Optimal Stiffness/Damping for Dynamic Loading	121
3.1	Introduction	122
3.2	Dynamic Response - MDOF	122
3.2.1	Modal Equations - MDOF System	123
3.2.2	General Solution - Convolution Integral	131
3.2.3	Periodic Excitation	132
3.2.4	Seismic Loading; Response Spectra	135
3.2.5	Selection of Modes	142
3.3	Stiffness Distribution for a Cantilever Beam: Dy- namic Response	151
3.4	Stiffness Distribution for a Discrete Shear Beam: Dynamic Response	156
3.5	Stiffness Calibration- Fundamental Mode Response	159
3.5.1	Discrete Shear Beam	159
3.5.2	Continuous Beam	164
3.5.3	Periodic Excitation	169
3.5.4	Seismic Excitation	175
3.5.5	Construction of Spectral Displacement Re- sponse Spectra	177
3.5.6	Calibration Examples	184
3.6	Stiffness Modification for Seismic Excitation	190
3.6.1	Iterative Procedure	190
3.6.2	Multiple Mode Response	190

4	Optimal Passive Damping Distribution	207
4.1	Introduction	208
4.2	Viscous, Frictional, and Hysteretic Damping . . .	215
4.2.1	Viscous Damping	215
4.2.2	Friction Damping	220
4.2.3	Hysteretic Damping	222
4.3	Viscoelastic Material Damping	228
4.4	Equivalent Viscous Damping	233
4.5	Damping Parameters: Discrete Shear Beam . . .	242
4.5.1	Damping Systems	242
4.5.2	Rigid Structural Members: Linear Viscous Behavior	246
4.5.3	Rigid Structural Members: Linear Vis- coelastic Behavior	249
4.5.4	Flexible Structural Members: Linear Vis- coelastic Behavior	257
4.6	Damping Parameters: Truss Beam	263
4.6.1	Linear Viscous Behavior	264
4.6.2	Linear Viscoelastic Behavior	266
5	Tuned Mass Damper Systems	287
5.1	Introduction	288
5.2	An Introductory Example	289
5.3	Examples of existing tuned mass damper systems	294
5.3.1	Translational tuned mass dampers	294
5.3.2	Pendulum tuned mass damper	301
5.4	Tuned Mass Damper Theory for SDOF Systems .	308
5.4.1	Undamped structure - undamped TMD . .	309
5.4.2	Undamped structure - damped TMD . . .	312
5.4.3	Damped structure - damped TMD	326
5.5	Case studies - SDOF systems	338

CONTENTS

5.6	Tuned mass damper theory for MDOF systems	346
5.7	Tuned Liquid Column Dampers	366
5.7.1	Design methodology for TLCD	378
6	Base Isolation Systems	391
6.1	Introduction	392
6.2	Isolation for SDOF Systems	393
6.2.1	SDOF Examples	393
6.2.2	Bearing Terminology	398
6.2.3	Modified SDOF Model	404
6.2.4	Periodic Excitation: Modified SDOF Model	406
6.2.5	Seismic Excitation: Modified SDOF Model	410
6.3	Design Issues for Structural Isolation Systems	414
6.3.1	Flexibility	414
6.3.2	Rigidity Under Low-level Lateral Loads	416
6.3.3	Energy Dissipation/Absorption	421
6.3.4	Applicability of Base Isolation Systems	422
6.4	Modeling Strategies for Rubber Bearings	424
6.4.1	Modeling of a Natural Rubber Bearing (NRB)	424
6.4.2	Modeling of a Lead Rubber Bearing (LRB)	428
6.5	Examples of Existing Base Isolation Systems	432
6.5.1	USC University Hospital [75, 10]	432
6.5.2	Fire Department Command and Control Facility [71]	433
6.5.3	Evans and Sutherland Manufacturing Fa- cility [88]	434
6.5.4	Salt Lake City Building [72, 108]	435
6.5.5	The Toushin 24 Ohmori Building [23]	436
6.5.6	Bridgestone Toranomon Building	439
6.5.7	San Francisco City Hall	440

6.5.8	Long Beach V.A. Hospital	440
6.5.9	Mills-Peninsula Health Services New Hos- pital	441
6.5.10	Benicia-Martinez Bridge [29]	442
6.5.11	The Cathedral of Christ the Light [91] . .	443
6.6	Optimal Stiffness Distribution: Discrete Shear Beam	444
6.6.1	Scaled Stiffness Distribution	444
6.6.2	Stiffness Calibration for Seismic Isolation .	450
6.7	Optimal Stiffness Distribution: Continuous Can- tilever Beam	454
6.7.1	Stiffness Distribution: Undamped Response	454
6.7.2	Fundamental Mode Equilibrium Equation	462
6.7.3	Rigidity Calibration: Seismic Excitation .	464
7	Applications of Active Control	481
7.1	The Nature of Active and Semi-Active Control . .	482
7.1.1	Active versus Passive Control	482
7.1.2	The Role of Feedback	487
7.1.3	Computational Requirements and Models for Active Control	488
7.1.4	An Introductory Example of Dynamic Feed- back Control	489
7.2	Active and Semi-Active Device Technologies . . .	497
7.2.1	Active versus Semi-Active Devices	497
7.2.2	Force Application Schemes	499
7.2.3	Large-Scale Linear Actuators	505
7.2.4	Semi-Active Device Technologies	509
7.2.5	Smart Materials	523
7.2.6	Hybrid Systems	531

CONTENTS

8	Structural Control Dynamics	539
8.1	Introduction	540
8.2	State-Space Formulation: Linear Time-Invariant SDOF Systems	540
8.2.1	Governing Equations	540
8.2.2	Free Vibration Uncontrolled Response	542
8.2.3	General Solution: Linear Time-Invariant Systems	545
8.2.4	Stability Criterion	547
8.2.5	Linear Negative Feedback	550
8.2.6	Effect of Time Delay on Feedback Control	552
8.2.7	Stability Analysis for Time Delay	556
8.3	Discrete Time Formulation: SDOF Systems	565
8.3.1	Governing Equation	565
8.3.2	Linear Negative Feedback Control	568
8.3.3	Stability Analysis for Time-Invariant Linear Feedback Control	569
8.4	State-Space Formulation for MDOF Systems	587
8.4.1	Notation and Governing Equations	587
8.4.2	Free Vibration Response: Time-Invariant Uncontrolled System	589
8.4.3	Orthogonality Properties of the State Eigenvectors	596
8.4.4	Determination of \mathbf{W} and f_j	598
8.4.5	General Solution: Time-Invariant System	600
8.4.6	Modal State-Space Formulation: Uncoupled Damping	602
8.4.7	Modal State-Space Formulation: Arbitrary Damping	605

8.4.8	Stability Analysis: Discrete Modal Formulation	623
8.4.9	Controllability of a Particular Modal Response	633
8.4.10	Observability of a Particular Modal Response	649
9	Linear Control	657
9.1	Introduction	658
9.2	Optimal Linear Feedback: Time-Invariant SDOF Systems	658
9.2.1	Quadratic Performance Index	658
9.2.2	An Example: Linear Quadratic Regulator Control Algorithm	661
9.2.3	The Continuous Time Algebraic Riccati Equation	667
9.2.4	The Discrete Time Algebraic Riccati Equation	673
9.2.5	Finite Interval Discrete Time Algebraic Riccati Equation	684
9.2.6	Continuous Time Riccati Differential Equation	687
9.2.7	Variational Formulation of the Continuous Time Riccati Equation	688
9.3	LQR Control Algorithm: MDOF Time-Invariant Systems	700
9.3.1	Continuous Time Modal Formulation	701
9.3.2	Discrete Time Modal Formulation	703
9.3.3	Application Studies: LQR Control	705
10	Advanced Control Theory	741
10.1	Introduction	742

CONTENTS

10.2 State Controllability	742
10.3 State Observability	745
10.4 State Observer	749
10.5 Input-Output Relations: H_2 and H_∞ Control . . .	759
10.5.1 SDOF Input-Output Relations	759
10.5.2 Norm of Functions	765
10.5.3 Input-Output Relationships Revisited . . .	767
10.5.4 MDOF Input-Output Relations	774
10.6 Introduction to Nonlinear Control	778
10.6.1 Lyapunov Stability Theory	779
10.6.2 Sliding Mode Control	784
10.7 Applications to Semi-Active and Hybrid Systems	793
10.7.1 Linear Controller for a Semi-Active TLCD	793
10.7.2 Variable stiffness	801
10.7.3 Variable Fluids	809
Bibliography	819

1

Introduction

1.1 Source of Motion Problems

In general, a “designed” structure has to satisfy a set of requirements pertaining to *safety* and *serviceability*. Safety relates to extreme loadings that have a low probability of occurring during a structure's life. The concerns here are the collapse of the structure, major damage to the structure and its contents, and loss of life. Serviceability pertains to moderate loadings that may occur several times during a structure's lifetime. For service loadings, the structure should remain fully operational (i.e., the structure should suffer negligible damage and, furthermore, the motion experienced by the structure should not exceed specified *comfort limits* for humans and motion-sensitive equipment mounted on the structure). An example of a human comfort limit is the restriction on the acceleration; humans begin to feel uncomfortable when the acceleration reaches about 0.02 g . A comprehensive discussion of human comfort criteria is given by [12].

Safety concerns are satisfied by requiring the resistance (i.e., strength) of the individual structural elements to be greater than the demand associated with the extreme loading. The conventional structural design process proportions the structure based on strength requirements, establishes the corresponding stiffness properties, and then checks the various serviceability constraints such as elastic behavior. Iteration is usually necessary for convergence to an acceptable structural design. This approach is referred to as *strength-based design* since the elements are proportioned according to strength requirements.

Applying a strength-based approach for preliminary design is appropriate when strength is the dominant design requirement. In the past, most structural design problems have fallen in this

1.1. SOURCE OF MOTION PROBLEMS

category. However, a number of developments have occurred recently that have limited the effectiveness of the strength-based approach.

Firstly, the trend toward more flexible structures such as tall buildings and longer span horizontal structures has resulted in more structural motion under service loading, thus shifting the emphasis from safety toward serviceability. For instance, the wind-induced lateral deflection of the Empire State Building in New York City, one of the earliest tall buildings in the United States, is several inches whereas the wind-induced lateral deflection of the former World Trade Center towers was several feet, an order of magnitude increase. This difference is due mainly to the increased height and slenderness of the former World Trade Center towers in comparison with the Empire State tower. Furthermore, satisfying the limitation on acceleration is a difficult design problem for tall, slender buildings.

Secondly, some of the new types of facilities such as space platforms and micro-structure manufacturing centers have more severe design constraints on motion than the typical civil structure. In the case of micro-device manufacturing, the environment has to be essentially motion free. Space platforms used to support mirrors have to maintain a certain shape within a small tolerance in order for the mirror to properly function. The design strategy for *motion-sensitive structures* is to proportion the members based on the stiffness needed to satisfy the motion constraints, and then check if the strength requirements are satisfied.

Thirdly, recent advances in material science and engineering have resulted in significant increases in the strength of traditional civil engineering materials such as steel and concrete, as well as a new generation of composite materials. Although the strength

CHAPTER 1. INTRODUCTION

of structural steel has essentially doubled, its elastic modulus has remained constant. Also, there has been some percentage increase in the elastic modulus for concrete, but this improvement is still small in comparison to the increase in strength. The lag in material stiffness versus material strength has resulted in additional structural motion, shifting design constraints from strength to serviceability. Indeed, for very high strength materials, the serviceability requirements may dominate.

		Damage			
		Negligible	Minor	Moderate	Extreme
Earthquake Design Load	Small			Unacceptable Performance (for new constructions)	
	Medium	<i>Essential/Hazardous Objective</i>		<i>Basic Objective</i>	
	Large	<i>Safety Critical Objective</i>		<i>Basic Objective</i>	
	Extreme	<i>Safety Critical Objective</i>		<i>Basic Objective</i>	

Figure 1.1: Performance-based design objective matrix for seismic excitation.

Fourthly, experience with recent earthquakes has shown that repairing the damages resulting from two motion related effects, high floor acceleration and inelastic deformation, can be very expensive, often exceeding the initial cost of the structure. Therefore, the focus in Seismic Design is shifting toward dual objectives: preventing the loss of life; and minimizing the total cost of damage over the life of the structure. The latter goal is associated with *performance based design*. Fig. 1.2 shows the objectives of this approach, which is rapidly gaining acceptance within the seismic design community.

1.2 Structural motion Engineering Methodology

Structural motion engineering is an approach that is more effective for the motion related design problems just described. This approach takes as its primary objective the satisfaction of motion requirements, and views strength as a constraint, not as a primary requirement. Motion engineering employs structural motion control methods to deal with the broad range of issues associated with the motion of structural systems, such as the specification of motion requirements governed by human and equipment comfort and the use of energy storage, dissipation, and absorption devices to control the motion generated by design loadings. Structural motion control provides the conceptual framework for the design of structural systems where motion is the dominant design constraints. Generally, one seeks the optimal deployment of material and motion control mechanisms to achieve the design targets on motion as well as satisfy the constraints on strength.

In what follows, examples are presented that reinforce the need for an alternate paradigm having motion rather than strength as its primary focus. These examples deal with the issue of strength versus serviceability from a static perspective for building-type structures. The dynamic case is treated later in Chapter 2.

1.3 Motion versus Strength Issues - Static Loading

1.3.1 Building Type Structures

Building configurations must simultaneously satisfy the requirements of site (location and geometry), building functionality

CHAPTER 1. INTRODUCTION

(occupancy needs), appearance, and economics. These requirements significantly influence the choice of the structural system and the corresponding design loads. Buildings are subjected to two types of loadings: *gravity loads*, consisting of the actual weight of the structural system and the material, equipment, and people contained in the building; and *lateral loads*, consisting mainly of wind and earthquake loads. Both wind and earthquake loadings are dynamic in nature and produce significant amplification over their static counterpart. The relative importance of wind versus earthquake depends on the site location, building height, and structural makeup. For steel buildings, the transition from *earthquake dominant* to *wind dominant* loading for a seismically active region occurs when the building height reaches approximately 150 m. Concrete buildings, because of their larger mass, are controlled by earthquake loading up to at least a height of 250 m, since the additional gravity load increases the seismic forces. In regions where the earthquake action is low (e.g., Chicago, Illinois), the transition occurs at a much lower height, and the design is governed primarily by wind loading.

1.3. MOTION VERSUS STRENGTH ISSUES - STATIC LOADING

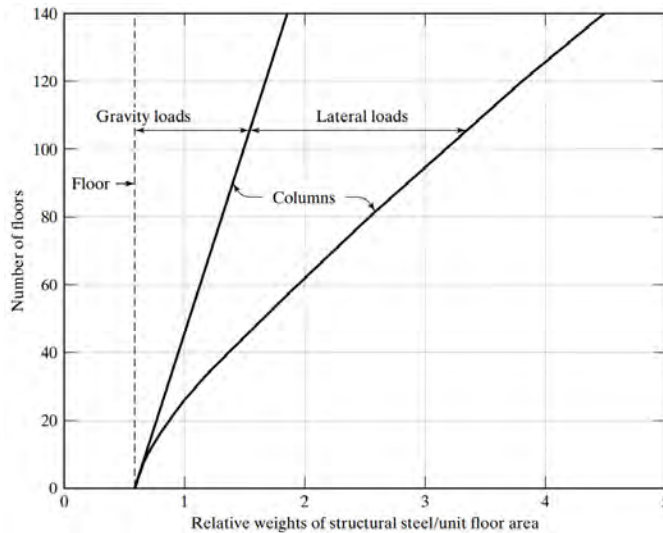


Figure 1.2: Structural steel quantities for gravity and wind systems.

When a low-rise building is designed for gravity loads, it is very likely that the underlying structure can carry most of the lateral loads. As the building height increases, the overturning moment and lateral deflection resulting from the lateral loads increase rapidly, requiring additional material over and above that needed for the gravity loads alone. Fig. 1.2 illustrates how the unit weight of the structural steel required for the different loadings varies with the number of floors. There is a substantial structural weight cost associated with lateral loading for tall buildings [102].

To illustrate the dominance of motion over strength as the slenderness of the structure increases, the uniform cantilever beam shown in Fig. 1.3 is considered. A cantilever beam is a reasonable model for a rectangular building. The lateral load is taken as a concentrated force p applied to the tip of the beam and is assumed to be static. The limiting cases of a pure shear ($d/H \approx 1$) beam and a pure bending beam ($d/H \approx 0.1$) are

CHAPTER 1. INTRODUCTION

examined.

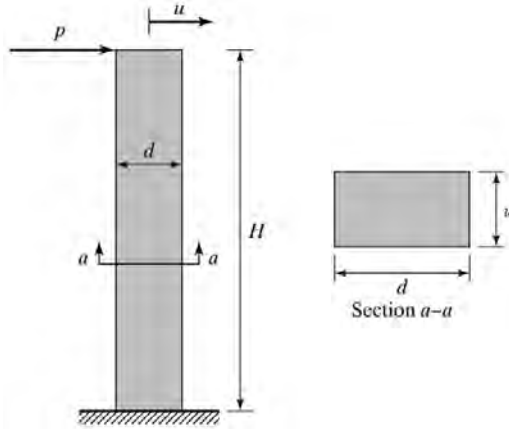


Figure 1.3: Building modeled as a uniform cantilever beam.

Example 1.1 - Cantilever shear beam

The shear stress τ is given by

$$\tau = \frac{p}{A_s} \quad (1)$$

where A_s is the cross-sectional area over which the shear stress can be considered to be constant. When the bending rigidity is very large, the displacement, u , at the tip of the beam is due mainly to shear deformation and can be estimated as

$$u = \frac{pH}{GA_s} \quad (2)$$

where G is the shear modulus and H is the height of the beam. This model is called a *shear beam*. The shear area needed to satisfy the strength requirement follows from Eq. (1):

$$A_s|_{\text{strength}} \geq \frac{p}{\tau^*} \quad (3)$$

1.3. MOTION VERSUS STRENGTH ISSUES - STATIC LOADING

where τ^* is the allowable stress. Noting Eq. (2), the shear area needed to satisfy the serviceability requirement on displacement is

$$A_s|_{\text{serviceability}} \geq \frac{p}{G} \cdot \frac{H}{u^*} \quad (4)$$

where u^* denotes the allowable displacement. The ratio of the area required to satisfy serviceability to the area required to satisfy strength provides an estimate of the relative importance of the motion design constraints versus the strength design constraints

$$r = \frac{A_s|_{\text{serviceability}}}{A_s|_{\text{strength}}} = \frac{\tau^*}{G} \cdot \frac{H}{u^*} \quad (5)$$

Fig. E1.1a shows the variation of r with H/u^* . Increasing H/u^* places more emphasis on the motion constraint since it corresponds to a decrease in the allowable displacement, u^* . Furthermore, an increase in the allowable shear stress, τ^* , also increases the dominance of the displacement constraint.

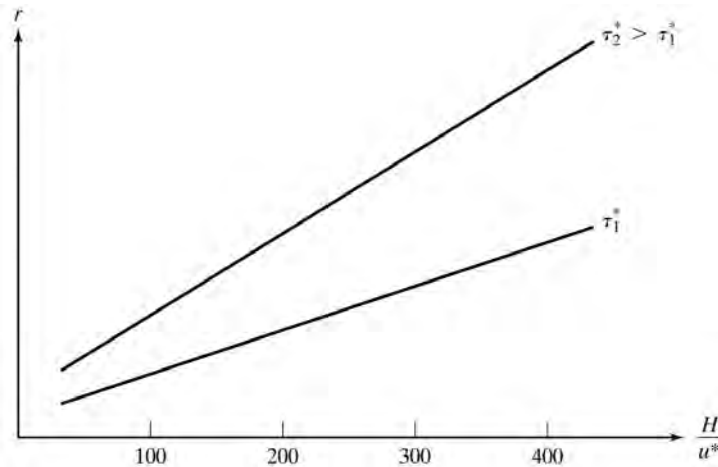


Figure E1.1a: Plot of r versus H/u^* for a pure shear beam.

Example 1.2 - Cantilever bending beam

When the shear rigidity is very large, shear deformation is negligible, and the beam is called a “bending” beam. The maximum bending moment M in the structure occurs at the base and equals

$$M = pH \quad (1)$$

The resulting maximum stress σ is

$$\sigma = \frac{M}{S} = \frac{Md}{2I} = \frac{pHd}{2I} \quad (2)$$

where S is the section modulus, I is the moment of inertia of the cross section about the bending axis, and d is the depth of the cross section (see Fig. 1.3). The corresponding displacement at the tip of the beam, u , becomes

$$u = \frac{pH^3}{3EI} \quad (3)$$

The moment of inertia needed to satisfy the strength requirement is given by

$$I_{\text{strength}} \geq \frac{pHd}{2\sigma^*} \quad (4)$$

Using Eq. (3), the moment of inertia needed to satisfy the serviceability requirement is

$$I_{\text{serviceability}} \geq \frac{pH^3}{3Eu^*} \quad (5)$$

Here, u^* and σ^* denote the allowable displacement and stress respectively. The ratio of the moment of inertia required to

1.3. MOTION VERSUS STRENGTH ISSUES - STATIC LOADING

satisfy serviceability to the moment of inertia required to satisfy strength has the form

$$r = \frac{I_{\text{serviceability}}}{I_{\text{strength}}} = \frac{pH^3}{3Eu^*} \cdot \frac{2\sigma^*}{pHd} = \frac{2H}{3d} \cdot \frac{\sigma^*}{E} \cdot \frac{H}{u^*} \quad (6)$$

Fig. E1.2a shows the variation of r with H/u^* for a constant value of the aspect ratio H/d ($H/d \approx 7$ for tall buildings). Similar to the case of the shear beam, an increase in H/u^* places more emphasis on the displacement since it corresponds to a decrease in the allowable displacement, u^* , for a constant H . Also, an increase in the allowable stress, σ^* , increases the importance of the displacement constraint.

For example, consider a standard strength steel beam with an allowable stress of $\sigma^* = 200$ MPa, a modulus of elasticity of $E = 200,000$ MPa, and an aspect ratio of $H/d = 7$. The value of H/u^* at which a transition from strength to serviceability occurs is

$$\frac{H}{u^*} \Big|_{r=1} = \frac{3}{2} \cdot \frac{E}{\sigma^*} \cdot \frac{d}{H} \approx 200 \quad (7)$$

For $H/u^* > 200$, $r > 1$ and motion controls the design. On the other hand, if medium-strength steel is utilized ($\sigma^* = 400$ MPa and $E = 200,000$ MPa),

$$\frac{H}{u^*} \Big|_{r=1} \approx 100 \quad (8)$$

and motion essentially controls the design for the full range of allowable displacement.

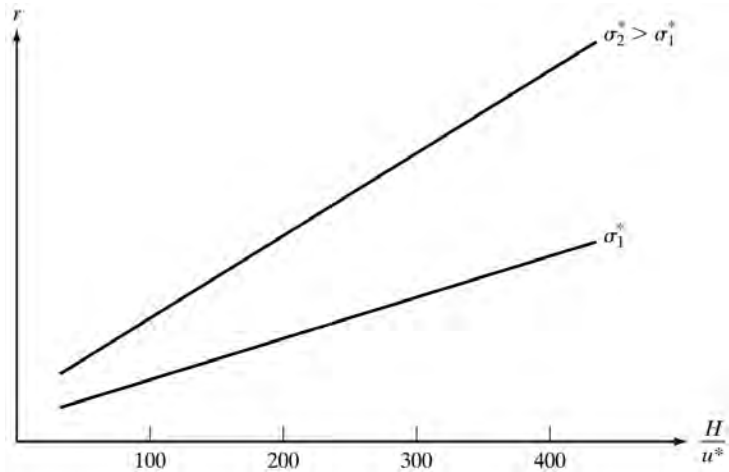


Figure E1.2a: Plot of r versus H/u^* for a pure bending beam.

Example 1.3 - Interstory drift

This example examines the interstory displacement constraint for a single bay frame of height H and load p (see Fig. E1.3a). For simplicity, a very stiff girder is assumed, resulting in a frame that displays quasi-shear beam behavior. Furthermore, the columns are considered to be identical, each characterized by a modulus of elasticity, E_c , and a moment of inertia about the bending axis, I_c . The maximum moment, M , in each column is equal to

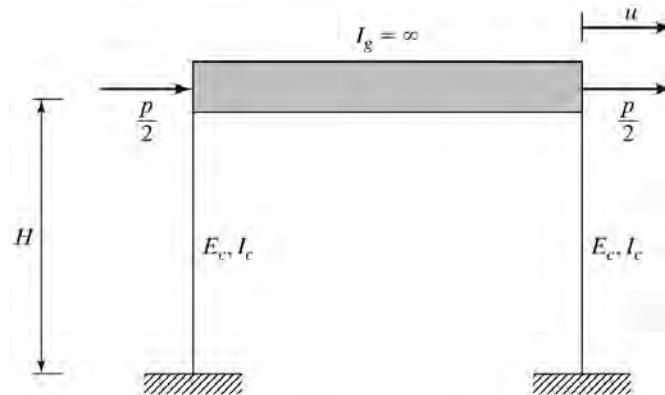


Figure E1.3a: Interstory displacement example.

1.3. MOTION VERSUS STRENGTH ISSUES - STATIC LOADING

$$M = \frac{pH}{4} \quad (1)$$

The lateral displacement of the frame under the load is expressed as

$$u = \frac{pH}{D_T} \quad (2)$$

where D_T denotes the equivalent shear rigidity which, for this structure, is given by

$$D_T = \frac{24E_c I_c}{H^2} \quad (3)$$

The strength constraint requires that the maximum stress in the column be less than the allowable stress σ^* :

$$\frac{Md}{2I_c} = \frac{pHd}{8I_c} \leq \sigma^* \quad (4)$$

where d represents the depth of the column in the bending plane. Eq. (4) is written as

$$I_c|_{\text{strength}} \geq \frac{pHd}{8\sigma^*} \quad (5)$$

The serviceability requirement constrains the maximum displacement to be less than the allowable displacement u^* , which is expressed as:

$$\frac{pH^3}{24E_c I_c} \leq u^* \leq \frac{H}{\alpha} \quad (6)$$

The corresponding requirement for I_c is

$$I_c|_{\text{serviceability}} \geq \frac{pH^2\alpha}{24E_c} \quad (7)$$

CHAPTER 1. INTRODUCTION

Forming the ratio of the moment of inertia required to satisfy the serviceability requirement to the moment of inertia required to satisfy the strength requirement,

$$r = \frac{I_c|_{\text{serviceability}}}{I_c|_{\text{strength}}} = \frac{\sigma^*}{3E_c} \cdot \frac{H}{d} \cdot \alpha \quad (8)$$

leads to the value of α for which motion dominates the design:

$$\alpha \geq \frac{3E_c}{\sigma^*} \cdot \frac{d}{H} \quad (9)$$

Using nominal values

$$\sigma^* = 200 \text{ MPa} \quad E = 200,000 \text{ MPa} \quad \frac{d}{H} = \frac{1}{20} \quad (10)$$

provides an estimate of the value of α for which motion dominates the design:

$$\alpha \geq 3(1000) \left(\frac{1}{20} \right) \geq 150 \quad (11)$$

A typical “code” value of α ranges from 300 to 500. It follows that the drift constraint limits typical code-based design.

1.3.2 Bridge Type Structures

A similar analysis can be carried out for bridge type structures. Gravity tends to be the dominant loading for a bridge. A key difference between bridges and buildings is the ability to offset the deflection due to dead load by initially deforming the bridge so one needs to consider only the live load deflection. In what follows, we illustrate the analysis procedure using a uniformly loaded simply supported bridge girder as the typical bridge structure.

1.3. MOTION VERSUS STRENGTH ISSUES - STATIC LOADING

Example 1.4 - Simply supported girder

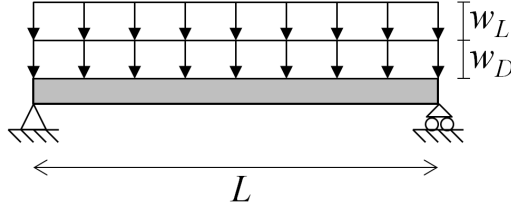


Figure E1.4a: Single-degree-of-freedom system.

The key response measures for the simply supported girder illustrated in Fig. E1.4a are:

$$\begin{aligned} M \left(x = \frac{L}{2} \right) &= (w_D + w_L) \frac{L^2}{8} \\ u \left(x = \frac{L}{2} \right) &= \frac{5(w_D + w_L)L^4}{384EI} \end{aligned} \quad (1)$$

These quantities are constrained by:

$$u|_{w_L} = \frac{5w_L L^4}{384EI} \leq \frac{L}{\alpha} \quad (2)$$

and

$$\sigma = \frac{Md}{2I} = \frac{(w_D + w_L)L^2}{10I} \leq \sigma^* \quad (3)$$

Solving for I leads to

$$\begin{aligned} I_d &> \frac{5w_L L^3 \alpha}{384E} \\ I_\sigma &> \frac{(w_D + w_L)L^2 d}{16\sigma^*} \end{aligned} \quad (4)$$

CHAPTER 1. INTRODUCTION

where I_d and I_σ represent the moments of inertia due to the displacement and strength constraints, respectively. Forming the ratio,

$$r = \frac{I_d}{I_\sigma} = \frac{80}{384} \left(\frac{w_L}{w_D + w_L} \right) \frac{\sigma^* L}{E d} \alpha \quad (5)$$

A typical value for α is $\alpha \approx 800$. Then, setting $r = 1$, and solving for σ^* ,

$$\sigma^*|_{\text{cr}} = \frac{1}{167} \frac{E \cdot d}{L} \frac{1}{1 + \frac{w_D}{w_L}} \quad (6)$$

When $\sigma^* > \sigma^*|_{\text{cr}}$, the live load displacement constraint controls the magnitude of I . Values of $\sigma^*|_{\text{cr}}$ for a range of values of w_D/w_L and d/L are listed in Table E1.4a. A typical lower bound value of the allowable stress for steel is 200 MPa. *It follows that a design based on high strength steel is limited by the constraint on displacement.*

Table E1.4a: Typical values of $\sigma^*|_{\text{cr}}$

w_D/w_L	$\sigma^* _{\text{cr}}$ (MPa)	
	$\frac{d}{L} = \frac{1}{12}$	$\frac{d}{L} = \frac{1}{24}$
0.5	157	78
1.0	210	105
2.0	320	154
3.0	420	210

1.4 Motion-Induced Problems - Periodic Loading

1.4.1 Resonance-Related Problems

A periodic loading applied to a structure excites a periodic response. If the forcing frequency is due to one of the natural frequencies of the structure, which depend on the structural properties, the magnitude of the response quantities such as the displacement, velocity, and acceleration will become excessive and damage will occur. This phenomenon is called **resonance**. In order to avoid resonance, one must select appropriate values for the stiffness and damping parameters in the design phase. Motion issues completely control the design process. There are many sources of excitation. In what follows, we describe some common sources. In a later section, we examine in more detail the response.

Rotating machinery mounted on a floor produces a periodic excitation when the rotating masses are not balanced. Fig. 1.4 illustrates this case. Assuming the mechanism is rotating with a constant angular velocity Ω , the forces acting on the support beam are equal to

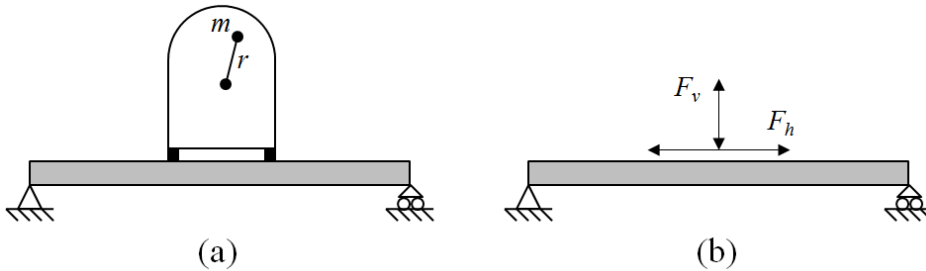


Figure 1.4: Rotating machinery producing a periodic excitation.

$$\begin{aligned} F_v &= (rm\Omega^2) \cos \Omega t \\ F_h &= (rm\Omega^2) \sin \Omega t \end{aligned} \tag{1.1}$$

One needs to design the beam so as to avoid resonance. Alternatively, one can insert additional supports between the machinery and the beam to reduce the magnitude of these forces. The latter approach is called *isolating* the equipment.

Steady fluid flow acting on an object initiates a process where vortices are periodically shed off the leeward face, resulting in a periodic force acting transverse to the direction of flow, as indicated in Fig. 1.5.

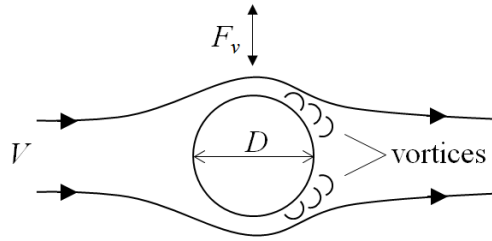


Figure 1.5: Steady flow acting on a circular object of diameter D .

The force is related to the shedding frequency by

$$\begin{aligned} F_v &= F \sin \Omega t \\ \Omega &= 2\pi \left(\frac{0.2V}{D} \right) \end{aligned} \tag{1.2}$$

Steady wind acting on a building produces this effect. Depending on the shedding frequency, Ω , which is a function of the wind speed, the resulting motion, especially the acceleration, may lead to human discomfort. Tall flexible buildings are vulnerable to vortex shedding induced motion, and generally have

1.4. MOTION-INDUCED PROBLEMS - PERIODIC LOADING

some form of motion control installed. Long span horizontal structures, such as suspension bridge decks, are also vulnerable to wind induced lateral/torsional motion.

Offshore platforms, such as shown in Fig. 1.6, are subjected to wave action which is usually modeled as a single sinusoidal wave. The interaction of the wave with the vertical legs is approximated as a periodic force having the same frequency (Fig. 1.6(a)). A reasonable estimate of the response can be generated using a single degree-of-freedom (SDOF) idealization (Fig. 1.6(b)).

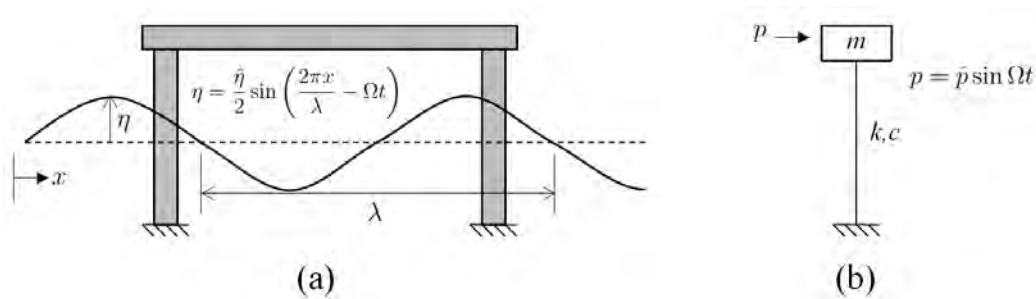


Figure 1.6: Wave load acting on an offshore platform. The *hat* indicates the magnitude.

Given data on wave frequencies for the site, one needs to select the stiffness (k) and damping (c) to avoid becoming close to resonance. The offshore industry has accumulated considerable experience related to designing offshore platforms in severe wave environments.

1.4.2 Response for Periodic Excitation

In this section, the analytical relationship between the excitation and the response is described using, as an illustrative example, a SDOF system. Chapter 2 contains an extensive treatment of multi-degree-of-freedom (MDOF) systems. Consider the SDOF

CHAPTER 1. INTRODUCTION

system shown in Fig. 1.7. The governing equation of motion of the system has the form

$$m\ddot{u}(t) + c\dot{u}(t) + ku(t) = p(t) \quad (1.3)$$

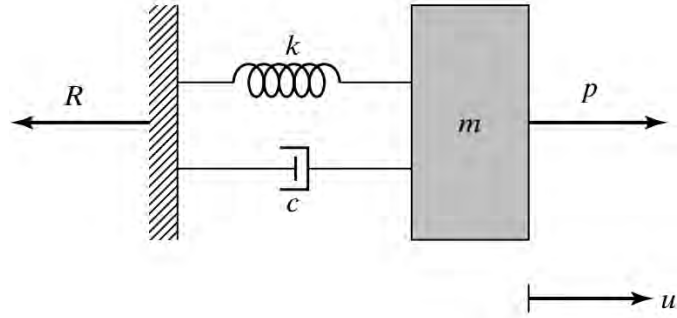


Figure 1.7: Single-degree-of-freedom system.

where m , k , c are the mass, stiffness, and viscous damping parameters of the system, respectively; p is the applied loading; u is the displacement; and t is the independent time variable. The *dot* operator denotes differentiation with respect to time. Taking p to be sinusoidal in time with frequency Ω , and magnitude \hat{p} ,

$$p(t) = \hat{p} \sin \Omega t \quad (1.4)$$

the corresponding forced vibration response is given by

$$u(t) = \hat{u} \sin (\Omega t - \delta) \quad (1.5)$$

where \hat{u} and δ characterize the response. They are related to the system and loading parameters as follows:

1.4. MOTION-INDUCED PROBLEMS - PERIODIC LOADING

$$\begin{aligned}
 \hat{u} &= \frac{\hat{p}}{k} H_1 \\
 H_1 &= \frac{1}{\sqrt{(1 - \rho^2)^2 + (2\xi\rho)^2}} \\
 \omega &= \sqrt{\frac{k}{m}} \\
 \xi &= \frac{c}{2\omega m} = \frac{c}{2\sqrt{km}} \\
 \rho &= \frac{\Omega}{\omega} = \Omega \sqrt{\frac{m}{k}} \\
 \tan \delta &= \frac{2\xi\rho}{1 - \rho^2}
 \end{aligned} \tag{1.6}$$

The term \hat{p}/k is the displacement response that would occur if \hat{p} were applied statically; H_1 represents the effect of the time varying nature of the response. Fig. 1.8 shows the variation of H_1 with the frequency ratio, ρ , for various levels of damping. The maximum value of H_1 and corresponding frequency ratio are related to the damping ratio ξ by

$$\begin{aligned}
 H_1|_{\max} &= \frac{1}{2\xi\sqrt{1 - \xi^2}} \\
 \rho_{\max} &= \sqrt{1 - 2\xi^2}
 \end{aligned} \tag{1.7}$$

When $\xi^2 \ll 1$,

$$\begin{aligned}
 \rho_{\max} &\approx 1 \\
 H_1|_{\max} &\approx \frac{1}{2\xi}
 \end{aligned} \tag{1.8}$$

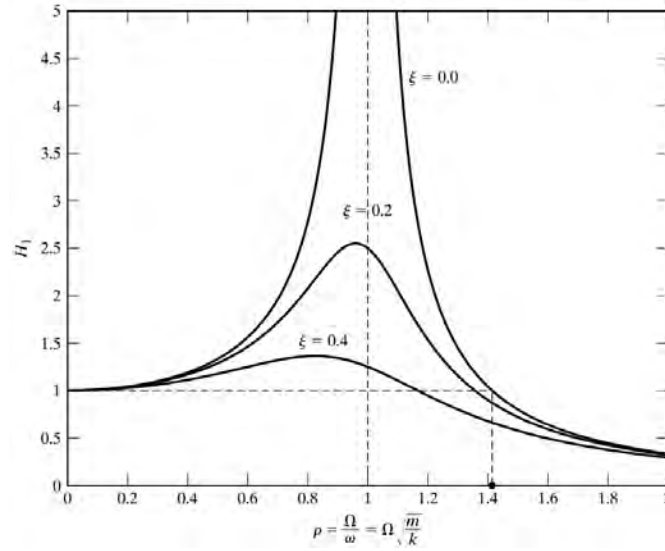


Figure 1.8: Plot of H_1 versus ρ and ξ .

For small ξ , the maximum dynamic response is significantly greater than the static response when ρ is close to 1. This condition is called **resonance**. For example, for $\xi = 0.2$, which corresponds to an upper bound on ξ , the peak response is still quite high: $H_1|_{\max} \approx 2.55$. If the forcing frequency, Ω , is close to the natural frequency, ω , the response depends only on the damping. Outside of this region, damping has less influence and has essentially no effect for $\rho < 0.4$ and $\rho > 1.6$.

The acceleration response a is obtained by differentiating u twice with respect to time

$$a(t) = \ddot{u}(t) = -\Omega^2 \hat{u} \sin(\Omega t - \delta) = -\hat{a} \sin(\Omega t - \delta) \quad (1.9)$$

Noting Eq. (1.6), the magnitude of a can be written as

$$\hat{a} = \frac{\hat{p}}{k} \Omega^2 H_1 = \frac{\hat{p}}{m} H_2 \quad (1.10)$$

1.4. MOTION-INDUCED PROBLEMS - PERIODIC LOADING

where

$$H_2 = \rho^2 H_1 = \sqrt{\frac{\rho^4}{(1 - \rho^2)^2 + (2\xi\rho)^2}} \quad (1.11)$$

The variation of H_2 with ρ for different damping ratios is shown in Fig. 1.9. Note that the behavior of H_2 in the region of $\rho \approx 1$ is similar to H_1 . Both exhibit the **resonance** characteristic, i.e., high amplification:

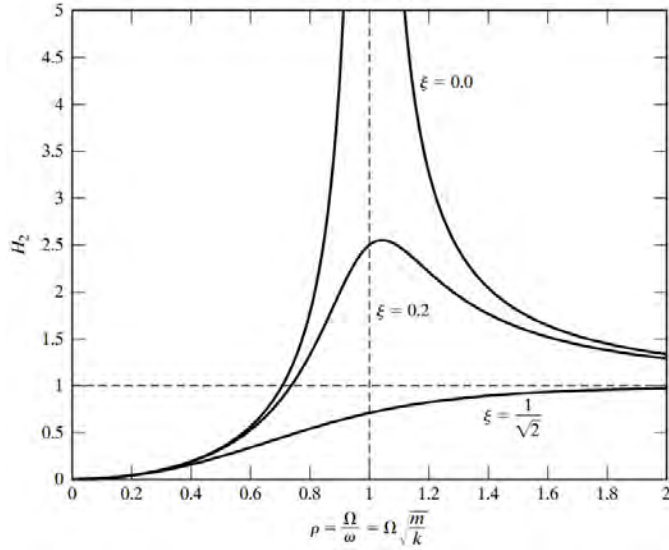


Figure 1.9: Plot of H_2 versus ρ and ξ .

$$H_2|_{\max} = \frac{1}{2\xi\sqrt{1 - 2\xi^2}} \quad (1.12)$$

$$\rho_{\max} = \frac{1}{\sqrt{1 - 2\xi^2}}$$

The ratio \hat{p}/m is the acceleration the mass would experience if it were unrestrained and subjected to a constant force of

CHAPTER 1. INTRODUCTION

magnitude \hat{p} . One can interpret H_2 as a modification factor that takes into account the time-varying nature of the loading and the system restraints associated with stiffness and damping.

Noting Eq. (1.11), the displacement amplitude can be expressed as

$$\hat{u} = \frac{\hat{p}}{k} H_1 = \frac{\hat{p}}{m\omega^2} H_1 = \frac{\hat{p}}{\Omega^2 m} H_2 \quad (1.13)$$

Now, both the displacement and acceleration responses are defined in terms of H_2 . If the loading and system parameters are specified, one determines the response with

$$\hat{u} = \left(\frac{\hat{p}}{\Omega^2 m} \right) H_2$$
$$\hat{a} = \left(\frac{\hat{p}}{m} \right) H_2$$

where $H_2 = H_2(\xi, \rho) = H_2(\xi, m, k, \Omega)$.

The opposite scenario is when the loading and response are specified, say:

$$\hat{a} \leq a^*$$

$$\hat{u} \leq u^*$$

p, Ω, m given

and the appropriate system parameters (k, ξ) need to be determined. This case is discussed in the next section.

The previous examples dealt with determining the displacement or acceleration of the single-degree-of-freedom system. Another design scenario is associated with the concept of isolation

1.4. MOTION-INDUCED PROBLEMS - PERIODIC LOADING

(i.e., where one wants to limit the internal force that is generated by the applied force and transmitted to the support). The reaction force, R , shown in Fig. 1.7, is given by

$$R = p - ma = ku + c\dot{u} \quad (1.14)$$

Expressing R as

$$R = \hat{R} \sin(\Omega t - \delta + \delta_1) \quad (1.15)$$

and using Eqs. (1.4) through (6), the magnitude and phase shift are given by

$$\begin{aligned} \hat{R} &= H_3 \hat{p} \\ H_3 &= \sqrt{\frac{1 + (2\xi\rho)^2}{(1 - \rho^2)^2 + (2\xi\rho)^2}} \\ \tan \delta_1 &= 2\xi\rho \end{aligned} \quad (1.16)$$

Fig. 1.10 shows the variation of H_3 with ρ and ξ . Of particular interest is the case where $H_3 < 1$ which results in $\hat{R} < \hat{p}$. The plot shows that at $\rho = \sqrt{2}$, $H_3 = 1$ for all values of ξ . When $\rho > \sqrt{2}$, the minimum value of H_3 corresponds to $\xi = 0$, which implies that damping magnifies rather than decreases the response in this region. The strategy for reducing the reaction is to take the stiffness as

$$k < \Omega^2 m / 2 \quad (1.17)$$

Decreasing k “softens” the system, reduces the internal force, and causes the displacement and acceleration to approach the following limiting values:

$$\hat{u} = \frac{\hat{p}}{\Omega^2 m}$$

$$\hat{a} = \frac{\hat{p}}{m}$$

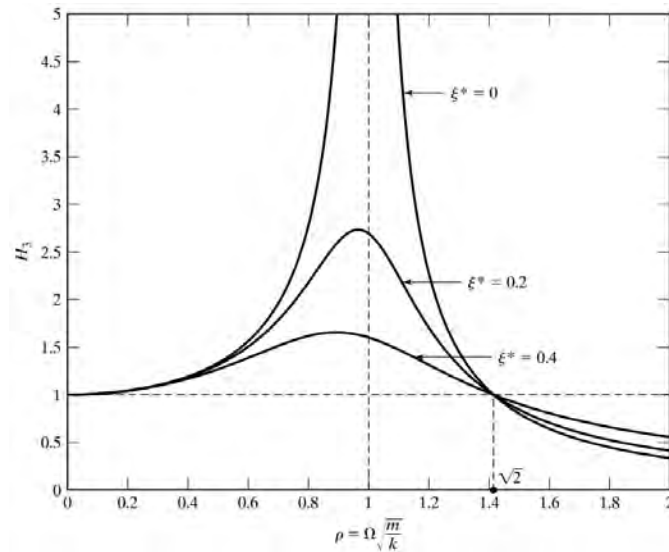


Figure 1.10: Plot of H_3 versus ρ and ξ .

The last scenario relates to seismic excitation. Assuming the ground motion can be represented as a single periodic function, and a structure as a SDOF, one can easily generate an estimate of the response. Consider the SDOF system shown in Fig. 1.11. The equation of motion is:

1.4. MOTION-INDUCED PROBLEMS - PERIODIC LOADING

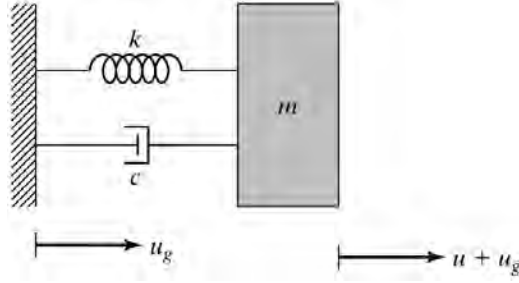


Figure 1.11: Single-degree-of-freedom system.

$$m\ddot{u}(t) + c\dot{u}(t) + ku(t) = -m\ddot{u}_g(t) \quad (1.18)$$

where u is now considered to be the relative displacement with respect to the support, and u_g denotes the motion of the support. Assuming periodic ground excitation,

$$u_g(t) = \hat{u}_g \sin(\Omega t) \quad (1.19)$$

the relative and total displacements are given by

$$u(t) = \hat{u} \sin(\Omega t - \delta) \quad (1.20)$$

$$u_t(u) = u(t) + u_g(t) = \hat{u}_t \sin(\Omega t + \delta_1 - \delta) \quad (1.21)$$

where

$$\hat{u} = H_2 \hat{u}_g \quad (1.22)$$

$$\hat{u}_t = H_3 \hat{u}_g$$

The total acceleration is related to the support acceleration by a similar expression:

$$\begin{aligned} \ddot{u}_t(t) = a_t(t) &= \hat{a}_t \sin(\Omega t + \delta_1 - \delta) \\ \hat{a}_t &= H_3[-\Omega^2 \hat{u}_g] = H_3 \hat{a}_g \end{aligned} \quad (1.23)$$

CHAPTER 1. INTRODUCTION

There are a number of design scenarios for support motion. If the system is sensitive to the total acceleration, one can limit the response by requiring H_3 to be small with respect to unity. In effect, one *isolates* the mass from the support motion. From Fig. 1.10, ρ must be greater than $\sqrt{2}$ for *isolation* to be feasible. The corresponding constraint on stiffness is $k < m\Omega^2/2$.

If the support motion is interpreted as seismic excitation and the system represents a structure, one wants to limit both the relative motion of the structure and the total acceleration of the equipment attached to the structure. One approach is to isolate the structure so that the acceleration constraint is satisfied. The relative motion will be essentially equal to the ground motion, so an additional mechanism is needed to localize the motion. An example of this approach is a *rigid* building supported by low-stiffness springs; the motion in this structure is confined to the support springs. A detailed discussion of isolation of building structures for seismic excitation is presented in Chapter 6.

1.5 Motion Control Methodologies

1.5.1 Passive and Active Control

The previous sections dealt with the problem of determining the response of a single-degree-of-freedom system subjected to periodic excitation. In what follows, using the SDOF case as an example, strategies for controlling the motion, i.e., limiting the response, are introduced.

Consider the linear elastic SDOF system shown in Fig. 1.12. Suppose the design loading is static, and the motion criteria is $u < u^*$. Enforcing equilibrium leads to an expression for the required stiffness:

1.5. MOTION CONTROL METHODOLOGIES

$$k \geq \frac{p}{u^*} \equiv k^* \quad (1.24)$$

From a stiffness perspective, control for static loading is realized by adjusting the stiffness such that k is greater than a certain limiting value, which depends on the design criteria for displacement.

Another way of expressing the motion control requirement is in terms of energy. In general, the work done by the external forces acting on a system is equal to the sum of the mechanical energy stored in the system and the energy transformed to another form, through either energy dissipation or absorption mechanisms. This system is elastic, and the loading is static. It follows that the stored energy is equal to the strain energy, and since no energy is dissipated, the work done by the external loading must be balanced by the strain energy. Expanding these quantities leads to:

$$\begin{aligned} \text{External work} &\leq \text{Strain energy} \\ \frac{1}{2}pu^* &\leq \frac{1}{2}k(u^*)^2 \Rightarrow \frac{p}{u^*} \leq k \end{aligned} \quad (1.25)$$

From an energy perspective, static control is achieved by providing sufficient energy storage capacity to satisfy the energy demand.

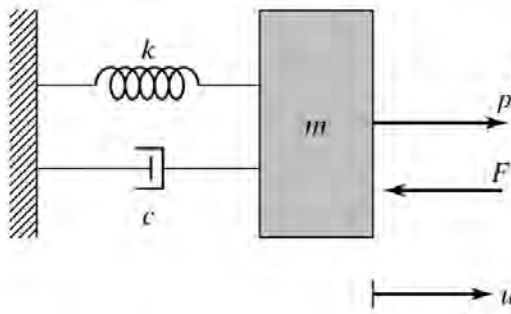


Figure 1.12: Single-degree-of-freedom model for passive and active control.

The design value of stiffness defined by Eq. (1.24) is based on the hypothesis that the system properties (k, m) remain constant as the load is being applied, and there is no other agent that assists in resisting the load. Control is achieved solely by the action of the stiffness embedded within the system. This type of control action is called *passive control* since the system responds in a passive manner, i.e., it does not change its properties during the loading process.

A different strategy for limiting the displacement is based on using an external energy source to counteract some of the energy input. In this approach, the energy requirement is taken as

$$\text{Net external work} - \text{Supplied energy} \leq \text{Strain energy} \quad (1.26)$$

Energy can be supplied in different ways. For the SDOF system, a force actuator can be used to generate the force, F , shown in Fig. 1.12. Force actuators are devices that convert energy into a mechanical force and provide the ability to implement this control strategy. The work done by F as the mass displaces is negative, and represents the supplied energy which offsets the external work done by p .

1.5. MOTION CONTROL METHODOLOGIES

$$\text{Work}|_F = -\frac{1}{2}Fu^*$$

Equation (1.26) expands to

$$\frac{1}{2}pu^* - \frac{1}{2}Fu^* \leq \frac{1}{2}k(u^*)^2 \quad (1.27)$$

and it follows that

$$p - F \leq ku^* \quad (1.28)$$

One can also arrive at this result by enforcing equilibrium. Controlling motion by supplying external energy is referred to as *active control*.

One of the key decisions in motion engineering is the selection of the control strategy. Fully passive static control is simple to implement, since it involves only providing stiffness and damping initially. Active control employs actuator technology and changes in physical properties, which is costly and less reliable. However, active control has considerable potential, particularly for structural applications where weight is a critical issue, such as aerospace vehicles and long-span structures.

The concepts just discussed are also applicable for dynamic loading. When the loading is periodic, the response amplitudes are given by

$$\begin{aligned} \hat{u} &= \frac{\hat{p}}{\Omega^2 m} H_2 \\ \hat{a} &= \frac{\hat{p}}{m} H_2 \end{aligned} \quad (1.29)$$

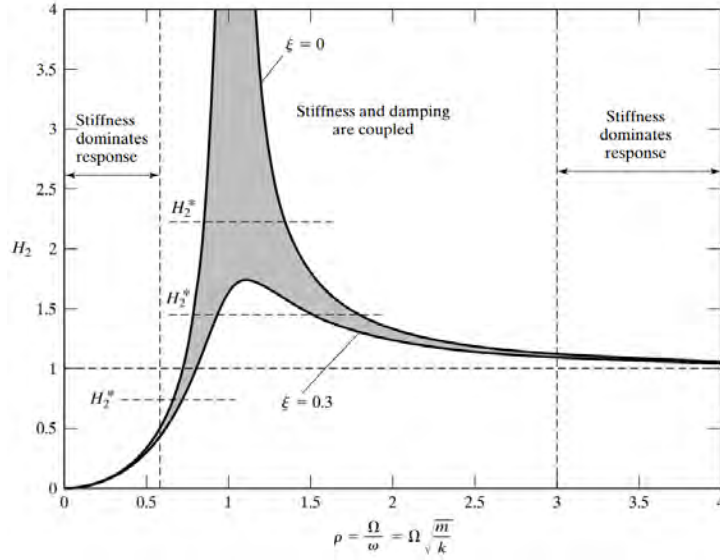


Figure 1.13: Response function for periodic excitation.

where H_2 is plotted in Fig. 1.13. Since civil structures are generally lightly damped, a realistic upper limit for ξ is 0.3. Assuming that \hat{p} , Ω , and m are specified, passive control involves selecting initial values for stiffness and damping that satisfy the design motion criteria:

$$H_2 < H_2^* \tag{1.30}$$

where the value of H_2^* depends on whether displacement or acceleration is the limiting motion constraint.

$$\begin{aligned} H_2^* &= \frac{m\Omega^2 u^*}{\hat{p}} && \text{(displacement)} \\ H_2^* &= \frac{ma^*}{p} && \text{(acceleration)} \end{aligned} \tag{1.31}$$

Fig. 1.13 shows that H_2^* is essentially independent of damping for $H_2^* < \approx 0.5$ and stiffness is the only parameter that can be

1.5. MOTION CONTROL METHODOLOGIES

adjusted to satisfy the design constraint. In this case, the design process is essentially quasi-static. For $0.5 < H_2^* < 1.0$, both stiffness and damping are available as control variables. One can generate a spectrum of designs by specifying stiffness (ρ) and determining the corresponding damping (ξ) that satisfies $H_2 = H_2^*$. When $H_2^* > 1$, there are two possible design zones, one for $\rho < 1$ and the other for $\rho > 1$. As H_2^* increases, these zones merge into a single zone centered at $\rho = 1$, the resonant state of the system. Damping dominates the response in the neighborhood of $\rho = 1$. The strategy employed for $0.5 < H_2^* < 1.0$ can also be applied for $H_2^* > 1.0$. Given H_2^* , we select a value for ρ within the stiffness range defined by the specified value of H_2^* , and the boundary curves $\xi = 0$ and $\xi = 0.3$, and then determine the required value of ξ . For $1.0 \leq H_2^* \leq 1.25$, the second stiffness range is outside $\rho = 3.0$. Designs for this region are controlled by stiffness and are characterized by their low stiffness. Designs for the first region are controlled by both stiffness and damping and have a higher stiffness.

The response for periodic ground excitation is given by $\hat{u}_t = H_3 \hat{u}_g$, where H_3 is plotted in Fig. 1.14. This function also relates the applied periodic force and the corresponding reaction, $\hat{R} = H_3 \hat{p}$. These equations are used to establish a passive control strategy for isolating a system from an external action, either an applied loading or a support motion. In general, one wants $H_3 < 1$ for isolation. Defining H_3^* as the design requirement, the allowable stiffness range is bounded by the curves for $\xi = 0$ (upper bound) and $\xi = 0.3$ (lower bound), as indicated in Fig. 1.14. The absolute upper limit on stiffness is

$$\rho = \sqrt{2} \Rightarrow k_{\max} = \frac{\Omega^2 m}{2} \quad (1.32)$$

CHAPTER 1. INTRODUCTION

Isolation is achieved by reducing the stiffness below the critical level, k_{\max} . Designs are generated by specifying the damping, and then determining the corresponding value of k . Taking $\xi = 0$ leads to an upper bound estimate for k .

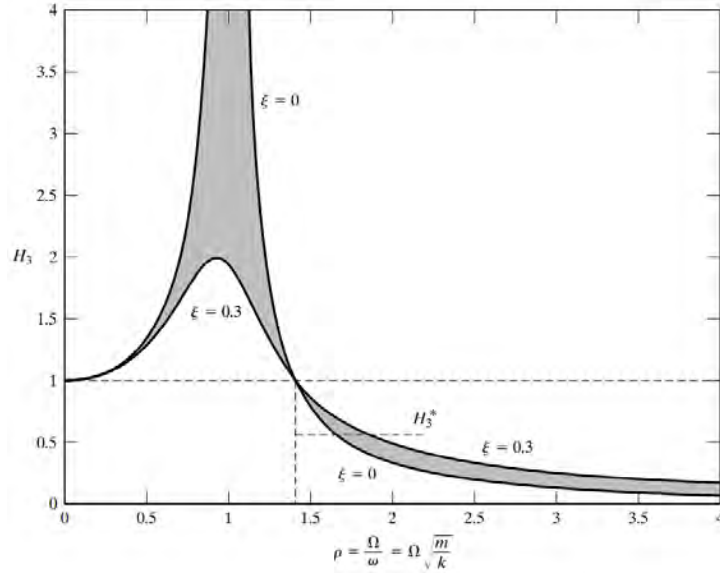


Figure 1.14: Response function for periodic ground excitation.

Active control of a SDOF system for dynamic loading involves applying a control force, $F(t)$, and adjusting its magnitude over time in such a manner that the resulting motion is constrained within the desired limits. A force actuator that responds essentially in real time is required. Specifying the magnitude and sense of $F(t)$ is the key issue for active control. Various approaches are discussed later in the text. In general, F is selected to oppose the motion and does negative work on the mass. This work has to be supplied by an external energy source.

Taking F to be proportional to the displacement and velocity,

$$F(t) = k_d u(t) + k_v \dot{u}(t) \quad (1.33)$$

1.5. MOTION CONTROL METHODOLOGIES

corresponds to increasing the stiffness and damping of the original system. This observation follows by substituting for F in the equilibrium equation. Then, active control based on Eq. (1.33) can be interpreted as introducing virtual stiffness and damping.

From an energy perspective, stable active control reduces the energy demand for the system. The energy balance equation for a linear SDOF system initially at rest is given by (Fig. 1.12 defines the notation used here)

$$\int_0^t p\dot{u} dt + \int_0^t (-F\dot{u}) dt = \frac{1}{2}m\dot{u}^2 + \frac{1}{2}ku^2 + \int_0^t c\dot{u}^2 dt \quad (1.34)$$

The last term is the energy dissipated through linear viscous action. Passive control provides energy storage and energy dissipation mechanisms to resist the demand. When $F(t)$ is taken to have the same sense as \dot{u} , active control decreases the energy input to the system since the integral is always negative. The effect of this action is a lower energy demand than the demand which has to be met by passive control mechanisms.

Selecting a motion control strategy for dynamic excitation involves a number of decisions. Firstly, should the strategy be purely passive or a combination of passive and active control? Secondly, what percentage of the energy demand should be met by energy storage (stiffness) versus energy dissipation (damping)? Thirdly, the type and properties of the passive energy dissipation device needs to be specified. There are a number of passive energy dissipation devices that are appropriate for structural systems. Fourthly, if active control is used to supplement passive control, the type and capacity of the force actuator need to be established.

Although the discussion has focused on a SDOF system, the

concepts introduced here are also applicable for a general multi-degree-of-freedom structural system. The only difference is that now we are dealing with sets of stiffness and damping parameters, and motion criteria involving the displacement variables associated with the degrees of freedom. Using vector notation, the problem can be stated as follows: Given a desired displacement response vector, $\mathbf{u}^*(t)$, determine \mathbf{k} , \mathbf{c} , and \mathbf{F} , the vectors containing the stiffness, damping, and active control force variables. These vectors are functions when the system is continuous.

1.5.2 Desired Response

The desired response for a structure is related to the nature of the loading and the critical performance measures chosen for the structure. For **service loading**, the damage that nonstructural elements, such as wall panels of buildings and fixtures, can experience constrains the magnitude and distribution of displacements, while human and equipment comfort limits the peak acceleration. The controlling criterion for wind-dominant design tends to be the peak velocity and acceleration. Motion is the controlling criterion for earthquake-dominant designs. In general, the structure is required to remain elastic under **service loading**, and non-structural damage is limited.

Under **extreme loading**, structural performance and stability requirements constrain the magnitude and distribution of inelastic deformation that the structural components can experience. Structural deformation is the key measure for earthquake-dominant design. Although design codes allow a structure to experience inelastic deformation under an extreme earthquake with no collapse or loss of life, the current trend is to reduce the **allowable** inelastic deformation [30]. This shift is driven by the

need to lower the cost of repair.

1.6 Scope of Text

This text presents a systematic treatment of the concepts and computational procedures for limiting the motion of civil structures. The material is organized according to the nature of the control process. Part I concerns passive control and includes Chapters 2 through 6. Methodologies for stiffness and damping-based control are presented and applied to typical building-type structures. Part II consists of Chapters 7 through 9. These chapters are intended to provide an introduction to active control concepts and computational algorithms. Quasi-static control is discussed first, since it is easier to deal with analytically. Classical dynamic control algorithms are treated next. Their application to civil structures is illustrated with a series of computer simulation studies.

Problems

Problem 1.1

Refer to Ex. 1.2 and Eq. (5). Construct plots of $(H/u^*)_{\gamma=1}$, as a function of the aspect ratio (H/d) for the following ranges:

- $E = 200,000$ MPa
- σ^* from 200 MPa to 600 MPa
- (H/d) from 3 to 8

Recommended design values of for H/u^* a building are in the region 400 to 500. Comment on when motion rather than strength controls the design.

Problem 1.2

Refer to Ex. 1.3. A typical value for the ratio of column depth to story height is 0.10. Using Eq. (9), determine the value of (H/u^*) for which the constraint on displacement controls the design taking the following ranges for E^c and σ^* :

- $E^c = 200,000$ MPa
- σ^* from 200 MPa to 600 MPa

Problem 1.3

Refer to Ex. 1.3. Suppose a mass, m , is attached to the “infinitely stiff” girder. Assuming the columns have negligible mass, determine the expression for the natural frequency, ω , for lateral vibration in terms of the material and geometric properties of the frame.

Problem 1.4

Consider a SDOF system having $m = 1000$ kg and subjected to a sinusoidal force with amplitude $\hat{p} = 500$ N and frequency 2π r/s. Recommend design values for stiffness, k , and damping, c , corresponding to the following limiting values for peak acceleration:

- $a^* = 0.1$ m/s²
- $a^* = 1$ m/s²
- $a^* = 3$ m/s²

Problem 1.5

Consider a SDOF system with mass of 5000 kg. The system is to be subjected to a periodic loading having a magnitude of 4 kN and frequency 2 Hz. Recommend design values for stiffness and damping corresponding to the following limiting values of peak displacement:

- $u^* = 1$ mm
- $u^* = 10$ mm
- $u^* = 20$ mm

Problem 1.6

Suppose the mass of a SDOF system is known, but the stiffness, k , and damping, c , are unknown. Discuss how you would determine the stiffness by applying a periodic loading for which both the frequency and magnitude can be varied, and monitoring the response. How would you determine the damping parameter, c ?

Problem 1.7

CHAPTER 1. INTRODUCTION

Consider a SDOF system having $m = 1000$ kg. The system is to be subjected to a periodic force with a magnitude of 5 kN and frequency 3 Hz. Recommend design values for k and c such that the magnitude of the reaction force is less than

- 10 kN
- 3 kN

Problem 1.8

A SDOF system having $m = 1000$ kg is to be subjected to the following ground motion:

$$u_g = 0.3 \sin 4\pi t \text{ m}$$

Recommend values for k and c for the following design values of peak relative displacement:

- $u^* = 0.2m$
- $u^* = 0.4m$

Problem 1.9

Recommend values for k and c for a SDOF system with mass of 2000 kg subjected to the following ground motion:

$$u_g = 0.5 \sin 3\pi t \text{ m}$$

The motion constraint is $\hat{u}_t \leq 0.1m$. What is the corresponding value for the peak relative motion, \hat{u} ? Discuss how the response measures, \hat{u}_t and \hat{u} , vary as the spring stiffness is reduced from the value you select.

Problem 1.10

1.6. SCOPE OF TEXT

Consider a SDOF system subjected to ground excitation. Take $m = 3000$ kg and the ground acceleration as

$$u_g = 0.5 \sin 3\pi t \text{ m}$$

Recommend values for k and c such that the peak total acceleration is less than 1.0 m/s^2 .

Problem 1.11

A machine represented by the mass m is to be supported by the spring and dashpot shown in the Fig. P1.11a. The machine is sensitive to total acceleration and therefore needs to be isolated from the ground motion.

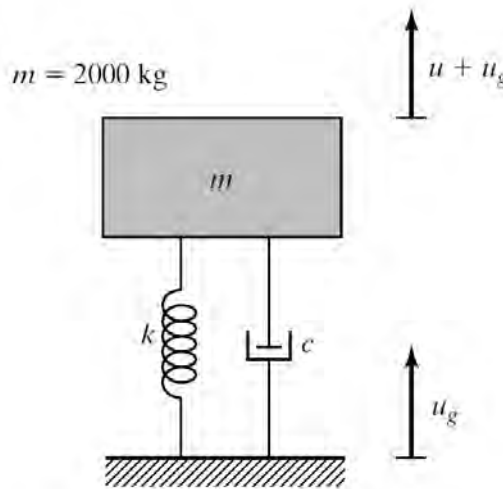


Figure P1.11a

Consider the ground acceleration to consist of two dominant components:

$$\frac{a_g}{g} = 0.1 \sin(2\pi t + \delta_1) + 0.2 \sin(4\pi t + \delta_2)$$

CHAPTER 1. INTRODUCTION

where

g is the gravitational acceleration (9.81 m/s^2) and

δ_1, δ_2 are random phase angles that can range from 0 to 2π

A reasonable approximation for the peak acceleration of the combined response is

$$a_t = \sqrt{(a_{t,1})^2 + (a_{t,2})^2}$$

where $a_{t,1}$ and $a_{t,2}$ are the total accelerations due to the individual harmonic excitations with random phasing.

Suppose the desired maximum total acceleration is $0.005g$. Describe how you would establish design values for k and c .

PART ONE

Passive Control

2

Optimal Stiffness Distribution - Static Loading

2.1 Introduction

This chapter is concerned with the first step in passive motion control, establishing a distribution of structural stiffness that produces the desired displacement profile. When the design loading is quasi-static, the stiffness parameters are determined by solving the equilibrium equations in an inverse way. Discrete systems are governed by algebraic equations, and the problem reduces to finding the elements of the system stiffness matrix, \mathbf{K} . The static case involves solving

$$\mathbf{K}\mathbf{U}^* = \mathbf{P}^* \quad (2.1)$$

for \mathbf{K} , where \mathbf{U}^* and \mathbf{P}^* are the prescribed displacement and loading vectors. Some novel numerical procedures for solving Eq. (2.1) are presented in a later section.

Continuous systems such as beams are governed by differential equations, and the degree of complexity that can be dealt with analytically is limited. The general strategy of working with equilibrium equations is the same, but now one has to determine analytic functions rather than discrete values for the stiffness. Analytical solutions are useful since they allow the key dimensionless parameters to be identified and contain generic information concerning the behavior.

In what follows, the topics discussed concern establishing the stiffness distribution for static loading applied to a set of structures consisting of continuous cantilever beams, building-type structures modeled as equivalent discontinuous beams with lumped masses, and truss-type structures. Closed form solutions are generated for the continuous cantilever beam example.

2.2. GOVERNING EQUATIONS: TRANSVERSE BENDING OF PLANAR BEAMS

2.2 Governing Equations: Transverse Bending of Planar Beams

In this section, the governing equations for a specialized form of a beam are developed. The beam is considered to have a straight centroidal axis and a cross-section that is symmetrical with respect to a plane containing the centroidal axis. Fig. 2.1 shows the notation for the coordinate axes and the displacement measures (translations and rotations) that define the motion of the member. The beam cross section is assumed to remain a plane under loading. This restriction is the basis for the technical theory of beams and reduces the number of displacement variables to three translations and three rotations, which are functions of x and time.

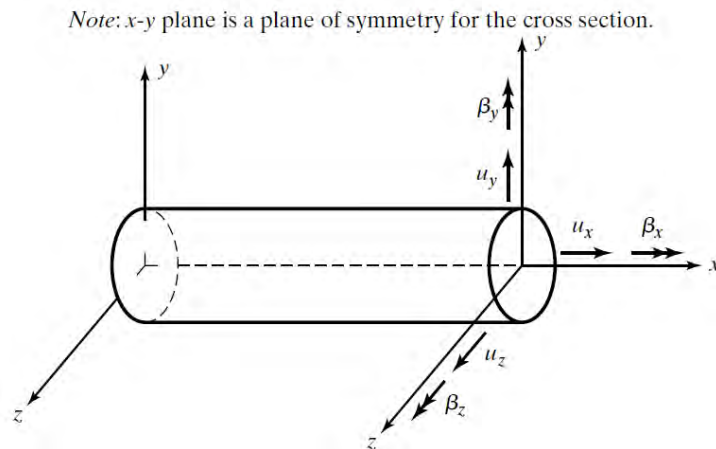


Figure 2.1: Notation - planar beam.

When the loading is constrained to act in the symmetry plane for the cross section, the behavior involves only those motion measures associated with this plane. In this discussion, the $x - y$ plane is taken as the plane of symmetry, and u_x , u_y , and β_z

CHAPTER 2. OPTIMAL STIFFNESS DISTRIBUTION - STATIC LOADING

are the relevant displacement variables. If the loading is further restricted to act only in the y direction, the axial displacement measure, u_x , is identically equal to zero. The behavior for this case is referred to as transverse bending. In what follows, the governing equations for transverse bending of a continuous planar beam are derived. The derivation is then extended to deal with discontinuous structures such as trusses and frames that are modeled as equivalent beams.

2.2.1 Planar Deformation-Displacement Relations

Fig. 2.2 shows the initial and deformed configurations of a differential beam element. The cross-sectional rotation, β_z , is assumed to be sufficiently small such that $\beta_z^2 \ll 1$. In this case, linear strain-displacement relations are acceptable. Letting γ denote the transverse shearing strain and ε the extensional strain at an arbitrary location y from the reference axis, and taking $\beta \equiv \beta_z$ and $u \equiv u_y$, the deformation relations take the form

$$\varepsilon = -y\chi \quad (2.2)$$

$$\gamma = \frac{\delta u}{\delta x} - \beta \quad (2.3)$$

$$\chi = \frac{\delta \beta}{\delta x} \quad (2.4)$$

where χ denotes the bending deformation parameter.

2.2. GOVERNING EQUATIONS: TRANSVERSE BENDING OF PLANAR BEAMS

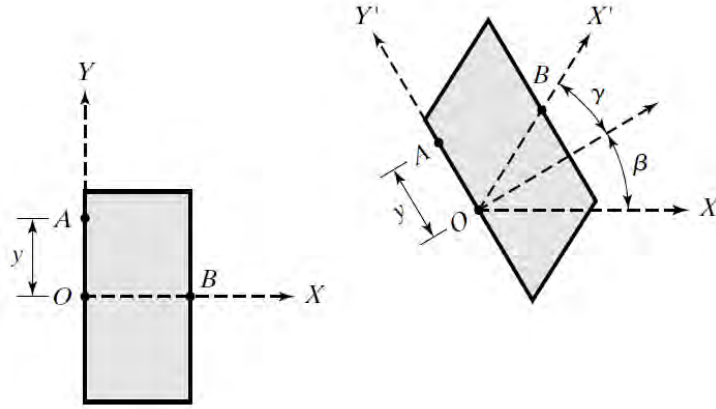


Figure 2.2: Initial and deformed elements.

2.2.2 Optimal Deformation and Displacement Profiles

Optimal behavior from a motion perspective is defined as the state of uniform shear and bending deformation under the design loading. This goal is expressed as

$$\gamma = \gamma^* \quad (2.5)$$

$$\chi = \chi^* \quad (2.6)$$

Uniform deformation states are possible only for statically determinate structures. Building-type structures can be modeled as cantilever beams, and therefore the goal of uniform deformation can be achieved for these structures.

Consider the vertical cantilever beam shown in Fig. 2.3. Integrating Eqs. (2.3) and (2.4) and enforcing the boundary conditions at $x = 0$ leads to

$$\beta = \chi^* x \quad (2.7)$$

CHAPTER 2. OPTIMAL STIFFNESS DISTRIBUTION - STATIC LOADING

$$u = \gamma^* x + \frac{\chi^* x^2}{2} \quad (2.8)$$

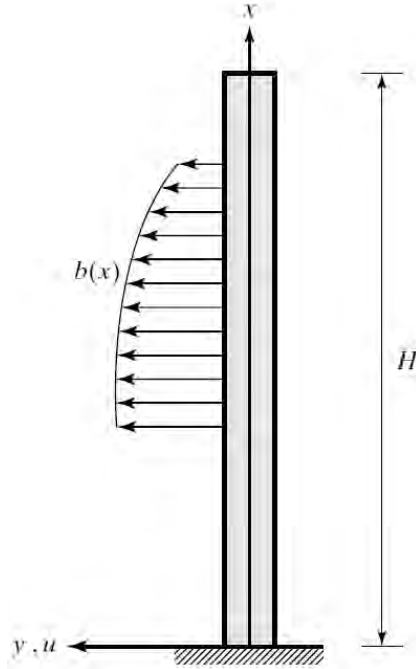


Figure 2.3: Simple cantilever beam.

The deflection at the end of the beam is given by

$$u(H) = \gamma^* H + \frac{\chi^* H^2}{2} \quad (2.9)$$

where $\gamma^* H$ is the contribution from shear deformation and $\chi^* H^2/2$ is the contribution from bending deformation. For actual buildings, the ratio of height to width (i.e., aspect ratio) provides an indication of the relative contribution of shear versus bending deformation. Buildings with aspect ratios on the order of unity tend to display shear beam behavior and $\chi \approx 0$. On the other

2.2. GOVERNING EQUATIONS: TRANSVERSE BENDING OF PLANAR BEAMS

hand, buildings with aspect ratios greater than about 7 display bending beam behavior and $\gamma \approx 0$.

One establishes the values of γ^* , χ^* based on the performance constraints imposed on the motion, and selects the stiffness such that these target deformations are reached. Introducing a dimensionless factor s , which is equal to the ratio of the displacement due to bending to the displacement due to shear at $x = H$,

$$s = \left(\frac{H^2 \chi^*}{2} \right) / (\gamma^* H) = \frac{H \chi^*}{2 \gamma^*} \quad (2.10)$$

transforms Eq. (2.9) to a form that is more convenient for low-rise buildings.

$$u(H) = (1 + s) \gamma^* H \quad (2.11)$$

A shear beam is defined by $s = 0$. Tall buildings tend to have $s \approx 1$.

2.2.3 Equilibrium Equations

Fig. 2.4 shows a differential beam element subjected to an external transverse loading, b , and restrained by the internal transverse shear, V , and bending moment, M . By definition,

$$V = \int \tau dA \quad (2.12)$$

$$M = - \int y \sigma dA \quad (2.13)$$

CHAPTER 2. OPTIMAL STIFFNESS DISTRIBUTION - STATIC LOADING

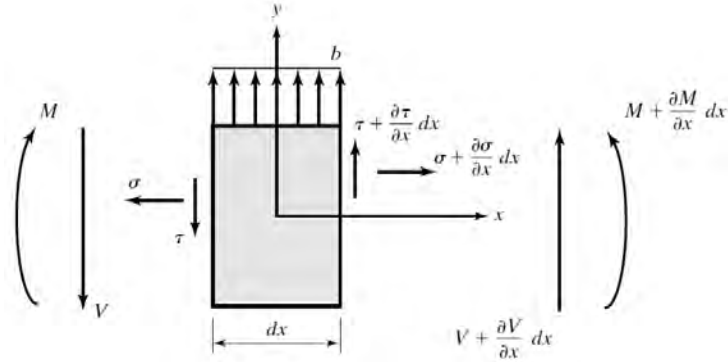


Figure 2.4: Forces acting on a differential element.

where τ and σ are the stresses acting on the cross section. Summing forces and moments leads to

$$\frac{\delta V}{\delta x} + b = \rho_m \frac{\delta^2 u}{\delta t^2} \quad (2.14)$$

$$\frac{\delta M}{\delta x} + V = J \frac{\delta^2 \beta}{\delta t^2} \quad (2.15)$$

where ρ_m , J are the mass and rotatory inertia per unit length. When the member is supported only at $x = 0$ (see Fig. 2.3), the equilibrium equations can be expressed in the following integral form:

$$V(x) = \int_x^H \left(b - \rho_m \frac{\delta^2 u}{\delta t^2} \right) dx \quad (2.16)$$

$$M(x) = \int_x^H \left(V - J \frac{\delta^2 \beta}{\delta t^2} \right) dx \quad (2.17)$$

In the case of static loading, since the acceleration terms are equal to 0, V and M can be determined by integrating Eqs. (2.16) and (2.17).

2.2. GOVERNING EQUATIONS: TRANSVERSE BENDING OF PLANAR BEAMS

2.2.4 Force-Deformation Relations

The force-deformation relations, also referred to as the constitutive relations, depend on the characteristics of the materials that make up the beam. For the case of static loading and linear elastic behavior, the expressions relating the shear force and bending moment to the shear deformation and bending deformation, respectively, are expressed as

$$V(x) = D_T(x)\gamma(x) \quad (2.18)$$

$$M(x) = D_B(x)\chi(x) \quad (2.19)$$

where D_T and D_B are defined as the transverse shear and bending rigidities. These equations have to be modified when the deformation varies with time. This aspect is addressed in Sect. 2.4.2. Examples that illustrate how to determine the rigidity coefficients for a range of beam cross sections are presented next.

Example 2.1 - Composite sandwich beam

Fig. E2.1a shows a sandwich beam composed of two face plates and a core. The face material is usually much stiffer than the core material, and therefore the core is assumed to carry only shear stress. Noting Eq. (2.2), the strains in the face and core are

$$\varepsilon_f = \pm \frac{d}{2}\chi \quad (1)$$

$$\gamma_c = \gamma \quad (2)$$

CHAPTER 2. OPTIMAL STIFFNESS DISTRIBUTION - STATIC LOADING

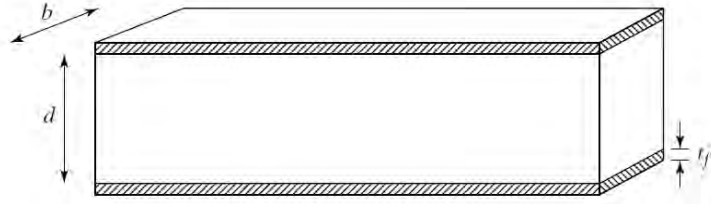


Figure E2.1a: Composite beam cross section.

The face thickness is also assumed to be small in comparison to the depth. Considering the material to be linear elastic, the expressions for shear and moment are

$$V = (bd)\tau_c = (bdG_c)\gamma \quad (3)$$

$$M = (bt_f d)\sigma_f = \left(\frac{bt_f d^2}{2}E_f\right)\chi \quad (4)$$

where G_c is the shear modulus for the core and E_f is the Young's modulus for the face plate. The corresponding rigidity coefficients are

$$D_T = bdG_c \quad (5)$$

$$D_B = \frac{bt_f d^2}{2}E_f \quad (6)$$

Example 2.2 - Equivalent rigidities for a discrete truss beam

The term *truss beam* refers to a beam-type structure composed of a pair of chord members and a diagonal bracing system. Fig. E2.2a illustrates an X-bracing scheme. Truss beams are used as girders for long-span horizontal systems. Truss beams are also deployed to form rectangular space structures, which are the

2.2. GOVERNING EQUATIONS: TRANSVERSE BENDING OF PLANAR BEAMS

primary lateral load-carrying mechanisms for very tall buildings. The typical “mega-truss” has large columns located at the four corners of a rectangular cross section, and diagonal bracing systems placed on the perimeter planes. These structures are usually symmetrical, and the behavior in one of the symmetry directions can be modeled using an equivalent truss beam. When the vertical spacing, h , is small in comparison to the overall length, we can approximate the discrete structure as a continuous beam having equivalent properties. In this example, approximate expressions for these equivalent properties are derived for the case of X-bracing.

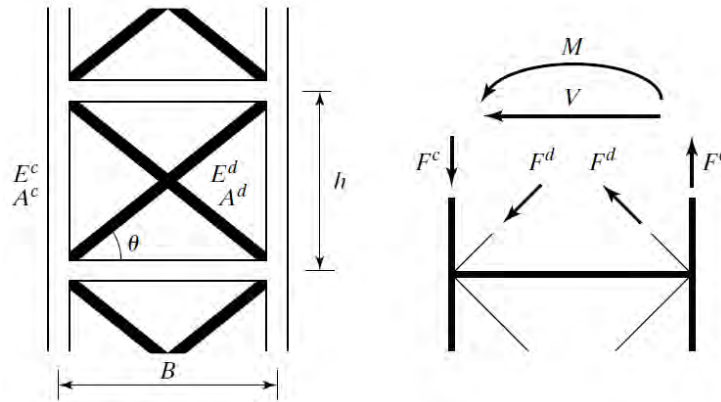


Figure E2.2a: Parameters and internal forces: truss beam.

The key assumption is that the members carry only axial force. This approximation is reasonable when the members are slender, and diagonal or chevron bracing is used. Noting Fig. E2.2a, the cross-section force quantities are related to the member forces by

$$M = BF^c \quad (1)$$

$$V = 2F^d \cos \theta \quad (2)$$

CHAPTER 2. OPTIMAL STIFFNESS DISTRIBUTION - STATIC LOADING

Assuming linear elastic behavior, the member forces are also related to the extensional strains by

$$F^c = A^c E^c \varepsilon^c \quad (3)$$

$$F^d = A^d E^d \varepsilon^d \quad (4)$$

It remains to express the extensional strains in terms of the bending and shear deformation measures.

Fig. E2.2b shows the deformed shapes of a panel of the truss beam. The extensional strain in the diagonals, ε^d , due to the relative motion between adjacent nodes, Δ_h , is a function of Δ_h , and θ .

$$\varepsilon^d |_{\Delta_h} = \pm \frac{\Delta_h \cos \theta \sin \theta}{h} \quad (5)$$

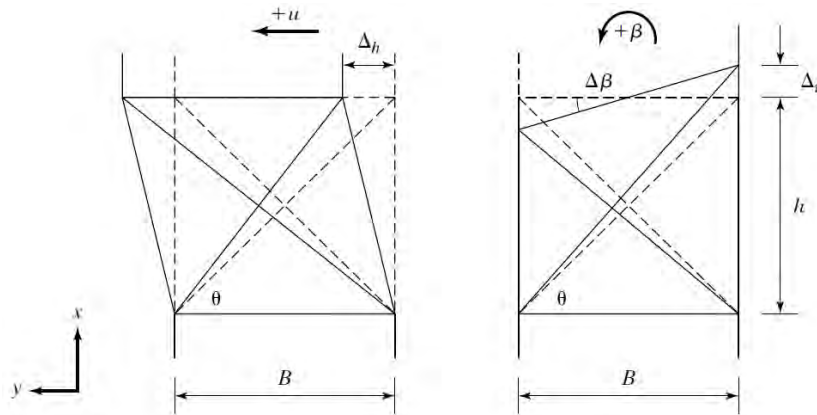


Figure E2.2b: Deformed truss beam section.

Neglecting the extensional strain in the diagonal due to $\Delta\beta$ and approximating γ as

2.2. GOVERNING EQUATIONS: TRANSVERSE BENDING OF PLANAR BEAMS

$$\frac{\Delta_h}{h} \approx \gamma \quad (6)$$

one obtains the following approximation for the total extensional strain:

$$\varepsilon^d \approx \varepsilon^d|_{\Delta_h} \approx \gamma \cos \theta \sin \theta \approx \frac{\gamma \sin 2\theta}{2} \quad (7)$$

Similarly, the extensional strain in the chord, ε^c , is related to the change in angle, $\Delta\beta$, between adjacent sections by

$$\varepsilon^c = \frac{\Delta_v}{2} = \frac{B\Delta\beta}{2h} \quad (8)$$

Noting that $\Delta\beta/h$ is related to the bending deformation χ ,

$$\chi = \frac{\Delta\beta}{h} \quad (9)$$

the strain can be expressed as

$$\varepsilon^c = \frac{B\chi}{2} \quad (10)$$

Substituting for ε^c and ε^d and combining Eqs. (1) through (4) results in

$$M = \left(\frac{A^c E^c B^2}{2} \right) \chi \quad (11)$$

$$V = (A^d E^d \sin 2\theta \cos \theta) \gamma \quad (12)$$

Comparing these expressions with the definition equations for the rigidity parameters leads to the following relations for the equivalent continuous beam properties:

CHAPTER 2. OPTIMAL STIFFNESS DISTRIBUTION - STATIC LOADING

$$D_B = \frac{A^c E^c B^2}{2} \quad (13)$$

$$D_T = A^d E^d \sin 2\theta \cos \theta \quad (14)$$

When the truss beam model is used to represent a tall building, the chords correspond to the columns of the building. These elements are required to carry both gravity and lateral loading whereas the diagonals carry only lateral loading. Since the column force required by the gravity loading is usually larger than the force generated by the lateral loading, the allowable incremental deformation in the column due to lateral loading should be less than the corresponding value for the diagonal. To allow for this reduction, a factor, f^* , which is defined as the ratio of the diagonal strain to the chord strain for lateral loading, is introduced.

$$f^* = \frac{\varepsilon^d}{\varepsilon^c} \quad (15)$$

This factor is greater than 1. Substituting for the strain measures from Eqs. (7) and (10) results in

$$\chi = \frac{\gamma \sin 2\theta}{f^* B} \quad (16)$$

Once the shear deformation level γ^* is specified, the bending deformation is determined with

$$\chi^* = \frac{\gamma^* \sin 2\theta}{f^* B} \quad (17)$$

Substituting for χ^* in Eq. (2.10), the ratio of the contributions from bending and shear deformation expands to

2.3. STIFFNESS DISTRIBUTION FOR A CONTINUOUS CANTILEVER BEAM UNDER STATIC LOADING

$$s = \frac{H \sin 2\theta}{2f^*B} \quad (18)$$

Typical values of f^* for buildings range from about 3 for elastic behavior to 6 for inelastic behavior. Eq. (18) shows that the bending contribution becomes more important as the aspect ratio, H/B , increases. The shear and bending contributions to the elastic displacement at the top of the building are essentially equal when $H \approx 6B$.

2.3 Stiffness Distribution for a Continuous Cantilever Beam under Static Loading

Once the shear and bending moment distributions are specified, the rigidity distributions required to produce a specific deformation profile can be evaluated using Eqs. (2.18) and (2.19). The equations corresponding to uniform deformation reduce to

$$D_T = \frac{V}{\gamma^*} \quad (2.20)$$

$$D_B = \frac{M}{\chi^*} \quad (2.21)$$

For example, taking a uniform loading $b(x) = b$ as shown in Fig. 2.5, which is a reasonable assumption for the wind action on a tall building, results in

$$\begin{aligned} V(x) &= b(H - x) \\ M(x) &= \frac{b(H - x)^2}{2} \end{aligned} \quad (2.22)$$

and

CHAPTER 2. OPTIMAL STIFFNESS DISTRIBUTION - STATIC LOADING

$$\begin{aligned}
 D_T(x) &= \frac{b(H-x)}{\gamma^*} = \frac{bH}{\gamma^*} \left(1 - \frac{x}{H}\right) \\
 D_B(x) &= \frac{b(H-x)^2}{2\chi^*} = \frac{bH^3}{4s\gamma^*} \left(1 - \frac{x}{H}\right)^2
 \end{aligned}
 \tag{2.23}$$

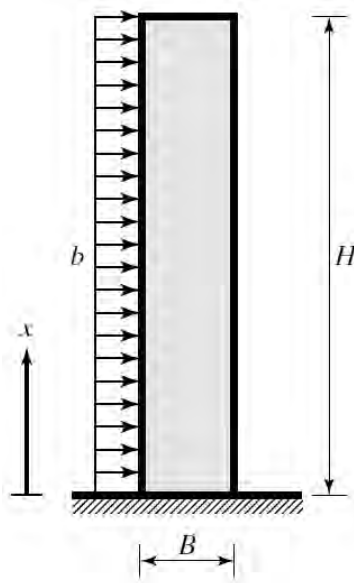


Figure 2.5: Continuous cantilever beam.

A cantilever beam having a linear shear rigidity distribution and a quadratic bending rigidity distribution will be in a state of uniform deformation under uniform transverse loading.

Taking typical values for γ^* , f^* , and the aspect ratio B/H for a tall building modeled as a truss beam,

$$\gamma^* = \frac{1}{400} \quad f^* = 3 \quad \frac{B}{H} = \frac{1}{6}$$

and evaluating s ,

2.3. STIFFNESS DISTRIBUTION FOR A CONTINUOUS CANTILEVER BEAM UNDER STATIC LOADING

$$s = \frac{H}{2f^*B} = 1$$

leads to

$$u(H) = \gamma^*H + \frac{\chi^*H^2}{2} = \gamma^*H(1 + s) = \frac{H}{200}$$
$$\gamma^* = \frac{1}{200}$$

This result for γ^* corresponds to the upper bound value for shear strain. We would use this value together with b and H to establish an appropriate value for D_T at $x = 0$. As will be seen later, the rigidity distributions need to be modified near $x = H$ in order to avoid excessive deformation under dynamic load.

Example 2.3 - Cantilever beam: quasi-static seismic loading

The cantilever beam loading shown in Fig. E2.3a is used to simulate, in a quasi-static way, seismic excitation for low rise buildings. The triangular loading is related to the inertia forces associated with the fundamental mode response, and the concentrated force is included to represent the effect of the higher modes. Evaluating V and applying Eq. (2.20) leads to

$$D_T = \frac{1}{\gamma^*} \left\{ P + \frac{b_0H}{2} \left[1 - \left(\frac{x}{H} \right)^2 \right] \right\} \quad \textcircled{1}$$

CHAPTER 2. OPTIMAL STIFFNESS DISTRIBUTION - STATIC LOADING

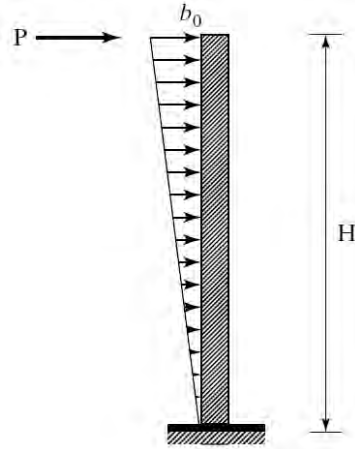


Figure E2.3a: Cantilever beam: quasi-static seismic loading.

A combination of constant and quadratic terms is a reasonable starting point for the transverse shear rigidity distribution.

Example 2.4 - Truss beam revisited

This example extends the treatment of the truss beam discussed in Ex. 2.2 and focuses on comparing the cross-sectional parameters required to satisfy the strength-based versus the stiffness-based performance criteria.

Considering elastic behavior and given the desired design deformations γ^* and χ^* , the corresponding extensional strains ε^{d*} and ε^{c*} must be less than the yield strains for the element materials, ε_y^d and ε_y^c , respectively. That is,

$$\varepsilon_y^d \geq \varepsilon^{d*} = \gamma^* \cos \theta \sin \theta = \frac{\gamma^* \sin 2\theta}{2} \quad (1)$$

$$\varepsilon_y^c \geq \varepsilon^{c*} = \frac{B\chi^*}{2} \quad (2)$$

Once the dimensions and the design deformations are specified, the structural material can be chosen to satisfy the motion design

2.3. STIFFNESS DISTRIBUTION FOR A CONTINUOUS CANTILEVER BEAM UNDER STATIC LOADING

constraints defined by Eqs. (1) and (2). When the column strain is constrained to be related to the diagonal strain by

$$\varepsilon^{c^*} = \frac{\varepsilon^{d^*}}{f^*} \quad (3)$$

Eq. (2) can be written as

$$\varepsilon_y^c \geq \frac{\varepsilon_y^d}{f^*} \quad (4)$$

To provide more options in satisfying the design requirements, different materials may be used. We must also ensure that the stresses due to the design forces, V and M , are less than the yield stresses.

The axial forces in the columns, F^c , and diagonals, F^d , are related to the transverse shear and moment by

$$V = 2F^d \cos \theta \quad (5)$$

$$M = BF^c \quad (6)$$

The cross-sectional areas required to provide the strength capacity follow from Eqs. (5) and (6):

$$A_{\text{strength}}^d \geq \frac{V}{2\sigma^{d^*} \cos \theta} \quad (7)$$

$$A_{\text{strength}}^c \geq \frac{M}{B\sigma^{c^*}} \quad (8)$$

where σ^* denotes the allowable stresses based on strength considerations.

The rigidity terms for this model are

CHAPTER 2. OPTIMAL STIFFNESS DISTRIBUTION - STATIC LOADING

$$D_T = 2A^d E^d \sin \theta \cos^2 \theta \quad (9)$$

$$D_B = \frac{A^c E^c B^2}{2} \quad (10)$$

Substituting Eqs. (9) and (10) in the motion-based design criteria,

$$D_T = \frac{V}{\gamma^*} \quad (11)$$

$$D_B = \frac{M}{\chi^*} \quad (12)$$

we obtain the following expressions for the cross-sectional areas required to satisfy the stiffness requirement:

$$A_{\text{stiffness}}^d \geq \frac{V}{2E^d \gamma^* \sin \theta \cos^2 \theta} \quad (13)$$

$$A_{\text{stiffness}}^c \geq \frac{2M}{E^c B^2 \chi^*} = \frac{f^* M}{E^c B \gamma^* \sin \theta \cos \theta} \quad (14)$$

The ratio of areas provides a measure of the relative importance of strength versus stiffness:

$$\frac{A_{\text{strength}}^d}{A_{\text{stiffness}}^d} = \frac{\gamma^* E^d \sin \theta \cos \theta}{\sigma^{d*}} = \frac{\varepsilon^{d*} E^d}{\sigma^{d*}} \quad (15)$$

$$\frac{A_{\text{strength}}^c}{A_{\text{stiffness}}^c} = \frac{\chi^* E^c B}{2\sigma^{c*}} = \frac{\varepsilon^{c*} E^c}{\sigma^{c*}} \quad (16)$$

Stiffness controls when the ratios are less than unity. The limit on γ^* follows from Eq. (15):

$$\bar{\gamma}^* = \frac{\sigma^{d*}}{E^d \sin \theta \cos \theta} \quad (17)$$

2.4. BUILDINGS MODELED AS SHEAR BEAMS

Table E2.4a: $\bar{\gamma}^*$ values for various steel strengths

σ^* (MPa)	$\bar{\gamma}^*$
250	1/400
500	1/200
1000	1/100

For $\gamma^* < \bar{\gamma}^*$, the cross-sectional area is governed by the deformation constraint, and Eqs. (13) and (14) apply. When $\gamma^* > \bar{\gamma}^*$, the allowable stress is the controlling factor, and Eqs. (7) and (8) apply. Inelastic behavior occurs in this case. Values of $\bar{\gamma}^*$ for a range of allowable stress levels for steel calculated using an angle of 45° are listed in Table E2.4a. With high-strength steel, the structure can experience substantial transverse shear deformation and still remain elastic.

2.4 Buildings Modeled as Shear Beams

2.4.1 Governing Equations for Buildings Modeled as Pseudo Shear Beams

In this section, we consider a class of planar rectangular building frames having aspect ratios of order $O(1)$ and moment resisting connections. Fig. 2.6 shows a typical case. This type of structure is the exact opposite to the truss beam with respect to the way the lateral loading is carried. In the case of the truss beam, the transverse shear is provided by the axial forces in the braces. Here, the shear is produced by bending of the columns. The axial deformation of the columns is usually small for low rise frames, so it is reasonable to assume that the “floors” experience only lateral displacement and slide with respect to each other. Considering the structure as a pseudo-beam, there is no rotation of the cross

CHAPTER 2. OPTIMAL STIFFNESS DISTRIBUTION - STATIC LOADING

section (i.e., $\beta = 0$); there is only one displacement variable per floor; and the transverse shearing strain at a story location is equal to the interstory displacement divided by the story height. In what follows, the formulation of the governing equations is illustrated using a simple structure and then generalized for more complex structures.

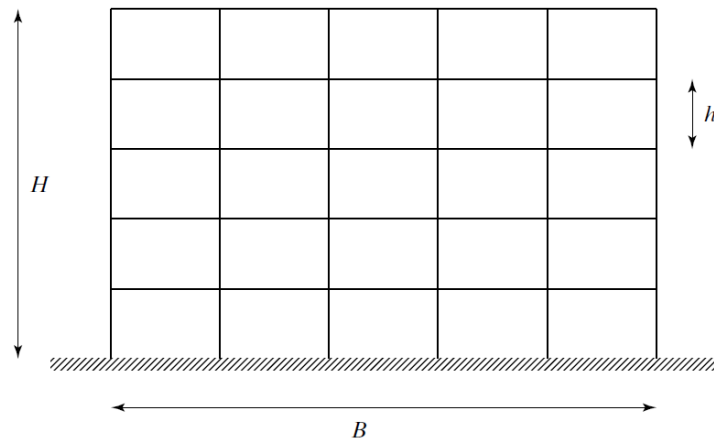


Figure 2.6: Low-rise rigid frame.

The two-story frame shown in Fig. 2.7 is modeled as a 2DOF system having masses concentrated at the floor locations and shear beam segments which represent the action of the columns and beams in resisting lateral displacement. The shear forces in the equivalent beam segments (see Fig. 2.8) are expressed in terms of shear stiffness factors:

$$V_1 = k_1 u_1 \quad V_2 = k_2 (u_2 - u_1) \quad (2.24)$$

2.4. BUILDINGS MODELED AS SHEAR BEAMS

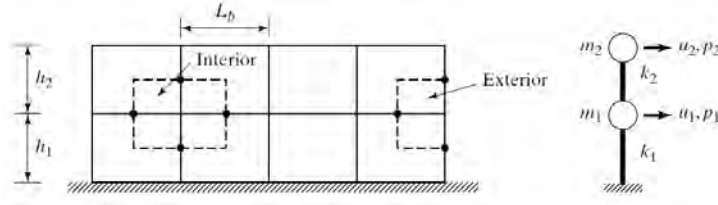


Figure 2.7: A discrete shear beam model.

Noting the definition of transverse shear strain,

$$\gamma_1 = u_1/h_1 \quad \gamma_2 = \frac{u_2 - u_1}{h_2} \quad (2.25)$$

we can relate the k 's to the equivalent transverse shear rigidity factors:

$$V_1 = D_{T,1}\gamma_1 \quad V_2 = D_{T,2}\gamma_2 \quad \Rightarrow \quad D_{T,i} = h_i k_i, \quad i = 1, 2 \quad (2.26)$$

The equivalent shear stiffness factors are determined by displacing the floors of the actual frame, determining the shear forces in the columns, summing these forces for each story, and equating the total shear forces to V_1 and V_2 as defined by Eq. (2.24). The shear force in the j^{th} column of story i is expressed as

$$V_{i,j} = k_{i,j}(u_i - u_{i,j}) \quad (2.27)$$

where $k_{i,j}$ depends on the frame geometry and member properties. Then, summing the column shears for story i and generalizing Eq. (2.24) leads to

$$k_i = \sum_j k_{i,j} \quad (2.28)$$

CHAPTER 2. OPTIMAL STIFFNESS DISTRIBUTION - STATIC LOADING

For this example, $i = 1, 2$ and j ranges from 1 to 5.

An approximate expression for the column shear stiffness factors can be obtained by assuming the location of the inflection points in the columns and beams. Taking these points at the midpoints, as indicated in Fig. 2.7, leads to the following estimates for interior and exterior columns:

$$k_{\text{interior column}} = \frac{12EI_c}{h^3(1 + \frac{1}{2}r)} \quad (2.29)$$

$$k_{\text{exterior column}} = \frac{12EI_c}{h^3(1 + r)} \quad (2.30)$$

where r is a dimensionless parameter,

$$r = \frac{I_c}{h} \cdot \frac{L_b}{I_b} \quad (2.31)$$

and the subscripts denote column and beam properties. A typical frame has $r = O(1)$.

The equilibrium equations for the discrete beam are established by enforcing equilibrium for the lumped masses shown in Fig. 2.8.

$$p_1 = V_1 - V_2 + m_1\ddot{u}_1 \quad p_2 = V_2 + m_2\ddot{u}_2 \quad (2.32)$$

2.4. BUILDINGS MODELED AS SHEAR BEAMS

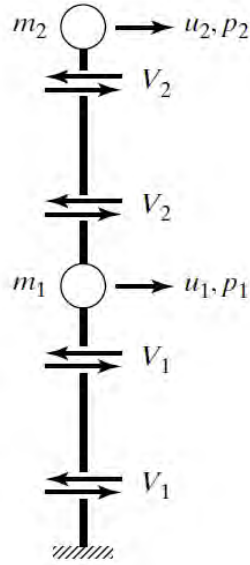


Figure 2.8: External and internal forces for discrete shear beam model.

Substituting for V_1 and V_2 , Eq. (2.32) expands to

$$\begin{aligned} p_1 &= k_1 u_1 + k_2(u_1 - u_2) + m_1 \ddot{u}_1 \\ p_2 &= k_2(u_2 - u_1) + m_2 \ddot{u}_2 \end{aligned} \quad (2.33)$$

It is convenient to express Eq. (2.33) in matrix form. The various matrices are defined as

$$\mathbf{U} = \begin{bmatrix} u_1 \\ u_2 \end{bmatrix} \quad (2.34)$$

$$\mathbf{P} = \begin{bmatrix} p_1 \\ p_2 \end{bmatrix} \quad (2.35)$$

$$\mathbf{M} = \begin{bmatrix} m_1 & 0 \\ 0 & m_2 \end{bmatrix} \quad (2.36)$$

$$\mathbf{K} = \begin{bmatrix} k_1 + k_2 & -k_2 \\ -k_2 & k_2 \end{bmatrix} \quad (2.37)$$

With these definitions, Eq. (2.33) takes the form

$$\mathbf{P} = \mathbf{K}\mathbf{U} + \mathbf{M}\ddot{\mathbf{U}} \quad (2.38)$$

Eq. (2.16) expresses the shear force in a continuous beam as an integral of the applied lateral loading. The corresponding equations for this discrete system are obtained from Eq. (2.32) by combining the individual equations:

$$\begin{aligned} V_2 &= p_2 - m_2\ddot{u}_2 \\ V_1 &= p_1 + p_2 - m_1\ddot{u}_1 - m_2\ddot{u}_2 \end{aligned} \quad (2.39)$$

In general, the shear force in a particular story is determined by summing the forces acting on the stories above this story.

A building having n stories is considered next. The building is modeled as an n DOF system with lumped mass and equivalent shear springs, as shown in Fig. 2.9. The strategy for determining the equivalent shear stiffness factors is the same as discussed previously. The only difference for this case is the form of the system matrices. They are now of order n .

2.4. BUILDINGS MODELED AS SHEAR BEAMS

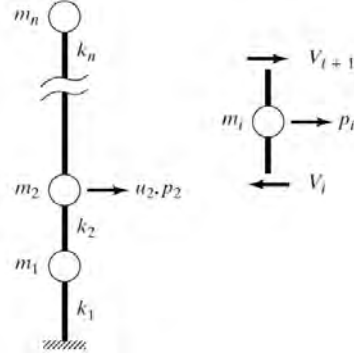


Figure 2.9: General shear beam model.

The equilibrium equation for mass i is given by

$$p_i = m_i \ddot{u}_i + V_i - V_{i+1} \quad (2.40)$$

Expressing the shear forces in terms of the nodal displacements

$$V_j = k_j (u_j - u_{j-1}) \quad (2.41)$$

and substituting in Eq. (2.40) results in

$$p_i = m_i \ddot{u}_i - k_i u_{i-1} + (k_i + k_{i+1}) u_i - k_{i+1} u_{i+1} \quad (2.42)$$

This equation defines the entries in the i^{th} row of \mathbf{M} and \mathbf{K} . The expanded forms are as follows:

$$\mathbf{M} = \begin{bmatrix} m_1 & & & \\ & m_2 & & \\ & & \dots & \\ & & & m_n \end{bmatrix}$$

CHAPTER 2. OPTIMAL STIFFNESS DISTRIBUTION - STATIC LOADING

$$\mathbf{K} = \begin{bmatrix} k_1 + k_2 & -k_2 & 0 & \cdots & 0 & 0 & 0 \\ -k_2 & k_2 + k_3 & -k_3 & \cdots & 0 & 0 & 0 \\ \vdots & \vdots & \vdots & \ddots & \vdots & \vdots & \vdots \\ 0 & 0 & 0 & \cdots & -k_{n-1} & k_{n-1} + k_n & -k_n \\ 0 & 0 & 0 & \cdots & 0 & -k_n & k_n \end{bmatrix} \quad (2.43)$$

2.4.2 Stiffness Distribution for a Discrete Shear Beam: Static Loading

Consider the set of equilibrium equations relating the nodal forces and story displacements for an n^{th} -order discrete shear beam:

$$\begin{bmatrix} p_1 \\ p_2 \\ \vdots \\ p_n \end{bmatrix} = \begin{bmatrix} k_1 + k_2 & -k_2 & \cdots & 0 \\ -k_2 & k_2 + k_3 & \cdots & 0 \\ \vdots & \vdots & \ddots & \vdots \\ 0 & 0 & \cdots & k_n \end{bmatrix} \begin{bmatrix} u_1 \\ u_2 \\ \vdots \\ u_n \end{bmatrix} \quad (2.44)$$

For the normal analysis problem, one specifies \mathbf{P} and \mathbf{K} and solves for \mathbf{U} . The problem is statically determinate since there are n equations for the n unknown displacements. In the motion based approach, one specifies \mathbf{U} and \mathbf{P} and attempts to determine the n stiffness factors. Since there are n linear algebraic equations, it should be possible to solve for the n stiffness coefficients by rearranging the equations such that the k 's are the unknowns. The vector containing the stiffness coefficients is denoted by \mathbf{k} .

2.4. BUILDINGS MODELED AS SHEAR BEAMS

$$\mathbf{k} = \begin{bmatrix} k_1 \\ k_2 \\ \vdots \\ k_n \end{bmatrix} \quad (2.45)$$

With this definition, Eq. (2.44) is written as

$$\mathbf{S}\mathbf{k} = \mathbf{P}^* \quad (2.46)$$

where the elements of \mathbf{S} are linear combinations of the prescribed displacement components, u_i^* , and \mathbf{P}^* contains the prescribed loads. The entries in the i^{th} row of \mathbf{S} follow from Eq. (2.42).

$$\begin{aligned} S(i, i) &= u_i^* - u_{i-1}^* \\ S(i, i + 1) &= u_i^* - u_{i+1}^* \\ S(i, j) &= 0 \quad \text{for } j \neq i, i + 1 \end{aligned} \quad (2.47)$$

These entries define \mathbf{S} to be an upper triangular matrix. The diagonal entries for \mathbf{S} are interstory displacements. Normally, we would not specify an interstory displacement to be 0 since it would require an infinite shear stiffness. It follows that \mathbf{S} will be nonsingular, and there will be a unique solution for \mathbf{k} .

Example 2.5 - 3DOF shear beam

Consider a 3DOF cantilever beam subjected to uniform nodal loading and required to have a linear displacement profile. The design values are

$$\mathbf{P}^* = \begin{bmatrix} 19.6 \\ 19.6 \\ 19.6 \end{bmatrix} \text{ kN} \quad (1)$$

CHAPTER 2. OPTIMAL STIFFNESS DISTRIBUTION - STATIC LOADING

$$\mathbf{U}^* = \begin{bmatrix} 0.025 \\ 0.050 \\ 0.075 \end{bmatrix} \text{ m} \quad (2)$$

Applying Eq. (2.47) results in

$$\begin{bmatrix} 0.025 & -0.025 & 0 \\ 0 & 0.025 & -0.025 \\ 0 & 0 & 0.025 \end{bmatrix} \begin{bmatrix} k_1 \\ k_2 \\ k_3 \end{bmatrix} = \begin{bmatrix} 19.6 \\ 19.6 \\ 19.6 \end{bmatrix} \quad (3)$$

Since the coefficient matrix is upper triangular, we solve for k_3 , k_2 , and then k_1 by backsubstitution. The solution is

$$\mathbf{k} = \begin{bmatrix} 2352 \\ 1568 \\ 784 \end{bmatrix} \text{ kN/m} \quad (4)$$

As illustrated with the preceding example, solving Eq. (2.46) is relatively simple, and we can easily handle arbitrary loading and permissible (nonzero interstory drift) displacement profiles.

2.5 Stiffness Distribution: Truss under Static Loading

2.5.1 An Introductory Example

The approach discussed in the previous sections can be extended to deal with other types of structures such as trusses and frames. Since trusses involve simple equations, the approach is illustrated using a planar truss. A more general discussion is contained in [35].

2.5. STIFFNESS DISTRIBUTION: TRUSS UNDER STATIC LOADING

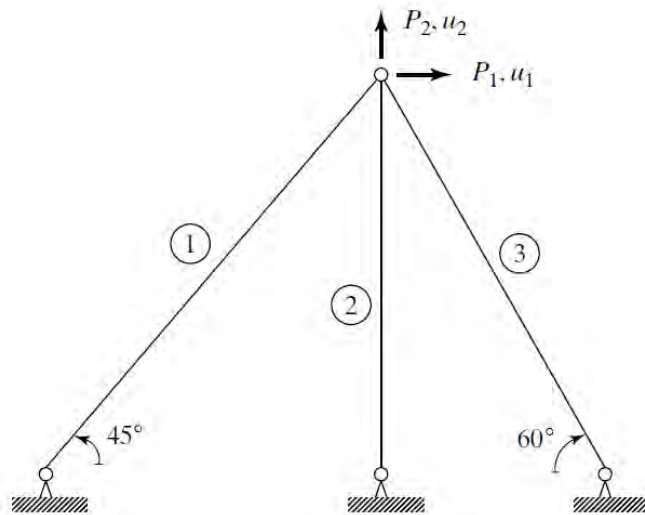


Figure 2.10: Planar truss.

The truss shown in Fig. 2.10 has three members and two displacement variables; the supports are assumed to be rigid so there are *no* support movements. Each member has an extension, e , and corresponding force, F . Assuming linear elastic behavior, the force-displacement relation for member i is

$$F_i = k_i e_i \quad (2.48)$$

where k is the member stiffness factor,

$$k_i = \left(\frac{AE}{L} \right)_{\text{member } i} \quad (2.49)$$

Using a geometric analysis, the member extensions are expressed in terms of the nodal displacements:

CHAPTER 2. OPTIMAL STIFFNESS DISTRIBUTION - STATIC LOADING

$$\begin{aligned}e_1 &= \frac{\sqrt{2}}{2}(u_1 + u_2) \\e_2 &= u_2 \\e_3 &= -\frac{1}{2}u_1 + \frac{\sqrt{3}}{2}u_2\end{aligned}\tag{2.50}$$

The nodal and member forces are related by the nodal force equilibrium equations

$$\begin{aligned}P_1 &= \frac{\sqrt{2}}{2}F_1 - \frac{1}{2}F_3 \\P_2 &= \frac{\sqrt{2}}{2}F_1 + F_2 + \frac{\sqrt{3}}{2}F_3\end{aligned}\tag{2.51}$$

Since there are three extensions and only two displacements, one cannot arbitrarily specify values for all three extensions. They are constrained by the geometric compatibility equation that follows by combining the first and third rows of Eq. (2.50) and substituting for u_2 in terms of e_2 :

$$\frac{\sqrt{2}}{2}e_1 + e_3 = \frac{1}{2}(1 + \sqrt{3})e_2\tag{2.52}$$

In general, a state of uniform deformation in a statically indeterminate system is not possible.

One possible strategy is to specify u_1 and u_2 and evaluate the extensions. Once the extensions are known, we can substitute for the forces in the equilibrium equations and establish a set of equations relating the member stiffness factors. The result is

2.5. STIFFNESS DISTRIBUTION: TRUSS UNDER STATIC LOADING

$$\mathbf{Sk} = \mathbf{P}^*$$

$$\begin{bmatrix} P_1^* \\ P_2^* \end{bmatrix} = \begin{bmatrix} \frac{\sqrt{2}}{2}e_1^* & 0 & -\frac{1}{2}e_3^* \\ \frac{\sqrt{2}}{2}e_1^* & e_2^* & \frac{\sqrt{3}}{2}e_3^* \end{bmatrix} \begin{bmatrix} k_1 \\ k_2 \\ k_3 \end{bmatrix} \quad (2.53)$$

Since there are three unknown stiffness factors and only two equations, Eq. (2.53) represents an under-determined system of equations which does not have a unique solution for \mathbf{k} . This situation is typical of indeterminate structures. A solution of Eq. (2.53) can be generated by selecting two stiffness factors as the primary variables, such as k_1 and k_2 , and solving for these variables in terms of P_1^* , P_2^* , and the third stiffness factor, k_3 . The result is written as

$$\begin{aligned} k_1 &= \bar{k}_1 + a_1 k_3 \\ k_2 &= \bar{k}_2 + a_2 k_3 \end{aligned} \quad (2.54)$$

where \bar{k}_1 , \bar{k}_2 depend on the forces, P_1 and P_2 . Eq. (2.54) represents a constraint on the stiffness parameters. An additional condition must be introduced in order to determine k_3 . This additional condition is usually established by formulating an optimization problem.

One possibility is to work with a weighted volume measure that is related to the member stiffness factor, and seek the solution that corresponds to the minimum value of the sum of the weighted volumes. For example, suppose one takes

$$V_i = (AEL)_i \quad (2.55)$$

as the member volume variable. Expressing k_i in terms of V_i ,

CHAPTER 2. OPTIMAL STIFFNESS DISTRIBUTION - STATIC LOADING

$$k_i = \left(\frac{AE}{L} \right)_i = \frac{1}{L_i^2} V_i \quad (2.56)$$

and substituting for k_i in Eq. (2.54) transforms the constraint equations to

$$\begin{aligned} V_1 &= L_1^2 \bar{k}_1 + a_1 (L_1/L_3)^2 V_3 \\ V_2 &= L_2^2 \bar{k}_2 + a_2 (L_2/L_3)^2 V_3 \end{aligned} \quad (2.57)$$

The optimization problem can be stated as

$$\text{minimize } f(V) = V_1 + V_2 + V_3 \quad (2.58)$$

Using Eq. (2.57), the objective function reduces to

$$f = b_0 + b_1 V_3 \quad (2.59)$$

where b_0 and b_1 are constants. Since f is a linear function, there is no minimum value and it follows that the approach does not introduce an additional independent constraint.

Another possibility is to use a least square approach (i.e., to select V_3 such that the sum of the squares of the weighted member volumes is a minimum). The objective function for this optimization problem is

$$f = \frac{1}{2} (V_1^2 + V_2^2 + V_3^2) \quad (2.60)$$

Substituting for V_1 and V_2 transforms f to

$$f = c_0 + c_1 V_3 + c_2 V_3^2 \quad (2.61)$$

Requiring f to be stationary with respect to a change in V_3 ,

2.5. STIFFNESS DISTRIBUTION: TRUSS UNDER STATIC LOADING

$$\frac{\delta f}{\delta V_3} = c_1 + 2c_2V_3 = 0 \quad (2.62)$$

leads to

$$V_3 = -\frac{c_1}{2c_2} \quad (2.63)$$

The problem with this approach is that it tends to eliminate redundant members, such as member three for this example. This tendency is evidenced by “optimal” volume values, which are low and may even be negative. A negative value for the volume indicates that the member should be deleted.

A third approach partially overcomes the limitation of the least squares approach by working with the deviation from the mean value as the member variable. Let V_m denote the mean value.

$$V_m = \frac{1}{3}(V_1 + V_2 + V_3) \quad (2.64)$$

and \bar{V}_i represent the deviation from the mean value for member i ,

$$\bar{V}_i = V_i - V_m \quad (2.65)$$

The optimization problem is stated as

$$\text{minimize } f = \frac{1}{2}(\bar{V}_1^2 + \bar{V}_2^2 + \bar{V}_3^2) \quad (2.66)$$

subject to the constraints on V_1 and V_2 . Substituting for V_1 and V_2 using Eq. (2.57) transforms f to

$$f = d_0 + d_1 - \bar{V}_3 + d_2\bar{V}_3^2 \quad (2.67)$$

CHAPTER 2. OPTIMAL STIFFNESS DISTRIBUTION - STATIC LOADING

The remaining steps are the same as for the classical least square approach. This approach generates a solution that tends toward the same value for each member. However, as will be illustrated in the following example, it does not eliminate the possibility of negative volume members.

Example 2.6 - Application of least squares approaches

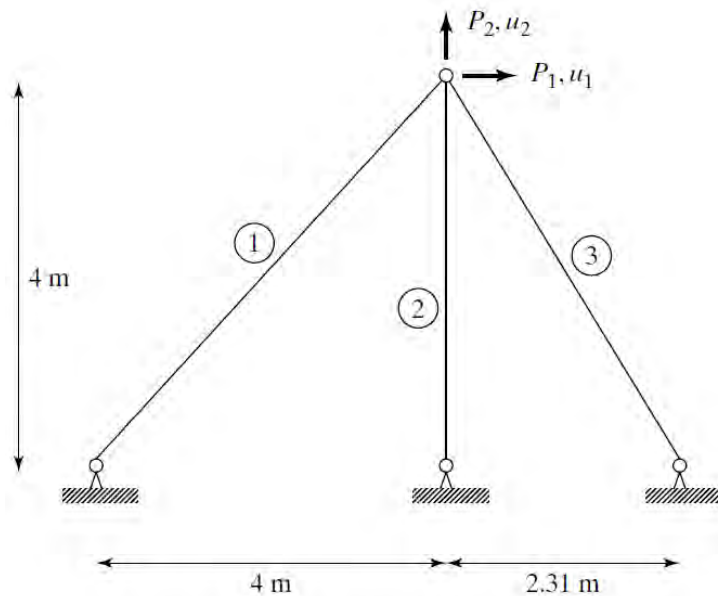


Figure E2.6a

The procedures just described are applied using the data defined in Fig. E2.6a:

$$\begin{aligned} P_1 &= 100 \text{ kN} & P_2 &= 300 \text{ kN} \\ u_1 &= 0.01 \text{ m} & u_2 &= 0.01 \text{ m} \end{aligned} \quad (1)$$

Using Eq. (2.50), the extensions are

2.5. STIFFNESS DISTRIBUTION: TRUSS UNDER STATIC LOADING

$$\begin{aligned}e_1 &= \frac{\sqrt{2}}{2}(0.01 + 0.01) = 0.01414 \text{ m} \\e_2 &= 0.01 \text{ m} \\e_3 &= -\frac{1}{2}(0.01) + \frac{\sqrt{e}}{2}(0.01) = 0.00366 \text{ m}\end{aligned}\tag{2}$$

Substituting for the e 's in Eq. (2.53) results in

$$\begin{aligned}0.01k_1 - 0.00183k_3 &= 100,000 \\0.01k_1 + 0.01k_2 + 0.00317k_3 &= 300,000\end{aligned}\tag{3}$$

Solving for k_1 and k_2 in terms of k_3 leads to

$$\begin{aligned}k_1 &= 0.183k_3 + 10^7 \\k_2 &= -0.500k_3 + 2 \cdot 10^7\end{aligned}\tag{4}$$

Eq. 4 represents the constraint on k_1 and k_2 . Substituting for k in terms of the weighted volume measure, $V = AEL$, using Eq. (2.56) transforms Eq. (4) to

$$\begin{aligned}V_1 &= 0.275V_3 + 32 \cdot 10^7 \\V_2 &= -0.375V_3 + 32 \cdot 10^7\end{aligned}\tag{5}$$

Least Squares Procedure

The objective function is

$$f = \frac{1}{2}(V_1^2 + V_2^2 + V_3^2) = f(V_3)\tag{6}$$

Differentiating with respect to V_3 ,

CHAPTER 2. OPTIMAL STIFFNESS DISTRIBUTION - STATIC LOADING

$$\frac{\delta f}{\delta V_3} = V_1 \frac{\delta V_1}{\delta V_3} + V_2 \frac{\delta V_2}{\delta V_3} + V_3 \quad (7)$$

substituting for V_1 and V_2 , and then setting the resulting expression equal to zero results in

$$1.216V_3 - 3.222 \cdot 10^7 = 0 \quad (8)$$

The “optimal” least squares values are

$$\begin{aligned} V_3 &= 2.65 \cdot 10^7 \text{ Nm} \\ V_1 &= 32.71 \cdot 10^7 \text{ Nm} \\ V_2 &= 31.00 \cdot 10^7 \text{ Nm} \end{aligned} \quad (9)$$

The low value for V_3 indicates that this member is redundant and could be removed.

Mean Value Least Squares Procedure

We start by establishing the mean value. Noting Eq. (5) leads to

$$V_m = \frac{1}{3}(V_1 + V_2 + V_3) = 0.3V_3 + 21.33 \cdot 10^7 \quad (10)$$

and the deviations,

$$\begin{aligned} \bar{V}_1 &= V_1 - V_m = -0.025V_3 + 10.71 \cdot 10^7 \\ \bar{V}_2 &= V_2 - V_m = -0.675V_3 + 10.67 \cdot 10^7 \\ \bar{V}_3 &= V_3 - V_m = 0.700V_3 - 21.33 \cdot 10^7 \end{aligned} \quad (11)$$

The objective function for this case is

$$f = \frac{1}{2}(\bar{V}_1^2 + \bar{V}_2^2 + \bar{V}_3^2) = f(V_3) \quad (12)$$

2.5. STIFFNESS DISTRIBUTION: TRUSS UNDER STATIC LOADING

Setting the derivative of f with respect to V_3 equal to zero,

$$\frac{\delta f}{\delta V_3} = \bar{V}_1 \frac{\delta \bar{V}_1}{\delta V_3} + \bar{V}_2 \frac{\delta \bar{V}_2}{\delta V_3} + \bar{V}_3 \frac{\delta \bar{V}_3}{\delta V_3} = 0 \quad (13)$$

and noting Eq. (11) reduces Eq. (13) to

$$0.946V_3 - 22.40 \cdot 10^7 = 0 \quad (14)$$

The final mean value least squares results are

$$\begin{aligned} V_3 &= 23.67 \cdot 10^7 \text{ Nm} \\ V_1 &= 38.50 \cdot 10^7 \text{ Nm} \\ V_2 &= 23.10 \cdot 10^7 \text{ Nm} \end{aligned} \quad (15)$$

Note that now V_3 is the same order of magnitude as V_1 and V_2 .

The solution is sensitive to the prescribed loading and displacement quantities. To illustrate this point, the computation is repeated taking the same imposed displacements but different sets of nodal forces. The results are as follows:

Case 1 $P_1 = 100 \text{ kN}$ $P_2 = 200 \text{ kN}$

Least squares:

$$\begin{aligned} V_1 &= 31.37 \cdot 10^7 \text{ Nm} \\ V_2 &= 16.86 \cdot 10^7 \text{ Nm} \\ V_3 &= -2.29 \cdot 10^7 \text{ Nm} \end{aligned} \quad (16)$$

Mean value least squares:

$$\begin{aligned} V_1 &= 35.37 \cdot 10^7 \text{ Nm} \\ V_2 &= 11.40 \cdot 10^7 \text{ Nm} \\ V_3 &= 12.26 \cdot 10^7 \text{ Nm} \end{aligned} \quad (17)$$

CHAPTER 2. OPTIMAL STIFFNESS DISTRIBUTION - STATIC LOADING

Case 2 $P_1 = 100$ kN $P_2 = 100$ kN

Least squares:

$$\begin{aligned} V_1 &= 30.02 \cdot 10^7 \text{ Nm} \\ V_2 &= 2.71 \cdot 10^7 \text{ Nm} \\ V_3 &= -7.25 \cdot 10^7 \text{ Nm} \end{aligned} \tag{18}$$

Mean value least squares:

$$\begin{aligned} V_1 &= 32.23 \cdot 10^7 \text{ Nm} \\ V_2 &= -0.32 \cdot 10^7 \text{ Nm} \\ V_3 &= 0.86 \cdot 10^7 \text{ Nm} \end{aligned} \tag{19}$$

The Case 2 result indicates that members 2 and 3 should be deleted. This is the correct solution for the specified loading and displacement. Taking $P_1 = P_2$ corresponds to a load at 45° , which coincides with the direction of member 1. Furthermore, an extension of member 1 corresponds to $u_1 = u_2$, which is the specified displacement condition. However, deleting members 2 and 3 results in an unstable structure.

2.5.2 A General Procedure

The procedures just described can be generalized to deal with an arbitrary truss. Suppose there are degrees of freedom and m members. It follows that there are n equilibrium equations relating the m stiffness factors and the n prescribed nodal forces. These equations are written as

$$\mathbf{Sk} = \mathbf{P} \tag{2.68}$$

2.5. STIFFNESS DISTRIBUTION: TRUSS UNDER STATIC LOADING

where \mathbf{S} is of order $n \times m$. When $m > n$, the structure is indeterminate, and Eq. (2.68) does not have a unique solution for \mathbf{k} . In this case the problem is undetermined, and an optimization statement has to be formulated. We can work with either stiffness or weighted volume measures as the variables. To allow for different choices, the form of Eq. (2.68) is generalized to

$$\mathbf{A}\mathbf{X} = \mathbf{P} \quad (2.69)$$

where \mathbf{X} is an m^{th} -order vector containing the selected variables, and \mathbf{A} is of order $n \times m$ with $m > n$. If we select V defined by Eq. (2.56) as the measure, \mathbf{A} is obtained by multiplying the i^{th} column of \mathbf{S} by $1/L_i^2$, and taking i from 1 to m .

Background material on computational techniques for solving linear algebraic equations is contained in [100]. In what follows, the use of one of these techniques to solve Eq. (2.69) is described in general terms.

The least squares approach works with a scalar quantity, f , that is equal to the sum of the squares of the elements of \mathbf{X} . Using matrix notation, f is given by

$$f = \frac{1}{2}\mathbf{X}^T\mathbf{X} \quad (2.70)$$

The elements of \mathbf{X} are constrained by Eq. (2.69). It follows that elements can be expressed in terms of $m - n$ elements, which can be interpreted as the unknowns that need to be selected such that f is a minimal value. Assuming the first n columns of \mathbf{A} are independent, Eq. (2.69) can be expressed in partitioned form

$$[\mathbf{A}_1 \quad \mathbf{A}_2] \left\{ \begin{array}{c} \mathbf{X}_1 \\ \mathbf{X}_2 \end{array} \right\} = \mathbf{P} \quad (2.71)$$

where \mathbf{A}_1 is of order $n \times n$. Solving Eq. (2.71) for \mathbf{X}_1 leads to

CHAPTER 2. OPTIMAL STIFFNESS DISTRIBUTION - STATIC LOADING

$$\mathbf{X}_1 = \bar{\mathbf{X}}_1 + \mathbf{B}\mathbf{X}_2 \quad (2.72)$$

where \mathbf{X}_2 represents the unknown elements. Using Eq. (2.72), \mathbf{X} is expressed in terms of \mathbf{X}_2 ,

$$\mathbf{X} = \begin{bmatrix} \bar{\mathbf{X}}_1 \\ \mathbf{0} \end{bmatrix} + \begin{bmatrix} \mathbf{B} \\ \mathbf{I} \end{bmatrix} \mathbf{X}_2 = \bar{\mathbf{X}} + \mathbf{C}\mathbf{X}_2 \quad (2.73)$$

Substituting for \mathbf{X} , the objective function expands to

$$f = \frac{1}{2} (\bar{\mathbf{X}} + \mathbf{C}\mathbf{X}_2)^T (\bar{\mathbf{X}} + \mathbf{C}\mathbf{X}_2) \quad (2.74)$$

Requiring f to be stationary with respect to \mathbf{X}_2 leads to the following set of $m - n$ equations:

$$\mathbf{C}^T \mathbf{C}\mathbf{X}_2 = -\mathbf{C}^T \bar{\mathbf{X}} \quad (2.75)$$

We solve Eq. (2.75) for \mathbf{X}_2 and then determine \mathbf{X}_1 with Eq. (2.72). This solution corresponds to an absolute minimum value of f (see [100]). The MATLAB statement, $\mathbf{X} = \text{pinv}(\mathbf{A}) * \mathbf{P}$, generates this least squares solution.

The mean value least squares approach works with the deviation from the mean,

$$e_i = x_i - x_{\text{mean}} \quad (2.76)$$

For this case, there are m members, and x_{mean} is given by

$$x_{\text{mean}} = \frac{1}{m} (x_1 + x_2 + \cdots + x_m) \quad (2.77)$$

Using matrix notation, the deviation vector, \mathbf{e} , can be expressed as

2.5. STIFFNESS DISTRIBUTION: TRUSS UNDER STATIC LOADING

$$\mathbf{e} = \mathbf{D}\mathbf{X} = \mathbf{D}(\bar{\mathbf{X}} + \mathbf{C}\mathbf{X}_2) \quad (2.78)$$

where the entries in row i of \mathbf{D} are

$$\begin{aligned} D(i, i) &= 1 - \frac{1}{m} \\ D(i, j) &= -\frac{1}{m} \quad \text{for } j \neq i \end{aligned} \quad (2.79)$$

The objective function is a quadratic form in \mathbf{e} .

$$f = \frac{1}{2}\mathbf{e}^T\mathbf{e} \quad (2.80)$$

Substituting for \mathbf{e} using Eq. (2.78) and enforcing stationarity with respect to \mathbf{X}_2 leads to the equation for \mathbf{X}_2 .

$$\mathbf{C}^T\mathbf{D}^T\mathbf{D}\mathbf{C}\mathbf{X}_2 = -\mathbf{C}^T\mathbf{D}^T\mathbf{D}\bar{\mathbf{X}} \quad (2.81)$$

An alternative way of generating the solution is based on using Lagrangian multipliers to incorporate the constraint equations in the objective function ([100]). The “generalized” function is defined as

$$\begin{aligned} J &= \frac{1}{2}\mathbf{e}^T\mathbf{e} + \lambda^T(\mathbf{A}\mathbf{X} - \mathbf{P}) \\ &= \frac{1}{2}\mathbf{X}^T(\mathbf{D}^T\mathbf{D})\mathbf{X} + \lambda^T(\mathbf{A}\mathbf{X} - \mathbf{P}) \end{aligned} \quad (2.82)$$

where λ is a vector containing the n Lagrangian multipliers. Requiring J to be stationary with respect to both \mathbf{X} and λ leads to the following set of equations:

CHAPTER 2. OPTIMAL STIFFNESS DISTRIBUTION - STATIC LOADING

$$\begin{aligned} \mathbf{D}^T \mathbf{D} \mathbf{X} + \mathbf{A}^T \lambda &= \mathbf{0} \\ \mathbf{A} \mathbf{X} &= \mathbf{P} \end{aligned} \quad (2.83)$$

These equations can be combined,

$$\begin{bmatrix} \mathbf{D}^T \mathbf{D} & \mathbf{A}^T \\ \mathbf{A} & \mathbf{0} \end{bmatrix} \begin{Bmatrix} \mathbf{X} \\ \lambda \end{Bmatrix} = \begin{Bmatrix} \mathbf{0} \\ \mathbf{P} \end{Bmatrix} \quad (2.84)$$

and solved in a single step using a linear equation solver such as one of the MATLAB functions.

Example 2.7 - Comparison of strength-versus displacement-based design

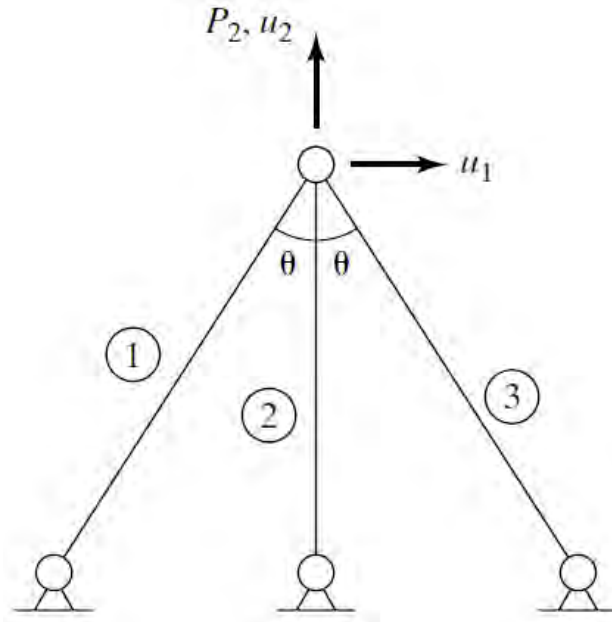


Figure E2.7a

Consider the three-member truss shown in Fig. E2.7a. Suppose members 1 and 3 to have the same properties. It follows that $u_1 = 0$ and $e_3 \equiv e_1$. The member elongations are

2.5. STIFFNESS DISTRIBUTION: TRUSS UNDER STATIC LOADING

$$\begin{aligned}e_1 &= u_2 \cos \theta \\e_2 &= u_2\end{aligned}\tag{1}$$

Noting Eq. (1), the elongations are constrained by

$$e_1 = e_2 \cos \theta\tag{2}$$

The member flexibility factor, f , is defined as

$$f = \frac{1}{k} = \frac{L}{AE}\tag{3}$$

Then the member force-deformation relation can be expressed as

$$e = fF\tag{4}$$

Using Eq. (4), the geometric compatibility equation expressed in terms of member forces has the form

$$f_1 F_1 = \cos \theta f_2 F_2\tag{5}$$

The solutions for F_1 and F_2 are

$$\begin{aligned}F_1 &= \cos \theta \frac{f_2}{f_1} F_2 \\F_2 &= \frac{P_2}{1 + 2 \cos^2 \theta \frac{f_2}{f_1}}\end{aligned}\tag{6}$$

Strength-Based Design

Ideally, we would want the member stresses to be equal to an allowable stress, σ_a . However, a state of uniform stress is not

CHAPTER 2. OPTIMAL STIFFNESS DISTRIBUTION - STATIC LOADING

possible because of the indeterminate nature of the structure. Noting that

$$e = L\varepsilon \quad (7)$$

for a member, Eq. (1) can be written as

$$L_1\varepsilon_1 = \cos\theta L_2\varepsilon_2 \quad (8)$$

Then assuming the same material for members 1 and 2 and substituting $L_2 = L_1 \cos\theta$ results in the constraint equation for the member stresses:

$$\sigma_1 = (\cos^2\theta)\sigma_2 \quad (9)$$

According to Eq. (9), $\sigma_1 \leq \sigma_2$.

Let

$$\begin{aligned} \sigma_2 &= \sigma_a \\ \sigma_1 &= \sigma_a \cos^2\theta \end{aligned} \quad (10)$$

represent the design values for the stresses. The member cross-sectional areas are

$$\begin{aligned} A_2 &= \frac{F_2}{\sigma_a} \\ A_1 &= \frac{F_1}{\sigma_1} = \frac{F_1}{\sigma_a \cos^2\theta} \end{aligned} \quad (11)$$

Substituting for F_1 and F_2 in the equilibrium equation,

$$F_2 + 2F_1 \cos\theta = P_2 \quad (12)$$

leads to a relationship between the cross-sectional areas:

2.5. STIFFNESS DISTRIBUTION: TRUSS UNDER STATIC LOADING

$$A_2 + (2 \cos^3 \theta)A_1 \geq \frac{P_2}{\sigma_a} \quad (13)$$

The allowable solutions lie *outside* the triangle shaded in Fig. E2.7b.

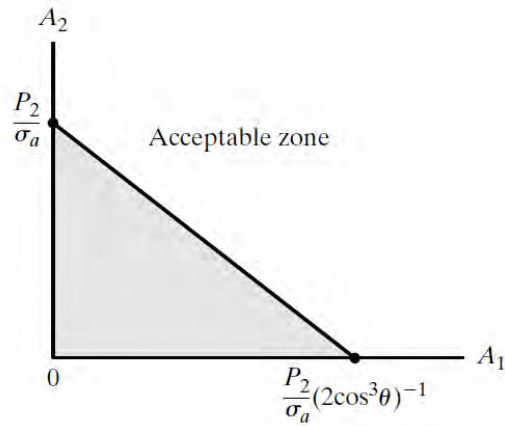


Figure E2.7b

The constraint equation is expressed as

$$A_2 + \alpha A_1 = \beta \quad (14)$$

There is no unique solution for the areas. One approach is to apply a least square approach to the member areas. Minimizing the function

$$J = (A_1^2 + A_2^2 + A_3^2) \quad (15)$$

subject to the constraint, Eq. (14), results in the following design:

$$\begin{aligned} A_1 &= \frac{\alpha\beta}{2 + \alpha^2} \\ A_2 &= \frac{2\beta}{2 + \alpha^2} \end{aligned} \quad (16)$$

Motion-Based Design

The member forces are expressed in terms of the displacement, u_2 , by using Eqs. (1) and (4).

$$\begin{aligned} F_1 &= \frac{A_1 E}{L_1} e_1 = A_1 E \frac{u_2}{L_1} \cos \theta \\ F_2 &= \frac{A_2 E}{L_2} e_2 = A_2 E \frac{u_2}{L_2} \end{aligned} \quad (17)$$

Substituting for the forces in Eq. (12) leads to

$$A_2 + (2 \cos^3 \theta) A_1 \geq \frac{P_2 L_2}{E u_2} \quad (18)$$

This equation is similar to the strength-based constraint equation. The equations differ only with respect to the right-hand sides. Comparing these terms, it follows that motion-based design controls when

$$\frac{P_2 L_2}{E u_2} > \frac{P_2}{\sigma_a} \quad (19)$$

which translates to

$$u_2^* < L_2 \frac{\sigma_a}{E} \quad (20)$$

2.5. STIFFNESS DISTRIBUTION: TRUSS UNDER STATIC LOADING

Problems

Problem 2.1

Determine the transverse shear and bending deformations corresponding to the following displacement distributions:

1.

$$u = \sin \frac{n\pi x}{2L}$$
$$\beta = 0$$
$$n = 1, 3, \dots$$

2.

$$u = x^2 + a_1x^3 + a_2x^4$$
$$\beta = 2x + 3a_1x^2 + 4a_2x^3$$

3.

$$u = a_1x + a_2x^2 + a_3x^3$$
$$\beta = 2a_2x + 3a_3x^2$$

4.

$$u = a_1 \left(x - \frac{x^2}{2L} \right) + a_2 \left(\frac{x^2}{2} - \frac{x^4}{12L^2} \right)$$
$$\beta = a_2 \left(x - \frac{x^3}{3H^2} \right)$$

Problem 2.2

Determine the shear and bending rigidity coefficients for the cross section shown in Fig. P2.2a. The dimensions are in centimeters.

CHAPTER 2. OPTIMAL STIFFNESS DISTRIBUTION - STATIC LOADING

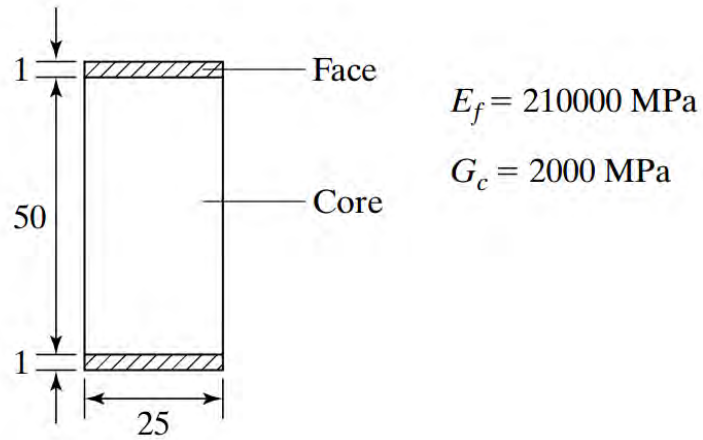


Figure P2.2a

Problem 2.3

Consider the chevron bracing scheme shown in Fig. P2.3a. Determine an expression for D_T . Assume the members carry only axial force.

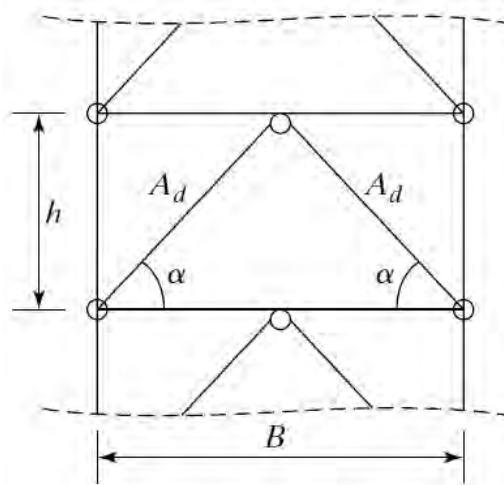


Figure P2.3a

Problem 2.4

2.5. STIFFNESS DISTRIBUTION: TRUSS UNDER STATIC LOADING

The force-displacement relationship for the structures shown in Fig. 2.4(a), (b), and (c) is written as $P = ku$.

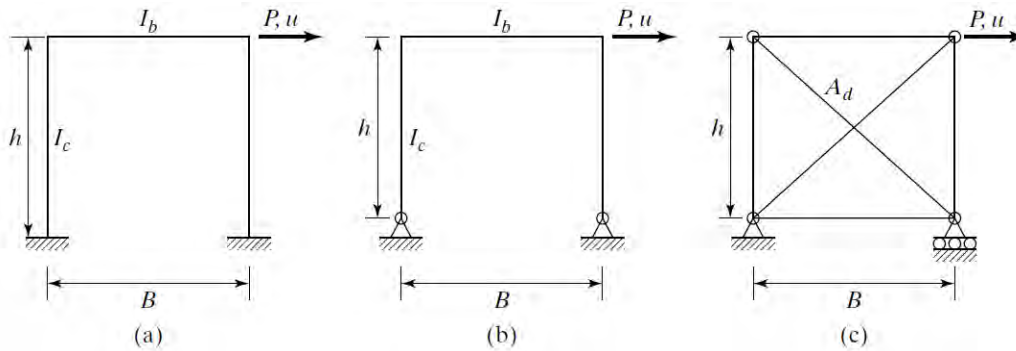


Figure P2.4a

Establish the expression for k for each structure. Comment on the relative efficiency of the structures for resisting lateral loading.

Problem 2.5

Consider a five-story, five-bay rigid frame modeled as a shear beam (Fig. P2.5a). Assume that all the columns in a story have the same properties, but allow for variation in column size over the stories. Establish an approximate expression for the equivalent shear beam stiffness for a typical story.

CHAPTER 2. OPTIMAL STIFFNESS DISTRIBUTION - STATIC LOADING

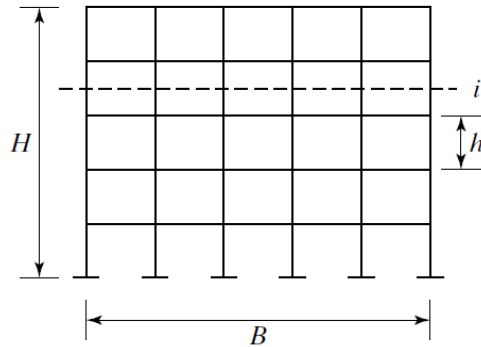


Figure P2.5a

Problem 2.6

Diagonal bracing is added to a rigid frame as indicated in Fig. P2.6a.

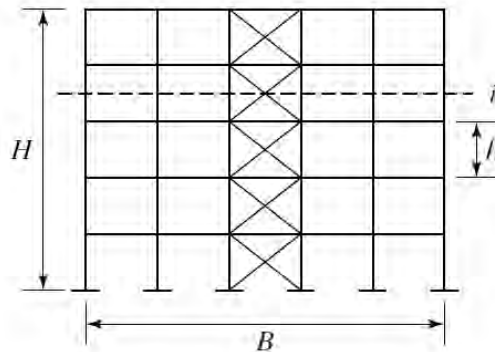


Figure P2.6a

1. Establish an approximate expression for the equivalent shear beam stiffness for a typical story. Assume the column properties are constant in a story, but vary from story to story.
2. Suppose the diagonal bracing system is expected to carry a specified fraction of the total shear in a story. Discuss how

2.5. STIFFNESS DISTRIBUTION: TRUSS UNDER STATIC LOADING

you would select the cross-sectional area of the diagonal braces and moment of inertia for the columns in a typical story.

Problem 2.7

Determine the expressions for the distribution of shear and bending rigidities corresponding to constant deformations γ^* and χ^* (Fig. P2.7a).

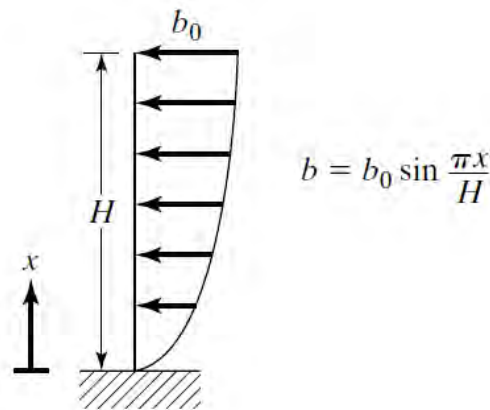


Figure P2.7a

Problem 2.8

Determine the shear and bending rigidity distributions (Fig. P2.8a). Take

$$\gamma^* = \frac{1}{400}$$
$$\chi^* = \frac{1}{20,000}$$

Note: These values correspond to $s = 0.1$ (see Eq. (2.10)).

CHAPTER 2. OPTIMAL STIFFNESS DISTRIBUTION - STATIC LOADING

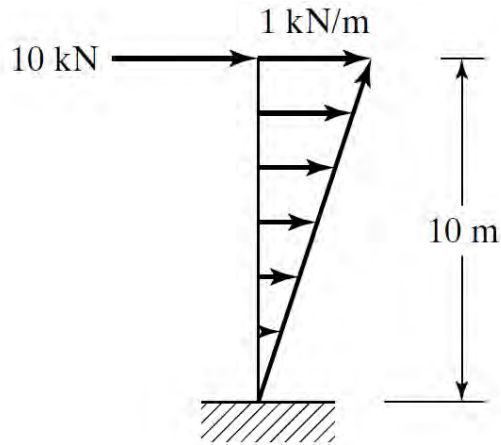


Figure P2.8a

Problem 2.9

A particular steel having an allowable stress of 600 MPa and Young's modulus equal to 210,000 MPa has been selected as the "design" material. Assuming the material is to be used in 45° bracing members, for what range of transverse shear strains will the design be controlled by motion constraints rather than strengths?

Problem 2.10

1. Refer to Problem 2.5. Consider a uniform lateral loading of 30 kN/m, a story height of 4 m, and a design shear strain, γ^* , equal to 1/300 for each story. Estimate the value of I_c for each story, assuming steel is selected as the material.
2. Refer to Problem 2.6. Using the loading defined in part (a), select the bracing properties such that the bracing carries 25% of the total story shear.

2.5. STIFFNESS DISTRIBUTION: TRUSS UNDER STATIC
LOADING

Problem 2.11

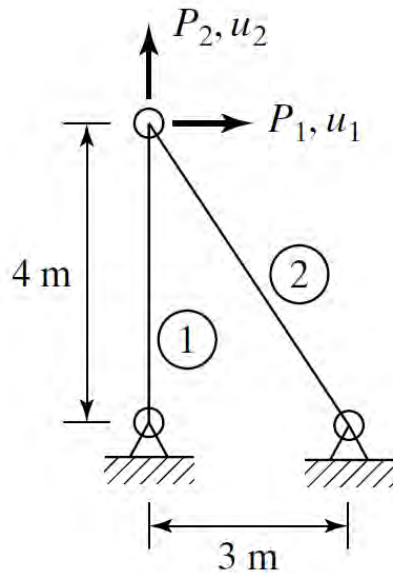


Figure P2.11a

Determine the member stiffness factors for the following prescribed loading and displacement quantities (Fig. P2.11a):

$$P_1 = 100 \text{ kN} \quad P_2 = 50 \text{ kN} \quad u_1 = 0.01 \text{ m} \quad u_2 = 0.005 \text{ m}$$

Problem 2.12

CHAPTER 2. OPTIMAL STIFFNESS DISTRIBUTION - STATIC LOADING

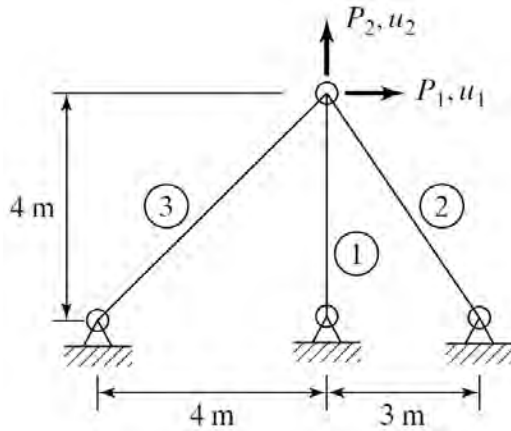


Figure P2.12a

The design objective is to determine the member stiffness factors for the truss shown in Fig. P2.12a such that the nodal displacements corresponding to $P_1 = 25$ kN, $P_2 = 50$ kN are $u_1 = 0.01$ m, $u_2 = 0.01$ m. Generate solutions using the least squares and mean value least squares approaches.

Problem 2.13

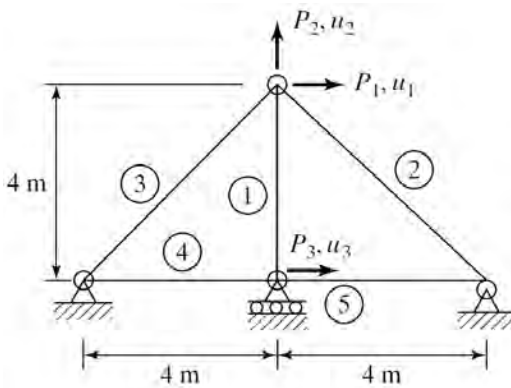


Figure P2.13a

2.5. STIFFNESS DISTRIBUTION: TRUSS UNDER STATIC LOADING

Recommend stiffness factors for the truss shown in Fig. P2.13a based on the following requirements:

$$u_1 = -0.0087 \text{ m} \quad u_2 = 0.0012 \text{ m} \quad u_3 = -0.0019 \text{ m}$$

$$P_1 = -100 \text{ kN} \quad P_2 = 50 \text{ kN} \quad P_3 = -100 \text{ kN}$$

Problem 2.14

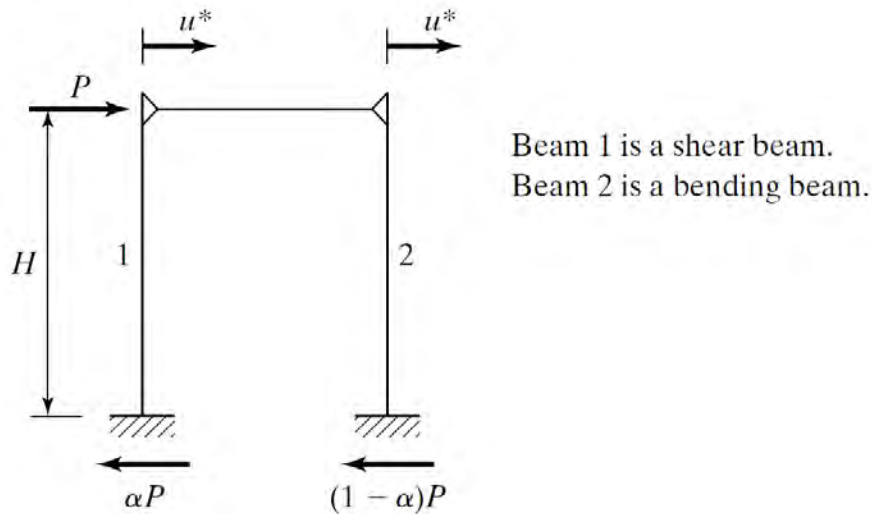


Figure P2.14a

Consider two cantilever beams coupled with a rigid link at the top (Fig. P2.14a). Assume that beam 1 is a shear beam and beam 2 is a bending beam.

Determine the optimal rigidity distributions that satisfy the displacement requirement $u^* = H/\beta$ and divide the lateral load between the two beams as indicated.

3

Optimal Stiffness/Damping for Dynamic Loading

CHAPTER 3. OPTIMAL STIFFNESS/DAMPING FOR DYNAMIC LOADING

3.1 Introduction

This chapter presents a strategy for establishing the structural stiffness distribution which produces the desired deformation profile for a specified dynamic loading. The approach is similar to that developed for static loading; one only needs to include the additional inertia forces in the equilibrium equations. The basic steps are the same; one assumes there is a dominant lateral loading and specifies the corresponding deformation profile. For buildings, either wind or seismic load may dominate, depending on the site and the height of the building. Selecting the deflected shape that corresponds to the desired deformation profile is critical for the success of this strategy.

In what follows, we first describe how one generates the linear dynamic response of a MDOF system using modal superposition and illustrate its application for periodic and seismic excitation. Based on analytical solutions and simulation results, one can establish the contribution of the individual modes to the total response. Our findings indicate that the fundamental mode usually dominates the response, and therefore the deflection profile can be taken as the fundamental mode shape. Once this assumption is introduced, the remaining steps are essentially the same as for the static loading case except that now one needs to include damping. The final result consist of two distributions, one for stiffness and one for damping.

3.2 Dynamic Response - MDOF

Using matrix notation, the governing equilibrium equations for a MDOF are expressed as:

$$\mathbf{M}\ddot{\mathbf{U}} + \mathbf{P}_d + \mathbf{K}\mathbf{U} = \mathbf{P} - \mathbf{M}\mathbf{E}a_g(t) \quad (3.1)$$

where \mathbf{M} and \mathbf{K} are the mass and stiffness matrices, \mathbf{P}_d contains the nodal forces due to damping, \mathbf{P} is the external nodal force, \mathbf{U} is the displacement vector relative to ground, $a_g(t)$ is the ground acceleration, and \mathbf{E} is a vector representing the rigid body motion of the system due to a unit translation at the base. We assume the system is of order n , i.e., Eq. (3.1) represents n equations relating the n nodal displacements.

3.2.1 Modal Equations - MDOF System

Eq. (3.1) can be transformed into a set of uncoupled equations by expressing \mathbf{U} in terms of a “special” set of vectors, Φ_j , and assuming a particular form for the nodal damping force, \mathbf{P}_d . These special vectors are solutions of the eigenvalue problem,

$$\mathbf{K}\Phi_j = \omega_j^2 \mathbf{M}\Phi_j \quad j = 1, 2, \dots, n \quad (3.2)$$

and satisfy the following set of orthogonality relations:

$$\begin{aligned} \Phi_k^T \mathbf{M}\Phi_j &= \tilde{m}_j \delta_{jk} \\ \Phi_k^T \mathbf{K}\Phi_j &= \omega_j^2 \tilde{m}_j \delta_{jk} \\ \delta_{jk} &= 1 \quad \text{if } k = j; \text{ otherwise } \delta_{jk} = 0 \end{aligned} \quad (3.3)$$

The expression for \mathbf{U} is written as:

$$\mathbf{U} = \sum_{j=1}^n q_j(t) \Phi_j \quad (3.4)$$

One envisions the response as a superposition of individual responses corresponding to the different Φ_j 's. In this approach, Φ_j

CHAPTER 3. OPTIMAL STIFFNESS/DAMPING FOR DYNAMIC LOADING

defines the spatial distribution over the structure, and q_j defines the magnitude. It is customary to call Φ_j the j^{th} mode shape and q_j the corresponding modal coordinate.

Substituting for \mathbf{U} in Eq. (3.1), and premultiplying by Φ_j^T leads to an equation for q_j .

$$\tilde{m}_j \ddot{q}_j + \Phi_j^T \mathbf{P}_d + \omega_j^2 \tilde{m}_j q_j = \Phi_j^T (\mathbf{P} - \mathbf{M} \mathbf{E} a_g) \quad (3.5)$$

The damping force depends on $\dot{\mathbf{U}}$. We assume Rayleigh damping here and express \mathbf{P}_d as

$$\mathbf{P}_d = (\alpha \mathbf{K} + \beta \mathbf{M}) \dot{\mathbf{U}} = \mathbf{C} \dot{\mathbf{U}} \quad (3.6)$$

where α and β are parameters. Noting the orthogonality relations, the expression for $\Phi_j^T \mathbf{P}_d$ reduces to

$$\Phi_j^T \mathbf{P}_d = \sum_{j=1}^n (\alpha \omega_j^2 + \beta) \tilde{m}_j \dot{q}_j = \sum_{j=1}^n \tilde{c}_j \dot{q}_j \quad (3.7)$$

Lastly, we express \tilde{c}_j as

$$\begin{aligned} \tilde{c}_j &= 2\xi_j \omega_j \tilde{m}_j \\ \xi_j &= \frac{1}{2} \alpha \omega_j + \frac{1}{2} \frac{\beta}{\omega_j} \end{aligned} \quad (3.8)$$

where ξ_j is the equivalent modal damping factor for mode j . One determines α and β by specifying ξ_j for 2 modes, usually the first two modes. Lastly, we substitute for $\Phi_j^T \mathbf{P}_d$ in Eq. (3.5) and divide by \tilde{m}_j , leading to the uncoupled modal modal equations

$$\ddot{q}_j + 2\xi_j \omega_j \dot{q}_j + \omega_j^2 q_j = \frac{1}{\tilde{m}_j} p_j - \Gamma_j a_g \quad (3.9)$$

where

$$\begin{aligned} p_j &= \Phi_j^T \mathbf{P} \\ \Gamma_j &= \frac{\Phi_j^T (\mathbf{M}\mathbf{E})}{\tilde{m}_j} \end{aligned} \quad (3.10)$$

We interpret p_j as the modal force for the j^{th} mode. The dimensionless factor, Γ_j , defines the influence of ground acceleration on the response of the j^{th} mode. Typically, Γ_j decreases with increasing mode number, which implies that the higher mode responses are less significant.

Example 3.1 - 3DOF System

Consider the 3DOF system shown in Fig. E3.1a. We assume the first mode shape is a linear function (which corresponds to uniform transverse shear deformation),

$$\Phi_1 = \frac{1}{3} \{1, 2, 3\} \quad (1)$$

and generate the modal coefficients. Starting with the mass and stiffness matrices,

$$\begin{aligned} \mathbf{M} &= \begin{bmatrix} m_1 & 0 & 0 \\ 0 & m_2 & 0 \\ 0 & 0 & m_3 \end{bmatrix} \\ \mathbf{K} &= \begin{bmatrix} k_1 + k_2 & -k_2 & 0 \\ -k_2 & k_2 + k_3 & -k_3 \\ 0 & -k_3 & k_3 \end{bmatrix} \end{aligned} \quad (2)$$

CHAPTER 3. OPTIMAL STIFFNESS/DAMPING FOR DYNAMIC LOADING

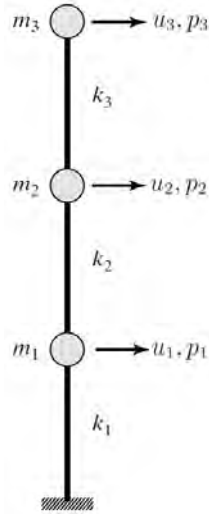


Figure E3.1a

we pre and post multiply by Φ_1 .

$$\begin{aligned}\tilde{m}_1 &= \Phi_1^T \mathbf{M} \Phi_1 = \frac{m_1}{9} + \frac{4m_2}{9} + m_3 \\ \tilde{p}_1 &= \Phi_1^T \mathbf{P} = \frac{1}{3}p_1 + \frac{2}{3}p_2 + p_3 \\ \tilde{k}_1 &= \Phi_1^T \mathbf{K} \Phi_1 = \frac{1}{9}(k_1 + k_2 + k_3) \equiv \omega_1^2 \tilde{m}_1\end{aligned}\quad (3)$$

The nodal forces due to seismic excitation are proportional to the nodal masses. A typical force is

$$p_i = -m_i a_g \quad (4)$$

where a_g is the ground acceleration. Substituting for p_i in Eq. (3) results in

$$\tilde{p}_1 = -\left(\frac{m_1}{3} + \frac{2m_2}{3} + m_3\right) a_g \quad (5)$$

3.2. DYNAMIC RESPONSE - MDOF

It is convenient to express \tilde{p} due to seismic acceleration as

$$\tilde{p}_1 = -\Gamma_1 \tilde{m}_1 a_g \quad (6)$$

where Γ_1 is a dimensionless factor. For this example, Γ_1 is given by

$$\Gamma_1 = \frac{\frac{m_1}{3} + \frac{2m_2}{3} + m_3}{\frac{m_1}{9} + \frac{4m_2}{9} + m_3} \quad (7)$$

When the masses are equal, $\Gamma_1 = 9/7$.

In order to evaluate the one-dimensional damping coefficient, \tilde{c} , the system damping matrix, \mathbf{C} , must be specified. The form of \mathbf{C} depends on how the viscous damping elements are located throughout the structure. Fig. E3.1b shows an arrangement consisting of viscous dampers inserted between adjacent masses.

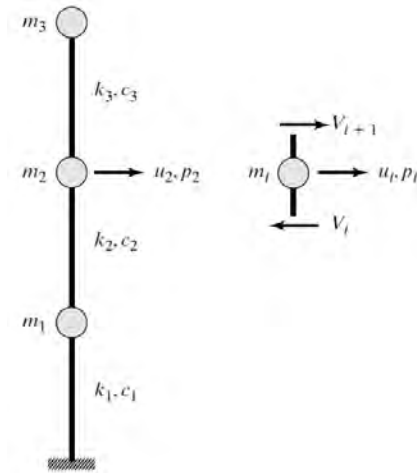


Figure E3.1b: Dampers included in shear beam elements.

In this case, the shear force in an element depends on both the shear deformation and the time rate of change of the shear

CHAPTER 3. OPTIMAL STIFFNESS/DAMPING FOR DYNAMIC LOADING

deformation. Assuming linear behavior, the typical equations have the form

$$\begin{aligned} V_i &= k_i(u_i - u_{i-1}) + c_i(\dot{u}_i - \dot{u}_{i-1}) \\ p_i &= m_i\ddot{u}_i + V_i - V_{i-1} \end{aligned} \quad (8)$$

Eq. (8) shows that the forms of \mathbf{K} and \mathbf{C} are similar; we replace k_i with c_i . Taking \mathbf{C} as

$$\mathbf{C} = \begin{bmatrix} c_1 + c_2 & -c_2 & 0 \\ -c_2 & c_2 + c_3 & -c_3 \\ 0 & -c_3 & c_3 \end{bmatrix} \quad (9)$$

leads to

$$\tilde{c}_1 = \Phi_1^T \mathbf{C} \Phi_1 = \frac{1}{9}(c_1 + c_2 + c_3) \quad (10)$$

The contribution of the individual dampers to \tilde{c} is the *same* since the assumed displacement profile corresponds to *constant* shear deformation.

When c_i is taken proportional to k_i , Eq. (10) takes this form

$$\tilde{c}_1 = \alpha \left[\frac{1}{9}(k_1 + k_2 + k_3) \right] = \alpha \tilde{k}_1 \equiv \alpha \omega_1^2 \tilde{m}_1 \quad (11)$$

Noting Eq. (3.8), \tilde{c}_1 is defined as

$$\tilde{c}_1 = 2\xi_1 \omega_1 \tilde{m}_1 \quad (12)$$

Then

$$\alpha \omega_1^2 \tilde{m}_1 = 2\xi_1 \omega_1 \tilde{m}_1$$

and it follows that

3.2. DYNAMIC RESPONSE - MDOF

$$\xi_1 = \frac{1}{2}\alpha\omega_1 \quad (13)$$

The damper arrangement shown in Fig. E3.1c produces nodal forces that depend on the nodal velocities. Assuming linear behavior, the typical equations are

$$\begin{aligned} V_i &= k_i(u_i - u_{i-1}) \\ p_i &= m_i\ddot{u}_i + c'_i\dot{u}_i + V_i - V_{i-1} \end{aligned} \quad (14)$$

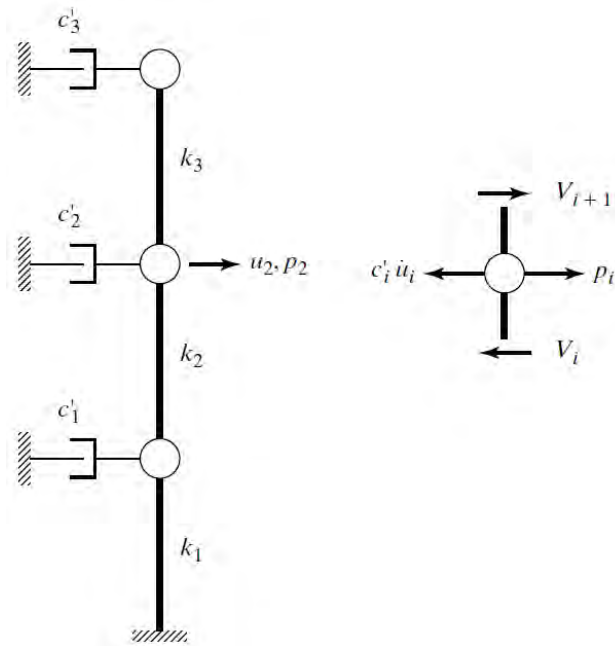


Figure E3.1c: Dampers attached to nodal masses.

With this arrangement, \mathbf{C} is similar to \mathbf{M} . Then

$$\mathbf{C} = \begin{bmatrix} c'_1 & 0 & 0 \\ 0 & c'_2 & 0 \\ 0 & 0 & c'_3 \end{bmatrix} \quad (15)$$

CHAPTER 3. OPTIMAL STIFFNESS/DAMPING FOR DYNAMIC LOADING

and

$$\tilde{c} = \Phi^T \mathbf{C} \Phi = \frac{c'_1}{9} + \frac{4}{9}c'_2 + c'_3 \quad (16)$$

Eq. (14) shows that the most effective damper location is node 3. This result is deduced by examining the assumed displacement profile. Node 3 corresponds to the maximum element in Φ^* and therefore has the largest velocity.

When \mathbf{C} is taken proportional to \mathbf{M} , say $\mathbf{C} = \beta\mathbf{M}$, Eq. (16) becomes

$$\tilde{c}_1 = \beta\tilde{m}_1 \quad (17)$$

Then, noting Eq. (12),

$$\xi_1 = \frac{1}{2} \frac{\beta}{\omega_1} \quad (18)$$

This result confirms Eq. (3.8).

Given the external loading and ground acceleration, one solves for the modal coordinates, $q_j(t)$, and then generates the structural displacement response by superimposing the modal responses. Theoretically one needs to include all the modal responses to obtain the exact solution. However, one can obtain a reasonable estimate with a limited set of modes. The critical issue concerns what modes to retain in the approximate solution. Comparing the magnitudes of p_j and Γ_j provides a reasonable indication of the significance of the different modal responses. We discuss this strategy further in a later section.

3.2.2 General Solution - Convolution Integral

The complete solution for q_j involves 2 terms, one associated with free vibration, and the other due to the loading defined by p_j and a_g . Their general forms are listed below.

Homogeneous solution

$$q_j = e^{-\xi_j \omega_j t} \left[q_j(0) \cos \omega'_j t + \frac{1}{\omega'_j} (\dot{q}_j(0) + \xi_j \omega_j q_j(0)) \sin \omega'_j t \right]$$

$$\omega'_j = \omega_j \sqrt{1 - \xi_j^2}$$

(3.11)

Particular solution

$$q_j = \frac{1}{\omega'_j} \int_0^t \left[\frac{p_j(\tau)}{\tilde{m}_j} - \Gamma_j a_g(\tau) \right] e^{-\xi_j \omega_j (t-\tau)} \sin \omega'(t - \tau) d\tau$$

(3.12)

$$\dot{q}_j = \frac{\omega_j}{\omega'_j} \int_0^t \left[\frac{p_j(\tau)}{\tilde{m}_j} - \Gamma_j a_g(\tau) \right] e^{-\xi_j \omega_j (t-\tau)} \sin[\omega'(t - \tau) + \delta_j] d\tau$$

(3.13)

$$\ddot{q}_j = \frac{p_j(t)}{\tilde{m}_j} - \Gamma_j a_g(t)$$

$$+ \frac{\omega_j^2}{\omega'_j} \int_0^t \left[\frac{p_j(\tau)}{\tilde{m}_j} - \Gamma_j a_g(\tau) \right] e^{-\xi_j \omega_j (t-\tau)} \sin[\omega'(t - \tau) + \delta_{j1}] d\tau$$

(3.14)

$$\begin{aligned}\tan \delta_j &= \frac{-\sqrt{1 - \xi_j^2}}{\xi_j} \\ \tan \delta_{j1} &= \frac{2\xi_j \sqrt{1 - \xi_j^2}}{1 - 2\xi_j^2}\end{aligned}\tag{3.15}$$

Given the initial conditions on \mathbf{U} ,

$$\begin{aligned}\mathbf{U}(0) &= \mathbf{U}_0 \\ \dot{\mathbf{U}}(0) &= \dot{\mathbf{U}}_0\end{aligned}\tag{3.16}$$

one can establish the initial conditions on q by noting the orthogonality conditions. The resulting expressions are:

$$\begin{aligned}q_j(0) &= \frac{\Phi_j^T \mathbf{M} \mathbf{U}_0}{\tilde{m}_j} \\ \dot{q}_j(0) &= \frac{\Phi_j^T \mathbf{M} \dot{\mathbf{U}}_0}{\tilde{m}_j}\end{aligned}\tag{3.17}$$

Given $a_g(t)$, one evaluates the convolution integrals with a numerical integration procedure. We describe this approach in more detail in a later section. When the loading is periodic, it is possible to obtain analytical solutions.

3.2.3 Periodic Excitation

We suppose the external loading is periodic with forcing frequency Ω .

$$\mathbf{P} = e^{i\Omega t} \mathbf{F}\tag{3.18}$$

3.2. DYNAMIC RESPONSE - MDOF

where \mathbf{F} defines the nodal force magnitudes. When the loading is uniform, \mathbf{F} is expressed as

$$\mathbf{F} = f\mathbf{E} = f \{1, 1, \dots, 1\} \quad (3.19)$$

Of interest is the response of the j^{th} mode. Noting Eq. (3.10), the governing equation is:

$$\begin{aligned} \ddot{q}_j + 2\omega_j\xi_j\dot{q}_j + \omega_j^2q_j &= \frac{1}{\tilde{m}_j}p_j \\ p_j = \Phi_j^T\mathbf{P} = e^{i\Omega t}(f\Phi_j^T\mathbf{E}) &= \bar{p}_je^{i\Omega t} \end{aligned} \quad (3.20)$$

Note that the scalar $\Phi_j^T\mathbf{E}$ decreases with increasing mode number since Φ_j had both positive and negative entries when $j > 1$. We express q_j as

$$q_j = \bar{q}_je^{i\Omega t} \quad (3.21)$$

Substituting in Eq. (3.20) leads to

$$\begin{aligned} \bar{q}_j(-\Omega^2 + 2\xi_j\omega_j\Omega_ji + \omega_j^2) &= \frac{1}{\tilde{m}_j}\bar{p}_j \\ \Downarrow & \\ \bar{q}_j &= \frac{1}{-\Omega^2 + 2\xi_j\omega_j\Omega_ji + \omega_j^2} \frac{1}{\tilde{m}_j}\bar{p}_j \end{aligned} \quad (3.22)$$

The modal coordinate is complex. Shifting to complex notation, we write:

$$\bar{q}_j = \hat{q}_je^{-i\delta_j} \quad (3.23)$$

The solution follows from Eq. (3.22).

CHAPTER 3. OPTIMAL STIFFNESS/DAMPING FOR DYNAMIC LOADING

$$\hat{q}_j = \frac{1}{\sqrt{\left[1 - \left(\frac{\Omega}{\omega_j}\right)^2\right]^2 + \left[2\xi_j \frac{\Omega}{\omega_j}\right]^2}} \cdot \frac{1}{\omega_j^2 \tilde{m}_j} \bar{p}_j$$

$$\tan \delta_j = \frac{2\xi_j \left(\frac{\Omega}{\omega_j}\right)}{1 - \left(\frac{\Omega}{\omega_j}\right)^2} \quad (3.24)$$

$$q_j = \hat{q}_j e^{i(\Omega t - \delta_j)}$$

The corresponding nodal displacement vector for mode j is

$$\mathbf{U}|_j = q_j \Phi_j = \hat{q}_j \Phi_j e^{i(\Omega t - \delta_j)} \quad (3.25)$$

The response is a scaled version of Φ_j with a periodic scale factor.

Using the H notation introduced in Chapter 1, the terms in Eq. (3.24) are expressed as

$$H_{j1} = \frac{1}{\sqrt{\left[1 - \left(\frac{\Omega}{\omega_j}\right)^2\right]^2 + \left[2\xi_j \frac{\Omega}{\omega_j}\right]^2}} \quad (3.26)$$

$$H_{j2} = \left(\frac{\Omega}{\omega_j}\right)^2 H_{j1}$$

Then, Eq. (3.24) simplifies to

$$\hat{q}_j = H_{j1} \frac{\bar{p}_j}{\omega_j^2 \tilde{m}_j}$$

$$= H_{j2} \frac{\bar{p}_j}{\Omega^2 \tilde{m}_j} \quad (3.27)$$

3.2. DYNAMIC RESPONSE - MDOF

Typical plots for H_{j1} and H_{j2} are shown in Fig. 3.1. The peak value of H occurs at $\Omega \approx \omega_j$ and is approximately equal to $\approx 1/2\xi_j$. Note that the influence of damping is confined to a narrow zone, $0.6\omega_j < \Omega < 1.4\omega_j$, centered on ω_j .

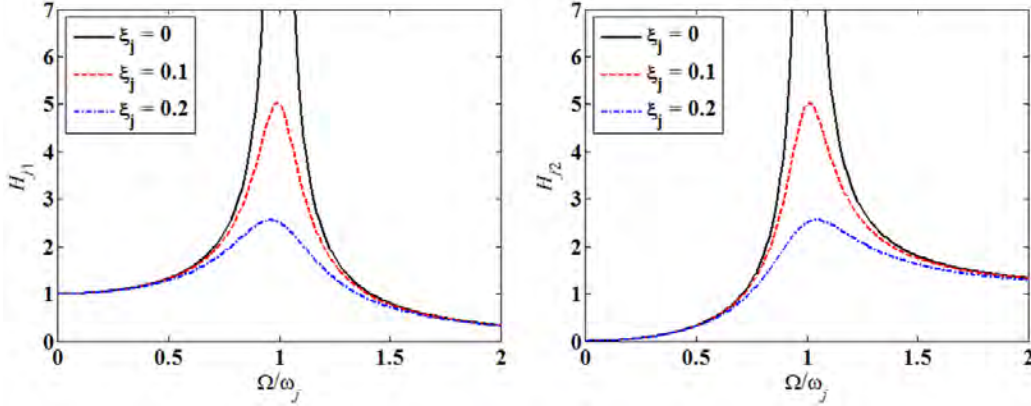


Figure 3.1: Plots of H_1 and H_2 for mode j .

The complete solution is obtained by summing the contributions of the individual modes

$$\mathbf{U} = \sum_{j=1}^n q_j \Phi_j = \sum_{j=1}^n \frac{\bar{p}_j}{\Omega^2 \tilde{m}_j} H_{j2} \Phi_j e^{i(\Omega t - \delta_j)} \quad (3.28)$$

Given Ω , one compares Ω with the set of modal frequencies $(\omega_1, \omega_2, \dots, \omega_n)$, and determines whether one of the modes dominates the response, i.e., whether a resonance condition exists. Resonance is avoided by either adding damping or modifying the stiffness to shift ω .

3.2.4 Seismic Loading; Response Spectra

Specializing Eq. (3.9) for only seismic excitation leads to the following set of equations relating the modal coordinates and the

CHAPTER 3. OPTIMAL STIFFNESS/DAMPING FOR DYNAMIC LOADING

ground acceleration:

$$\ddot{q}_j + 2\xi_j\omega_j\dot{q}_j + \omega_j^2q_j = -\Gamma_j a_g \quad j = 1, 2, \dots, n \quad (3.29)$$

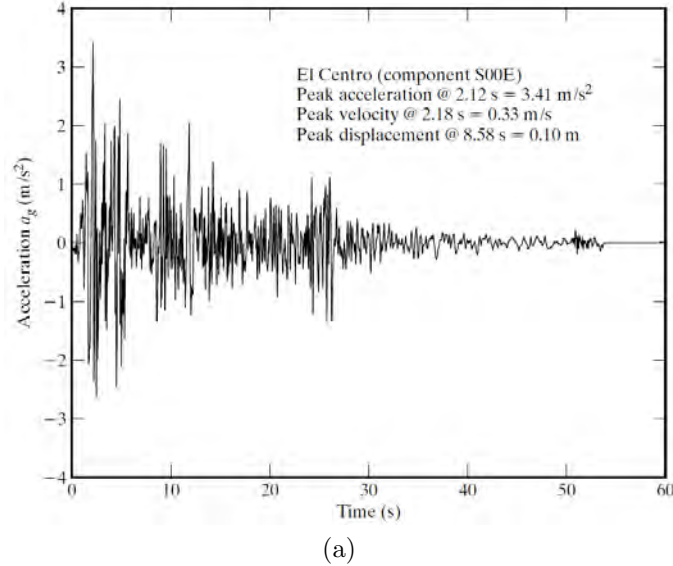


Figure 3.2: Ground motion time histories: (a) El Centro accelerogram (component S00E);

Typical ground acceleration time history plots are shown in Fig. 3.2. Since the governing equation is linear, one can generate the individual modal time histories, $q(t)$, and superimpose these responses in order to obtain the total time history response.

$$\mathbf{U}(x, t) = \sum_{r=1}^n q_r(t)\Phi_r(x) \quad (3.30)$$

An alternate strategy is to work with the equilibrium equation for a 1 DOF system:

$$\ddot{v} + 2\xi\omega\dot{v} + \omega^2v = -a_g \quad (3.31)$$

3.2. DYNAMIC RESPONSE - MDOF

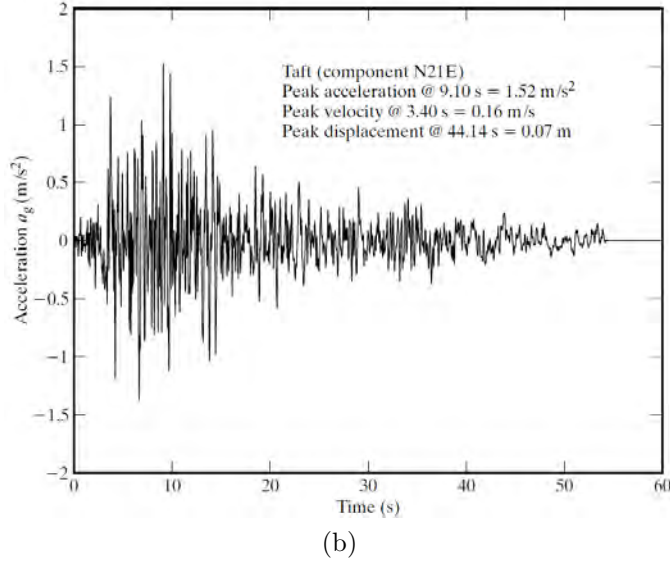


Figure 3.2: Ground motion time histories: (b) Taft accelerogram (component N21E).

Given an earthquake time history, Eq. (3.31) is solved for a range of values of ω and ξ . The solution for the j^{th} modal response is determined by scaling the 1 DOF solution

$$q_j(t) = \Gamma_j v(t, \omega_j, \xi_j) \quad (3.32)$$

corresponding to ω_j, ξ_j with Γ_j .

The general solution of Eq. (3.31) can be expressed in terms of convolution integrals

$$\begin{aligned} v(t, \omega, \xi) &= \frac{1}{\omega'} \Psi_1(\xi, \omega, t) \\ \dot{v}(t, \omega, \xi) &= \frac{\omega}{\omega'} \Psi_2(\xi, \omega, t) \\ \ddot{v}(t, \omega, \xi) &= -a_g(t) + \frac{\omega^2}{\omega'} \Psi_3(\xi, \omega, t) \end{aligned} \quad (3.33)$$

where

CHAPTER 3. OPTIMAL STIFFNESS/DAMPING FOR DYNAMIC LOADING

$$\begin{aligned}\Psi_1(\xi, \omega, t) &= - \int_0^t a_g(t) e^{-\xi\omega(t-\tau)} \sin[\omega'(t-\tau)] d\tau \\ \Psi_2(\xi, \omega, t) &= - \int_0^t a_g(t) e^{-\xi\omega(t-\tau)} \sin[\omega'(t-\tau) + \delta] d\tau \\ \Psi_3(\xi, \omega, t) &= - \int_0^t a_g(t) e^{-\xi\omega(t-\tau)} \sin[\omega'(t-\tau) + \delta_1] d\tau \\ \tan \delta &= \frac{\sqrt{1-\xi^2}}{\xi} \\ \tan \delta_1 &= \frac{2\xi\sqrt{1-\xi^2}}{1-2\xi^2} \\ \omega' &= \omega(1-\xi^2)^{1/2}\end{aligned}$$

For lightly damped structures, $\xi < \approx 0.10$, and one can assume

$$\begin{aligned}\omega' &\approx \omega \\ \delta &\approx \pi/2 \\ \tan \delta_1 &\approx \delta_1 \approx 2\xi\end{aligned}\tag{3.34}$$

in Eq. (3.33).

For given values of $a_g(t)$, ω , and ξ , the time history solutions are generated, and the *peak values* of v and its derivatives are determined. They are denoted as follows (for lightly damped structures):

$$\begin{aligned}S_D(\omega, \xi) &= \text{spectral displacement} = |v(\omega, \xi, t)|_{\max} = \left| \frac{1}{\omega} \Psi_1(\omega, \xi, t) \right|_{\max} \\ PS_V(\omega, \xi) &= \text{pseudo spectral velocity} = \omega S_D(\omega, \xi) \\ S_A(\omega, \xi) &= \text{spectral acceleration} = |\omega \Psi_3(\omega, \xi, t)|_{\max}\end{aligned}\tag{3.35}$$

3.2. DYNAMIC RESPONSE - MDOF

Typical spectral plots corresponding to the Northridge Earthquake are listed in Fig. 3.3. Increasing the damping tends to smoothen out the oscillations in the plots. When ξ is small ($\xi \ll 1$), the spectral acceleration can be approximated by

$$S_A \approx \omega^2 S_D \quad (3.36)$$

The peak values for modal coordinate q_j are related to the spectral quantities by scaling with Γ_j .

$$\begin{aligned} q_j|_{\max} &= \Gamma_j S_D(\omega_j, \xi_j) \\ \ddot{q}_j|_{\max} &= \Gamma_j [-a_g + \omega \Psi_3]_{\max} \end{aligned} \quad (3.37)$$

For a 1 DOF system, the total acceleration is

$$\ddot{v}_t = \ddot{v} + \ddot{u}_g = \ddot{v} + a_g = \omega \Psi_3(\omega, \xi, t) \quad (3.38)$$

Noting the definition of S_A , it follows that S_A is the *peak total acceleration* for a 1 DOF system.

Extending this analysis to a MDOF system, the total nodal acceleration at node i is:

$$\ddot{\mathbf{U}}_T(i) = \ddot{\mathbf{U}}(i) + a_g = a_T(x_i, t) \quad (3.39)$$

Expanding $\ddot{\mathbf{U}}(i)$ in terms of its modal contributions leads to

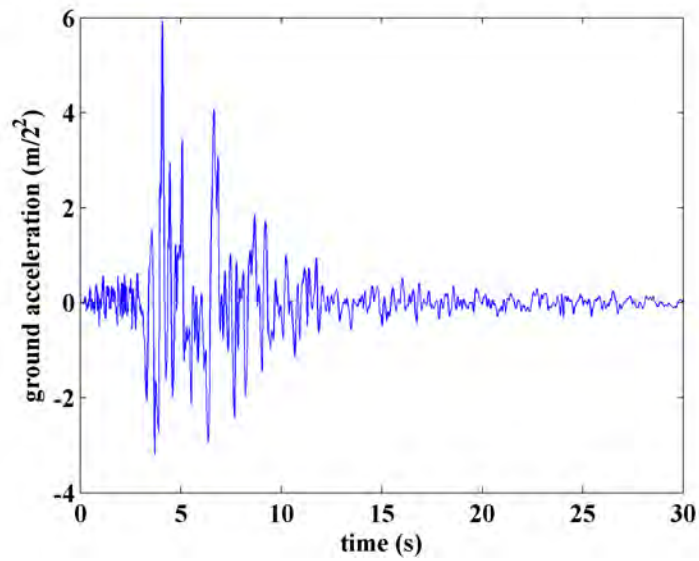
$$\ddot{\mathbf{U}}(i) = \sum_r \ddot{q}_r(t) \Phi_r(x_i) \quad (3.40)$$

where

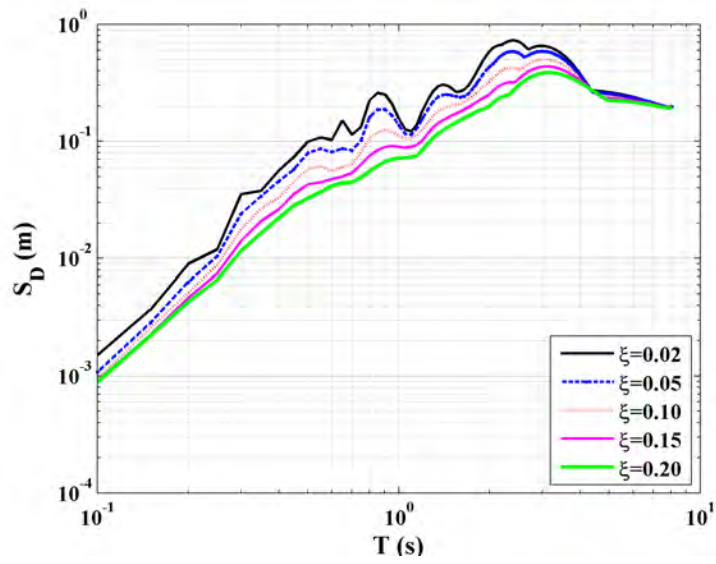
$$\ddot{q}_r(t) = -\Gamma_r a_g(t) + \Gamma_r \omega_r \Psi_3(\xi_r, \omega_r, t)$$

Combining terms leads to

CHAPTER 3. OPTIMAL STIFFNESS/DAMPING FOR DYNAMIC LOADING



(a)



(b)

Figure 3.3: Spectral plots - Northridge Earthquake: (a) acceleration time history; (b) spectral displacement;

3.2. DYNAMIC RESPONSE - MDOF

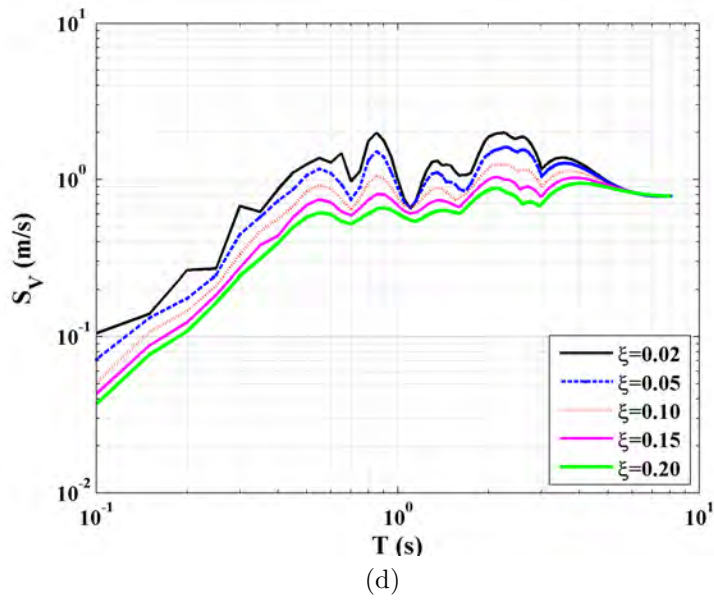
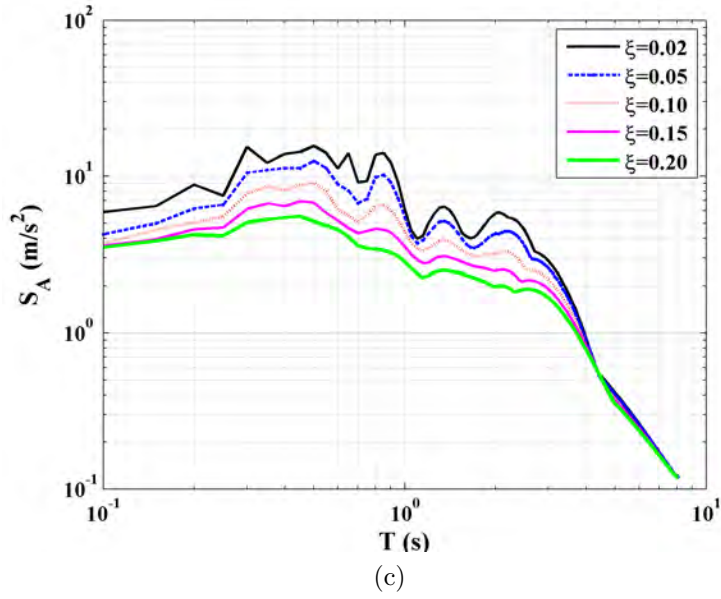


Figure 3.3: (c) spectral acceleration; and (d) pseudo spectral velocity.

$$a_T(x_i, t) = a_g(t) \left[1 - \sum_r \Gamma_r \Phi_r(x_i) \right] + \left[\sum_r \Gamma_r \omega_r \Phi_r(x_i) \Psi_3(\xi_r, \omega_r, t) \right] \quad (3.41)$$

Since the peak acceleration values for the individual modes occur at different times, one cannot just sum up the modal spectral acceleration terms in order to obtain an estimate of the peak acceleration at a node. Eq. (3.41) is useful for evaluating the inertia forces acting on the nodes. For node i , the force is

$$P_i|_{\text{inertia}} = m_i a_T(x_i, t) \quad (3.42)$$

Eq. 3.42 is used to develop the seismic nodal loading distribution for an approximate quasi-static analysis procedure called the “pushover test” which is commonly applied in seismic design.

3.2.5 Selection of Modes

The general solution for the response of an n^{th} order structural system is given by Eq. (3.30) which is listed below for convenience.

$$\mathbf{U}(x, t) = \sum_{r=1}^n q_r(t) \Phi_r(x)$$

Retaining all n modes is computationally expensive, and therefore one needs a strategy for identifying the relative importance of the modal contributions toward the response. With this strategy, one can generate a reasonable estimate of the solution using only a limited number of modes.

We encountered this issue in Sect. 3.2.3 which deals with periodic loading. We observed that when the forcing frequency is

3.2. DYNAMIC RESPONSE - MDOF

close to one of the modal frequencies, say ω_j , the corresponding modal response coordinate, q_j , is significantly greater than the other modal responses, and essentially dominates the response. Therefore, one could retain only mode j . Extending this approach to an arbitrary loading; one first examines the frequency content of the loading using an FFT procedure, and identifies whether there are dominant frequencies. Next, one compares these dominant frequencies with the set of modal frequencies to see if there are reasonable matches. If so, one retains the *matched* modes in the response calculation.

The following example illustrates the different modal responses for a range of structures subjected to various earthquakes scaled to the same ground peak acceleration. The spectral acceleration response spectrum is used to identify the frequency content of a seismic time history record.

Example 3.2 - Selection of modes

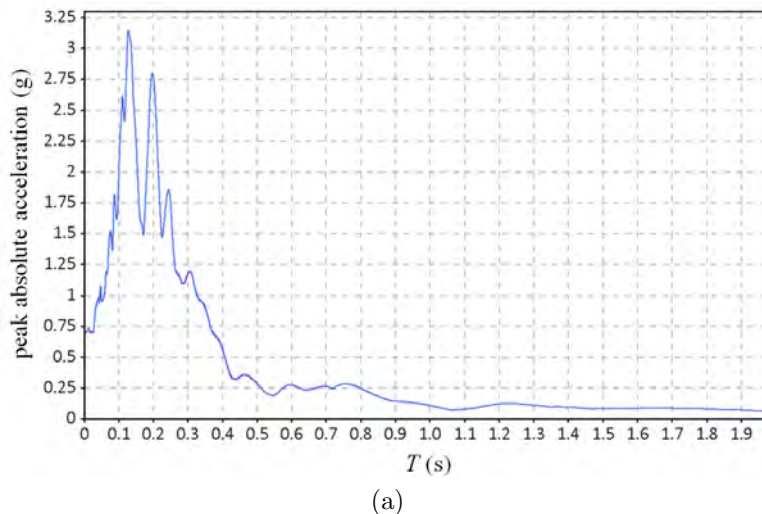
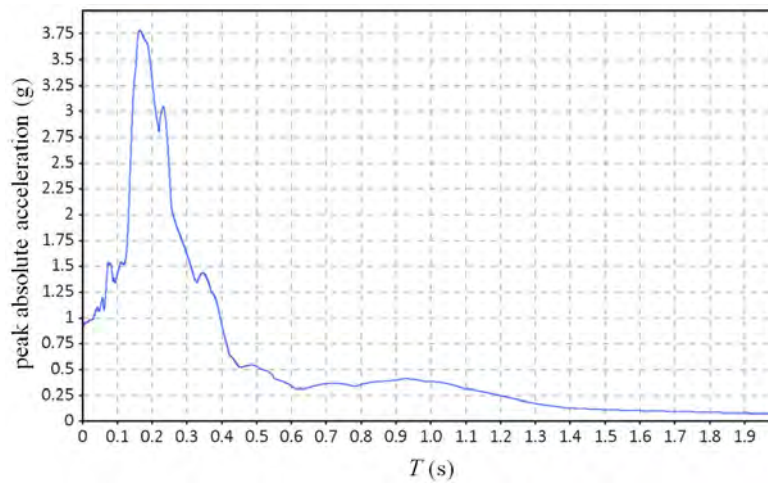


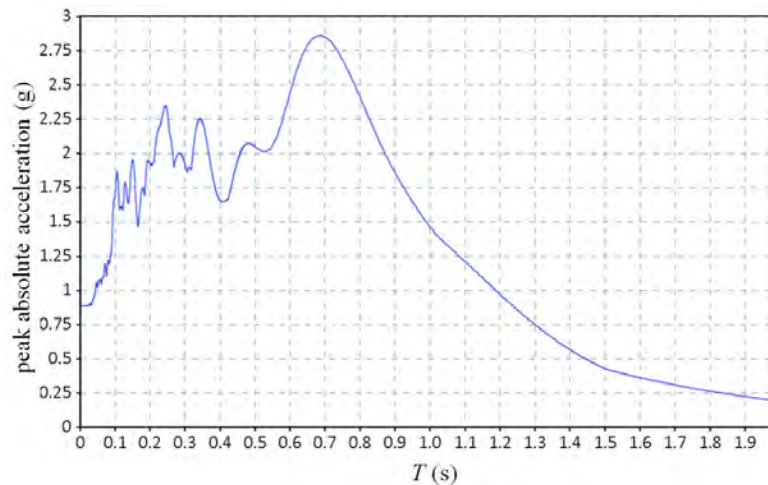
Figure 3.4: Peak absolute acceleration response: (a) earthquake 1;

CHAPTER 3. OPTIMAL STIFFNESS/DAMPING FOR DYNAMIC LOADING

The response spectra in Figs. 3.4a to 3.4e show the peak absolute acceleration response to various earthquakes assuming 5% structural damping. All earthquake records are scaled so that the peak ground acceleration (PGA) = 0.5 g.



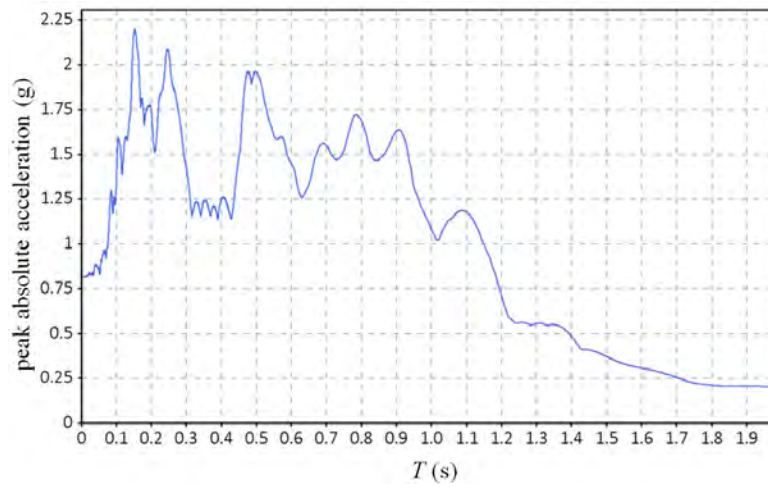
(b)



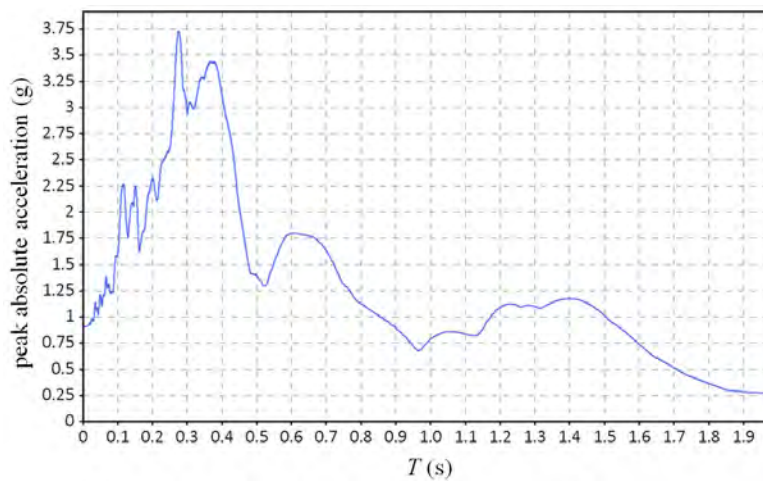
(c)

Figure 3.4: Peak absolute acceleration response: (b) earthquake 2; (c) earthquake 3;

3.2. DYNAMIC RESPONSE - MDOF



(d)



(e)

Figure 3.4: Peak absolute acceleration response: (d) earthquake 4; and (e) earthquake 5.

Listed below are the displacement time history responses based on retaining only the first mode and retaining all the modes for various structures.

CHAPTER 3. OPTIMAL STIFFNESS/DAMPING FOR DYNAMIC LOADING

Structure 1

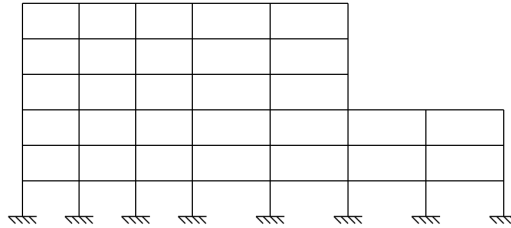


Figure 3.5: Structure 1.

Table E3.2a: Dynamic properties - structure 1

N	T (sec)	Γ	Norm. ξ	Φ_1	Φ_2	Φ_3	Φ_4	Φ_5	Φ_6
1	0.87	1.52	1.00	0.15	0.31	0.50	0.71	0.89	1.00
2	0.38	0.76	1.00	-0.27	-0.50	-0.55	-0.20	0.44	1.00
3	0.23	0.34	1.34	-0.53	-0.66	-0.02	1.00	0.42	-0.99
4	0.16	0.27	1.78	0.67	0.33	-0.81	0.16	1.00	-0.62
5	0.13	0.15	2.08	-0.27	0.00	0.33	-0.61	1.00	-0.40

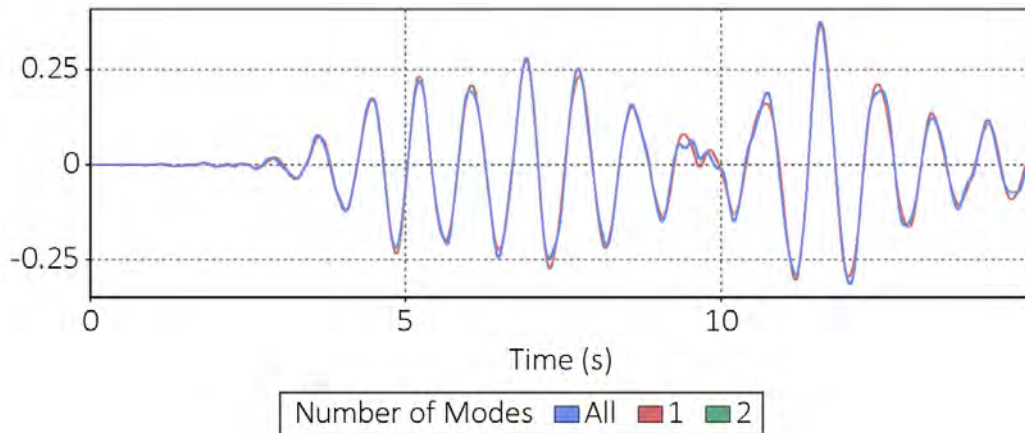


Figure 3.6: Time history response - displacement (ft); structure 1, floor 4, earthquake 4.

3.2. DYNAMIC RESPONSE - MDOF

Structure 2

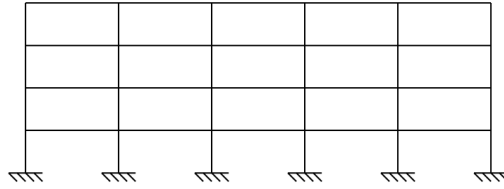


Figure 3.7: Structure 2.

Table E3.2b: Dynamic properties - structure 2

N	T (sec)	Γ	Norm. ξ	Φ_1	Φ_2	Φ_3	Φ_4
1	0.64	1.36	1.00	0.18	0.42	0.70	1.00
2	0.25	0.45	1.00	-0.52	-0.94	-0.70	1.00
3	0.13	0.34	1.48	-0.78	-0.60	1.00	-0.30
8	0.07	0.25	2.48	1.00	-0.81	0.29	-0.04

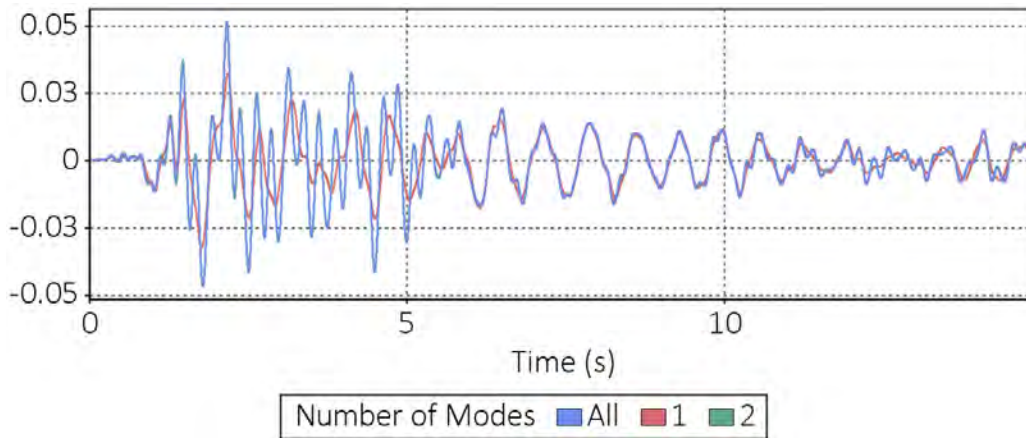


Figure 3.8: Time history response - displacement (ft); structure 2, floor 3, earthquake 2.

CHAPTER 3. OPTIMAL STIFFNESS/DAMPING FOR DYNAMIC LOADING

Structure 2 | Floor 3 | Earthquake 6 | Displacement (ft)

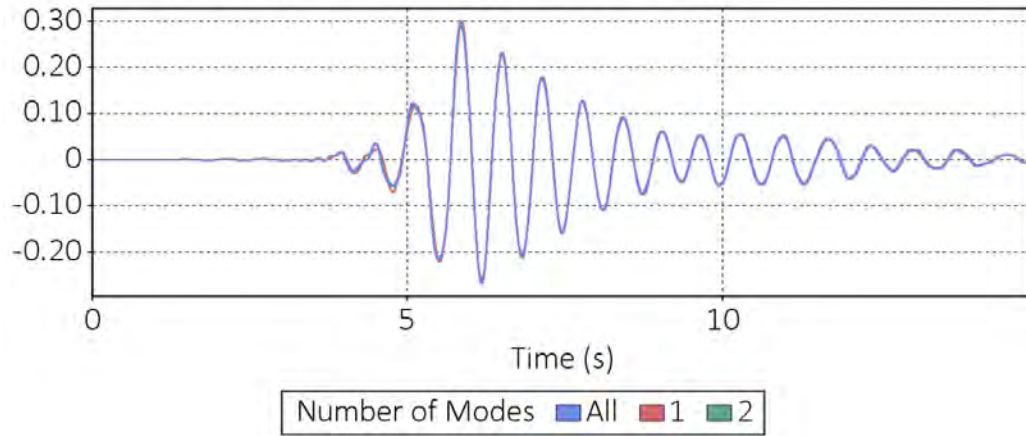


Figure 3.9: Time history response - displacement (ft); structure 2, floor 3, earthquake 3.

Structure 3

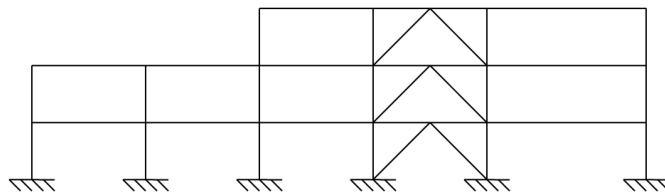


Figure 3.10: Structure 3.

Table E3.2c: Dynamic properties - structure 3

N	T (sec)	Γ	Norm. ξ	Φ_1	Φ_2	Φ_3
1	0.36	1.32	1.00	0.35	0.73	1.00
2	0.15	0.38	1.00	-0.93	-0.49	1.00
6	0.10	0.18	1.29	1.00	-0.77	0.23
9	0.08	0.02	1.46	0.18	-0.73	1.00

3.2. DYNAMIC RESPONSE - MDOF

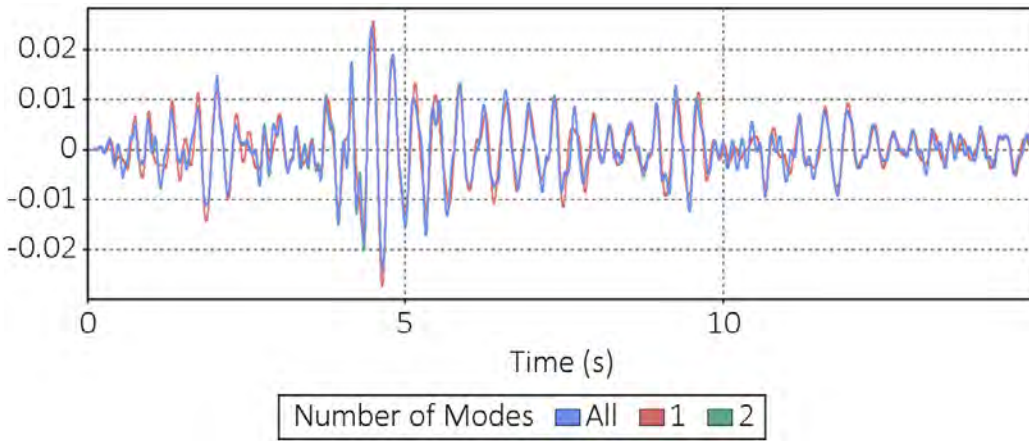


Figure 3.11: Time history response - displacement (ft); structure 3, floor 2, earthquake 1.

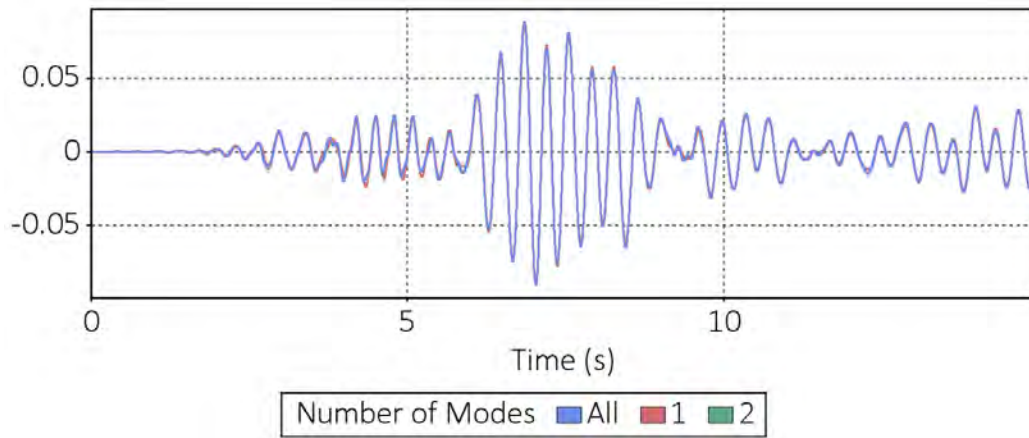


Figure 3.12: Time history response - displacement (ft); structure 3, floor 2, earthquake 5.

CHAPTER 3. OPTIMAL STIFFNESS/DAMPING FOR DYNAMIC LOADING

Structure 4

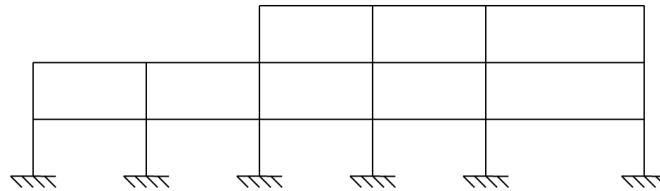


Figure 3.13: Structure 4.

Table E3.2d: Dynamic properties - structure 4

N	T (sec)	Γ	Norm. ξ	Φ_1	Φ_2	Φ_3
1	0.64	1.47	1.00	0.24	0.54	1.00
2	0.32	0.52	1.00	-0.56	-0.80	1.00
3	0.18	0.36	1.39	1.00	-0.60	0.14

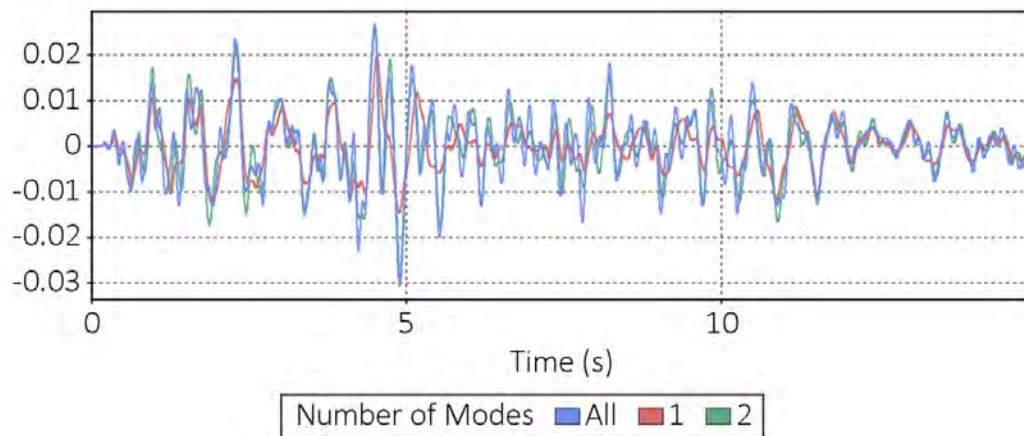


Figure 3.14: Time history response - displacement (ft); structure 4, floor 2, earthquake 1.

These results show that the second mode may be as significant as the first mode for certain earthquakes. One can detect this trend by comparing the peak period values for the spectral acceleration with the modal periods. However, in most cases,

3.3. STIFFNESS DISTRIBUTION FOR A CANTILEVER BEAM: DYNAMIC RESPONSE

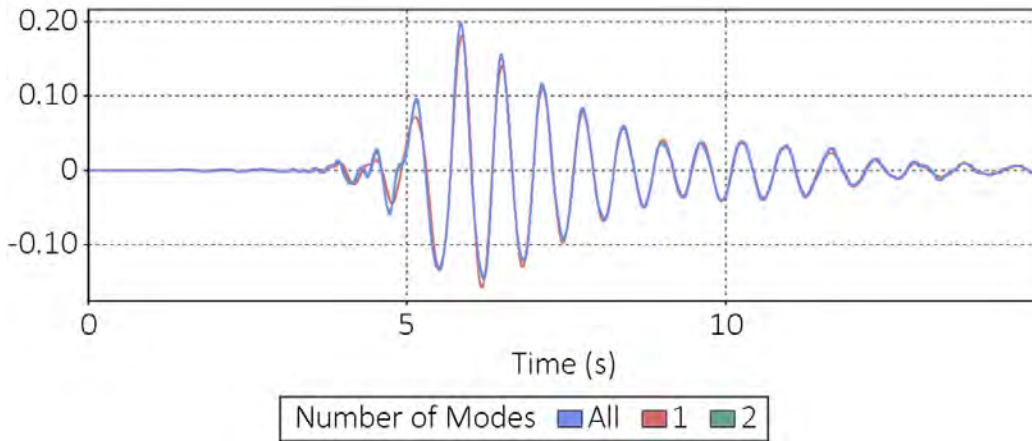


Figure 3.15: Time history response - displacement (ft); structure 4, floor 2, earthquake 3.

retaining only the first mode leads to a reasonable estimate for the seismic response. In what follows, we shall adopt this strategy to generate the stiffness distribution for dynamic loading.

3.3 Stiffness Distribution for a Cantilever Beam: Dynamic Response

The distribution of rigidity is established by requiring the fundamental mode for a dynamically loaded cantilever beam to have a certain profile. For undamped free vibration, the distributed loading consists only of the inertia terms

$$\begin{aligned}
 b(x, t) &= -\rho_m(x) \frac{\delta^2 u(x, t)}{\delta t^2} = -\rho_m(x) \ddot{u}(x, t) \\
 m(x, t) &= -J(x) \frac{\delta^2 \beta(x, t)}{\delta t^2} = -J(x) \ddot{\beta}(x, t)
 \end{aligned}
 \tag{3.43}$$

For simplicity, a uniform mass distribution is assumed. The

CHAPTER 3. OPTIMAL STIFFNESS/DAMPING FOR DYNAMIC LOADING

equilibrium equations specialized for uniform mass, elastic behavior, and no rotatory inertia loading take the form

$$\begin{aligned} V(x, t) &= -\rho_m \int_x^H \ddot{u}(x, t) dx = D_T(x) \gamma(x, t) \\ M(x, t) &= \int_x^H V(x, t) dx = D_B(x) \chi(x, t) \end{aligned} \quad (3.44)$$

The desired behavior is periodic vibration with uniform shear and bending deformation throughout the length. Requiring periodic vibration with uniform deformation modes is achieved by specifying the deformations as follows:

$$\begin{aligned} \gamma(x, t) &= \gamma^* \cos(\omega_1 t + \delta) \\ \chi(x, t) &= \chi^* \cos(\omega_1 t + \delta) \end{aligned} \quad (3.45)$$

where ω_1 is the fundamental circular frequency of the beam and δ is an arbitrary scalar. The displacement expressions which define the fundamental mode are generated using Eqs. (2.7) and (2.8)

$$\begin{aligned} u &= \left[\gamma^* x + \frac{\chi^* x^2}{2} \right] \cos(\omega_1 t + \delta) \\ \beta &= (\chi^* x) \cos(\omega_1 t + \delta) \\ \chi^* &= \frac{2s}{H} \gamma^* \end{aligned} \quad (3.46)$$

Substituting for u , γ , and χ in Eq. (3.44), canceling out the cosine terms, and evaluating the integrals leads to the following expressions for the rigidity distributions:

3.3. STIFFNESS DISTRIBUTION FOR A CANTILEVER BEAM: DYNAMIC RESPONSE

$$D_T \left(\frac{x}{H} \right) = \frac{\rho_m \omega_1^2 H^2}{2} \left[1 - \left[\frac{x}{H} \right]^2 + \frac{2s}{3} \left(1 - \left[\frac{x}{H} \right]^3 \right) \right] \quad (3.47)$$

$$D_B \left(\frac{x}{H} \right) = \frac{\rho_m \omega_1^2 H^4}{2} \left[\frac{1}{4} \left(1 - \frac{4x}{3H} + \frac{1}{3} \left[\frac{x}{H} \right]^4 \right) + \frac{1}{6s} \left(2 - 3 \frac{x}{H} + \left[\frac{x}{H} \right]^3 \right) \right] \quad (3.48)$$

The magnitude of D_T at $x = 0$ can be determined by specifying representative values of base shear and transverse shear deformation:

$$D_T(0) = \frac{[V(0)]_{\max}}{\gamma^*} \quad (3.49)$$

Once $D_T(0)$ is defined, the fundamental frequency can be obtained with Eq. (3.47) specialized for $x = 0$. The final expressions are

$$D_T(0) = \frac{\rho_m \omega_1^2 H^2}{2} \left(1 + \frac{2s}{3} \right) \quad (3.50)$$

$$\omega_1 = \sqrt{\frac{2[V(0)]_{\max}}{\gamma^* \rho_m H^2 \left(1 + \frac{2s}{3} \right)}}$$

Figs. 3.16 and 3.17 show the normalized distribution of D_T and D_B for typical low- and high-rise buildings. Fig. 3.18 contains plots of the first five mode shapes corresponding to the preceding rigidity distributions, and Fig. 3.19 shows the shear deformation profiles of those modes. The results are relatively insensitive to the parameter s , which ranges from 0 for a pure shear beam to about 1 for a tall building. It should be noted

CHAPTER 3. OPTIMAL STIFFNESS/DAMPING FOR DYNAMIC LOADING

that the mode shape and frequency expressions are the *exact solution* for the fundamental modal response of the beam having the rigidity distributions defined by Eqs. (3.47) and (3.48).

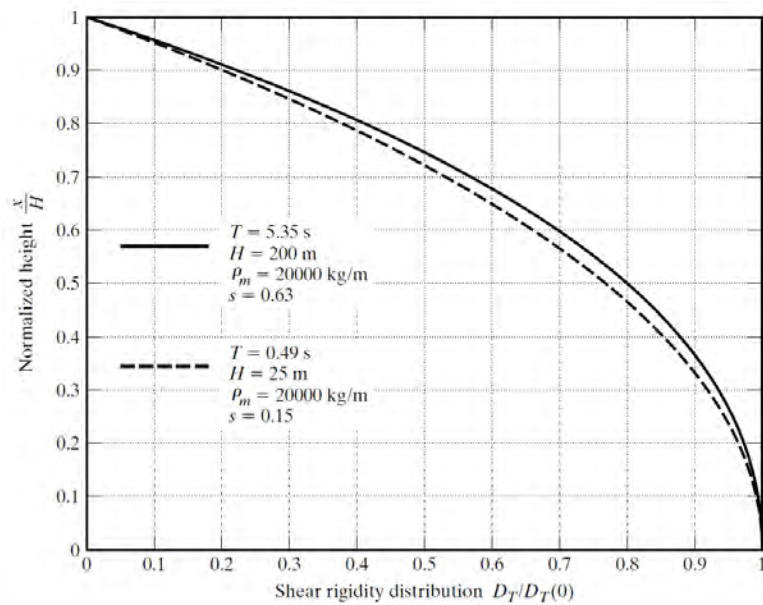


Figure 3.16: Normalized shear rigidity distribution.

3.3. STIFFNESS DISTRIBUTION FOR A CANTILEVER BEAM: DYNAMIC RESPONSE

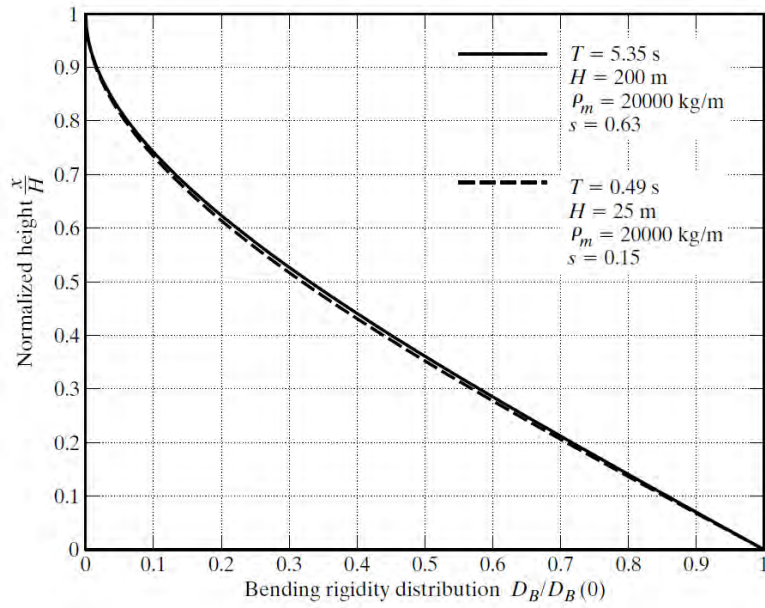


Figure 3.17: Normalized bending rigidity distribution.

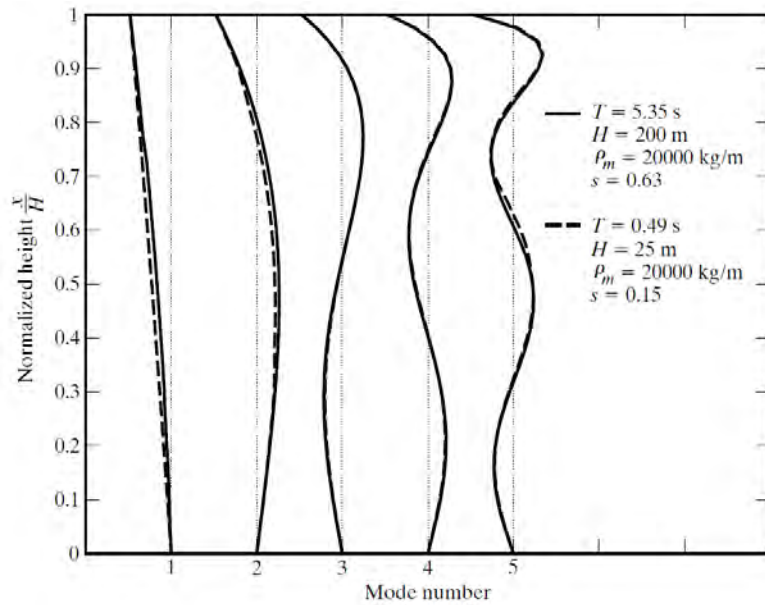


Figure 3.18: Mode shapes.

CHAPTER 3. OPTIMAL STIFFNESS/DAMPING FOR DYNAMIC LOADING

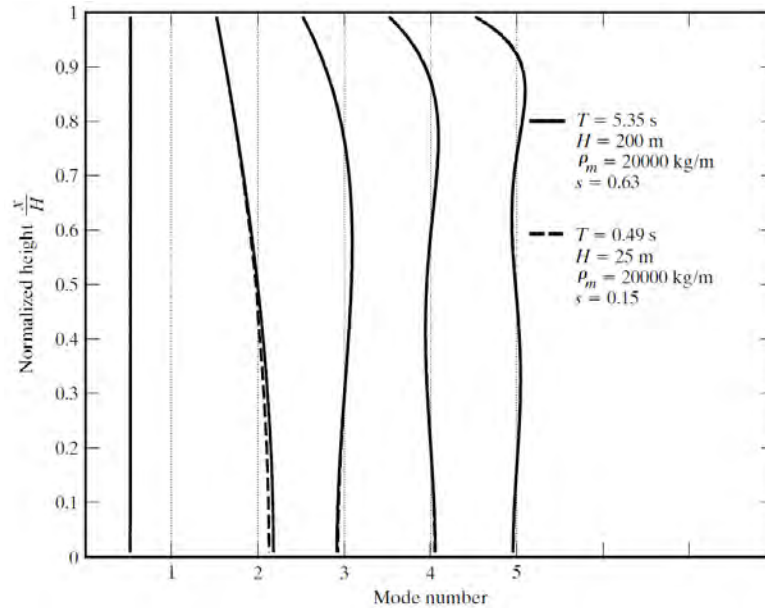


Figure 3.19: Mode shear deformation profiles.

This approach leads to the proper distribution of rigidities, but the actual magnitude is not defined since we have to specify $D_T(0)$ using a representative value of base shear. In effect, we have to calibrate the rigidities for a particular loading. The calibration procedure is discussed in detail in later sections.

3.4 Stiffness Distribution for a Discrete Shear Beam: Dynamic Response

Our starting point is Eq. (3.2), the equation for the undamped eigenvalue problem for an n^{th} order system:

$$\mathbf{K}\Phi = \omega^2\mathbf{M}\Phi$$

Solutions of Eq. (3.2) define the frequencies (ω_j) and mode shapes (Φ_j) corresponding to a particular beam (i.e., when \mathbf{M}

3.4. STIFFNESS DISTRIBUTION FOR A DISCRETE SHEAR BEAM: DYNAMIC RESPONSE

and \mathbf{K} are specified). In the motion based approach, one specifies the fundamental mode shape and determines \mathbf{K} .

Let

$$\Phi_1 = \Phi^* \quad (3.51)$$

denote the specified fundamental mode profile. Substituting in Eq. (3.2) leads to

$$\mathbf{K}\Phi^* = \omega_1^2 \mathbf{M}\Phi^* \quad (3.52)$$

where ω_1 is the fundamental modal frequency. Defining a scaled version of \mathbf{K} ,

$$\mathbf{K}' = \frac{1}{\omega_1^2} \mathbf{K} \quad (3.53)$$

reduces Eq. (3.52) to

$$\mathbf{K}'\Phi^* = \mathbf{M}\Phi^* = \mathbf{P}' \quad (3.54)$$

The remaining steps are the same as for the static case discussed in Sect. 2.4.2. Equation (3.54) is written as

$$\mathbf{S}'\mathbf{k}' = \mathbf{P}' \quad (3.55)$$

where \mathbf{k}' contains the n scaled stiffness factors, and \mathbf{S}' is an upper triangular matrix containing the elements of Φ^* .

$$\begin{aligned} \mathbf{S}'(i, i) &= \Phi_i^* - \Phi_{i-1}^* \\ \mathbf{S}'(i, i+1) &= \Phi_i^* - \Phi_{i+1}^* \\ \mathbf{S}'(i, j) &= 0 \quad \text{for } j \neq i, i+1 \end{aligned} \quad (3.56)$$

We solve Eq. (3.55) for \mathbf{k}' . Once ω_1 is specified, the actual values of the stiffness parameters can be determined with

$$k_j = \omega_1^2 k'_j \quad (3.57)$$

Example 3.3 - 3DOF shear beam

This example illustrates the determination of the stiffness distribution that produces the following linear profile for the fundamental mode.

$$\Phi^* = \begin{bmatrix} 1/3 \\ 2/3 \\ 1 \end{bmatrix} \quad (1)$$

It is convenient to scale Φ^* so that the magnitude of the maximum element is equal to 1. The corresponding forms of \mathbf{P}' and \mathbf{S}' are

$$\mathbf{P}' = \mathbf{M}\Phi^* = \begin{bmatrix} m_1/3 \\ 2m_2/3 \\ m_3 \end{bmatrix} \quad (2)$$

$$\mathbf{S}' = \begin{bmatrix} \frac{1}{3} & -\frac{1}{3} & 0 \\ 0 & \frac{1}{3} & -\frac{1}{3} \\ 0 & 0 & \frac{1}{3} \end{bmatrix} \quad (3)$$

Solving Eq. (3.55) results in

$$\begin{aligned} k'_3 &= 3m_3 \\ k'_2 &= 2m_2 + 3m_3 \\ k'_1 &= m_1 + 2m_2 + 3m_3 \end{aligned} \quad (4)$$

When all the elements of Φ^* are positive, one can show that Φ^* is actually the fundamental mode shape for the system having

3.5. STIFFNESS CALIBRATION- FUNDAMENTAL MODE RESPONSE

the stiffness distribution defined by Eq. (3.55), and ω_1 is the corresponding fundamental frequency.

3.5 Stiffness Calibration- Fundamental Mode Response

The procedure described in Sect. 3.4 generates a rigidity distribution which involves the *unknown* fundamental frequency, ω_1 . We determine ω_1 by first reducing the governing equations down to a single equation, specializing the loading for this equation, and then imposing a constraint on the solution which involves ω_1 . We refer to this process as “calibrating” the rigidity.

3.5.1 Discrete Shear Beam

For the discrete shear beam, we assume the response is dominated by the first mode.

$$\mathbf{U}(x, t) \approx q_1(t)\Phi_1(x) \quad (3.58)$$

where $\Phi_1(x)$ is taken as Φ^* , the shape function used to establish the rigidity distribution. The corresponding modal equation follows from Eq. (3.10).

$$\ddot{q}_1 + 2\xi_1\omega_1\dot{q}_1 + \omega_1^2q = \frac{1}{\tilde{m}_1}p_1 - \Gamma_1a_g \quad (3.59)$$

where the modal coefficients are derived using Φ^* . For example,

$$\begin{aligned}
 \tilde{m}_1 &= \Phi^{*T} \mathbf{M} \Phi^* \\
 \Gamma_1 &= \frac{\Phi^{*T} \mathbf{M} \mathbf{E}}{\tilde{m}_1} \\
 2\xi_1 \omega_1 &= \frac{\Phi^{*T} \mathbf{C} \Phi^*}{\tilde{m}_1} = \frac{\tilde{c}_1}{\tilde{m}_1} \\
 p_1 &= \Phi^{*T} \mathbf{P}
 \end{aligned} \tag{3.60}$$

Later, we will drop the subscript 1 for convenience. The basis for retaining only the first mode is justified in Sect. 3.2.5.

Example 3.4 - 3DOF shear beam revisited

Consider the 3DOF system defined in Ex. 3.3. Taking Φ^* according to Eq. (1), the one-dimensional mass and force measures are

$$\tilde{m} = \begin{bmatrix} \frac{1}{3} & \frac{2}{3} & 1 \end{bmatrix} \begin{bmatrix} \frac{m_1}{3} \\ \frac{2m_2}{3} \\ m_3 \end{bmatrix} = \frac{m_1}{9} + \frac{4}{9}m_2 + m_3 \tag{1}$$

$$\tilde{p} = \begin{bmatrix} \frac{1}{3} & \frac{2}{3} & 1 \end{bmatrix} \begin{bmatrix} p_1 \\ p_2 \\ p_3 \end{bmatrix} = \frac{1}{3}p_1 + \frac{2}{3}p_2 + p_3 \tag{2}$$

The nodal forces due to seismic excitation are proportional to the nodal masses. A typical force is

$$p_i = -m_i a_g \tag{3}$$

where a_g is the ground acceleration. Substituting for p_i in Eq. (2) results in

3.5. STIFFNESS CALIBRATION- FUNDAMENTAL MODE RESPONSE

$$\tilde{p} = - \left(\frac{m_1}{3} + \frac{2m_2}{3} + m_3 \right) a_g \quad (4)$$

It is convenient to express \tilde{p} due to seismic acceleration as

$$\tilde{p} = -\Gamma \tilde{m} a_g \quad (5)$$

where Γ is a dimensionless factor. For this example, Γ is given by

$$\Gamma = \frac{\frac{m_1}{3} + \frac{2m_2}{3} + m_3}{\frac{m_1}{9} + \frac{4m_2}{9} + m_3} \quad (6)$$

When the masses are equal, $\Gamma = 9/7$.

In order to evaluate the one-dimensional damping coefficient, \tilde{c} , the system damping matrix, \mathbf{C} , must be specified. The form of \mathbf{C} depends on how the viscous damping elements are located throughout the structure. Fig. E3.4a shows an arrangement consisting of viscous dampers inserted between adjacent masses.

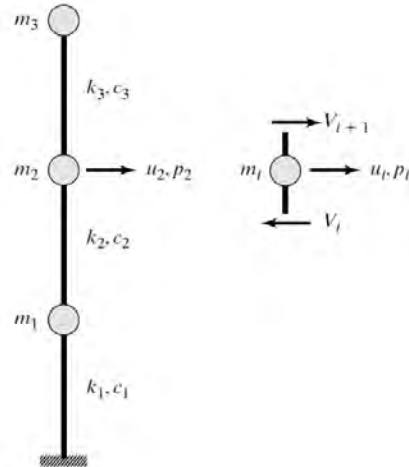


Figure E3.4a: Dampers included in shear beam elements.

CHAPTER 3. OPTIMAL STIFFNESS/DAMPING FOR DYNAMIC LOADING

In this case, the shear force in an element depends on both the shear deformation and the time rate of change of the shear deformation. Assuming linear behavior, the typical equations have the form

$$\begin{aligned} V_i &= k_i(u_i - u_{i-1}) + c_i(\dot{u}_i - \dot{u}_{i-1}) \\ p_i &= m_i\ddot{u}_i + V_i - V_{i-1} \end{aligned} \quad (7)$$

Eq. (7) shows that the forms of \mathbf{K} and \mathbf{C} are similar; we replace k_i with c_i . Taking \mathbf{C} as

$$\mathbf{C} = \begin{bmatrix} c_1 + c_2 & -c_2 & 0 \\ -c_2 & c_2 + c_3 & -c_3 \\ 0 & -c_3 & c_3 \end{bmatrix} \quad (8)$$

leads to

$$\tilde{c} = \frac{1}{9}(c_1 + c_2 + c_3) \quad (9)$$

The contribution of the individual dampers to \tilde{c} is the same since the assumed displacement profile corresponds to constant shear deformation.

The damper arrangement shown in Fig. E3.4b produces nodal forces that depend on the nodal velocities. Assuming linear behavior, the typical equations are

$$\begin{aligned} V_i &= k_i(u_i - u_{i-1}) \\ p_i &= m_i\ddot{u}_i + c'_i\dot{u} + V_i - V_{i-1} \end{aligned} \quad (10)$$

3.5. STIFFNESS CALIBRATION- FUNDAMENTAL MODE RESPONSE

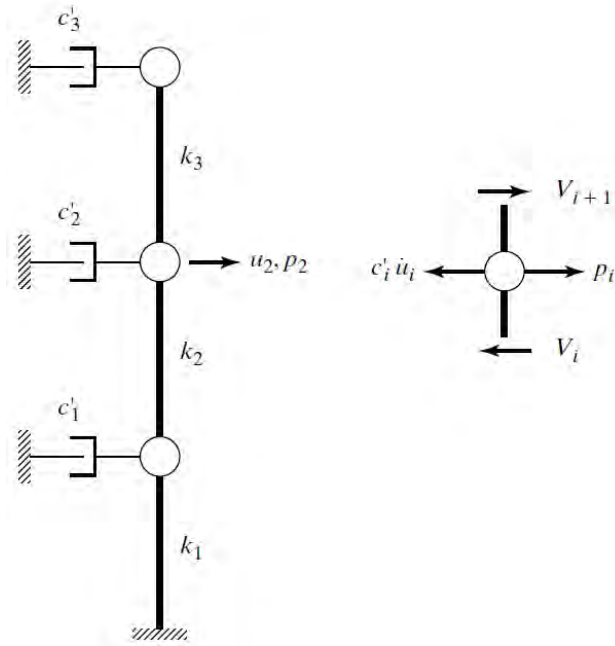


Figure E3.4b: Dampers attached to nodal masses.

With this arrangement, \mathbf{C} is similar to \mathbf{M} . Then

$$\mathbf{C} = \begin{bmatrix} c'_1 & 0 & 0 \\ 0 & c'_2 & 0 \\ 0 & 0 & c'_3 \end{bmatrix} \quad (11)$$

and

$$\tilde{c} = \frac{c'_1}{9} + \frac{4}{9}c'_2 + c'_3 \quad (12)$$

Eq. (12) shows that the most effective damper location is node 3. This result can also be deduced by examining the assumed displacement profile. Node 3 corresponds to the maximum element in Φ^* and therefore has the largest velocity.

CHAPTER 3. OPTIMAL STIFFNESS/DAMPING FOR DYNAMIC LOADING

3.5.2 Continuous Beam

The following developments are based on the material presented in Sect. 3.3. The displacement variables for a continuous beam are the translation, u , and rotation, β , of the cross section. Noting Eq. (3.46), the displacement expressions corresponding to *uniform shear* and *bending deformation* are expressed as

$$\begin{aligned}u &= q(t)\phi(x) \\ \beta &= q(t)\psi(x)\end{aligned}\tag{3.61}$$

where ϕ , ψ are the fundamental mode shape functions,

$$\begin{aligned}\phi &= \frac{x}{H} + s \left(\frac{x}{H}\right)^2 \\ \psi &= \frac{2s}{H} \left(\frac{x}{H}\right)\end{aligned}\tag{3.62}$$

q is the modal amplitude parameter, and $2s/H$ is the ratio of prescribed bending deformation to prescribed shear deformation. A pure shear beam has $s = 0$. The uniform deformations and maximum displacement are related to q by

$$\begin{aligned}\gamma &= \frac{\delta u}{\delta x} - \beta = q \left(\frac{1}{H}\right) \\ \chi &= \frac{\delta \beta}{\delta x} = q \left(\frac{2s}{H^2}\right) \\ u(H) &= q(1 + s)\end{aligned}\tag{3.63}$$

Lastly, these equations lead to the rigidity distribution defined by Eqs. (3.47) and (3.48).

3.5. STIFFNESS CALIBRATION- FUNDAMENTAL MODE RESPONSE

The equilibrium equation expressed in terms of $q(t)$ can be generated using the *principle of virtual displacements* [22]. This principle is used to transform continuous equilibrium equations into a set of discrete equations and can be interpreted as a variational statement. We start by introducing an expansion for the displacement variables in terms of generalized coordinates. For this case, $\phi(x)$ and $\psi(x)$ are the prescribed displacement fields, and $q(t)$ is the generalized coordinate. A virtual displacement is defined as a displacement distribution generated by perturbing the generalized coordinate by a small amount, δq . According to this principle, the first-order work done by the external loads during this virtual displacement is equal to the first-order work done by the internal forces during the corresponding virtual deformation. The transverse shear force and bending moment are the internal forces for a beam; the corresponding deformations are γ and χ . Assuming the external loading consists only of the transverse load, b , the mathematical form of the principle is

$$\int_0^H (M\delta\chi + V\delta\gamma)dx = \int_0^H b\delta u dx \quad (3.64)$$

Taking u according to Eq. (3.61), the virtual terms are related to δq by

$$\begin{aligned} \delta u &= \delta q \phi \\ \delta \gamma &= \delta q \left(\frac{1}{H} \right) \\ \delta \chi &= \delta q \left(\frac{2s}{H^2} \right) \end{aligned} \quad (3.65)$$

Using Eq. (3.65) and requiring the equality to be satisfied for arbitrary δq results in

CHAPTER 3. OPTIMAL STIFFNESS/DAMPING FOR DYNAMIC LOADING

$$\int_0^H \left(\frac{2s}{H^2} M + \frac{1}{H} V \right) dx = \int_0^H b \phi dx \quad (3.66)$$

To proceed further, M , V , and b must be related to q .

Assuming linear behavior and including viscous damping in both the material and external loading terms, the expressions for the internal shear force and moment reduce to

$$\begin{aligned} V &= D_T \gamma + C_T \dot{\gamma} = \frac{1}{H} (D_T q + C_T \dot{q}) \\ M &= D_B \chi + C_B \dot{\chi} = \frac{2s}{H^2} (D_B q + C_B \dot{q}) \end{aligned} \quad (3.67)$$

where C_T , C_B are material damping parameters. Including inertia and damping contributions, the external distributed loading expands to

$$b = -\rho_m \ddot{u} - c' \dot{u} + \bar{b} - \rho_m a_g = -\rho_m \phi \ddot{q} - c' \phi \dot{q} + \bar{b} - \rho_m a_g \quad (3.68)$$

where c' is a damping parameter and \bar{b} is the prescribed loading. We substitute in Eq. (3.66), and write the resulting equation in the “same” form as Eq. (3.59),

$$\ddot{q} + \tilde{c} \dot{q} + \omega^2 q = \frac{1}{\tilde{m}} \tilde{p} - \Gamma a_g \quad (3.69)$$

Eq. (3.69) is the modal equation for the fundamental mode. The corresponding modal coefficients are:

3.5. STIFFNESS CALIBRATION- FUNDAMENTAL MODE RESPONSE

$$\begin{aligned}
 \tilde{m} &= \int_0^H \rho_m \phi^2 dx \\
 \tilde{p} &= \int_0^H \phi \bar{b} dx \\
 \Gamma &= \frac{\int_0^H \rho_m \phi dx}{\int_0^H \rho_m \phi^2 dx} \\
 \tilde{k} &= \int_0^H \left(\frac{1}{H^2} D_T + \frac{4s^2}{H^4} D_B \right) dx = \omega_1^2 \tilde{m} \\
 \tilde{c} &= \int_0^H \left(\frac{1}{H^2} C_T + \frac{4s^2}{H^4} C_B + c' \phi^2 \right) dx = 2\xi \omega_1 \tilde{m}
 \end{aligned} \tag{3.70}$$

The expression for \tilde{k} follows from the definition of the rigidity distributions (see Eqs. (3.47) and (3.48)). The other terms depend on the mass density distribution and prescribed loading. The following example considers various cases.

Example 3.5 - Modal parameters: continuous beam

1. Uniform mass density

$$\begin{aligned}
 \rho_m &= \text{constant} = \rho_m^* \\
 \tilde{m} &= \rho_m^* H \left(\frac{1}{3} + \frac{s}{2} + \frac{s^2}{5} \right)
 \end{aligned} \tag{1}$$

2. Uniform loading

$$\begin{aligned}
 \bar{b} &= b^*(t) \\
 \tilde{p} &= \frac{b^* H}{2} \left(1 + \frac{2s}{3} \right)
 \end{aligned} \tag{2}$$

CHAPTER 3. OPTIMAL STIFFNESS/DAMPING FOR DYNAMIC LOADING

3. Linear loading

$$\begin{aligned}\bar{b} &= b_0(t) \frac{x}{H} \\ \tilde{p} &= \frac{b_0 H}{3} \left(1 + \frac{3s}{4} \right)\end{aligned}\tag{3}$$

4. Seismic loading

$$\begin{aligned}\bar{b} &= -\rho_m a_g \\ \tilde{p} &= -a_g \int_0^H \rho_m \phi dx\end{aligned}\tag{4}$$

A more convenient form of \tilde{p} is

$$\begin{aligned}\tilde{p} &= -a_g \tilde{m} \Gamma \\ \Gamma &= \frac{\int_0^H \rho_m \phi dx}{\int_0^H \rho_m \phi^2 dx}\end{aligned}\tag{5}$$

When ρ_m is constant, Γ depends only on ϕ .

$$\Gamma|_{\rho_m = \text{constant}} = \Gamma^* = \frac{\int_0^H \phi dx}{\int_0^H \phi^2 dx} = \frac{1 + \frac{2s}{3}}{\frac{2}{3} + s + \frac{2s^2}{5}}\tag{6}$$

3.5. STIFFNESS CALIBRATION- FUNDAMENTAL MODE RESPONSE

Table E3.5a: Variation of Γ^* with s

s	Γ^*
0.00	1.50
0.125	1.36
0.25	1.24
0.50	1.05
0.75	0.91
1.00	0.81

3.5.3 Periodic Excitation

Eq. (3.69) is the governing 1DOF equation for both discrete and continuous beams. We just have to use the appropriate mass, damping stiffness, and loading terms. The solution for a 1DOF system subjected to periodic excitation is developed in Sect. 1.4. That solution is applicable here with a change in notation to account for the difference in notation between Eqs. (1.3) and (3.70). The response due to the loading,

$$\tilde{p} = \hat{p} \sin(\Omega t)$$

is written as

$$q = \hat{q} \sin(\Omega t - \delta)$$

where \hat{q} is related to \hat{p} by

$$\begin{aligned}
 \hat{q} &= \frac{\hat{p}}{\tilde{m}\Omega^2} H_2 \\
 H_2 &= \sqrt{\frac{\rho^4}{(1-\rho^2)^2 + (2\xi\rho)^2}} \\
 \rho^2 &= \frac{\Omega^2 \tilde{m}}{\tilde{k}} = \frac{\Omega^2}{\omega^2} \\
 \xi &= \frac{\tilde{c}}{2\omega\tilde{m}}
 \end{aligned} \tag{3.71}$$

The terms \tilde{p} , Ω , and \tilde{m} are assumed to be prescribed. The constraint on displacement, say $u(x) = u^*(x)$, is converted to a constraint on \hat{q} using the assumed displacement expansion, $u = q\phi$. Taking

$$\hat{q} \leq q^* \tag{3.72}$$

in Eq. (3.71), the calibration problem reduces to determining ρ and ξ that satisfy the following constraint:

$$H_2 \leq H_2^{**} = \frac{\Omega^2 \tilde{m} q^*}{\hat{p}} \tag{3.73}$$

One assumes a value for ξ and then determines ρ from Eq. (3.73). Once ρ is known, the frequency is calculated with

$$\omega^2 = \frac{\Omega^2}{\rho^2} \tag{3.74}$$

Lastly, we scale the stiffness parameters with ω^2 .

Example 3.6 - 3DOF shear beam revisited again

Consider the case of equal nodal masses and loads for the system defined in Ex. 3.4.

3.5. STIFFNESS CALIBRATION- FUNDAMENTAL MODE RESPONSE

$$m_1 = m_2 = m_3 = 1000 \text{ kg}$$
$$\hat{p}_1 = \hat{p}_2 = \hat{p}_3 = 10 \text{ kN}$$

Applying Eqs. (1) and (2) of Ex. 3.4 leads to

$$\tilde{m} = \frac{14}{9}(1000) = 1555 \text{ kg}$$
$$\hat{p} = 2(10) = 20 \text{ kN}$$

The displacement constraint is taken as $u_3 = 0.1m$. Since $\Phi^*(3) \equiv 1$, it follows that $q^* = 0.1m$. Evaluating H_2^{**} results in

$$H_2^{**} = 0.007775\Omega^2$$

Various values for Ω are considered.

1. $\Omega = 2\pi \quad H_2^{**} = 0.307$

Since H_2^{**} is less than 1, there is only one value for ρ . Stiffness dominates the response, and we can neglect ξ in the expression for H_2 . Then, using Eq. (3.71),

$$\frac{1}{\rho_1^2} = 1 + \frac{1}{H_2^{**}} = 4.257$$

and

$$\omega = (2\pi)(4.257)^{1/2} = 12.96 \text{ rad/s}$$

The stiffness parameters are derived in Ex. 3.3. For equal nodal masses, Eq. (4) of Ex. 3.3 reduces to

$$\mathbf{k}' = \begin{bmatrix} 3000 \\ 5000 \\ 6000 \end{bmatrix} \text{ kg}$$

CHAPTER 3. OPTIMAL STIFFNESS/DAMPING FOR DYNAMIC LOADING

Finally, the scaled stiffnesses are

$$\mathbf{k} = \omega^2 \mathbf{k}' = \begin{bmatrix} 504 \\ 840 \\ 1067 \end{bmatrix} \text{ kN/m}$$

2. $\Omega = 4\pi \quad H_2^{**} = 1.228$

Since H_2^{**} is greater than 1, there are two values for ρ . Results for different values of ξ are listed in the following table. Selecting ω_2 generates the lowest stiffness and shifts the response away from the resonance zone.

ξ	ρ_1	ω_1 (rad/s)	ρ_2	ω_2 (rad/s)
0	0.633	19.85	2.383	5.27
0.1	0.656	19.16	2.300	5.46
0.2	0.742	16.93	2.033	6.18

Example 3.7 - Stiffness calibration: continuous beam; periodic excitation

Consider a continuous beam model of a moderately tall building having the following properties

$$H = 100 \text{ m}$$
$$\rho_m = 20000 \text{ kg/m}$$

Let $s = 0.4$, which corresponds to allocating 40% of the deflection at the top of the building to bending deformation. The modal mass follows from Eq. (1) of Ex. 3.5.

$$\tilde{m} = (20000)(100)(0.541) = 1.082 \times 10^6 \text{ kg}$$

3.5. STIFFNESS CALIBRATION- FUNDAMENTAL MODE RESPONSE

Assuming the displacement at the top is prescribed and noting Eq. (3.63), the nodal amplitude is determined with

$$q^* = \frac{1}{1+s} u^*(H)$$

A representative value for $u^*(H)$ is $H/400$. Then $q^* = \frac{1}{1.4} \left(\frac{100}{400}\right) = 0.178$ m. Lastly, the loading is assumed to be uniform over the building height. Applying Eq. 2 of Ex. 3.5,

$$\tilde{p} = \frac{b^*(100)}{2} \left(1 + \frac{0.8}{3}\right) = 63.33b^*$$

where b^* has units of N/m. Combining these terms, the constraint condition is given by

$$\begin{aligned} H_2 &\leq H_2^{**} \\ H_2^{**} &= \frac{\Omega^2}{b^*} (3043) \end{aligned}$$

The remaining steps are the same as for the previous example. For example, assuming $\Omega = 1$ rad/s and $b^* = 6086$ N/m, $H_2^{**} = 0.5$ and the appropriate value of ω is $\sqrt{3}$ rad/s. Substituting for the various parameters in Eqs. (3.47) and (3.48), the corresponding rigidity distributions are

$$\begin{aligned} D_T &= 3 \times 10^5 \left(1 - \left(\frac{x}{H}\right)^2 + \frac{2s}{3} \left[1 - \left(\frac{x}{H}\right)^3\right]\right) \text{ kN} \\ D_B &= 3 \times 10^9 \left(\frac{1}{4} \left[1 - \frac{4x}{3H} + \frac{1}{3} \left(\frac{x}{H}\right)^4\right] + \frac{1}{6s} \left[2 - 3\frac{x}{H} + \left(\frac{x}{H}\right)^3\right]\right) \text{ kNm} \end{aligned}$$

CHAPTER 3. OPTIMAL STIFFNESS/DAMPING FOR DYNAMIC LOADING

The previous examples dealt with the case where the displacement controls the design. When acceleration is the limiting condition, we work with the differentiated form of Eq. (3.71)

$$\ddot{q} = -\Omega^2 \hat{q} \sin(\Omega t - \delta) \quad (3.75)$$

and establish a relation between the maximum allowable acceleration, $(\ddot{u})_{\max}$, and $(\ddot{q})_{\max}$ using Eq. (3.61). Letting

$$(\ddot{q})_{\max} = a^* \quad (3.76)$$

the constraint condition for acceleration controlled design is

$$\begin{aligned} H_2 &< H_2^* \\ H_2^* &= \frac{\tilde{m}a^*}{\tilde{p}} \end{aligned} \quad (3.77)$$

The remaining steps are the same as before. We select a value for ξ , determine the allowable values of ρ , and then convert to values for ω .

Example 3.8 - Example 3.7 revisited

Consider the continuous beam model introduced in Ex. 3.7. Suppose the acceleration at the top of the building is the critical motion parameter. This acceleration is expressed as a fraction of the gravitational acceleration,

$$\ddot{u}(H) \leq fg \quad (1)$$

Noting Eq. (3.61), $\ddot{u}(H)$ is related to \ddot{q} by

$$\ddot{u}(H) = (1 + s)\ddot{q}$$

Then the limiting value for \ddot{q} is

3.5. STIFFNESS CALIBRATION- FUNDAMENTAL MODE RESPONSE

$$(\ddot{q})_{\max} = a^* = \frac{f}{1+s}g \quad (2)$$

Substituting for a^* , Eq. (3.77) takes the form

$$H_2^* = \frac{\tilde{m}g}{\tilde{p}} \left(\frac{f}{1+s} \right) \quad (3)$$

The limiting acceleration for human comfort is about 1.5% of g . Taking $f = 0.015$ and using the values of \tilde{m} , \tilde{p} , and s for Ex. 3.7, the design constraint is

$$H_2^* = \frac{1805}{b^*}$$

where b^* has units of N/m.

To illustrate the computational aspects, the case where $b^* = 3610$ N/m is considered. The corresponding value of H_2^* is 0.5. Taking $\xi = 0$ and using Eq. (3.71), we obtain

$$\rho_1^2 = \frac{1}{3}$$
$$\omega_1^2 = \frac{\Omega^2}{\rho_1^2} = 3\Omega^2$$

The acceleration constraint requires $\omega \geq \omega_1$.

3.5.4 Seismic Excitation

The strategy we employ here is based on selecting the fundamental frequency such that the peak displacement due to the seismic design loading (referred to as the design basis earthquake (DBE)) is equal to or less than the prescribed displacement. Assuming the response is dominated by the first mode, the maximum displacement occurs at the top of the beam.

CHAPTER 3. OPTIMAL STIFFNESS/DAMPING FOR DYNAMIC LOADING

$$u(H) = q(t)\phi(H) \leq u^* \quad (3.78)$$

For a shear beam, u^* is due to transverse shear

$$u^* = \gamma^* H \quad (3.79)$$

For a general beam, u^* is due to both bending and shear deformation, and is expressed as

$$u^* = \frac{H}{\alpha} \quad (3.80)$$

The parameters, γ^* and α , depend on the severity of the seismic excitation which is defined by the return period. Noting Eq. (3.62),

$$\phi(H) = 1 + s$$

and substituting in Eq. (3.78) leads to

$$q|_{\max} = \frac{u^*}{1 + s} \equiv q^* \quad (3.81)$$

We relate $q|_{\max}$ to ω_1 using the definition of the Spectral Displacement response spectrum. Noting Eq. (3.37),

$$q|_{\max} = \Gamma_1 S_D(\omega_1, \xi_1) \quad (3.82)$$

Given $q|_{\max}$ and Γ_1 , one selects a value for ξ_1 , and then determines T_1 . A typical design response spectrum plot is shown in Fig. 3.20. Details pertaining to how this type of plot is created are discussed in the following section.

3.5. STIFFNESS CALIBRATION- FUNDAMENTAL MODE RESPONSE

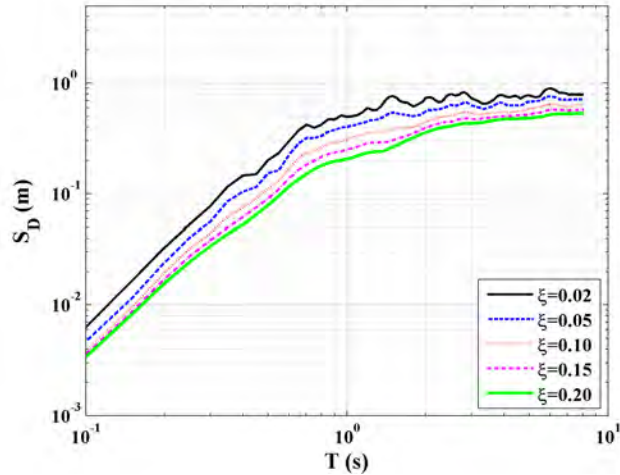


Figure 3.20: Typical spectral displacement response spectrum.

3.5.5 Construction of Spectral Displacement Response Spectra

The first step is to establish the design basis earthquake, the seismic event which has a specified probability of exceedance during the design life of the structure. Most codes consider the maximum credible earthquake to correspond to a 2% probability of exceedance in 50 years. This corresponds to a return period of 2500 years. Given the return period, one uses a hazard curve specialized for the particular region to determine the expected maximum peak ground acceleration corresponding to the return period. Fig. 3.21 shows curves for various locations in the U.S. In what follows, we choose to use the data for Los Angeles, and take 40 ft/sec^2 as the expected peak ground acceleration over 2500 years.

The next step is to assemble an ensemble of typical earthquakes for this region (in this case, the Los Angeles area), scale their intensities such that their resultant peak ground accel-

CHAPTER 3. OPTIMAL STIFFNESS/DAMPING FOR DYNAMIC LOADING

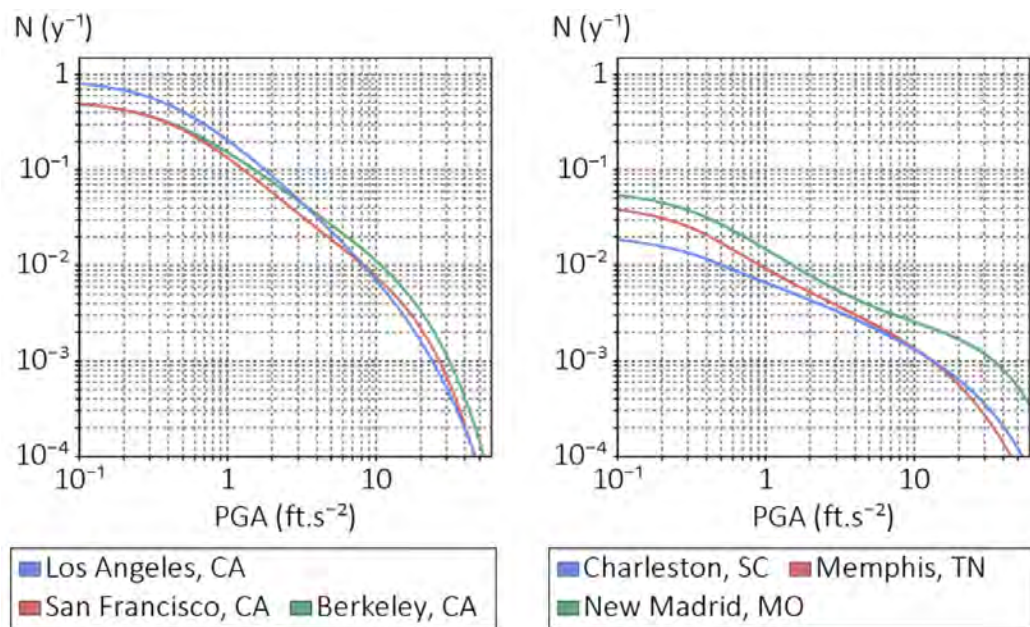


Figure 3.21: Annual exceedance frequency of the peak ground acceleration at various U.S. locations [38].

3.5. STIFFNESS CALIBRATION- FUNDAMENTAL MODE RESPONSE

ation is equal to 40 ft/sec^2 , and then generate spectral density plots for a range of damping values. Fig. 3.22 contains the spectral displacement plots for five earthquakes and $\xi = 0.02, 0.05, 0.10, 0.15,$ and 0.20 .

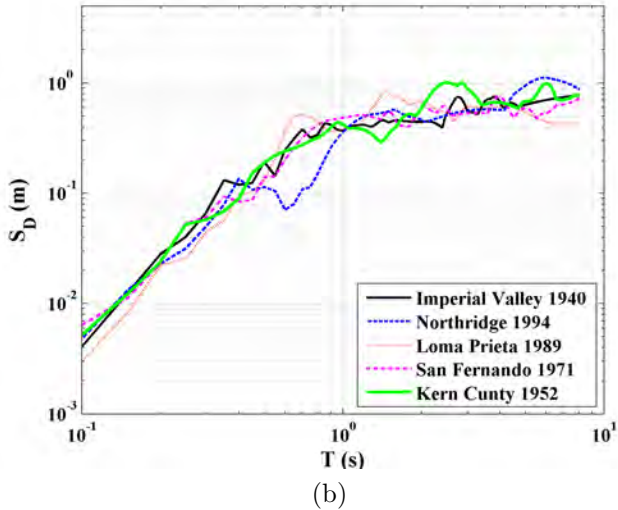
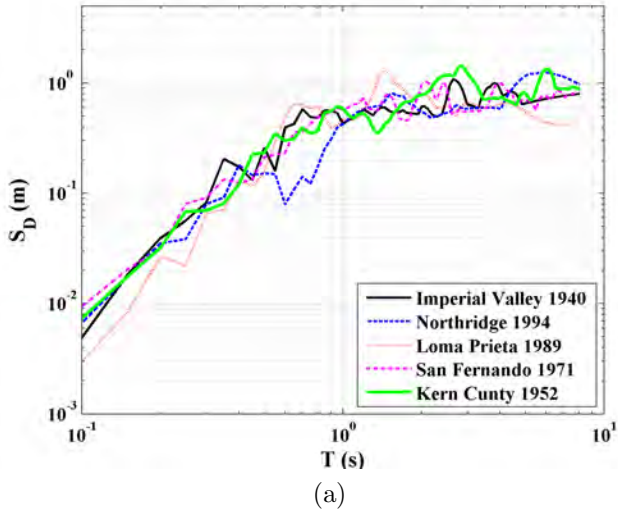


Figure 3.22: Spectral displacement plots: (a) $\xi = 0.02$; (b) $\xi = 0.05$;

CHAPTER 3. OPTIMAL STIFFNESS/DAMPING FOR DYNAMIC LOADING

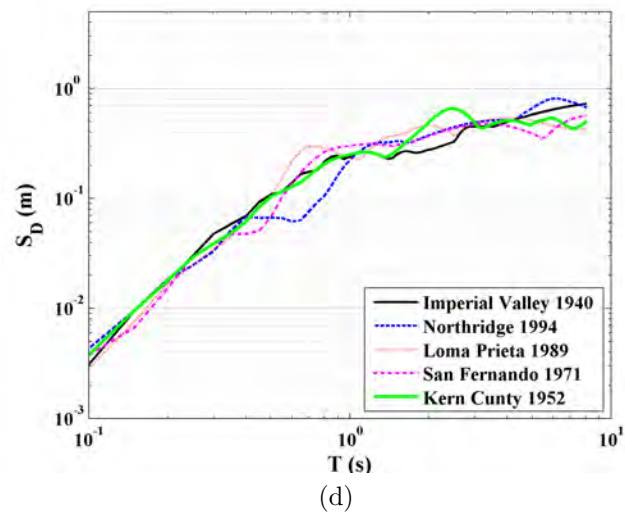
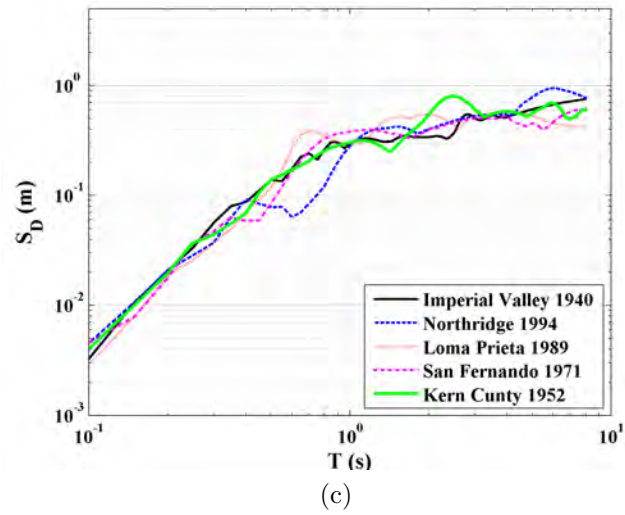


Figure 3.22: Spectral displacement plots: (c) $\xi = 0.10$; (d) $\xi = 0.15$;

3.5. STIFFNESS CALIBRATION- FUNDAMENTAL MODE RESPONSE

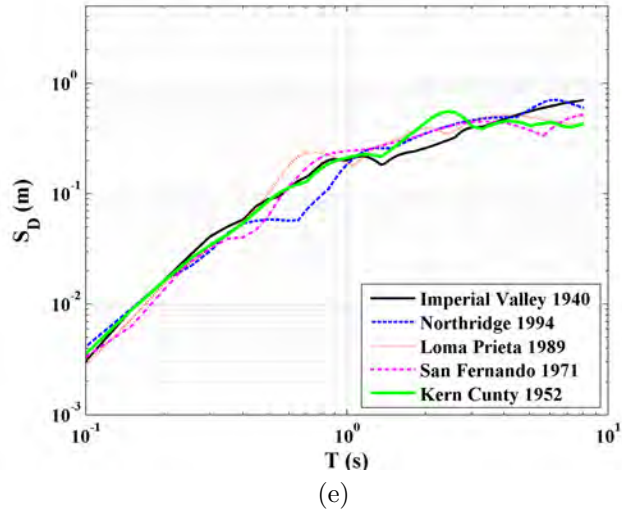


Figure 3.22: Spectral displacement plots: (e) $\xi = 0.20$.

The last step is to establish “average” plots for each value of ξ . These plots are contained in Fig. 3.23. We use these plots to evaluate Eq. 3.82.

CHAPTER 3. OPTIMAL STIFFNESS/DAMPING FOR DYNAMIC LOADING

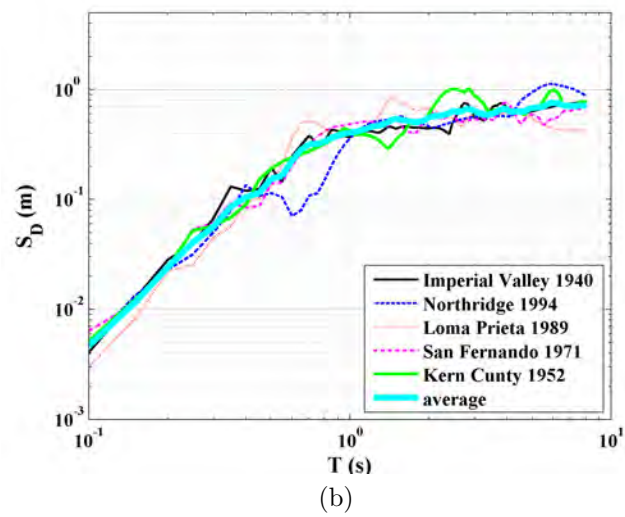
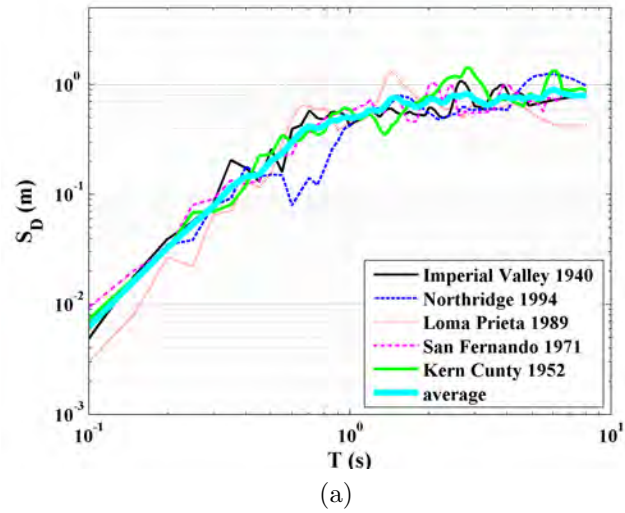


Figure 3.23: Average of spectral displacement plots: (a) $\xi = 0.02$; (b) $\xi = 0.05$;

3.5. STIFFNESS CALIBRATION- FUNDAMENTAL MODE RESPONSE

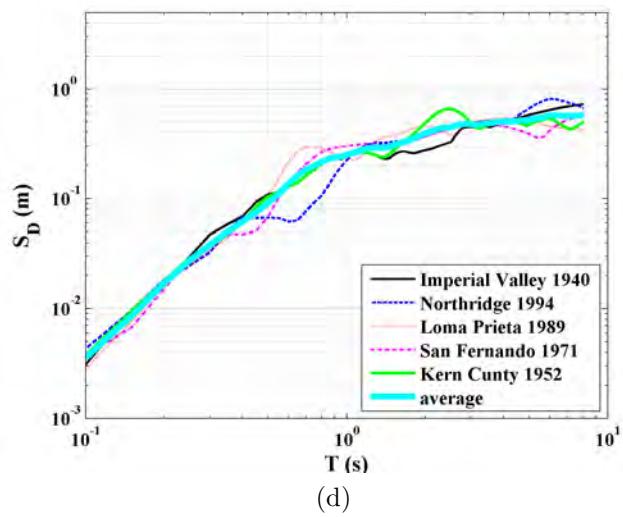
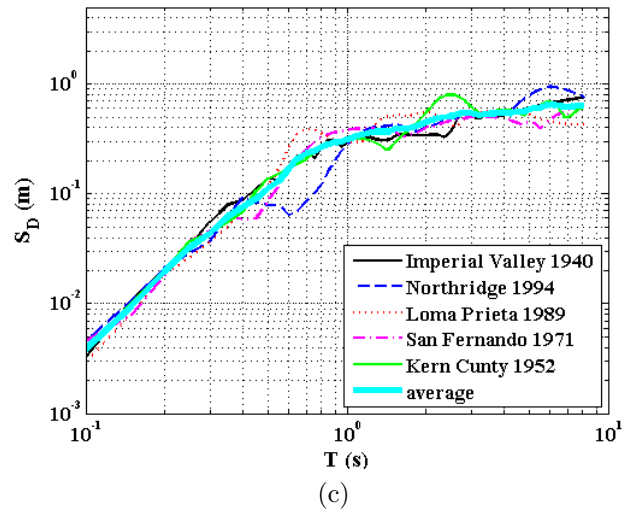


Figure 3.23: Average of spectral displacement plots: (c) $\xi = 0.10$; (d) $\xi = 0.15$;

CHAPTER 3. OPTIMAL STIFFNESS/DAMPING FOR DYNAMIC LOADING

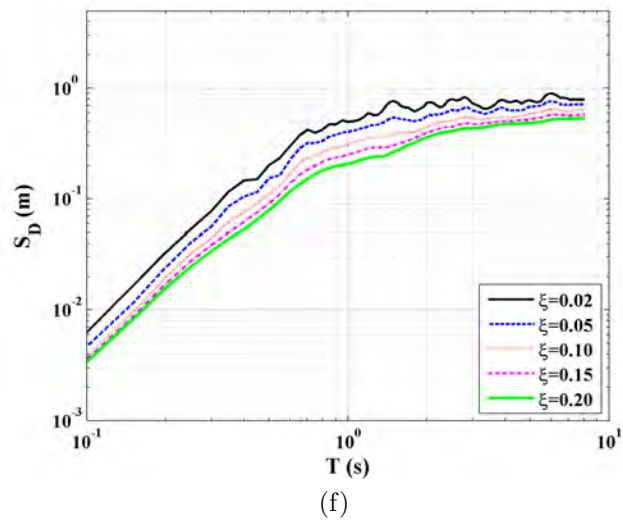
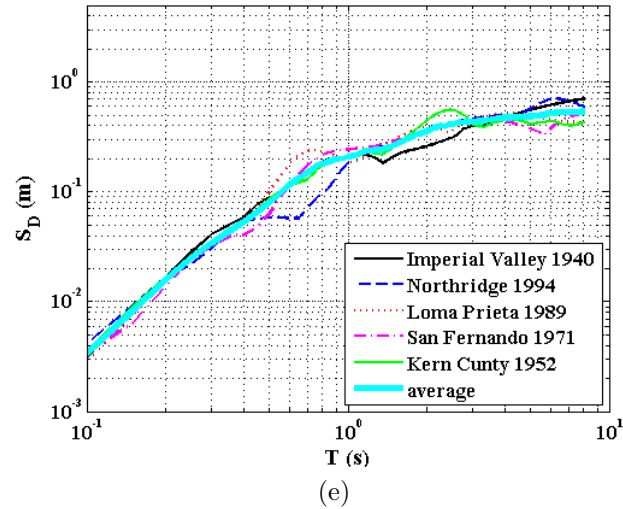


Figure 3.23: Average of spectral displacement plots: (e) $\xi = 0.20$; and (f) results summary.

3.5.6 Calibration Examples

Example 3.9 - Example 3.7 revisited

The properties of the continuous beam considered in Ex. 3.7

3.5. STIFFNESS CALIBRATION- FUNDAMENTAL MODE RESPONSE

are:

$$H = 100 \text{ m}$$

$$\rho_m = 20000 \text{ kg/m}$$

$$s = 0.4$$

$$\tilde{m} = 1.082 \times 10^6 \text{ kg}$$

$$\Gamma_1 = 1.12$$

The design value for the peak displacement is determined with Eq. (3.80).

$$u^* = \frac{H}{200} = 0.50$$

Then, noting Eq. (3.81),

$$q^* = \frac{u^*}{1 + s} = 0.36$$

and the required value of $S_D(\omega_1, \xi_1)$ is

$$S_D(\omega_1, \xi_1) = \frac{q^*}{\Gamma_1} = 0.32$$

The value of ω_1 depends on the value of ξ_1 that we assume. Several choices are considered below.

Case 1 $\xi = 0.02$

Using Fig. 3.23(a), an estimate for T is

$$T \approx 0.61 \text{ sec} \Rightarrow \omega = 10.3 \text{ rad/s}$$

The modal damping parameter is

CHAPTER 3. OPTIMAL STIFFNESS/DAMPING FOR DYNAMIC LOADING

$$\begin{aligned}\tilde{c} &= 2\xi\omega\tilde{m} = 2(0.02)(10.3)(1.082)10^6 \\ &= 446 \text{ kN} \cdot \text{s/m}\end{aligned}$$

When the material damping is constant, the distributed viscous damping parameter, C_T , follows from Eq. (3.70)

$$\begin{aligned}\tilde{c} &= \frac{1}{H}c_T \\ C_T &= 44.6 \text{ MN} \cdot \text{s}\end{aligned}$$

Case 2 $\xi = 0.10$

Using Fig. 3.23(c), an estimate for T is

$$T \approx 1.0 \text{ sec} \Rightarrow \omega = 6.28 \text{ rad/s}$$

$$\tilde{c} = 272 \text{ kN} \cdot \text{s/m}$$

The rigidity distributions are evaluated by substituting for ω^2 in Eqs. (3.47) and (3.48). One should note that *increasing the damping reduces the required stiffness*.

Example 3.10 - 5DOF shear beam

Consider a 5DOF shear beam having equal nodal masses. The fundamental mode vector is specified such that the differential nodal displacements for the five elements are equal. Its form is

$$\mathbf{U} = q\Phi^*$$

3.5. STIFFNESS CALIBRATION- FUNDAMENTAL MODE RESPONSE

$$\Phi^* = \frac{1}{5} \begin{bmatrix} 1 \\ 2 \\ 3 \\ 4 \\ 5 \end{bmatrix}$$

The equivalent modal mass follows from Eq. (3.60):

$$\tilde{m} = (\Phi^*)^T \mathbf{M} \Phi^* = 2.2 m$$

where m is the “constant” nodal mass. Substituting for Φ^* and \mathbf{M} in Eq. (3.55) leads to the following set of stiffness coefficients:

$$k'_1 = 15 m \quad k'_2 = 14 m \quad k'_3 = 12 m \quad k'_4 = 9 m \quad k'_5 = 5 m$$

The actual stiffness values depend on ω (i.e., $k = \omega^2 k'$).

Noting the definition of Γ , the modal participation factor is

$$\Gamma = \frac{\sum m_i \phi_i}{\sum m_i \phi_i^2} = \frac{3m}{2.2m} = 1.36$$

The maximum displacement at node 5 (the top level) is considered to be the controlling motion measure.

$$u_5|_{\max} = q_{\max} \equiv q^*$$

Assuming the beam is a model of a building, $u_5|_{\max}$ is related to the height of the building and the story shear deformation.

$$u_5|_{\max} = \gamma^* H$$

To illustrate the remaining steps, suppose H and γ^* have the following values:

CHAPTER 3. OPTIMAL STIFFNESS/DAMPING FOR DYNAMIC LOADING

$$H = 20 \text{ meters}$$

$$\gamma^* = 1/200$$

Then, $q^* = 0.1$ meters and the required value of $S_D(\omega, \xi)$ is

$$S_D(\omega, \xi) = \frac{0.1}{1.36} = 0.074$$

Case 1 $\xi = 0.2$

Taking $\xi = 0.02$ and using Fig. 3.23(a),

$$\begin{aligned} T \approx 0.33 \text{ sec} &\Rightarrow \omega = 19 \text{ rad/s} \\ \tilde{c} &= 1.67 \times 10^4 \text{ N} \cdot \text{s/m} \end{aligned}$$

Case 2 $\xi = 0.10$

Taking $\xi = 0.10$ and using Fig. 3.23(c),

$$\begin{aligned} T \approx 0.41 \text{ sec} &\Rightarrow \omega = 15.3 \text{ rad/s} \\ \tilde{c} &= 6.73 \times 10^4 \text{ N} \cdot \text{s/m} \end{aligned}$$

Case 3 $\xi = 0.20$

Taking $\xi = 0.20$ and using Fig. 3.23(e),

$$\begin{aligned} T \approx 0.48 \text{ sec} &\Rightarrow \omega = 13.09 \text{ rad/s} \\ \tilde{c} &= 11.52 \times 10^4 \text{ N} \cdot \text{s/m} \end{aligned}$$

The modal damping parameter is related to the system damping matrix by Eq. (3.61):

3.5. STIFFNESS CALIBRATION- FUNDAMENTAL MODE RESPONSE

$$\tilde{c} = (\Phi^*)^T \mathbf{C}(\Phi^*)$$

Given \tilde{c} , we need to establish \mathbf{C} . When linear viscous dampers are connected to adjacent nodes, \mathbf{C} is similar in form to the stiffness matrix \mathbf{K} . Using Φ^* defined previously, the triple matrix product evaluates to

$$\tilde{c} = \frac{1}{25}(c_1 + c_2 + c_3 + c_4 + c_5)$$

where c_i is the damping coefficient for element i . Since there is only one equation relating the five coefficients, there is no unique solution for the c 's. Additional equations can be derived by imposing conditions on the damping ratios for the higher modes and optimizing “cost” and “performance”. Establishing the optimal damping distribution is addressed in Chapter 4.

Using the stiffness and viscous damping values generated for $\xi = 0.02$ and $\xi = 0.10$, we evaluate the stiffness and damping parameters for the elements, and subject the resulting structures to the set of scaled accelerograms used to compute the Spectral Displacement Response Spectrum. The results for the peak displacement are listed in Table 3.1. Note that we specified $u|_{\max} = 0.1$ m in the calibration process. The deviation in displacement for different earthquakes decreases with increasing damping, as expected.

Table 3.1: $u|_{\max}$ for Maximum Considered Earthquake (MCE)

Relative stiffness	ξ	ω^2	Loma				Average
			ElCentro	Northridge	Prieta	Pacoima	
1	0.02	361	0.113	0.142	0.078	0.070	0.101
0.65	0.10	234	0.100	0.092	0.110	0.121	0.106
0.49	0.20	178	0.134	0.115	0.122	0.109	0.120

3.6 Stiffness Modification for Seismic Excitation

3.6.1 Iterative Procedure

Numerical studies show that the method for establishing the shear and bending rigidities based on the fundamental mode is adequate for low-rise buildings but may need to be modified for moderate-rise buildings. This section presents a procedure for adjusting the stiffness that is based on updating the shear and bending deformation profiles by including the contribution of the higher modes and then determining improved estimates for the rigidity measures with

$$\begin{aligned} D_T^{(i+1)}(x) &= D_T^{(i)} \frac{[\gamma^{(i)}(x)]_{\max}}{\gamma^*} \\ D_B^{(i+1)}(x) &= D_B^{(i)} \frac{[\chi^{(i)}(x)]_{\max}}{\chi^*} \end{aligned} \tag{3.83}$$

The iteration is continued until the change in the rigidity is within the acceptable range. In what follows, we present details of the procedure for seismic excitation applied to beam type structures.

3.6.2 Multiple Mode Response

This section draws on the material presented in Sect. 3.2. Given the mass distribution ρ_m , we specify the following: γ^* , the desired deformation; $S_D(\omega_1, \xi_1)$, corresponding to the level of earthquake to be designed for; and the parameter s relating the shear and bending deformations. An initial estimate of $D_T^{(0)}(x)$ and $D_B^{(0)}(x)$ is generated using the fundamental mode response approach

3.6. STIFFNESS MODIFICATION FOR SEISMIC EXCITATION

presented in the previous sections. The structure is then discretized as an n^{th} -order MDOF system, leading to the following governing equation:

$$\mathbf{M}\ddot{\mathbf{U}}(t) + \mathbf{C}\dot{\mathbf{U}}(t) + \mathbf{K}\mathbf{U}(t) = \mathbf{P}(t) = -\mathbf{M}\mathbf{E}a_g(t) \quad \text{(a)}$$

where \mathbf{M} , \mathbf{C} , and \mathbf{K} represent the mass, damping, and stiffness matrices of the discrete system; \mathbf{U} is the displacement vector relative to the base; and \mathbf{E} is a vector representing the rigid body motion of the system due to a unit translation at the base.

Eq. (a) is transformed into a set of uncoupled equations by expressing \mathbf{U} in terms of modal vectors, ϕ_j , and assuming a particular form for \mathbf{C} .

$$\mathbf{U}(t) = \sum_{j=1}^n \Phi_j q_j(t) = \Phi \mathbf{q}(t) \quad \text{(b)}$$

$$\mathbf{C} = \alpha \mathbf{K} \quad \text{(c)}$$

This equation leads to the following set of uncoupled scalar equations:

$$\ddot{q}_j + 2\xi_j \omega_j \dot{q}_j + \omega_j^2 q_j = -\Gamma_j a_g \quad j = 1, 2, 3, \dots, n \quad \text{(d)}$$

The damping ratio and modal participation factor for the j^{th} mode are

$$\xi_j = \frac{\alpha \omega_j}{2} \quad \text{(e)}$$

$$\Gamma_j = \frac{\Phi_j^T \mathbf{M} \mathbf{E}}{\Phi_j^T \mathbf{M} \Phi_j}$$

To determine an estimate of the earthquake response of a lumped MDOF system, we make use of the response spectra

CHAPTER 3. OPTIMAL STIFFNESS/DAMPING FOR DYNAMIC LOADING

method. The maximum response for a mode is obtained from the response spectrum for the SDOF system using the corresponding values of frequency, damping, and participation factor. The expressions for the j^{th} mode are

$$q_j|_{\max} = \Gamma_j S_D(\omega_j, \xi_j) \quad \text{(f)}$$

$$\mathbf{U}_j|_{\max} = \Phi_j q_j|_{\max} \quad \text{(g)}$$

where $S_D(\omega_j, \xi_j)$ is the spectral displacement corresponding to the damping and frequency of the j^{th} mode. The shear and bending deformations in the i^{th} element due to the maximum response of the j^{th} mode are determined with the following differential approximations:

$$\begin{aligned} \gamma(i)|_{j_{\max}} &= \frac{1}{h_i} |u(i+1) - u(i)|_{j_{\max}} \\ &\quad - \frac{1}{2} |\beta(i+1) - \beta(i)|_{j_{\max}} \\ \chi(i)|_{j_{\max}} &= \frac{1}{h_1} |\beta(i+1) - \beta(i)|_{j_{\max}} \end{aligned} \quad \text{(3.84)}$$

where the displacement measures are for the nodes at the base and upper end of element i .

The individual modal time histories are generally not in phase, so we need to introduce an assumption as to the relative phasing. Taking the algebraic sum assumes they are all in phase. Using a square root sum of squares (SRSS) procedure assumes the phase lag is a uniformly distributed random variable and tends to place more emphasis on the dominant terms. The latter procedure is discussed here.

The maximum value of a variable, say ν , is determined with

3.6. STIFFNESS MODIFICATION FOR SEISMIC EXCITATION

$$\nu|_{\max} = \left\{ (\nu_{1_{\max}})^2 + (\nu_{2_{\max}})^2 + \cdots + (\nu_{N_{\max}})^2 \right\}^{1/2} \quad (3.85)$$

where N is the number of modes retained for the stiffness modification. This computational algorithm is used to determine γ_{\max} and χ_{\max} for each segment.

We start with $D^{(0)}$, compute the peak modal responses using Eq. (f), and then evaluate the peak deformations with Eq. (3.84). The rigidity coefficients are then updated with Eq. (3.83).

The process is now repeated. Given $D_T^{(1)}(x)$ and $D_B^{(1)}(x)$, the system stiffness matrix is generated, and updated mode shapes, frequencies, and participation factors are evaluated, leading to revised peak deformation distributions and ultimately to new estimates for rigidities.

CHAPTER 3. OPTIMAL STIFFNESS/DAMPING FOR DYNAMIC LOADING

Problems

Problem 3.1

The bending beam model is based on the assumption of no transverse shear strain (i.e., $\gamma = 0$). Theoretically, we set $D_T = \infty$, which results in $s = \infty$. The displacement distributions for periodic vibration with constant curvature, χ^* , and $\gamma = 0$ are

$$\begin{aligned}u &= q_B \left[\left(\frac{x}{H} \right)^2 \right] \\ \beta &= q_B \left[\frac{2x}{H^2} \right] \\ q_B &= \frac{H^2}{2} \chi^* \cos(\omega_1 t + \delta)\end{aligned}$$

Consider uniform mass density. Determine $D_B(x)$ for this prescribed mode shape.

Problem 3.2

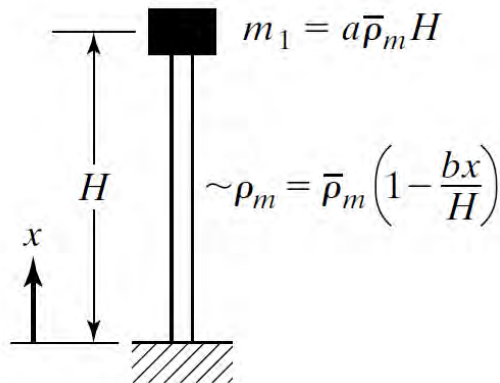


Figure P3.2a

3.6. STIFFNESS MODIFICATION FOR SEISMIC EXCITATION

Consider a cantilever beam having the mass distribution indicated in Fig. P3.2a. Assuming the beam acts as a shear beam, determine the transverse shear rigidity distribution required in order that the fundamental mode shape have the following form:

$$\phi(x) = \frac{x}{H}$$

Investigate how the shear rigidity varies with a , taking $b = 0$.

Problem 3.3

The structure shown in Fig. P3.3a consists of a cantilever beam and a rigid weightless link connecting two masses to the top end of the beam. Assume the cantilever beam has uniform mass density ρ_m and negligible transverse shear deformation.

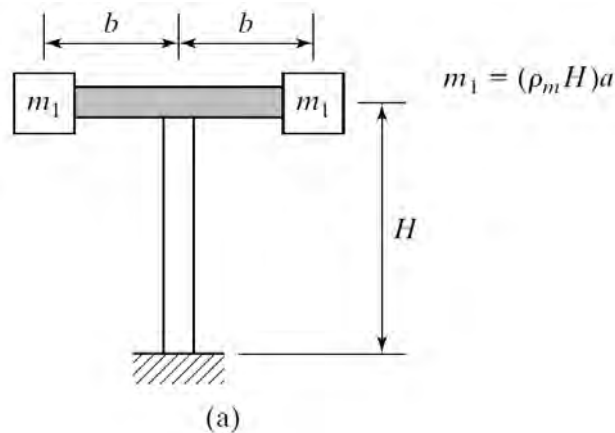


Figure P3.3a

1. Determine the bending rigidity distribution required to produce the fundamental mode shape corresponding to constant curvature. The displacement expressions for this case are

CHAPTER 3. OPTIMAL STIFFNESS/DAMPING FOR DYNAMIC LOADING

$$u = q_B \left[\left(\frac{x}{H} \right)^2 \right]$$
$$\beta = q_B \left[\frac{2x}{H^2} \right]$$
$$q_B = \frac{H^2}{2} \chi^* \cos(\omega_1 t + \delta)$$

- Investigate the sensitivity of the solution to a variation of a .
- Suppose outriggers are attached to the rigid links and the beam is extended as shown in Fig. P3.3b. Determine the bending rigidity distribution for the case where a uniform static loading is applied, and the design objective is constant curvature.

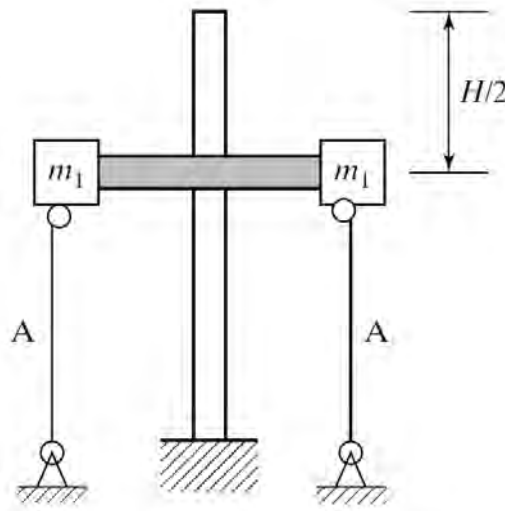


Figure P3.3b

- Repeat part 1. using the structure defined in part 3.

3.6. STIFFNESS MODIFICATION FOR SEISMIC EXCITATION

Problem 3.4

Consider a cantilever shear beam having uniform mass density and constant transverse shear rigidity. Allowing for material damping and external damping, the equilibrium equation for free vibration has the following form:

$$D_T u_{,xx} + C_T u_{,xxt} - \rho_m u_{,tt} - C' u_{,t} = 0 \quad (1)$$

The boundary conditions are

$$\begin{aligned} u(x=0) &= 0 \\ V(x=L) &= 0 \end{aligned} \quad (2)$$

Substituting for V in Eq. (2) leads to

$$D_T u_{,x}(L) + C_T u_{,xt}(L) = 0 \quad (3)$$

The general solution of Eq. (1) that satisfies the boundary conditions at $x=0, L$ is

$$\begin{aligned} u &= e^{\alpha t} \sin \lambda x \\ \lambda &= \frac{2n-1}{2L} \pi \quad n = 1, 2, \dots \end{aligned} \quad (4)$$

Let

$$\begin{aligned} \omega &= \lambda \left[\frac{D_T}{\rho_m} \right]^{1/2} \\ \frac{\lambda^2 C_T + C'}{\rho_m} &= 2\xi\omega \end{aligned} \quad (5)$$

CHAPTER 3. OPTIMAL STIFFNESS/DAMPING FOR DYNAMIC LOADING

1. Derive the expression for α in terms of ω and ξ . Assume $\xi < 1$. The solution corresponding to $n = 1$ is the fundamental solution. Comment on the nature of this solution.
2. Compare the mode shapes with the profiles based on constant shear deformation for the fundamental mode. Consider n from 1 to 3.
3. Let ξ_n be the value of ξ corresponding to $\lambda = \lambda_n$ (i.e., the n^{th} mode). Comment on how ξ_n varies with n .

Problem 3.5

Refer to Problem 2.5 (Fig. P2.5a). Assume the structure is a discrete shear beam. Determine the distribution of equivalent shear beam stiffness based on a linear profile for the fundamental mode and the following floor masses:

$$\begin{aligned}m_1 &= m_2 = m_3 = m_4 = 10,000 \text{ kg} \\m_5 &= 5,000 \text{ kg}\end{aligned}$$

Relate the shear beam stiffness to the column size for each story.

Problem 3.6

Repeat Problem 3.5 using the structure defined in Problem 2.6. Assume that the bracing contributes 25% of the story stiffness.

Problem 3.7

3.6. STIFFNESS MODIFICATION FOR SEISMIC EXCITATION

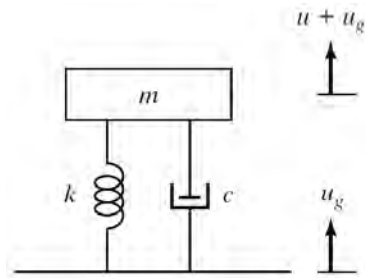


Figure P3.7a

The single-degree-of-freedom system shown in Fig. P3.7a is to be designed to displace a given amount, u_{\max} , under a specified seismic excitation. Use the response spectrum for the spectral displacement shown in Fig. 3.23(f), and take $m = 10,000$ kg. Determine design values for k and c for a range of damping coefficients ($\xi = 0.05, 0.10, 0.20$) and two values of u_{\max} :

$$u_{\max} = 0.1 \text{ m}, 0.2 \text{ m}$$

Also determine the maximum values of the stiffness and damper forces.

Problem 3.8

CHAPTER 3. OPTIMAL STIFFNESS/DAMPING FOR DYNAMIC LOADING

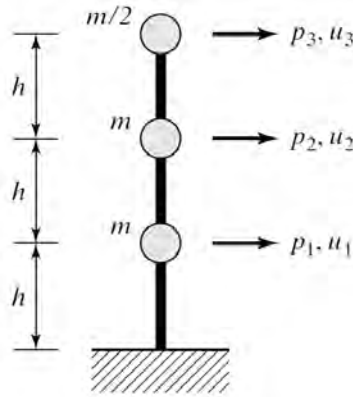


Figure P3.8a

The structure shown in Fig. P3.8a consists of three shear beam segments and lumped masses. Take

$$h = 4 \text{ m} \quad m = 1000 \text{ kg}$$

1. Determine the shear stiffness distribution required for the fundamental mode vector to have the form

$$\Phi = \left\{ \frac{1}{3}, \frac{2}{3}, 1 \right\}$$

2. Assume a periodic force, $p = \hat{p} \sin(\Omega t)$, is applied at node 3. Calibrate the rigidity for the following conditions:

$$\hat{p} = 10 \text{ kN} \quad \Omega = 4\pi \quad q_{\max} = \frac{h}{150} \quad \xi = 0.05$$

3. Calibrate the shear stiffness for the following conditions:

$$q_{\max} = \frac{h}{100} \quad \xi = 0.02$$

3.6. STIFFNESS MODIFICATION FOR SEISMIC EXCITATION

4. Assume that linear viscous dampers having the same property, $c_1 = c_2 = c_3 = c$, are installed. Determine c based on the results of part 3.

Problem 3.9

Refer to Problem 3.5.

1. Calibrate the stiffness for the following seismic excitation criteria (use the S_D plot from Fig. 3.23(f)):

$$u(H)_{\max} = 0.125 \text{ m}$$
$$\xi = 0.05$$

2. Assume that viscous dampers are installed in the third, fourth, and fifth stories. Take the damper coefficient to be the same for each story. Determine the coefficient required by the calibration specified in part 1.

Problem 3.10

Refer to Problem 3.6.

1. Calibrate the structure for the following seismic criteria:

$$u(H)_{\max} = 0.125 \text{ m}$$
$$\xi = 0.02$$

2. Assume a uniform distribution of damping over the height. Determine the damping coefficient required by part 1.
3. Suppose a single damper is connected to the top node (node 5). Determine the value of c required by part (a).

CHAPTER 3. OPTIMAL STIFFNESS/DAMPING FOR DYNAMIC LOADING

Problem 3.11

Refer to Problem 3.1. Take $H = 200$ m and $\rho_m = 10,000$ kg/m.

1. Determine \tilde{m} and Γ .
2. Assume the following loading:

$$b = b_0 \frac{x \sin \Omega t}{H} \quad \text{where } b_0 = 6 \text{ kN/m}$$

is applied. Calibrate the stiffness based on limiting $u(H)$ to 0.5 m for a frequency of 1 radian per second.

3. Suppose the design is constrained by the peak acceleration at $x = H$ under periodic loading. Calibrate the stiffness for $\ddot{u}(H)_{\max} = 0.015$ g, where $g = 9.86$ m/s². Consider ξ to be equal to 0.05 and use the loading defined in part 2.
4. Assume the stiffness calibration is dictated by seismic excitation. Take $u(H)_{\max} = 1$ m, $\xi = 0.05$. Determine $D_B(x)$. Assume $C_T(x) = \alpha D_B(x)$, where α is a constant. Determine α corresponding to $\xi = 0.05$. Use Fig. 3.23.

Problem 3.12

Refer to Problem 3.2.

1. Determine \tilde{m} and Γ in terms of ρ_m , a , and b .
 2. Assume that a uniform periodic loading is applied to the beam. Calibrate the shear rigidity for the following specifications:
-

3.6. STIFFNESS MODIFICATION FOR SEISMIC EXCITATION

$$H = 10 \text{ m} \quad u(H)_{\max} = H/300$$

$$\rho_m = 100 \text{ kg/m}$$

$$a = 1 \quad b = 0.5$$

$$\Omega = 2\pi \text{ rad/s}$$

3. Calibrate the rigidity for the case of seismic loading. Take

$$u(H)_{\max} = H/300$$

$$\xi = 0.02$$

Use Fig. 3.23(f).

Problem 3.13

Refer to Problem 3.3. Determine \tilde{m} and Γ .

Problem 3.14

Let $q^* = H/\alpha$, where α is a design parameter. Express H as $H = nh$, where h is the typical story height and n is the number of stories. This leads to $T = fn$. Estimate a typical value of f .

Problem 3.15

CHAPTER 3. OPTIMAL STIFFNESS/DAMPING FOR DYNAMIC LOADING

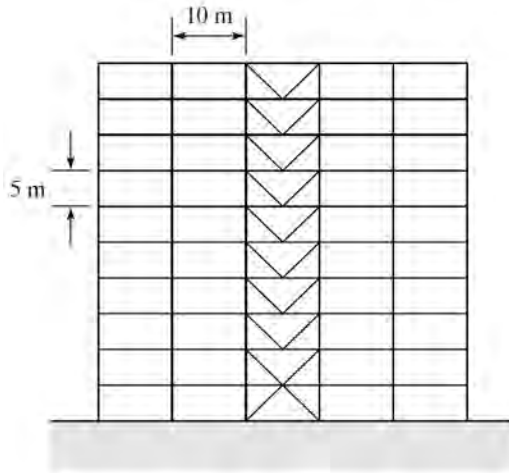


Figure P3.15a

This problem concerns the preliminary design of the lateral stiffness system for a 10-story rectangular rigid frame Fig. P3.15a. The frame properties and design criteria are as follows:

- Height = 5 m/story
- Width = 10 m/bay
- Mass/floor = 10,000 kg
- Seismic loading: $\xi = 0.02$
- Max. Deflection at top = 0.25 m
- $\gamma_{\max} = 1/200$

Model the frame as a 10DOF shear beam.

1. Determine an initial estimate for the lateral stiffness at each story level, considering a single mode response and $\xi = 0.02$. Use the spectrum shown in Fig. 3.23(f).

3.6. STIFFNESS MODIFICATION FOR SEISMIC EXCITATION

2. Consider linear viscous dampers to be installed at each story level. Take $c_i = \alpha k_i$ for story i . Using the stiffness distribution established in part 1. (frequencies and mode shapes), establish the modal equations for a modal decomposition in terms of the first three modes. Determine α such that $\xi_1 = 0.02$. Determine ξ_2 and ξ_3 corresponding to this value of α . Estimate the maximum mean square deformation response using the spectral displacement response spectrum shown Fig. 3.23(f), and modify the initial stiffness distribution using Eq. (3.83). Carry out this computation for two iterations.
3. Suppose the lateral stiffness is maintained constant over two story heights; that is,

$$\begin{aligned}k_2 &= k_1 \\k_4 &= k_3, \text{ etc}\end{aligned}$$

Discuss how you would determine initial estimates for k_1, k_3, \dots considering a single mode response and $\xi = 0.02$. Also discuss how you would modify the stiffness distribution.

4

Optimal Passive Damping Distribution

4.1 Introduction

Damping is the process by which physical systems such as structures dissipate the energy input from external excitations. Damping reduces the build-up of kinetic and strain energy and the system response, especially near resonance conditions, where damping governs the response. Fig. 4.1 illustrates the influence of damping on the time history of the energy for a system with a period of 1 second subjected to an unscaled El Centro accelerogram. The symbols in Fig. 4.1. refer to the energy input (E_I), the strain energy stored (E_S), and the energy dissipated (E_D). During the early stage of the response, there is a rapid build-up of the input energy, similar to an impulsive loading. Damping dissipates energy over the response cycle, in this case, 1 second. For low damping ratio, the energy dissipated per cycle is small, and many cycles are required before the input energy is eventually dissipated. As ξ is increased, the energy dissipated per cycle increases, and the stored energy build-up is reduced. Shifting from $\xi = 0.02$ to $\xi = 0.1$ reduces the peak strain energy demand by a factor of 3.7 for this particular system and earthquake excitation. It should be noted that seismic accelerograms differ with respect to their frequency content and intensity, and therefore one needs to carry out energy time history studies for individual excitations applied to a specific system. For example, Fig. 4.2 shows the response of the same system for a typical Northridge accelerogram. The input energy build-up for the Northridge loading is quite different from that for the El Centro loading.

4.1. INTRODUCTION

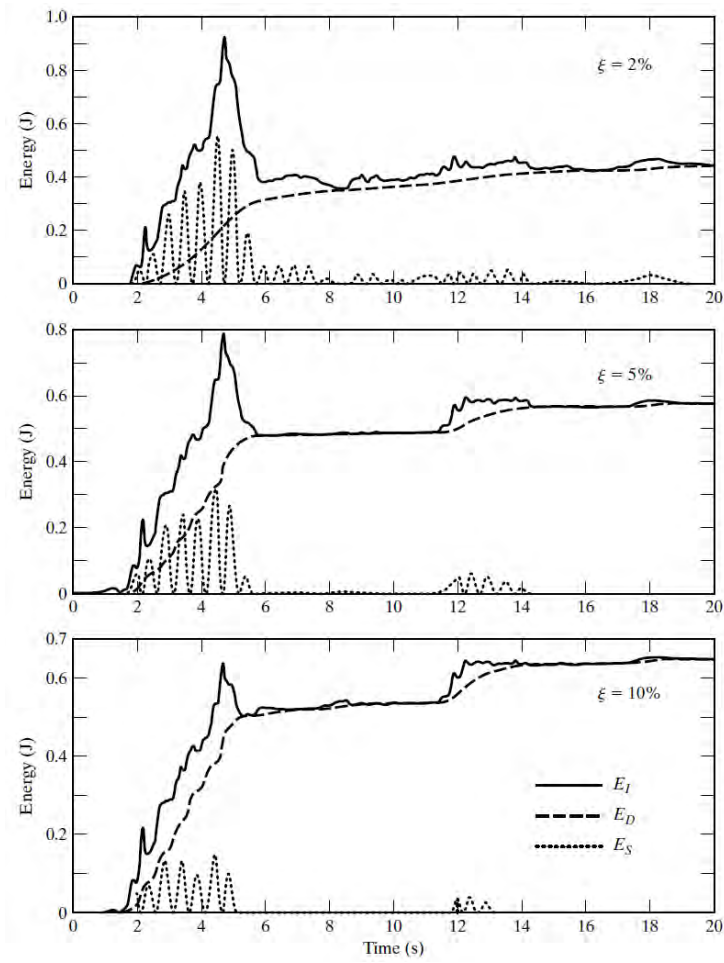


Figure 4.1: Energy build-up, El Centro (S00E), Imperial Valley, 1940.

CHAPTER 4. OPTIMAL PASSIVE DAMPING DISTRIBUTION

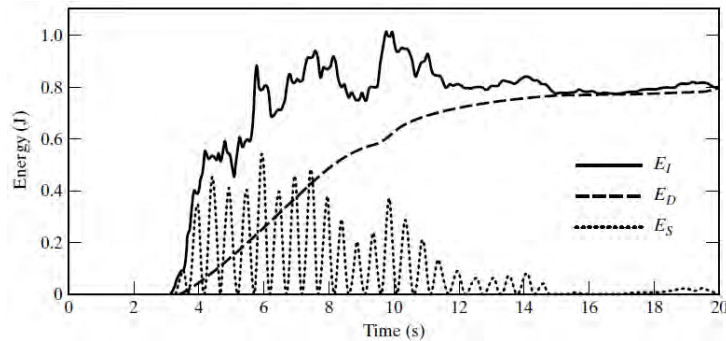


Figure 4.2: Energy build-up, Arleta Station (90 DEG), Northridge, 1994, $\xi = 2\%$.

The motion based seismic design process described in the last chapter is based on utilizing damping to limit the stiffness required for seismic excitation. Typically, the stiffness is reduced as damping is increased. Fig. 4.3 shows this trend. Given cost data for stiffness and damping, one can convert Fig. 4.3 to a plot showing cost trends, as illustrated in Fig. 4.4. The optimal value of damping depends on many factors such as the seismic design loading, type of structure, and choice of dampers.

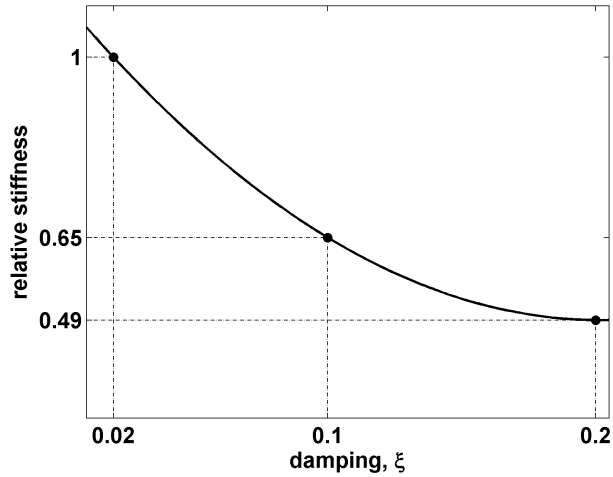
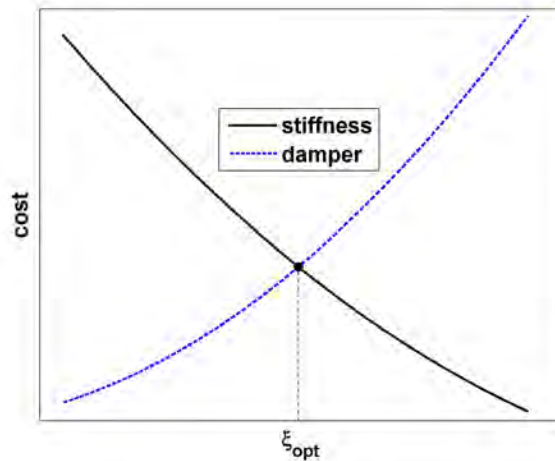
Figure 4.3: Relative stiffness versus damping ξ .

Figure 4.4: Stiffness versus damper cost functions.

Fig. 4.5 shows the Torre Mayor, a 55 story building constructed in Mexico City which is noted for its high seismic risk and poor soil conditions. Ninety eight viscous dampers are deployed in a unique way; they are installed within mega brace

CHAPTER 4. OPTIMAL PASSIVE DAMPING DISTRIBUTION

elements that span over six floors. This damper layout produces a damping ratio of 0.1 for the fundamental mode. Without this damping system, the 55 story structural concept would not have been feasible.



Figure 4.5: Torre Mayor Building [119].

Dissipation and absorption are attributed to a number of external and internal mechanisms, including the following:

- Energy dissipation due to the viscosity of the material. This process depends on the time rate of change of the deformations and is referred to as material damping. *Viscoelastic* materials belong to this category.
- Energy dissipation and absorption caused by the material undergoing cyclic inelastic deformation and ending up with

some residual deformation. The cyclic inelastic deformation path forms a hysteresis loop that corresponds to energy dissipation; the residual deformation is a measure of the energy absorption. This process is generally termed *hysteretic damping*.

- Energy dissipation associated with overcoming the friction between moving bodies in contact, such as flexible connections. *Coulomb damping* refers to the case where the magnitude of the friction force is constant. *Structural damping* is a more general *friction damping* mechanism that allows for a variable magnitude of the friction force.
- Energy dissipation resulting from the interaction of the structure with its surrounding environment. Relative motion of the structure generates forces that oppose the motion and extract energy from the structure. Fluid-structure interaction is a typical case. The fluid exerts a *drag force* that depends on the relative velocity and functions as an equivalent viscous damping force.
- Damping devices installed at discrete locations in structures to supplement their natural energy dissipation/absorption capabilities. These mechanisms may be passive or active. Passive mechanisms require no external energy, whereas active mechanisms cannot function without an external source of energy. Passive devices include viscous, friction, tuned mass, and liquid sloshing dampers. Active damping is achieved by applying external control forces to the structure over discrete time intervals. The magnitudes of the control forces are adjusted at each time point according to a *control* algorithm.

CHAPTER 4. OPTIMAL PASSIVE DAMPING DISTRIBUTION

- Passive damping removes energy from the response and therefore cannot cause the response to become unstable. Since active control involves an external source of energy, there is the potential for introducing an instability in the system. The term *semiactive* refers to a particular class of active devices that require a relatively small amount of external energy and apply the control force in such a way that the resulting motion is always stable. Chapter 7 discusses active and semi-active control devices.

In this chapter, the response characteristics for material, hysteretic, and friction damping mechanisms are examined for a single-degree-of-freedom (SDOF) system. The concept of *equivalent viscous damping* is introduced and is used to express viscoelastic, structural, and hysteretic damping in terms of their equivalent viscous counterpart. Numerical simulations are presented to demonstrate the validity of this concept for SDOF systems subjected to seismic excitation. This introductory material is followed by a discussion of the influence of distributed viscous damping on the deformation profiles of multi-degree-of-freedom (MDOF) systems. The damping distribution is initially taken to be proportional to the stiffness distribution generated in the previous chapter, and then modified to allow for nonproportional damping. Numerical results and deformation profiles for a range of structures subjected to seismic loading are presented, and the adequacy of this approach for distributing damping is assessed.

Distributed passive damping is usually supplemented with discrete damping devices to improve the response profile. Discrete viscous dampers inserted in beam-type structures are considered in this chapter; the basic theory for tuned mass dampers is

4.2. VISCOUS, FRICTIONAL, AND HYSTERETIC DAMPING

presented in the next chapter. Subsequent chapters deal with base isolation, a form of passive stiffness/damping control, and active control.

4.2 Viscous, Frictional, and Hysteretic Damping

4.2.1 Viscous Damping

Viscous damping is defined as the energy dissipation mechanism where the damping force is a function of the time rate of change of the corresponding displacement measure:

$$F = f(\dot{u}) \quad (4.1)$$

where F is the damping force and \dot{u} is the velocity in the direction of F . The linearized form is written as

$$F = c\dot{u} \quad (4.2)$$

where c , the *damping coefficient*, is a property of the damping device. Linear viscous damping is convenient to deal with mathematically and therefore is the preferred way of representing energy dissipation.

In general, the work W done on the device during the time interval $[t_1, t_2]$ is given by

$$W = \int_{u(t_1)}^{u(t_2)} F du = \int_{t_1}^{t_2} F \dot{u} dt \quad (4.3)$$

Considering periodic excitation

$$u = \hat{u} \sin \Omega t \quad (4.4)$$

CHAPTER 4. OPTIMAL PASSIVE DAMPING DISTRIBUTION

and evaluating Eq. (4.3) for one full cycle under linear viscous damping leads to

$$W_{\text{viscous}} = c\pi\Omega\hat{u}^2 \quad (4.5)$$

This term represents the energy dissipated per cycle by the damping device, as the system to which it is attached undergoes a periodic motion of amplitude \hat{u} and frequency Ω . Fig. 4.6 shows the force-displacement relationship for periodic excitation; the enclosed area represents W .

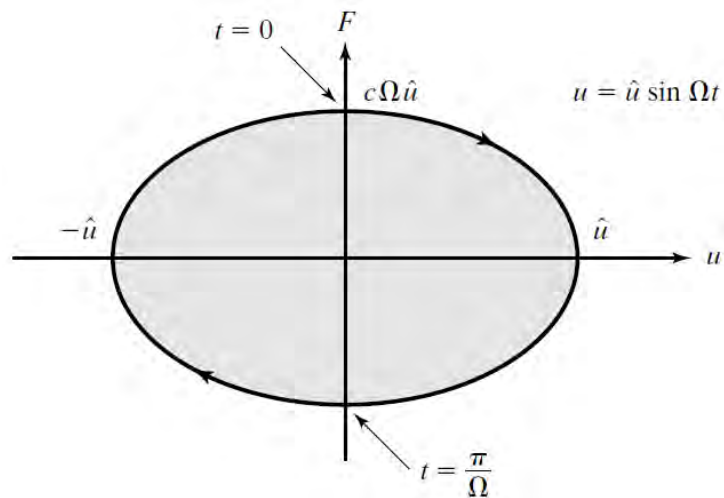


Figure 4.6: Linear viscous response: periodic excitation.

Example 4.1 - Viscous damper

Fig. E4.1a shows a possible design for a viscous damping device. The gap between the plunger and external plates is filled with a linear viscous fluid characterized by

$$\tau = G_v \dot{\gamma} \quad (1)$$

4.2. VISCOUS, FRICTIONAL, AND HYSTERETIC DAMPING

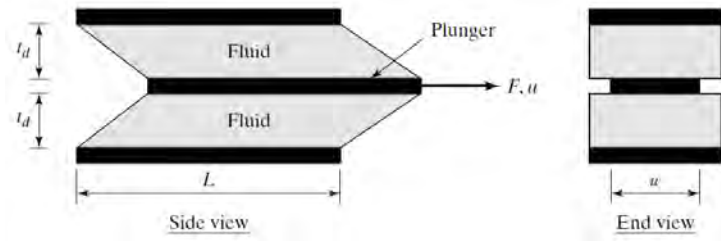


Figure E4.1a: Viscous damping device.

where τ and γ are the shearing stress and strain measures respectively and G_v is the viscosity coefficient. Assuming no slip between the fluid and plunger, the shear strain is related to the plunger motion by

$$\gamma = \frac{u}{t_d} \quad (2)$$

where t_d is the thickness of the viscous layer. Letting L and w represent the initial wetted length and width of the plunger respectively, the damping force is equal to

$$F = 2wL\tau \quad (3)$$

Substituting for results in

$$F = \left(\frac{2wLG_v}{t_d} \right) \dot{u} \quad (4)$$

Finally, Eq. (4) is written as

$$F = c\dot{u} \quad (5)$$

where c represents the viscous coefficient of the device,

$$c = \left(\frac{2wL}{t_d} \right) G_v \quad (6)$$

CHAPTER 4. OPTIMAL PASSIVE DAMPING DISTRIBUTION

The design parameters are the geometric measures w , L , t_d and the fluid viscosity, G_v .

A schematic diagram of a commercial viscous damper employed for structural applications is contained in Fig. 4.7a; an actual damper is shown in Fig. 4.7b. This product is engineered and manufactured by Taylor Devices, a leading provider of large scale viscous dampers for civil structures. As of 2012, Taylor Devices has supplied 339 structures with dampers, including 231 building and bridges. Fluid is forced through orifices located in the piston head as the piston rod position is changed, creating a resisting force that depends on the velocity of the rod. The damping coefficient can be varied by adjusting the control valve.

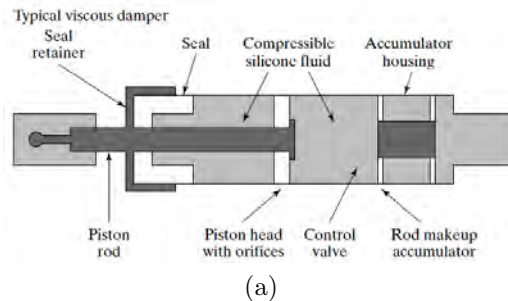


Figure 4.7: Viscous damper: (a) schematic diagram; (b) 450 kN capacity (Courtesy of Taylor Devices Inc.).

4.2. VISCOUS, FRICTIONAL, AND HYSTERETIC DAMPING

The force generated by a viscous damping device is characterized by the following equation,

$$F = c(\dot{u})^n \quad (4.6)$$

Properties specific to the device are the damping coefficient, c ; the exponent, n ; and the capacity, F_{\max} . Typical values of n for a Taylor device range from 0.3 to 1.95; the corresponding response plots are shown in Fig. 4.8. Taking $n < 1$ allows one to “limit” the damping force in order to prevent overloading when dampers are used to retrofit existing structures. The damper cost depends on c and F_{\max} ; it is essentially independent of n .

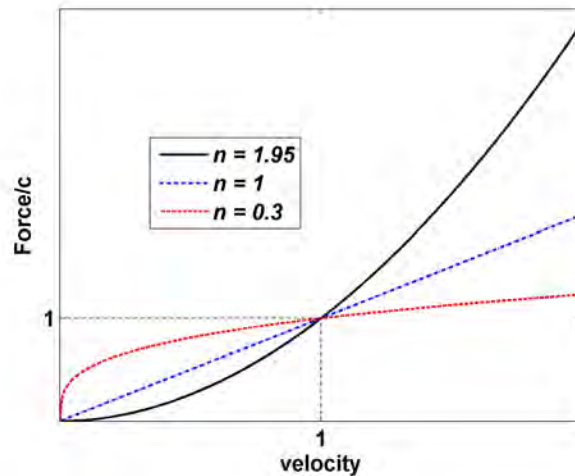


Figure 4.8: Damping force versus velocity for different values of n .

Eq. (4.5) shows that the energy loss per cycle for viscous damping depends on the frequency of the excitation. This dependency is at variance with observations for real structural systems, which indicate that the energy loss per cycle tends to be independent of the frequency. In what follows, a number of damping models that exhibit the latter property are presented.

4.2.2 Friction Damping

Coulomb damping is characterized by a damping force that is in phase with the velocity and has constant magnitude. Mathematically, the force can be expressed as

$$F = \bar{F} \operatorname{sgn}(\dot{u}) \quad (4.7)$$

where $\operatorname{sgn}(\dot{u})$ denotes the sign of \dot{u} . Fig. 4.9 shows the variation of F with u for periodic excitation. The work per cycle is the area enclosed by the response curve

$$W_{\text{coulomb}} = 4\bar{F}\bar{u} \quad (4.8)$$

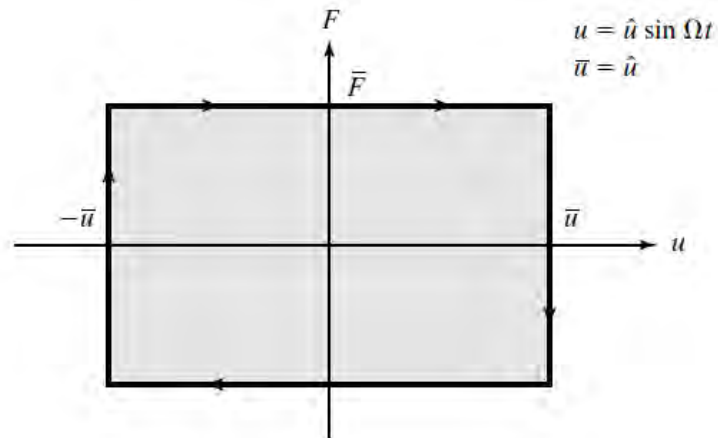


Figure 4.9: Coulomb damping force versus displacement.

Fig. 4.10 shows a Coulomb friction device used with diagonal bracing in frames. Friction pads are inserted between the plates, then the connecting bolt is tensioned, producing a compressive normal force, N , on the pads. Slotted holes are provided to allow for relative motion between the left and right segments. The resulting Coulomb force is

4.2. VISCOUS, FRICTIONAL, AND HYSTERETIC DAMPING

$$\bar{F} = 2N\mu \quad (4.9)$$

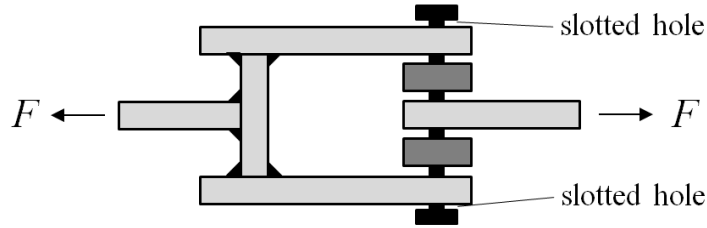


Figure 4.10: Coulomb friction device.

where μ is the coefficient of friction for the pad/plate interface. Devices of this type are said to be passive since N is constant. Incorporating a mechanism which allows N to vary transforms the device to a *semi-active* friction damper. Chapter 7 deals with this topic.

Observations indicate that the frictional damping force tends to increase with displacement [20]. Structural damping removes the restriction on the magnitude of the damping force and considers the force to be proportional to the displacement amplitude. The definition equation for this friction model has the form

$$F = k_s |u| \operatorname{sgn}(\dot{u}) \quad (4.10)$$

where k_s is a pseudostiffness factor. Fig. 4.11 shows the corresponding cyclic response path. The energy dissipated per cycle is equal to

$$W_{\text{structural}} = 4 \left(\frac{k_s \bar{u}^2}{2} \right) = 2k_s \bar{u}^2 \quad (4.11)$$

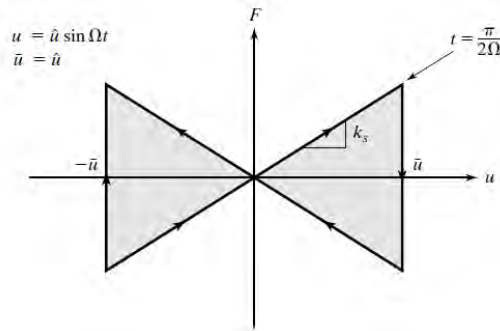


Figure 4.11: Structural damping force versus displacement.

4.2.3 Hysteretic Damping

Hysteretic damping is due to the inelastic deformation of the material composing the device. The form of the damping force-deformation relationship depends on the stress-strain relationship for the material and the makeup of the device. Fig. 4.12 illustrates the response path for the case where the material force-deformation relationship is elastic-perfectly plastic.

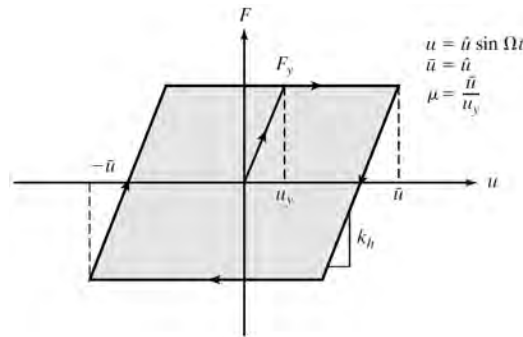


Figure 4.12: Hysteretic damping force versus displacement.

The limiting values are F_y , the yield force, and u_y , the displacement at which the material starts to yield; k_h is the elastic damper stiffness. The ratio of the maximum displacement to

4.2. VISCOUS, FRICTIONAL, AND HYSTERETIC DAMPING

the yield displacement is referred to as the ductility ratio and is denoted by μ . With these definitions, the work per cycle for hysteretic damping has the form

$$W_{\text{hysteretic}} = 4k_h u_y^2 (\mu - 1) = 4F_y \bar{u} \left(\frac{\mu - 1}{\mu} \right) \quad (4.12)$$

Fig. 4.13 shows a schematic of a bracing element that also functions as an hysteretic damper [112]. The element is composed of a core member fabricated with highly ductile low-strength steel (yield strength of 100 MPa, maximum percent strain of 60%), a cylindrical jacket, and material placed between the core member and the jacket. The jacket functions as an additional bending element, and its cross-sectional moment of inertia is selected such that the buckling load is equal to the yield force. This design feature allows the brace to be used for both tensile and compressive loading. Fig. 4.14 shows a picture of an actual hysteretic damper brace element. Triangular shaped steel plate hysteretic dampers that dissipate energy through inelastic action have also been used for buildings [105].

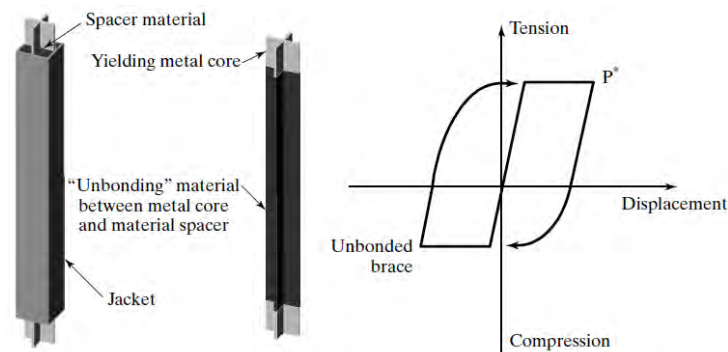


Figure 4.13: Hysteretic damper brace element [112].



Figure 4.14: Hysteretic damper brace element (Courtesy of J. Connor).

Devices that behave as energy dissipating elasto-plastic elements, such as the unbonded brace, are also used as “replaceable structural fuses” which serve to trigger a different response mechanism. One of the structural systems that has recently been proposed to provide cost effective resistance to earthquake excitation is a steel braced frame system with controlled rocking and energy dissipating fuses [25], shown in Fig. 4.15. The fuses are activated when the brace force equals the yield force, resulting in the structure “rocking” about the foundation; the lifting motion counteracts the overturning moment due to the lateral seismic loading. The basic strategy here is to use gravity to offset the lateral seismic action.

4.2. VISCOUS, FRICTIONAL, AND HYSTERETIC DAMPING

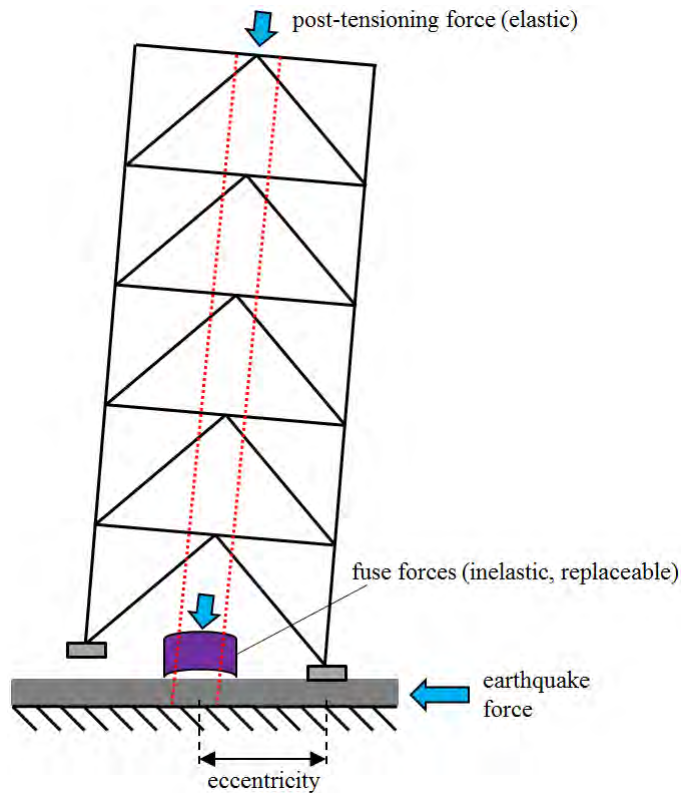


Figure 4.15: Schematic of a controlled rocking frame with steel fuses (adapted from [25]).

Unbounded braces combined with beam-column connections that act as structural fuses, are used to develop damage controlled structures [107]. The basic concept of a damage controlled structure is that by separating the main frame from the energy absorption system, the main frame is kept within the elastic range and the energy due to seismic excitation is absorbed by the members.

Example 4.2 - Stiffness of a rod hysteretic damper

Consider a damping device consisting of a cylindrical rod of length L and area A . Suppose the material is elastic-perfectly

CHAPTER 4. OPTIMAL PASSIVE DAMPING DISTRIBUTION

plastic, as shown in Fig. E4.2a.

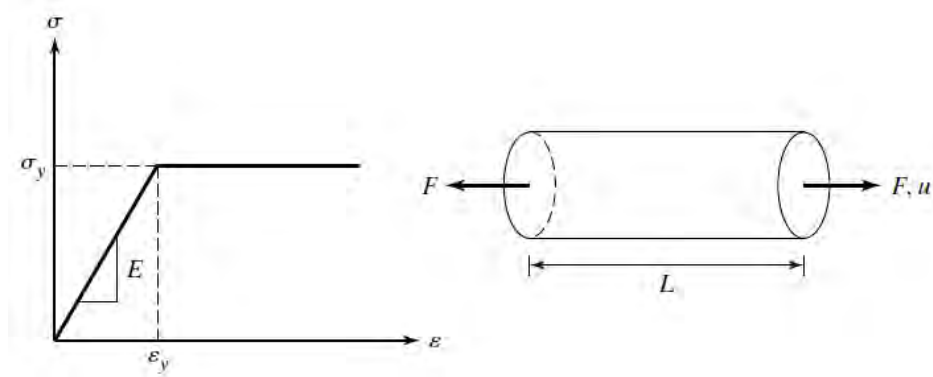


Figure E4.2a: Elastic-perfectly plastic damper device.

The relevant terms are

$$\varepsilon = \frac{u}{L} \quad (1)$$

$$F = A\sigma \quad (2)$$

Then

$$u_y = L\varepsilon_y \quad (3)$$

$$F_y = A\sigma_y = k_h u_y \quad (4)$$

$$k_h = \frac{AE}{L} \quad (5)$$

Example 4.3 - Stiffness of two hysteretic dampers in series

4.2. VISCOUS, FRICTIONAL, AND HYSTERETIC DAMPING

The device treated in Ex. 4.2 is modified by adding a second rod in series, as shown in Fig. E4.3a. The yield force for the second rod is assumed to be greater than the yield force for the first rod,

$$A_2\sigma_{y,2} > A_1\sigma_{y,1} \equiv F_{y,1} \quad (1)$$

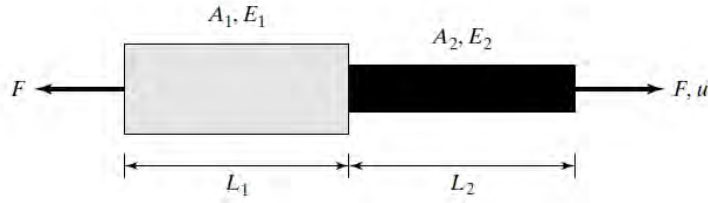


Figure E4.3a: Two-rod hysteretic damping device.

Since the force is the same for both devices, the total elastic displacement is the sum of the individual contributions.

$$u = \left(\frac{L_1}{A_1 E_1} + \frac{L_2}{A_2 E_2} \right) F = \left(\frac{1}{k_h} \right) F \quad (2)$$

Specializing Eq. (2) for the onset of yielding, we obtain

$$u_y = \frac{F_{y,1}}{k_h} = L_1 \varepsilon_{y,1} \left(1 + \frac{A_1 L_2 E_1}{A_2 L_1 E_2} \right) \quad (3)$$

$$k_h = \frac{A_1 E_1}{L_1} \left(\frac{1}{1 + \frac{A_1 L_2 E_1}{A_2 L_1 E_2}} \right) \quad (4)$$

When two elements are used, we can vary both the yield force, F_y , and the elastic stiffness. The energy dissipation increases with decreasing u_y for a given deformation amplitude \bar{u} .

4.3 Viscoelastic Material Damping

A material is considered to be elastic when the stresses due to an excitation are unique functions of the associated deformation. Similarly, a material is said to be viscous when the stress state depends only on the deformation rates. For simple shear, these definitions translate to

Elastic

$$\tau = G_e \gamma \quad (4.13)$$

Viscous

$$\tau = G_v \dot{\gamma}$$

The stress-deformation paths for periodic strain are illustrated in Fig. 4.16(a) and Fig. 4.16(b). There is no time lag between stress and strain for elastic behavior, whereas the stress is $\pi/2$ radians out of phase with the strain for viscous behavior. If these relations are linearly combined, we obtain the path shown in Fig. 4.16(c).

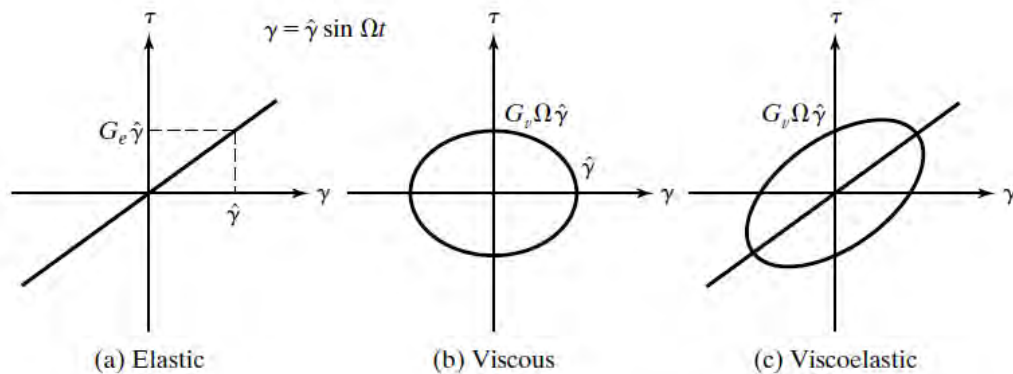


Figure 4.16: Stress-deformation relations.

4.3. VISCOELASTIC MATERIAL DAMPING

Materials that behave similar to Fig. 4.16(c) are called *viscoelastic*. The properties of a linear viscoelastic material are determined by applying a periodic excitation and observing the response, which involves both an amplification and a phase shift. The basic relations are expressed as

$$\begin{aligned}\gamma &= \hat{\gamma} \sin \Omega t \\ \tau &= \hat{\gamma}(G_s \sin \Omega t + G_l \cos \Omega t)\end{aligned}\tag{4.14}$$

where G_s is the *storage modulus* and G_l is the *loss modulus*. The ratio of the loss modulus to the storage modulus is defined as the *loss factor*, η :

$$\eta = \frac{G_l}{G_s} = \tan \delta\tag{4.15}$$

An alternate form for Eq. (4.14) is

$$\begin{aligned}\tau &= \hat{\gamma} \hat{G} \sin(\Omega t + \delta) \\ \hat{G} &= \sqrt{G_s^2 + G_l^2} = G_s \sqrt{1 + \eta^2}\end{aligned}\tag{4.16}$$

The angle δ is the phase shift between stress and strain. Delta ranges from 0 for elastic behavior to $\pi/2$ for pure viscous behavior.

Experimental observations show that the material properties G_s and η vary with temperature and the excitation frequency. Fig. 4.17 illustrates these trends for ISD110, a 3M product. The dependency on frequency makes it difficult to generalize the stress-strain relationships based on periodic excitation to allow for an arbitrary time-varying loading such as seismic excitation. This problem is addressed in the next section.

CHAPTER 4. OPTIMAL PASSIVE DAMPING DISTRIBUTION

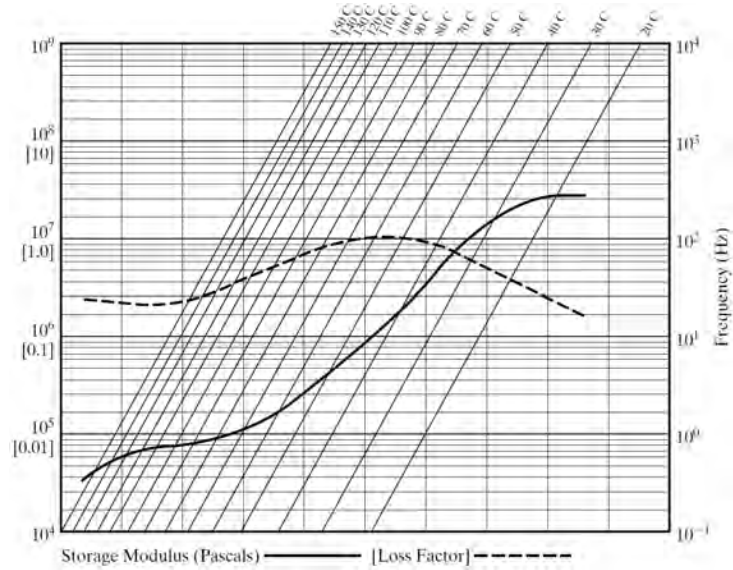


Figure 4.17: Variation of 3M viscoelastic material, ISD110, with frequency and temperature. To determine the damping properties at the desired temperature and frequency from the data graph shown above, proceed as follows: 1) Locate the desired frequency on the RIGHT vertical scale; 2) follow the chosen frequency line to the desired temperature isotherm; 3) from this intersect, go vertically up and/or down until crossing both the shear (storage) modulus G_s and loss factor curves η ; and 4) read the storage modulus and loss factor values from the appropriate LEFT-hand scale.

The energy dissipated per unit volume of material for one cycle of deformation is determined from

□

$$W_{\text{viscoelastic}} = \int_0^{2\pi/\Omega} \tau \dot{\gamma} dt \quad \text{(a)}$$

Substituting for τ and γ using Eq. (4.14) results in

$$W_{\text{viscoelastic}} = \pi G_l \hat{\gamma}^2 \quad \text{(4.17)}$$

The corresponding expression for a pure viscous material is

4.3. VISCOELASTIC MATERIAL DAMPING

$$W_{\text{viscous}} = \pi G_v \Omega \hat{\gamma}^2 \quad \text{b)}$$

This expression involves the frequency explicitly, whereas the effect of frequency is embedded in G_1 for the viscoelastic case.

Example 4.4 - Viscoelastic damper

A damper device is fabricated by bonding thin sheets of a viscoelastic material to steel plates, as illustrated in Fig. E4.4a.

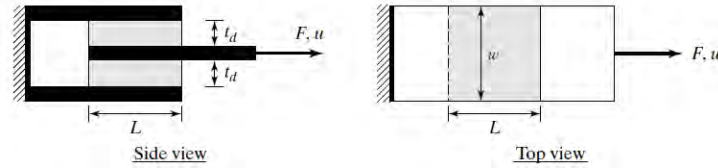


Figure E4.4a: Viscoelastic damper device.

Since the elastic modulus for steel is considerably greater than the shear modulus G_s for the sheet material, we can consider all the motion to be due to shear deformation of the sheets. Defining u as the relative displacement of the ends of the damper device, the shearing strain is

$$\gamma = \frac{u}{t_d} \quad \text{1)}$$

Given γ , we evaluate τ with the stress-strain relation and then F using the equilibrium equation for the system

$$F = 2wL\tau \quad \text{2)}$$

Applying a periodic excitation

$$u = \hat{u} \sin \Omega t \quad \text{3)}$$

and taking τ according to Eq. (4.14), we obtain

$$F = f_d G_s \hat{u} (\sin \Omega t + \eta \cos \Omega t) \quad (4)$$

$$f_d = \frac{2wL}{t_d} \quad (5)$$

Eq. (4) can also be written as

$$F = f_d \hat{G} \hat{u} \sin(\Omega t + \delta) \quad (6)$$

$$\hat{G} = G_s \sqrt{1 + \eta^2} \quad (7)$$

Finally, the energy dissipated per cycle is given by

$$W = \pi \eta f_d G_s \hat{u}^2 \quad (8)$$

Typical polymer materials have G_s in the range of 1.5 MPa and $\eta \approx 1$.

Based on the result of the previous example, the expressions defining the response of a viscoelastic damper due to periodic excitation can be written in a generalized form:

$$\begin{aligned} u &= \hat{u} \sin \Omega t \\ F &= f_d G_s \hat{u} (\sin \Omega t + \eta \cos \Omega t) \\ W_{\text{viscoelastic}} &= \pi \eta f_d G_s \hat{u}^2 \end{aligned} \quad (4.18)$$

where f_d depends on the geometric configuration of the device, G_s is the storage modulus, and η is the material loss factor. Fig. 4.18 shows the variation of F with u over the loading cycle.

4.4. EQUIVALENT VISCOUS DAMPING

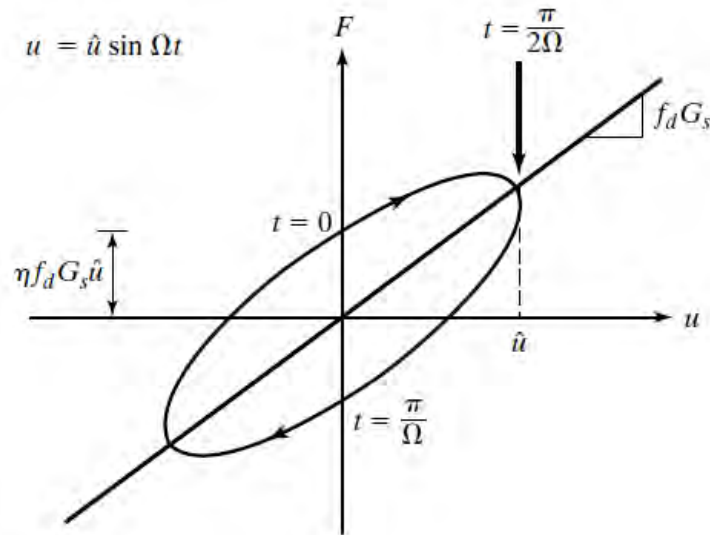


Figure 4.18: Variation of F_d with u_d for viscoelastic material.

4.4 Equivalent Viscous Damping

The expression for the damping force corresponding to linear viscous damping is the most convenient mathematical form, in comparison to the other damping force expressions, for deriving approximate analytical solutions to the force equilibrium equations. Therefore, one way of handling the different damping models is to convert them to *equivalent viscous* damping models. In what follows, a conversion strategy based on equating the energy dissipated per cycle of *periodic* excitation to the corresponding value for linear viscous damping is described.

Linear viscous damping is defined as:

$$F = c\dot{u} \quad \text{(a)}$$

Specializing Eq. (a) for periodic excitation

CHAPTER 4. OPTIMAL PASSIVE DAMPING DISTRIBUTION

$$u = \hat{u} \sin \Omega t \quad \text{(b)}$$

leads to

$$F = c\Omega\hat{u} \cos \Omega t \quad \text{(c)}$$

and the energy loss per cycle

$$W = c\pi\Omega\hat{u}^2 \quad \text{(d)}$$

The force and energy loss for the other models are expressed in terms of an equivalent damping coefficient, c_{eq} :

$$\begin{aligned} F &= c_{\text{eq}}\Omega\hat{u} \cos \Omega t \\ W &= c_{\text{eq}}\pi\Omega\hat{u}^2 \end{aligned} \quad \text{(4.19)}$$

Substituting W for a particular damping model in Eq. (4.19) and taking $\bar{u} = \hat{u}$, we obtain the equivalent damping coefficient. The coefficients for the various models are as follows:

Coulomb

$$c_{\text{eq}} = \frac{4\bar{F}}{\pi\Omega\hat{u}} \quad \text{(4.20)}$$

Structural

$$c_{\text{eq}} = \frac{2k_s}{\pi\Omega} \quad \text{(4.21)}$$

4.4. EQUIVALENT VISCOUS DAMPING

Hysteretic

$$c_{\text{eq}} = \frac{4F_y}{\pi\Omega\hat{u}} \left(\frac{\mu - 1}{\mu} \right) \quad (4.22)$$

Viscoelastic

$$c_{\text{eq}} = \frac{f_d\eta G_d}{\Omega} = \frac{f_d G_l}{\Omega} \quad (4.23)$$

These expressions are valid for periodic excitation of amplitude \hat{u} and frequency Ω . They can be used to approximate structural and hysteretic damping as pseudoviscous damping but require specifying a representative frequency, Ω_r , and amplitude, u_r . In this case, Eqs. (4.21) and (4.22) are written as

Structural

$$c_{\text{eq}} = \frac{2k_s}{\pi\Omega_r} \quad (4.24)$$

Hysteretic

$$\begin{aligned} c_{\text{eq}} &= \frac{4F_y}{\pi\Omega_r u_r} \left(\frac{\mu - 1}{\mu} \right) \\ u_y &= \frac{F_y}{k_h} \\ \mu &= \frac{u_r}{u_y} \end{aligned} \quad (4.25)$$

CHAPTER 4. OPTIMAL PASSIVE DAMPING DISTRIBUTION

Numerical simulations illustrating the accuracy of this approximation are provided by the following examples.

Example 4.5 - Structural and hysteretic damping comparison: seismic excitation

A 1DOF shear beam having the following properties is considered:

$$\begin{aligned} m &= 4 \times 10^6 \text{ kg} & \omega_1 &= 1.17 \text{ rad/s} \\ k &= 5517 \text{ kN/m} & T_1 &= 5.35 \text{ s} \\ c &= 187.9 \text{ kN}\cdot\text{s/m} & \xi_1 &= 2.0 \% \end{aligned}$$

The equivalent structural stiffness is generated using Eq. (4.24), taking $c = c_e$ and Ω_r equal to the fundamental frequency ω_1 . The corresponding structural stiffness is

$$k_s = \frac{\pi\omega_1 c_e}{2} = \frac{\pi(1.17)(187.9)}{2} = 346.6 \text{ kN/m} \quad \textcircled{1}$$

Results for this model subjected to Taft excitation are compared with the corresponding results for the linear viscous model in Figs. E4.5a and E4.5b. Close agreement is observed.

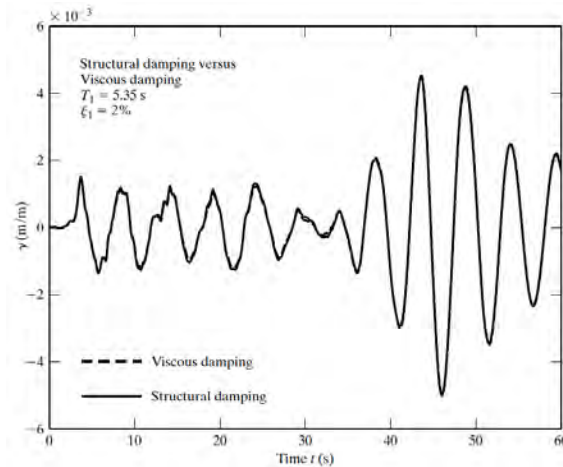


Figure E4.5a: Response of SDOF with structural damping.

4.4. EQUIVALENT VISCOUS DAMPING

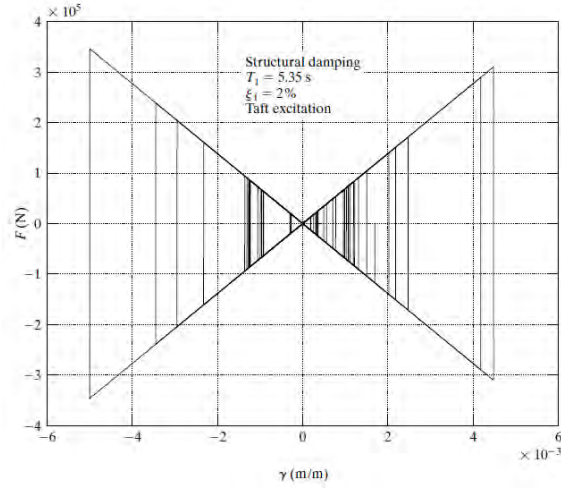


Figure E4.5b: Structural damping force versus deformation.

The hysteretic model calibration defined by Eq. (4.25) is not as straightforward since both the yield force and the ductility are involved. For periodic motion, the maximum displacement $\bar{u}_d = \hat{u}_d$ is known. Then we can specify the desired ductility μ^* and compute the required force level and initial stiffness with

$$F_y = \frac{\pi\omega_1\bar{u}c_{\text{eq}}}{4} \left(\frac{\mu^*}{\mu^* - 1} \right) \quad (2)$$

$$u_y = \frac{\bar{u}}{\mu^*} \quad (3)$$

$$k_h = \frac{F_y}{u_y} \quad (4)$$

For nonperiodic motion, we need to specify the limiting elastic displacement u_y and estimate the maximum amplitude \bar{u} . This leads to estimates for the ductility ratio μ^* and the peak force F_y . Figs. E4.5c and E4.5d show the results based on taking \bar{u} equal to the peak amplitude observed for pure viscous damping and

CHAPTER 4. OPTIMAL PASSIVE DAMPING DISTRIBUTION

a ductility ratio $\mu^* = 7.5$. We can adjust μ^* and F_y to obtain closer agreement. *Since the energy is dissipated only during this inelastic phase, hysteretic damping is generally less effective than either viscous or structural damping for low-intensity loading.*

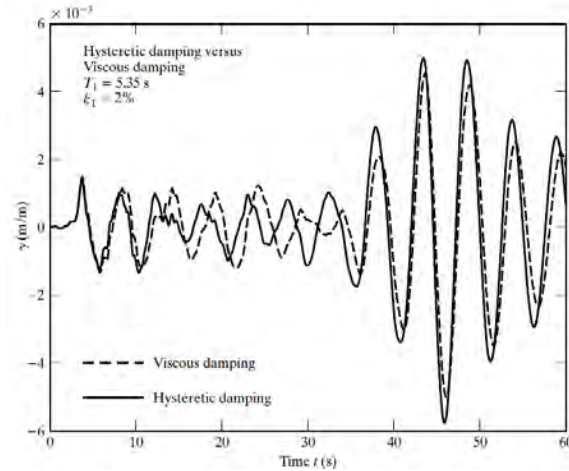


Figure E4.5c: Response of SDOF with hysteretic damping.

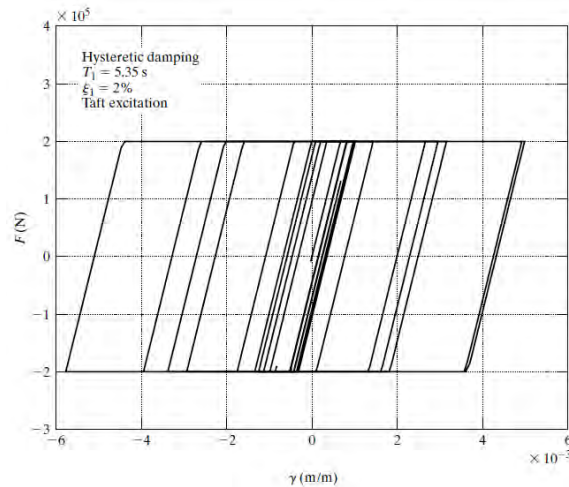


Figure E4.5d: Hysteretic damping force versus deformation.

The calibration of the equivalent viscous damping coefficient

4.4. EQUIVALENT VISCOUS DAMPING

was based on assuming a periodic excitation. As discussed previously, nonperiodic excitation requires some assumptions as to the response. An improved estimate of the equivalent damping coefficient can be obtained by evaluating the actual work done by the damping force. Starting with

$$E_D|_{\text{actual}} = \int_0^t F \dot{u} dt \quad (5)$$

and writing

$$E_D|_{\text{eq. viscous}} = c_{\text{eq}} \int_0^t \dot{u}^2 dt \quad (6)$$

leads to

$$c_{\text{eq}}(t) = \frac{\int_0^t F \dot{u} dt}{\int_0^t \dot{u}^2 dt} = 2\xi_{\text{eq}} \omega m \quad (7)$$

Eq. 7 can be used to evaluate the variation over time of the equivalent damping ratio. Taking $t = t_{\text{end}}$, the total duration of the response, provides an estimate of the effective damping ratio. Fig. E4.5e shows results generated for a range of seismic excitations and hysteretic damper yield force levels. As expected, the effective damping increases with increasing seismic excitation. For a given seismic excitation, there is an optimal value of the ratio of yield force to total weight. Typical values are between 0.03 and 0.05.

CHAPTER 4. OPTIMAL PASSIVE DAMPING DISTRIBUTION

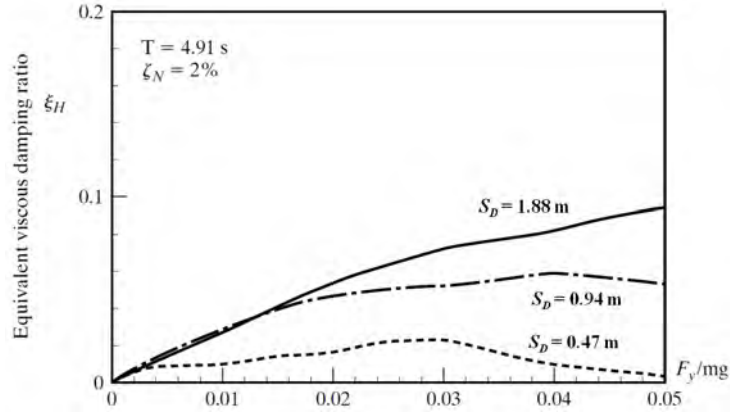


Figure E4.5e: Equivalent viscous damping ratio versus yield force.

The viscoelastic model calibration is more involved since the material properties are also frequency dependent. Referring back to Eq. (4.18), the damping force for periodic excitation

$$u = \hat{u} \sin \Omega t \quad \text{(a)}$$

was expressed as

$$F = \hat{u} f_d G_s (\sin \Omega t + \eta \cos \Omega t) \quad \text{(b)}$$

where f_d is a geometric factor defined by the geometry of the device. Our objective is to express F as

$$F = k_{\text{eq}} u + c_{\text{eq}} \dot{u} \quad \text{(4.26)}$$

where k_{eq} and c_{eq} are equivalent stiffness and damping terms. Considering periodic excitation, Eq. (4.26) takes the form

$$F = \hat{u} (k_{\text{eq}} \sin \Omega t + \Omega c_{\text{eq}} \cos \Omega t) \quad \text{(4.27)}$$

We can obtain estimates for k_{eq} and c_{eq} with a least squares approach. Assuming there are N material property data sets

4.4. EQUIVALENT VISCOUS DAMPING

and summing the squares of the errors for k_{eq} and c_{eq} over the ensemble results in

$$J_k = \sum_{i=1}^N [k_{\text{eq}} - f_d G_s(\Omega_i)]^2 \quad (4.28)$$

$$J_c = \sum_{i=1}^N \left[c_{\text{eq}} - \frac{f_d G_s(\Omega_i) \cdot \eta(\Omega_i)}{\Omega_i} \right]^2 \quad (4.29)$$

Minimizing Eq. (4.28) with respect to k_{eq} yields

$$k_{\text{eq}} = f_d \left[\left(\frac{1}{N} \right) \sum_{i=1}^N G_s(\Omega_i) \right] = f_d \hat{G}_s \quad (4.30)$$

Similarly, minimizing Eq. (4.29) with respect to c_{eq} results in

$$c_{\text{eq}} = f_d \left[\left(\frac{1}{N} \right) \sum_{i=1}^N \frac{G_s(\Omega_i) \eta(\Omega_i)}{\Omega_i} \right] \quad (4.31)$$

The form of Eq. (4.31) suggests that c_{eq} be expressed as

$$c_{\text{eq}} = \alpha_d k_{\text{eq}} \quad (4.32)$$

Substituting for k_{eq} and c_{eq} leads to the definition equation for α_d :

$$\alpha_d = \frac{\sum_{i=1}^N \left(\frac{G_s \eta}{\Omega} \right)_i}{\sum_{i=1}^N G_s(\Omega_i)} \quad (4.33)$$

Note that α_d depends only on the material (i.e., it is independent of the geometry of the device).

With this notation, the equivalent viscous force-deformation relation for a linear viscoelastic damper is written as

$$F = k_{\text{eq}}u + \alpha_d k_{\text{eq}}\dot{u} \quad (4.34)$$

Example 4.6 - Determining α_d for 3M ISD110 damping material

This example illustrates how the procedure discussed above can be applied to compute the parameters for the 3M Scotchdamp ISD110 material. Using Fig. 4.17, data corresponding to five frequencies is generated. Table E4.6a contains this data.

Applying Eqs. (4.30), (4.31), and (4.33), we obtain

$$k_{\text{eq}} = 5.7f_d \quad \alpha_d = 0.104 \quad c_{\text{eq}} = 0.593f_d$$

Table E4.6a: Data for ISD110 Scotchdamp material (from Fig. 4.17)

Ω (rad/s)	G_s (MPa)	η
0.628	1.0	1.0
3.14	2.5	1.0
6.28	3.7	0.93
12.56	5.0	0.85
31.4	9.0	0.65
62.8	13.0	0.55

4.5 Damping Parameters: Discrete Shear Beam

4.5.1 Damping Systems

This section extends the treatment of discrete shear beams to include damping devices located between the floors Fig. 4.19 illustrates two different placement schemes of viscous-type dampers for a typical panel. Scheme (a) combines the damper with a

4.5. DAMPING PARAMETERS: DISCRETE SHEAR BEAM

structural element and deploys the composite element on the diagonal between floors. Scheme (b) places the damper on a roller support at the floor level and connects the device to the adjacent floor with structural elements. An actual installation of a scheme (a) system is shown in Fig. 4.20. This is a toggle brace damper system, which magnifies the effect of diagonal extension on the device so it can be used at low levels of interstory displacement. The structural elements are modeled as linear springs and the representations defined in Fig. 4.21 are used for schemes (a) and (b).

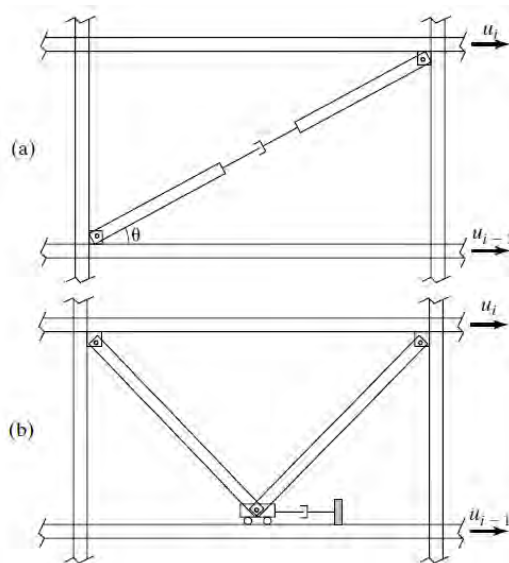


Figure 4.19: Damper placement schemes.

CHAPTER 4. OPTIMAL PASSIVE DAMPING DISTRIBUTION



Figure 4.20: Toggle brace damper system (Courtesy of J. Connor).

4.5. DAMPING PARAMETERS: DISCRETE SHEAR BEAM

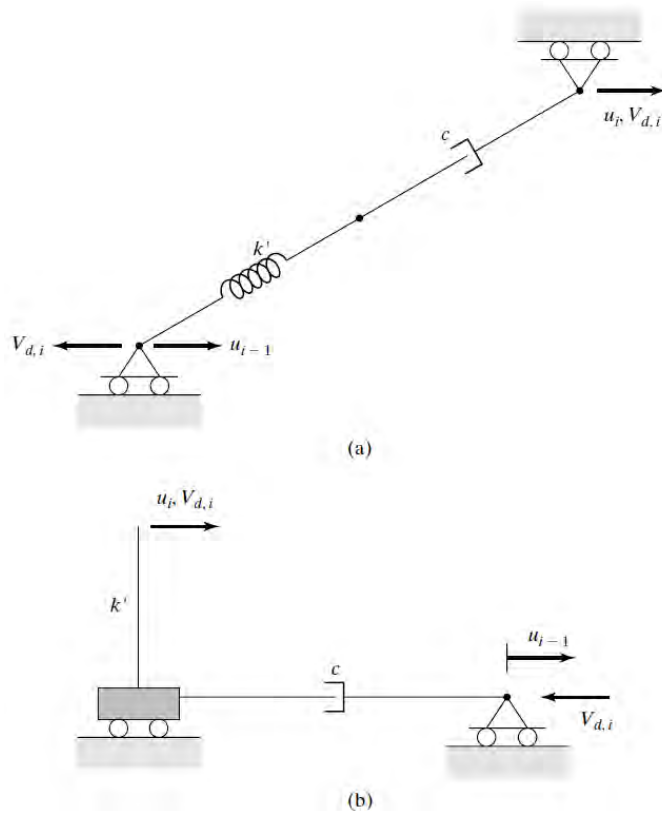


Figure 4.21: Idealized models of structures with viscous dampers.

A differential story displacement generates a deformation of the damper, resulting in a damper force that produces the story shear, $V_{d,i}$. A subscript d is used to denote quantities associated with the damper. The total story shear is the sum of the elastic shear force due to elastic frame/brace action and the damper shear force. The former was considered in Chapter 2. This contribution is written as

$$V_{e,i} = k_{e,i}(u_i - u_{i-1}) \quad (4.35)$$

where subscript e refers to elastic frame/brace action. The damper shear force is a function of both the relative displacement

and the relative velocity. This term is expressed in a form similar to Eq. (4.34):

$$V_{d,i} = k_{d,i}(u_i - u_{i-1}) + c_{d,i}(\dot{u}_i - \dot{u}_{i-1}) \quad (4.36)$$

where k_d and c_d are equivalent properties that depend on the makeup of the damping system. Various cases are considered in the following sections.

4.5.2 Rigid Structural Members: Linear Viscous Behavior

Consider first the case where the stiffness, k' , of the structural members contained in the damping system is sufficiently large so that the extension of the member is negligible in comparison to the extension of the damper. Defining e_d as the extension of the damper and considering scheme (a) shown in Fig. 4.21, the damper force for linear viscous behavior is given by

$$F_d = c_d \dot{e}_d = c_d(\dot{u}_i - \dot{u}_{i-1}) \cos \theta \quad (4.37)$$

The corresponding shear force is

$$V_{d,i} = F_d \cos \theta = c_d(\dot{u}_i - \dot{u}_{i-1}) \cos^2 \theta \quad (4.38)$$

The equivalent damping coefficient for story i is obtained by summing the contributions of the dampers present in story i .

$$c_{d,i} = \sum_{\text{story } i} (c_d \cos^2 \theta) \quad (4.39)$$

Eq. (4.39) also applies for scheme (b); $\theta = 0$ for this arrangement of structural members and dampers. Scheme (b) is more

4.5. DAMPING PARAMETERS: DISCRETE SHEAR BEAM

effective than scheme (a) (a factor of 2 for 45° bracing) and is more frequently adopted.

The general spring-dashpot model shown in Fig. 4.22 is useful for representing the different contributions to the story shear force. For this case, the damper (C) acts in parallel with the elastic shear stiffness of the frame/bracing system (K) and e is equal to the interstory displacement. An extended version of this model is used to study other damping systems.

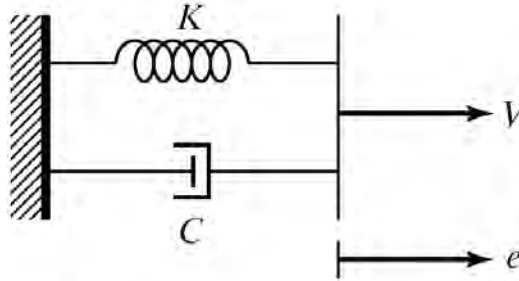


Figure 4.22: Spring and dashpot in parallel model.

Example 4.7 - Example 3.10 revisited

Consider the 5DOF shear beam defined in Ex. 3.10. Taking the constant nodal mass as 10,000 kg, and using the stiffness calibration based on $S_D = 0.24$ m, $\xi = 0.1$ results in the following values for the element shear stiffness factors, fundamental frequency, nodal mass, and damping:

$$\begin{aligned}
 k_1 &= 13.59 \text{ MN/m} & k_2 &= 12.68 \text{ MN/m} & k_3 &= 10.87 \text{ MN/m} \\
 k_4 &= 8.15 \text{ MN/m} & k_5 &= 4.53 \text{ MN/m} & & \\
 \omega_1 &= 9.52 \text{ rad/s} & \tilde{m} &= 22,000 \text{ kg} & \tilde{c} &= 41.9 \text{ kN} \cdot \text{s/m}
 \end{aligned}$$

①

The element damping coefficients are related to \tilde{c} by

CHAPTER 4. OPTIMAL PASSIVE DAMPING DISTRIBUTION

$$\tilde{c} = \frac{1}{25}(c_1 + c_2 + c_3 + c_4 + c_5) \quad (2)$$

Taking c_i constant leads to

$$c_1 = c_2 = \cdots = c_5 = 5\tilde{c} = 210 \text{ kN} \cdot \text{s/m} \quad (3)$$

Assuming damping is proportioned to the element stiffness, $c_i = \alpha k_i$, and selecting α according to $\alpha = 2\xi_1/\omega_1$ (the basis for this equation is established in Sect. 3.2.1), we obtain the following:

$$\begin{aligned} \alpha &= 0.0210 \\ c_1 &= 285 \text{ kN} \cdot \text{s/m} & c_2 &= 266 \text{ kN} \cdot \text{s/m} & c_3 &= 228 \text{ kN} \cdot \text{s/m} \\ c_4 &= 171 \text{ kN} \cdot \text{s/m} & c_5 &= 95 \text{ kN} \cdot \text{s/m} \end{aligned} \quad (4)$$

Suppose the chevron brace scheme [scheme (b)] is used, and two dampers are deployed per floor. The design values for the dampers are obtained by dividing the preceding results by a factor equal to 2. For the uniform case, $c = 105 \text{ kN} \cdot \text{s/m}$. In order to design the damper, we also need to specify the peak value of the damper force. This quantity is determined with $F_{\max} = cv_{\max}$ where v_{\max} is the maximum relative velocity of the damper piston. For this damper deployment scheme, the relative damper displacement is equal to the interstory displacement. It follows that v_{\max} for level i is equal to

$$v_{\max}|_{\text{level } i} = (\dot{u}_i - \dot{u}_{i-1})_{\max} = h_i(\dot{\gamma}_i)_{\max} \quad (5)$$

The nodal displacements for this 5DOF model are considered to vary linearly with height:

4.5. DAMPING PARAMETERS: DISCRETE SHEAR BEAM

$$u_i - u_{i-1} = \frac{1}{5}q \quad (6)$$

where q is the modal amplitude. Then

$$v_{\max} = \frac{1}{5}(\dot{q})_{\max} \quad (7)$$

The peak amplitude is determined with

$$q_{\max} = \Gamma S_D \quad (8)$$

We can estimate \dot{q}_{\max} by assuming the response is periodic, with frequency ω_1 .

$$\dot{q}_{\max} \approx \Gamma S_D(\omega, \xi)\omega_1 \quad (9)$$

Using the problem data,

$$\dot{q}_{\max} \approx (1.36)(0.24)(9.52) = 3.10 \text{ m/s} \quad (10)$$

and the peak damper force is estimated as

$$F_{\max} \approx (105) \left(\frac{3.10}{5} \right) = 65.1 \text{ kN} \quad (11)$$

4.5.3 Rigid Structural Members: Linear Viscoelastic Behavior

The case where the damping mechanism is viscoelastic is represented by the model shown in Fig. 4.23. Here, the damping force has an elastic component as well as a viscous component. Noting Eq. (4.34), the damping force is expressed as

$$V_d = K_1 e + C \dot{e} = K_1 e + \alpha_d K_1 \dot{e} \quad (4.40)$$

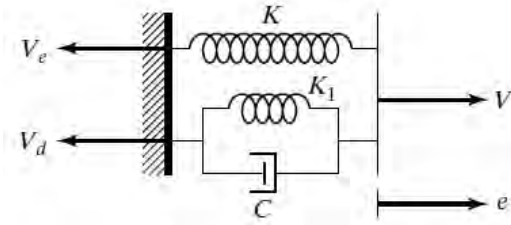


Figure 4.23: Spring-dashpot model for viscoelastic damping.

where K_1 and C (or α_d) are the *equivalent* stiffness and damping parameters for the viscoelastic device, and e is the interstory displacement. This formulation assumes the viscous device is attached to a *rigid* element so that all the deformation occurs in the device. The more general case is treated later. Using Eq. (4.40), we obtain

$$V = (K + K_1)e + C \dot{e} = (K + K_1)e + \alpha_d K_1 \dot{e} \quad (4.41)$$

When K_1/K is small with respect to unity, the contribution of the viscoelastic damper to the stiffness can be neglected.

Example 4.8 -

Consider a SDOF system having an elastic spring and a viscoelastic damper modeled as shown in Fig. E4.8a. Suppose m , ω , and ξ are specified, and the objective is to establish values for the spring stiffness and damper properties.

4.5. DAMPING PARAMETERS: DISCRETE SHEAR BEAM

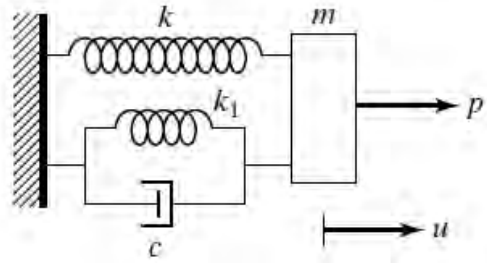


Figure E4.8a

The governing equation has the form

$$m\ddot{u} + c\dot{u} + (k + k_1)u = p \quad (1)$$

By definition,

$$\omega^2 = \frac{k + k_1}{m} \quad (2)$$

$$c = 2\xi\omega m \quad (3)$$

Given ξ and ω , c is determined with Eq. (3). The stiffness factors are related by

$$k_1 + k = m\omega^2 \quad (4)$$

Our strategy for dealing with a viscoelastic device is based on expressing the equivalent damper coefficient as [see Eq. (4.34)]:

$$c = \alpha_d k_1 \quad (5)$$

where α_d is a material property. Ex. 4.6 illustrates how to evaluate α_d for a typical viscoelastic material. The procedure followed here is to first determine k_1 , using Eqs. (3) and (5),

CHAPTER 4. OPTIMAL PASSIVE DAMPING DISTRIBUTION

$$k_1 = \frac{2\xi\omega m}{\alpha_d} \equiv \frac{c}{\alpha_d} \quad (6)$$

and then substitute for k_1 in Eq. (4). This operation results in an equation for k .

$$k = m\omega^2 - \frac{2\xi\omega m}{\alpha_d} = m\omega \left(\omega - \frac{2\xi}{\alpha_d} \right) \quad (7)$$

Suppose $m = 10,000$ kg, $\omega = 2\pi$ rad/s, and $\xi = 0.1$. Then

$$x = 2(0.1)(2\pi)(10^4) = 12.56 \text{ mN} \cdot \text{s/m}$$

Using a typical value for α_d ,

$$\alpha_d = 0.15$$

leads to

$$k_1 = 84 \text{ kN/m}$$

$$k = 394 - 84 = 310 \text{ kN/m}$$

For these parameters, the viscoelastic element contributes approximately 20% of the stiffness.

Example 4.9 - Example 4.7 revisited

Suppose viscoelastic dampers are used for the 5DOF system considered in Ex. 4.7. The damper force is taken as

$$F_d = k_d u_d + c_d \dot{u}_d = k_d u_d + \alpha_d k_d \dot{u}_d \quad (1)$$

where α_d and k_d depend on the device, and u_d is the displacement of the damper. Consider the case where a chevron brace with two dampers is installed in each floor and the damping distribution

4.5. DAMPING PARAMETERS: DISCRETE SHEAR BEAM

defined by Ex. 4.7 Eq. (4) is used. The damper coefficients are determined by dividing the values listed in Ex. 4.7 Eq. (4) by 2 (two dampers per floor):

$$\begin{aligned} c_{d_1} &= 142.5 \text{ kN} \cdot \text{s/m} & c_{d_2} &= 133 \text{ kN} \cdot \text{s/m} & c_{d_3} &= 114 \text{ kN} \cdot \text{s/m} \\ c_{d_4} &= 85.5 \text{ kN} \cdot \text{s/m} & c_{d_5} &= 47.5 \text{ kN} \cdot \text{s/m} \end{aligned} \quad (2)$$

The damper stiffness is determined with

$$k_d = \frac{1}{\alpha_d} c_d \quad (3)$$

Assuming $\alpha_d = 0.15$, the corresponding values of damper stiffness are

$$\begin{aligned} k_{d_1} &= 950 \text{ kN/m} & k_{d_2} &= 887 \text{ kN/m} & k_{d_3} &= 760 \text{ kN/m} \\ k_{d_4} &= 570 \text{ kN/m} & k_{d_5} &= 317 \text{ kN/m} \end{aligned} \quad (4)$$

The total story shear stiffness distribution is given by Ex. 4.7 Eq. (1). This value is the sum of the elastic stiffness due to frame/brace action and the stiffness due to the two dampers:

$$k = k_e + 2k_d \quad (5)$$

Using (6) and the data from Ex. 4.7, the frame/brace story shear stiffness factors for this choice of α_d are

$$\begin{aligned} k_{e_1} &= 11.69 \text{ MN/m} & k_{e_2} &= 10.93 \text{ MN/m} & k_{e_3} &= 9.35 \text{ MN/m} \\ k_{e_4} &= 7.01 \text{ MN/m} & k_{e_5} &= 3.89 \text{ MN/m} \end{aligned} \quad (6)$$

CHAPTER 4. OPTIMAL PASSIVE DAMPING DISTRIBUTION

The contribution of the damper stiffness is about 14% of the total stiffness for this example.

Example 4.10 - Viscoelastic damper design

Referring back to Eq. (4.30), the elastic stiffness of the damper depends on the *average* storage modulus of the viscoelastic material and a geometric parameter f_d .

$$K_1 = f_d \hat{G}_s \quad (1)$$

Given K_1 and \hat{G}_s , we solve for f_d :

$$f_d = \frac{K_1}{\hat{G}_s} \quad (2)$$

To proceed further, we need to specify the geometry of the device. Fig. E4.10a shows a system consisting of $2n$ layers of a viscoelastic material located between metal plates. Considering the metal elements to be rigid with respect to the viscoelastic elements, the shape factor is given by

$$f_d = 2n \left(\frac{wL_d}{t_d} \right) \quad (3)$$

The layer thickness is usually fixed by the material manufacturer, and therefore the design variables are the number, length, and width of the viscous plates.

4.5. DAMPING PARAMETERS: DISCRETE SHEAR BEAM

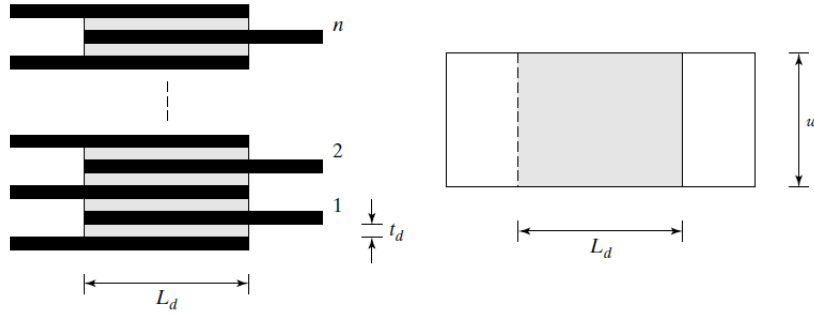


Figure E4.10a

As an illustration, suppose

$$k_{d,1} = 10,000 \text{ kN/m} \quad (4)$$

Taking $\hat{G}_s = 2.5 \text{ MPa}$ as the “average” modulus for 3M ISD110, the corresponding shape factor is

$$f_d = \frac{10,000 \times 10^3}{2.5 \times 10^6} = 4.0 \text{ m} \quad (5)$$

Substituting for f_d in Eq. (3), the variables are related by

$$2n(wL_d) = t_d \cdot f_d = 4.0t_d \text{ (meters)} \quad (6)$$

Suppose $n = 2$ and $t_d = 10^{-2} \text{ m} = 1 \text{ cm}$.

$$wL_d = 1.0 \times 10^{-2} \text{ m}^2 \quad (7)$$

Taking $w = L_d$ results in

$$w = L_d = 0.1 \text{ m} = 10 \text{ cm} \quad (8)$$

Example 4.11 - Hysteretic damper design: diagonal element

CHAPTER 4. OPTIMAL PASSIVE DAMPING DISTRIBUTION

Eq. (4.25) defines the equivalent viscous damping parameter for hysteretic damping. Substituting the extension, e , for the displacement measure u , and solving for the yield force, F_y , results in

$$F_y = \frac{\pi\Omega_r e_r}{4} \left(\frac{\mu}{\mu - 1} \right) C \quad (1)$$

where e_r and Ω_r are *representative* extension and frequency values, and μ is given by

$$\mu = \frac{e_r}{e_y} = \frac{e_r}{L\varepsilon_y} = \frac{e_r \sin \theta}{h\varepsilon_y} \quad (2)$$

where e_y is the extension at which the diagonal material yields.

The representative extension is a function of the representative transverse shear deformation γ_r . Taking γ_r equal to γ^* , the design level for γ , leads to

$$e_r = \gamma^* h \cos \theta \quad (3)$$

and

$$\mu = \left(\frac{\sin 2\theta}{2} \right) \frac{\gamma^*}{\varepsilon_y} \quad (4)$$

A typical design value for γ^* is 1/200. Ideally, we should use a low-strength material so that the response is essentially inelastic throughout the loading duration, thus maximizing the energy dissipation. One potential candidate material is the 100 MPa yield strength steel developed by Nippon Steel [81]; the corresponding yield strain is 1/2000. Using these values and taking $\theta = 45^\circ$ provides an upper bound estimate for the ductility ratio

4.5. DAMPING PARAMETERS: DISCRETE SHEAR BEAM

$$\mu = \frac{2000}{2} \left(\frac{1}{200} \right) = 5 \quad (5)$$

4.5.4 Flexible Structural Members: Linear Viscoelastic Behavior

For completeness, the analysis for the refined viscoelastic model shown in Fig. 4.24 is presented. The component attached to the damper device is modeled as a spring in series with the damper, which is considered to be linear viscoelastic with frequency-dependent properties G_s and η . It is convenient to deal first with a periodic excitation and then average the properties over the appropriate frequency range.

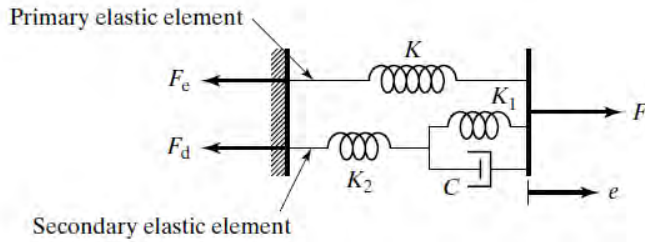


Figure 4.24: General spring-dashpot model.

Letting e_d represent the *displacement* of the damper and considering e_d to be periodic, the corresponding damper force, F_d , follows from Eq. (4.18):

$$\begin{aligned} e_d &= \hat{e}_d \sin \Omega t \\ F_d &= G_s f_d \hat{e}_d (\sin \Omega t + \eta \cos \Omega t) = G_s f_d \hat{e}_d \sin(\Omega t + \delta) \end{aligned} \quad (4.42)$$

where f_d is a characteristic geometric parameter for the device and $\tan \delta = \eta$.

CHAPTER 4. OPTIMAL PASSIVE DAMPING DISTRIBUTION

Since the force in the secondary elastic element must be equal to the damping force, the extensions are related by

$$e - e_d = \frac{F_d}{K_2} \quad (4.43)$$

Substituting for e_d and F_d leads to the expression for the total displacement e :

$$e = e_d + \frac{F_d}{K_2} = \hat{e}_d \left(1 + \frac{G_d f_d}{K_2} \right) \sin \Omega t + \hat{e}_d \left(\frac{G_s f_d}{K_2} \right) \eta \cos \Omega t \quad (4.44)$$

Eq. (4.44) can also be written as

$$e = \hat{e} \sin(\Omega t + \delta_1) \quad (4.45)$$

where

$$\hat{e} = \hat{e}_d \sqrt{\left(1 + \frac{G_s f_d}{K_2} \right)^2 + \left(\frac{\eta G_s f_d}{K_2} \right)^2} = \aleph \hat{e}_d \quad (4.46)$$

$$\tan \delta_1 = \eta \left(\frac{1}{1 + \frac{K_2}{G_s f_d}} \right)$$

The force in the primary elastic element depends only on e :

$$F_e = K e = K \hat{e} \sin(\Omega t + \delta_1) \quad (4.47)$$

Combining F_e and F_d , the total force is given by

$$F = F_e + F_d = K \hat{e} \sin(\Omega t + \delta_1) + G_s f_d \hat{e}_d \sin(\Omega t + \delta) \quad (4.48)$$

A more compact form for F is

4.5. DAMPING PARAMETERS: DISCRETE SHEAR BEAM

$$F = \hat{K} \hat{e} \sin(\Omega t + \delta_1 + \delta_2) \quad (4.49)$$

where δ_2 represents the phase shift between the excitation and the force response, and \hat{K} is the total stiffness measure. The definition equations are

$$\hat{K} = \sqrt{\left(K \cos \delta_1 + \frac{G_s f_d}{\aleph} \cos \delta\right)^2 + \left(K \sin \delta_1 + \frac{G_s f_d}{\aleph} \sin \delta\right)^2} \quad (4.50)$$

$$\tan(\delta_1 + \delta_2) = \frac{K \sin \delta_1 + \frac{G_s f_d}{\aleph} \sin \delta}{K \cos \delta_1 + \frac{G_s f_d}{\aleph} \cos \delta} = \aleph \quad (4.51)$$

$$\tan \delta_2 = \frac{\frac{\aleph}{\tan \delta_1} - 1}{\aleph + \frac{1}{\tan \delta_1}} \quad (4.52)$$

The equations can be expressed in conventional form by shifting the time reference point. Defining t' as

$$t = t' - \frac{\delta_1}{\Omega} \quad (4.53)$$

transforms Eqs. (4.45) and (4.49) to

$$\begin{aligned} e &= \hat{e} \sin \Omega t' \\ F &= \hat{K} \hat{e} \sin(\Omega t' + \delta_2) \end{aligned} \quad (4.54)$$

Finally, expanding Eq. (4.54), the result can be expressed in a form similar to the conventional viscoelastic form:

$$F = K_s \hat{e} \sin \Omega t' + \bar{\eta} K_s \hat{e} \cos \Omega t' \quad (4.55)$$

CHAPTER 4. OPTIMAL PASSIVE DAMPING DISTRIBUTION

where

$$\begin{aligned} K_s &= \hat{K} \cos \delta_2 \\ \bar{\eta} &= \tan \delta_2 \end{aligned} \tag{4.56}$$

We can interpret K_s as the *storage* stiffness and $\bar{\eta}$ as the loss factor for the assemblage.

Equivalent parameters can be generated following the procedure described in Sect. 4.4. We write

$$F = K_{\text{eq}}e + C_{\text{eq}}\dot{e} \tag{4.57}$$

and equate Eq. (4.57) with (4.55). The error terms for a periodic excitation are

$$E_1 = K_{\text{eq}} - K_s \tag{4.58}$$

$$E_2 = C_{\text{eq}} - \frac{\bar{\eta}K_s}{\Omega} \tag{4.59}$$

Minimizing the sum of the square of these terms over the frequency range with respect to K_{eq} and C_{eq} produces the following expressions:

$$K_{\text{eq}} = K_s|_{\text{average}} \equiv \frac{1}{N} \sum_{i=1}^N K_s(\Omega_i) \tag{4.60}$$

$$C_{\text{eq}} = \frac{1}{N} \sum_{i=1}^N \frac{\bar{\eta}_i K_{s,i}(\Omega_i)}{\Omega_i} \tag{4.61}$$

where N is the number of frequencies composing the data set. If we consider K_2 to be very large with respect to the viscoelastic damper stiffness, $G_s f_d$, the various terms simplify to

4.5. DAMPING PARAMETERS: DISCRETE SHEAR BEAM

$$\begin{aligned} \aleph &\approx 1 \\ \delta_1 &\approx 0 \\ \hat{K} &\approx K \sqrt{1 + \frac{2G_s f_d}{K} \cos \delta + \left(\frac{G_s f_d}{K}\right)^2} \\ \bar{\eta} = \tan \delta_2 = \aleph &= \eta \left(\frac{1}{1 + \frac{K}{G_s f_d \cos \delta}} \right) \end{aligned} \quad (4.62)$$

Example 4.12 - Coupled spring-damper model

This example considers the case where the damper is viscous, and the structural element connecting the damper to the floors is flexible. This is a simplified version of the model considered previously; the stiffness component of the viscoelastic device is deleted (Fig. E4.12a).

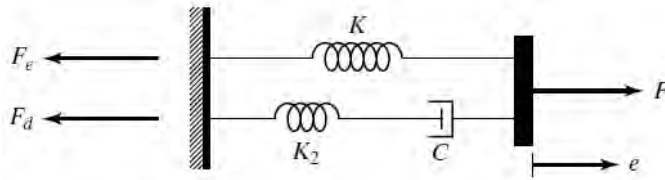


Figure E4.12a

The steps are similar to the previous steps. We take

$$e_d = \hat{e}_d \sin \Omega t \quad (1)$$

Then,

$$\begin{aligned}
 F_d &= C\Omega\hat{e}_d \cos \Omega t \\
 e &= \hat{e} \sin(\Omega t + \delta_1) \\
 \hat{e} &= \hat{e}_d \left[1 + \left(\frac{C\Omega}{K_2} \right)^2 \right]^{1/2} \\
 \tan \delta_1 &= \frac{C\Omega}{K_2}
 \end{aligned} \tag{2}$$

The total force is expressed as

$$F = \hat{K} \hat{e} \sin(\Omega t + \delta_1 + \delta_2) \tag{3}$$

where

$$\hat{K} = K \cos \delta_1 \left[1 + \left(\tan \delta_1 + \frac{C\Omega}{K} \right)^2 \right]^{1/2} \tag{4}$$

$$\tan \delta_2 = \frac{C\Omega}{K} \cdot \frac{1}{1 + (C\Omega)^2 \left(\frac{1}{K_2} \right) \left(\frac{1}{K_2} + \frac{1}{K} \right)} \tag{5}$$

The remaining steps are the same. We express F as

$$F = K_{\text{eq}} e + C_{\text{eq}} \dot{e} \tag{6}$$

and determine K_{eq} and C_{eq} using Eq. (4.61).

When $K_2 = \infty$, $\delta_1 = 0$ and

$$\tan \delta_2 = \frac{C\Omega}{K} \quad \cos \delta_2 = \frac{K}{\hat{K}} \tag{7}$$

Then

$$K_s = K \quad \bar{\eta} K_s = C\Omega \tag{8}$$

4.6. DAMPING PARAMETERS: TRUSS BEAM

and

$$K_{\text{eq}} \equiv K \quad C_{\text{eq}} \equiv C \quad (9)$$

4.6 Damping Parameters: Truss Beam

This section extends the treatment of the truss-beam discussed in Ex. 2.2 to include damping. The typical panel shown in Fig. 4.25. is considered to be composed of *two* sets of elements: an elastic system, which provides the stiffness (shear and bending), and a second system, which functions as a distributed energy dissipation/ absorption mechanism.

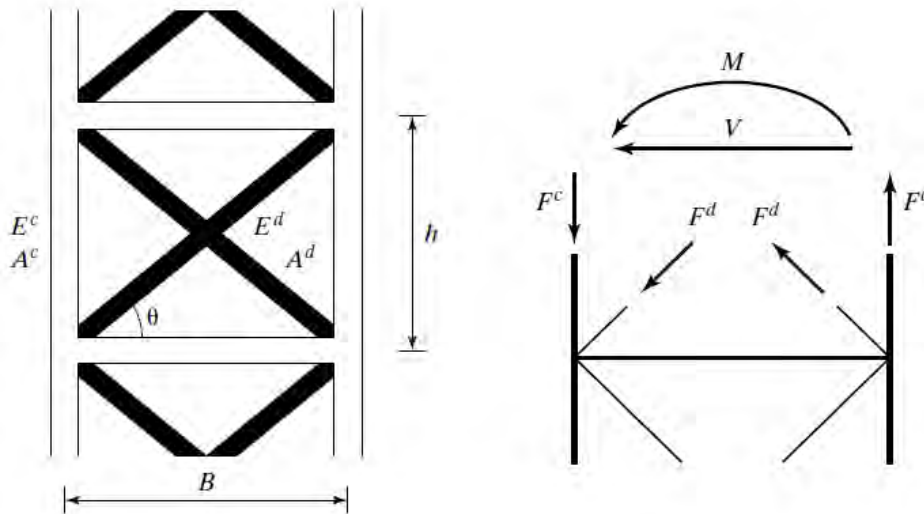


Figure 4.25: Truss-beam structure: geometry and forces.

The various force quantities are determined with

$$\begin{aligned}
 F^d &= F_e^d + F_d^d \\
 F^c &= F_e^c + F_d^c \\
 V &= 2F^d \cos \theta \\
 M &= BF^c
 \end{aligned}
 \tag{4.63}$$

where superscripts c and d refer to the column and diagonal elements, and subscripts e and d denote the elastic and damping force components.

Defining e as the extension (i.e., the total change in length of a structural element), and noting Ex. 2.2 Eqs. (7) and (10), the extensions for the diagonal and chord elements are related to the transverse shear and bending deformations by

$$\begin{aligned}
 e^d &= \gamma h \cos \theta \\
 e^c &= \frac{Bh}{2} \chi
 \end{aligned}
 \tag{4.64}$$

The elastic force is a function of e and the element properties

$$F_e = \left(\frac{AE}{L} \right) e = K \cdot e
 \tag{4.65}$$

where L denotes the length, A the cross-sectional area, and E the Young's modulus for the elastic element.

4.6.1 Linear Viscous Behavior

The *dissipative* force-deformation relation depends on the nature of the damping device. For viscous behavior, F_d is a function of \dot{e} . The linear viscous force is expressed as

$$F_d = C\dot{e}
 \tag{4.66}$$

4.6. DAMPING PARAMETERS: TRUSS BEAM

where C is a property of the device, which may be an actual viscous damper, or an *equivalent* viscous coefficient. Summing the elastic and damping forces leads to the element force-extension relations

$$\begin{aligned} F^c &= K^c e^c + C^c \dot{e}^c \\ F^d &= K^d e^d + C^d \dot{e}^d \end{aligned} \quad (4.67)$$

We can associate these relations with the parallel spring/dashpot model shown in Fig. 4.22. The member force-deformation relations are obtained by introducing these expressions into the definition equations for V and M . They are written as

$$\begin{aligned} V &= D_T \gamma + C_T \dot{\gamma} \\ M &= D_B \chi + C_B \dot{\chi} \end{aligned} \quad (4.68)$$

where

$$\begin{aligned} D_T &= (2h \cos^2 \theta) K^d \\ C_T &= (2h \cos^2 \theta) C^d \\ D_B &= \frac{B^2 h}{2} K^c \\ C_B &= \frac{B^2 h}{2} C^c \end{aligned}$$

It is convenient to express the damping coefficients in terms of the stiffness parameters,

$$\begin{aligned} C_T &= \alpha_T D_T \\ C_B &= \alpha_B D_B \end{aligned} \quad (4.69)$$

where α_T and α_B follow from the previous equations:

$$\begin{aligned}\alpha_T &= \frac{C^d}{K^d} \\ \alpha_B &= \frac{C^c}{K^c}\end{aligned}\tag{4.70}$$

Note that α_T and α_B depend on the damping device configuration and stiffness of the diagonal and chord elements. Expressing C in terms D of and taking α constant over the height simplifies the analysis of the beam as a continuum using modal shape functions by uncoupling the equations for the modal coordinates.

4.6.2 Linear Viscoelastic Behavior

The case where the damping mechanism is viscoelastic is represented by the model shown in Fig. 4.23. Here, the damping force has an elastic component as well as a viscous component and is expressed as

$$F_d = K_1 e + C \dot{e} = K_1 e + \alpha_d K_1 \dot{e}\tag{4.71}$$

where K_1 and α_d are the *equivalent* stiffness and damping parameters for the device, and e is the total extension of the member. This formulation assumes the viscous device is attached to a rigid element so that all the deformation occurs in the device. Using Eq. (4.71), we obtain

$$\begin{aligned}F^c &= (K^c + K_1^c) e^c + \alpha_d^c K_1^c \dot{e}^c \\ F^d &= (K^d + K_1^d) e^d + \alpha_d^d K_1^d \dot{e}^d\end{aligned}\tag{4.72}$$

Substituting for the forces and deformations leads to

4.6. DAMPING PARAMETERS: TRUSS BEAM

$$\begin{aligned}D_T &= (2h \cos^2 \theta) (K^d + K_1^d) \\C_t &= (2h \cos^2 \theta) \alpha_d^d K_1^d \\D_B &= \frac{B^2 h}{2} (K^c + K_1^c) \\C_B &= \frac{B^2 h}{2} \alpha_d^c K_1^c\end{aligned}\tag{4.73}$$

The proportionality factors in this case are given by

$$\begin{aligned}\alpha_B &= \frac{C_B}{D_B} = \alpha_d^c \left(\frac{K_1^c / K^c}{1 + K_1^c / K^c} \right) \\ \alpha_T &= \frac{C_T}{D_T} = \alpha_d^d \left(\frac{K_1^d / K^d}{1 + K_1^d / K^d} \right)\end{aligned}\tag{4.74}$$

Problems

Problem 4.1

Consider a SDOF system. The total stored energy is the sum of the kinetic energy and the strain energy.

$$\begin{aligned}\text{Stored energy} &= E_S + E_K \\ &= \left(\frac{1}{2}ku^2 + \frac{1}{2}m\dot{u}^2 \right)\end{aligned}$$

Note that E_S and E_K are out of phase for periodic excitation. Suppose there is a rapid build-up of strain energy during the initial phase of a seismic excitation, and the design objective is to limit u_{\max} to a target value, u^* . What strategy would you apply? Assume the mass cannot be varied. Illustrate your strategy for a SDOF system subjected to an Impulse, I_0 at time $t = 0$. The corresponding solution is

$$u(t) = \frac{I_0}{m\omega'} e^{-\xi\omega t} \sin \omega' t \quad \text{where } \omega' = \omega \sqrt{1 - \xi^2}$$

Problem 4.2

Give examples of energy dissipation and absorption devices that are used in structures such as vehicles, crash barriers, machine supports, buildings, and bridges.

Problem 4.3

Consider a SDOF system having a linear spring and linear viscous damper. Suppose the initial conditions at $t = 0$ are

$$u(0) = 0 \quad \dot{u}(0) = \dot{u}^*$$

4.6. DAMPING PARAMETERS: TRUSS BEAM

and there is no external loading (Fig. P4.3a).

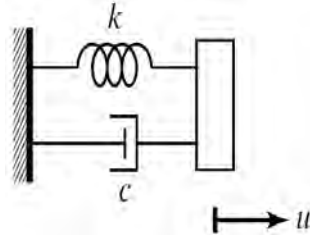


Figure P4.3a

1. Determine the expression for the free vibration response corresponding to these initial conditions.
2. Construct a plot of \dot{u} versus u for t ranging from 0 to $4\pi/\omega$. Comment on the influence of damping on the time history response. Illustrate for $m = 1,000$ kg, $k = 9,000$ kN/m.

Problem 4.4

Refer to Problem 4.3. Suppose the device is a Coulomb function damper.

1. Determine the free vibration response. Since the sense of the friction force is determined by the sense of the velocity, we need to generate solutions for different time intervals. During the first interval, $0 \leq t \leq t_1$, the velocity is positive.
2. Construct a plot of \dot{u} versus u for t sufficient to include one full cycle.

Problem 4.5

The SDOF system shown in Fig. P4.5a is subjected to a periodic

CHAPTER 4. OPTIMAL PASSIVE DAMPING DISTRIBUTION

force. Determine the expressions for the spring and damper forces. Let F denote the total internal force.

$$F = F_s + F_d$$

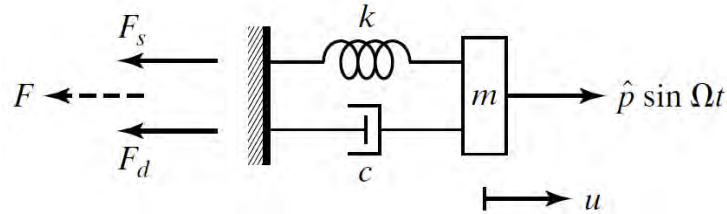


Figure P4.5a

Determine the expression for F . Compare the magnitude of F with the magnitudes of F_s and F_d .

Problem 4.6

Refer to Ex. 4.3. Consider material 1 to be low-strength steel with $\sigma_y = 200$ MPa, and material 2 to have $\sigma_y = 500$ MPa steel. Design a hysteretic damper for the following criteria:

$$F_y = 100 \text{ kN}$$

$$L_1 + L_2 = 5 \text{ m}$$

$$k_h = 6000 \text{ kN/m}$$

Problem 4.7

Design a viscoelastic damper for the following conditions:

- Temperature = 20°
- Frequency excitation = 1 Hz
- Material 3M-ISD110

4.6. DAMPING PARAMETERS: TRUSS BEAM

- Maximum displacement = 0.025 m
- Maximum force = 10 kN

Problem 4.8

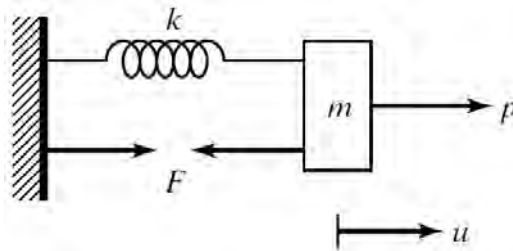


Figure P4.8a

The SDOF system shown in Fig. P4.8a has a linear viscoelastic damper that produces the force F . Assume $u = \hat{u} \sin \Omega t$ and use F given by Eq. (4.18). Determine p .

Problem 4.9

A convenient way of dealing with periodic excitation is to introduce complex notation. The basic identity is

$$e^{i\theta} = \cos \theta + i \sin \theta$$

where θ is an arbitrary scalar. Using this notation, an arbitrary periodic forcing can be expressed in terms of a complex amplitude, \bar{p} :

$$\begin{aligned} p &= \bar{p}e^{i\Omega t} = (\hat{p}e^{i\delta}) e^{i\Omega t} = \hat{p}e^{i(\Omega t + \delta)} \\ &= \hat{p} (\cos(\Omega t + \delta) + i \sin(\Omega t + \delta)) \end{aligned}$$

CHAPTER 4. OPTIMAL PASSIVE DAMPING DISTRIBUTION

We can work with the complex form and then retain either the real term (for cosine forcing) or the imaginary term (for sine forcing).

1. Consider a 1DOF system having a spring and linear viscous damper in parallel (Fig. P4.9a). Suppose p is a general periodic excitation, $p = \bar{p}e^{i\Omega t}$. Let $u = \bar{u}e^{i\Omega t}$ represent the response. Express the relationship between p and u as $\bar{p} = \bar{K}\bar{u}$, where \bar{K} is the complex system stiffness. Determine \bar{K} .

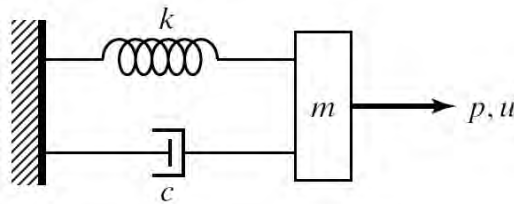


Figure P4.9a

2. Consider a linear spring and viscous damper in series (Fig. P4.9b). Determine \bar{K} .

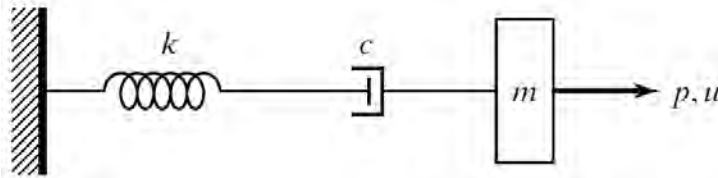


Figure P4.9b

3. Refer to part 1. Express the relationship between p and u as $\bar{u} = \bar{H}\bar{p}$. Determine $\bar{H} = \hat{H}e^{i\alpha}$. Suppose the loading consists of a set of periodic excitations,

4.6. DAMPING PARAMETERS: TRUSS BEAM

$$p = \bar{p}_1 e^{i\Omega_1 t} + \bar{p}_2 e^{i\Omega_2 t} + \dots + \bar{p}_n e^{i\Omega_n t}$$

Express u in terms of \bar{p}_j and \bar{H}_j . Discuss how you would evaluate u at some time t for a cosine forcing (i.e., the loading corresponding to the real part of p).

Problem 4.10

Eqs. (4.14) and (4.15) define the stress-strain response of a linear viscoelastic material to periodic sinusoidal excitation. Using complex notation, we can generalize these equations for arbitrary periodic excitation, $\gamma = \bar{\gamma} e^{i\Omega t}$, where $\bar{\gamma}$ is the complex amplitude. The complex shear modulus is defined as

$$\bar{G} = \hat{G} e^{i\delta}$$

where

$\tan \delta = \eta$, the loss factor

$$\hat{G} = [G_s^2 + G_l^2]^{1/2}$$

With these definitions, the shear stress can be written as

$$\tau = \bar{\tau} e^{i\Omega t}$$

$$\bar{\tau} = \bar{G} \bar{\gamma}$$

1. Consider a linear viscoelastic damper subjected to periodic excitation, $u = \bar{u} e^{i\Omega t}$. Express the damper force as $F = \bar{F} e^{i\Omega t}$ and let $\bar{F} = \bar{k}_v \bar{u}$. Determine \bar{k}_v by generalizing Eq. (4.18).

CHAPTER 4. OPTIMAL PASSIVE DAMPING DISTRIBUTION

2. Consider a SDOF system having a spring and linear viscoelastic device in parallel (Fig. P4.10a). Assume is a general periodic excitation and let $\bar{p} = \bar{K}\bar{u}$. Determine \bar{K} . Equate this result to the result for a linear spring and linear viscous damper in parallel (see Fig. P4.10b), and determine the equivalent stiffness and damping factors, k' and c' .

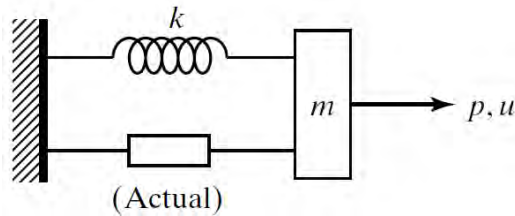


Figure P4.10a

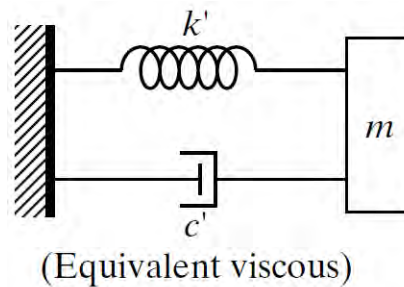


Figure P4.10b

3. Consider a linear spring and linear viscoelastic device in series (Fig. P4.10c). Determine \bar{K} .

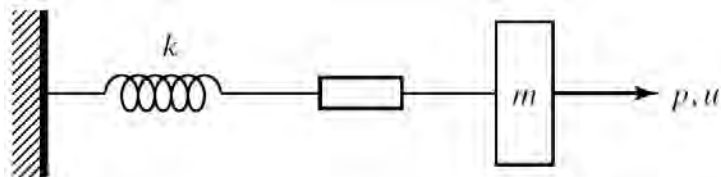


Figure P4.10c

4.6. DAMPING PARAMETERS: TRUSS BEAM

4. Consider a SDOF system having a linear spring in parallel with a linear spring/linear viscoelastic device (Fig. P4.10d). Determine \bar{K} .

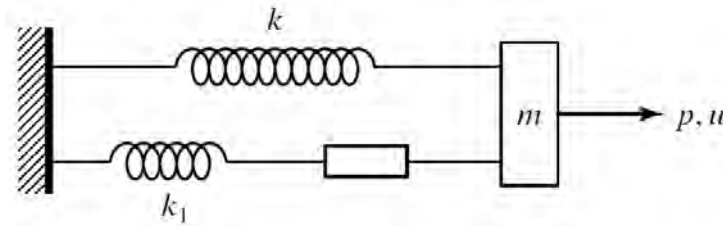


Figure P4.10d

Problem 4.11

Consider a single-degree-of-freedom system having $m = 1000$ kg and $k = 36$ kN/m. This problem concerns designing various types of damping devices. Assume the system is to be subjected to seismic excitation, and the design objective is a damping ratio of 0.1. Take $S_D = 0.25$ m as the response for pure viscous damping with $\xi = 0.1$. Propose damper properties for the following cases:

1. Viscous
2. Structural
3. Coulomb
4. Hysteretic with $\mu = 5$

Discuss the basis for your recommendations.

Problem 4.12

Refer to Problem 4.10, part 2. Take $m = 2000$ kg and $k = 25$ kN/m. Determine the equivalent stiffness and viscous damping

CHAPTER 4. OPTIMAL PASSIVE DAMPING DISTRIBUTION

coefficients for the case where the material is 3M ISD110, the excitation frequency ranges from 0.5 Hz to 5 Hz, and $f_d = 10^{-2}m$.

Problem 4.13

Refer to Problem 4.10, part 2. Suppose $m = 4000$ kg and $k = 50$ kN/m. Design a viscoelastic damper to produce an equivalent viscous damping of 3 kN·s/m at an excitation frequency of 2 Hz. Use 3M ISD110 material. Also determine the corresponding equivalent stiffness.

Problem 4.14

Refer to Problem 4.10, part 2. The equivalent stiffness and viscous damping coefficients corresponding to a periodic excitation of frequency Ω are

$$k' = k + f_d G_s \quad (10)$$

$$c' = \frac{\eta f_d G_s}{\Omega} \quad (11)$$

where G_s and η are functions of Ω . Suppose we want to approximate these coefficients with constant values over the frequency range of interest.

$$k'(\Omega) \approx k^* \quad (12)$$

$$c'(\Omega) \approx c^* \quad (13)$$

Show that a least squares approximation leads to

$$k^* = k + k_{\text{eq}} \quad (14)$$

$$c^* = c_{\text{eq}} \quad (15)$$

where k_{eq} and c_{eq} are defined by Eqs. (4.30) and (4.31).

Problem 4.15

4.6. DAMPING PARAMETERS: TRUSS BEAM

Consider a SDOF system having a spring and a viscoelastic damper modeled as shown in Fig. P4.15a. Take $c = \alpha_d k_1$.

1. Determine expressions for the fundamental frequency, ω , and damping ratio, ξ .
2. Suppose $m = 1000$ kg and $k = 9$ kN/m. Determine the damper properties c and k_1 that correspond to a damping ratio of 0.1. Take $\alpha_d = 0.15$. Also determine the fundamental frequency.
3. Suppose $m = 1000$ kg and the total stiffness, $k + k_1$, is equal to 9 kN/m. Determine the stiffness and damping parameters required for $\xi = 0.1$. Take $\alpha_d = 0.15$.

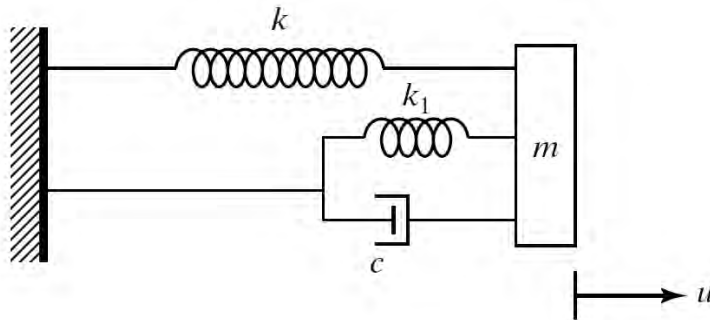


Figure P4.15a

Problem 4.16

Refer to Ex. 4.12.

1. Take $C = 600$ N·s/m. Determine K_{eq} and C_{eq} corresponding to a periodic excitation, $\Omega = 2\pi$ rad/s, and the following values for stiffness:
(a) $K = 9$ kN/m; $K_2 = 4.5$ kN/m

CHAPTER 4. OPTIMAL PASSIVE DAMPING DISTRIBUTION

(b) $K = 9 \text{ kN/m}$; $K_2 = 18 \text{ kN/m}$

(c) $K = 9 \text{ kN/m}$; $K_2 = \infty \text{ kN/m}$

2. Suppose $m = 1000 \text{ kg}$. Determine ω and ξ corresponding to the values of K_{eq} and C_{eq} obtained in part 1.

Problem 4.17

Consider the truss beam segment shown in Fig. P4.17a. Assume the diagonal bracing system consists of elastic elements and linear viscous dampers attached to rigid links connecting the end nodes. Dimension the elastic element and damper for the following requirements:

$$D_T = 260 \times 10^3 \text{ kN}$$

$$C_T = 4 \times 10^3 \text{ kN} \cdot \text{s/m}$$

Use steel for the elastic element.

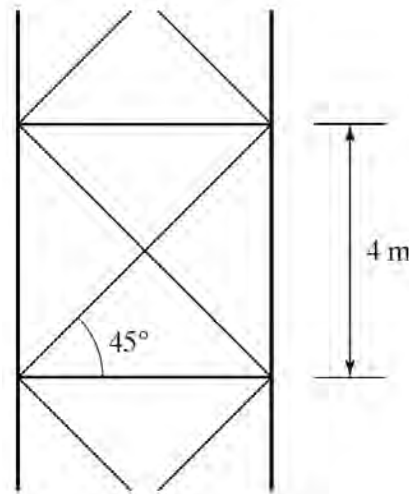


Figure P4.17a

4.6. DAMPING PARAMETERS: TRUSS BEAM

Problem 4.18

Refer to Problem 4.17. Assume the diagonal bracing system consists of elastic elements and linear viscoelastic elements. Dimension the components for the requirements specified in Problem 4.17. Use equivalent stiffness and damping parameters for the viscoelastic component, and take $\alpha_d = 0.15$.

Problem 4.19

Consider a structural system composed of two subsystems: The first is linear elastic and provides only stiffness; the second system is linear viscoelastic and provides both stiffness and damping. Let \mathbf{K}_e denote the stiffness matrix for the elastic component and \mathbf{K}_1, \mathbf{C} the stiffness and damping matrices for the viscoelastic component. The equations of motion are

$$\mathbf{M}\ddot{\mathbf{U}} + \mathbf{C}\dot{\mathbf{U}} + (\mathbf{K}_e + \mathbf{K}_1)\mathbf{U} = \mathbf{P} \quad \text{(P19.1)}$$

where \mathbf{C} is related to \mathbf{K}_1 . Specializing Eq. (P19.1) for free vibration and expressing the solution as

$$\mathbf{U} = A e^{\lambda t} \Phi \quad \text{(P19.2)}$$

leads to the following equation:

$$[\lambda^2 \mathbf{M} + \lambda \mathbf{C} + (\mathbf{K}_e + \mathbf{K}_1)] \Phi = \mathbf{0} \quad \text{(P19.3)}$$

The solution for the primary elastic system is expressed as

$$\begin{aligned} \lambda &= \pm i\omega & |\omega| > 0 \\ (\mathbf{K}_e - \omega^2 \mathbf{M})\Phi_e &= \mathbf{0} \end{aligned} \quad \text{(P19.4)}$$

1. Consider the pure elastic case, $\mathbf{C} = \mathbf{0}$ and $\mathbf{K}_1 \neq \mathbf{0}$. Determine the corresponding λ and Φ for the case where \mathbf{K}_1 is a scalar multiple of \mathbf{K}_e , say $\mathbf{K}_1 = \alpha_1 \mathbf{K}_e$.

CHAPTER 4. OPTIMAL PASSIVE DAMPING DISTRIBUTION

2. Consider the pure viscous case $\mathbf{C} \neq \mathbf{0}$ and $\mathbf{K}_1 = \mathbf{0}$. Take $\mathbf{C} = \alpha_2 \mathbf{K}_e$. Determine λ and Φ . Express λ as

$$\lambda = -\xi\omega \pm i\omega' \quad \text{(P19.5)}$$

3. Consider the linear viscoelastic case. Take $\mathbf{C} = \alpha_d \mathbf{K}_1$, where α_d is a material parameter. Assume stiffness proportional damping and consider two cases:

- (a) $\mathbf{C} = \alpha_2 \mathbf{K}_e$
(b) $\mathbf{C} = \alpha_3 (\mathbf{K}_e + \mathbf{K}_1)$

Determine expressions for the corresponding λ and Φ .

Problem 4.20

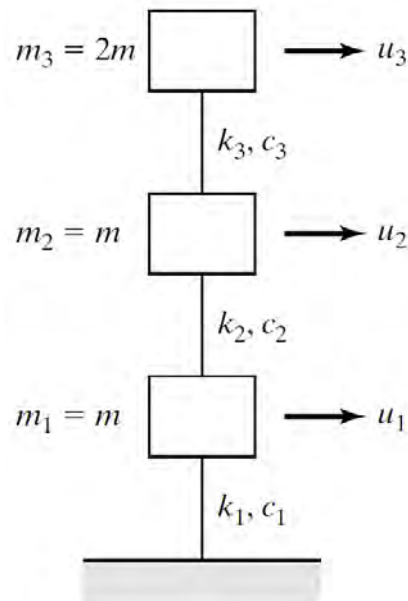


Figure P4.20a

Consider the 3DOF system shown in Fig. P4.20a.

4.6. DAMPING PARAMETERS: TRUSS BEAM

1. Determine the magnitudes of k_1 , k_2 , and k_3 such that the first mode has the form

$$\Phi_1 = \left\{ \frac{1}{3}, \frac{2}{3}, 1 \right\}$$

and the fundamental frequency is 2π rad/s. Take $m = 2000$ kg.

2. Determine the viscous damping coefficients c_1 , c_2 , and c_3 such that the damping ratio, ξ_1 , for the first mode is 0.1. Consider both stiffness proportional damping and uniform damping. Use MATLAB to determine the modal properties for the case of nonproportional damping.
3. Suppose viscoelastic dampers are used. Let k_d and c_d denote the equivalent stiffness and damping coefficients, and take $c_d = \alpha_d k_d$, where α_d is a material property. Determine $c_{d,i}$ and the elastic stiffness $k_{e,i}$ for each element. Assume $\alpha_d = 0.15$. Consider stiffness proportional damping and uniform damping. Compare the modal properties for these two cases.

Problem 4.21

Refer to Ex. 4.7. Use MATLAB to determine the modal properties for the first three modes. Take k_i according to Ex. 4.7 Eq. (1) and based on

1. Damping proportional to stiffness
2. Uniform damping
3. $c_1 = c_2 = 0$ and $c_3 = c_4 = c_5$

CHAPTER 4. OPTIMAL PASSIVE DAMPING DISTRIBUTION

4. Other combinations of the c' that you believe may be more optimal in the sense of resulting in higher damping ratios for the higher modes.

Problem 4.22

Refer to Ex. 4.7. Suppose viscoelastic dampers are used for elements 3, 4, 5 and there is no damping in elements 1 and 2. Assume uniform viscoelastic damper properties and take $\alpha_d = 0.15$. Starting with the data contained in Ex. 4.7 Eq. (1), determine the damper properties and modified elastic stiffness that correspond to a damping ratio of 0.1 for the fundamental mode. Using MATLAB, assess the effect of nonproportional damping on the mode shape for this design value of ξ_1 . What would be the effect if ξ_1 is increased to 0.2 and the stiffness is maintained at the level defined by Eq. (1) of Ex. 4.7?

Problem 4.23

This problem concerns the preliminary design of a 10-story rectangular rigid frame for seismic excitation (Fig. P4.23a). The frame properties and design criteria are

- Height = 5 m/story
- Width = 10 m/bay
- Mass/floor = 10,000 kg
- Max. deflection at top = 0.25 m
- Max. story shear deformation = 1/200
- Response spectrum defined by Fig. 3.23.

4.6. DAMPING PARAMETERS: TRUSS BEAM

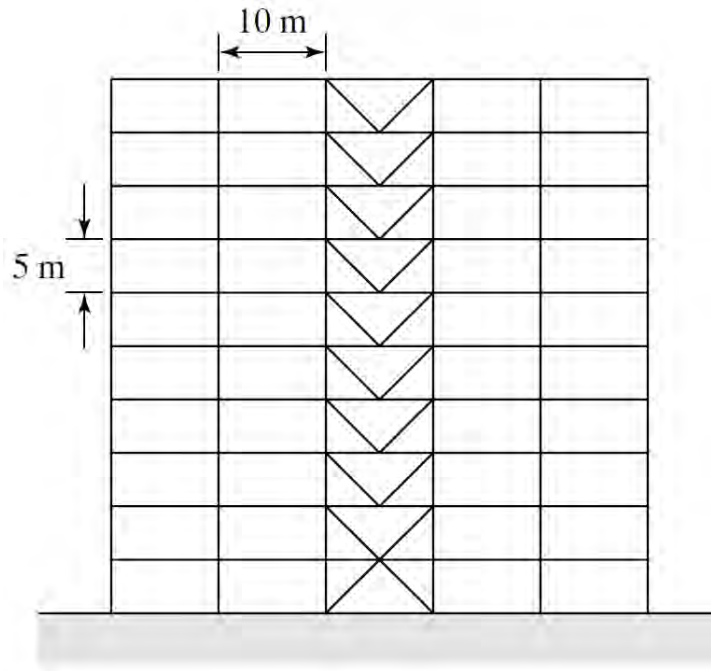


Figure P4.23a

The chevron bracing system is similar to the scheme shown in Fig. 4.19(b); it allows two viscous dampers to be placed on each floor.

1. Determine the stiffness distributions based on a linear fundamental mode profile and ξ equal to 0.02, 0.10, and 0.20. Evaluate the stiffness cost, $\sum k_i$, for each distribution.
2. Assume stiffness proportional damping. Determine the corresponding distributions for the story damping coefficients and the damping cost, $\sum c_1$.
3. Repeat part 2. for uniform damping. Using MATLAB, determine the properties for the fundamental mode. Compare the displacement profiles .

CHAPTER 4. OPTIMAL PASSIVE DAMPING DISTRIBUTION

- Repeat part 2. for $c_1 = c_2 = c_3 = c_4 = c_5 = 0$ and $c_6 = c_7 = c_8 = c_9 = c_{10} = c^*$, where c^* is a constant value. Determine the actual damping ratio and profile for the fundamental mode.
- The damper cost increases nonlinearly with the damper coefficient (i.e., the cost for $2c$ is more than twice the cost for c). Also, the damper force increases with c and places more loading on the brace-floor connection. With these limitations, discuss how you would select a damper placement that satisfies the performance requirement on the maximum transverse shear deformation for each story and minimizes a “cost” function.

Problem 4.24

Consider a 5DOF shear beam having equal masses and equal nodal forces. Suppose the force consists of a combination of a static component and a periodic excitation,

$$p = p_s + p_d \sin \omega t$$

where ω is a random quantity. Take

$$m_i = 10,000 \text{ kg}$$

$$p_s = 100 \text{ kN}$$

$$p_d = 1 \text{ kN}$$

- Determine the stiffness distribution such that the interstory displacement under the static loading is 0.02 m for each story.

4.6. DAMPING PARAMETERS: TRUSS BEAM

2. Assume ω coincides with the frequency for the fundamental mode corresponding to the stiffness distribution generated in part 1. Suppose the design objective is to have the peak acceleration less than $0.02g$, where g is the acceleration due to gravity and is equal to 9.87 m/s^2 . Suggest various schemes for generating the required energy dissipation. Comment on what you consider to be the optimal solution.

5

Tuned Mass Damper Systems

5.1 Introduction

A tuned mass damper (TMD) is a device consisting of a mass, a spring, and a damper that is attached to a structure in order to reduce the dynamic response of the structure. The frequency of the damper is tuned to a particular structural frequency so that when that frequency is excited, the damper will resonate out of phase with the structural motion. Energy is dissipated by the damper inertia force acting on the structure. The TMD concept was first applied by Frahm in 1911 [32] to reduce the rolling motion of ships as well as ship hull vibrations. A theory for the TMD was presented later in the paper by Ormondroyd & Den Hartog [82], followed by a detailed discussion of optimal tuning and damping parameters in Den Hartog's book on Mechanical Vibrations [26]. The initial theory was applicable for an undamped SDOF system subjected to a sinusoidal force excitation. Extension of the theory to damped SDOF systems has been investigated by numerous researchers. Significant contributions were made by Randall et al. [87], Warburton [111, 109, 110], and Tsai & Lin [104]. More recently, the theory has been extended to include new types of dampers that rely on liquid motion to generate the inertia force.

This chapter starts with an introductory example of a TMD design and a brief description of some of the implementations of tuned mass dampers in building structures. A rigorous theory of tuned mass dampers for SDOF systems subjected to harmonic force excitation and harmonic ground motion is discussed next. Various cases including a damped TMD attached to an undamped SDOF system, and a damped TMD attached to a damped SDOF system are considered. Time history responses for a range of

5.2. AN INTRODUCTORY EXAMPLE

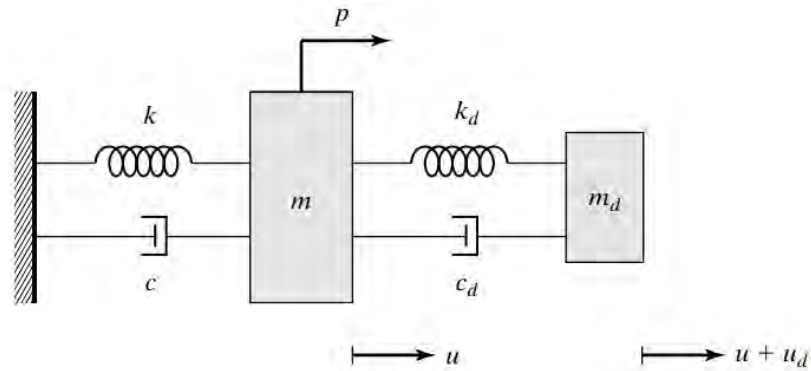


Figure 5.1: SDOF - TMD system.

SDOF systems connected to optimally tuned TMD and subjected to harmonic and seismic excitations are presented. The theory is then extended to MDOF systems where the TMD is used to dampen out the vibrations of a specific mode. Lastly, a theory for tuned liquid column dampers is presented and design procedures are suggested.

5.2 An Introductory Example

In this section, the concept of the tuned mass damper is illustrated using the two-mass system shown in Fig. 5.1. Here, the subscript d refers to the *tuned mass damper*; the structure is idealized as a single degree of freedom system. Introducing the following notation

$$\omega^2 = \frac{k}{m} \quad (5.1)$$

$$c = 2\xi\omega m \quad (5.2)$$

$$\omega_d^2 = \frac{k_d}{m_d} \quad (5.3)$$

CHAPTER 5. TUNED MASS DAMPER SYSTEMS

$$c_d = 2\xi_d\omega_d m_d \quad (5.4)$$

and defining \bar{m} as the mass ratio,

$$\bar{m} = \frac{m_d}{m} \quad (5.5)$$

the governing equations of motion are given by

$$\text{primary mass} \quad (1 + \bar{m})\ddot{u} + 2\xi\omega\dot{u} + \omega^2 u = \frac{p}{m} - \bar{m}\ddot{u}_d \quad (5.6)$$

$$\text{tuned mass} \quad \ddot{u}_d + 2\xi_d\omega_d\dot{u}_d + \omega_d^2 u_d = -\ddot{u} \quad (5.7)$$

The purpose of adding the mass damper is to limit the motion of the structure when it is subjected to a particular excitation. The design of the mass damper involves specifying the mass m_d , stiffness k_d , and damping coefficient c_d . The optimal choice of these quantities is discussed in Section 5.4. In this example, the near-optimal approximation for the frequency of the damper,

$$\omega_d = \omega \quad (5.8)$$

is used to illustrate the design procedure. The stiffnesses for this frequency combination are related by

$$k_d = \bar{m}k \quad (5.9)$$

Eq. (5.8) corresponds to tuning the damper to the fundamental period of the structure.

Considering a periodic excitation,

$$p = \hat{p} \sin \Omega t \quad (5.10)$$

the response is given by

5.2. AN INTRODUCTORY EXAMPLE

$$u = \hat{u} \sin(\Omega t + \delta_1) \quad (5.11)$$

$$u_d = \hat{u}_d \sin(\Omega t + \delta_1 + \delta_2) \quad (5.12)$$

where \hat{u} and δ denote the displacement amplitude and phase shift respectively. The critical loading scenario is the resonant condition, $\Omega = \omega$. The solution for this case has the following form

$$\hat{u} = \frac{\hat{p}}{k\bar{m}} \sqrt{\frac{1}{1 + \left(\frac{2\xi}{\bar{m}} + \frac{1}{2\xi_d}\right)^2}} \quad (5.13)$$

$$\hat{u}_d = \frac{1}{2\xi_d} \hat{u} \quad (5.14)$$

$$\tan \delta_1 = - \left[\frac{2\xi}{\bar{m}} + \frac{1}{2\xi_d} \right] \quad (5.15)$$

$$\tan \delta_2 = -\frac{\pi}{2} \quad (5.16)$$

Note that the response of the tuned mass is 90° out of phase with the response of the primary mass. This difference in phase produces the *energy dissipation* contributed by the damper inertia force.

The response for *no* damper is given by

$$\hat{u} = \frac{\hat{p}}{k} \left(\frac{1}{2\xi} \right) \quad (5.17)$$

$$\delta_1 = -\frac{\pi}{2} \quad (5.18)$$

To compare these two cases, we can express Eq. (5.13) in terms of an equivalent damping ratio

$$\hat{u} = \frac{\hat{p}}{k} \left(\frac{1}{2\xi_e} \right) \quad (5.19)$$

where

$$\xi_e = \frac{\bar{m}}{2} \sqrt{1 + \left(\frac{2\xi}{\bar{m}} + \frac{1}{2\xi_d} \right)^2} \quad (5.20)$$

Equation (5.20) shows the relative contribution of the damper parameters to the total damping. Increasing the mass ratio magnifies the damping. However, since the added mass also increases, there is a practical limit on \bar{m} . Decreasing the damping coefficient for the damper also increases the damping. Noting Eq. (5.14), the relative displacement also increases in this case, and just as for the mass, there is a practical limit on the relative motion of the damper. Selecting the final design requires a compromise between these two constraints.

Example 5.1 - Preliminary design of a TMD for a SDOF system

Suppose $\xi = 0$ and we want to add a tuned mass damper such that the equivalent damping ratio is 10%. Using Eq. (5.20), and setting $\xi_e = 0.1$, the following relation between \bar{m} and ξ_d is obtained.

$$\frac{\bar{m}}{2} \sqrt{1 + \left(\frac{1}{2\xi_d} \right)^2} = 0.1 \quad (5.21)$$

The relative displacement constraint is given by Eq. (5.14)

$$\hat{u}_d = \frac{1}{2\xi_d} \hat{u} \quad (5.22)$$

5.2. AN INTRODUCTORY EXAMPLE

Combining Eq. (5.21) and Eq. (5.22), and setting $\xi = 0$ leads to

$$\frac{\bar{m}}{2} \sqrt{1 + \left(\frac{\hat{u}_d}{\hat{u}}\right)^2} = 0.1 \quad (5.23)$$

Usually, \hat{u}_d is taken to be an order of magnitude greater than \hat{u} . In this case Eq. (5.23) can be approximated as

$$\frac{\bar{m}}{2} \left(\frac{\hat{u}_d}{\hat{u}}\right) \approx 0.1 \quad (5.24)$$

The generalized form of Eq. (5.24) follows from (5.20)

$$\bar{m} \approx 2\xi_e \left(\frac{1}{\hat{u}_d/\hat{u}}\right) \quad (5.25)$$

Finally, taking $\hat{u}_d = 10\hat{u}$ yields an estimate for m

$$\bar{m} = \frac{2(0.1)}{10} = 0.02 \quad (5.26)$$

This magnitude is typical for \bar{m} . The other parameters are

$$\xi_d = \frac{1}{2} \left(\frac{\hat{u}}{\hat{u}_d}\right) = 0.05 \quad (5.27)$$

and from Eq. (5.9)

$$k_d = \bar{m}k = 0.02k \quad (5.28)$$

It is important to note that with the addition of only 2% of the primary mass, we obtain an effective damping ratio of 10%. The negative aspect is the large relative motion of the damper mass; in this case, 10 times the displacement of the primary mass. How to accommodate this motion in an actual structure is an important design consideration.

A description of some applications of tuned mass dampers to building structures is presented in the following section to provide additional background on this type of device prior to entering into a detailed discussion of the underlying theory.

5.3 Examples of existing tuned mass damper systems

Although the majority of applications have been for mechanical systems, tuned mass dampers have been used to improve the response of building structures under wind excitation. A short description of the various types of dampers and several building structures that contain tuned mass dampers follows.

5.3.1 Translational tuned mass dampers

Figure 5.2 illustrates the typical configuration of a unidirectional translational tuned mass damper. The mass rests on bearings that function as rollers and allow the mass to translate laterally relative to the floor. Springs and dampers are inserted between the mass and the adjacent vertical support members which transmit the lateral *out-of-phase* force to the floor level, and then into the structural frame. Bidirectional translational dampers are configured with springs/dampers in two orthogonal directions and provide the capability for controlling structural motion in two orthogonal planes. Some examples of early versions of this type of damper are described below.

- **John Hancock Tower** [1]

Two dampers were added to the 60-story John Hancock Tower in Boston to reduce the response to wind loading. The dampers

5.3. EXAMPLES OF EXISTING TUNED MASS DAMPER SYSTEMS

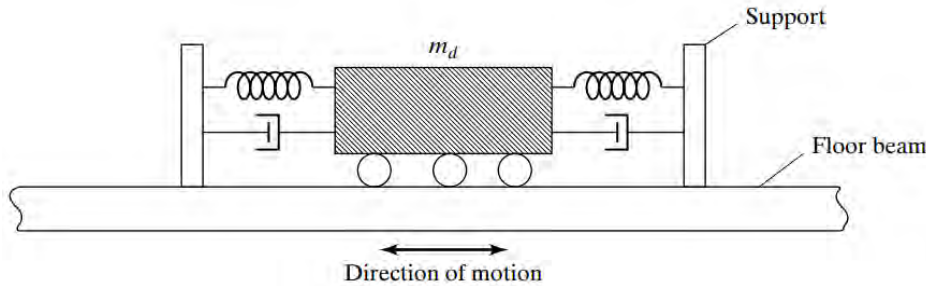


Figure 5.2: Schematic diagram of a translational tuned mass damper.

are placed at opposite ends of the 58th story, 67 m apart, and move to counteract sway as well as twisting due to the shape of the building. Each damper weighs 2700 kN and consists of a lead-filled steel box about 5.2 m square and 1m deep that rides on a 9-m-long steel plate. The lead-filled weight, laterally restrained by stiff springs anchored to the interior columns of the building and controlled by servo-hydraulic cylinders, slides back and forth on a hydrostatic bearing consisting of a thin layer of oil forced through holes in the steel plate. Whenever the horizontal acceleration exceeds 0.003g for two consecutive cycles, the system is automatically activated. This system was designed and manufactured by LeMessurier Associates/SCI in association with MTS System Corp., at a cost of around 3 million dollars, and is expected to reduce the sway of the building by 40 to 50%.

- **Citicorp Center** [2, 73, 85]

The Citicorp (Manhattan) TMD was also designed and manufactured by LeMessurier Associates/SCI in association with MTS System Corp. This building is 279m high, has a fundamental period of around 6.5s with an inherent damping ratio of 1% along each axis. The Citicorp TMD, located on the 63rd floor in the crown of the structure, has a mass of 366 Mg, about 2% of the

CHAPTER 5. TUNED MASS DAMPER SYSTEMS

effective modal mass of the first mode, and was 250 times larger than any existing tuned mass damper at the time of installation. Designed to be biaxially resonant on the building structure with a variable operating period of $6.25 \text{ s} \pm 20\%$, adjustable linear damping from 8% to 14%, and a peak relative displacement of $\pm 1.4 \text{ m}$, the damper is expected to reduce the building sway amplitude by about 50%. This reduction corresponds to increasing the basic structural damping by 4%. The concrete mass block is about 2.6m high with a plan cross-section of 9.1 m by 9.1 m and is supported on a series of twelve 60 cm diameter hydraulic pressure-balanced bearings. During operation, the bearings are supplied oil from a separate hydraulic pump which is capable of raising the mass block about 2 cm to its operating position in about 3 minutes. The damper system is activated automatically whenever the horizontal acceleration exceeds 0.003g for two consecutive cycles, and will automatically shut itself down when the building acceleration does not exceed 0.00075g in either axis over a 30-minute interval. LeMessurier estimates Citicorps TMD, which cost about 1.5 million dollars, saved 3.5 to 4 million dollars. This sum represents the cost of some 2,800 tons of structural steel that would have been required to satisfy the deflection constraints.

- **Canadian National Tower [3]**

The 102-m steel antenna mast on top of the Canadian National Tower in Toronto (553 m high including the antenna) required two lead dampers to prevent the antenna from deflecting excessively when subjected to wind excitation. The damper system consists of two doughnut-shaped steel rings, 35 cm wide, 30 cm deep, and 2.4 m and 3 m in diameter, located at elevations 488 m

5.3. EXAMPLES OF EXISTING TUNED MASS DAMPER SYSTEMS

and 503 m. Each ring holds about 9 metric tons of lead and is supported by three steel beams attached to the sides of the antenna mast. Four bearing universal joints that pivot in all directions connect the rings to the beams. In addition, four separate hydraulically activated fluid dampers mounted on the side of the mast and attached to the center of each universal joint dissipate energy. As the lead-weighted rings move back and forth, the hydraulic damper system dissipates the input energy and reduces the towers response. The damper system was designed by Nicolet, Carrier, Dressel, and Associates, Ltd, in collaboration with Vibron Acoustics, Ltd. The dampers are tuned to the second and fourth modes of vibration in order to minimize antenna bending loads; the first and third modes have the same characteristics as the prestressed concrete structure supporting the antenna and did not require additional damping.

- **Chiba Port Tower** [54]

Chiba Port Tower (completed in 1986) was the first tower in Japan to be equipped with a TMD. Chiba Port Tower is a steel structure 125 m high weighing 1950 metric tons and having a rhombus shaped plan with a side length of 15 m. The first and second mode periods are 2.25 s and 0.51 s respectively for the x direction and 2.7 s and 0.57 s for the y direction. Damping for the fundamental mode is estimated at 0.5%. Damping ratios proportional to frequencies were assumed for the higher modes in the analysis. The purpose of the TMD is to increase damping of the first mode for both the x and y directions. Fig. 5.3 shows the damper system. Manufactured by Mitsubishi Steel Manufacturing Co., Ltd, the damper has: mass ratios with respect to the modal mass of the first mode of about 1/120 in

CHAPTER 5. TUNED MASS DAMPER SYSTEMS

the x direction and $1/80$ in the y direction; periods in the x and y directions of 2.24 s and 2.72 s respectively; and a damper damping ratio of 15%. The maximum relative displacement of the damper with respect to the tower is about ± 1 m in each direction. Reductions of around 30% to 40% in the displacement of the top floor and 30% in the peak bending moments are expected.



Figure 5.3: Tuned mass damper for Chiba-Port Tower. (Courtesy of J. Connor.)

The early versions of TMDs employ complex mechanisms for the bearing and damping elements, have relatively large masses, occupy considerably space, and are quite expensive. Recent versions, such as the scheme shown in Fig. 5.4, have been designed to minimize these limitations. This scheme employs a multi-assembly of elastomeric rubber bearings, which function as shear springs, and bitumen rubber compound (BRC) elements, which provide viscoelastic damping capability. The device is compact in size, requires unsophisticated controls, is multidirectional, and is easily assembled and modified. Fig. 5.5 shows a full scale damper being subjected to dynamic excitation by a

5.3. EXAMPLES OF EXISTING TUNED MASS DAMPER SYSTEMS

shaking table. An actual installation is contained in Fig. 5.6.

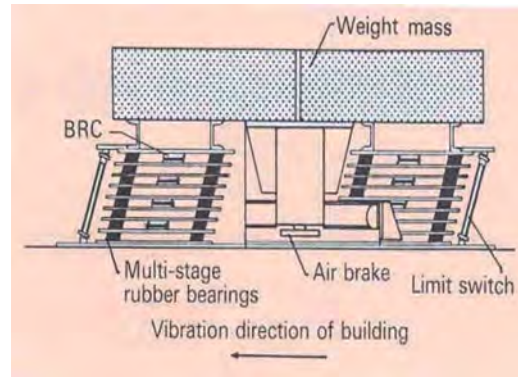


Figure 5.4: Tuned mass damper with spring and damper assemblage.

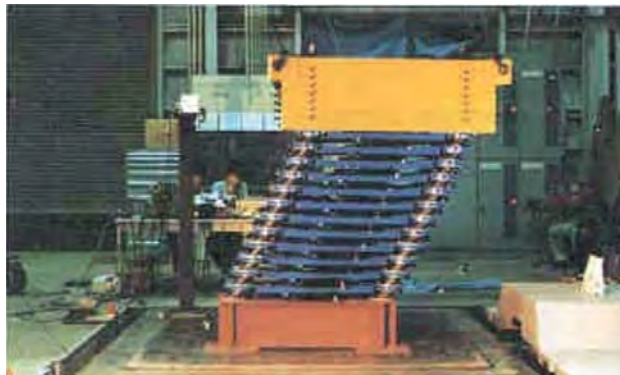


Figure 5.5: Deformed position - tuned mass damper. (Courtesy of J. Connor.)

CHAPTER 5. TUNED MASS DAMPER SYSTEMS



Figure 5.6: Tuned mass damper - Huis Ten Bosch Tower, Nagasaki. (Courtesy of J. Connor.)

The effectiveness of a tuned mass damper can be increased by attaching an auxiliary mass and an actuator to the tuned mass and driving the auxiliary mass with the actuator such that its response is out of phase with the response of the tuned mass. Fig. 5.7 illustrates this scheme. The effect of driving the auxiliary mass is to produce an additional force which complements the force generated by the tuned mass, and therefore increases the equivalent damping of the TMD (we can obtain the same behavior by attaching the actuator directly to the tuned mass, thereby eliminating the need for an auxiliary mass). Since the actuator requires an external energy source, this system is referred to as an active tuned mass damper. The scope of this chapter is restricted to passive TMDs. Active TMDs are discussed in Chapter 7.

5.3. EXAMPLES OF EXISTING TUNED MASS DAMPER SYSTEMS

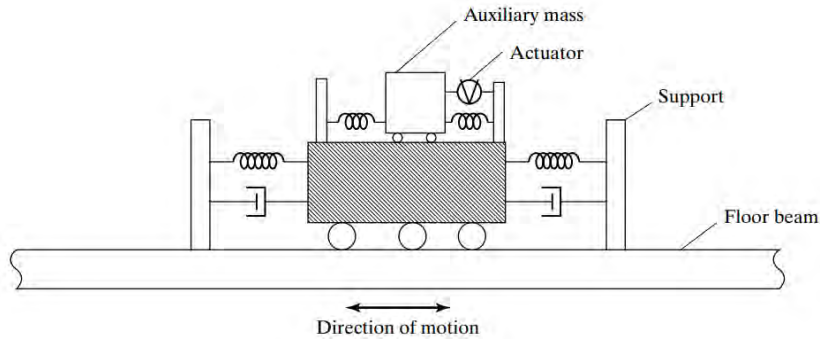


Figure 5.7: An active tuned mass damper configuration.

5.3.2 Pendulum tuned mass damper

The problems associated with the bearings can be eliminated by supporting the mass with cables which allow the system to behave as a pendulum. Fig. 5.8a shows a simple pendulum attached to a floor. Movement of the floor excites the pendulum. The relative motion of the pendulum produces a horizontal force which opposes the floor motion. This action can be represented by an equivalent SDOF system which is attached to the floor as indicated in Fig. 5.8b.

The equation of motion for the horizontal direction is

$$T \sin \theta + \frac{W_d}{g}(\ddot{u} + \ddot{u}_d) = 0 \quad (5.29)$$

where T is the tension in the cable. When Θ is small, the following approximations apply

$$\begin{aligned} u_d &= L \sin \theta \approx L\theta \\ T &\approx W_d \end{aligned} \quad (5.30)$$

Introducing these approximations transforms Eq. (5.29) to

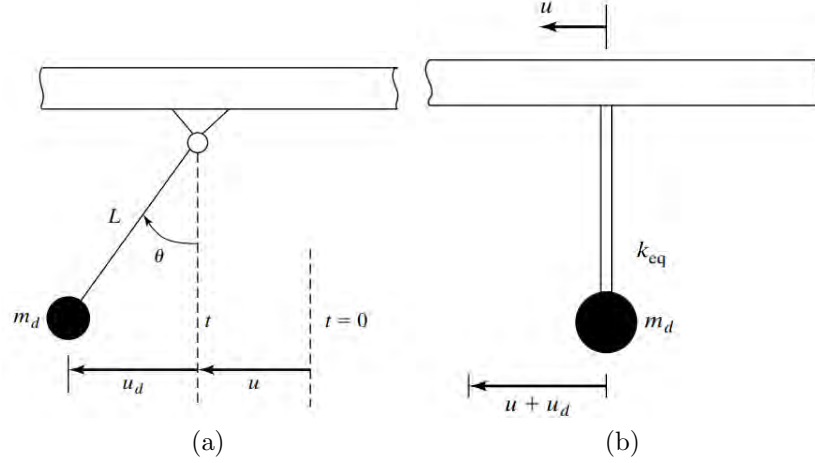


Figure 5.8: A simple pendulum tuned mass damper. (a) Actual system; and (b) equivalent system.

$$m_d \ddot{u}_d + \frac{W_d}{L} u_d = -m_d \ddot{u} \quad (5.31)$$

and it follows that the equivalent shear spring stiffness is

$$k_{eq} = \frac{W_d}{L} \quad (5.32)$$

The natural frequency of the pendulum is related to k_{eq} by

$$\omega_d^2 = \frac{k_{eq}}{m_d} = \frac{g}{L} \quad (5.33)$$

Noting Eq. 5.33, the natural period of the pendulum is

$$T_d = 2\pi \sqrt{\frac{L}{g}} \quad (5.34)$$

The simple pendulum tuned mass damper concept has a serious limitation. Since the period depends on L , the required

5.3. EXAMPLES OF EXISTING TUNED MASS DAMPER SYSTEMS

length for large T_d may be greater than the typical story height. For instance, the length for $T_d=5$ s is 6.2 meters whereas the story height is between 4 to 5 meters. This problem can be eliminated by resorting to the scheme illustrated in Fig. (5.9). The interior rigid link magnifies the support motion for the pendulum, and results in the following equilibrium equation

$$m_d(\ddot{u} + \ddot{u}_1 + \ddot{u}_d) + \frac{W_d}{L}u_d = 0 \quad (5.35)$$

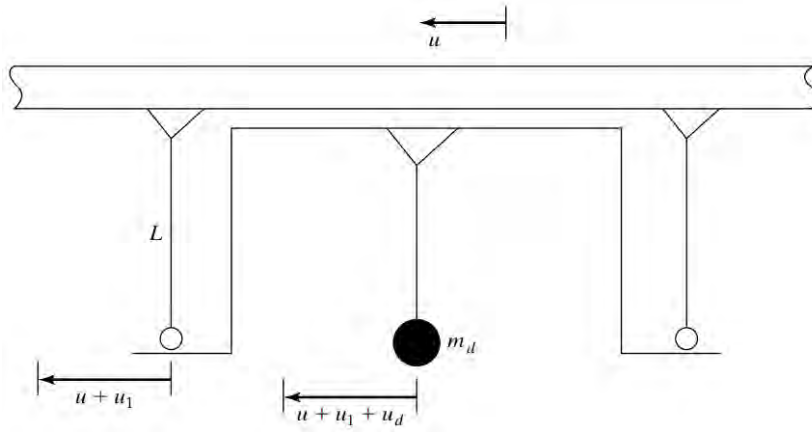


Figure 5.9: Compound pendulum.

The rigid link moves in phase with the damper, and has the same displacement amplitude. Then, taking $u_1 = u_d$ in Eq. (5.35) results in

$$m_d\ddot{u}_d + \frac{W_d}{2L}u_d = -\frac{m_d}{2}\ddot{u} \quad (5.36)$$

The equivalent stiffness is $W_d/2L$, and it follows that the effective length is equal to $2L$. Each additional link increases the effective length by L . An example of a pendulum type damper is described below.

- Crystal Tower [77]

The tower, located in Osaka Japan, is 157 m high and 28 m by 67 m in plan, weighs 44,000 metric tons, and has a fundamental period of approximately 4 s in the north-south direction and 3 s in the east-west direction. A tuned pendulum mass damper was included in the early phase of the design to decrease the wind-induced motion of the building by about 50%. Six of the nine air cooling and heating ice thermal storage tanks (each weighing 90 tons) are hung from the top roof girders and used as a pendulum mass. Four tanks have a pendulum length of 4 m and slide in the north-south direction; the other two tanks have a pendulum length of about 3 m and slide in the east-west direction. Oil dampers connected to the pendulums dissipate the pendulum energy. Fig. 5.10 shows the layout of the ice storage tanks that were used as damper masses. Views of the actual building and one of the tanks are presented in Fig. 5.11. The cost of this tuned mass damper system was around \$350,000, less than 0.2% of the construction cost.

5.3. EXAMPLES OF EXISTING TUNED MASS DAMPER SYSTEMS

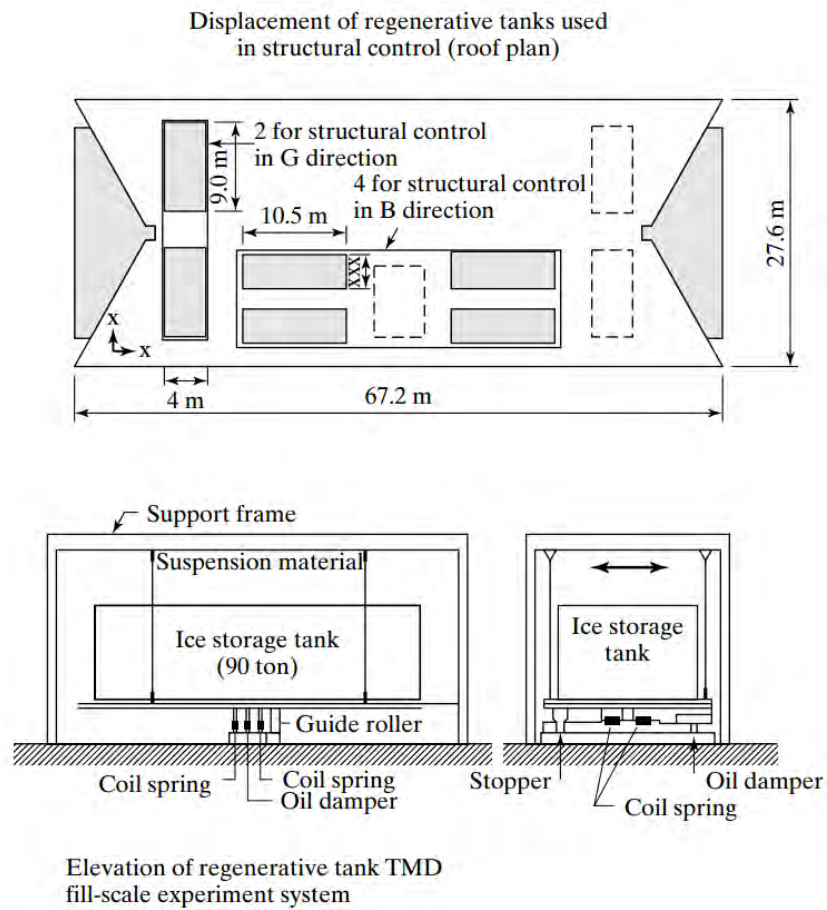


Figure 5.10: Pendulum damper layout - Crystal Tower. (Courtesy of Takenaka Corporation.)

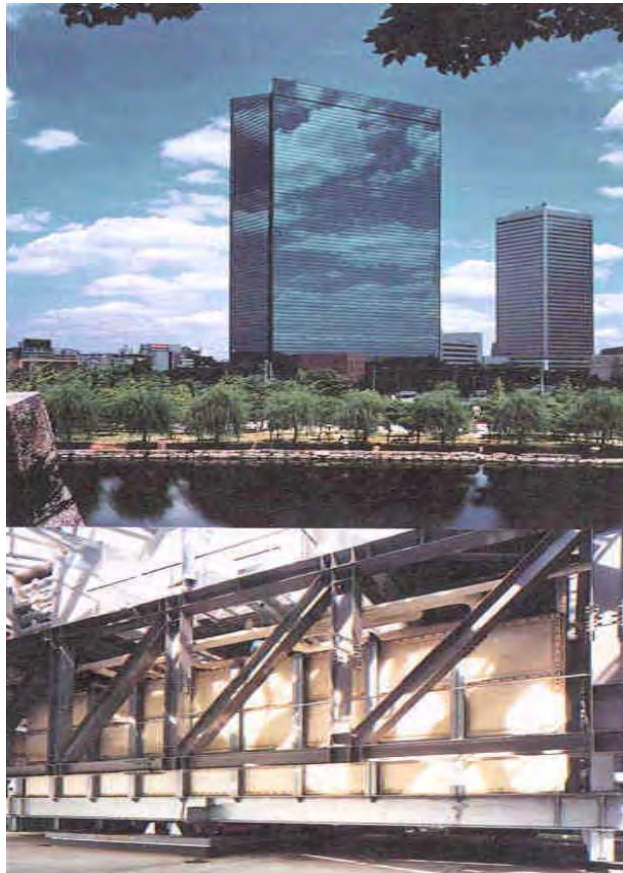


Figure 5.11: Ice storage tank - Crystal Tower. (Courtesy of Takenaka Corporation.)

A modified version of the pendulum damper is shown in Fig. 5.12. The restoring force provided by the cables is generated by introducing curvature in the support surface and allowing the mass to roll on this surface. The vertical motion of the weight requires an energy input. Assuming θ is small, the equations for the case where the surface is circular are the same as for the conventional pendulum with the cable length L , replaced with the surface radius R .

5.3. EXAMPLES OF EXISTING TUNED MASS DAMPER SYSTEMS

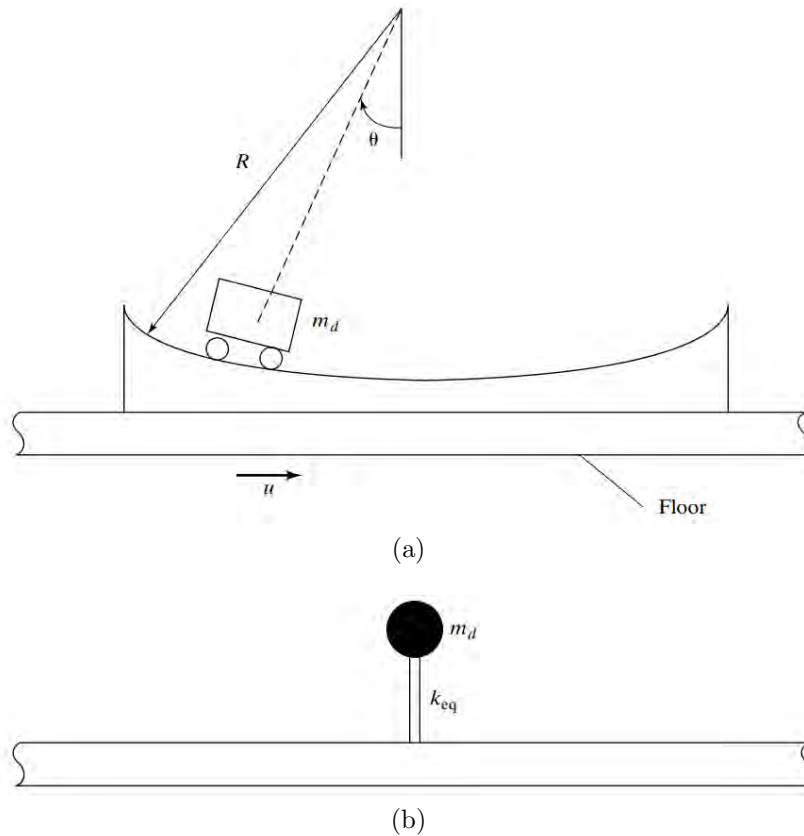


Figure 5.12: Rocker pendulum.

- **Taipei 101 Tower** [40, 46]

The Taipei 101 tower, located in Taipei, Taiwan is a 101-story building, 508 m tall, which includes a pinnacle of 53 m. The structure is equipped with a 660-tonne steel pendulum damper. At the time of construction, the pendulum damper was the largest passive TMD to be completed. While the pendulum damper is designed to dampen wind-induced vibrations, it is also engineered to withstand seismic forces from a 2 500-year event. The pinnacle is also equipped with passive dampers to mitigate vortex induced oscillation at common wind speeds that occur

CHAPTER 5. TUNED MASS DAMPER SYSTEMS

at three frequencies. Three passive TMDs are installed in the pinnacle, each tuned at a one of these particular frequencies. Fig. 5.13 shows the schematic of the TMD systems installed in the tower. The pendulum TMD also constitutes an attraction for visitors.

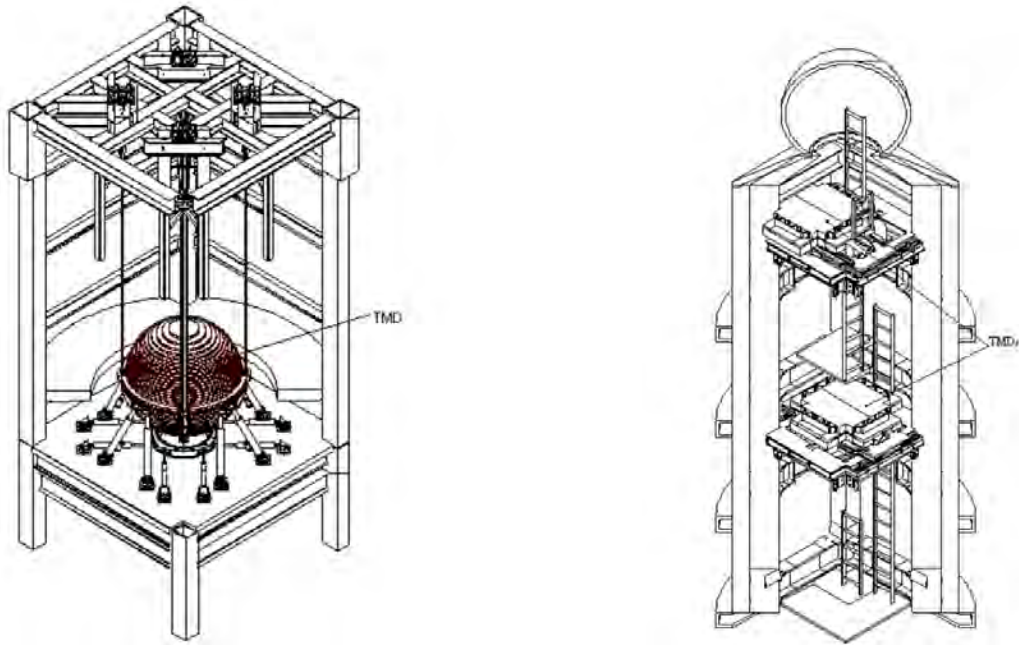


Figure 5.13: Schematic of the TMD systems installed in Taipei 101. Left: the pendulum TMD on the main tower. Right: three TMDs in the pinnacle [40], reprinted with permission of Motioneer Inc.

5.4 Tuned Mass Damper Theory for SDOF Systems

In what follows, various cases ranging from fully undamped to fully damped conditions are analyzed and design procedures are presented.

5.4. TUNED MASS DAMPER THEORY FOR SDOF SYSTEMS

5.4.1 Undamped structure - undamped TMD

Fig. 5.14 shows a SDOF system having mass m and stiffness k , subjected to both external forcing and ground motion. A tuned mass damper with mass m_d and stiffness k_d is attached to the primary mass. The various displacement measures are: u_g , the absolute ground motion; u , the relative motion between the primary mass and the ground; and u_d , the relative displacement between the damper and the primary mass. With this notation, the governing equations take the form

$$m_d(\ddot{u}_d + \ddot{u}) + k_d u_d = -m_d a_g \quad (5.37)$$

$$m\ddot{u} + ku - k_d u_d = -ma_g + p \quad (5.38)$$

where a_g is the absolute ground acceleration and p is the force loading applied to the primary mass.

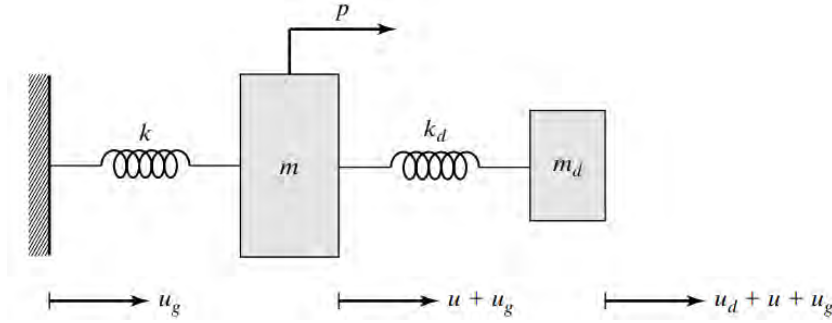


Figure 5.14: SDOF system coupled with a TMD.

The excitation is considered to be periodic of frequency Ω ,

$$a_g = \hat{a}_g \sin \Omega t \quad (5.39)$$

$$p = \hat{p} \sin \Omega t \quad (5.40)$$

Expressing the response as

$$u = \hat{u} \sin \Omega t \quad (5.41)$$

$$u_d = \hat{u}_d \sin \Omega t \quad (5.42)$$

and substituting for these variables, the equilibrium equations are transformed to

$$(-m_d \Omega^2 + k_d) \hat{u}_d - m_d \Omega^2 \hat{u} = -m_d \hat{a}_g \quad (5.43)$$

$$-k_d \hat{u}_d + (-m \Omega^2 + k) \hat{u} = -m \hat{a}_g + \hat{p} \quad (5.44)$$

The solutions for \hat{u} and \hat{u}_d are given by

$$\hat{u} = \frac{\hat{p}}{k} \left(\frac{1 - \rho_d^2}{D_1} \right) - \frac{m \hat{a}_g}{k} \left(\frac{1 + \bar{m} - \rho_d^2}{D_1} \right) \quad (5.45)$$

$$\hat{u}_d = \frac{\hat{p}}{k_d} \left(\frac{\bar{m} \rho^2}{D_1} \right) - \frac{m \hat{a}_g}{k_d} \left(\frac{\bar{m}}{D_1} \right) \quad (5.46)$$

where

$$D_1 = (1 - \rho^2)(1 - \rho_d^2) - \bar{m} \rho^2 \quad (5.47)$$

and the ρ terms are dimensionless frequency ratios,

$$\rho = \frac{\Omega}{\omega} = \frac{\Omega}{\sqrt{k/m}} \quad (5.48)$$

$$\rho_d = \frac{\Omega}{\omega_d} = \frac{\Omega}{\sqrt{k_d/m_d}} \quad (5.49)$$

Selecting the mass ratio and damper frequency ratio such that

$$1 - \rho_d^2 + \bar{m} = 0 \quad (5.50)$$

reduces the solution to

5.4. TUNED MASS DAMPER THEORY FOR SDOF SYSTEMS

$$\hat{u} = \frac{\hat{p}}{k} \quad (5.51)$$

$$\hat{u}_d = -\frac{\hat{p}}{k_d}\rho^2 + \frac{m\hat{a}_g}{k_d} \quad (5.52)$$

This choice isolates the primary mass from ground motion and reduces the response due to external force to the pseudo-static value, \hat{p}/k . A typical range for \bar{m} is 0.01 to 0.1. Then, the *optimal* damper frequency is very close to the forcing frequency. The exact relationship follows from Eq. (5.50).

$$\omega_d|_{\text{opt}} = \frac{\Omega}{\sqrt{1 + \bar{m}}} \quad (5.53)$$

We determine the corresponding damper stiffness with

$$k_d|_{\text{opt}} = (\omega_d|_{\text{opt}})^2 m_d = \frac{\Omega^2 m \bar{m}}{1 + \bar{m}} \quad (5.54)$$

Finally, substituting for k_d , Eq. (5.52) takes the following form

$$\hat{u}_d = \frac{1 + \bar{m}}{\bar{m}} \left(\left| \frac{\hat{p}}{k} \right| + \left| \frac{\hat{a}_g}{\Omega^2} \right| \right) \quad (5.55)$$

One specifies the amount of relative displacement for the damper and determines \bar{m} with Eq. (5.55). Given \bar{m} and Ω , the stiffness is found using Eq. (5.54). It should be noted that this stiffness applies for a *particular* forcing frequency. Once the mass damper properties are defined, Eq. (5.45) and (5.46) can be used to determine the response for a *different* forcing frequency. The primary mass will move under ground motion excitation in this case.

5.4.2 Undamped structure - damped TMD

The next level of complexity has damping included in the mass damper, as shown in Fig. 5.15. The equations of motion for this case are

$$m_d \ddot{u}_d + c_d \dot{u}_d + k_d u_d + m_d \ddot{u} = -m_d a_g \quad (5.56)$$

$$m \ddot{u} + k u - c_d \dot{u}_d - k_d u_d = -m a_g + p \quad (5.57)$$

The inclusion of the damping terms in Eq. (5.56) and (5.57) produces a phase shift between the periodic excitation and the response. It is convenient to work initially with the solution expressed in terms of complex quantities. We express the excitation as

$$a_g = \hat{a}_g e^{i\Omega t} \quad (5.58)$$

$$p = \hat{p} e^{i\Omega t} \quad (5.59)$$

where \hat{a}_g and \hat{p} are real quantities. The response is taken as

$$u = \bar{u} e^{i\Omega t} \quad (5.60)$$

$$u_d = \bar{u}_d e^{i\Omega t} \quad (5.61)$$

where the response amplitudes, \bar{u} and \bar{u}_d are considered to be complex quantities. The real and imaginary parts of a_g correspond to cosine and sinusoidal input. Then, the corresponding solution is given by either the real (for cosine) or imaginary (for sine) parts of u and u_d . Substituting Eq. (5.60) and (5.61) in the set of governing equations and canceling $e^{i\Omega t}$ from both sides results in

$$(-m_d \Omega^2 + i c_d \Omega + k_d) \bar{u}_d - m_d \Omega^2 \bar{u} = -m_d \hat{a}_g \quad (5.62)$$

5.4. TUNED MASS DAMPER THEORY FOR SDOF SYSTEMS

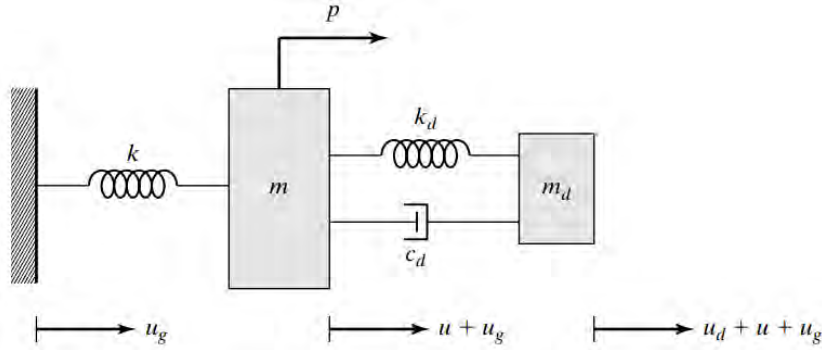


Figure 5.15: Undamped SDOF system coupled with a damped TMD system.

$$-(ic_d\Omega + k_d)\bar{u}_d + (-m\Omega^2 + k)\bar{u} = -m\hat{a}_g + \hat{p} \quad (5.63)$$

The solution of the governing equations is

$$\bar{u} = \frac{\hat{p}}{kD_2}(f^2 - \rho^2 + i2\xi_d\rho f) - \frac{\hat{a}_g m}{kD_2}[(1 + \bar{m})f^2 - \rho^2 + i2\xi_d\rho f(1 + \bar{m})] \quad (5.64)$$

$$\bar{u}_d = \frac{\hat{p}\rho^2}{kD_2} - \frac{\hat{a}_g m}{kD_2} \quad (5.65)$$

where

$$D_2 = (1 - \rho^2)(f^2 - \rho^2) - \bar{m}\rho^2 f^2 + i2\xi_d\rho f[1 - \rho^2(1 + \bar{m})] \quad (5.66)$$

$$f = \frac{\omega_d}{\omega} \quad (5.67)$$

and ρ was defined earlier as the ratio of Ω to ω (see Eq. (5.48)).

Converting the complex solutions to polar form leads to the following expressions

$$\bar{u} = \frac{\hat{p}}{k}H_1e^{i\delta_1} - \frac{\hat{a}_g m}{k}H_2e^{i\delta_2} \quad (5.68)$$

CHAPTER 5. TUNED MASS DAMPER SYSTEMS

$$\bar{u}_d = \frac{\hat{p}}{k} H_3 e^{-i\delta_3} - \frac{\hat{a}_g m}{k} H_4 e^{-i\delta_3} \quad (5.69)$$

where the H factors define the amplification of the pseudo-static responses, and the δ 's are the phase angles between the response and the excitation. The various H and δ terms are listed below

$$H_1 = \frac{\sqrt{(f^2 - \rho^2)^2 + (2\xi_d \rho f)^2}}{|D_2|} \quad (5.70)$$

$$H_2 = \frac{\sqrt{[(1 + \bar{m})f^2 - \rho^2]^2 + [2\xi_d \rho f(1 + \bar{m})]^2}}{|D_2|} \quad (5.71)$$

$$H_3 = \frac{\rho^2}{|D_2|} \quad (5.72)$$

$$H_4 = \frac{1}{|D_2|} \quad (5.73)$$

$$|D_2| = \sqrt{[(1 - \rho^2)(f^2 - \rho^2) - \bar{m}\rho^2 f^2]^2 + [2\xi_d \rho f(1 - \rho^2[1 + \bar{m}])]^2} \quad (5.74)$$

Also

$$\delta_1 = \alpha_1 - \delta_3 \quad (5.75)$$

$$\delta_2 = \alpha_2 - \delta_3 \quad (5.76)$$

$$\tan \delta_3 = \frac{2\xi_d \rho f[1 - \rho^2(1 + \bar{m})]}{(1 - \rho^2)(f^2 - \rho^2) - \bar{m}\rho^2 f^2} \quad (5.77)$$

$$\tan \alpha_1 = \frac{2\xi_d \rho f}{f^2 - \rho^2} \quad (5.78)$$

$$\tan \alpha_2 = \frac{2\xi_d \rho f(1 + \bar{m})}{(1 + \bar{m})f^2 - \rho^2} \quad (5.79)$$

For most applications, the mass ratio is less than about 0.05. Then, the amplification factors for external loading (H_1) and

5.4. TUNED MASS DAMPER THEORY FOR SDOF SYSTEMS

ground motion (H_2) are essentially equal. A similar conclusion applies for the phase shift. In what follows, the solution corresponding to ground motion is examined and the optimal values of the damper properties for this loading condition are established. An in-depth treatment of the external forcing case is contained in Den Hartog's text [26].

Fig. 5.16 shows the variation of H_2 with forcing frequency for specific values of damper mass \bar{m} and frequency ratio f , and various values of the damper damping ratio, ξ_d . When $\xi_d = 0$, there are two peaks with infinite amplitude located on each side of $\rho = 1$. As ξ_d is increased, the peaks approach each other and then merge into a single peak located at $\rho \approx 1$. The behavior of the amplitudes suggests that there is an optimal value of ξ_d for a given damper configuration (m_d and k_d , or equivalently, \bar{m} and f). Another key observation is that all the curves pass through two common points, P and Q . Since these curves correspond to different values of ξ_d , the location of P and Q must depend only on \bar{m} and f .

Proceeding with this line of reasoning, the expression for H_2 can be written as

$$H_2 = \sqrt{\frac{a_1^2 + \xi_d^2 a_2^2}{a_3^2 + \xi_d^2 a_4^2}} = \frac{a_2}{a_4} \sqrt{\frac{a_1^2/a_2^2 + \xi_d^2}{a_3^2/a_4^2 + \xi_d^2}} \quad (5.80)$$

where the a terms are functions of \bar{m} , ρ , and f . Then, for H_2 to be independent of ξ_d , the following condition must be satisfied

$$\left| \frac{a_1}{a_2} \right| = \left| \frac{a_3}{a_4} \right| \quad (5.81)$$

The corresponding values for H_2 are

CHAPTER 5. TUNED MASS DAMPER SYSTEMS

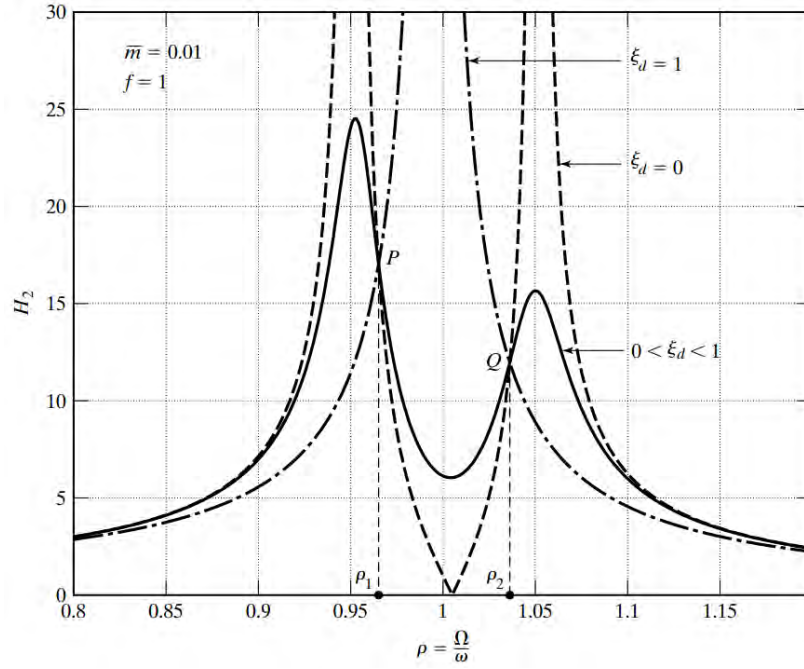


Figure 5.16: Plot of H_2 versus ρ .

$$H_2|_{P,Q} = \left| \frac{a_2}{a_4} \right| \quad (5.82)$$

Substituting for the a terms in Eq. (5.81), we obtain a quadratic equation for ρ^2

$$\rho^4 - \left[(1 + \bar{m})f^2 + \frac{1 + 0.5\bar{m}}{1 + \bar{m}} \right] \rho^2 + f^2 = 0 \quad (5.83)$$

The two positive roots ρ_1 and ρ_2 are the frequency ratios corresponding to points P and Q . Similarly, Eq. (5.82) expands to

$$H_2|_{P,Q} = \frac{1 + \bar{m}}{|1 - \rho_{1,2}^2(1 + \bar{m})|} \quad (5.84)$$

5.4. TUNED MASS DAMPER THEORY FOR SDOF SYSTEMS

Fig. 5.16 shows different values for H_2 at points P and Q . For *optimal* behavior, we want to minimize the maximum amplitude. As a first step, we require the values of H_2 for ρ_1 and ρ_2 to be equal. This produces a distribution which is symmetrical about $\rho^2 = 1/(1 + \bar{m})$, as illustrated in Fig. 5.17. Then, by increasing the damping ratio, ξ_d , we can lower the peak amplitudes until the peaks coincide with points P and Q . This state represents the *optimal* performance of the TMD system. A further increase in ξ_d causes the peaks to merge and the amplitude to increase beyond the optimal value.

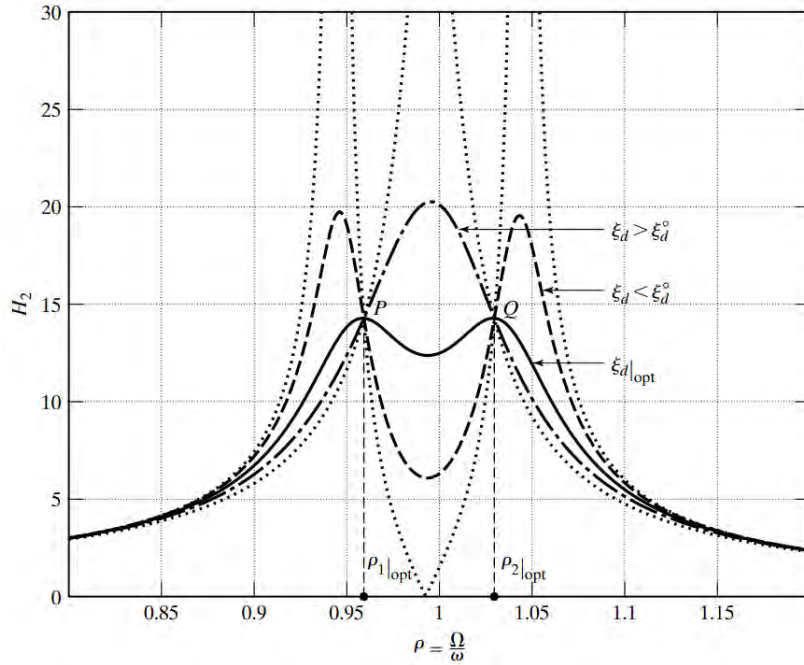


Figure 5.17: Plot of H_2 versus ρ for f_{opt} .

Requiring the amplitudes to be equal at P and Q is equivalent to the following condition on the roots

$$|1 - \rho_1^2(1 + \bar{m})| = |1 - \rho_2^2(1 + \bar{m})| \quad (5.85)$$

CHAPTER 5. TUNED MASS DAMPER SYSTEMS

Then, substituting for ρ_1 and ρ_2 using Eq. (5.83), we obtain a relation between the optimal tuning frequency and the mass ratio

$$f_{\text{opt}} = \frac{\sqrt{1 - 0.5\bar{m}}}{1 + \bar{m}} \quad (5.86)$$

$$\omega_d|_{\text{opt}} = f_{\text{opt}}\omega \quad (5.87)$$

The corresponding roots and optimal amplification factors are

$$\rho_{1,2}|_{\text{opt}} = \sqrt{\frac{1 \pm \sqrt{0.5\bar{m}}}{1 + \bar{m}}} \quad (5.88)$$

$$H_2|_{\text{opt}} = \frac{1 + \bar{m}}{\sqrt{0.5\bar{m}}} \quad (5.89)$$

The expression for the optimal damping at the optimal tuning frequency is

$$\xi_d|_{\text{opt}} = \sqrt{\frac{\bar{m}(3 - \sqrt{0.5\bar{m}})}{8(1 + \bar{m})(1 - 0.5\bar{m})}} \quad (5.90)$$

Fig. 5.18 through 5.21 show the variation of the *optimal* parameters with the mass ratio, \bar{m} .

5.4. TUNED MASS DAMPER THEORY FOR SDOF SYSTEMS

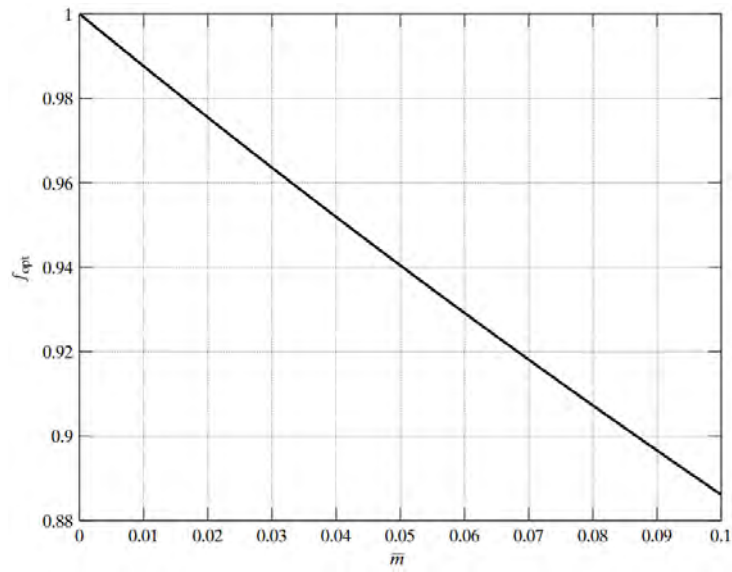


Figure 5.18: Optimum tuning frequency ratio, f_{opt} .

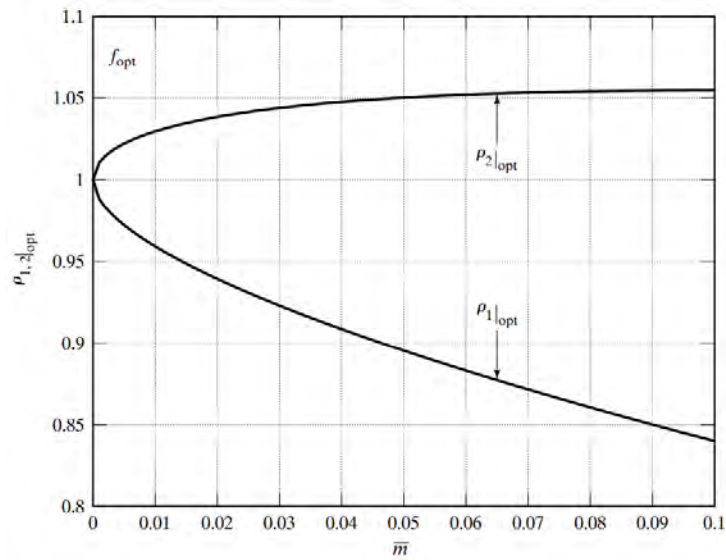


Figure 5.19: Input frequency ratios at which the response is independent of damping.

CHAPTER 5. TUNED MASS DAMPER SYSTEMS

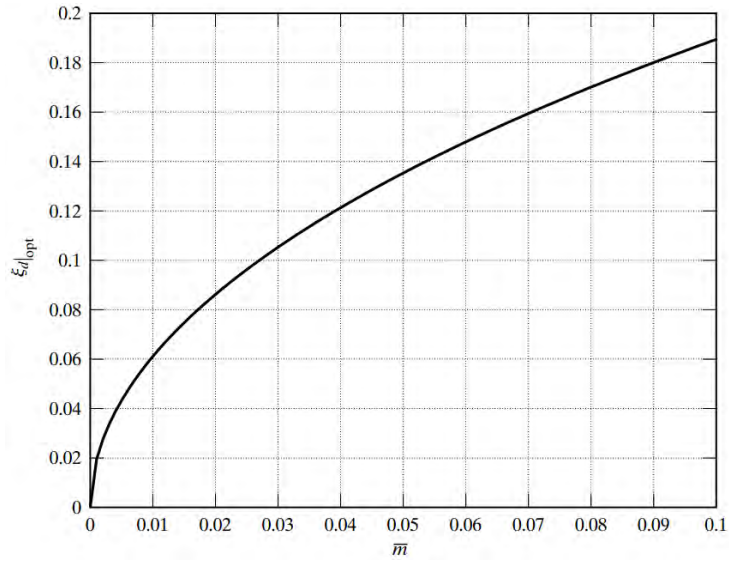


Figure 5.20: Optimal damping ratio for TMD.

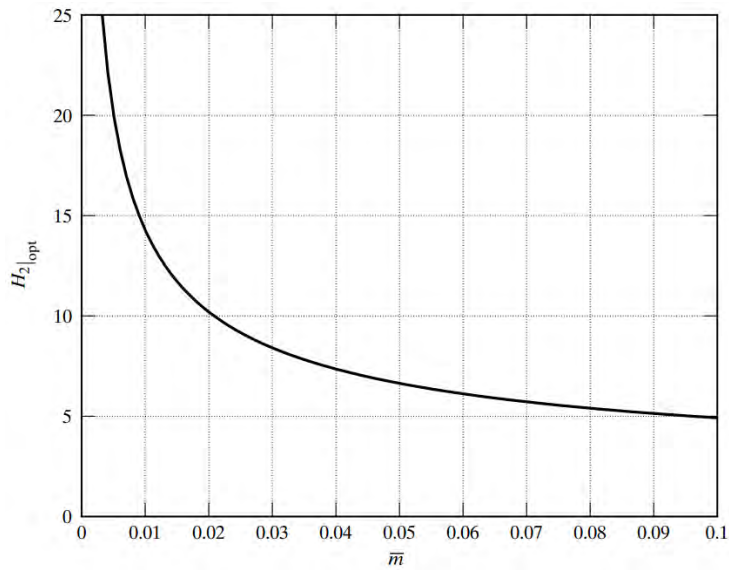


Figure 5.21: Maximum dynamic amplification factor for SDOF system (optimal tuning and damping).

The response of the damper is defined by Eq. (5.61). Spe-

5.4. TUNED MASS DAMPER THEORY FOR SDOF SYSTEMS

cializing this equation for the optimal conditions leads to the plot of amplification versus mass ratio contained in Fig. 5.22. A comparison of the damper motion with respect to the motion of the primary mass for optimal conditions is shown in Fig. 5.23.

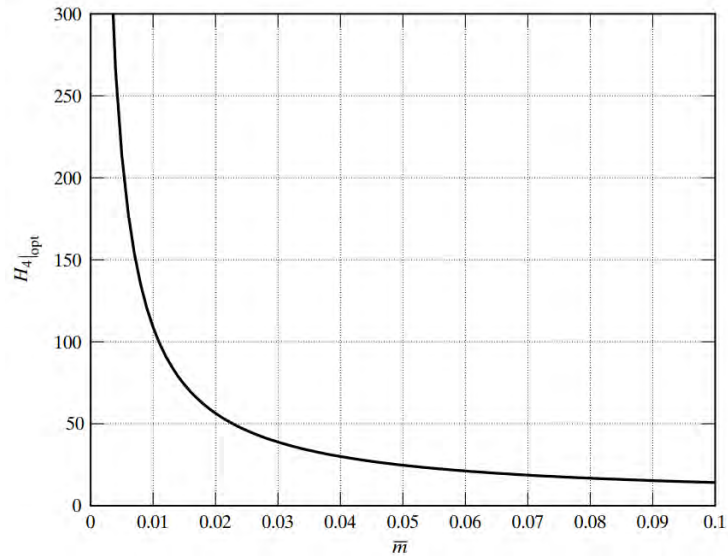


Figure 5.22: Maximum dynamic amplification factor for TMD.

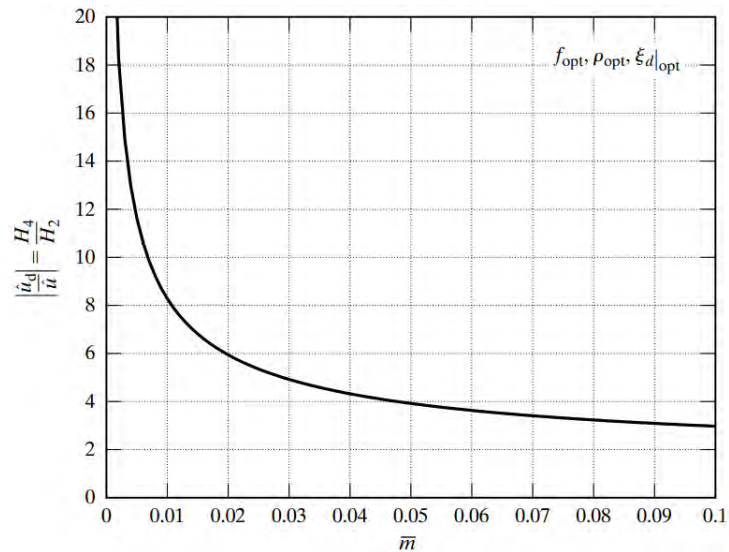


Figure 5.23: Ratio of maximum TMD amplitude to maximum system amplitude.

Lastly, response curves for a typical mass ratio, $\bar{m} = 0.01$, and optimal tuning are plotted in Fig. 5.24 and 5.25. The response for no damper is also plotted in Fig. 5.24. We observe that the effect of the damper is to limit the motion in a frequency range centered on the natural frequency of the primary mass and extending about 0.15ω . Outside of this range, the motion is not significantly influenced by the damper.

5.4. TUNED MASS DAMPER THEORY FOR SDOF SYSTEMS

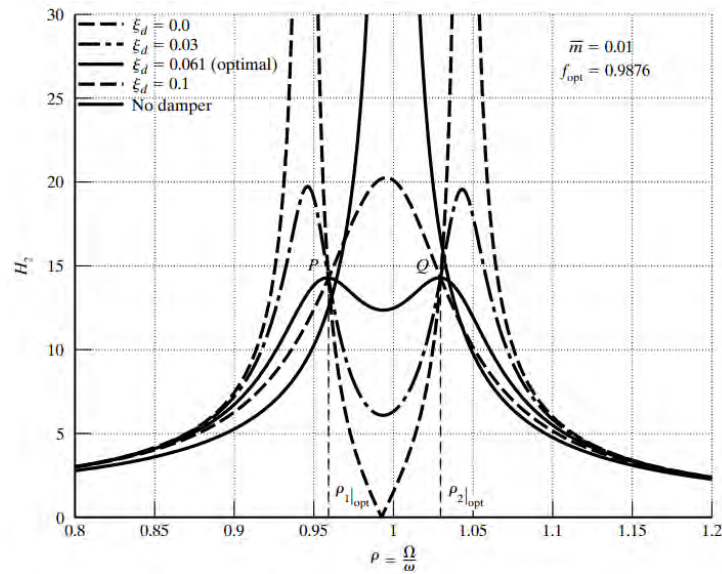


Figure 5.24: Response curves for amplitude of system with optimally tuned TMD.

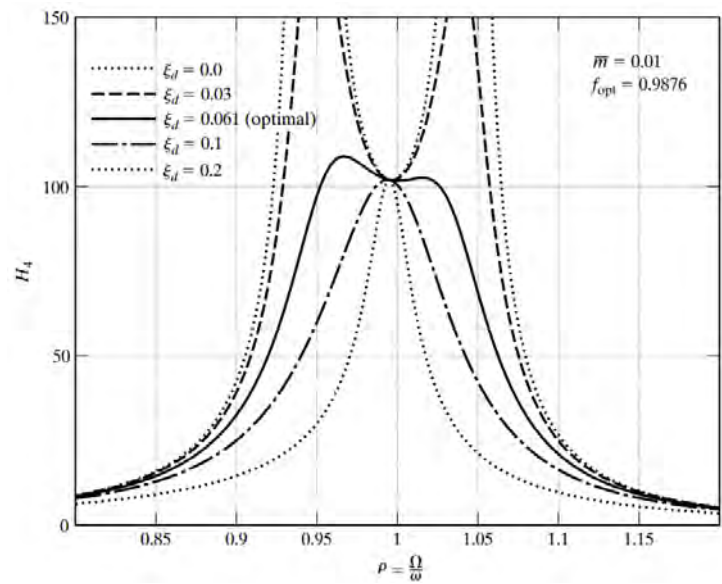


Figure 5.25: Response curves for amplitude of optimally tuned TMD.

The maximum amplification for a damped SDOF system

CHAPTER 5. TUNED MASS DAMPER SYSTEMS

without a TMD, undergoing harmonic excitation is given by Eq. (1.7).

$$H = \frac{1}{2\xi\sqrt{1-\xi^2}} \quad (5.91)$$

Since ξ is small, a reasonable approximation is

$$H \approx \frac{1}{2\xi} \quad (5.92)$$

Expressing the optimal H_2 in a similar form provides a measure of the equivalent damping ratio ξ_e for the primary mass

$$\xi_e = \frac{1}{2H_2|_{\text{opt}}} \quad (5.93)$$

Fig. 5.26 shows the variation of ξ_e with the mass ratio. A mass ratio of 0.02 is equivalent to about 5% damping in the primary system.

5.4. TUNED MASS DAMPER THEORY FOR SDOF SYSTEMS

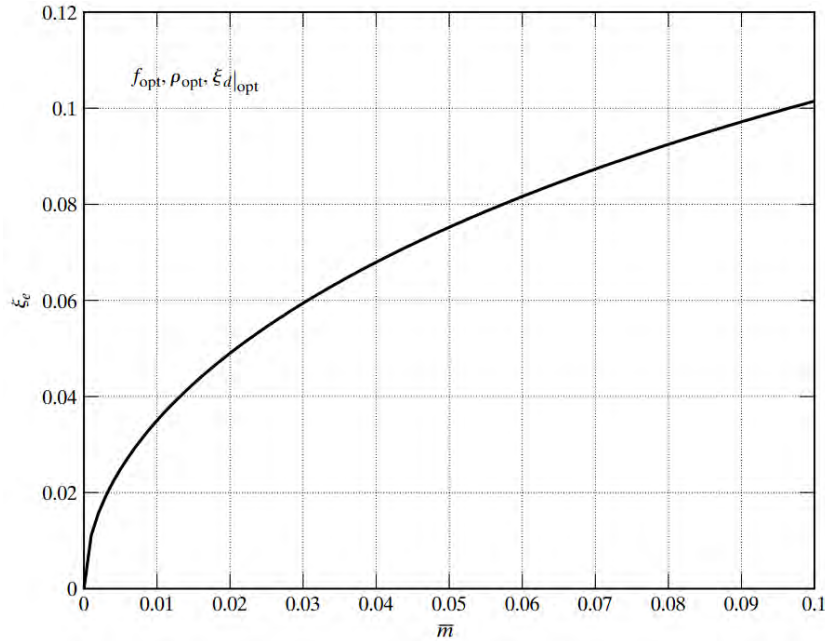


Figure 5.26: Equivalent damping ratio for optimally tuned TMD.

The design of a TMD involves the following steps:

- Establish the allowable values of displacement of the primary mass and the TMD for the design loading. This data provides the *design* values for $H_2|_{opt}$ and $H_4|_{opt}$.
- Determine the mass ratios required to satisfy these motion constraints from Fig. 5.21 and 5.22. Select the largest value of \bar{m} .
- Determine f_{opt} from Fig. 5.18.

- Compute ω_d

$$\omega_d = f_{opt}\omega \quad (5.94)$$

- Compute k_d

$$k_d = m_d\omega_d^2 = \bar{m}k f_{opt}^2 \quad (5.95)$$

- Determine $\xi_d|_{\text{opt}}$ from Fig. 5.20.
- Compute c_d

$$c_d = 2\xi_d|_{\text{opt}}\omega_d m_d = \bar{m} f_{\text{opt}}(2\xi_d|_{\text{opt}}\omega m) \quad (5.96)$$

Example 5.2 - Design of a TMD for an undamped SDOF system

Consider the following motion constraints

$$H_2|_{\text{opt}} < 7 \quad (5.97)$$

$$\frac{H_4}{H_2|_{\text{opt}}} < 6 \quad (5.98)$$

Constraint Eq. (5.97) requires $\bar{m} \geq 0.05$. For constraint Eq. (5.98), we need to take $\bar{m} \geq 0.02$. Therefore, $\bar{m} \geq 0.05$ controls the design. The relevant parameters are:

$$\bar{m} = 0.05 \quad f_{\text{opt}} = 0.94 \quad \xi_d|_{\text{opt}} = 0.135$$

Then

$$m_d = 0.05m \quad \omega_d = 0.94\omega \quad k_d = \bar{m} f_{\text{opt}}^2 k = 0.044k$$

5.4.3 Damped structure - damped TMD

All real systems contain some damping. Although an absorber is likely to be added only to a lightly damped system, assessing the effect of damping in the real system on the optimal tuning of the absorber is an important design consideration.

The main system in Fig. 5.27 consists of the mass m , spring stiffness k , and viscous damper c . The TMD system has mass

5.4. TUNED MASS DAMPER THEORY FOR SDOF SYSTEMS

m_d , stiffness k_d , and viscous damper c_d . Considering the system to be subjected to both external forcing and ground excitation, the equations of motion are

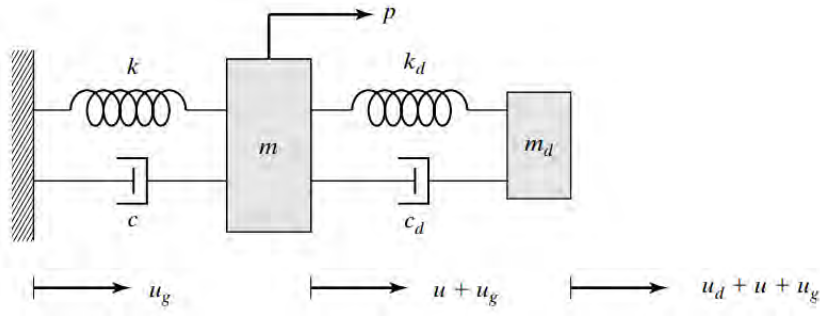


Figure 5.27: Damped SDOF system coupled with a damped TMD system.

$$m_d \ddot{u}_d + c_d \dot{u}_d + k_d u_d + m_d \ddot{u} = -m_d a_g \quad (5.99)$$

$$m \ddot{u} + c \dot{u} + k u - c_d \dot{u}_d - k_d u_d = -m a_g + p \quad (5.100)$$

Proceeding in the same way as for the undamped case, the solution due to periodic excitation (both p and u_g) is expressed in polar form

$$\bar{u} = \frac{\hat{p}}{k} H_5 e^{i\delta_5} - \frac{\hat{a}_g m}{k} H_6 e^{i\delta_6} \quad (5.101)$$

$$\bar{u}_d = \frac{\hat{p}}{k} H_7 e^{-i\delta_7} - \frac{\hat{a}_g m}{k} H_8 e^{-i\delta_8} \quad (5.102)$$

The various H and δ terms are defined below

$$H_5 = \frac{\sqrt{(f^2 - \rho^2)^2 + (2\xi_d \rho f)^2}}{|D_3|} \quad (5.103)$$

$$H_6 = \frac{\sqrt{[(1 + \bar{m})f^2 - \rho^2]^2 + [2\xi_d \rho f(1 + \bar{m})]^2}}{|D_3|} \quad (5.104)$$

$$H_7 = \frac{\rho^2}{|D_3|} \quad (5.105)$$

$$H_8 = \frac{\sqrt{1 + [2\xi\rho]^2}}{|D_3|} \quad (5.106)$$

$$|D_3| = \{[-f^2\rho^2\bar{m} + (1 - \rho^2)(f^2 - \rho^2) - 4\xi\xi_d f\rho^2]^2 + 4[\xi\rho(f^2 - \rho^2) + \xi_d f\rho(1 - \rho^2(1 + \bar{m}))]^2\}^{1/2} \quad (5.107)$$

$$\delta_5 = \alpha_1 - \delta_7 \quad (5.108)$$

$$\delta_6 = \alpha_2 - \delta_7 \quad (5.109)$$

$$\delta_8 = \alpha_3 - \delta_7 \quad (5.110)$$

$$\tan \delta_7 = 2 \frac{\xi\rho(f^2 - \rho^2) + \xi_d f\rho(1 - \rho^2(1 + \bar{m}))}{-f^2\rho^2\bar{m} + (1 - \rho^2)(f^2 - \rho^2) - 4\xi\xi_d f\rho^2} \quad (5.111)$$

$$\tan \alpha_3 = 2\xi\rho \quad (5.112)$$

The α_1 and α_2 terms are defined by Eq. (5.78) and (5.79).

In what follows, the case of an external force applied to the primary mass is considered. Since $|D_3|$ involves ξ , we cannot establish analytical expressions for the optimal tuning frequency and optimal damping ratio in terms of the mass ratio. In this case, these parameters also depend on ξ . Numerical simulations can be applied to evaluate H_5 and H_7 for a range of ρ , given the values for \bar{m} , ξ , f , and ξ_d . Starting with specific values for \bar{m} and ξ , plots of H_5 versus ρ can be generated for a range of f and ξ_d . Each $H_5 - \rho$ plot has a peak value of H_5 . The particular combination of f and ξ_d that correspond to the *lowest* peak value of H_5 is taken as the *optimal* state. Repeating this process for different values of \bar{m} and ξ produces the behavioral data needed to design the damper system.

Example 5.3 -

5.4. TUNED MASS DAMPER THEORY FOR SDOF SYSTEMS

Eq. (5.101) defines the displacement of the primary structure. Also of interest is the acceleration of the primary structure since this measure usually controls the design for wind vibration. Starting with

$$u = \bar{u}e^{i\Omega t} \quad (1)$$

and differentiating with respect to time leads to

$$\begin{aligned} a = \ddot{u} &= -\Omega^2 \bar{u}e^{i\Omega t} = \Omega^2 \bar{u}e^{i(\Omega t + \pi)} \\ &= Ae^{i(\Omega t + \pi)} \end{aligned} \quad (2)$$

Noting Eq. (5.101), A is given by

$$\begin{aligned} A = \Omega^2 \bar{u} &= \frac{\Omega^2 p}{k} H_5 e^{i\delta_5} = \frac{p}{m} \left(\frac{\Omega}{\omega} \right)^2 H_5 e^{i\delta_5} \\ &= \left(\frac{p}{m} e^{i\delta_5} \right) (\rho^2 H_5) \end{aligned} \quad (3)$$

Finally,

$$\begin{aligned} a &= \frac{p}{m} (\rho^2 H_5) e^{i(\Omega t + \pi + \delta_5)} \\ &= \frac{p}{m} A e^{i(\Omega t + \pi + \delta_5)} \end{aligned} \quad (4)$$

One can apply numerical simulations to evaluate the optimal values of f and ξ_d , given the mass ratio and the initial damping. The following plots (Figs. E5.3a to E5.3f) illustrate the convergence process for two values of \bar{m} .

CHAPTER 5. TUNED MASS DAMPER SYSTEMS

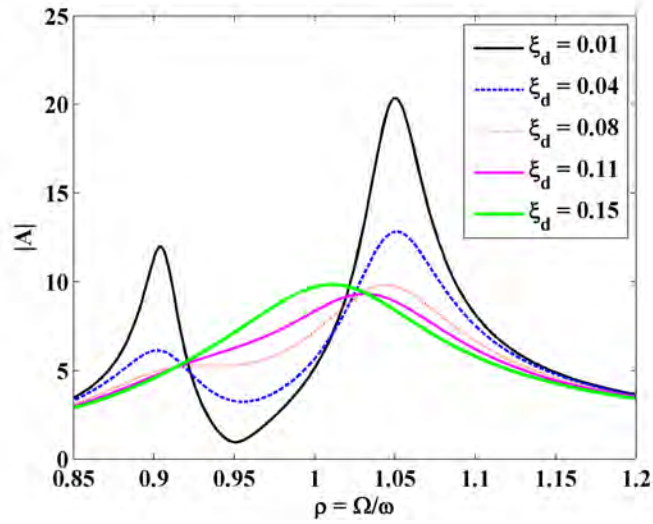


Figure E5.3a: Damped SDOF. $\bar{m} = 0.02$, $f = 0.95$, $\xi = 0.02$.

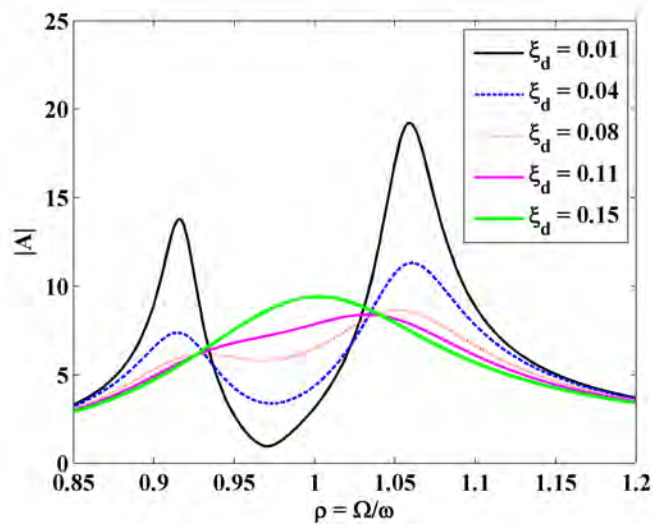


Figure E5.3b: Damped SDOF. $\bar{m} = 0.02$, $f = 0.97$, $\xi = 0.02$.

5.4. TUNED MASS DAMPER THEORY FOR SDOF SYSTEMS

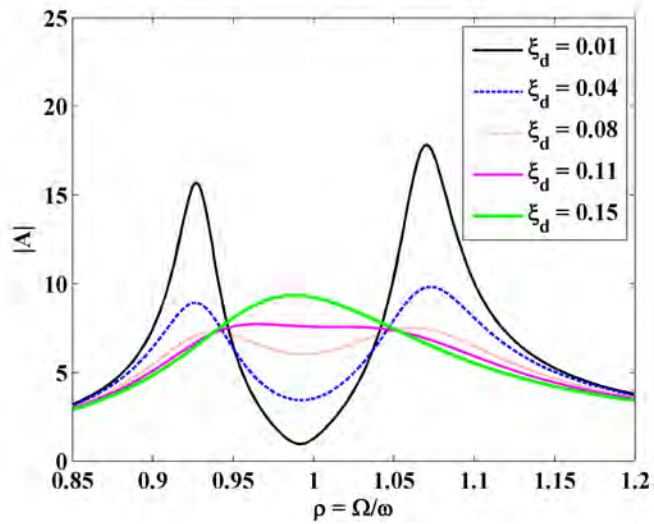


Figure E5.3c: Damped SDOF. $\bar{m} = 0.02$, $f = 0.9915$, $\xi = 0.02$.

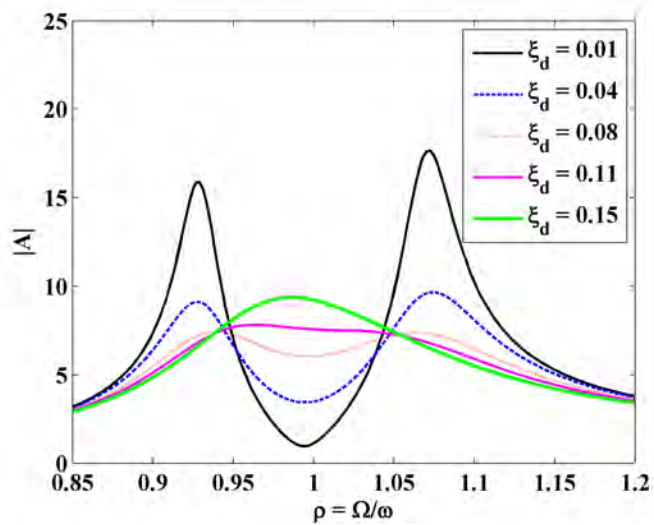


Figure E5.3d: Damped SDOF. $\bar{m} = 0.02$, $f = 0.994$, $\xi = 0.02$.

CHAPTER 5. TUNED MASS DAMPER SYSTEMS

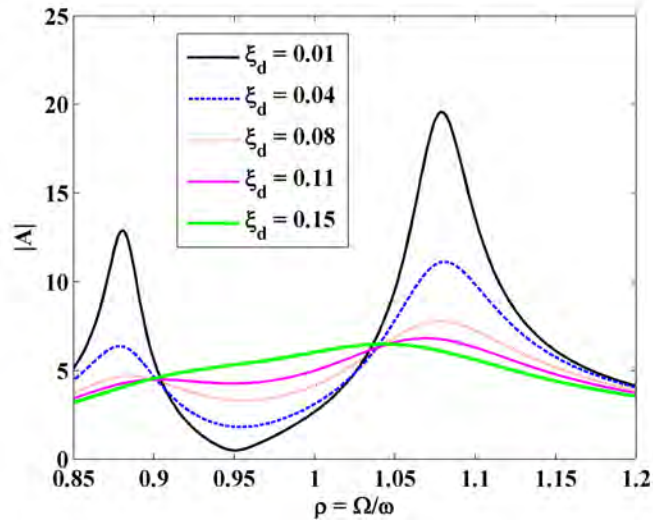


Figure E5.3e: Damped SDOF. $\bar{m} = 0.04$, $f = 0.95$, $\xi = 0.02$.

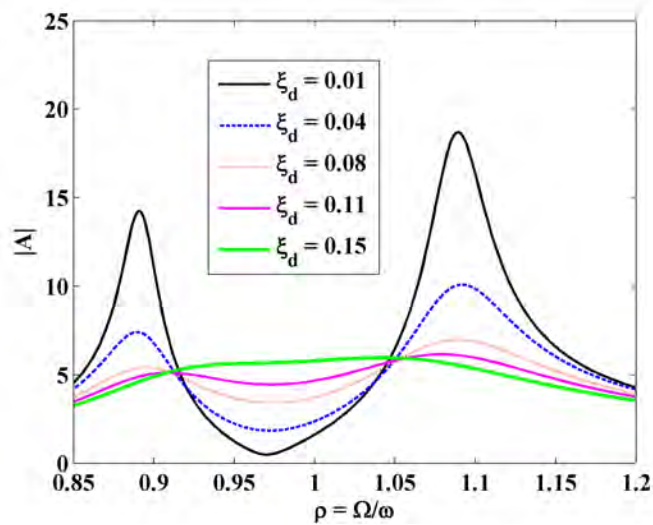


Figure E5.3f: Damped SDOF. $\bar{m} = 0.04$, $f = 0.97$, $\xi = 0.02$.

5.4. TUNED MASS DAMPER THEORY FOR SDOF SYSTEMS

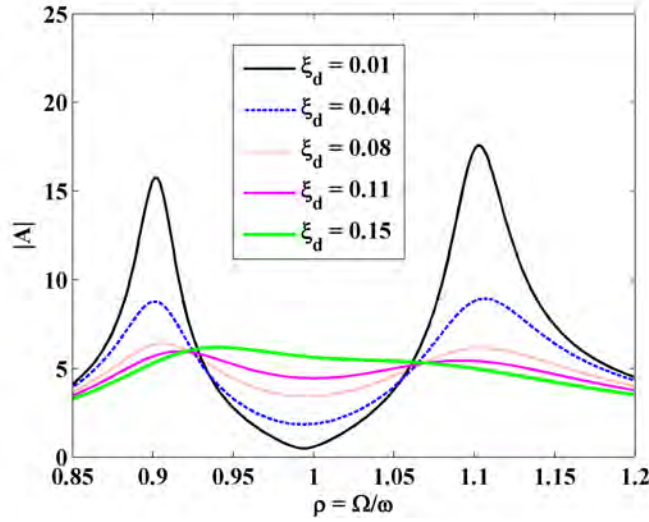


Figure E5.3g: Damped SDOF. $\bar{m} = 0.04$, $f = 0.994$, $\xi = 0.02$.

Fig. 5.28 shows the variation of the maximum value of H_5 for the optimal state. The corresponding response of the damper is plotted in Fig. 5.29. Adding damping to the primary mass has an appreciable effect for small \bar{m} . Noting Eq. (5.101) and (5.102), the ratio of damper displacement to primary mass displacement is given by

$$\frac{|\hat{u}_d|}{|\hat{u}|} = \frac{H_7}{H_5} = \frac{\rho^2}{\sqrt{(f^2 - \rho^2)^2 + (2\xi_d \rho f)^2}} \quad (5.113)$$

Since ξ is small, this ratio is essentially independent of ξ . Fig. 5.30 confirms this statement. The optimal values of the frequency and damping ratios generated through simulation are plotted in Fig. 5.31 and 5.32. Lastly, using Eq. (5.93), $H_5|_{\text{opt}}$ can be converted to an equivalent damping ratio for the primary system.

$$\xi_e = \frac{1}{2H_5|_{\text{opt}}} \quad (5.114)$$

Fig. 5.33 shows the variation of ξ_e with \bar{m} and ξ .

Tsai & Lin [105] suggest equations for the optimal tuning parameters f and ξ_d determined by curve fitting schemes. The equations are listed below for completeness

$$\begin{aligned} f = & \left(\frac{\sqrt{1 - 0.5\bar{m}}}{1 + \bar{m}} + \sqrt{1 - 2\xi^2} - 1 \right) \\ & - (2.375 - 1.034\sqrt{\bar{m}} - 0.426\bar{m})\xi\sqrt{\bar{m}} \\ & - (3.730 - 16.903\sqrt{\bar{m}} + 20.496\bar{m})\xi^2\sqrt{\bar{m}} \end{aligned} \quad (5.115)$$

$$\begin{aligned} \xi_d = & \sqrt{\frac{3\bar{m}}{8(1 + \bar{m})(1 - 0.5\bar{m})}} + (0.151\xi - 0.170\xi^2) \\ & + (0.163\xi + 4.980\xi^2)\bar{m} \end{aligned} \quad (5.116)$$

5.4. TUNED MASS DAMPER THEORY FOR SDOF SYSTEMS

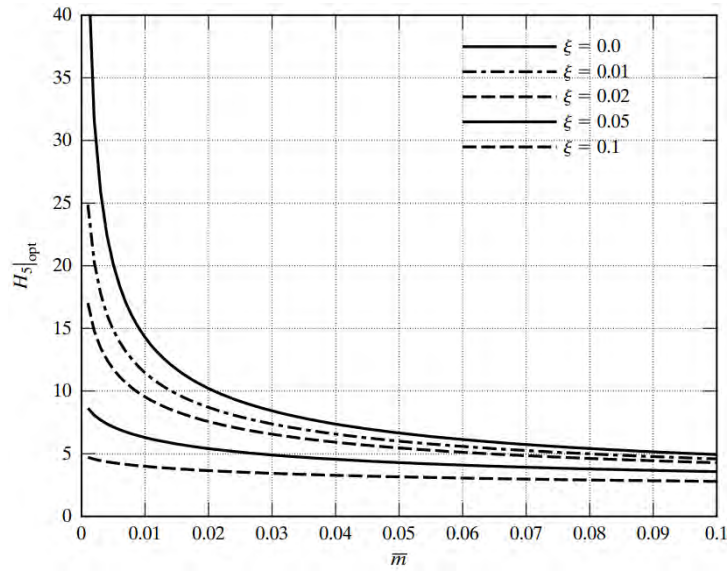


Figure 5.28: Maximum dynamic amplification factor for damped SDOF system.

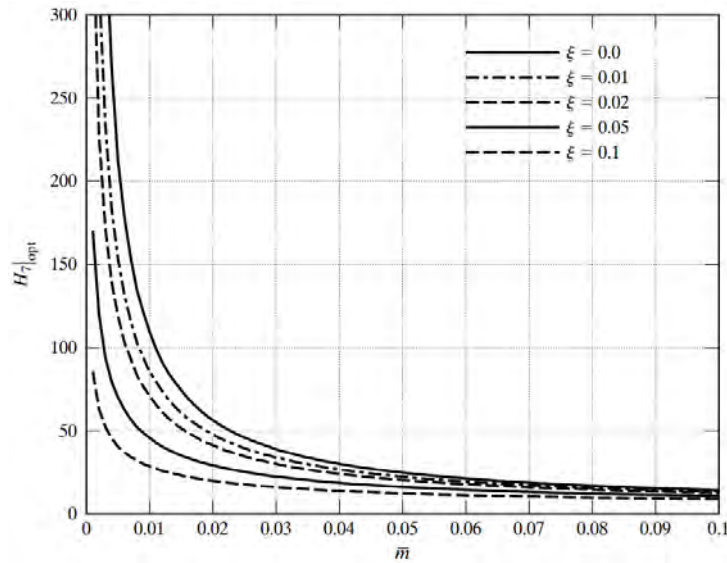


Figure 5.29: Maximum dynamic amplification factor for TMD.

CHAPTER 5. TUNED MASS DAMPER SYSTEMS

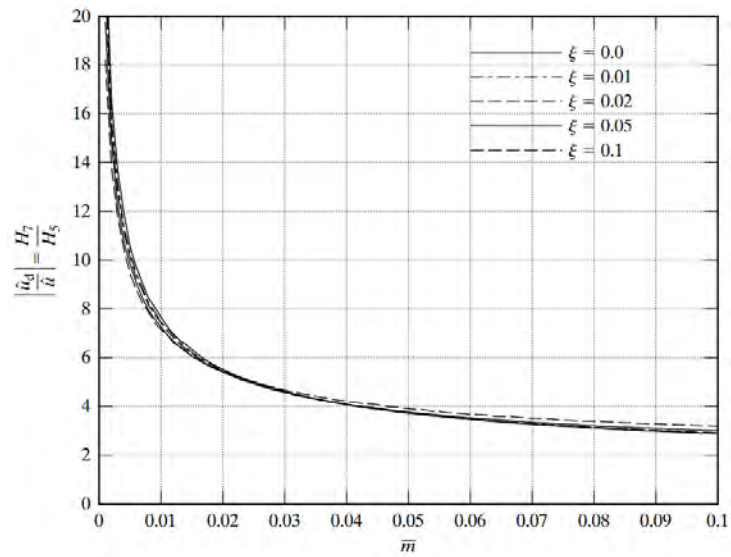


Figure 5.30: Ratio of maximum TMD amplitude to maximum system amplitude.

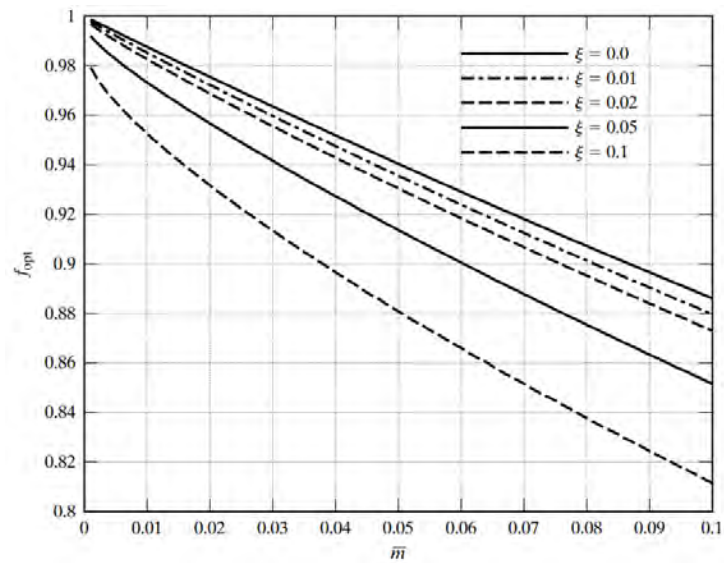


Figure 5.31: Optimum tuning frequency ratio for TMD, f_{opt} .

5.4. TUNED MASS DAMPER THEORY FOR SDOF SYSTEMS

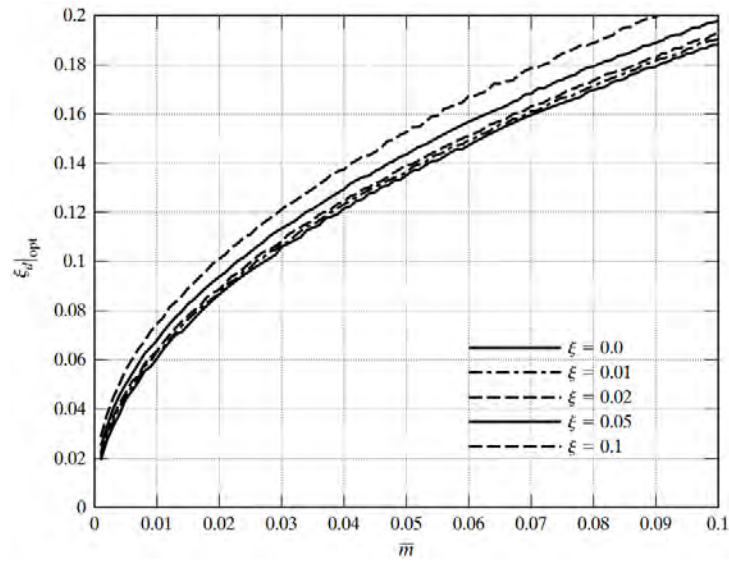


Figure 5.32: Optimal damping ratio for TMD.

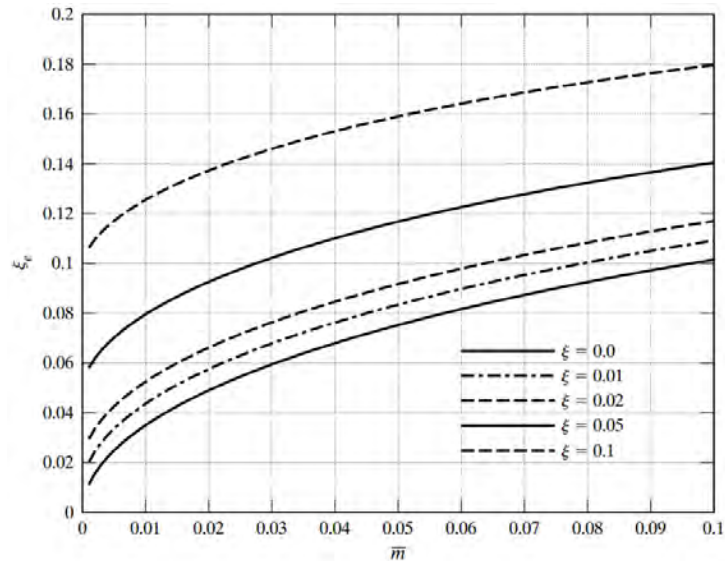


Figure 5.33: Equivalent damping ratio for optimally tuned TMD.

Example 5.4 - Design of a TMD for a damped SDOF system

CHAPTER 5. TUNED MASS DAMPER SYSTEMS

Ex. 5.2 is reworked here, allowing for 2% damping in the primary system. The same design motion constraints are considered:

$$H_5|_{\text{opt}} < 7 \quad (5.117)$$

$$\frac{H_7}{H_5|_{\text{opt}}} < 6 \quad (5.118)$$

Using Fig. 5.28, the required mass ratio for $\xi = 0.02$ is $\bar{m} = 0.03$. The other optimal values are $f_{\text{opt}} = 0.965$ and $\xi_d|_{\text{opt}} = 0.105$.

Then

$$m_d = 0.03m \quad \omega_d = 0.955\omega \quad k_d = \bar{m}f_{\text{opt}}^2 k = 0.027k$$

In this case, there is a significant reduction in the damper mass required for this set of motion constraints. The choice between including damping in the primary system versus incorporating a tuned mass damper depends on the relative costs and reliability of the two alternatives, and the nature of the structural problem. A TMD system is generally more appropriate for upgrading an existing structure where access to the structural elements is difficult.

5.5 Case studies - SDOF systems

Fig. 5.34 to 5.45 show the time history responses for two SDOF systems with periods of 0.49s and 5.35s respectively under harmonic (at resonance conditions), El Centro, and Taft ground excitations. All examples have a system damping ratio of 2% and an optimally tuned TMD with a mass ratio of 1%. The

5.5. CASE STUDIES - SDOF SYSTEMS

excitation magnitudes have been scaled so that the peak amplitude of the response of the system without the TMD is unity. The plots show the response of the system without the TMD (the dotted line) as well as the response of the system with the TMD (the solid line). Figures showing the time history of the relative displacement of the TMD with respect to the system are also presented. Significant reduction in the response of the primary system under harmonic excitation is observed. However, optimally tuned mass dampers are relatively ineffective under seismic excitation, and in some cases produce a negative effect, i.e. they amplify the response slightly. This poor performance is attributed to the ineffectiveness of tuned mass dampers for impulsive loadings as well as their inability to reach a resonant condition under random excitation, and therefore dissipate energy. The results for $T = 5.35$ s show essentially no effect of the TMD. This is due to the nature of the seismic excitation; their energy (amplitude) is concentrated in the neighborhood of $T = 1$ s. These results are in close agreement with the data presented by Kaynia *et al.* [51].

CHAPTER 5. TUNED MASS DAMPER SYSTEMS

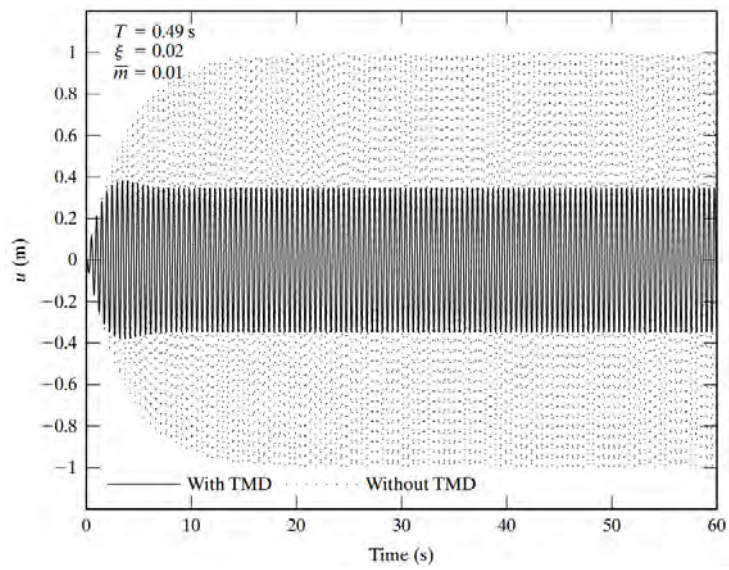


Figure 5.34: Response of SDOF to harmonic excitation.

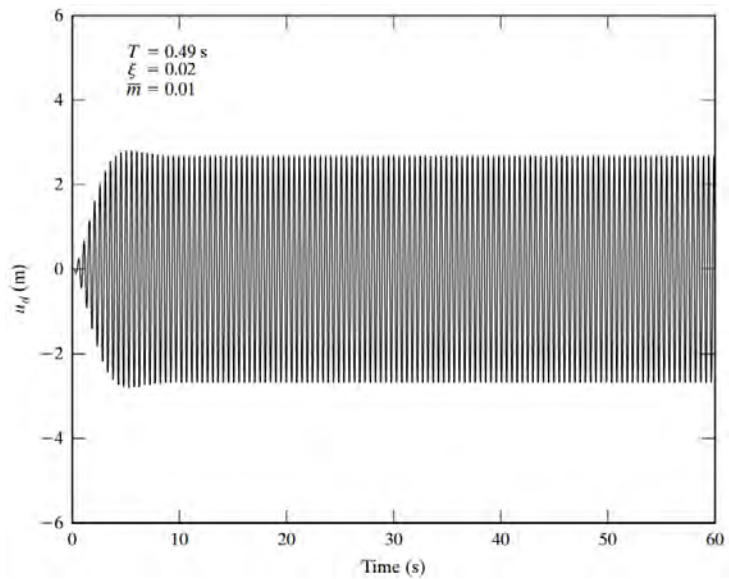


Figure 5.35: Relative displacement of TMD under harmonic excitation.

5.5. CASE STUDIES - SDOF SYSTEMS

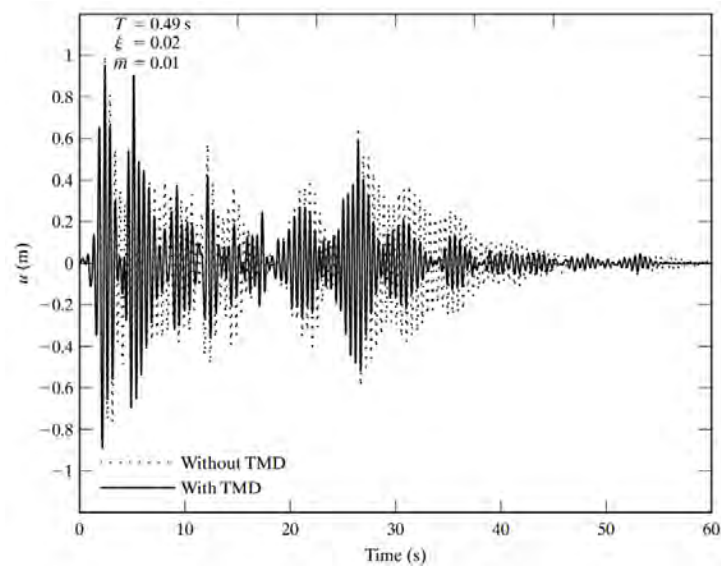


Figure 5.36: Response of SDOF to El Centro excitation.

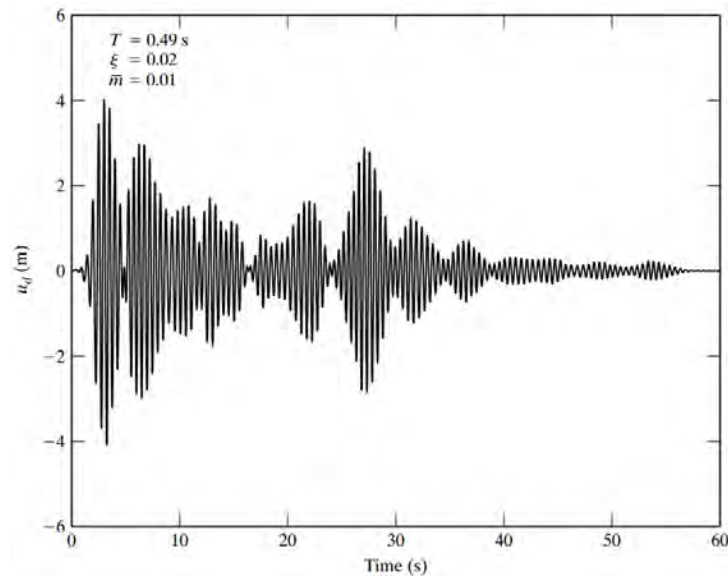


Figure 5.37: Relative displacement of TMD under El Centro excitation.

CHAPTER 5. TUNED MASS DAMPER SYSTEMS

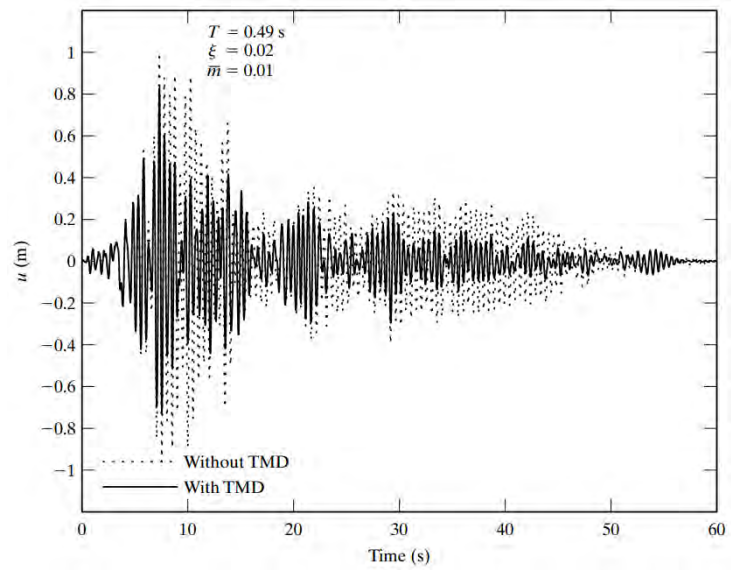


Figure 5.38: Response of SDOF to Taft excitation.

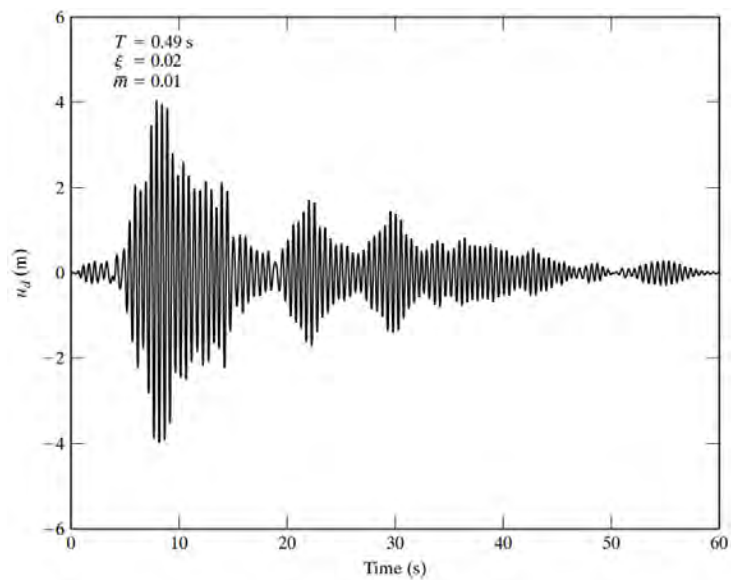


Figure 5.39: Relative displacement of TMD under Taft excitation.

5.5. CASE STUDIES - SDOF SYSTEMS

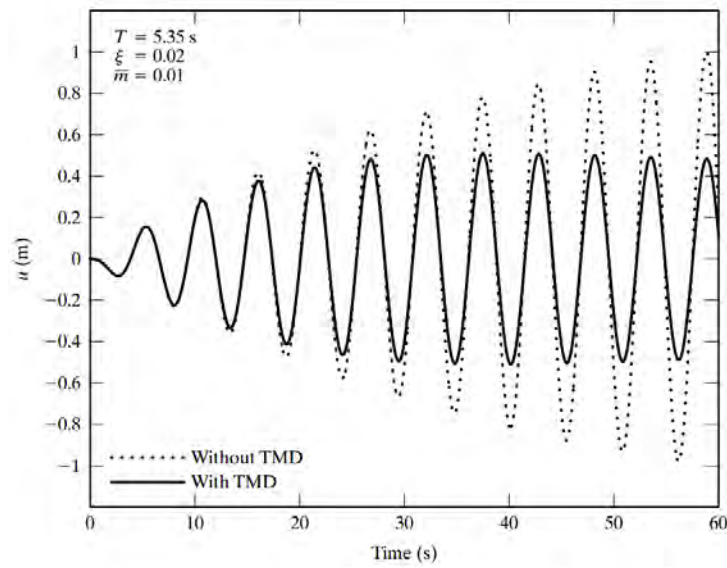


Figure 5.40: Response of SDOF to harmonic excitation.

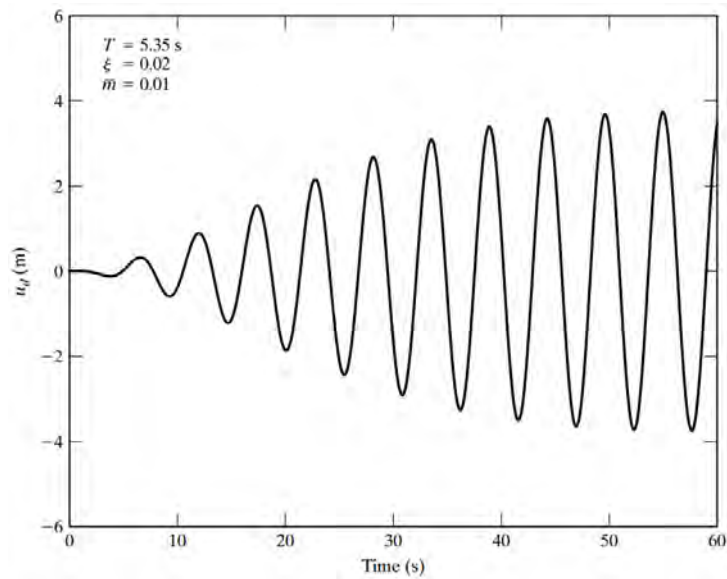


Figure 5.41: Relative displacement of TMD under harmonic excitation.

CHAPTER 5. TUNED MASS DAMPER SYSTEMS

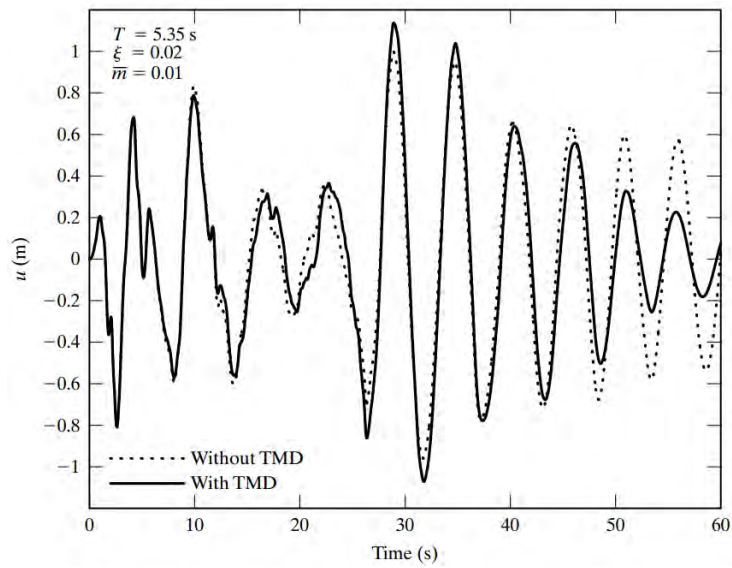


Figure 5.42: Response of SDOF to El Centro excitation.

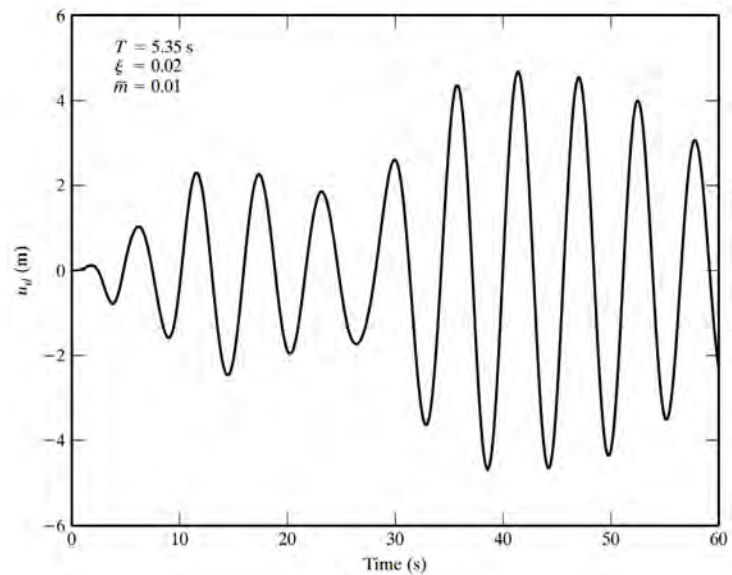


Figure 5.43: Relative displacement of TMD under El Centro excitation.

5.5. CASE STUDIES - SDOF SYSTEMS

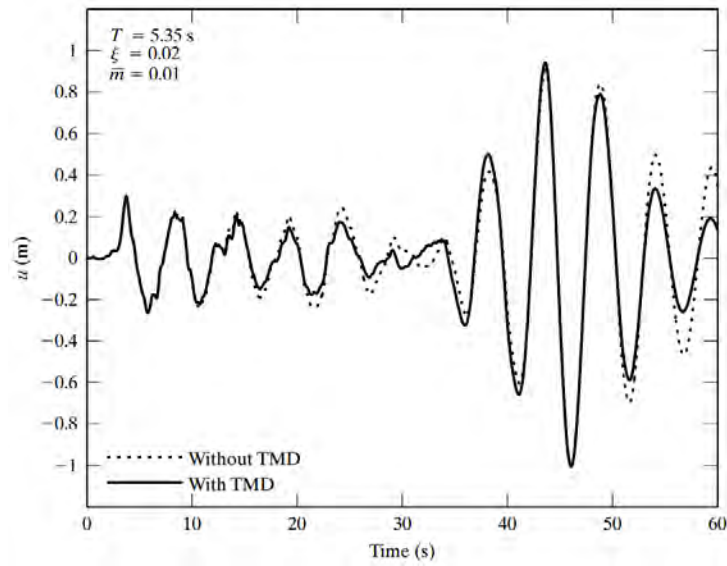


Figure 5.44: Response of SDOF to Taft excitation.

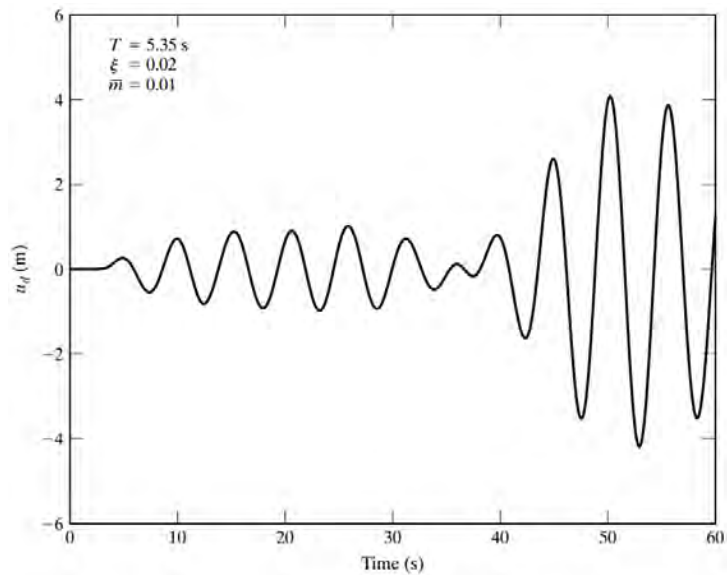


Figure 5.45: Relative displacement of TMD under Taft excitation.

5.6 Tuned mass damper theory for MDOF systems

The theory of a SDOF system presented earlier is extended here to deal with a MDOF system having a number of tuned mass dampers located throughout the structure. Numerical simulations, which illustrate the application of this theory to example building structures are presented in the next section.

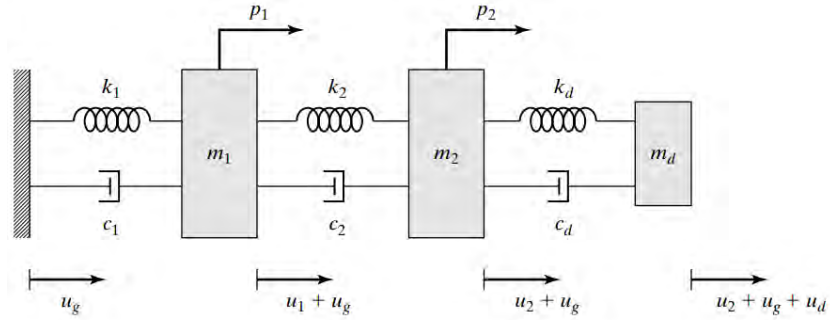


Figure 5.46: 2DOF system with TMD.

A 2DOF system having a damper attached to mass 2 is considered first to introduce the key ideas. The governing equations for the system shown in Fig. 5.46 are

$$m_1 \ddot{u}_1 + c_1 \dot{u}_1 + k_1 u_1 - k_2 (u_2 - u_1) - c_2 (\dot{u}_2 - \dot{u}_1) = p_1 - m_1 \ddot{u}_g \quad (5.119)$$

$$m_2 \ddot{u}_2 + c_2 (\dot{u}_2 - \dot{u}_1) + k_2 (u_2 - u_1) - c_d \dot{u}_d - k_d u_d = p_2 - m_2 \ddot{u}_g \quad (5.120)$$

$$m_d \ddot{u}_d + c_d \dot{u}_d + k_d u_d = -m_d (\ddot{u}_2 + \ddot{u}_g) \quad (5.121)$$

The key step is to combine Eqs. (5.119) and (5.120) and express the resulting equation in a form similar to the SDOF case defined by Eq. 5.100. This operation reduces the problem to

5.6. TUNED MASS DAMPER THEORY FOR MDOF SYSTEMS

an equivalent SDOF system, for which the theory of Sect. 5.4 is applicable. The approach followed here is based on transforming the original matrix equation to scalar modal equations.

Introducing matrix notation, Eqs. (5.119) and (5.120) are written as

$$\mathbf{M}\ddot{\mathbf{U}} + \mathbf{C}\dot{\mathbf{U}} + \mathbf{K}\mathbf{U} = \begin{bmatrix} p_1 - m_1 a_g \\ p_2 - m_2 a_g \end{bmatrix} + \begin{bmatrix} 0 \\ c_d \dot{u}_d + k_d u_d \end{bmatrix} \quad (5.122)$$

where the various matrices are

$$\mathbf{U} = \begin{bmatrix} u_1 \\ u_2 \end{bmatrix} \quad (5.123)$$

$$\mathbf{M} = \begin{bmatrix} m_1 & 0 \\ 0 & m_2 \end{bmatrix} \quad (5.124)$$

$$\mathbf{K} = \begin{bmatrix} k_1 + k_2 & -k_2 \\ -k_2 & k_2 \end{bmatrix} \quad (5.125)$$

$$\mathbf{C} = \begin{bmatrix} c_1 + c_2 & -c_2 \\ -c_2 & c_2 \end{bmatrix} \quad (5.126)$$

We substitute for \mathbf{U} in terms of the modal vectors and coordinates

$$\mathbf{U} = \Phi_1 q_1 + \Phi_2 q_2 \quad (5.127)$$

The modal vectors satisfy the following orthogonality relations (see Sect. 3.2.1)

$$\Phi_j^T \mathbf{K} \Phi_i = \delta_{ij} \omega_j^2 \Phi_j^T \mathbf{M} \Phi_i \quad (5.128)$$

Defining modal mass, stiffness, and damping terms,

$$\tilde{m}_j = \Phi_j^T \mathbf{M} \Phi_j \quad (5.129)$$

$$\tilde{k}_j = \Phi_j^T \mathbf{K} \Phi_j = \omega_j^2 \tilde{m}_j \quad (5.130)$$

$$\tilde{c}_j = \Phi_j^T \mathbf{C} \Phi_j \quad (5.131)$$

expressing the elements of Φ_j as

$$\Phi_j = \begin{bmatrix} \Phi_{j1} \\ \Phi_{j2} \end{bmatrix} \quad (5.132)$$

and assuming damping is proportional to stiffness

$$\mathbf{C} = \alpha \mathbf{K} \quad (5.133)$$

we obtain a set of uncoupled equations for q_1 and q_2

$$\begin{aligned} \tilde{m}_j \ddot{q}_j + \tilde{c}_j \dot{q}_j + \tilde{k}_j q_j = & \Phi_{j1} (p_1 - m_1 a_g) \\ & + \Phi_{j2} (p_2 - m_2 a_g + c_d \dot{u}_d + k_d u_d) \quad j = 1, 2 \end{aligned} \quad (5.134)$$

With this assumption, the modal damping ratio is given by

$$\xi_j = \frac{\tilde{c}_j}{2\omega_j \tilde{m}_j} = \frac{\alpha \omega_j}{2} \quad (5.135)$$

Eq. (5.134) represents two equations. Each equation defines a particular SDOF system having mass, stiffness, and damping equal to \tilde{m} , \tilde{k} , and ξ . Since a TMD is effective for a narrow frequency range, we have to decide on which *modal* resonant response is to be controlled with the TMD. Once this decision is made, the analysis can proceed using the *selected* modal equation and the initial equation for the TMD, i.e. Eq. (5.121).

5.6. TUNED MASS DAMPER THEORY FOR MDOF SYSTEMS

Suppose the *first* modal response is to be controlled. Taking $j = 1$ in Eq. (5.134) leads to

$$\begin{aligned} \tilde{m}_1 \ddot{q}_1 + \tilde{c}_1 \dot{q}_1 + \tilde{k}_1 q_1 = & \Phi_{11} p_1 + \Phi_{12} p_2 \\ & - (m_1 \Phi_{11} + m_2 \Phi_{12}) a_g + \Phi_{12} (c_d \dot{u}_d + k_d u_d) \end{aligned} \quad (5.136)$$

In general, u_2 is obtained by superposing the modal contributions

$$u_2 = \Phi_{12} q_1 + \Phi_{22} q_2 \quad (5.137)$$

However, when the external forcing frequency is close to ω_1 , the first mode response will dominate, and it is reasonable to assume

$$u_2 \approx \Phi_{12} q_1 \quad (5.138)$$

Solving for q_1

$$q_1 = \left[\frac{1}{\Phi_{12}} \right] u_2 \quad (5.139)$$

and then substituting in Eq. (5.136), we obtain

$$\tilde{m}_{1e} \ddot{u}_2 + \tilde{c}_{1e} \dot{u}_2 + \tilde{k}_{1e} u_2 = c_d \dot{u}_d + k_d u_d + \tilde{p}_{1e} - \Gamma_{1e} \tilde{m}_{1e} a_g \quad (5.140)$$

where \tilde{m}_{1e} , \tilde{c}_{1e} , \tilde{k}_{1e} , \tilde{p}_{1e} , and Γ_{1e} represent the *equivalent* SDOF parameters for the combination of mode 1 and node 2, the node at which the TMD is attached.

Their definition equations are

$$\tilde{m}_{1e} = \left[\frac{1}{\Phi_{12}^2} \right] \tilde{m}_1 \quad (5.141)$$

$$\tilde{k}_{1e} = \left[\frac{1}{\Phi_{12}^2} \right] \tilde{k}_1 \quad (5.142)$$

$$\tilde{c}_{1e} = \alpha \tilde{k}_{1e} \quad (5.143)$$

$$\tilde{p}_{1e} = \frac{\Phi_{11}p_1 + \Phi_{12}p_2}{\Phi_{12}} \quad (5.144)$$

$$\Gamma_{1e} = \frac{\Phi_{12}}{\tilde{m}_1} (m_1\Phi_{11} + m_2\Phi_{22}) \quad (5.145)$$

Eq. (5.121) and (5.140) are similar in form to the SDOF equations treated in the previous section. Both set of equations are compared below.

TMD equation

$$\begin{aligned} m_d\ddot{u}_d + c_d\dot{u}_d + k_d u_d &= -m_d(\ddot{u} - a_g) \\ \text{versus} & \\ m_d\ddot{u}_d + c_d\dot{u}_d + k_d u_d &= -m_d(\ddot{u}_2 - a_g) \end{aligned} \quad (5.146)$$

Primary mass equation

$$\begin{aligned} m\ddot{u} + c\dot{u} + ku &= c_d\dot{u}_d + k_d u_d + p - ma_g \\ \text{versus} & \\ \tilde{m}_{1e}\ddot{u}_2 + \tilde{c}_{1e}\dot{u}_2 + \tilde{k}_{1e}u_2 &= c_d\dot{u}_d + k_d u_d + \tilde{p}_{1e} - \Gamma_{1e}\tilde{m}_{1e}a_g \end{aligned} \quad (5.147)$$

Taking

$$\begin{aligned} u_2 \equiv u \quad \tilde{m}_{1e} \equiv m \quad \tilde{c}_{1e} \equiv c \quad \tilde{k}_{1e} \equiv k \\ \tilde{p}_{1e} \equiv p \quad \Gamma_{1e} \equiv \Gamma \end{aligned} \quad (5.148)$$

transforms the primary mass equation for the MDOF case to

5.6. TUNED MASS DAMPER THEORY FOR MDOF SYSTEMS

$$m\ddot{u} + c\dot{u} + ku = c_d\dot{u}_d + k_d u_d + p - \Gamma m a_g \quad (5.149)$$

which differs from the corresponding SDOF equation by the factor Γ . Therefore, the solution for ground excitation generated earlier has to be modified to account for the presence of Γ .

The generalized solution is written in the same form as the SDOF case. We need only to modify the terms associated with a_g (i.e. H_6 , H_8 and δ_6 , δ_8). Their expanded form is listed below.

$$H_6 = \frac{\sqrt{[(\Gamma + \bar{m})f^2 - \Gamma\rho^2]^2 + [2\xi_d\rho f(\Gamma + \bar{m})]^2}}{|D_3|} \quad (5.150)$$

$$H_8 = \frac{\sqrt{[1 + \rho^2(\Gamma - 1)]^2 + [2\xi\rho]^2}}{|D_3|} \quad (5.151)$$

$$\tan \alpha_2 = \frac{2\xi_d f \rho (\Gamma + \bar{m})}{f^2(\Gamma + \bar{m}) - \Gamma\rho^2} \quad (5.152)$$

$$\tan \alpha_3 = \frac{2\xi\rho}{1 + (\Gamma - 1)\rho^2} \quad (5.153)$$

$$\delta_6 = \alpha_2 - \delta_7 \quad (5.154)$$

$$\delta_8 = \alpha_3 - \delta_7 \quad (5.155)$$

where $|D_3|$ is defined by Eq. (5.107), and δ_7 is given by Eq. 5.111.

From this point on, we proceed as described in Sect. 5.4. The mass ratio is defined in terms of the *equivalent* SDOF mass.

$$\bar{m} = \frac{m_d}{\tilde{m}_{1e}} \quad (5.156)$$

Given \bar{m} and ξ_1 , we find the tuning frequency and damper damping ratio using Fig. 5.31 and 5.32. The damper parameters are determined with

$$m_d = \bar{m}\tilde{m}_{1e} \quad (5.157)$$

$$\omega_d = f_{\text{opt}}\omega_1 \quad (5.158)$$

$$c_d = 2\xi_d|_{\text{opt}}\omega_d m_d \quad (5.159)$$

Expanding the expression for the damper mass,

$$m_d = \bar{m}\tilde{m}_{1e} = \frac{\bar{m}[\Phi_1^T \mathbf{M} \Phi_1]}{\Phi_{12}^2} \quad (5.160)$$

shows that we should select the TMD location to coincide with the maximum amplitude of the mode shape that is being controlled. In this case, the first mode is the target mode, and Φ_{12} is the maximum amplitude for Φ_1 .

This derivation can be readily generalized to allow for tuning on the i^{th} modal frequency. We write Eq. (5.139) as

$$q_i = \left[\frac{1}{\Phi_{i2}} \right] u_2 \quad (5.161)$$

where i is either 1 or 2. The equivalent parameters are

$$\tilde{m}_{ie} = \left[\frac{1}{\Phi_{i2}^2} \right] \tilde{m}_i \quad (5.162)$$

$$\tilde{k}_{ie} = \omega_i^2 \tilde{m}_{1e} \quad (5.163)$$

Given \tilde{m}_{ie} and ξ_e , we specify \bar{m} and find the optimal tuning with

$$\omega_d = f_{\text{opt}}\omega_i \quad (5.164)$$

Example 5.5 - Design of a TMD for a damped MDOF system

5.6. TUNED MASS DAMPER THEORY FOR MDOF SYSTEMS

To illustrate the above procedure, a two DOF system having $m_1 = m_2 = 1$ is considered. Designing the system for a fundamental period of $T_1 = 1$ sec and a uniform deformation fundamental mode profile yields the following stiffnesses

$$k_1 = 12\pi^2 = 118.44$$
$$k_2 = 8\pi^2 = 78.96$$

Requiring a fundamental mode damping ratio of 2%, and taking damping proportional to stiffness ($\mathbf{C} = \alpha\mathbf{K}$), the corresponding α is

$$\alpha = \frac{2\xi_2}{\omega_1} = \frac{0.02}{\pi} = 0.0064$$

The mass, stiffness, and damping matrices for these design conditions are:

$$\mathbf{M} = \begin{bmatrix} 1 & 0 \\ 0 & 1 \end{bmatrix}$$
$$\mathbf{K} = \begin{bmatrix} 197.39 & -78.96 \\ -78.96 & 78.96 \end{bmatrix}$$
$$\mathbf{C} = \begin{bmatrix} 1.26 & -0.51 \\ -0.51 & 0.51 \end{bmatrix}$$

Performing an eigenvalue analysis yields the following frequencies and mode shapes

$$\omega_1 = 6.28 \text{ rad/s} \quad \omega_2 = 15.39 \text{ rad/s}$$
$$\Phi_1 = \begin{bmatrix} 0.5 \\ 1.0 \end{bmatrix} \quad \Phi_2 = \begin{bmatrix} 1.0 \\ -0.5 \end{bmatrix}$$

CHAPTER 5. TUNED MASS DAMPER SYSTEMS

The corresponding modal mass, stiffness, and damping terms are

$$\begin{aligned}\tilde{m}_1 &= \mathbf{\Phi}_1^T \mathbf{M} \mathbf{\Phi}_1 = 1.25 & \tilde{m}_2 &= \mathbf{\Phi}_2^T \mathbf{M} \mathbf{\Phi}_2 = 1.25 \\ \tilde{k}_1 &= \mathbf{\Phi}_1^T \mathbf{K} \mathbf{\Phi}_1 = 49.35 & \tilde{k}_2 &= \mathbf{\Phi}_2^T \mathbf{K} \mathbf{\Phi}_2 = 296.09 \\ \tilde{c}_1 &= \mathbf{\Phi}_1^T \mathbf{C} \mathbf{\Phi}_1 = 0.32 & \tilde{c}_2 &= \mathbf{\Phi}_2^T \mathbf{C} \mathbf{\Phi}_2 = 1.90 \\ \xi_1 &= \frac{\tilde{c}_1}{2\omega_1 \tilde{m}_1} = 0.02 & \xi_2 &= \frac{\tilde{c}_2}{2\omega_2 \tilde{m}_2} = 0.049\end{aligned}$$

When a TMD is added, the number of DOF is increased; in this case from 2 to 3. This results in another mode shape which is close to the mode that is being controlled. Fig. E5.5b shows the case for mode 1 with a damper applied to node 2; the additional mode denoted as 2 (the second mode) is close to mode 1. Results for the response based on calibrating the TMD to correspond to an equivalent modal damping of 0.1 are listed in Figs. E5.5c to E5.5f. Note that Fig. E5.5e shows the damper to be out of phase with the node.

5.6. TUNED MASS DAMPER THEORY FOR MDOF SYSTEMS

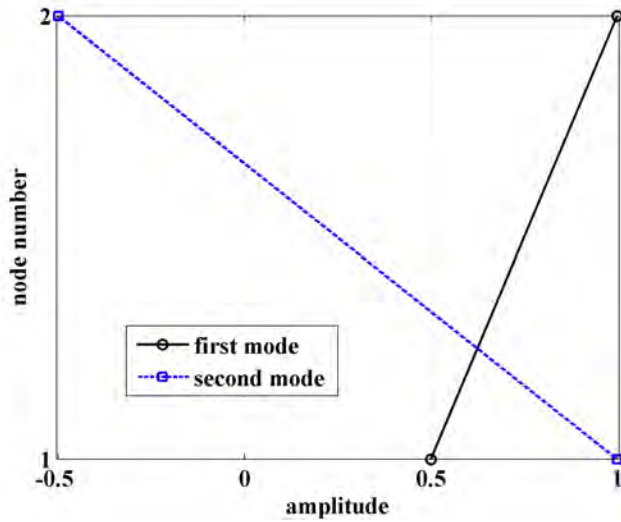


Figure E5.5a: Mode shapes - without TMD

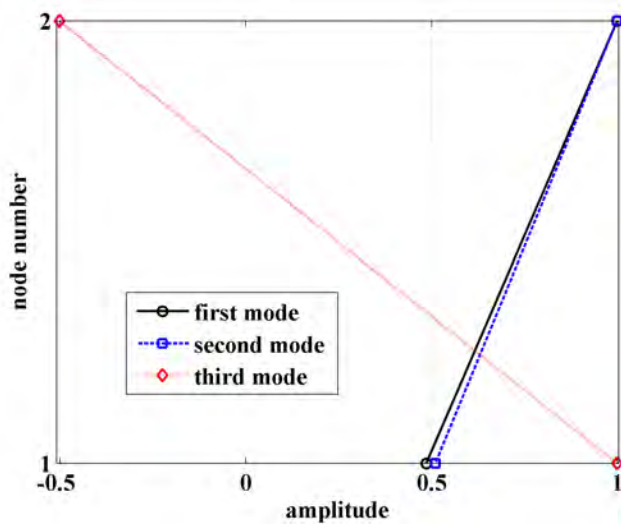


Figure E5.5b: Mode shapes - with TMD

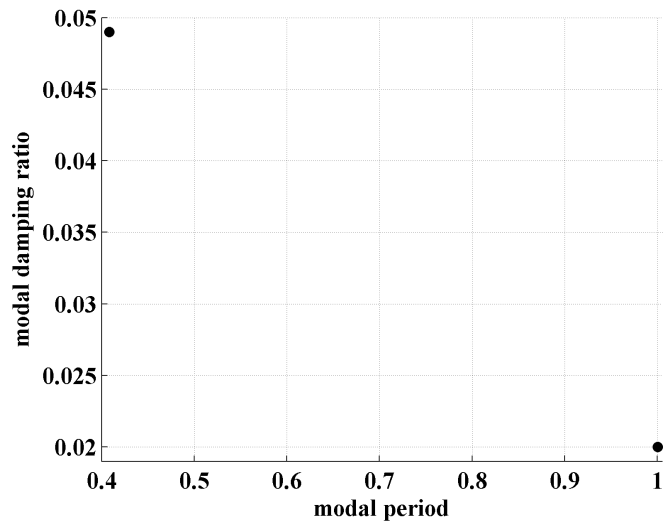


Figure E5.5c: Modal damping ratio without TMD

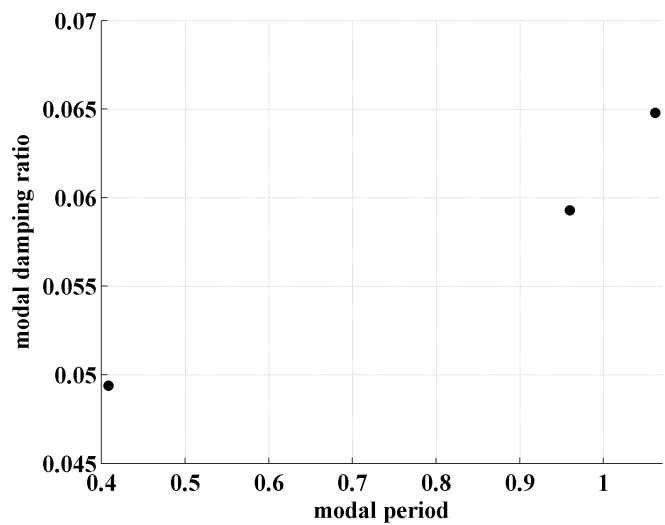


Figure E5.5d: Modal damping ratio with TMD

5.6. TUNED MASS DAMPER THEORY FOR MDOF SYSTEMS

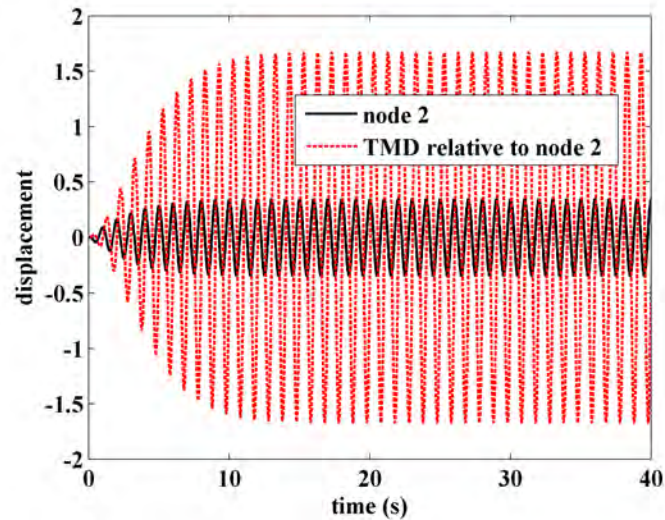


Figure E5.5e: Time history of the nodal and TMD displacements.

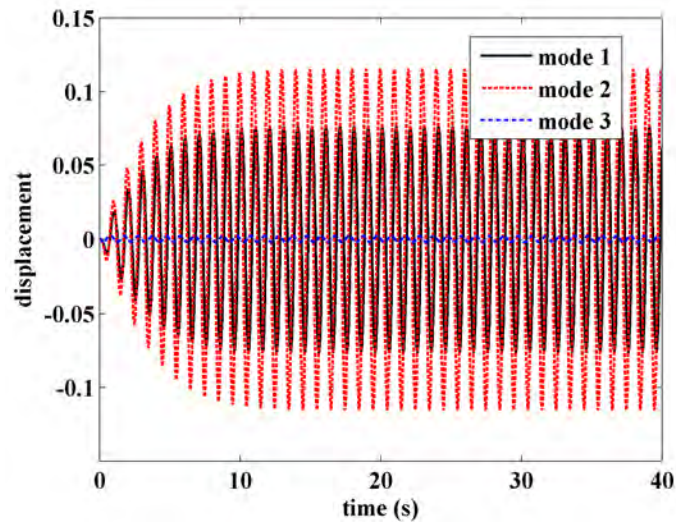


Figure E5.5f: Time history of modal displacements - node 1.

The general case of a MDOF system with a tuned mass damper connected to the n^{th} degree of freedom is treated in a

CHAPTER 5. TUNED MASS DAMPER SYSTEMS

similar manner. Using the notation defined above, the j^{th} modal equation can be expressed as

$$\tilde{m}_j \ddot{q}_j + \tilde{c}_j \dot{q}_j + \tilde{k}_j q_j = \tilde{p}_j + \Phi_{jn} [c_d \dot{u}_d + k_c u_d] \quad j = 1, 2, \dots \quad (5.165)$$

where \tilde{p}_j denotes the modal force due to ground motion and external forcing, and Φ_{jn} is the element of Φ_j corresponding to the n^{th} displacement variable. To control the i^{th} modal response, we set $j = i$ in Eq. (5.165), and introduce the approximation

$$q_i \approx \left[\frac{1}{\Phi_{in}} \right] u_n \quad (5.166)$$

This leads to the following equation for u_n

$$\tilde{m}_{ie} \ddot{u}_n + \tilde{c}_{ie} \dot{u}_n + \tilde{k}_{ie} u_n = \tilde{p}_{ie} + c_d \dot{u}_d + k_d u_d \quad (5.167)$$

where

$$\tilde{m}_{ie} = \left[\frac{1}{\Phi_{in}^2} \right] \tilde{M}_i = \left[\frac{1}{\Phi_{in}^2} \right] \Phi_i^T \mathbf{M} \Phi_i \quad (5.168)$$

$$\tilde{k}_{ie} = \omega_i^2 \tilde{m}_{ie} \quad (5.169)$$

$$\tilde{c}_{ie} = \alpha \tilde{k}_{ie} \quad (5.170)$$

$$\tilde{p}_{ie} = \frac{1}{\Phi_{in}} \tilde{p}_i \quad (5.171)$$

The remaining steps are the same as described above. We specify \bar{m} and ξ_i , determines the optimal tuning and damping values with Fig. 5.31 and 5.32, and then compute m_d and ω_d .

$$m_d = \bar{m} \tilde{m}_{ie} = \left[\frac{\bar{m}}{\Phi_{in}^2} \right] \Phi_i^T \mathbf{M} \Phi_i \quad (5.172)$$

5.6. TUNED MASS DAMPER THEORY FOR MDOF SYSTEMS

$$\omega_d = f_{\text{opt}}\omega_i \quad (5.173)$$

The optimal mass damper for mode i is obtained by selecting n such that Φ_{in} is the maximum element in Φ_i

Example 5.6 - Design of TMDs for a simply supported beam

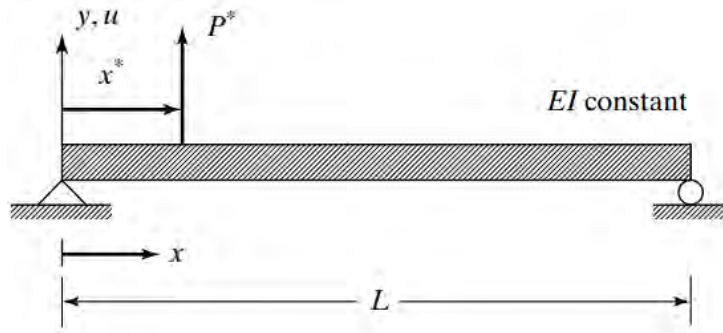


Figure 5.47

Consider the simply supported beam shown in Fig. 5.47. The modal shapes and frequencies for the case where the cross sectional properties are constant and the transverse shear deformation is negligible are

$$\Phi_n(x) = \sin \frac{n\pi x}{L} \quad n = 1, 2, \dots \quad (5.174)$$

$$\omega_n^2 = \frac{EI}{\rho_m} \left(\frac{n\pi}{L} \right)^4 \quad (5.175)$$

We obtain a set of N equations in terms of N modal coordinates by expressing the transverse displacement, $u(x, t)$, as

$$u = \sum_{j=1}^N q_j(t) \Phi_j(x) \quad (5.176)$$

CHAPTER 5. TUNED MASS DAMPER SYSTEMS

and substituting for u in the Principle of Virtual Displacements specialized for negligible transverse shear deformation (see Eq. (3.64)),

$$\int_0^L M \delta \chi dx = \int b \delta u dx \quad (5.177)$$

Substituting for $\delta \chi$

$$\delta \chi = -\frac{d^2}{dx^2}(\delta u) \quad (5.178)$$

and taking

$$\delta u = \delta q_j \Phi_j \quad (5.179)$$

leads to the following equations

$$-\int M \Phi_{j,xx} dx = \int b \Phi_j dx \quad j = 1, 2, \dots, N \quad (5.180)$$

Lastly, we substitute for M and b in terms of Φ and q , and evaluate the integrals. The expressions for M and b are

$$M = EI \chi = -EI \sum_{l=1}^N \ddot{q}_l \Phi_{l,xx} \quad (5.181)$$

$$b = -\rho_m \ddot{u} + \bar{b}(x, t) = -\rho_m \sum_{l=1}^N \ddot{q}_l \Phi_l + \bar{b}(x, t)$$

Noting the orthogonality properties of the modal shape functions

$$\int_0^L \Phi_j \Phi_k dx = \delta_{jk} \frac{L}{2} \quad (5.182)$$

5.6. TUNED MASS DAMPER THEORY FOR MDOF SYSTEMS

$$\int_0^L \Phi_{j,xx} \Phi_{k,xx} dx = \left(\frac{j\pi}{L} \right)^4 \delta_{jk} \frac{L}{2} \quad (5.183)$$

the modal equations uncouple and reduce to

$$\tilde{m}_j \ddot{q}_j + \tilde{k}_j q_j = \tilde{p}_j \quad (5.184)$$

where

$$\tilde{m}_j = \frac{L\rho_m}{2} \quad (5.185)$$

$$\tilde{k}_j = EI \left(\frac{j\pi}{L} \right)^4 \frac{L}{2} \quad (5.186)$$

$$\tilde{p}_j = \int_0^L \bar{b} \sin \frac{j\pi x}{L} dx \quad (5.187)$$

When the external loading consists of a concentrated force applied at the location $x = x^*$ (see Fig. 5.47), the corresponding modal load for the j^{th} mode is

$$\tilde{p}_j = P^* \sin \frac{j\pi x^*}{L} \quad (5.188)$$

In this example, the force is considered to be due to a mass attached to the beam as indicated in Fig. 5.48. The equations for the tuned mass and the force are

$$m_d(\ddot{u}^* + \ddot{u}_d) + c_d \dot{u}_d + k_d u_d = 0 \quad (5.189)$$

$$m_d(\ddot{u}^* + \ddot{u}_d) = -P^* \quad (5.190)$$

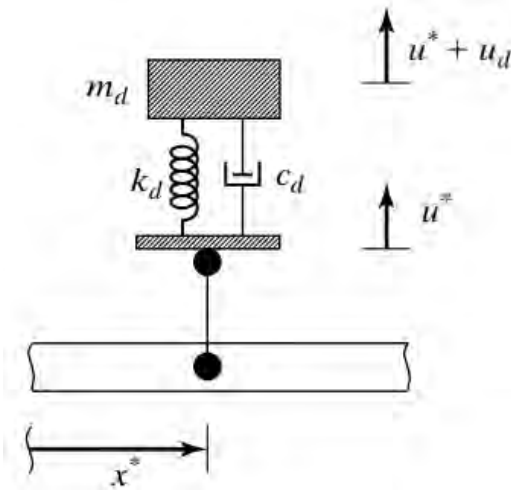


Figure 5.48

Suppose we want to control the i^{th} modal response with a tuned mass damper attached at $x = x^*$. Taking j equal to i in Eq. (5.184) and (5.185), the i^{th} modal equation has the form

$$\tilde{m}_i \ddot{q}_i + \tilde{k}_i q_i = (c_d \dot{u}_d + k_d u_d) \sin \frac{i\pi x^*}{L} \quad (5.191)$$

Assuming the response is dominated by the i^{th} mode, $u^*(x^*, t)$ is approximated by

$$u^*(x^*, t) \approx q_j \sin \frac{i\pi x^*}{L} \quad (5.192)$$

and Eq. (5.191) is transformed to an equation relating u^* and u_d

$$\tilde{m}_{ie} \ddot{u}^* + \tilde{k}_{ie} u^* = c_d \dot{u}_d + k_d u_d \quad (5.193)$$

where

5.6. TUNED MASS DAMPER THEORY FOR MDOF SYSTEMS

$$\begin{aligned}\tilde{m}_{ie} &= \frac{1}{\left(\sin \frac{i\pi x^*}{L}\right)^2} \tilde{m}_i \\ \tilde{k}_{ie} &= \frac{1}{\left(\sin \frac{i\pi x^*}{L}\right)^2} \tilde{k}_i\end{aligned}\tag{5.194}$$

The remaining steps utilize the results generated for the SDOF undamped structure - damped TMD system considered in Sect. 5.3. We use \tilde{m}_{ie} and \tilde{k}_{ie} as the mass and stiffness parameters for the primary system.

To illustrate the procedure, consider the damper to be located at mid-span, and the first mode is to be controlled. Taking $i = 1$ and $x^* = L/2$, the corresponding parameters are

$$\sin \frac{i\pi x^*}{L} = 1\tag{5.195}$$

$$\tilde{m}_{ie} = \tilde{m}_1 = \frac{L\rho_m}{2}\tag{5.196}$$

$$\tilde{k}_{ie} = \tilde{k}_1 = \frac{EIL}{2} \left(\frac{\pi}{L}\right)^4\tag{5.197}$$

We specify the equivalent damping ratio, ξ_e , and determines the required mass ratio from Fig. 5.33. For example, taking $\xi_e = 0.06$ requires $\bar{m} = 0.03$. The other parameters corresponding to $\bar{m} = 0.03$ follow from Figs. 5.30, 5.31, and 5.32.

$$f_{\text{opt}} = \frac{\omega_d}{\omega_1} = 0.965\tag{5.198}$$

$$\xi_d|_{\text{opt}} = 0.105\tag{5.199}$$

$$\frac{\hat{u}_d}{\hat{u}^*} = 5\tag{5.200}$$

CHAPTER 5. TUNED MASS DAMPER SYSTEMS

Using these parameters, the corresponding expression for the damper properties are

$$m_d = 0.03\tilde{m}_1 \quad (5.201)$$

$$\omega_d = 0.965\omega_1 \quad (5.202)$$

$$k_d = \omega_d^2 m_d \quad (5.203)$$

$$c_d = 2\xi_d \omega_d m_d \quad (5.204)$$

Once \tilde{m}_1 and ω_1 are specified, the damper properties can be evaluated. For example, consider the beam to be a steel beam having the following properties

$$\begin{aligned} L &= 20 \text{ m} \\ \rho_m &= 1000 \text{ kg/m} \\ I &= 8 \times 10^{-4} \text{ m}^4 \\ E &= 2 \times 10^{11} \text{ N/m}^2 \end{aligned} \quad (5.205)$$

The beams parameters are

$$\begin{aligned} \tilde{m}_1 &= 10,000 \text{ kg} \\ \omega_1 &= 9.87 \text{ ras/s} \end{aligned} \quad (5.206)$$

Applying Eq. (5.201)-(5.204), results in

$$m_d = 300 \text{ kg} \quad (5.207)$$

$$\omega_d = 9.52 \text{ ras/s} \quad (5.208)$$

$$k_d = 27,215 \text{ N/m} \quad (5.209)$$

$$c_d = 599.8 \text{ Ns/m} \quad (5.210)$$

5.6. TUNED MASS DAMPER THEORY FOR MDOF SYSTEMS

The total mass of the girder is 20,000 kg. Adding 300 kg, which is just 1.5% of the total mass, produces an effective damping ratio of 0.06 for the first mode response.

The mode shape for the second mode has a null point at $x = L/2$, and therefore locating a tuned mass at this point would have no effect on the second modal response. The optimal locations are $x^* = L/4$ and $x^* = 3L/4$. Taking $x^* = L/4$ and $i = 2$, we obtain

$$\sin \frac{i\pi x^*}{L} = 1 \quad (5.211)$$

$$\tilde{m}_{2e} = \tilde{m}_2 = \frac{L\rho_m}{2} \quad (5.212)$$

$$\tilde{k}_{2e} = \tilde{k}_2 = 8EIL \left(\frac{\pi}{L}\right)^4 \quad (5.213)$$

$$\omega_2^2 = \frac{16EI}{\rho_m} \left(\frac{\pi}{L}\right)^4 \quad (5.214)$$

The procedure from here on is the same as before. We specify ξ_e , determines the required mass ratio, and then the frequency and damping parameters. It is of interest to compare the damper properties corresponding to the same equivalent damping ratio. Taking $\xi_e = 0.06$, the damper properties for the example steel beam are

$$m_d = 300 \text{ kg} \quad (5.215)$$

$$k_d = 435,440 \text{ N/m} \quad (5.216)$$

$$c_d = 2400 \text{ Ns/m} \quad (5.217)$$

The required damper stiffness is an order of magnitude greater than the corresponding value for the first mode response.

5.7 Tuned Liquid Column Dampers

We have seen in the previous sections that TMDs are simple, well accepted mechanical damping systems. In the late 1990's, new types of dampers that rely on liquid motion to mitigate vibrations have emerged, including the Tuned Liquid Dampers (TLD), and Tuned Liquid Column Dampers (TLCD). The main advantage of the liquid dampers over TMDs is that they may utilize pre-existing tanks for their damping function, consequently using less valuable space. They are also less expensive to incorporate in structural design, and have less maintenance requirements. Several research papers have examined the behavior of U-shape TLCD subjected to various types of excitations and suggested design procedures using parametric studies [36, 126, 122, 89, 43, 123]. U-shape TLCDs are one of the most popular types of liquid dampers. They dissipate vibration energy using the oscillation of water from one column of the U-shape structure to the other column while passing through an orifice at the base (see Fig. 5.50). Fig. 5.49 shows One Wall Centre, a 48 story building located in Vancouver, British Columbia. The building has a slenderness ratio of 7:1. Two tuned liquid column dampers containing 60,000 US gallons of water (230 tons) were installed to mitigate vibrations due to wind. The dampers were tuned to the fundamental frequency of the structure.

5.7. TUNED LIQUID COLUMN DAMPERS



Figure 5.49: One Wall Centre [118].

This section presents the theory for U-Shape TLCDs subjected to harmonic excitations, and suggests design procedures. Consider the dynamics of the TLCDD represented in Fig. 5.50. Assuming that the liquid is incompressible and the the TLCDD pipe is opened (no pressure created from the movement of the liquid u_d) and of constant area A_d , the total kinetic energy E_k and potential energy E_p of the U-shape tube are

$$E_k = \frac{1}{2}\rho' A_d B(\dot{u}^2 + \dot{u}_d^2) + \rho' A_d H(\dot{u}^2 + \dot{u}_d^2) \quad (5.218)$$

$$E_p = \rho' A_d g u_d^2 \quad (5.219)$$

where ρ' is the fluid density and g the gravitational acceleration. The equilibrium equation for the U-tube is obtained by enforcing conservation of energy.

CHAPTER 5. TUNED MASS DAMPER SYSTEMS

$$\frac{d}{dt}(\text{kinetic and potential energy}) = \text{input power} \quad (5.220)$$

For this case, Eq. (5.220) expands to

$$\frac{d}{dt}(E_k + E_p) = F\dot{u} - F_d\dot{u}_d \quad (5.221)$$

Substituting for E_k and E_p , and equating the coefficients of \dot{u} and \dot{u}_d leads to

$$\begin{aligned} F &= \rho' A_d(B + 2H)\ddot{u} + \rho' A_d B \ddot{u}_d \\ F_d &= -[\rho' A_d B \ddot{u} + \rho' A_d(B + 2H)\ddot{u}_d + 2\rho' g A_d u_g] \end{aligned} \quad (5.222)$$

The equation of motion for the primary mass is

$$m\ddot{u} + c\dot{u} + ku + F = p \quad (5.223)$$

Combining the above equations, the equilibrium equations for the TLCD and the primary mass reduce to

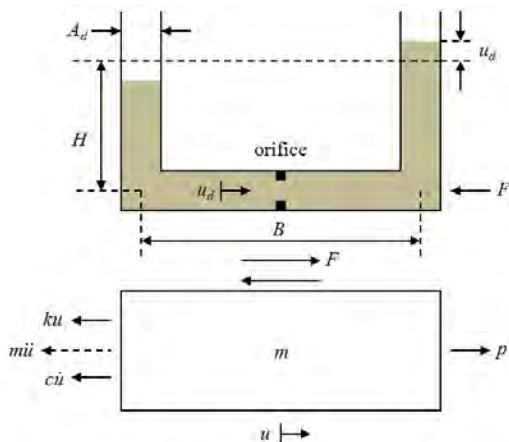


Figure 5.50: Tuned liquid column damper.

5.7. TUNED LIQUID COLUMN DAMPERS

$$(m + m_d)\ddot{u} + c\dot{u} + ku = p - \beta m_d \ddot{u}_d \quad (5.224)$$

$$m_d \ddot{u}_d + F_d + k_d u_d = -\beta m_d \ddot{u} \quad (5.225)$$

where $L_d = B + 2H$ is the equivalent length of the fluid, $m_d = \rho' A_d L_d$, $k_d = 2\rho' A_d g$, and $\beta = B/L_d = 1/(1 + 2H/B)$.

These equations apply for $\beta < 1$. When $\beta = 1$, one replaces k_d with $\rho' A_d g$ and L_d with B . The friction force induced by the orifice is expressed as

$$F_d = \frac{1}{2} \rho' A \eta |\dot{u}_d| \dot{u}_d \quad (5.226)$$

where η is referred to as the coefficient of head loss. Idelchik [43] proposed the following empirical formula for η ,

$$\eta = (\psi + 0.707\psi^{0.375})^2 (1 - \psi)^{-2} \quad (5.227)$$

Here, ψ is the fraction of the cross-sectional area that is blocked with the orifice. For example, $\psi = 1$ corresponds to fully blocked. Wu *et al.* [123] found better agreement with experimental results using the following formula

$$\eta = (-0.6\psi + 2.1\psi^{0.1})^{1.6} (1 - \psi)^{-2} \quad (5.228)$$

Fig. 5.51 shows a comparison between these predictions and experimental data.

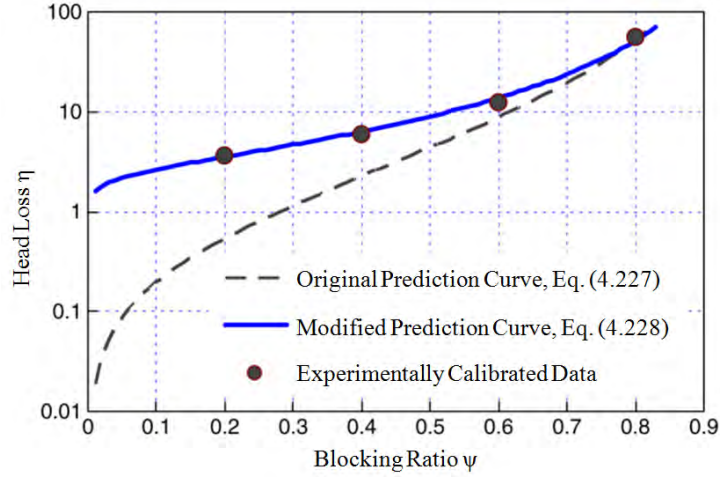


Figure 5.51: Comparison of head loss coefficients (adapted from [123]), reprinted with permission of Elsevier.

Eqs. (5.224) and (5.225) are rewritten in a more convenient form

$$\begin{aligned}
 (1 + \bar{m})\ddot{u} + 2\xi\omega\dot{u} + \omega^2u &= \frac{p}{m} - \beta\bar{m}\ddot{u}_d \\
 \ddot{u}_d + \bar{F}_d + \omega_d^2u_d &= -\beta\ddot{u} \\
 \bar{F}_d = \frac{F_d}{m_d} &= \frac{1}{2L_d}\eta|\dot{u}_d|\dot{u}_d
 \end{aligned} \tag{5.229}$$

These equations are difficult to solve due to the nonlinear damping term $\eta/(2L_d)|\dot{u}_d|\dot{u}_d$ which represents the TLCD damping force due to the orifice.

Consider that the structure is subjected to an harmonic excitation $p = \hat{p}e^{i\Omega t}$. The force dissipated by the TLCD in a full cycle can be calculated by considering the real part of the response over the ranges $0 - 2\pi$ where $u_d = \hat{u}_d \sin \Omega t$.

$$\bar{F}_d = \frac{F_d}{m_d} = \frac{\eta}{2L_d}\hat{u}_d^2\Omega^2|\cos \Omega t|\cos \Omega t \tag{5.230}$$

5.7. TUNED LIQUID COLUMN DAMPERS

The hysteretic loop of the damping force is shown in Fig. 5.52

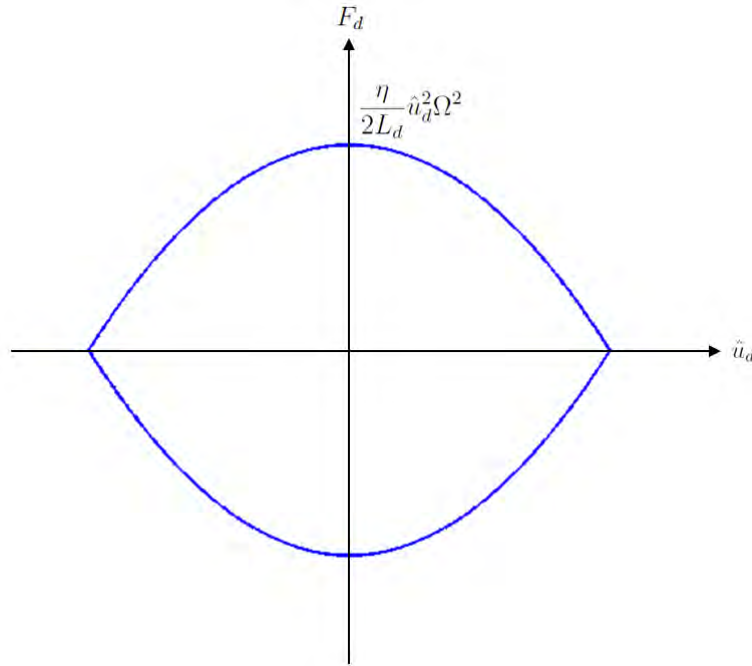


Figure 5.52: Damping force \bar{F}_d as a function of the fluid displacement u_d .

The work done by the TLCD in a full cycle is defined by the following integral

$$\begin{aligned}
 \frac{W}{m_d} &= 4 \int_0^{\pi/2\Omega} \bar{F}_d \dot{u}_d \, dt \\
 &= 4 \int_0^{\pi/2\Omega} \frac{\eta}{2L_d} \hat{u}_d^3 \Omega^3 \cos^3 \Omega t \, dt \quad (5.231) \\
 &= \frac{4\eta\Omega^2 \hat{u}_d^3}{3L_d}
 \end{aligned}$$

Equating this work to the equivalent work done by an equivalent linear viscous damper leads to an estimate for the equivalent damping coefficient, c_{eq}

$$F_d \approx c_{\text{eq}} \dot{u}_d \quad (5.232)$$

and

$$\begin{aligned} m_d \frac{4\eta\Omega^2 \hat{u}_d^3}{3L_d} &\approx c_{\text{eq}} \pi \Omega \hat{u}_d^2 \\ c_{\text{eq}} &\approx \frac{4\eta\Omega \hat{u}_d}{3L_d \pi} m_d \end{aligned} \quad (5.233)$$

Substituting for the damping term in Eq. (5.229), we obtain a more mathematically trackable set of equations;

$$\begin{aligned} (1 + \bar{m})\ddot{u} + 2\xi\omega\dot{u} + \omega^2 u &= \frac{p}{m} - \beta\bar{m}\ddot{u}_d \\ \ddot{u}_d + \frac{c_{\text{eq}}}{m_d}\dot{u}_d + \omega_d^2 u_d &= -\beta\ddot{u} \end{aligned} \quad (5.234)$$

Eq. (5.234) can be solved to find an analytical solution for u and u_d . Taking the same strategy as for the Damped TMD case, the excitation and responses are expressed as complex quantities

$$\begin{aligned} p &= \hat{p}e^{i\Omega t} \\ u &= \bar{u}e^{i\Omega t} \\ u_d &= \bar{u}_d e^{i\Omega t} \end{aligned} \quad (5.235)$$

where \hat{p} is a real quantity, and \bar{u} and \bar{u}_d are considered to be complex quantities. Eq. (5.234) takes the form

$$\begin{aligned} [1 - (1 + \bar{m})\rho^2 + 2i\xi\rho]\bar{u} &= \frac{\hat{p}}{k} + \beta\bar{m}\rho^2\bar{u}_d \\ [(f^2 - \rho^2) + 2i\xi_d\rho f]\bar{u}_d &= \beta\rho^2\bar{u} \end{aligned} \quad (5.236)$$

5.7. TUNED LIQUID COLUMN DAMPERS

where

$$\xi_d = \frac{2\eta\hat{u}_d}{3L_d\pi} \frac{\Omega}{\omega_d} \quad (5.237)$$

Assuming ξ_d is constant, solving Eq. 5.235 leads to

$$\begin{aligned} \bar{u} &= \frac{[(f^2 - \rho^2) + 2i\xi_d\rho]\hat{p}}{D_4k} \\ \bar{u}_d &= \frac{\beta\rho^2\hat{p}}{D_4k} \\ D_4 &= [1 - (1 + \bar{m})\rho^2 + 2i\xi_d\rho][(f^2 - \rho^2) + 2i\xi_d\rho f] - \beta^2\rho^4\bar{m} \end{aligned} \quad (5.238)$$

Finally, converting to polar form, one obtains

$$\bar{u} = \frac{\hat{p}}{k} H_9 e^{i\delta_9} = \hat{u} e^{i\delta_9} \quad (5.239)$$

$$\bar{u}_d = \frac{\hat{p}}{k} H_{10} e^{i\delta_{10}} = \hat{u}_d e^{i\delta_{10}} \quad (5.240)$$

where

$$H_9 = \frac{\sqrt{(f^2 - \rho^2)^2 + 4\xi_d^2\rho^2 f^2}}{|D_4|} \quad (5.241)$$

$$H_{10} = \frac{\beta\rho^2}{|D_4|} \quad (5.242)$$

$$\begin{aligned}
 |D_4| &= \sqrt{\frac{((f^2 - \rho^2)(1 - (1 + \bar{m})\rho^2) - 4\xi\xi_d\rho^2 f - \beta^2\rho^4\bar{m})^2}{+4(\xi_d\rho f(1 - (1 + \bar{m})\rho^2) + \xi\rho(f^2 - \rho^2))^2}} \\
 \delta_9 &= \beta_4 - \delta_{10} \\
 \tan \beta_4 &= \frac{2\xi_d\rho}{(f^2 - \rho^2)} \\
 \tan \delta_{10} &= 2\frac{\xi_d\rho(1 - (1 + \bar{m})\rho^2) + \xi\rho(f^2 - \rho^2)}{(f^2 - \rho^2)(1 - (1 + \bar{m})\rho^2) - 4\xi\xi_d\rho^4 - \beta^2\rho^4\bar{m}}
 \end{aligned}$$

5.243

The behavior of a TLCD is similar to that of a conventional TMD. Given the primary structure properties (ξ, ω, m) , one decides on values for β and \bar{m} , and determines through numerical simulation the corresponding optimal values for f and ξ_d . Fig. 5.53 illustrates the process. Firstly, one adjusts f such that the values of H_9 at points P and Q are equal. Then one adjusts ξ_d such that the peak values for H_9 occur at P and Q . These values are referred to as the “optimal” values. The response of the fluid in the column corresponding to these optimal values is plotted in Fig. 5.54. Note that this response is approximately 5 times the structural response. One needs to check that u_d is less than B (see Fig. 5.50). When $u_d > H$, this solution does not apply, since the damper frequency is reduced by $1/\sqrt{2}$ and consequently the damper is no longer in phase with the structure. The appropriate solution for this case corresponds to $\beta = 1$.

5.7. TUNED LIQUID COLUMN DAMPERS

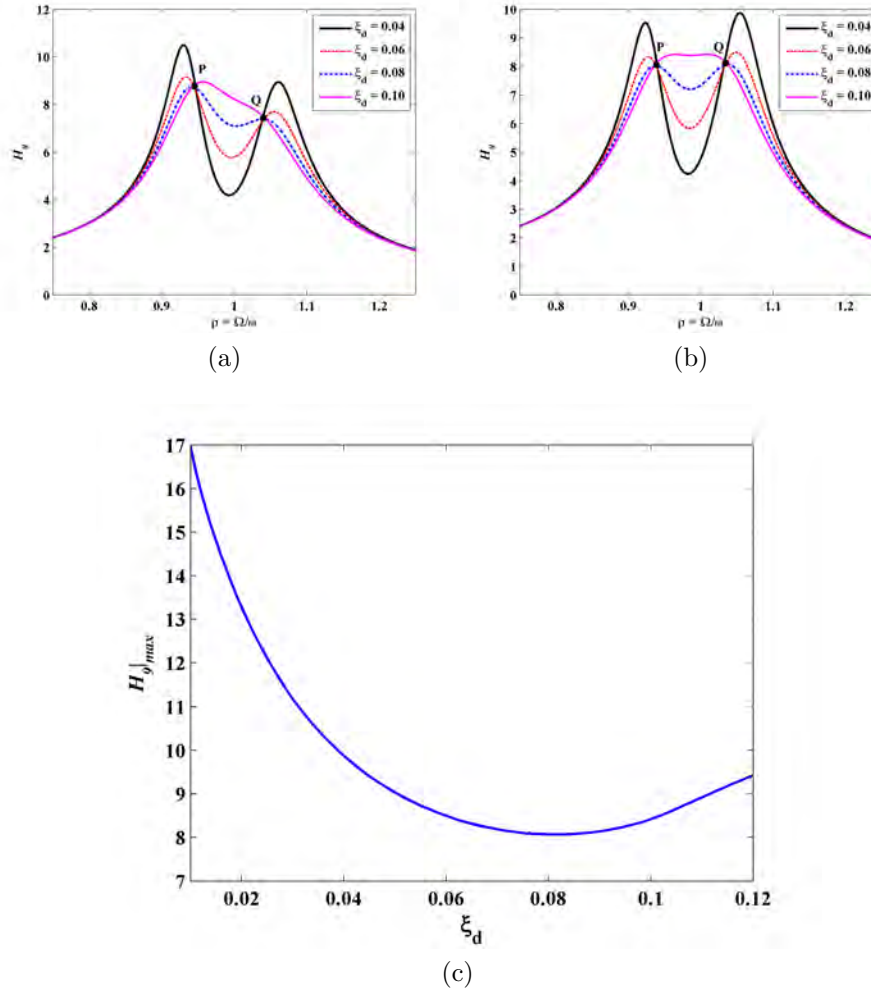
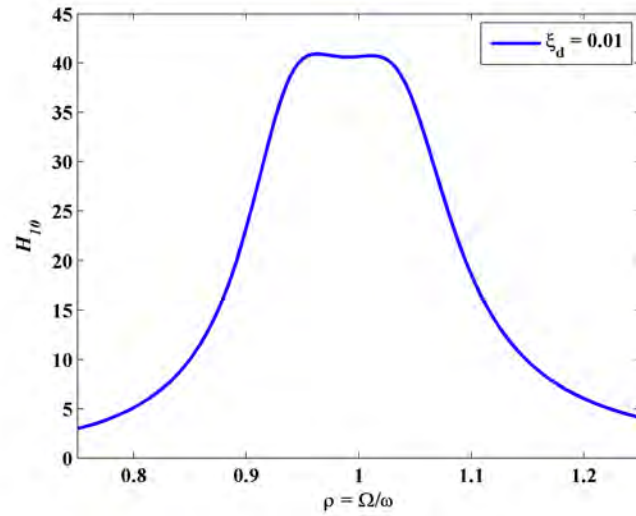
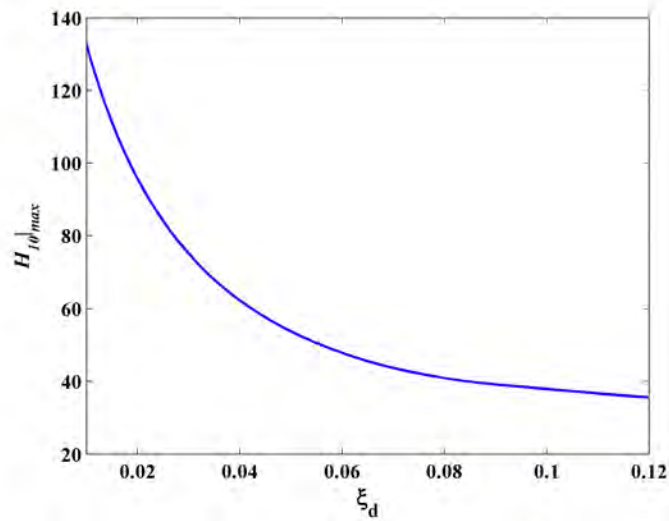


Figure 5.53: Response plots (H_9) ($\bar{m} = 0.02$, $B = 0.9$, $\xi = 0.02$): a) $f = 0.990$; b) $f|_{\text{opt}} = 0.978$ ($\xi_d|_{\text{opt}} = 0.08$); and c) variation of $H_9|_{\text{max}}$ versus ξ_d .



(a)



(b)

Figure 5.54: Response plots (H_{10}) ($\bar{m} = 0.02$, $B = 0.9$, $\xi = 0.02$): a) $f|_{\text{opt}} = 0.978$ and $\xi_d|_{\text{opt}} = 0.08$; and b) variation of $H_{10}|_{\text{textmax}}$ versus ξ_d .

Each of these plots is based on the assumption that ξ_d is constant and equal to the equivalent linearized damping ratio

5.7. TUNED LIQUID COLUMN DAMPERS

defined by Eq. (5.236).

$$\xi_d = \frac{2\eta\hat{u}_d}{3L_d\pi} \frac{\Omega}{\omega_d} = \frac{2\eta\hat{u}_d}{3L_d\pi} \frac{\rho}{f} \quad \text{(e)}$$

For optimal conditions, f and ρ are close to 1. The length is related to the natural frequency of the U-tube,

$$\omega_d^2 = \frac{2g}{L_d} = f^2\omega^2 \quad \text{(f)}$$

Combining these equations lead to

$$\xi_d = \frac{4\pi}{3} \frac{\eta\hat{u}_d\rho f}{gT^2} \quad \text{(5.244)}$$

Lastly, we substitute for \hat{u}_d using Eq. (5.240).

$$\begin{aligned} \xi_d &= \left(\frac{4\pi}{3gT^2} \right) (\rho f) \frac{\eta\hat{p}}{k} H_{10} \\ &= \left[\frac{\rho f H_{10}}{3\pi} \right] \frac{\hat{p}}{mg} \eta \end{aligned} \quad \text{(5.245)}$$

The nonlinear form of the damping force results in a coupling between the loading (\hat{p}) and the linearized damping ratio (ξ_d). One approach is to iterate on ξ_d given η . One assumes ξ_d , computes H_{10} , and updates ξ_d . Another strategy, which is more appealing, is to assume η is adaptive, i.e., the magnitude can be modified depending on the loading. In this case, we assume ξ_d and H_{10} are optimal, and compute the required value of η which leads to the appropriate value for the area blockage ratio, ψ .

$$\eta|_{\text{required}} = \frac{\xi_d|_{\text{opt}}}{\left[\frac{\rho f|_{\text{opt}} H_{10}|_{\text{opt}}}{3\pi} \right] \frac{\hat{p}}{mg}} \quad \text{(5.246)}$$

CHAPTER 5. TUNED MASS DAMPER SYSTEMS

Note that \hat{p}/mg is the ratio of the amplitude of the applied load to the weight of the primary structure.

When $\beta = 1$, Eqs. (5.239) through (5.244) still apply but one needs to use the following expression for L_d and $\eta|_{\text{required}}$.

$$L_d \equiv B = \frac{g}{(f\omega)^2} = \frac{g}{(2\pi f)^2} T^2 \quad (5.247)$$

$$\eta|_{\text{required}} = \frac{\xi_d|_{\text{opt}}}{\left[\frac{2\rho f|_{\text{opt}} H_{10}|_{\text{opt}}}{3\pi} \right] \frac{\hat{p}}{mg}} \quad (5.248)$$

5.7.1 Design methodology for TLCD

Given the properties and loading for the primary structure, one needs to select values for β and \bar{m} . Using numerical simulation, one can establish the corresponding optimal values for f , ξ_d , H_9 , and H_{10} . These results are summarized in Table 5.1. A typical value of structural damping ($\xi = 0.02$) was selected for this computation.

5.7. TUNED LIQUID COLUMN DAMPERS

Table 5.1: Optimal values for TLCD based on $\xi = 0.02$

β	\bar{m}	$f _{\text{opt}}$	$\xi_d _{\text{opt}}$	$H_9 _{\text{opt}}$	$H_{10} _{\text{opt}}$	$\xi _{\text{eq}}$
1.0	0.01	0.987	0.06	9.50	69.2	0.053
1.0	0.02	0.970	0.09	7.52	37.9	0.066
1.0	0.03	0.965	0.11	6.43	26.7	0.078
1.0	0.04	0.957	0.12	5.78	21.5	0.087
0.9	0.01	0.989	0.06	10.20	70.0	0.049
0.9	0.02	0.978	0.08	8.00	40.0	0.063
0.9	0.03	0.970	0.10	7.00	29.0	0.071
0.9	0.04	0.963	0.11	6.50	24.0	0.077
0.8	0.01	0.989	0.05	11.00	80.0	0.045
0.8	0.02	0.982	0.07	9.00	45.0	0.056
0.8	0.03	0.973	0.09	7.70	31.0	0.065
0.8	0.04	0.965	0.10	6.50	25.0	0.077
0.7	0.01	0.991	0.05	12.00	80.0	0.042
0.7	0.02	0.982	0.06	9.60	50.0	0.052
0.7	0.03	0.975	0.07	8.50	35.0	0.059
0.7	0.04	0.968	0.09	7.63	27.3	0.066
0.6	0.01	0.991	0.04	13.00	90.0	0.038
0.6	0.02	0.985	0.05	10.80	55.0	0.046
0.6	0.03	0.978	0.07	9.50	38.0	0.053
0.6	0.04	0.970	0.08	8.52	29.9	0.059
0.5	0.01	0.993	0.03	14.20	103.1	0.035
0.5	0.02	0.986	0.045	11.87	59.6	0.042
0.5	0.03	0.981	0.055	10.67	43.6	0.047
0.5	0.04	0.974	0.065	9.70	35.3	0.052

One selects values for β and \bar{m} , determines the corresponding optimal values from Table 5.1, then evaluates $\eta|_{\text{required}}$ and lastly, when $\beta < 1$, checks on whether $\bar{u}_d > H$. We note that

$$H = \frac{1}{2}(L_d - B) \tag{a}$$

and

$$\begin{aligned}\hat{u}_d &= \frac{\hat{p}}{k} H_{10} \\ &= \frac{\hat{p}}{mg} \frac{f^2 L_d}{2} H_{10}\end{aligned}\tag{b}$$

Then

$$\frac{H}{L_d} = \frac{1}{2}(1 - \beta)\tag{c}$$

$$\frac{\hat{u}_d}{L_d} = \frac{\hat{p}}{mg} \frac{f^2 H_{10}}{2}\tag{d}$$

Finally, the constraint takes the form:

$$\frac{\hat{p}}{mg} f^2 H_{10} < (1 - \beta) \quad \text{for } \beta < 1\tag{5.249}$$

Example 5.7 - Design example

We illustrate the design process for a structure having a mass of 4.61×10^7 kg, structural damping of 0.02, and fundamental period of 6 seconds which corresponds to $\omega = 1.047$ rad/sec. One approach is to specify the desired equivalent damping ratio, and using the data listed in Table 5.1, determine the appropriate values of β and \bar{m} . Comparing Eqs. (5.103) and (5.107) with Eqs. (5.241) and (5.243) shows that the TLCD solution is “identical” to the TMD solution when $\beta = 1$. Furthermore, Table 5.1 shows that ξ_{eq} “decreases” with β , for a given value of \bar{m} . Therefore, an obvious strategy point is to take $\beta = 1$ and consider different values of \bar{m} . Since the optimum tuning frequency ratio, f , is close to 1, Eq. (5.247) shows that the length, L_d , varies as T^2

5.7. TUNED LIQUID COLUMN DAMPERS

where T is the period of the structure. Then, it follows that A_d varies linearly with \bar{m} and is independent of β .

For completeness, an extensive set of damper configurations was considered to illustrate how the TLCD compares with the TMD. This data is listed in Table 5.2.

Table 5.2: Design parameters for $\xi = 0.02$, $m = 4.61 \times 10^7$ kg, $T = 6$ sec.

β	\bar{m}	B (m)	H (m)	A_d (m ²)	$\frac{\hat{u}_d}{\hat{p}/mg}$ (m)	$\frac{\hat{p}}{mg}\eta$	ξ_{eq}
1.0	0.01	9.37	0	49.30	631.6	0.004	0.053
1.0	0.03	9.80	0	142.00	243.6	0.020	0.078
0.8	0.01	14.92	1.87	24.80	729.7	0.006	0.045
0.8	0.03	15.42	1.93	72.00	282.8	0.028	0.065
0.7	0.01	13.00	2.80	24.90	729.0	0.006	0.042
0.7	0.03	13.40	2.90	72.00	319.4	0.019	0.059
0.6	0.01	11.20	3.72	24.90	822.0	0.004	0.038
0.6	0.03	11.44	3.82	73.00	346.6	0.018	0.053
0.5	0.01	9.26	4.63	25.00	940.4	0.003	0.035
0.5	0.03	9.51	4.76	73.00	399.0	0.012	0.047

If the objective is to maximize the effective damping ratio, the best option is to take $\beta = 1$ and $\bar{m} = 0.03$. The corresponding maximum damper displacement is $243.6\hat{p}/mg$. Either a TMD or a TLCD can be used here. One disadvantage of the TLCD is the large cross-sectional area required ($A_d = 142$ m²). A close alternative is to choose $\beta = 0.8$ and $\bar{m} = 0.03$. This design has $\xi_{\text{eq}} = 0.065$ (versus 0.078 for $\beta = 1$), $\hat{u}_d|_{\text{max}} = 282.8 \hat{p}/mg$, and $A_d = 72$ m². The available stem height is only 1.93 m so there is the potential of the fluid displacement exceeding its limit value, $H = 1.93$ m. A second choice is $\beta = 0.5$, $\bar{m} = 0.03$. The effective area is essentially the same, but constraint on fluid displacement is not as critical ($399 \hat{p}/mg < 4.76$).

Problems

Problem 5.1

Verify Eqs. (5.13) through (5.17). Hint: Express p , u , and u_d in complex form

$$\begin{aligned} p &= \hat{p}e^{i\Omega t} \\ u &= \bar{u}e^{i\Omega t} \\ u_d &= \bar{u}_d e^{i\Omega t} \end{aligned}$$

and solve Eqs. (5.6) and (5.7) for \bar{u} and \bar{u}_d . Then take

$$\begin{aligned} \bar{u} &= \hat{u}e^{i\delta_1} \\ \bar{u}_d &= \hat{u}_d e^{i(\delta_1+\delta_2)} \\ \omega &= \omega_d = \Omega \end{aligned}$$

Problem 5.2

Refer to Eqs. (5.14) and (5.20). Express ξ_e as a function of \bar{m} , ξ , and \hat{u}/\hat{u}_d . Take $\xi = 0.05$, and plot ξ_e versus \bar{m} for a representative range of the magnitude of the displacement ratio, \hat{u}/\hat{u}_d

Problem 5.3

Fig. 5.7 illustrates an active tuned mass damper configuration. The damper can be modeled with the 2DOF system shown in Fig. P5.3a. The various terms are as follows: u_s is the total displacement of the support attached to the floor beam; F_a is the self-equilibrating force provided by the actuator; m_d , k_d , c_d

5.7. TUNED LIQUID COLUMN DAMPERS

are parameters for the damper mass; k_a and m_a are parameters for the auxillary mass

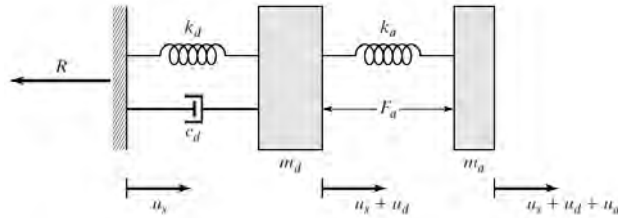


Figure P5.3a

1. Derive the governing equation for m_d and m_a . Also determine an expression for the resultant force, R , that the system applies to the floor beam.
2. Consider m_a to be several orders of magnitude smaller than m_d (e.g., $m_a = 0.01m_d$). Also take the actuator force to be a linear function of the relative velocity of the damper mass.

$$F_a = c_a \dot{u}_d$$

Specialize the equations for this case. How would you interpret the contribution of the actuator force to the governing equation for the damper mass?

Problem 5.4

Design a pendulum damper system having a natural period of 6 seconds and requiring less than 4 meters of vertical space.

Problem 5.5

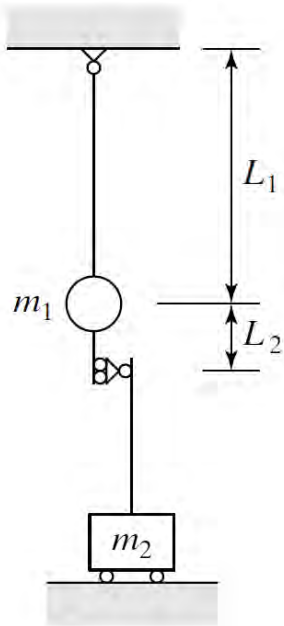


Figure P5.5a

The pendulum shown in Fig. P5.5a is connected to a second mass, which is free to move horizontally. The connection between mass 1 and mass 2 carries only shear. Derive an equation for the period of the compound pendulum and the length of an equivalent simple pendulum. Assume the links are rigid.

Problem 5.6

Refer to Fig. 5.12. Establish the equations of motion for the mass, m_d , considering θ to be small. Verify that the equivalent stiffness is equal to W_d/R .

Problem 5.7

Refer to Fig. 5.16 and Eq. (5.84). Derive the corresponding expression for $H_1|_{P,Q}$ starting with Eq. (5.62) and using the same reasoning strategy. Considering the mass ratio, \bar{m} , to be

5.7. TUNED LIQUID COLUMN DAMPERS

less than 0.03, estimate the difference in the “optimal” values for the various parameters.

Problem 5.8

Generate plots of H_1 versus ρ for ξ_d ranging from 0 to 0.2, $\bar{m} = 0.01$, and $f = 0.9876$. Compare the results with the plots shown in Fig. 5.24.

Problem 5.9

Consider a system composed of an undamped primary mass and a tuned mass damper. The solution for periodic force excitation is given by (see Eqs. (5.52) to (5.71))

$$u = \bar{u}e^{i\Omega t} \quad (1)$$

$$u_d = \bar{u}_d e^{i\Omega t} \quad (2)$$

$$\bar{u} = \frac{p}{k} H_1 e^{i\delta_1} \quad (3)$$

$$\bar{u}_d = \frac{p}{k} H_3 e^{i\delta_3} \quad (4)$$

$$H_1 = \frac{\sqrt{(f^2 - \rho^2)^2 + (2\xi_d \rho f)^2}}{|D_2|} \quad (5)$$

$$H_3 = \frac{\rho^2}{|D_2|} \quad (6)$$

$$|D_2| = \sqrt{([1 - \rho^2][f^2 - \rho^2] - \bar{m}\rho^2 f^2)^2 + (2\xi_d \rho f[1 - \rho^2(1 + \bar{m})])^2} \quad (7)$$

The formulation for the optimal damper properties carried out in Sect. 5.3 was based on minimizing the peak value of H_1 (actually H_2 but H_1 behaves in a similar way) (i.e., on controlling the displacement of the primary mass). Suppose the

CHAPTER 5. TUNED MASS DAMPER SYSTEMS

design objective is to control the acceleration of the primary mass. Noting Eqs. (1) and (3), the acceleration is given by

$$\ddot{u} = a = \bar{a}e^{i\Omega t} \quad (8)$$

$$\bar{a} = \frac{p\Omega^2}{k}H_1e^{i(\delta_1+\pi)} \quad (9)$$

Substituting for k transforms the equation to

$$\bar{a} = \frac{p}{m}H'_1e^{i(\delta_1+\pi)} \quad (10)$$

where

$$H'_1 = \rho^2H_1 \quad (11)$$

Investigate the behavior of H'_1 with ρ , f , \bar{m} , and ξ_d . If it behaves similar to H_2 , as shown in Fig. 5.16, describe how you would establish the optimal values for the various parameters, and also how you would design a tuned mass system when H'_1 is specified.

Problem 5.10

Design a TMD for a damped SDOF system having $\xi = 0.02$. The design motion constraints are

1.

$$\begin{aligned} H_5|_{\text{opt}} &< 10 \\ \frac{H_7}{H_5|_{\text{opt}}} &< 5 \end{aligned}$$

5.7. TUNED LIQUID COLUMN DAMPERS

2.

$$H_5|_{\text{opt}} < 5$$
$$\frac{H_7}{H_5|_{\text{opt}}} < 5$$

3. Repeat part 2., considering ξ to be equal to 0.05.

Problem 5.11

This problem concerns the design of a tuned-mass damper for a damped single degree of freedom system. The performance criteria are

$$\xi_{\text{eq}} = 0.1 \quad \hat{u}_d/\hat{u} = 5$$

1. Determine the damper properties for a system having $m = 10,000$ kg and $k = 395$ kN/m for the following values of ξ :
 - $\xi = 0.02$
 - $\xi = 0.05$
2. Will the damper be effective for an excitation with frequency 2.5π rad/s? Discuss the basis for your conclusion.

Problem 5.12

Refer to Ex. 4.7. Suppose a tuned mass damper is installed at the top level (at mass 5).

1. Determine the damper properties such that the equivalent damping ratio for the fundamental mode is 0.16. Use the values of m , k , c from Ex. 4.7. Assume stiffness proportional damping for c .

CHAPTER 5. TUNED MASS DAMPER SYSTEMS

2. Consider the tuned mass damper to be a pendulum attached to m_5 (Fig. P5.12a). Determine m_d and L for the damper properties established in part 1.

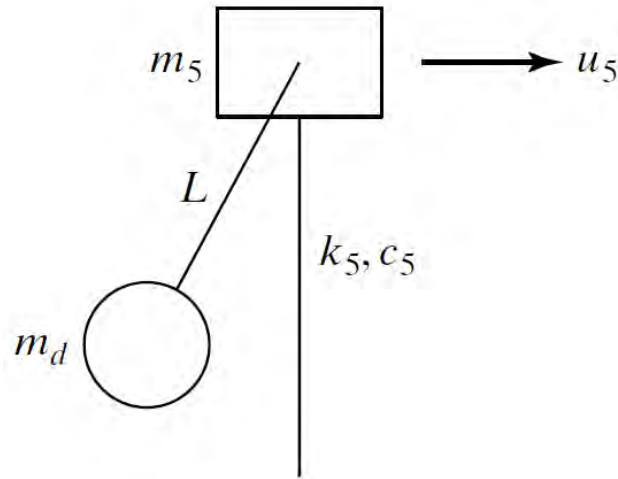


Figure P5.12a

3. Repeat part 1. for the case where the mass damper is tuned for the second mode rather than for the first mode, and the desired equivalent modal damping ratio is 0.3. Use the same values of m , k , c and assume stiffness proportional damping.

Problem 5.13

Consider a cantilever shear beam with the following properties:

$$\begin{aligned} H &= 50 \text{ m} \\ \rho_m &= 20,000 \text{ kg/m} \\ D_T &= 8 \times 10^5 \left(1 - \frac{0.6x}{H} \right) \text{ kN} \end{aligned}$$

5.7. TUNED LIQUID COLUMN DAMPERS

1. Model the beam as a 10DOF discrete shear beam having 5 m segments. Determine the first three mode shapes and frequencies. Normalize the mode shapes such that the peak amplitude is unity for each mode.
2. Design tuned mass dampers to provide an effective modal damping ratio of 0.10 for the first and third modes. Take $\xi_1 = 0.02$ and assume modal damping is proportional to stiffness.

Note: You need to first establish the “optimal location” of the tuned mass dampers for the different modes.

Problem 5.14

Consider a simply supported steel beam having the following properties:

$$\begin{aligned}L &= 30 \text{ m} \\ \rho_m &= 1500 \text{ kg/m} \\ I &= 1 \times 10^{-2} \text{ m}^4\end{aligned}$$

1. Design tuned mass damper systems that provide an equivalent damping of 0.05 for each of the first three modes.
2. Repeat part 1. with the constraint that an individual damper mass cannot exceed 300 kg. *Hint:* Utilize symmetry of a particular mode shape to locate a pair of dampers whose function is to control that mode.

Problem 5.15

CHAPTER 5. TUNED MASS DAMPER SYSTEMS

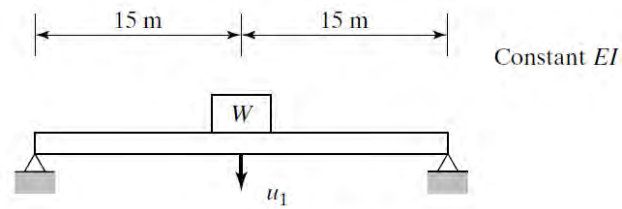


Figure P5.15a

Consider the simply supported beam shown in Fig. P5.15a. The beam has a uniform weight of 15 kN/m and a concentrated weight at midspan of 100 kN. The flexural rigidity is constant and equal to 200,000 kN·m².

1. Assume the first mode can be approximated by:

$$u = u_1 \sin\left(\frac{\pi}{L}\right)$$

Determine the governing equation for u_1 using the principle of virtual displacements.

2. Design a tuned mass damper to provide an equivalent damping ratio of 0.05 for the first mode. Assume no damping for the beam itself.
3. Will the damper designed in part 2. be effective for the second mode? Explain your answer.

Problem 5.16

Refer to Problem 4.24, part 2. Suggest a tuned mass damper for generating the required energy dissipation.

6

Base Isolation Systems

6.1 Introduction

The term *isolation* refers to the degree of interaction between objects. An object is said to be isolated if it has little interaction with other objects. The act of *isolating* an object involves providing an interface between the object and its neighbors, which minimizes interaction. These definitions apply directly to various physical systems. For example, we speak of isolating a piece of equipment from its support by mounting the equipment on an isolation system, which acts as a buffer between the equipment and the support. The design of isolation systems for vibrating machinery is a typical application. The objective here is to minimize the effect of the machine-induced loading on the support. Another application is concerned with minimizing the effect of support motion on the structure. This issue is becoming increasingly important for structures containing motion sensitive equipment and for structures located adjacent to railroad tracks or other sources of ground disturbance.

Although isolation as a design strategy for mounting mechanical equipment has been employed for over seventy years, only recently has the concept been seriously considered for civil structures, such as buildings and bridges, subjected to ground motion. This type of excitation interacts with the structure at the foundation level and is transmitted up through the structure. Therefore, it is logical to isolate the structure at its base and prevent the ground motion from acting on the structure. The idea of seismic isolation dates back to the late nineteenth century, but the application was delayed by the lack of suitable commercial isolation components. Substantial development has occurred since the mid-1980s [52], and base isolation for certain types of civil structures is now considered to be a highly viable

6.2. ISOLATION FOR SDOF SYSTEMS

design option by the seismic engineering community, particularly in Japan [107], for moderate to extreme seismic excitation.

A set of simple examples are presented in the next section to identify the key parameters and illustrate the quantitative aspects of base isolation. This material is followed by a discussion of practical aspects of seismic base isolation and a description of some seismically isolated buildings. The remaining sections deal with the behavioral and design issues for base isolated MDOF structural systems. Numerical results illustrating the level of performance feasible with seismic base isolation are included to provide a basis of comparison with the other *motion control* schemes considered in this text.

6.2 Isolation for SDOF Systems

The application of base isolation to control the motion of a SDOF system subjected to ground motion was discussed earlier in Sect. 1.4 as part of a general treatment of design for periodic excitation. The analytical formulation developed in that section provides the basis for designing an isolation system for simple structures that can be accurately represented with a SDOF model. Examples illustrating the reasoning process we follow are presented. The formulation is also extended to deal with a modified version of a SDOF model that is appropriate for a low-rise building isolated at its base. This model is useful for preliminary design.

6.2.1 SDOF Examples

The first example considers external periodic forcing of the SDOF system shown in Fig. 6.1. The solution of this problem is contained in Sect. 1.4. For convenience, the relevant equations

CHAPTER 6. BASE ISOLATION SYSTEMS

are listed below.

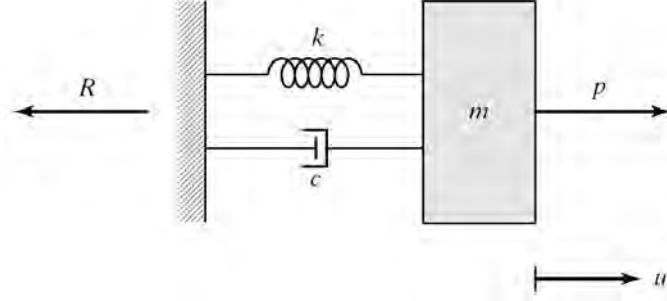


Figure 6.1: SDOF system.

$$p = \hat{p} \sin \Omega t \quad (6.1)$$

$$u = \hat{u} \sin(\Omega t - \delta) \quad (6.2)$$

$$\hat{u} = \left(\frac{H_1}{k} \right) \hat{p} \quad (6.3)$$

$$H_1 = \frac{1}{\sqrt{(1 - \rho^2)^2 + (2\xi\rho)^2}} \quad (6.4)$$

$$\rho = \frac{\Omega}{\omega} \quad (6.5)$$

$$\tan \delta = \frac{2\xi\rho}{1 - \rho^2} \quad (6.6)$$

Given \hat{p} and Ω , we can determine \hat{u} for a specific system having mass m , stiffness k , and damping c . With \hat{u} known, the forces in the spring and damper can be evaluated. The reaction can be found by either summing the internal forces, or combining p with the inertia force. With the latter approach, we write

$$R = p - m\ddot{u} \quad (6.7)$$

6.2. ISOLATION FOR SDOF SYSTEMS

and expand the various terms using Eqs. (6.1) through (6.6). The result is expressed as

$$R = \hat{R} \sin(\Omega t - \delta_r) \quad (6.8)$$

$$\hat{R} = H_3 \hat{p} \quad (6.9)$$

$$H_3 = \sqrt{\frac{1 + (2\xi\rho)^2}{(1 - \rho^2)^2 + (2\xi\rho)^2}} \quad (6.10)$$

$$\tan \delta_r = -\frac{\rho^2 H_1 \sin \delta}{1 + \rho^2 H_1 \cos \delta} \quad (6.11)$$

The function H_3 is referred to as the transmissibility of the system. It is a measure of how much of the load p is transmitted to the support. When $\xi = 0$, $\delta = 0$ and H_3 reduces to H_1 . Fig. 6.2 shows the variation of H_3 with ρ and ξ .

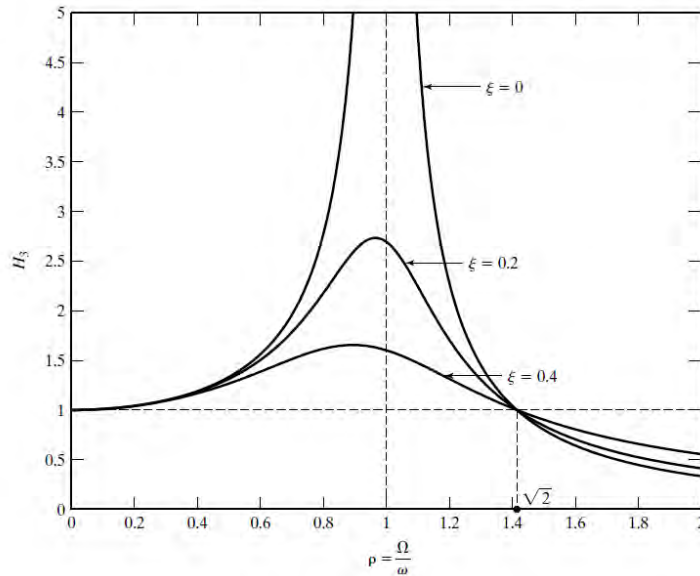


Figure 6.2: Plot of H_3 versus ρ .

CHAPTER 6. BASE ISOLATION SYSTEMS

The model just presented can be applied to the problem of designing a support system for a machine with an eccentric rotating mass. Here, we want to minimize the reaction force for a given \hat{p} (i.e., we take $H_3 < 1$). Noting Fig. 6.2, this constraint requires the frequency ratio, ρ , to be greater than $\sqrt{2}$, and it follows that

$$\omega < \frac{\Omega}{\sqrt{2}} \quad (6.12)$$

The corresponding periods are related by

$$T > T_f \sqrt{2} = \sqrt{2} \left(\frac{2\pi}{\Omega} \right) \quad (6.13)$$

where T_f is the forcing period. For example, taking $T = 3T_f$ results in $\hat{R} = 0.125\hat{p}$, a reduction of 87.5% from the static value.

The second example illustrates the strategy for isolating a system from support motion. Applying the formulation derived in Sect. 1.4 to the system shown in Fig. 6.3, the amplitudes of the relative and total displacement of the mass, \hat{u} and \hat{u}_t , are related to the support displacement by

$$\hat{u} = \rho^2 H_1 \hat{u}_g = H_2 \hat{u}_g \quad (6.14)$$

$$\hat{u}_t = H_3 \hat{u}_g \quad (6.15)$$

6.2. ISOLATION FOR SDOF SYSTEMS

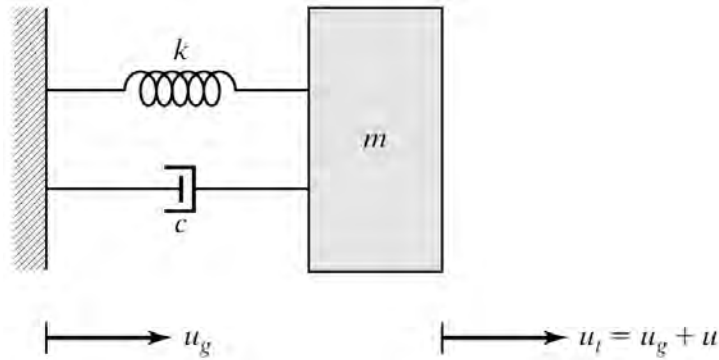


Figure 6.3: SDOF system subjected to support motion.

Taking H_3 small with respect to unity reduces the effect of support motion on the spatial position of the mass. The frequency and period criteria are the same as those of the previous example. We take $\rho > \sqrt{2}$ to reduce \hat{u}_t . However, since H_2 approaches unity as ρ increases, the magnitude of the relative motion increases and approaches the ground motion, \hat{u}_g . Therefore, this relative motion needs to be accommodated, i.e., one must allow sufficient clearance between the mass and its surroundings.

These examples show that isolation is obtained by taking the period of the SDOF system to be large in comparison to the forcing (either external or support) period. We express this requirement as

$$T \geq fT_f \quad \Rightarrow \quad \omega < \frac{\Omega}{f} \quad (6.16)$$

where f depends on the desired reduction in amplitude. The constraint on the stiffness of the spring is given by

$$k < m \left(\frac{\Omega}{f} \right)^2 = m \left(\frac{2\pi}{fT_f} \right)^2 \quad (6.17)$$

CHAPTER 6. BASE ISOLATION SYSTEMS

It should be noted that this derivation assumes that a single periodic excitation is applied. The result is applicable for *narrow band* excitations, which are characterized by a dominant frequency. A more complex analysis involving iteration on the stiffness is required to deal with *broad band* excitations. We have to ensure that the forcing near the fundamental frequency is adequately controlled by damping in this case.

6.2.2 Bearing Terminology

The spring and damper elements connecting the mass to the support are idealizations of physical objects called *bearings*. They provide a constraint against motion relative to a support plane, as illustrated in Fig. 6.4. The bearing in Fig. 6.4(a) functions as an axial element and resists the displacement normal to the plane with normal stresses (tension and compression). The bearing shown in Fig. 6.4(b) constrains relative tangential motion through shearing action over the height of the bearing. These elements are usually combined into a single compound bearing, but it is more convenient to view them as being uncoupled when modeling the system.

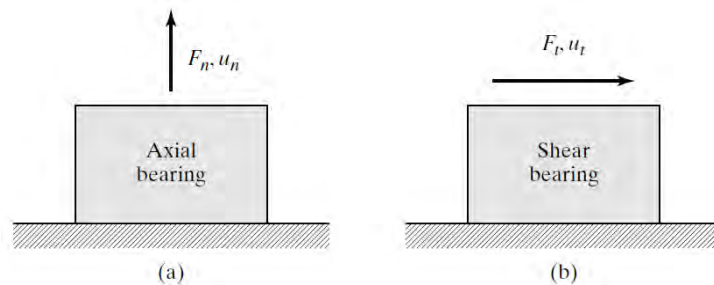


Figure 6.4: Axial and shear bearings.

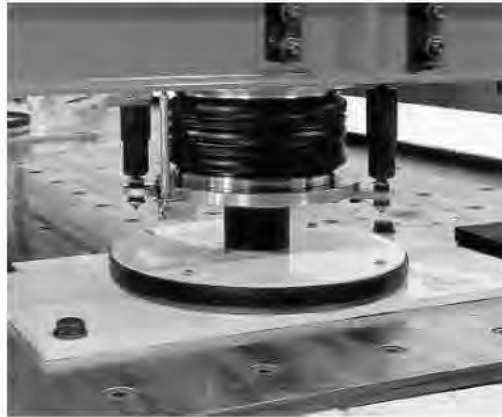
When applying the formulation just developed, we distinguish

6.2. ISOLATION FOR SDOF SYSTEMS

between normal and tangential support motion. For normal motion, axial-type bearings such as springs and rubber cushions are used; the k defined by Eq. (6.17) is the axial stiffness of the bearing F_n/u_n . Shear bearings such as laminated rubber cushions and friction pendulum-type sliding devices are used when the induced motion is parallel to the ground surface. In this case, k represents the required *shearing* stiffness of the bearing, F_t/u_t .

Fig. 6.5 shows an air spring/damper scheme used for vertical support. Single- and multiple-stage laminated rubber bearings are illustrated in Fig. 6.6. Rubber bearings used for seismic isolation can range up to 1 m in diameter and are usually inserted between the foundation footings and the base of the structure. A particular installation for a building is shown in Fig. 6.7.

CHAPTER 6. BASE ISOLATION SYSTEMS



Vertical section diagram

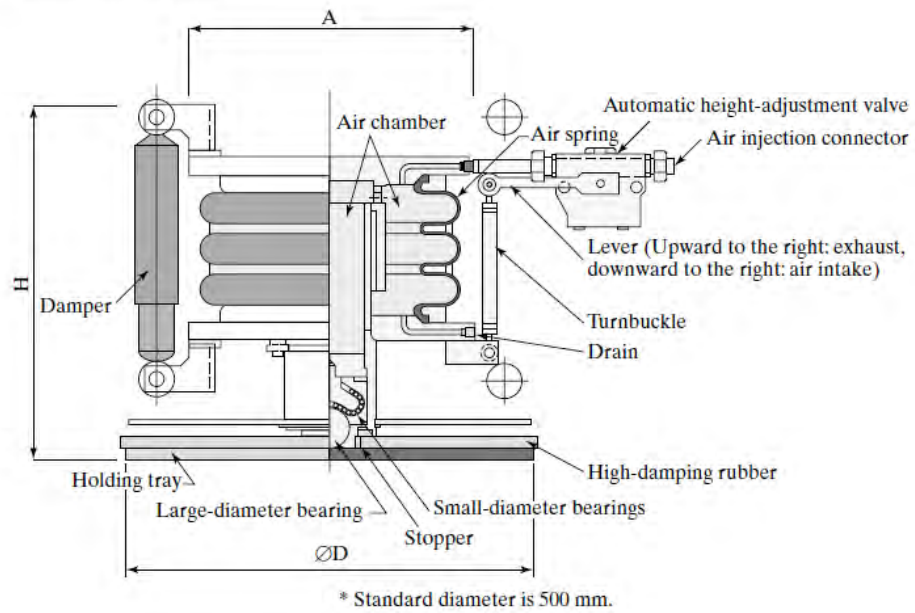
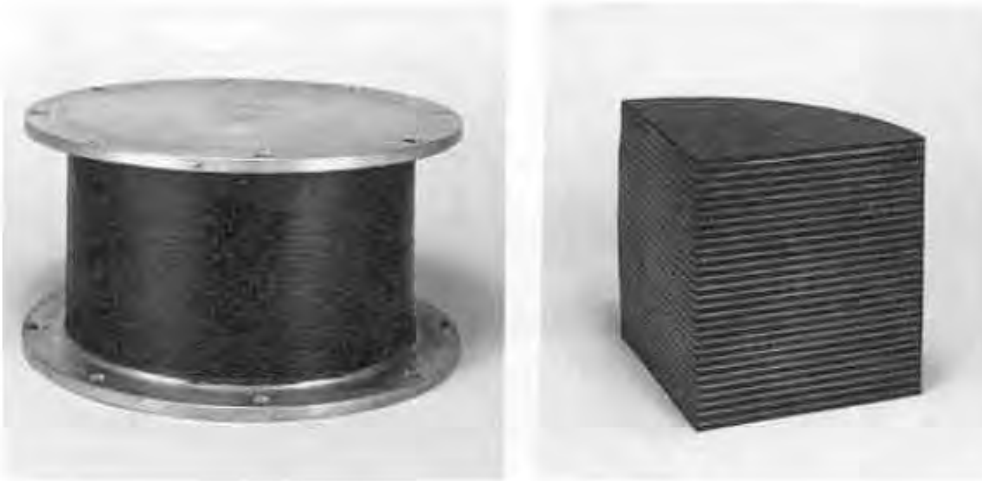
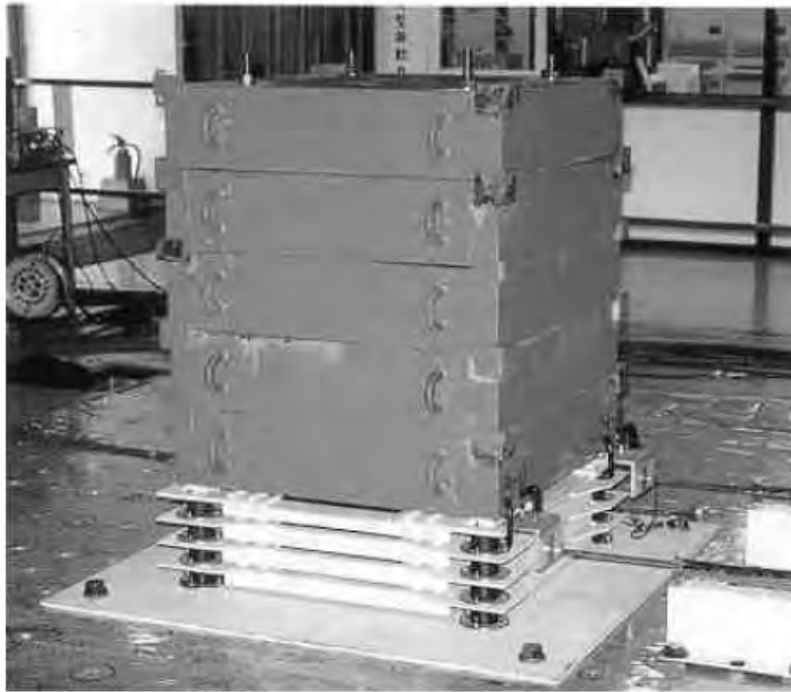


Figure 6.5: Air spring bearing. (Photo Courtesy of J. Connor).

6.2. ISOLATION FOR SDOF SYSTEMS



(a) Single stage



(b) Multiple stage

Figure 6.6: Laminated rubber bearings. (Courtesy of J. Connor). 401

CHAPTER 6. BASE ISOLATION SYSTEMS



(a)



(b)

Figure 6.7: Rubber bearing seismic isolation systems (Courtesy of J. Connor).

6.2. ISOLATION FOR SDOF SYSTEMS

Fig. 6.8 illustrates how the pendulum bearing system responds to lateral load. There are 3 components: a lower plate with a concave surface; an inner bearing; and an upper plate. As load is applied, the inner bearing slides up on the lower surface; the upper plate moves along with the bearing, rotating slightly so as to remain horizontal. Assuming the motion is small, one can show that the resistance force developed as the inner bearing translates on the lower surface is a linear function of the lateral displacement:

$$P = \left(\frac{W}{R} \right) u = k_{\text{eq}} u \quad (6.18)$$

Therefore, one can model the bearing system as an equivalent shear spring, shown in Fig. 6.8(c). The stiffness is adjusted by varying R .

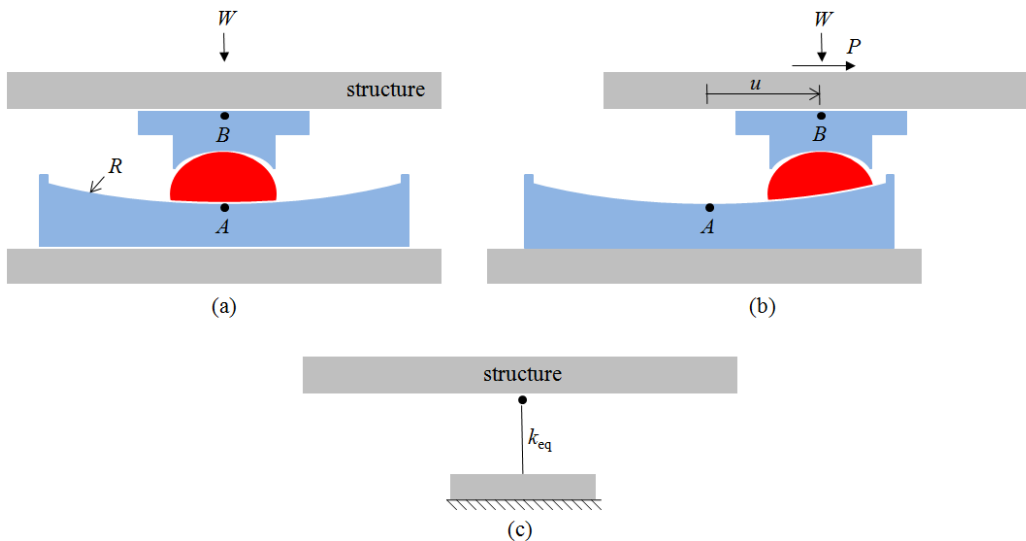


Figure 6.8: Friction pendulum system: (a) initial position; (b) deformed position under lateral load; and (c) equivalent system.

Fig. 6.9 shows a bearing system (a triple pendulum bearing)

CHAPTER 6. BASE ISOLATION SYSTEMS

installed in the Mills Peninsula Hospital.



Figure 6.9: Triple Pendulum bearing - Mills Peninsula Hospital (courtesy of Earthquake Protection Systems (EPS)).

6.2.3 Modified SDOF Model

In what follows, the support motion is considered to be due to seismic excitation. Although both normal (vertical) and tangential (horizontal) motions occur during a seismic event, the horizontal ground motion is generally more significant for structural systems since it leads to lateral loading. Typical structural systems are designed for vertical loading and then modified for lateral loading. Since the vertical motion is equivalent to additional vertical loading, it is not as critical as the horizontal motion.

6.2. ISOLATION FOR SDOF SYSTEMS

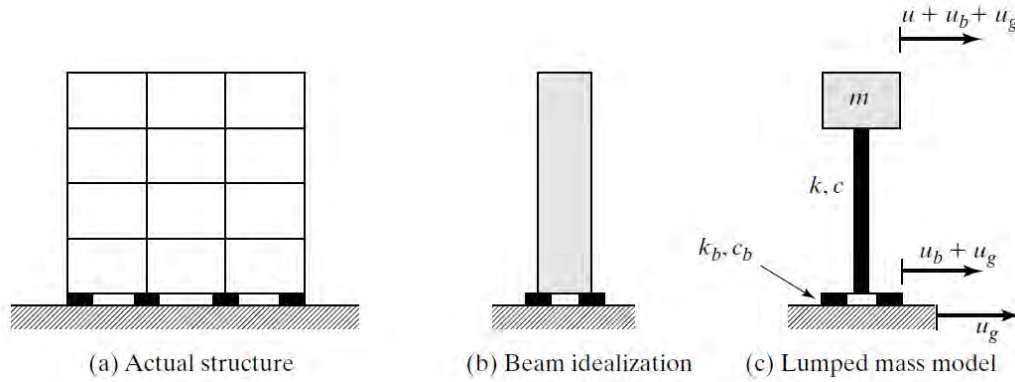


Figure 6.10: Base isolation models.

The model shown in Fig. 6.3 represents a rigid structure supported on flexible shear bearings. To allow for the flexibility of the structure, the structure can be modeled as a MDOF system. Fig. 6.10 illustrates a SDOF beam-type idealization. We can estimate the equivalent SDOF properties of the structure by assuming that the structural response is dominated by the fundamental mode. The data provided in earlier chapters shows that this assumption is reasonable for low-rise buildings subjected to seismic excitation.

An in-depth analysis of low rise buildings modeled as MDOF beams is presented later in this chapter. The objective here is to derive a simple relationship showing the effect of the bearing stiffness on the relative displacement of the structure, u , with respect to the base displacement, $u_b + u_g$. The governing equations for the lumped mass model consist of an equilibrium equation for the mass, and an equation relating the shear forces in the spring and the bearing.

$$m\ddot{u} + c\dot{u} + ku = -m(\ddot{u}_b + \ddot{u}_g) \quad (6.19)$$

$$k_b u_b + c_b \dot{u}_b = ku + c\dot{u} \quad (6.20)$$

CHAPTER 6. BASE ISOLATION SYSTEMS

Neglecting damping, Eq. (6.20) can be solved for u_b in terms of u .

$$u_b = \left(\frac{k}{k_b} \right) u \quad (6.21)$$

Then, substituting for u_b in Eq. (6.19) leads to

$$m \left(1 + \frac{k}{k_b} \right) \ddot{u} + ku = -m\ddot{u}_g \quad (6.22)$$

Eq. (6.22) is written in the conventional form for a SDOF system:

$$\ddot{u} + \omega_{\text{eq}}^2 u = -\Gamma \ddot{u}_g \quad (6.23)$$

where Γ is a participation factor,

$$\Gamma = \frac{k_b}{k + k_b} = \left(\frac{k_b}{k} \right) / \left(1 + \frac{k_b}{k} \right) \quad (6.24)$$

and ω_{eq} is an equivalent frequency measure:

$$\omega_{\text{eq}}^2 = \frac{\Gamma k}{m} = \Gamma \omega^2 \quad (6.25)$$

In this case, ω_{eq} is the fundamental frequency of the system consisting of the structure plus bearing. Taking k_b small with respect to k decreases the inertia loading on the structure as well as the effective frequency. Consequently, the structural response is reduced.

6.2.4 Periodic Excitation: Modified SDOF Model

To illustrate the effect of base stiffness on the response, the case of periodic ground motion, $u_g = \hat{u}_g \sin \Omega t$, is considered. The various response amplitudes are given by

6.2. ISOLATION FOR SDOF SYSTEMS

$$\hat{u} = \frac{\Gamma \rho_{\text{eq}}^2}{|1 - \rho_{\text{eq}}^2|} \hat{u}_g \quad (6.26)$$

$$\hat{u}_b = \left(\frac{k}{k_b} \right) \hat{u} \quad (6.27)$$

$$\hat{u}_t = \hat{u} + \hat{u}_b + \hat{u}_g = \frac{1}{|1 - \rho_{\text{eq}}^2|} \hat{u}_g \quad (6.28)$$

where the brackets indicate absolute values, and ρ_{eq} is the frequency ratio:

$$\rho_{\text{eq}} = \frac{\Omega}{\omega_{\text{eq}}} \quad (6.29)$$

Comparing Eq. (6.28) with Eq. (6.15) shows that the results are similar. We replace ω with ω_{eq} in the expression for H_3 . The limiting cases are $k_b = 0$ and $k_b = \infty$. The former is the fully isolated case, where $u_b \approx -\hat{u}_g$ and $u_t \approx 0$; the latter corresponds to a fixed support where $u_b \approx 0$ and $u_t \approx u + u_g$.

Suppose the structure is defined and the problem concerns selecting a bearing stiffness such that the total response satisfies

$$\hat{u}_t \leq \nu \hat{u}_g \quad \nu < 1$$

We need to take $\rho_{\text{eq}}^2 > 2$. Noting Eq. (6.28), the required value of ρ_{eq} is:

$$\rho_{\text{eq}}^2 = 1 + \frac{1}{\nu} \quad (6.30)$$

Substituting for ρ_{eq} in Eq. (6.29) leads to

$$\omega_{\text{eq}}^2 = \frac{\Omega^2}{1 + \frac{1}{\nu}} \quad (6.31)$$

CHAPTER 6. BASE ISOLATION SYSTEMS

Finally, using Eqs. (6.24) and (6.25), the required bearing stiffness is given by

$$k_b = k \frac{1}{\left(\frac{k}{\omega_{\text{eq}}^2 m}\right) - 1} = \frac{k}{\frac{k(1+(1/\nu))}{m\Omega^2} - 1} \quad (6.32)$$

The more general problem is the case where both structural stiffness and the bearing stiffness need to be established subject to the following constraints on the magnitudes of \hat{u} and \hat{u}_b .

$$\begin{aligned} \hat{u} &= \nu_s \hat{u}_g \\ \hat{u}_b &= \nu_b \hat{u}_g \end{aligned} \quad (6.33)$$

The typical design scenario has ν_b larger than ν_s . Noting Eq. (6.27), the stiffness factors are related by

$$k_b = \frac{\nu_s}{\nu_b} k \quad (6.34)$$

Eq. (6.26) provides the second equation relating the stiffness factors. It reduces to

$$\left| -1 + \frac{1}{\rho_{\text{eq}}^2} \right| = \frac{\Gamma}{\nu_s} \quad (6.35)$$

where

$$\Gamma = \frac{k_b/k}{1 + k_b/k} = \frac{\nu_s}{\nu_s + \nu_b} \quad (6.36)$$

Solving Eq. (6.35) for ρ_{eq}^2 leads to ω_{eq}^2 , and then k .

$$\omega_{\text{eq}}^2 = \frac{\Omega^2}{\rho_{\text{eq}}^2} = \Gamma \frac{k}{m} \quad (6.37)$$

6.2. ISOLATION FOR SDOF SYSTEMS

The following example illustrates the computational steps.

Example 6.1 - Stiffness factors for prescribed structure and base motion

Suppose $\nu_s = 0.1$ and $\nu_b = 1.0$. The relative motion of the base with respect to the ground is allowed to be 10 times greater than the relative motion of the structure with respect to the base.

$$\hat{u}_b = 10\hat{u} \quad (6.38)$$

The stiffness factors are related by

$$k_b = \frac{\nu_s}{\nu_b}k = 0.1k \quad (6.39)$$

Evaluating Γ and ρ_{eq} , using Eqs. (6.35) and (6.36),

$$\Gamma = \frac{\nu_s}{\nu_s + \nu_b} = \frac{0.1}{1.1} = 0.0909 \quad (6.40)$$

$$\left| 1 - \frac{1}{\rho_{\text{eq}}^2} \right| = \frac{\Gamma}{\nu_s} = \frac{1}{1.1} = 0.909 \quad (6.41)$$

leads to

$$\omega_{\text{eq}}^2 = 0.0909\Omega^2 \quad (6.42)$$

and finally to k :

$$k = \frac{m}{\Gamma}\omega_{\text{eq}}^2 = m\Omega^2 \quad (6.43)$$

6.2.5 Seismic Excitation: Modified SDOF Model

An estimate of the stiffness parameters required to satisfy the motion constraints under seismic excitation can be obtained with the response spectra approach described in Chapter 3. Taking \ddot{u}_g to be the seismic excitation, the solution of Eq. (6.23) is related to the spectral parameters by

$$|u|_{\max} = \Gamma S_D = \Gamma \frac{PS_V}{\omega_{\text{eq}}} \quad (6.44)$$

where S_D and PS_V are functions of the equivalent frequency, ω_{eq} , and the equivalent damping ratio for the structure/bearing system, ξ_{eq} . Substituting for Γ , and ω_{eq} , Eq. (6.44) expands to

$$|u|_{\max} = PS_V \sqrt{\frac{mk_b}{k(k+k_b)}} \quad (6.45)$$

The relation between the maximum relative displacement of the bearing and the maximum structural motion follows from Eq. (6.21):

$$|u_b|_{\max} = \left(\frac{k}{k_b} \right) |u|_{\max} \quad (6.46)$$

In this development, the criteria for motion based design of a base isolated structure are expressed as limits on the relative motion terms:

$$|u|_{\max} = u^* \quad (6.47)$$

$$|u_b|_{\max} = u_b^* \quad (6.48)$$

The values of k and k_b required to satisfy these constraints follow by solving Eqs. (6.45) and (6.46).

6.2. ISOLATION FOR SDOF SYSTEMS

$$k_b = \frac{ku^*}{u_b^*} \quad (6.49)$$

$$k = \frac{m(P S_V)^2}{u^*(u^* + u_b^*)} \quad (6.50)$$

We assume $P S_V$ is constant, evaluate k and k_b , determine the frequency ω_{eq} with Eq. (6.25), and then update $P S_V$ if necessary.

It is of interest to compare the stiffness required by the base isolated structure with the stiffness of the corresponding fixed base structure. Taking $k_b = \infty$ reduces Eq. (6.45) to

$$|u|_{\text{max}} = P S_V \sqrt{\frac{m}{k}} \quad (6.51)$$

The fixed base structural stiffness k_f follows from Eq. (6.51):

$$k_f = |k|_{k_b=\infty} = \frac{m(P S_V)^2}{(u^*)^2} \quad (6.52)$$

Using Eq. (6.52) and assuming the value of $P S_V$ is the same for both cases leads to the following estimates

$$\frac{k}{k_f} = \left(\frac{1}{1 + \frac{u_b^*}{u^*}} \right) \quad (6.53)$$

$$\frac{k_b}{k_f} = \left(\frac{\frac{u^*}{u_b^*}}{1 + \frac{u_b^*}{u^*}} \right) \quad (6.54)$$

The ratio of the isolated period to the fixed base period can be generated with Eq. (6.25):

$$\frac{T_{\text{eq}}}{T_f} = \frac{\omega_f}{\omega_{\text{eq}}} = 1 + \frac{u_b^*}{u^*} \quad (6.55)$$

CHAPTER 6. BASE ISOLATION SYSTEMS

Figs. 6.11 and 6.12 show the variation of k/k_f and k_b/k_f with u_b^*/u^* for a given constant PS_V . The increase in the period is plotted in Fig. 6.13. There is a significant reduction in the structural stiffness required by the seismic excitation when the base is allowed to move. For example, taking $u_b^* = 2u^*$ decreases the design stiffness by a factor of 3. However, we have to ensure that a potential resonant condition is not created by shifting the period. There may be a problem with wind gust loading as the period is increased beyond 3 seconds. This problem can be avoided by providing additional stiffness that functions under wind loading but not under seismic loading. Sect. 6.3 deals with this problem.

These scenarios provide an indication of the potential benefit of base isolation for seismic excitation. **However, we should note that the isolated structure is less stiff than the fixed base structure and therefore will experience larger displacement under other types of loading such as wind.** Also, the simplified model considered here is based on linear undamped behavior, whereas the actual bearings have some damping and may behave in a nonlinear manner. More complex models are considered later in this chapter.

6.2. ISOLATION FOR SDOF SYSTEMS

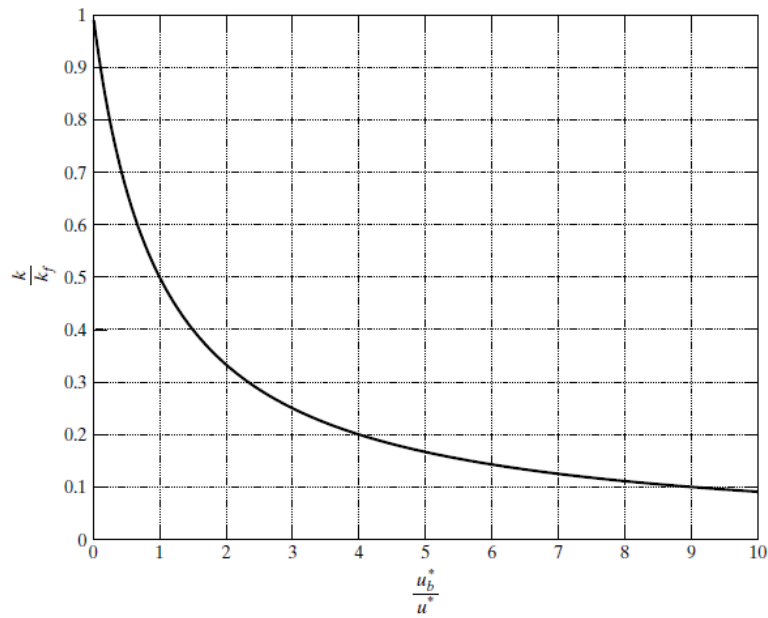


Figure 6.11: Variation of k/k_f with u_b^*/u^* .

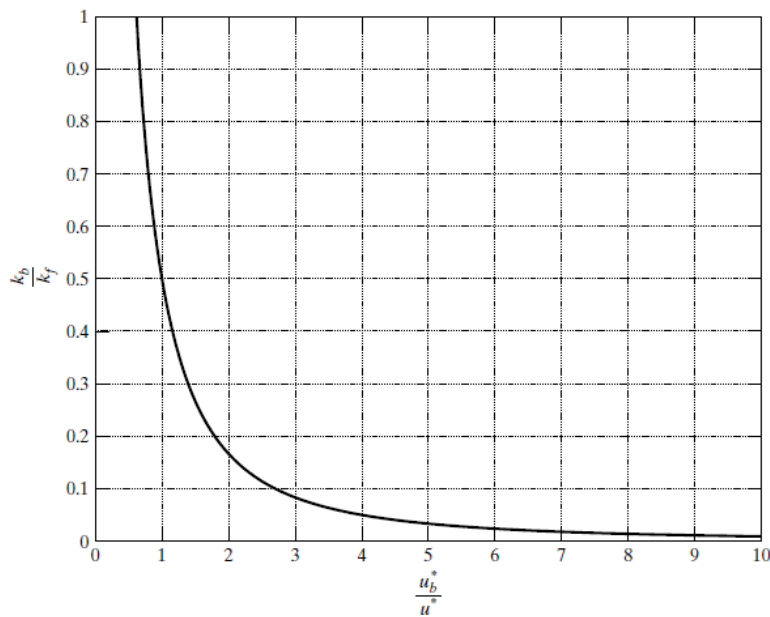


Figure 6.12: Variation of k_b/k_f with u_b^*/u^* .

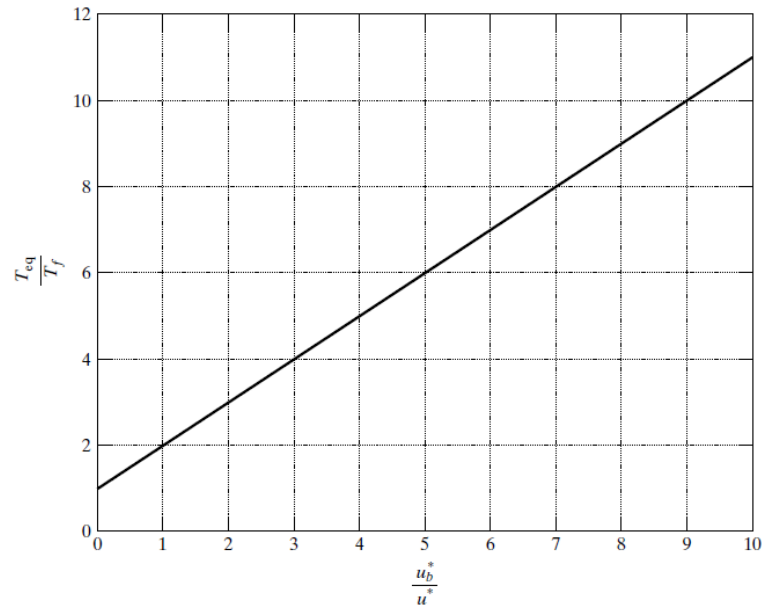


Figure 6.13: Variation of T_{eq}/T_f with u_b^*/u^* .

6.3 Design Issues for Structural Isolation Systems

The most important requirements for an isolation system concern flexibility, energy dissipation, and rigidity under low-level loading. A number of solutions have been proposed for civil-type structures over the past thirty years. The most significant aspects of these designs are discussed next.

6.3.1 Flexibility

A structural isolation system generally consists of a set of flexible support elements that are proportioned such that the period of vibration of the isolated structure is considerably greater than the dominant period of the excitation. Systems proposed to date employ plates sliding on a curved surface (e.g., an inverted pendulum), sleeved piles, and various types of rubber bearings.

6.3. DESIGN ISSUES FOR STRUCTURAL ISOLATION SYSTEMS

Popular choices at this time are the rubber bearing and inverted friction pendulum.

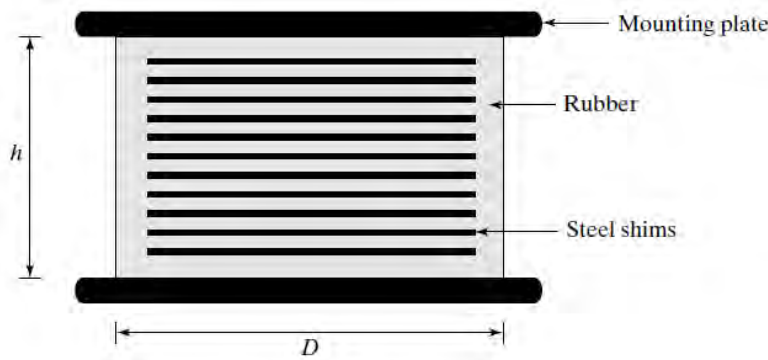


Figure 6.14: Typical natural rubber bearing (NRB).

Rubber bearings consist of layers of natural rubber sheets bonded to steel plates, as shown in Fig. 6.14. The steel plates constrain the lateral deformation of the rubber under vertical loading, resulting in a vertical stiffness several orders of magnitude greater than the horizontal stiffness. The lateral stiffness depends on the number and thickness of the rubber sheets. Increasing either quantity decreases the stiffness; usually, we work with a constant sheet thickness and increase the number of layers. As the height increases, buckling becomes the controlling failure mechanism, and therefore the height is usually limited to about half the diameter. Natural rubber is a nonlinear viscoelastic material and is capable of deforming up to about 300% without permanent damage. Shear strain on the order of 100% is a common design criterion. Bearing diameters up to 1 m and load capacities up to 5 MN are commercially available. Modeling of rubber bearing is discussed in Sect. 6.4.

Fig. 6.8 illustrates how the pendulum bearing responds to lateral loading. The key design parameters are the radius, R ,

which controls the stiffness, and the overall width, b , which is taken as twice the estimated peak ground displacement corresponding to the maximum credible earthquake. The bearings used for the San Francisco terminal were designed to provide a period of 3 seconds and to displace up to 20 inches in any horizontal direction.

6.3.2 Rigidity Under Low-level Lateral Loads

Increasing the lateral flexibility by incorporating a base isolation system provides an effective solution for high-level seismic excitation. Although the relative motion between the structure and the support may be large, the absolute structural motion is generally small, so that the structure does not feel the earthquake. The effect of other types of lateral loading such as wind is quite different. In this case, the loading is applied directly to the structure, and the low lateral stiffness can result in substantial lateral displacement of the structure relative to the fixed support.

To control the motion under service loading, we can incorporate an additional stiffness system that functions for service loading but is not operational for high-level loading. Systems composed of rods and/or springs that are designed to behave elastically up to a certain level of service loading and then yield have been developed and are commercially available. There are a variety of steel dampers having the aforementioned characteristics that can be combined with the rubber bearings. Fig. 6.15 illustrates particular schemes. The rods are dimensioned (length and area) such that they provide the initial stiffness and yield at the intended force level. The earliest solution and still the most popular approach for rubber bearings is to incorporate a lead rod in the rubber bearing, as illustrated in Fig. 6.16. The lead

6.3. DESIGN ISSUES FOR STRUCTURAL ISOLATION SYSTEMS

plug is dimensioned to yield at the service level load and to be approximately 10 times stiffer than the rubber bearing.

CHAPTER 6. BASE ISOLATION SYSTEMS



(a)



(b)

Figure 6.15: (a) Steel rod damper combined with a natural rubber bearing (NRB); and (b) lead rod damper combined with an NRB (courtesy of J. Connor).

6.3. DESIGN ISSUES FOR STRUCTURAL ISOLATION SYSTEMS

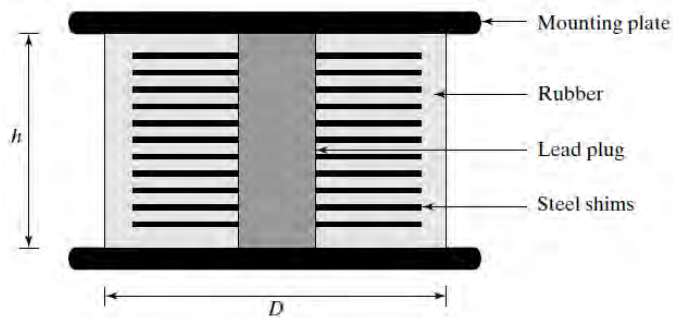


Figure 6.16: Typical lead rubber bearing (LRB).

In order to provide additional stiffness for low level loading, an innovative modification of the single pendulum scheme shown in Fig. 6.8 was introduced by the firm Earthquake Protection Systems (EPS). Their proposed scheme, shown in Fig. 6.17, consists of 3 friction pendulums, a lower unit, an upper unit, and an inner unit. As the lateral loading increases, the mechanisms are activated sequentially; friction between the individual surfaces controls the order in which the mechanism are triggered.

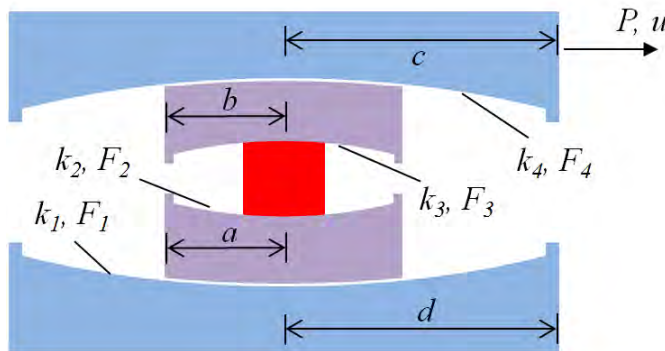


Figure 6.17: Triple pendulum system.

The load-displacement relationship based on $F_2 < F_1$, $F_3 > F_2$, $F_4 > F_1$, and $k_1 > k_2 > k_3 > k_4$ is plotted in Fig. 6.18(a). Fig. 6.18(b) shows the corresponding relative position of the individual

CHAPTER 6. BASE ISOLATION SYSTEMS

pendulums. Shifting to the triple pendulum system allows one to limit the low level motion as well as the forces generated by the design basis earthquake (DBE) and the maximum credible earthquake (MCE). Another benefit is the smaller required width; the double action characteristic of the triple pendulum system reduces the required width by 50%.

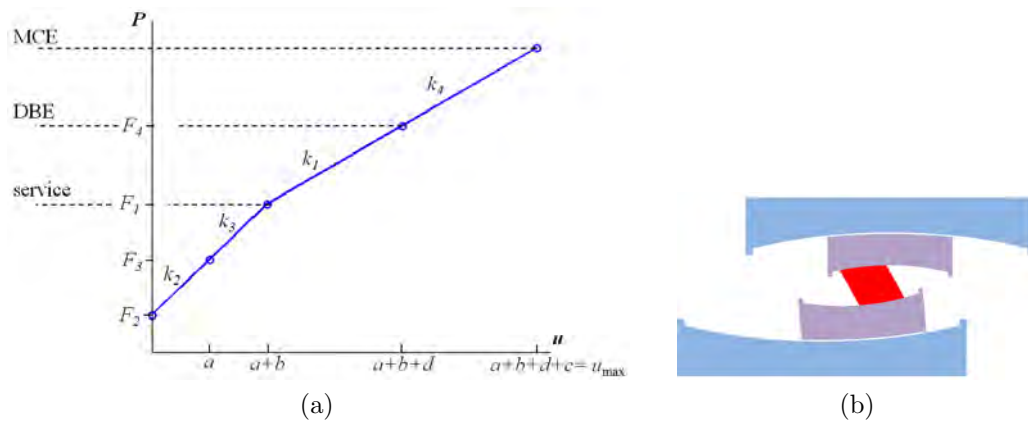


Figure 6.18

A typical design scenario is

$$k_3 = k_2 \quad k_4 = k_1 \quad F_2 = 0$$

Fig. 6.19 shows the corresponding force-displacement relationship and hysteresis loop for the MCE.

6.3. DESIGN ISSUES FOR STRUCTURAL ISOLATION SYSTEMS

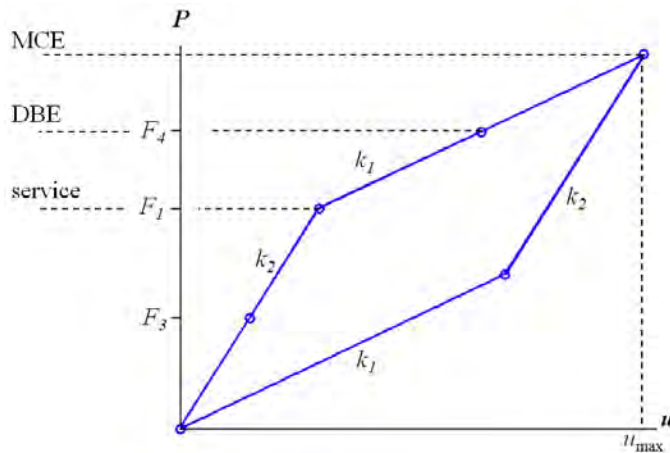


Figure 6.19: Hysteresis loop for MCE.

6.3.3 Energy Dissipation/Absorption

Rubber bearings behave in a viscoelastic manner and have some energy dissipation capacity. Additional damping can be provided by separate devices such as viscous, hysteretic, and friction dampers acting in parallel with the rubber bearings. The lead rubber bearing (LRB) is representative of this design approach; **the lead plug provides both initial stiffness and hysteretic damping**. Since hysteretic damping action occurs only at high-level loading, hysteretic-type systems require additional viscous damping to control the response for low-level loading. High damping natural rubber with a dissipation capacity about four times the conventional value is used together with other devices to improve the energy dissipation capacity of the isolation system. Figure 5.15 illustrates the deployment of a combination of NRBs, steel dampers, and viscous dampers. This scheme allows one to adjust both stiffness and damping for each load level (i.e., for both low- and high-level loading).

CHAPTER 6. BASE ISOLATION SYSTEMS



Figure 6.20: Isolation devices of Bridgestone Toranomon Building (courtesy of J. Connor).

The pendulum damper dissipates energy through friction between the sliding surfaces. One specifies the friction by adjusting the friction coefficients for the individual surfaces. Typical values range from 0.03 to 0.10.

6.3.4 Applicability of Base Isolation Systems

The feasibility of base isolation depends on whether it is needed, whether the proposed structure is suitable for base isolation, and whether it is cost effective compared with alternative solutions [71]. The need for base isolation may arise: if the location is an area of high seismicity; if increased building safety and post-earthquake operability are required; if reduced lateral design forces are desired; or if an existing structure needs upgrading to satisfy current safety requirements. A structure is considered suitable if 1) the subsoil conditions do not produce long period input motions to the structure, 2) the structure is less than about 10 to 15 stories and has a height-to-width ratio that prevents overturning, 3) the site permits the required level of motion of

6.3. DESIGN ISSUES FOR STRUCTURAL ISOLATION SYSTEMS

the base with respect to ground, and 4) the nonseismic lateral loads (such as wind) are less than approximately 10% of the weight of the structure.

The cost effectiveness of a base isolated structure can be assessed by assigning values to both the initial and life cycle costs and benefits. Examples of cost items are the bearings, changes to accommodate the isolation system, maintenance and inspection of the isolation system, and the cost of maintaining operability after earthquakes. Examples of savings are lower initial cost of the structural system, less construction time, lower insurance premium, reduction in earthquake structural and nonstructural damage, and the reduction in injuries, deaths, and lawsuits from related damages. When disruption costs and the value of the building contents are important, seismic isolation has a substantial economic advantage over other systems provided that such an isolation scheme is technically feasible. Under such conditions, initial cost savings of up to 5% of the building cost have been noticed. For conventional buildings where disruption of operation is not important, there may not be sufficient cost savings in the structural system to offset the cost of the isolators [71].

The greatest advantage of base isolation is achieved when it is considered in the early planning stages of the project, since it is possible to take advantage of the reduced response due to the isolation system. If the base isolation system is selected and added after completion of the structural design, many complications may arise since the construction techniques may have to be altered.

For bridge construction, on the other hand, the economic issues are very different from those for buildings. In bridges, the

implementation of seismic isolation simply requires the use of a seismic isolation bearing rather than a conventional bearing. Since bearings are only one or two percent of the cost of a bridge, an increase in the cost of isolation bearings will have very little impact on the overall construction cost and consequently, the use of a seismic isolation system is expected to reduce the overall construction cost [14].

6.4 Modeling Strategies for Rubber Bearings

6.4.1 Modeling of a Natural Rubber Bearing (NRB)

For the purpose of preliminary design, a NRB can be modeled as a simple shear element having a cylindrical shape and composed of a viscoelastic material. Fig. 6.21 defines the notation and shows the mode of deformation. The relevant equations are

$$\gamma = \frac{u}{h} \quad (6.56)$$

$$F = \tau A \quad (6.57)$$

$$h = nt_b \quad (6.58)$$

where A is the cross-sectional area, t_b is the thickness of an individual rubber sheet, and n is the total number of sheets. Each sheet is assumed to be in simple shear.

6.4. MODELING STRATEGIES FOR RUBBER BEARINGS

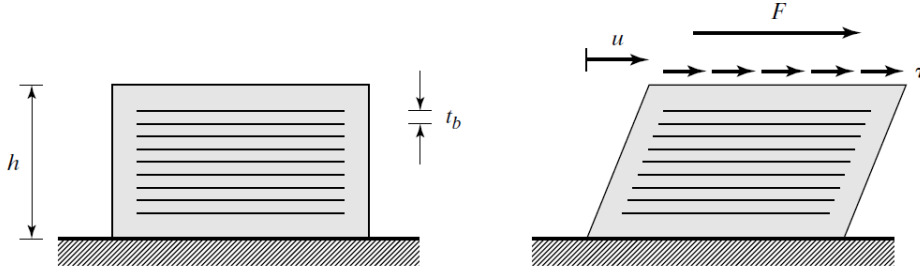


Figure 6.21: Natural rubber bearing under horizontal loading.

Applying the viscoelastic constitutive relations developed in Sect. 4.3, the behavior for harmonic shear strain is given by

$$\gamma = \hat{\gamma} \sin \Omega t \quad (6.59)$$

$$\tau = G_s \hat{\gamma} \sin \Omega t + \eta G_s \hat{\gamma} \cos \Omega t \quad (6.60)$$

where G_s is the storage modulus and η is the loss factor. In general, G_s and η are functions of the forcing frequency and temperature. They are also functions of the strain amplitude in the case of high damping rubbers that exhibit nonlinear viscoelastic behavior. Combining the preceding equations leads to

$$u = \hat{u} \sin \Omega t \quad (6.61)$$

$$F = f_d G_s \hat{u} (\sin \Omega t + \eta \cos \Omega t) \quad (6.62)$$

where

$$\hat{u} = \hat{\gamma} h = \hat{\gamma} n t_b \quad (6.63)$$

$$f_d = \frac{A}{h} = \frac{A}{n t_b} \quad (6.64)$$

Note that f_d depends on the bearing geometry whereas η and G_s are material properties.

CHAPTER 6. BASE ISOLATION SYSTEMS

The standard form of the linearized force-displacement relation is defined by Eq. (4.26):

$$F = k_{\text{eq}}u + c_{\text{eq}}\dot{u} \quad (6.65)$$

where k_{eq} and c_{eq} are the equivalent linear stiffness and viscous damping terms. Estimates for k_{eq} and c_{eq} can be obtained with a least squares approach. Assuming there are N material property data sets covering the expected range of strain amplitude and frequency, the resulting approximate expressions are Eqs. (4.30), (4.32), and (4.33), which are listed here for convenience.

$$k_{\text{eq}} = f_d \left[\frac{1}{N} \sum_{i=1}^N G_s(\Omega_i) \right] = f_d \hat{G}_s \quad (6.66)$$

$$c_{\text{eq}} = \alpha k_{\text{eq}} \quad (6.67)$$

$$\alpha = \frac{\sum_{i=1}^N \left(\frac{G_s \eta}{\Omega} \right)_i}{\sum_{i=1}^N G_s(\Omega_i)} \quad (6.68)$$

Eq. (6.65) is used in the MDOF analysis presented in a later section.

Figs. 6.22 and 6.23 show that the material properties for natural and filled rubber are essentially constant for the frequency range of interest. Assuming G_s and η are constant, the equivalent properties reduce to

6.4. MODELING STRATEGIES FOR RUBBER BEARINGS

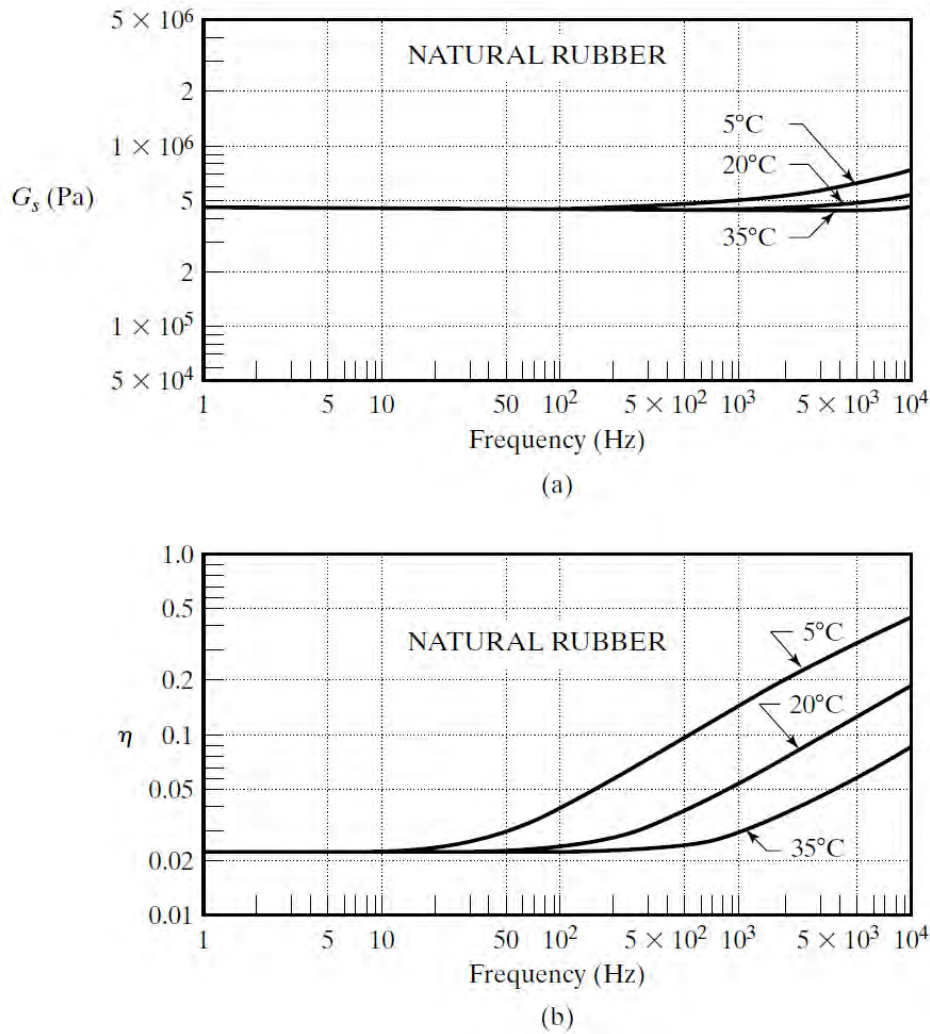


Figure 6.22: Storage modulus and loss factor for natural rubber versus frequency [95], reprinted with permission of AIP Publishing.

$$k_{\text{eq}} = f_d G_s \quad (6.69)$$

$$\alpha = \frac{\eta}{2\pi} T_{\text{av}} \quad (6.70)$$

where T_{av} is the average period for the excitation and G_s , η are the “constant” values.

CHAPTER 6. BASE ISOLATION SYSTEMS

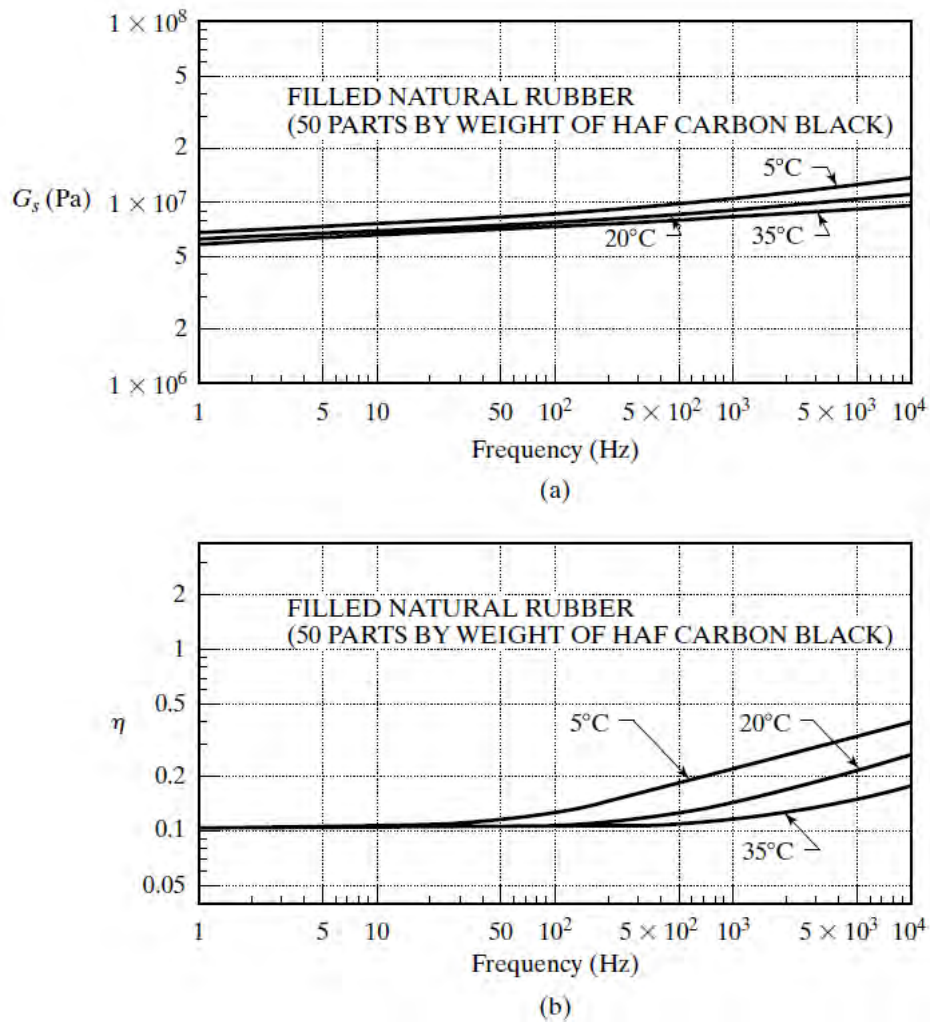


Figure 6.23: Storage modulus and loss factor for filled natural rubber versus frequency [95],reprinted with permission of AIP Publishing.

6.4.2 Modeling of a Lead Rubber Bearing (LRB)

As a first approximation, the LRB can be considered to consist of two elements: 1) a linear viscoelastic element representing the rubber component, and 2) a linear elastic perfectly plastic element simulating the lead plug. This model assumes that the

6.4. MODELING STRATEGIES FOR RUBBER BEARINGS

static force response relationship is bilinear, as indicated in Fig. 6.24. The stiffness defined by Eq. (6.69) can be used for the rubber bearing (i.e., for k_1).

$$k_{(\text{rubber})} \equiv k_1 = f_d G_s \quad (6.71)$$

Considering lead to behave in a linear elastic manner, the plug stiffness can be expressed as

$$k_{(\text{lead})} \equiv k_2 = \frac{A_p G_p}{h_p} \quad (6.72)$$

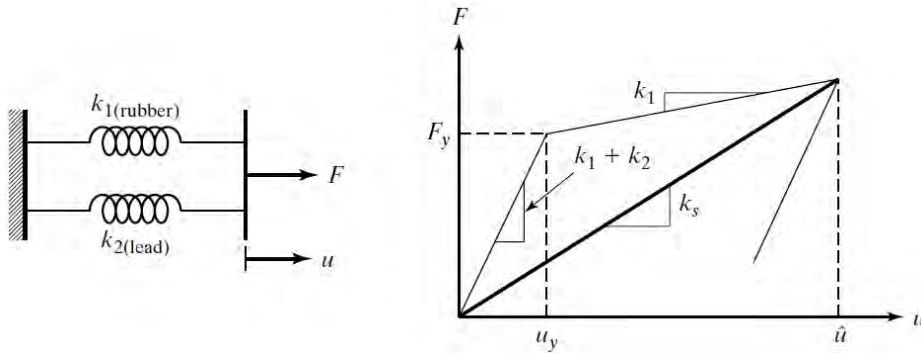


Figure 6.24: Lead rubber bearing model - quasi-static response.

where A_p , h_p , and G_p denote the cross-sectional area, height, and shear modulus for the plug. Lastly, the displacement corresponding to the onset of yielding is related to the yield strain for lead by

$$u_y = h_p \gamma_y \quad (6.73)$$

Interpreting the behavior of the lead rubber bearing for large deformation as viscoelastic, the response due to harmonic motion is expressed in terms of a secant stiffness, k_s , and equivalent loss factor, η ,

$$u = \hat{u} \sin \Omega t \quad (6.74)$$

$$F = k_s \hat{u} \sin \Omega t + \tilde{\eta} k_s \hat{u} \cos \Omega t \quad (6.75)$$

where k_s is related to the elastic energy storage capacity and η is a measure of the energy dissipated through hysteretic damping of the rubber and lead components. Defining μ as the ductility ratio

$$\mu = \frac{\hat{u}}{u_y} = \frac{\hat{\gamma}}{\gamma_y} \quad (6.76)$$

the secant stiffness is related to the individual stiffness terms by

$$k_s = k_1 + \frac{k_2}{\mu} \quad (6.77)$$

The equivalent loss factor is defined as

$$\tilde{\eta} = \frac{1}{2\pi} \left(\frac{W}{E_s} \right) \quad (6.78)$$

where W is the hysteretic work per cycle and E_s is the maximum strain energy. Evaluating the energy terms

$$W = 4(\mu - 1)k_2 u_y^2 + \pi \eta k_1 \mu^2 u_y^2 \quad (6.79)$$

$$E_s = \frac{1}{2} k_s (\mu u_y)^2 \quad (6.80)$$

and substituting in Eq. (6.78) leads to

$$\tilde{\eta} = \frac{4(\mu - 1)k_2}{\pi k_s \mu^2} + \eta \frac{k_1}{k_s} \quad (6.81)$$

Noting that γ_y is about 5×10^{-3} and the typical peak response strain is about 0.5, we can estimate μ as

6.4. MODELING STRATEGIES FOR RUBBER BEARINGS

$$\mu = \frac{\hat{\gamma}}{\gamma_y} \approx 100 \quad (6.82)$$

A typical value for the ratio of k_1 to k_2 is

$$k_1 \approx 0.1k_2 \quad (6.83)$$

Then reasonable estimates for k_s and η are

$$k_s = 1.1k_1 \quad (6.84)$$

$$\tilde{\eta} = \frac{4}{11\pi} + \frac{0.1}{0.11}\eta = 0.12 + 0.909\eta \quad (6.85)$$

The loss coefficient for high damping rubber can be as high as 0.15. Combining a high damping rubber bearing with a lead plug provides an effective solution for both initial stiffness and damping over the range from low to high excitation.

The last step involves transforming Eq. (6.75) to the standard form, Eq. (6.65). Applying a least squares approach and treating k_s and $\tilde{\eta}$ as functions of both the strain amplitude and frequency leads to

$$k_{\text{eq}} = \frac{1}{N} \sum_{i=1}^N k_s(\mu_i, \Omega_i) \quad (6.86)$$

$$c_{\text{eq}} = \frac{1}{N} \sum_{i=1}^N \frac{k_s(\mu_i, \Omega_i) \tilde{\eta}(\mu_i, \Omega_i)}{\Omega_i} \quad (6.87)$$

where N is the number of data sets (i.e., values of μ and Ω). It is reasonable to assume G_s and η are constant, and evaluate these parameters for a representative range of the ductility parameter, μ .

6.5 Examples of Existing Base Isolation Systems

The past few years, especially since the Kobe earthquake in Japan, have seen a significant increase in the number of base isolated structures, which suggests that the technology is gaining acceptance. A short description of some of the early implementations of base isolation systems is presented here to provide an indication of the type of buildings that are being isolated and the cost savings, if any, achieved by employing this technology. More comprehensive descriptions are contained in Ref. [52], the Architectural Institute of Japan Guide to Base Isolated Buildings in Japan (1993), and Ref. [101].

6.5.1 USC University Hospital [75, 10]

This eight-story structure, shown in Fig. 6.25, is used as a teaching hospital by the University of Southern California. It resists seismic forces with a steel braced frame located on the perimeter, and is supported on 68 LRB and 81 NRB isolators. The seismic design was based on a 0.4g response spectrum increased by 20% to account for near-fault effects. The decision to incorporate seismic isolation was made in the preliminary design phase of the project. Structural cost comparisons for conventional and isolated structures were developed and the benefits of seismic isolation were assessed. It was determined that the cost savings in the structural frame would be sufficient to pay for the new structural ground floor slab and the isolation system. The additional cost of mechanical and architectural details was 1.3%, and there was a 1.4% cost savings in the soil nailed retaining wall used in the isolation design versus the conventional retaining wall. Consequently, there was no net additional cost for incorporating

6.5. EXAMPLES OF EXISTING BASE ISOLATION SYSTEMS

seismic isolation on this hospital project.



Figure 6.25: USC University Hospital [114].

6.5.2 Fire Department Command and Control Facility [71]

This is a two-story, steel perimeter braced frame structure that uses 36 high-damping elastomeric isolation bearings. The decision to use seismic isolation on this project was based on a comparison of two designs (conventional and isolation) that required maintaining the functionality of the structure after the extreme design event. This project reflects the first such detailed comparison for two designs to meet a performance specification. In the case of this two-story structure, the isolated structure was found to be 6% less expensive than conventional design. A reduction in losses by a factor of 40 is expected with the seismic isolation.

6.5.3 Evans and Sutherland Manufacturing Facility [88]

The building (see Fig. 6.26) is a four-story manufacturing site for flight simulators located near the Warm Springs and East faults in Salt Lake City. The building measures 280 ft \times 160 ft in plan and rests on 40 LRB and 58 NRB isolators. Preliminary costs for conventional and isolated designs were developed and the benefits of seismic isolation assessed at the conceptual design phase. The structural engineers decided to design the structural framing system for the UBC code forces for conventional design and, consequently, there were no structural framing cost savings. The additional structural cost was the basement structural floor (versus a slab-on-grade) and the heavy fail-safe system used. Based on cost data developed by the contractors, the cost premium for incorporating seismic isolation was 5% or \$400,000 on an \$8 million project. An important factor in deciding to employ seismic isolation was the need to protect the building contents, including work in progress, the value of which exceeds \$100 million (approximately 12 times the cost of the structure).



Figure 6.26: Evans and Sutherland Facility. (courtesy of J. Connor).

6.5. EXAMPLES OF EXISTING BASE ISOLATION SYSTEMS

6.5.4 Salt Lake City Building [72, 108]

This facility, shown in Fig. 6.27, is a five-story, Richardson Romanesque Revival structure constructed between 1892 and 1894, 265 ft \times 130 ft in plan, and built of unreinforced brick and sandstone. Its 12-story tower is centrally located and is also constructed of unreinforced masonry. The building was restored, and a combination of 208 LRB and 239 NRB isolators were installed, separating the building from its foundation. The structure is now protected against damage for the 0.2g design earthquake event. This project was the subject of a detailed study of several retrofit schemes, among which were base isolation and UBC strengthening. The schemes were developed in sufficient detail to permit cost estimates and an evaluation of performance. Although the cost of these two alternatives was comparable, the decision to use seismic isolation was made based on the considerably better performance that results from the implementation of such a scheme. The complete architectural and historic restoration, and seismic rehabilitation work was estimated to be \$24 million. The approximate value of the seismic isolation work reported by the contractor was \$4,414,000 including the cost of the 447 seismic isolators.



Figure 6.27: Salt Lake City and County Building [116].

6.5.5 The Toushin 24 Ohmori Building [23]

This building has one underground story, which is used as a parking garage, and nine stories above ground. It is located adjacent to two of the busiest railway lines in Tokyo, and the isolation system was required to reduce the traffic induced vibration as well as seismic motion. Fig. 6.28 shows a view of the building, a sectional plan, and the isolation scheme. A combination of laminated natural rubber bearings and steel rod dampers were deployed. Thick layers of rubber were used to decrease the vertical stiffness and thus filter out vertical microtremors.

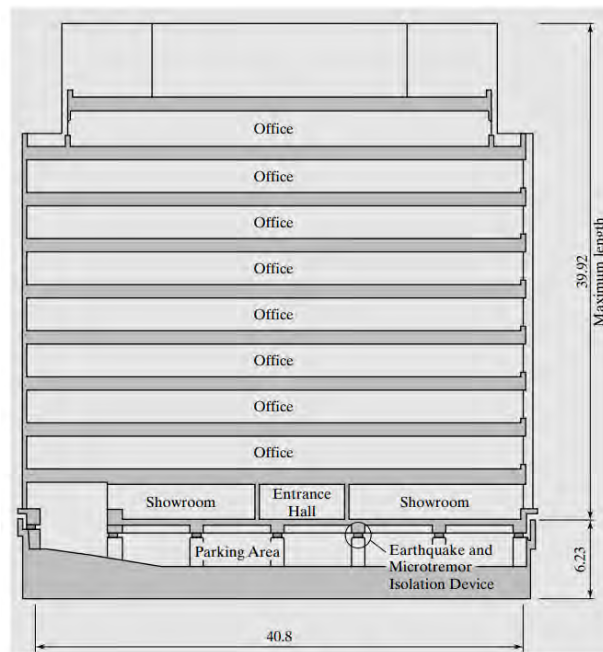
6.5. EXAMPLES OF EXISTING BASE ISOLATION SYSTEMS



(a) View of building

Figure 6.28: The Toushin 24 Ohmori Building (courtesy of J. Connor).

CHAPTER 6. BASE ISOLATION SYSTEMS



(b) Section

Figure 6.28: The Tou shin 24 Ohmori Building (courtesy of J. Connor) - (continued).



(c) Devices

Figure 6.28: The Tou shin 24 Ohmori Building. (courtesy of J. Connor) - (continued).

6.5. EXAMPLES OF EXISTING BASE ISOLATION SYSTEMS

6.5.6 Bridgestone Toranomom Building

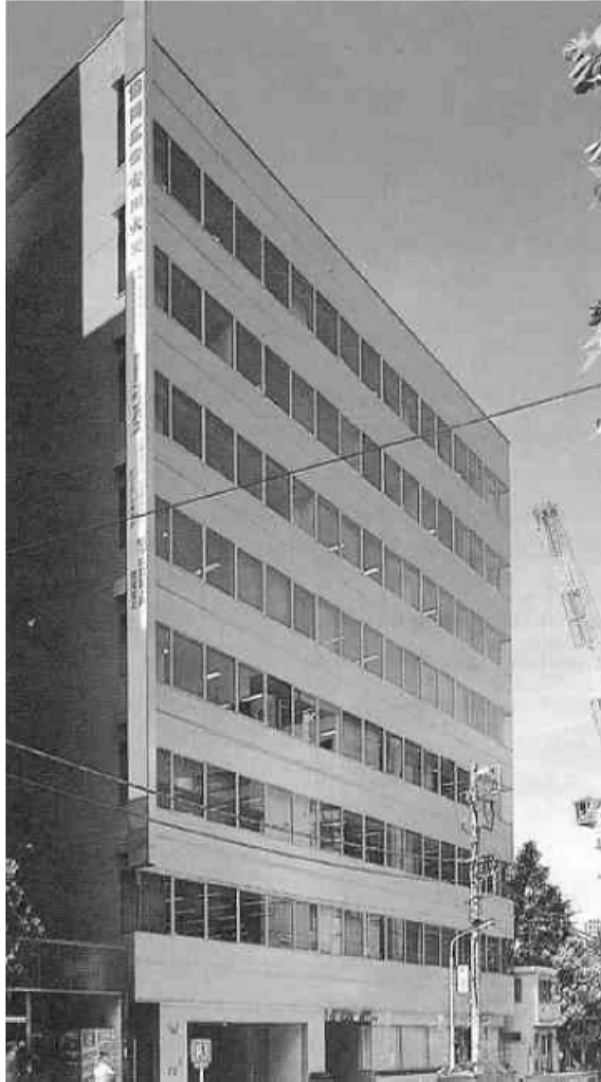


Figure 6.29: Bridgestone Toranomom Building (courtesy of J. Connor).

The Bridgestone Toranomom Building (see Fig. 6.29) is an office building of the Bridgestone Corporation, a major supplier of rubber products such as bearings. The base isolation system

CHAPTER 6. BASE ISOLATION SYSTEMS

consists of 12 laminated rubber bearings, 25 steel dampers, and 8 viscous (oil) dampers. Fig. 6.20 shows the layout of the devices. The viscous dampers are intended to dissipate the energy associated with wind and low intensity excitations. At this load level, the steel dampers are designed to behave elastically and provide stiffness. Energy associated with a large seismic excitation is dissipated/absorbed primarily by the steel dampers.

6.5.7 San Francisco City Hall

San Francisco City Hall (Fig. 6.30) is a historic structure that was retrofitted in 1994 with a seismic isolation system consisting of 530 lead rubber isolators. The design basis earthquake is 0.50g. Cost of retrofitting the structure is approximately \$105 million.



Figure 6.30: San Francisco City Hall [117].

6.5.8 Long Beach V.A. Hospital

The hospital is a 12-story concrete structure with shear walls (Fig. 6.31). A combination of 110 LRB, 18 NRB, and 18 sliding

6.5. EXAMPLES OF EXISTING BASE ISOLATION SYSTEMS

bearings were installed in the mechanical crawl spaces below the building to improve the building's ability to survive earthquakes up to magnitude 0.32g.



Figure 6.31: Long Beach V.A. Hospital [115].

6.5.9 Mills-Peninsula Health Services New Hospital

Located close to the San Andreas Fault, CA., the new medical facility has 176 triple pendulum bearings at the base of the columns. This bearing system allows up to 30 inches of displacement in any direction.

CHAPTER 6. BASE ISOLATION SYSTEMS



Figure 6.32: Mills-Peninsula Health Services New Hospital, CA (courtesy of Earthquake Protection Systems (EPS)).

6.5.10 Benicia-Martinez Bridge [29]

Friction pendulum bearings are installed at the top of the concrete piers of the Benicia-Martinez Bridge, CA. They allow up to 53 inches displacement. The isolated system has a period of 5 seconds.



Figure 6.33: Benicia-Martinez Bridge, CA (courtesy of Earthquake Protection Systems (EPS)).

6.5. EXAMPLES OF EXISTING BASE ISOLATION SYSTEMS

6.5.11 The Cathedral of Christ the Light [91]



Figure 6.34: The Cathedral of Christ the Light (courtesy of S. Laflamme).

The Cathedral of Christ the Light, located in Oakland, CA, has been erected in 2008 as a replacement to the St. Francis de Sales Cathedral, damaged during the 1989 Loma Prieta Earthquake. The new structure has been designed to withstand a 1,000-year earthquake. It is equipped with 36 double concave friction pendulum base isolators. The mitigation system provides up to 30 inches lateral displacement; Fig. 6.34(a) shows a picture of the cathedral. Fig. 6.34(b) shows the enclosed trench around the perimeter of the structure that allows structural motion during an earthquake.

6.6 Optimal Stiffness Distribution: Discrete Shear Beam

The theory developed earlier in this chapter for the SDOF case is extended here to deal with the more general case of a deformable beam-type structure supported by a base isolation system. Linear behavior is assumed since the objective is to generate results that are suitable for preliminary design. The approach followed to establish the stiffness distribution for the structure is similar to what was presented in Chapter 3. The only modification required is to include the effect of the stiffness and damping associated with the base isolation system. Most of the notation and relevant equations have been introduced in Chapter 3.

In what follows, the stiffness distribution corresponding to uniform deformation for the fundamental mode of the composite system consisting of a discrete shear beam and isolation system is derived. The theory is extended to deal with continuous beams in the next section.

6.6.1 Scaled Stiffness Distribution

Fig. 6.35 defines the notation used for the base isolated shear beam. The bearing system is represented by an equivalent linear spring, k_1 , and linear viscous damper, c_1 ; m_1 represents the mass lumped at the foundation level above the bearings; u_i is the displacement of the mass m_i with respect to the ground; k_i and c_i are the story stiffness and viscous damping coefficients for the actual structure. The governing equations for free undamped vibration are expressed as

$$\mathbf{M}\ddot{\mathbf{U}} + \mathbf{K}\mathbf{U} = \mathbf{0} \quad (6.88)$$

6.6. OPTIMAL STIFFNESS DISTRIBUTION: DISCRETE SHEAR BEAM

where the various matrices are the same as defined in Chapter 3.

In the previous development, the modal displacement profile was selected such that the interstory displacement was constant over the beam. That strategy is modified here to allow for a different interstory displacement for the first story, which, in this model, *represents the relative displacement of the bearing*.

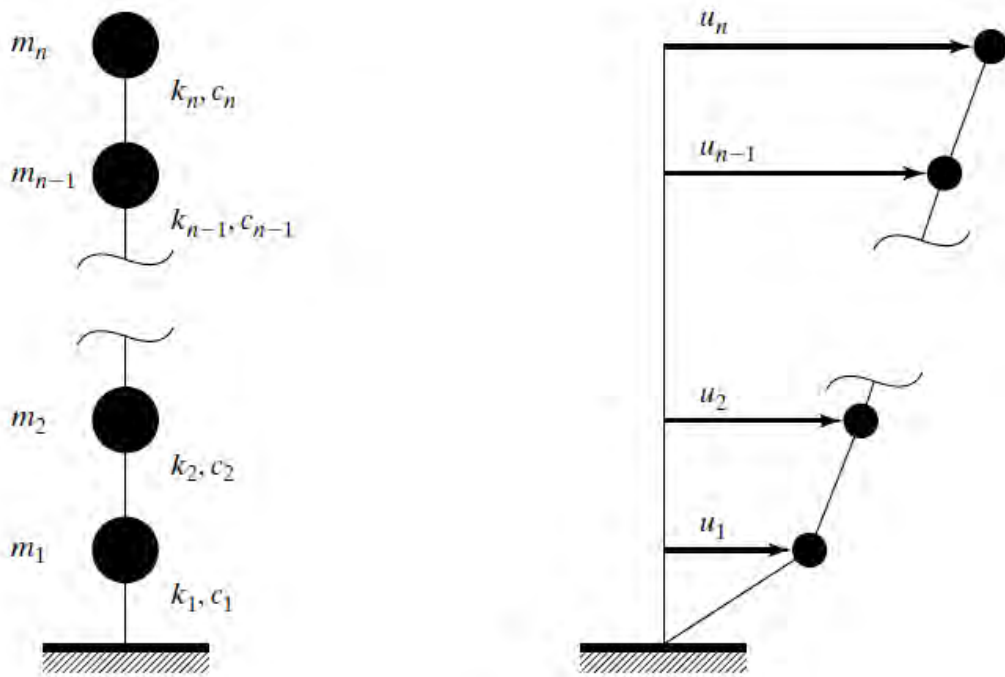


Figure 6.35: Notations for base isolated discrete shear beam.

Fig. 6.36(a) illustrates the choice of displacement profile; u_s is the displacement at the top node due to deformation of the beam; and u_b is the bearing displacement. For equal story height, the bilinear profile corresponds to uniform shear in the beam, $\gamma = u_s/H$. The bearing displacement is expressed as a multiple of the maximum structural displacement,

CHAPTER 6. BASE ISOLATION SYSTEMS

$$u_b = \nu u_s \tag{6.89}$$

and the profile is scaled by taking u_s as the independent displacement parameter. Fig. 6.36(b) shows the scaled profile. With this choice of displacement parameter, the displacement vector takes the form

$$\begin{aligned} \mathbf{U} &= q\Phi \\ &= u_s \left\{ \nu \quad \nu + \frac{1}{3} \quad \nu + \frac{2}{3} \quad \nu + 1 \right\} \end{aligned} \tag{6.90}$$

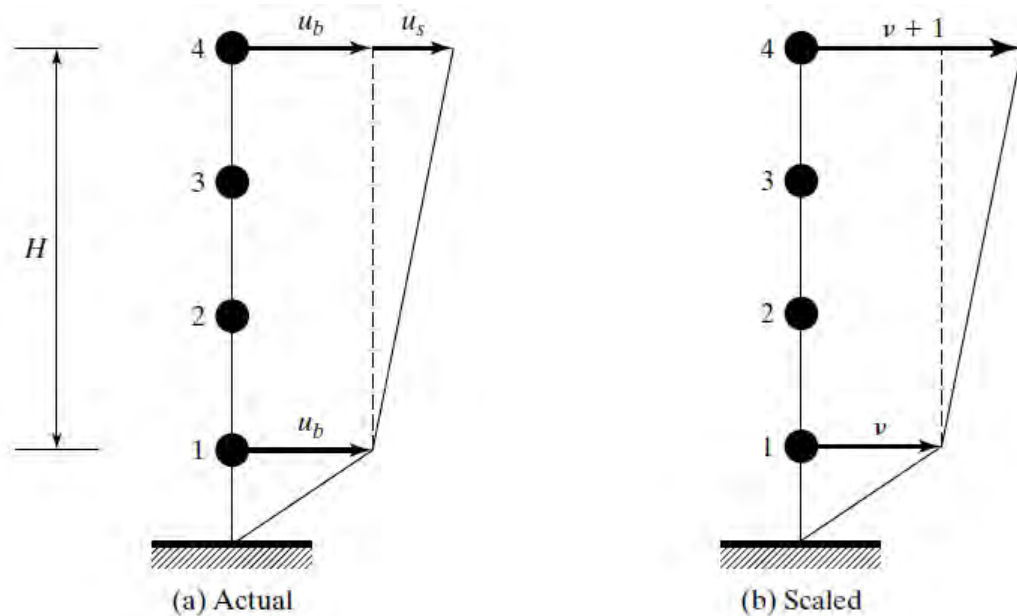


Figure 6.36: Example displacement profile.

Note that the choice of q as the maximum structural displacement due to deformation of the structure is consistent with the approach followed for the fixed base case. The modified displacement profile introduced here allows for an additional story at the

6.6. OPTIMAL STIFFNESS DISTRIBUTION: DISCRETE SHEAR BEAM

bottom of the beam and distinguishes between the deformation at the base and within the beam.

Generalizing this approach for an n^{th} -order system, the fundamental mode profile is taken as

$$\begin{aligned} \mathbf{U} &= q\Phi \\ \Phi &= \left\{ \nu \quad \nu + \frac{1}{n-1} \quad \nu + \frac{2}{n-1} \quad \cdots \quad \nu + 1 \right\} \end{aligned} \quad (6.91)$$

The remaining steps are the same as followed in Sect. 3.4. We write $\mathbf{U} = e^{\pm i\omega t}\Phi$ and substitute for \mathbf{U} in Eq. (6.88). This leads to

$$\mathbf{K}\Phi = \omega^2\mathbf{M}\Phi \quad (6.92)$$

Scaling \mathbf{K} and rearranging the equations results in

$$\mathbf{S}\mathbf{k}' = \mathbf{M}\Phi \quad (6.93)$$

where $k'_i = k_i/\omega^2$ and \mathbf{S} , defined by Eq. (3.56), is listed below for convenience.

$$\begin{aligned} \mathbf{S}'(i, i) &= \Phi_i - \Phi_{i-1} \\ \mathbf{S}'(i, i+1) &= \Phi_i - \Phi_{i+1} \\ \mathbf{S}'(i, j) &= 0 \quad \text{for } j \neq i, i+1 \end{aligned} \quad (6.94)$$

Given \mathbf{M} and Φ , we solve Eq. (6.93) for \mathbf{k}' . This procedure is illustrated with the following example.

Example 6.2 - Scaled stiffness for a 4DOF beam with base isolation

Consider the beam shown in Fig. 6.36. The various matrices are

$$\Phi = \left\{ \nu \quad \nu + \frac{1}{3} \quad \nu + \frac{2}{3} \quad \nu + 1 \right\} \quad (6.95)$$

$$\mathbf{M}\Phi = \left\{ m_1\nu \quad m_2 \left(\nu + \frac{1}{3} \right) \quad m_3 \left(\nu + \frac{2}{3} \right) \quad m_4(\nu + 1) \right\} \quad (6.96)$$

$$\mathbf{S} = \begin{bmatrix} \nu & -1/3 & & \\ & 1/3 & -1/3 & \\ & & 1/3 & -1/3 \\ & & & 1/3 \end{bmatrix} \quad (6.97)$$

$$\mathbf{k}' = \{ k'_1 \quad k'_2 \quad k'_3 \quad k'_4 \} \quad (6.98)$$

$$k'_4 = 3m_4(\nu + 1)$$

$$k'_3 = 3m_3 \left(\nu + \frac{2}{3} \right) + k'_4$$

$$k'_2 = 3m_2 \left(\nu + \frac{1}{3} \right) + k'_3 \quad (6.99)$$

$$k'_1 = m_1 + \frac{k'_2}{3\nu}$$

When the masses are equal, Eq. (6.99) reduces to

$$\begin{aligned} k'_1 &= m^* \left(4 + \frac{2}{\nu} \right) \\ k'_2 &= m^* (6 + 9\nu) \\ k'_3 &= m^* (5 + 6\nu) \\ k'_4 &= m^* (3 + 3\nu) \end{aligned} \quad (6.100)$$

Taking \mathbf{U} according to Eq. (6.91), the response of the fundamental mode is governed by

6.6. OPTIMAL STIFFNESS DISTRIBUTION: DISCRETE SHEAR BEAM

$$\tilde{m}\ddot{q} + \tilde{c}\dot{q} + \tilde{k}q = \tilde{p} - \tilde{m}\Gamma a_g \quad (6.101)$$

where the modal parameters are defined as

$$\begin{aligned} \tilde{m} &= \Phi^T \mathbf{M} \Phi & \tilde{c} &= \Phi^T \mathbf{C} \Phi & \tilde{k} &= \Phi^T \mathbf{K} \Phi \\ \tilde{p} &= \Phi^T \mathbf{P} & \Gamma &= \frac{\Phi^T \mathbf{M} \mathbf{E}}{\tilde{m}} & \tilde{\xi} &= \frac{\tilde{c}}{2\omega\tilde{m}} \end{aligned} \quad (6.102)$$

Since Φ now involves the relative displacement factor, ν , these terms will also depend on ν .

Example 6.3 - Example 6.2 revisited

Modal parameters for the 4DOF shear beam considered in Ex. 6.2 are as follows:

$$\begin{aligned} \tilde{m} &= m_1\nu^2 + m_2 \left(\nu^2 + \frac{2}{3}\nu + \frac{1}{9} \right) + m_3 \left(\nu^2 + \frac{4}{3}\nu + \frac{4}{9} \right) \\ &\quad + m_4(\nu^2 + 2\nu + 1) \\ \Phi^T \mathbf{M} \mathbf{E} &= m_1\nu + m_2 \left(\nu + \frac{1}{3} \right) + m_3 \left(\nu + \frac{2}{3} \right) + m_4(\nu + 1) \\ \tilde{c} &= \nu^2 c_1 + \frac{1}{9}(c_2 + c_3 + c_4) \\ \tilde{p} &= \nu p_1 + \left(\nu + \frac{1}{3} \right) p_2 + \left(\nu + \frac{2}{3} \right) p_3 + (\nu + 1)p_4 \end{aligned} \quad (6.103)$$

When the masses are equal, \tilde{m} and Γ simplify to

$$\begin{aligned} \tilde{m} &= m^* \left(4\nu^2 + 2\nu + \frac{14}{9} \right) \\ \Gamma &= \frac{2\nu + 1}{2\nu^2 + \nu + \frac{7}{9}} = \frac{9}{7} \left[\frac{1 + 2\nu}{1 + \frac{9}{7}\nu(1 + 2\nu)} \right] \end{aligned} \quad (6.104)$$

CHAPTER 6. BASE ISOLATION SYSTEMS

Values of \tilde{m}/m^* and Γ for a range of values of ν are listed in Table 6.1. There is a significant reduction in Γ with increasing ν , and this results in a reduced response to seismic excitation.

Table 6.1: Modal mass and participation factors for 4DOF shear beam with equal modal masses

ν	\tilde{m}/m^*	Γ
0	1.556	1.286
1	7.556	0.794
2	21.556	0.464
3	43.556	0.321
4	73.556	0.245
5	111.556	0.197

The modal damping parameter, \tilde{c} , depends on both the bearing damping c_1 and the structural damping (c_2, c_3, c_4) properties. Incorporating damping in the bearing is more effective than distributing damping over the structure for the fundamental mode response. Structural damping is needed mainly to control the higher modes.

6.6.2 Stiffness Calibration for Seismic Isolation

The peak fundamental mode response due to seismic excitation is given by

$$q_{\max} = \Gamma S_D(\omega, \xi) \quad (6.105)$$

We specify q_{\max} , ξ , and $S_D(\omega, \xi)$, and determine ω by iterating on Eq. (6.105). By definition, q_{\max} is the maximum structural displacement relative to the base motion due to deformation of the structure. It is evaluated using the design value for the maximum transverse shear strain and the structural height,

6.6. OPTIMAL STIFFNESS DISTRIBUTION: DISCRETE SHEAR BEAM

$$q_{\max} = \gamma^* H \quad (6.106)$$

The peak amplitude of the bearing displacement relative to the ground follows from Eq. (6.89):

$$u_b|_{\max} \equiv u_1|_{\max} = \nu q_{\max} \quad (6.107)$$

Given q_{\max} and $u_b|_{\max}$, ν is determined with Eq. (6.107). This approach has to be modified when the structure is taken to be rigid (i.e., when $q_{\max} \approx 0$). In this case, the system reduces to a SDOF model, and the formulation presented in Sect. 6.2 is applicable.

Example 6.4 - Stiffness calibration for Example 6.3

Returning to the 4DOF example structure, the following data are assumed.

$$\begin{aligned} H &= 15 \text{ m} \\ \gamma^* &= 1/200 \\ S_D(\omega, \xi) &\text{defined by Fig. 3.23} \end{aligned} \quad (6.108)$$

Using (6.108),

$$q_{\max} = (15)(1/200) = 0.075 \text{ m} \quad (6.109)$$

To proceed further, we need to specify ν . Various cases are considered next.

Case 1 $u_b|_{\max} = 0.3 \text{ m}$

The parameters corresponding to this bearing displacement are

$$\begin{aligned}\nu &= 0.3/0.075 = 4 \\ \Gamma &= 0.245\end{aligned}\tag{6.110}$$

Substituting in Eq. (6.105) leads to the value for S_D

$$S_D = \frac{q_{\max}}{\Gamma} = \frac{0.075}{0.245} = 0.30 \text{ m}\tag{6.111}$$

Suppose $\xi = 0.05$. From Fig. 3.23, $T \approx 0.65$ sec. Then

$$\omega = \frac{2\pi}{T} = 9.66 \text{ r/s}\tag{6.112}$$

The stiffness coefficients are generated using the results contained in Ex. 6.2. For the case of uniform mass, Eq. (6.100) applies. Taking $\nu = 4$ and ω according to Eq. (6.112) leads to

$$\begin{aligned}k_1 &= 403.1m^* \\ k_2 &= 3825m^* \\ k_3 &= 2641m^* \\ k_4 &= 1399m^*\end{aligned}\tag{6.113}$$

Damping is determined with Eq. (6.103). For $\nu = 4$ and $\xi = 0.05$,

$$\tilde{m} = 111.6m^*\tag{6.114}$$

$$\tilde{c} = 2\xi\omega\tilde{m} = 2(0.05)(9.66)(111.6m^*) = 107.8m^*\tag{6.115}$$

The individual damping coefficients are related to \tilde{c} by

$$\tilde{c} = 16c_1 + \frac{1}{9}(c_2 + c_3 + c_4) = 107.8m^*\tag{6.116}$$

6.6. OPTIMAL STIFFNESS DISTRIBUTION: DISCRETE SHEAR BEAM

We have to decide how to allocate damping to the various components. For example, assuming 75% of \tilde{c} is contributed by the bearing requires

$$\begin{aligned}c_1 &= 5.05m^* \\c_2 + c_3 + c_4 &= 242.5m^*\end{aligned}\tag{6.117}$$

Placing damping at the base is an order of magnitude more effective than distributing the damping throughout the structure for this degree of isolation.

Case 2 $u_b|_{\max} = 0.375 \text{ m}$

For this case, $\nu = 5$. The various parameters for $\xi = 0.05$, $\nu = 5$, and uniform mass are as follows.

$$\begin{aligned}\Gamma &= 0.197 \\T &= 0.85 \text{ s} \\\omega &= 7.85 \text{ rad/s} \\\tilde{m} &= 21.556m^* \\\tilde{c} &= 16.92m^*\end{aligned}\tag{6.118}$$
$$25c_1 + \frac{1}{9}(c_2 + c_3 + c_4) = 16.92m^*$$
$$\begin{aligned}k_1 &= 307m^* & k_2 &= 1476m^* \\k_3 &= 1045m^* & k_4 &= 553m^*\end{aligned}$$

Case 3 Fixed base

Treatment of the fixed base case is illustrated in Ex. 3.10. Considering uniform mass and $\xi = 0.05$ results in the following parameters and properties (note the system now has 3 degrees of freedom):

$$\begin{aligned}\Gamma &= 1.286 \\ T &= 0.35 \text{ s} \\ \omega &= 20.93 \text{ rad/s} \\ \tilde{m} &= 1.556m^* \\ \frac{1}{9}(c_2 + c_3 + c_4) &= 0.814m^* \\ k_1 &= \infty \quad k_2 = 7626m^* \\ k_3 &= 2187m^* \quad k_4 = 1313m^*\end{aligned}\tag{6.119}$$

6.7 Optimal Stiffness Distribution: Continuous Cantilever Beam

6.7.1 Stiffness Distribution: Undamped Response

The equilibrium equations for undamped motion of the base isolated continuous beam shown in Fig. 6.37 are

$$V(x, t) = -\rho_m \int_x^H \ddot{u}(x, t) dx \tag{6.120}$$

$$M(x, t) = \int_x^H V(x, t) dx \tag{6.121}$$

6.7. OPTIMAL STIFFNESS DISTRIBUTION: CONTINUOUS CANTILEVER BEAM

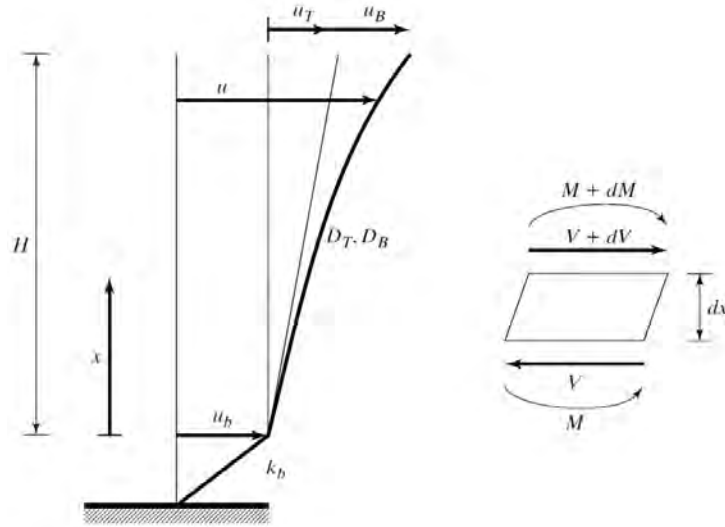


Figure 6.37: Base isolated continuous beam.

The transverse shear and bending deformation measures for the beam are related to the translation and rotation quantities by

$$\frac{\delta u}{\delta x} = \gamma + \beta \quad (6.122)$$

$$\chi = \frac{\delta \beta}{\delta x} \quad (6.123)$$

Considering γ and χ to be functions only of time, integrating the resulting equations with respect to x , and imposing the boundary conditions at $x = 0$, we obtain expressions for u and β in terms of $\gamma(t)$, $\chi(t)$, and $u_b(t)$:

$$u = \gamma x + \frac{1}{2} \chi x^2 + u_b \quad (6.124)$$

$$\beta = \chi x \quad (6.125)$$

where u_b denotes the displacement of the base of the structure with respect to ground. Taking

$$\gamma = \gamma^* e^{i\omega_1 t} \quad (6.126)$$

$$\chi = \chi^* e^{i\omega_1 t} \quad (6.127)$$

$$u_b = u_b^* e^{i\omega_1 t} \quad (6.128)$$

produces a periodic motion of the beam. Noting that the deformation amplitudes γ^* and χ^* are related by (see Fig. 6.37)

$$s = \frac{u_b}{u_T} = \frac{\chi^* H}{2\gamma^*} \quad (6.129)$$

and expressing u_b^* in terms of the displacement at $x = H$ due to shear deformation (see Fig. 6.37)

$$u_b^* = \nu u_T^* = \nu \gamma^* H \quad (6.130)$$

transforms Eq. (6.124) into

$$u = \left(\frac{x}{H} + \frac{sx^2}{H^2} + \nu \right) \gamma^* H e^{i\omega_1 t} = \Phi(x) (\gamma^* H e^{i\omega_1 t}) = q(t) \Phi(x) \quad (6.131)$$

The function $\Phi(x)$ defines the fundamental mode. Setting $\nu = 0$ results in the corresponding expression for the fixed base.

Differentiating with respect to time,

$$\ddot{u} = - \left(x + \frac{sx^2}{H} + \nu H \right) \gamma^* \omega_1^2 e^{i\omega_1 t} \quad (6.132)$$

and substituting for \ddot{u} in Eq. (6.120) leads to

$$V = \rho_m \omega_1^2 H^2 \left(\frac{1}{2} + \frac{s}{3} + \nu - \frac{x^2}{2H^2} - \frac{sx^3}{3H^3} - \frac{\nu x}{H} \right) \gamma^* e^{i\omega_1 t} \quad (6.133)$$

6.7. OPTIMAL STIFFNESS DISTRIBUTION: CONTINUOUS CANTILEVER BEAM

The corresponding relation for the bending moment is

$$M = \rho_m \omega_1^2 H^4 \chi^* e^{i\omega_1 t} \cdot \left[\frac{1}{6s} + \frac{1}{8} + \frac{\nu}{4s} - \left(\frac{1}{4s} + \frac{1}{6} + \frac{\nu}{2s} \right) \frac{x}{H} + \frac{\nu x^2}{4sH^2} + \frac{x^3}{12sH^3} + \frac{x^4}{24H^4} \right] \quad (6.134)$$

Lastly, the shear and bending rigidity distributions are determined with the definition equations

$$D_T = \frac{V}{\gamma^*} = \rho_m \omega_1^2 H^2 \left(\frac{1}{2} + \frac{s}{3} + \nu - \frac{x^2}{2H^2} - \frac{sx^3}{3H^3} - \frac{\nu x}{H} \right) \quad (6.135)$$

$$D_B = \frac{M}{\chi^*} = \rho_m \omega_1^2 H^4 \left[\frac{1}{6s} + \frac{1}{8} + \frac{\nu}{4s} - \left(\frac{1}{4s} + \frac{1}{6} + \frac{\nu}{2s} \right) \frac{x}{H} + \frac{\nu x^2}{4sH^2} + \frac{x^3}{12sH^3} + \frac{x^4}{24H^4} \right] \quad (6.136)$$

Eq. (6.135) is written as

$$D_T = \frac{D_T(0)}{\left(\frac{1}{2} + \frac{s}{3} + \nu \right)} \left(\frac{1}{2} + \frac{s}{3} + \nu - \frac{x^2}{2H^2} - \frac{sx^3}{3} - \frac{\nu x}{H} \right) \quad (6.137)$$

where $D_T(0)$ is the shear rigidity at the base.

$$D_t(0) = \rho_m \omega_1^2 H^2 \left(\frac{1}{2} + \frac{s}{3} + \nu \right) \equiv k_s H \quad (6.138)$$

The parameter, k_s , can be interpreted as an equivalent shear stiffness measure. The shear force at the base of the beam must equal the shear force in the bearing in order to satisfy the force

CHAPTER 6. BASE ISOLATION SYSTEMS

equilibrium condition for undamped motion. Equating these forces

$$D_t(0)\gamma^* = k_b u_b^* = k_b \nu \gamma^* H \quad (6.139)$$

and solving for k_b results in

$$k_b = \frac{D_T(0)}{\nu H} = \frac{1}{\nu} k_s \quad (6.140)$$

The fundamental frequency follows from Eq. (6.138):

$$\omega_1^2 = \frac{D_T(0)}{\rho_m H^2 \left(\frac{1}{2} + \frac{s}{3} + \nu \right)} \quad (6.141)$$

Figs 6.38 and 6.39 shows the mode shapes and shear deformation profiles for the first five modes of a typical low-rise building. The variation in the mode shape profiles with the ratio of the stiffness of the isolator, k_b , to the shear beam stiffness, k_s , are illustrated by Figs. 6.40, 6.41, and 6.42. This ratio is equal to $1/\nu$. Fig. 6.43 displays the variation in the periods of the highest three fundamental modes. The primary influence is on the period of the fundamental mode, which is significantly increased when the stiffness of the isolator is several orders of magnitude lower than the beam stiffness. The effect on the periods of the second and third modes is relatively insignificant. Fig. 6.44 shows the variation of the participation of the second and third modes relative to the first. The plot shows that the contribution of the second and third modes is also significantly reduced by decreasing the stiffness of the isolator with respect to the beam stiffness.

6.7. OPTIMAL STIFFNESS DISTRIBUTION: CONTINUOUS CANTILEVER BEAM

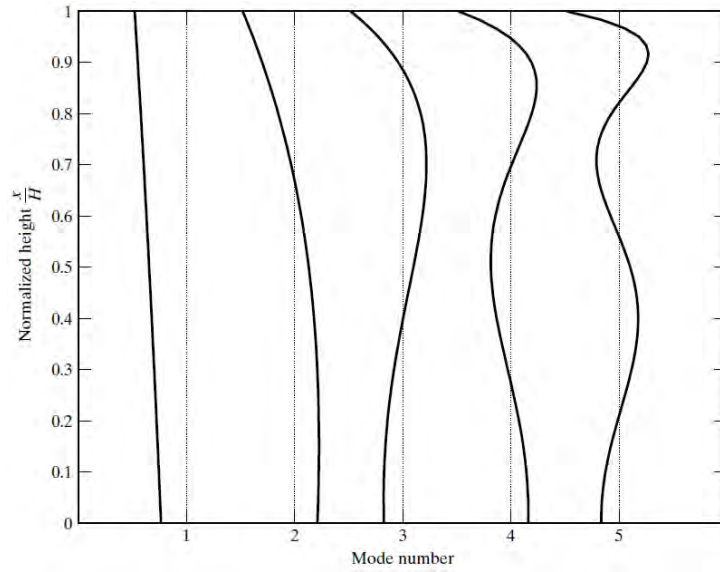


Figure 6.38: Mode shapes for a typical base isolated structure.

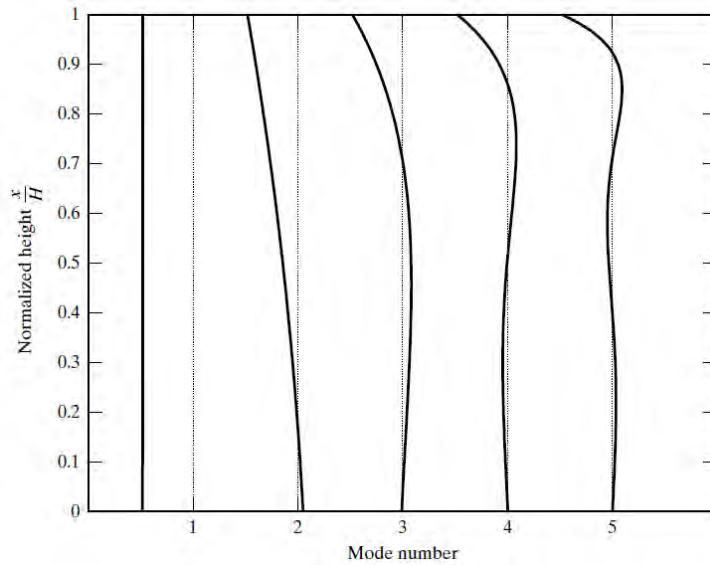


Figure 6.39: Shear deformation profiles for a typical base isolated structure.

CHAPTER 6. BASE ISOLATION SYSTEMS

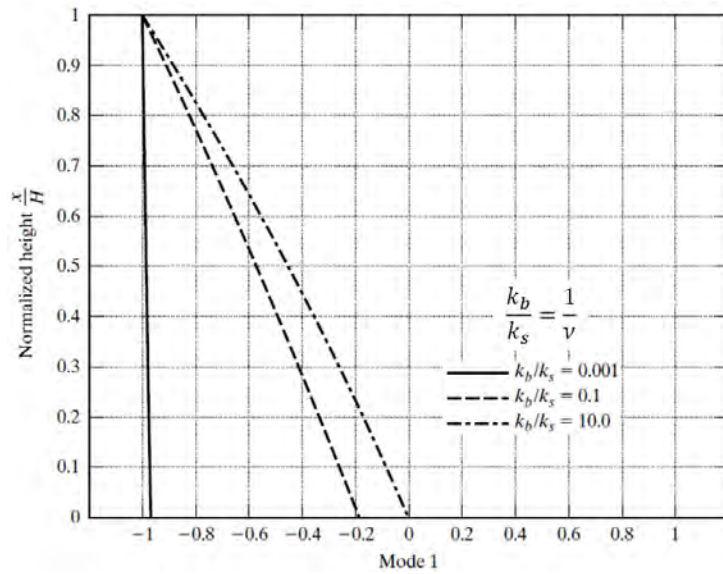


Figure 6.40: Variation of mode 1 shape with relative stiffness of isolator.

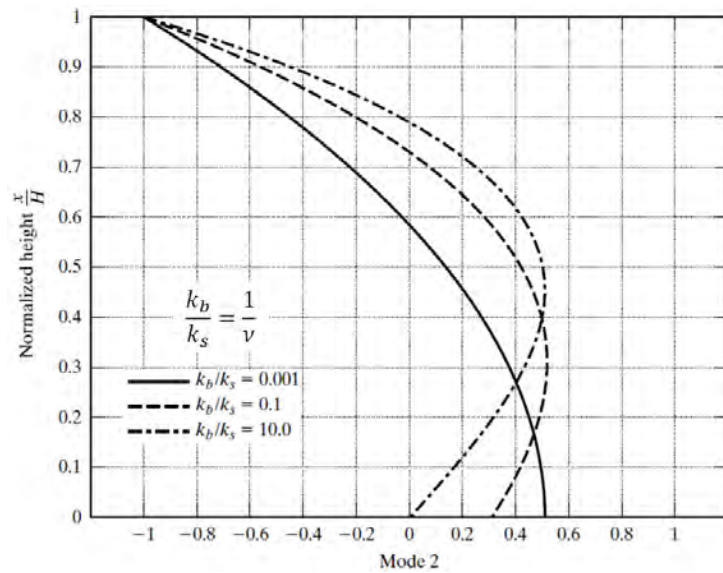


Figure 6.41: Variation of mode 2 shape with relative stiffness of isolator.

6.7. OPTIMAL STIFFNESS DISTRIBUTION: CONTINUOUS CANTILEVER BEAM

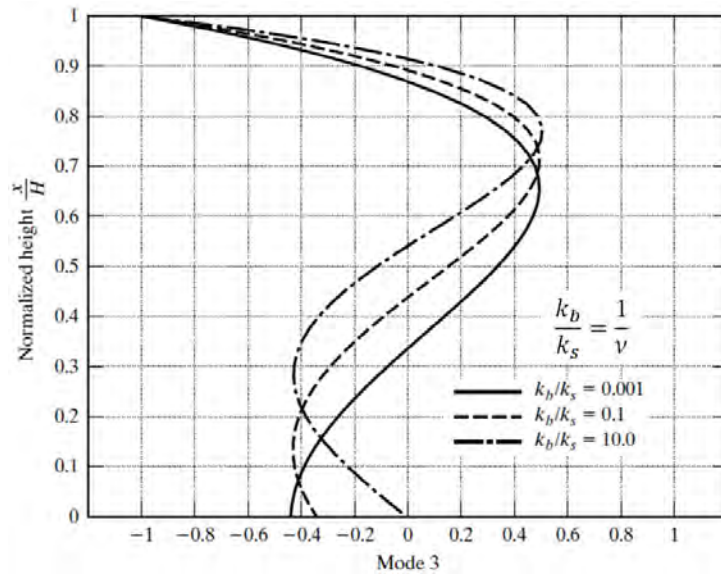


Figure 6.42: Variation of mode 3 shape with relative stiffness of isolator.

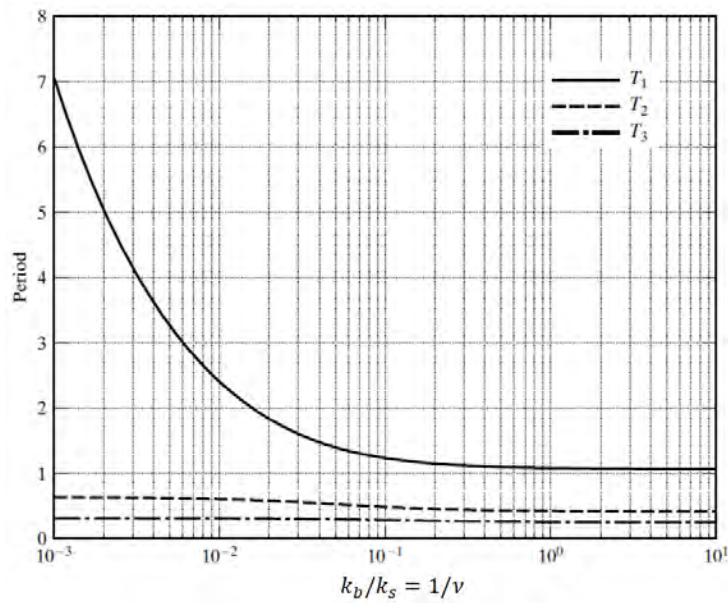


Figure 6.43: Variation of periods with relative stiffness of isolator.

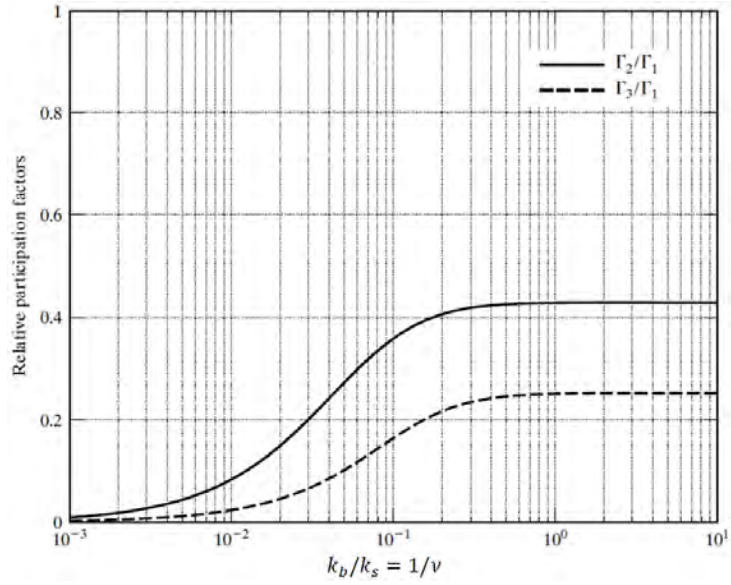


Figure 6.44: Variation of relative participation factors with relative stiffness of isolator.

6.7.2 Fundamental Mode Equilibrium Equation

Incorporating the contribution of the base isolation system, the principle of virtual displacements has the form

$$\int_0^H (M \cdot \delta\chi + V \cdot \delta\gamma) dx + F_b \cdot \delta u_b = \int_0^H (b \cdot \delta u) dx \quad (6.142)$$

where F_b is the shear force in the bearing. The equations relating internal forces to deformations and deformation rates are taken as

$$V = D_t \gamma + C_t \dot{\gamma} \quad (6.143)$$

$$M = D_B \chi + C_B \dot{\chi} \quad (6.144)$$

$$F_b = k_b u_b + c_b \dot{u}_b \quad (6.145)$$

6.7. OPTIMAL STIFFNESS DISTRIBUTION: CONTINUOUS CANTILEVER BEAM

The form of the modal expansion follows from Eq. (6.131).

$$u = q\Phi(x) = q \left(\frac{x}{H} + \frac{sx^2}{H^2} + \nu \right) \quad (6.146)$$

$$\beta = q\Psi(x) = q \left(\frac{2sx}{H^2} \right) \quad (6.147)$$

Assuming external loading and seismic excitation, the loading term is

$$b = -\rho_m a_g - \rho_m \ddot{u} + \bar{b}(x, t) \quad (6.148)$$

Finally, introducing the various terms in the principle of virtual displacements leads to the equilibrium equation for q :

$$\tilde{m}\ddot{q} + \tilde{c}\dot{q} + \tilde{k}q = \tilde{p} \quad (6.149)$$

where

$$\tilde{m} = \int_0^H \rho_m \left(\frac{x}{H} + \frac{sx^2}{H^2} + \nu \right)^2 dx = \rho_m H \left(\frac{1}{3} + \nu + \nu^2 + \frac{s}{2} + \frac{2s\nu}{3} + \frac{s^2}{5} \right) \quad (6.150)$$

$$\tilde{c} = \int_0^H \left(\frac{C_T}{H^2} + \frac{4s^2 C_B}{H^4} \right) dx + c_b \nu^2 \quad (6.151)$$

$$\tilde{k} = \int_0^H \left(\frac{D_T}{H^2} + \frac{4s^2 D_B}{H^4} \right) dx + k_b \nu^2 \quad (6.152)$$

$$\tilde{p} = \int_0^H (\bar{b} - \rho_m a_g) \left(\frac{x}{H} + \frac{sx^2}{H^2} + \nu \right) dx = -\rho_m H \left(\frac{1}{2} + \nu + \frac{s}{3} \right) a_g - \tilde{p}_e \quad (6.153)$$

Expressing \tilde{c} and \tilde{k} as

$$\tilde{c} = 2\xi\omega\tilde{m} \quad (6.154)$$

$$\tilde{k} = \omega^2\tilde{m} \quad (6.155)$$

transforms Eq. (6.149) to

$$\ddot{q} + 2\xi\omega\dot{q} + \omega^2q = -\Gamma a_g + \frac{1}{\tilde{m}}\tilde{p}_e \quad (6.156)$$

where

$$\Gamma = \frac{\nu + \frac{1}{2} + \frac{s}{3}}{\frac{1}{3} + \nu^2 + \nu + \frac{s^2}{5} + \frac{s}{2} + \frac{2s\nu}{3}} \quad (6.157)$$

For a pure shear beam, $s = 0$ and the participation factor for the fundamental mode reduces to

$$\Gamma = \frac{\nu + \frac{1}{2}}{\frac{1}{3} + \nu^2 + \nu} \quad (6.158)$$

The expression for the modal damping ratio depends on how we specify the damping over the beam.

6.7.3 Rigidity Calibration: Seismic Excitation

The calibration procedure presented in Chapter 3 is applied here to the base isolated model. One starts with

$$q_{\max} = \Gamma S_D(\omega, \xi) \quad (6.159)$$

and evaluates q_{\max}

$$q_{\max} = \gamma^* H = \frac{u_b^*}{\nu} \quad (6.160)$$

6.7. OPTIMAL STIFFNESS DISTRIBUTION: CONTINUOUS CANTILEVER BEAM

The one specifies in addition to the other parameters (γ^*, ξ, S_D) and determines ω . This value is used to determine $D_T(0)$ and k_b with Eqs. (6.138) and (6.140).

Example 6.5 - Stiffness calibration: Example Building

The design data are

$$\begin{aligned} H &= 50 \text{ m} & \rho_m &= 20,000 \text{ kg/m} \\ \gamma^* &= 1/200 & s &= 0.25 \\ \xi_1 &= 0.05 & S_D(T, \xi) &= \text{given by Fig. 3.23(b)} \end{aligned} \quad (6.161)$$

Using (6.161), the peak relative structural displacement is

$$q_{\max} = \gamma^* H = 0.25 \text{ m} \quad (6.162)$$

To proceed further, we need to specify the base displacement and then establish the value of ν with Eq. (6.130). We take

$$u_b = 0.25 \text{ m} \quad (6.163)$$

Then

$$\nu = \frac{u_b}{q_{\max}} = 1.0 \quad (6.164)$$

Given ν , the participation factor follows from Eq. (6.157):

$$\Gamma = 0.600 \quad (6.165)$$

The modal mass is determined with Eq. (6.150):

$$\tilde{m} = 2.638 \times 10^6 \text{ kg} \quad (6.166)$$

Assuming C_T constant and $C_B = 0$ in Eq. (6.151), the modal damping coefficient reduces to

$$\tilde{c} = \frac{C_T}{H} + \nu^2 c_b = 0.02C_T + c_b \quad (6.167)$$

Eq. (6.154) relates \tilde{c} to ω .

$$\tilde{c} = 2\xi\omega\tilde{m} = 0.2638 \times 10^6 \omega \quad \text{N} \cdot \text{s/m} \quad (6.168)$$

Lastly, the frequency is found using the design plot for $S_D(\xi = 0.05)$.

$$\begin{aligned} S_D &= \frac{q_{\max}}{\Gamma} = \frac{0.25}{0.6} = 0.42 \text{ m} \\ T &\approx 0.82 \text{ sec} \\ \omega &\approx 7.66 \text{ r/s} \end{aligned} \quad (6.169)$$

With ω known, the modal damping coefficient follows from Eq. (6.168):

$$\tilde{c} = 2.021 \text{ MN} \cdot \text{s/m} \quad (6.170)$$

and the transverse shear rigidity at the base of the beam is determined with Eq. (6.138).

$$D_T(0) = 4639 \text{ MN} \quad (6.171)$$

Finally, given $D_T(0)$, the isolator stiffness is estimated using Eq. (6.140), which is based on neglecting the contribution of the damping force in the bearing.

$$k_b = 92.8 \text{ MN} \quad (6.172)$$

**6.7. OPTIMAL STIFFNESS DISTRIBUTION: CONTINUOUS
CANTILEVER BEAM**

Problems

Problem 6.1

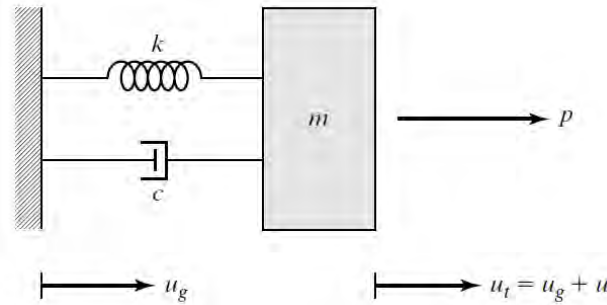


Figure P6.1a

Consider a SDOF system with $m = 1000$ kg (Fig. P6.1a). The design requirements for the system involve two nonconcurrent loading conditions, a periodic external forcing and a periodic ground motion. Under the external forcing, the relative motion is prescribed; the total motion is prescribed for the case of ground excitation. These design conditions are summarized next. The asterisk denotes a specified quantity.

$$(a) \quad p = p^* \sin \Omega_p^* t$$

$$u < u^*$$

$$(b) \quad u_g = u_g^* \sin \Omega_g^* t$$

$$u_t < u_t^* \equiv H_3^* u_g^*$$

The design problem involves determining k and c such that the preceding performance requirements are satisfied.

CHAPTER 6. BASE ISOLATION SYSTEMS

1. Recommend values for k and c corresponding to the following design data:

$$(a) \quad \Omega_g^* = 2\pi \text{ rad/s} \quad u_g^* = 0.2 \text{ m} \quad H_3^* = 0.125$$

$$p^* = 400 \text{ N} \quad \Omega_p^* = \frac{\pi}{2} \text{ rad/s} \quad u^* = 0.2 \text{ m}$$

$$(b) \quad \Omega_g^* = 2\pi \text{ rad/s} \quad H_3^* = 0.125$$

$$p^* = 800 \text{ N} \quad \Omega_p^* = \frac{\pi}{2} \text{ rad/s} \quad u^* = 0.2 \text{ m}$$

$$(c) \quad \Omega_g^* = 2\pi \text{ rad/s} \quad H_3^* = 0.125$$

$$p^* = 1600 \text{ N} \quad \Omega_p^* = \frac{\pi}{2} \text{ rad/s} \quad u^* = 0.2 \text{ m}$$

2. It may not be possible to satisfy both constraints with the same value of stiffness. When this problem arises, we can determine the stiffness corresponding to each design condition and design a spring mechanism that allows the stiffness to be varied. Suggest design concepts for such a mechanism. This situation may occur for lateral loading applied to a seismically isolated structure. Discuss how you would implement a variable stiffness scheme for non simultaneous wind and seismic loading.

Problem 6.2

Refer to the modified SDOF model defined by Fig. 6.10. Take $m = 10,000 \text{ kg}$ and $k = 400 \text{ kN/m}$. Suppose the system is to be subjected to a ground motion, $u_g(\text{meters}) = 0.5 \sin 4\pi t$, and the total displacement is required to be less than 0.2 m . Determine the appropriate bearing stiffness.

Problem 6.3

Refer to the modified SDOF model defined by Fig. 6.10. Take m

6.7. OPTIMAL STIFFNESS DISTRIBUTION: CONTINUOUS CANTILEVER BEAM

= 10,000 kg and the ground motion to be $u_g(\text{meters}) = 0.5 \sin 4\pi t$. Determine k and k_b such that

1. $u \leq 0.3$ m and $u_b \leq 0.3$ m
2. $u \leq 0.1$ m and $u_b \leq 0.3$ m

Problem 6.4

Refer to the modified SDOF model defined by Fig. 6.10. Take $m = 10,000$ kg and consider the system to be subjected to seismic excitation of intensity $S_D = 0.3$ m. Determine k , k_b , and T_{eq} for the following design conditions:

1. $u^* = 0.1$ m $u_n^* = 0.1$ m
2. $u^* = 0.1$ m $u_n^* = 0.2$ m
3. $u^* = 0.1$ m $u_n^* = 0.3$ m

Problem 6.5

Consider a cylindrical bearing having a diameter of 0.6 m, a height of 0.3 m, and composed of filled natural rubber. Take the rubber properties according to Fig. 6.23. Assume the frequency range is from 1 to 5 Hz, and the temperature is 20°C.

1. Estimate the equivalent linear stiffness and linear viscous damping parameters, k_{eq} and c_{eq} .
2. Determine the diameter of a lead plug for the case where the plug stiffness is 10 times the stiffness of the rubber bearing. Assume the lead plug and rubber cylinder have the same height. Take $G_P = 4 \times 10^3$ MPa.

CHAPTER 6. BASE ISOLATION SYSTEMS

3. Assume the bearing experiences periodic excitation resulting in a shear strain amplitude of 50%. Determine the secant stiffness, k_s , and loss factor, $\tilde{\eta}$, using Eqs. (6.77) and (6.81).
4. Instead of lead, consider using low strength steel as the material for the initial stiffness element, k_2 . Take $\tau_y = 150$ MPa and $G = 80 \times 10^3$ MPa for the steel plug. Repeat parts 2. and 3.

Problem 6.6

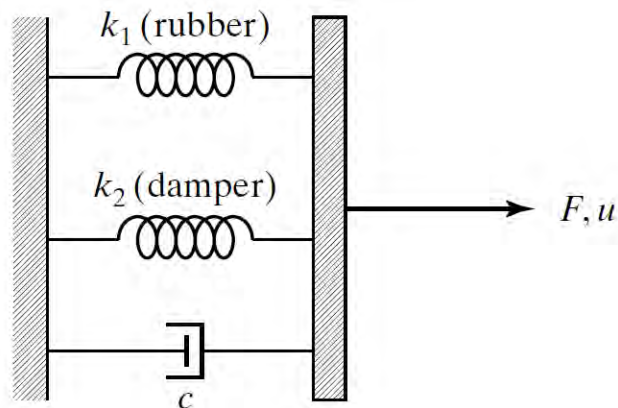


Figure P6.6a

**6.7. OPTIMAL STIFFNESS DISTRIBUTION: CONTINUOUS
CANTILEVER BEAM**

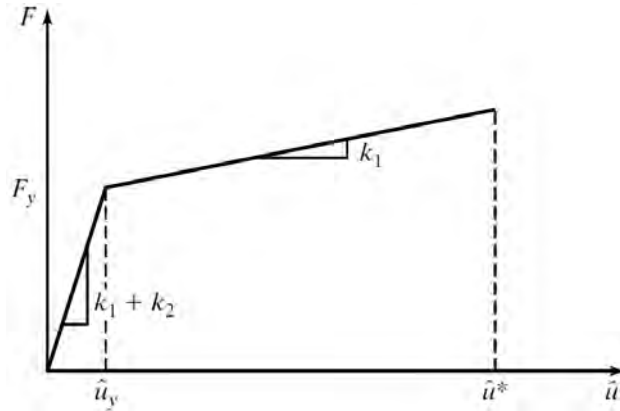


Figure P6.6b

Consider the isolation system composed of a NRB, a steel hysteretic damper, and a viscous damper shown in Fig. P6.6a. Neglect the damping provided by the NRB.

1. For low-level loading, we specify the initial stiffness, damping, and yield force level. Describe how you would design the steel damper.

2. For high-level loading, we specify the secant stiffness and equivalent viscous damping based on a seismic analysis. Describe how you would design the NRB. How would you select the viscous damper?

3. Suppose the isolation system is composed of spring and damper elements (see Fig. P6.6c) whose properties can be varied instantaneously. Assuming the elements behave linearly, the force is given by

$$F = k(t)u + c(t)\dot{u}$$

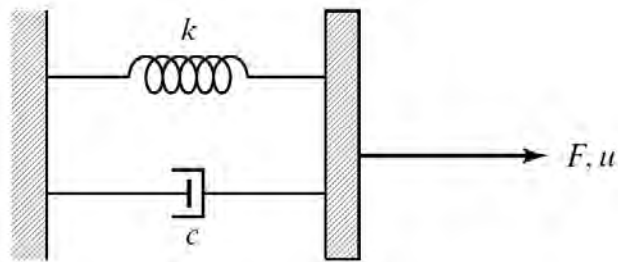


Figure P6.6c

where $k(t)$ and $c(t)$ are properties that can be “adjusted”. Describe how you would utilize this system for a building subjected (nonsimultaneously) to both wind and seismic excitation. How would you design these devices? *Note:* A system that has the ability to change its properties is said to be adaptive. Adaptive systems are discussed in Chapter 7.

Problem 6.7

6.7. OPTIMAL STIFFNESS DISTRIBUTION: CONTINUOUS CANTILEVER BEAM

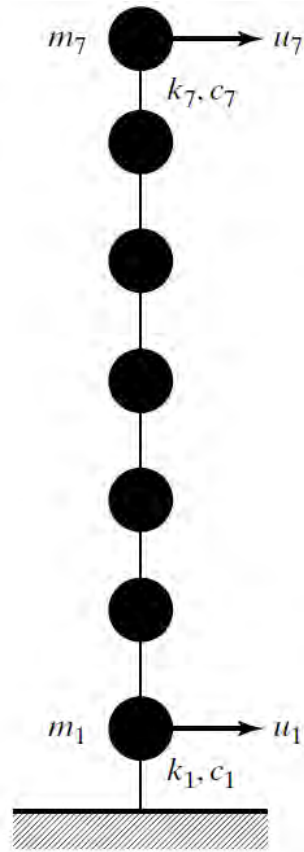


Figure P6.7a

Consider a six-story building with base isolation modeled as a 7DOF system (Fig. P6.7a). Take the floor masses as $m_1 = m_2 = \dots = m_6 = 10,000$ kg and $m_7 = 20,000$ kg.

1. Find the scaled stiffness for the profile based on Eq. (6.91). Take $\nu = 2.0$.
 2. Evaluate the expressions for \tilde{m} , \tilde{c} , \tilde{p} , and Γ .
 3. Calibrate the stiffness distribution for seismic excitation. Use the spectral displacement plot contained in Fig. 3.23.
-

CHAPTER 6. BASE ISOLATION SYSTEMS

Take $\xi = 0.05$, $u_s|_{\max} = 0.15$ m, and $u_b|_{\max} = 0.3$ m. Allocate 75% of the damping to the bearing.

- Repeat part 3., assuming the base is fixed. Take the sum of the stiffness factors as a measure of the cost of stiffness. Compare the costs of the fixed base and base isolation solutions.
- Suppose filled rubber bearings having a diameter of 0.5 m and a height of 0.25 m are to be used for the isolation system. Assume $G = 4$ MPa and $\eta = 0.15$ for the rubber. How many bearings are required for the design conditions specified in part 3.? Also discuss how you would provide the damping required for the isolation system.
- Discuss how you would deal with lateral wind loading. Assume the dominant wind gust frequency is 0.2 Hz.

Problem 6.8

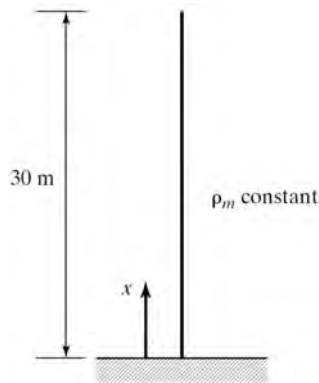


Figure P6.8a

6.7. OPTIMAL STIFFNESS DISTRIBUTION: CONTINUOUS CANTILEVER BEAM

Consider a base isolated continuous cantilever beam having a uniform mass density of 2000 kg/m and a height of 30 m (Fig. P6.8a).

1. Generate shear and bending rigidity distributions and isolation stiffness that correspond to a fundamental frequency of 0.33 Hz and various values for s and ν . Take $- \leq s \leq 0.25$ and $1 \leq \nu \leq 3$. Comment on the sensitivity of the rigidity parameters to variation in s and ν .
2. Approximate the continuous beam with six shear beam segments plus an additional segment to simulate the bearing. Determine the first three mode shapes and frequencies corresponding to $s = 0$ and $\nu = 0, 1.5, \text{ and } 3$. Consider the lumped masses to be equal. Comment on the sensitivity of the modal properties to the ratio of isolation stiffness, k_b , to the shear beam stiffness measure, k_s .

Problem 6.9

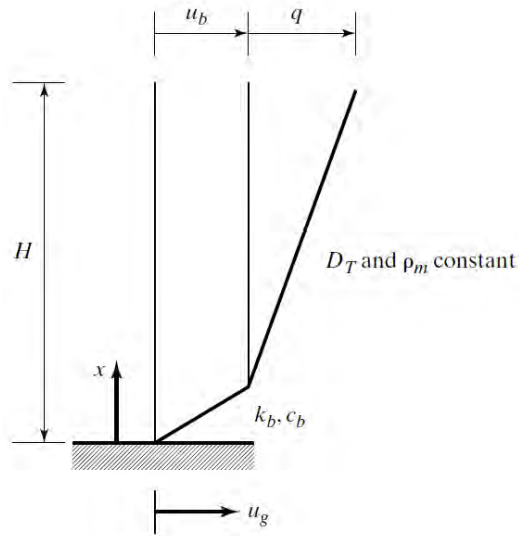


Figure P6.9a

Consider a base isolated continuous shear beam having a uniform mass density and constant transverse shear rigidity (Fig. P6.9a). Assume the lateral displacement is approximated by

$$u = u_g + u_b + q \frac{x}{H} = u_g + q \left(\nu + \frac{x}{H} \right)$$

1. Establish an equation for $q(t)$ using the principle of virtual displacements. Allow for linear viscous damping in the bearing and uniform material damping in the beam. Write the result in the same form as Eq. (6.149) and determine the expressions for \tilde{m} , \tilde{c} , \tilde{k} , \tilde{p} , ω , ξ , and Γ .
2. Suppose $H = 30$ m, $\rho_m = 2000$ kg/m, and $\nu = 2$. Calibrate the stiffness distribution (D_T and k_b) for $\xi = 0.05$, $q_{\max} = 0.15$, S_D and defined by Fig. 3.23. Determine the damping parameters assuming the bearing contributes 75% to \tilde{c} .

**6.7. OPTIMAL STIFFNESS DISTRIBUTION: CONTINUOUS
CANTILEVER BEAM**

3. Approximate the continuous beam with six shear beam segments plus an additional segment to simulate the bearing. Determine the first two mode shapes and frequencies, using the design data generated in part 2.

Problem 6.10

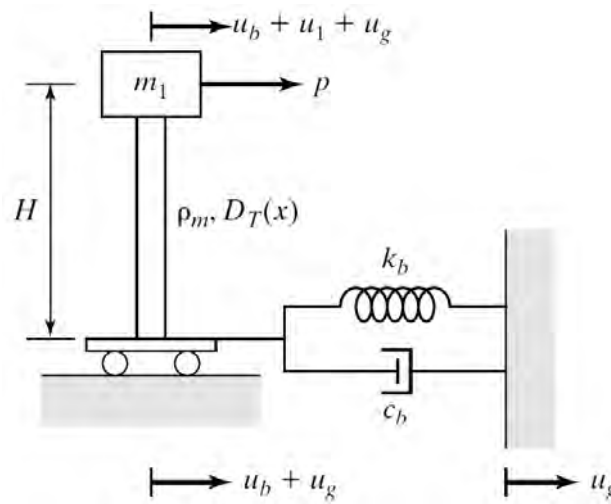


Figure P6.10a

Consider the base isolated shear beam shown in Fig. P6.10a. Assume uniform mass density, $m_1 = a(\rho_m H)$, and the shear rigidity to be defined as

$$D_T(x) = D^* \left(1 - \frac{x}{2H}\right)$$

1. Derive the equilibrium equation corresponding to the following approximate displacement expansion:

$$u = u_1(t) \frac{x}{H} + u_b(t)$$

CHAPTER 6. BASE ISOLATION SYSTEMS

Discuss how the undamped free vibration response behaves as D^* , k_b , and a are varied.

- Suppose the force, p , applied at the top of the structure is generated by a tuned mass damper as shown in Fig. P6.10b. How would you estimate the properties of the tuned mass damper to obtain an effective damping ratio of 0.05 for the mode shape approximation considered in part 1.?

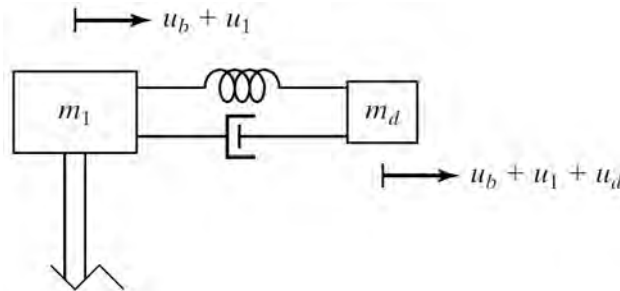


Figure P6.10b

- Suppose p has the form

$$p = -b_1 u_1 - b_2 \dot{u}_1 + \bar{p}(t)$$

where b_1 , b_2 are constants and \bar{p} is a prescribed function of time. Assume $c_b = 0$ and determine the equation for u_1 . What effect do b_1 and b_2 have on the response? Illustrate for the case where $\bar{p}(t)$ is periodic.

PART TWO

Active and Semi-Active Control

7

Applications of Active Control

7.1 The Nature of Active and Semi-Active Control

7.1.1 Active versus Passive Control

The design methodologies presented in the previous chapters provide systematic procedures for distributing passive motion control resources that, by definition, have fixed properties and do not require an external source of energy. Once installed, a passive system cannot be modified instantaneously, and therefore we need a reliable estimate of the design loading and an accurate numerical model of the physical system for any passive control scheme to be effective. The inability to change a passive control system dynamically to compensate for an unexpected loading tends to result in an overconservative design. When self-weight is an important design constraint, we cannot afford to be too conservative. Also, simulation studies on example building structures show that passive control is not always effective in fine tuning the response. Considering these limitations, the potential exists for improving the performance by dynamically modifying the loading and system properties. **An active structural control system is one that has the ability to determine the present state of the structure, decide on a set of actions that will change this state to a more desirable one, and carry out these actions in a controlled manner and in a short period of time.** Such control systems can theoretically accommodate unpredictable environmental changes, meet exacting performance requirements over a wide range of operating conditions, and compensate for the failure of a limited number of structural components. In addition, they may be able to offer more efficient solutions for a wide range of applications, from

7.1. THE NATURE OF ACTIVE AND SEMI-ACTIVE CONTROL

both technical and financial points of view.

Active motion control is obtained by incorporating within the structure a control system consisting of three main components: (1) *monitor*, a data acquisition system; (2) *controller*, a cognitive module that decides on a course of action in an intelligent manner; and (3) *actuator*, a set of physical devices that execute the instructions from the controller. Fig. 7.1 shows the interaction and function of these components; the information processing elements for active control are illustrated in Fig. 7.2 This control strategy is now possible due to significant recent advances in: sensor and actuator technologies; real-time information processing; and intelligent decision systems.

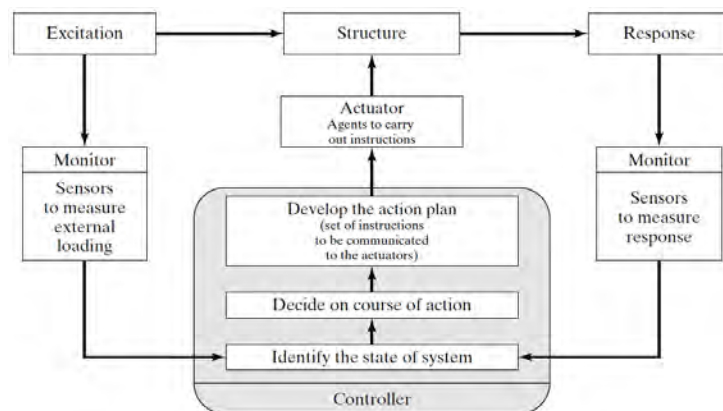


Figure 7.1: Components of an active control system.

CHAPTER 7. APPLICATIONS OF ACTIVE CONTROL

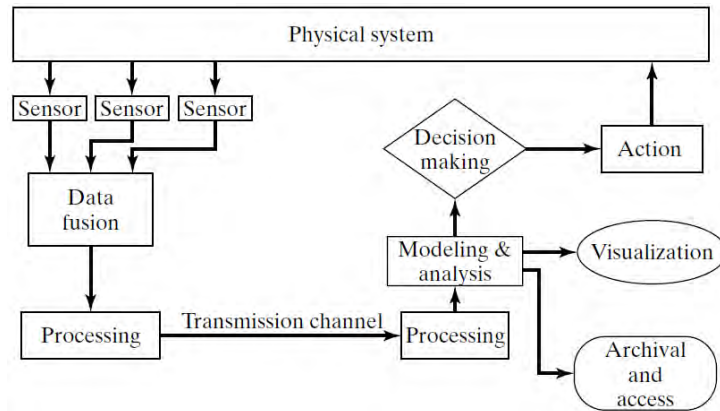


Figure 7.2: Information processing elements for an active control system.

The simple system shown in Fig. 7.3 is useful for comparing active and passive control. Fig. 7.3(a) corresponds to passive control. The input, p , is transformed to an output, u , by the operation $h(p)$:

$$u = h(p) \quad (7.1)$$

We can interpret this system as a structure with p denoting the loading, u the displacement, and h the flexibility of the structure. The strategy for passive motion control is to determine $h(p)$ such that the estimated output due to the expected loading is contained within the design limits, and then design the structure for this specific flexibility.

7.1. THE NATURE OF ACTIVE AND SEMI-ACTIVE CONTROL

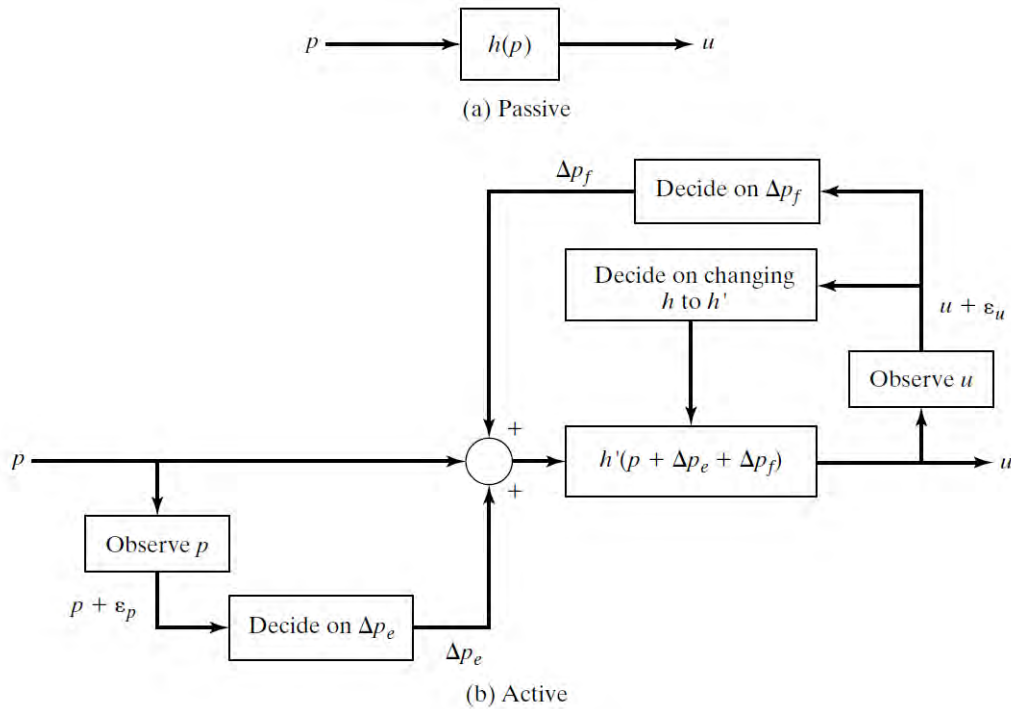


Figure 7.3: Passive and active feedback diagrams.

Active control involves monitoring the input and output, and adjusting the input and possibly also the system itself, to bring the response closer to the desired response. Fig. 7.3(b) illustrates the full range of possible actions. Assuming the input corrections and system modifications are introduced instantaneously, the input-output relation for the actively controlled system is given by

$$u = h'(p + \Delta p_e + \Delta p_f) \quad (7.2)$$

Monitoring the input and adjusting the loading is referred to as *open-loop control*. Observing the response, and using the information to apply a correction to the loading is called *feedback control*. The terminology *closed-loop control* is synonymous with

feedback control.

In addition to applying a correction to the input, the control system may also adjust certain properties of the actual system represented by the transformation $h(p)$. For example, we can envision changing the geometry, the connectivity, and the properties of structural elements in real time. We can also envision modifying the decision system. A system that can adjust its properties and cognitive processes is said to be *adaptive*. The distinguishing characteristic of an adaptive system is the self-adjustment feature. Nonadaptive active structural control involves monitoring and applying external forces using an invariant decision system. The makeup of the structure is not changed. Adaptive control is the highest level of active control.

Kajima Corporation has pioneered the research, design, experimentation, and implementation of active control of large scale building structures [90]. Their work has been concerned with the following active motion control schemes: active mass driver (AMD), active variable stiffness (AVS), and hybrid-mass damper (HMD), which are described later in this chapter. These schemes have been implemented in the set of buildings listed in Table 7.1. Other Japanese organizations such as Shimizu Corporation, Takenaka Corporation, and Mitsubishi have also carried out substantial research and implementation in the field of active structural control. Many other buildings have since been equipped with feedback control systems. For instance, a review paper in 2003 reported that over 40 buildings and 10 bridges have employed feedback control strategies [97].

7.1. THE NATURE OF ACTIVE AND SEMI-ACTIVE CONTROL

Table 7.1: Implementations of active and hybrid control systems in buildings designed by Kajima Corporation

Name of building	Kyobashi Seiwa	KaTRI No. 21	Ando Nishikicho	Shinjuku Park	Dowa Kasai Phoenix
Completion date	Aug. 1989	Nov. 1990	July 1993	April 1994	Jan. 1995
Number of floors	11+1(BG)	3+2(BG)	14+2(BG)	52+5(BG)	29+3(BG)
Building height (m)	33.10	16.30	68.00	232.60	144.45
Total floor area (m)	423.37	465.00	4,928.30	264,140.91	30,369.66
Typical floor area (m ²)	37.32	150.00	324.15	4,523.54	1,072.36
Control system	AMD	AVS	HMD	HMD	HMD
Type of disturbance	ME,SW	LE	ME,SW	ME,SW	ME,SW

BG: Below ground level.

AMD: Active mass driver.

ME: Moderate earthquake.

AVS: Active variable stiffness.

LE: Large earthquake.

MHD: Hybrid-mass damper.

SW: Strong wind.

7.1.2 The Role of Feedback

Feedback is a key element of the active control process. The importance of feedback can be demonstrated easily by considering a linear static system and taking the input correction to be a linear function of the output. For this case,

$$u = kp \quad (7.3)$$

$$\Delta p_f = k_f(u + \epsilon_u) \quad (7.4)$$

where h and k_f are constants. Substituting in Eq. (7.2) specialized for $h' = h$, and solving for u results in

$$u = \frac{h}{1 - hk_f}(p + \Delta p_e) + \frac{hk_f}{1 - hk_f}\epsilon_u \quad (7.5)$$

When k_f is positive, the sensitivity of the system to loading is increased by feedback (i.e., the response is amplified). Taking k_f negative has the opposite effect on the response. Specializing Eq. (7.5) for negative feedback ($k_f < 0$), the response becomes

$$u = \frac{h}{1 + |hk_f|}(p + \Delta p_e) + \frac{|hk_f|}{1 + |hk_f|}\epsilon_u \quad (7.6)$$

Increasing $|k_f|$ decreases the effect of external loading. However, the influence of ϵ_u , the noise in the response observation, increases with $|k_f|$ and, for sufficiently large $|k_f|$, is essentially independent of the feedback parameter. This result indicates that the accuracy of the monitoring system employed to observe the response is an important design issue for a control system.

7.1.3 Computational Requirements and Models for Active Control

The monitor component identified in Figs. 7.1 and 7.2 employs sensors to measure a combination of variables relevant to motion such as strain, acceleration, velocity, displacement, and other physical quantities such as pressure, temperature, and ground motion. These data are usually in the form of analog signals that are converted to discrete time sequences, fused with other data, and transmitted to the controller module. Data compression is an important issue for large-scale remote sensing systems. Wavelet-based data compression [8] has shown a promising approach for solving the data processing problem.

The functional requirements of the controller are to compare the observed response with the desired response, establish the control action such as the level of feedback force, and communicate the appropriate commands to the actuator, which then carries out the actual control actions such as apply force or modify a structural property. The controller unit is composed of a digital computer and software designed to evaluate the input and generate the instructions for the actuators.

7.1. THE NATURE OF ACTIVE AND SEMI-ACTIVE CONTROL

There are two information processing tasks: state identification and decision making. Given a limited amount of data on the response, we need to generate a more complete description of the state of the system. Some form of model characterizing the spatial distributions of the response and data analysis is required. Once the state has been identified, the corrective actions that bring the present state closer to the desired state can be established. In this phase, a model that defines the input-output relationship for the structure is used together with an optimization method to decide on an appropriate set of actions.

For algorithmic nonadaptive systems, the decision process is based on a numerical procedure that is invariant during the period when the structure is being controlled. Time-invariant linear feedback is a typical nonadaptive control algorithm. An adaptive controller may have, in addition to a numerical control algorithm, other symbolic computational models in the form of rule-based systems and neural networks, which modify the structure and the control algorithm in an intelligent manner when there is a change in the environmental conditions. An example illustrating time-invariant linear feedback control algorithms is presented in the following subsection; a detailed treatment of the algorithms is contained in Chapter 9, after Chapter 8 introduces structural control dynamics. A discussion of control algorithms follows in Chapter 9.

7.1.4 An Introductory Example of Dynamic Feedback Control

To gain further insight on the nature of feedback control, the simple SDOF system shown in Fig. 7.4 is considered. The system is assumed to be subjected to both an external force and

CHAPTER 7. APPLICATIONS OF ACTIVE CONTROL

ground motion, and controlled with the force F . Starting with the governing equation,

$$m\ddot{u} + c\dot{u} + ku = -ma_g + F + p \quad (7.7)$$

and introducing the definitions for frequency and damping ratio leads to the standardized form of the governing equation:

$$\ddot{u} + 2\xi\omega\dot{u} + \omega^2u = -a_g + \frac{F}{m} + \frac{p}{m} \quad (7.8)$$

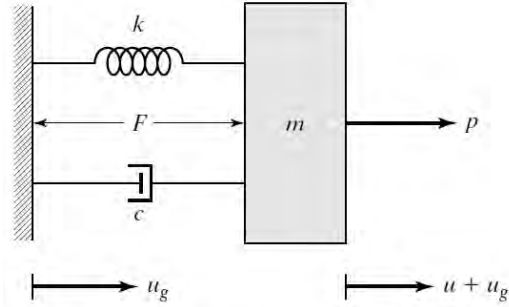


Figure 7.4: Single-degree-of-freedom system.

The free vibration response of the uncontrolled system has the general form

$$u = Ae^{\lambda t} \quad (7.9)$$

Substituting for u in Eq. (7.8), we obtain two possible solutions:

$$u = A_1e^{\lambda_1 t} + A_2e^{\lambda_2 t} \quad (7.10)$$

$$\lambda_{1,2} = -\xi\omega \pm i\omega\sqrt{1 - \xi^2} = -\xi\omega \pm i\omega' \quad (7.11)$$

Considering A_1 and A_2 to be complex conjugates,

7.1. THE NATURE OF ACTIVE AND SEMI-ACTIVE CONTROL

$$A_{1,2} = \frac{1}{2}(A_R \pm iA_I) \quad (7.12)$$

where A_R and A_I are real numbers representing the real and imaginary parts of A , the solution takes the form

$$u = e^{-\xi\omega t} [A_R \cos(\omega't) + A_t \sin(\omega't)] \quad (7.13)$$

We determine A_R and A_t with the initial conditions for u and \dot{u} . The resulting expressions are

$$\begin{aligned} A_R &= u(0) \\ A_I &= -\frac{1}{\omega'}(\dot{u}(0) + \xi\omega u(0)) \end{aligned} \quad (7.14)$$

Considering negative linear feedback, the control force is expressed as a linear combination of velocity and displacement:

$$F = -k_v \dot{u} - k_d u \quad (7.15)$$

where the subscripts v and d refer to the nature of the feedback (i.e., velocity or displacement). Feedback is implemented in the actual physical system by

- Observing the response
- Determining u and \dot{u}
- Calculating F with Eq. (7.15)
- Applying F with an actuator

CHAPTER 7. APPLICATIONS OF ACTIVE CONTROL

Mathematically, we incorporate feedback by substituting for F in Eq. (7.8). The result is

$$\ddot{u} + \left(2\xi\omega + \frac{k_v}{m}\right) \dot{u} + \left(\omega^2 + \frac{k_d}{m}\right) u = -a_g + \frac{p}{m} \quad (7.16)$$

Equation (7.16) can be transformed to the standardized form by defining equivalent damping and frequency parameters as follows:

$$\omega_{eq}^2 = \omega^2 + \frac{k_d}{m} \quad (7.17)$$

$$2\xi_{eq}\omega_{eq} = 2\xi\omega + \frac{k_v}{m} \quad (7.18)$$

With this notation, the solution for the free vibration response of the linear feedback controlled case has the same general form as for no control; we just replace ξ and ω with ξ_{eq} and ω_{eq} , respectively, in Eq. (7.13). It follows that the effect of linear feedback is to *change the fundamental frequency and damping ratio*. Solving Eqs. (7.17) and (7.18) results in

$$\omega_{eq} = \omega \sqrt{1 + \frac{k_d}{k}} \quad (7.19)$$

$$\xi_{eq} = \xi + \xi_a \quad (7.20)$$

where ξ_a is the increment in damping ratio due to active control:

$$\xi_a = \frac{1}{\left(1 + \frac{k_d}{k}\right)^{1/2}} \left\{ \frac{k_v}{2\omega m} - \xi \left[\left(1 + \frac{k_d}{k}\right)^{1/2} - 1 \right] \right\} \quad (7.21)$$

7.1. THE NATURE OF ACTIVE AND SEMI-ACTIVE CONTROL

Critical damping corresponds to $\xi_{eq} = 1$:

$$\frac{k_v}{2m\omega} \Big|_{\xi_{eq}=1} = \sqrt{1 + \frac{k_d}{k}} - \xi \quad (7.22)$$

Equation (7.19) shows that negative displacement feedback increases the frequency. According to Eq. (7.21), the damping ratio is *increased* by velocity feedback and *decreased* by displacement feedback. If the objective of including active control is to limit the response amplitude, velocity feedback is the appropriate mechanism. Displacement feedback is destabilizing in the sense that it reduces the effect of damping. Stability and other issues associated with feedback are discussed in Chapter 9.

Example 7.1 - Illustrative example: influence of velocity feedback

This example demonstrates the influence of pure velocity feedback on the response of two SDOF systems subjected to seismic excitation. The properties of the systems are as follows:

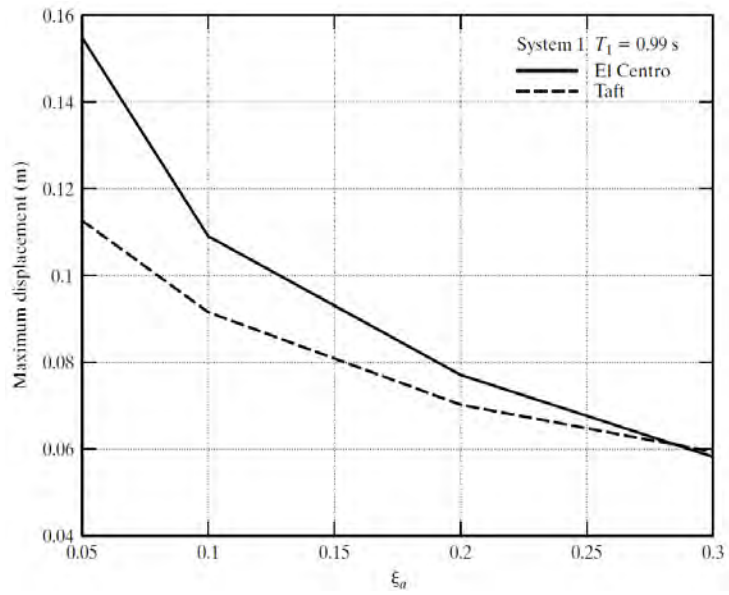
System 1:

$$\begin{aligned} m &= 10,000 \text{ kg} & \omega_1 &= 6.32 \text{ rad/s} \\ k &= 400,000 \text{ N/m} & T_1 &= 0.99 \text{ s} \\ c &= 2,500 \text{ N}\cdot\text{s/m} \end{aligned}$$

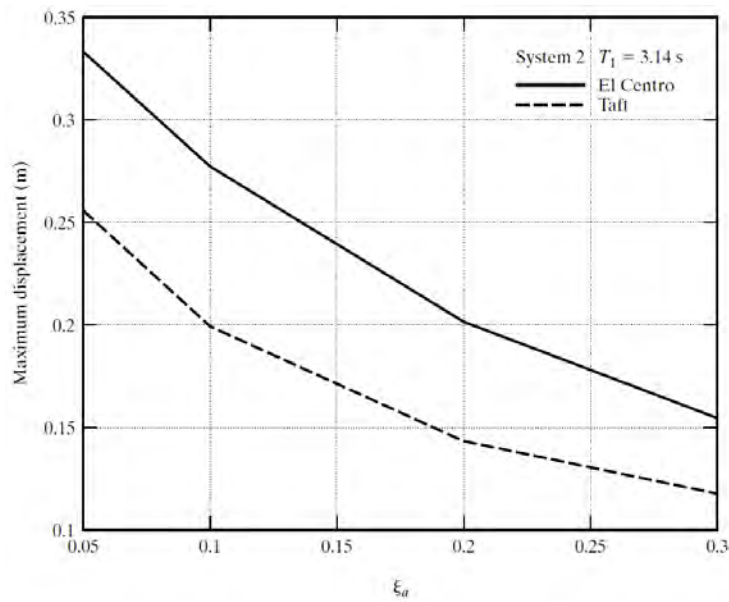
System 2:

$$\begin{aligned} m &= 10,000 \text{ kg} & \omega_1 &= 2 \text{ rad/s} \\ k &= 40,000 \text{ N/m} & T_1 &= 3.14 \text{ s} \\ c &= 830 \text{ N}\cdot\text{s/m} & \xi &= 0.0208 \end{aligned}$$

CHAPTER 7. APPLICATIONS OF ACTIVE CONTROL



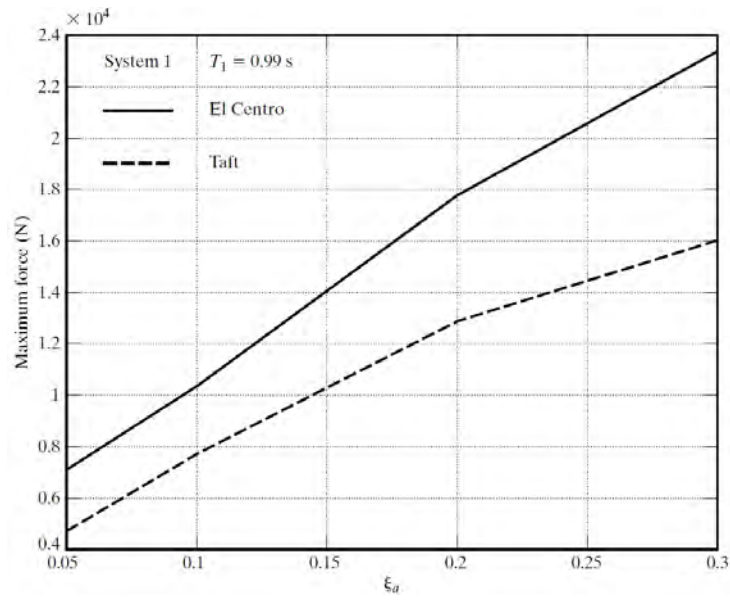
(a)



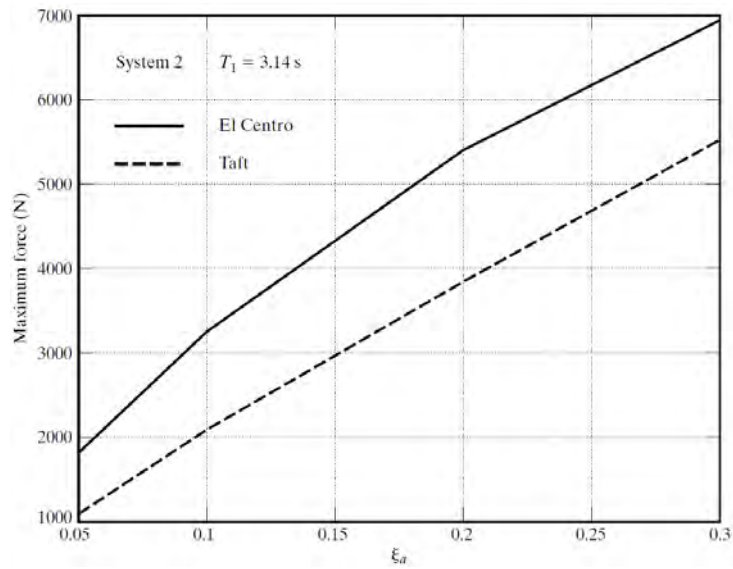
(b)

Figure 7.5: Variation of maximum displacement with active damping. (a) System 1; and (b) System 2.

7.1. THE NATURE OF ACTIVE AND SEMI-ACTIVE CONTROL



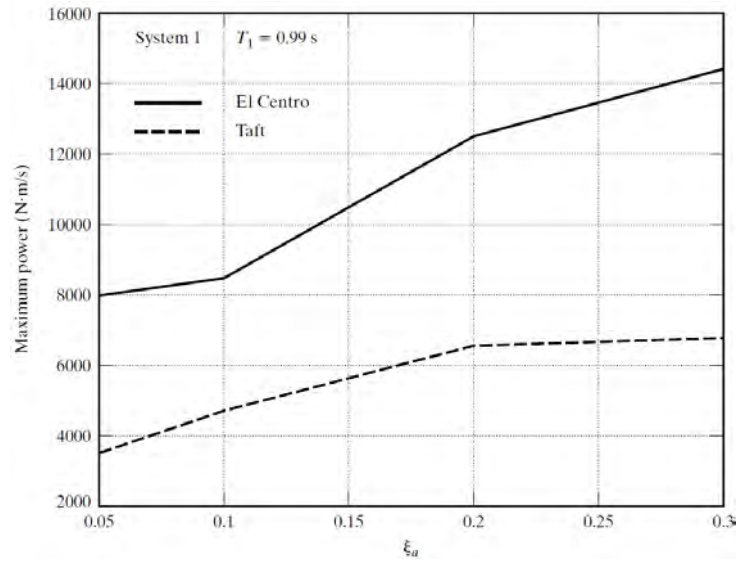
(a)



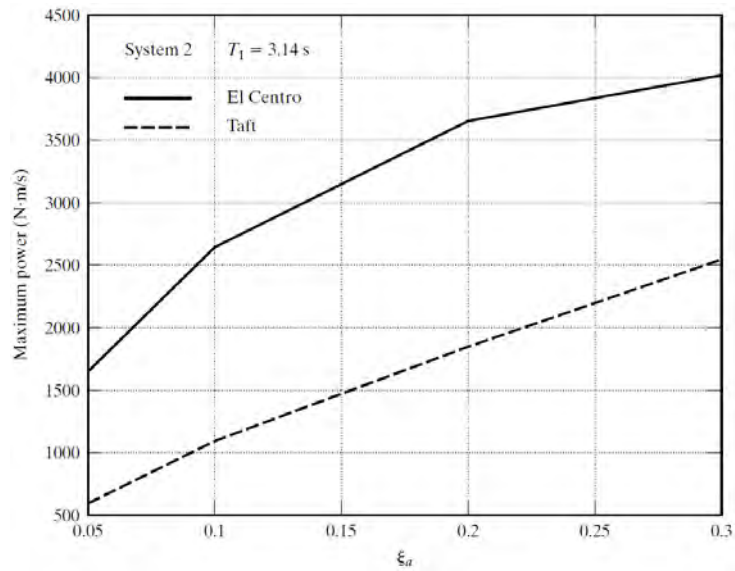
(b)

Figure 7.6: Variation of maximum control force level with active damping. (a) System 1; and (b) System 2.

CHAPTER 7. APPLICATIONS OF ACTIVE CONTROL



(a)



(b)

Figure 7.7: Variation of maximum power requirement with active damping. (a) System 1; and (b) System 2.

The models are excited with the El Centro and Taft accelero-

7.2. ACTIVE AND SEMI-ACTIVE DEVICE TECHNOLOGIES

grams scaled to $a_{\max} = 0.5$ g. Figures 7.5 through 7.7 contain plots of the maximum relative displacement, maximum control force magnitude, and maximum power requirement. The power requirement is computed using the following expression:

$$\text{Power} = \text{force} \times \text{velocity} = F\dot{u} = k_v(\dot{u})^2 \quad (7.23)$$

which assumes the control force is a set of self-equilibrating forces applied as shown in Fig. 7.4. Ground motion has no effect on the work done by F with this force scheme.

7.2 Active and Semi-Active Device Technologies

7.2.1 Active versus Semi-Active Devices

The actuator component of the control system generates and applies the control forces at specific locations on the structure according to instructions from the controller. Over the past several decades, a number of force generation devices have been developed for a broad range of motion control applications. These devices can be described in terms of performance parameters such as response time, peak force, and operating requirements such as peak power and total energy demand. The ideal device is one that can deliver a large force in a short period of time for a small energy input.

Civil structures generally require large control forces, on the order of a meganewton and, for seismic excitation, response times on the order of milliseconds. The requirement on peak force coupled with the constraint on energy demand is very difficult to achieve with a fully active force actuator system. There are force actuator systems that are capable of delivering large force, but they also have a high energy demand. Included in this group

CHAPTER 7. APPLICATIONS OF ACTIVE CONTROL

are hydraulic, electromechanical, and electromagnetic devices. All these types are based on very mature technology.

There is considerable ongoing research and development of new force actuators that have a *low energy* demand. One approach is based on modifying the physical makeup of the device in such a way that only a small amount of energy is required to vary the device properties, such as either stiffness or damping. For example, a typical viscous damper can deliver a force on the order of a meganewton; by adjusting the damping parameter, the force can be increased significantly.

These devices are termed *semi-active dampers*. They are designed so as to produce only a “resisting” force similar, in nature, to the behavior of a friction mechanism. Since the device’s force always acts to oppose the motion, a semi-active damper can never destabilize a structural system. Their main advantage is their low energy input requirement. Some devices operate with energy supplied by batteries, a desirable feature since power failures are likely to occur during a severe earthquake or wind event.

Despite the early application of semi-active technologies in the 1920s for vehicle shock absorbers, their introduction to civil engineering goes back only to 1983, in a research paper by Hrovat *et al.* [42]. They have since attracted a lot of interest in the research community. It has been demonstrated that semi-active damping systems can, in addition to enhanced earthquake and wind mitigation, have considerable economic benefits over passive energy dissipation systems. For instance, Laflamme [58] showed that the use of a semi-active damping system in lieu of an existing passive strategy currently installed in a high-rise building located in Boston, MA, *would result in savings on the order of 20% to*

7.2. ACTIVE AND SEMI-ACTIVE DEVICE TECHNOLOGIES

30% in the cost of the damping system. This reduction in cost is due to the significant reduction in the number of dampers required to attain a design performance. Other studies [50, 17] have demonstrated that designs of mid-rise steel buildings with either passive or semi-active damper systems can readily lead to a reduced interstory drift, while enabling the design to be lighter compared to a building without dampers. As a result, there is a reduction in the cost of construction while maintaining a high level of performance under the design earthquake.

Semi-active systems often employ adaptive materials, also termed *smart materials*, as the force generation mechanism. These materials respond to a low energy input by changing their properties and their state in a nonconventional manner that results in a force. Although these technologies are promising, the current devices can produce only low forces, and therefore their applicability for civil structures is limited.

When designing active and semi-active structural control systems, two issues need to be addressed: (1) how the force generation mechanism works, and (2) how the forces are applied to the structure. The first issue is related to the physical makeup and underlying physics of the device. The second question is concerned with how the device is attached to the structure so as to produce the “desired” control force. In what follows, the attachment issue is discussed first, then the state of the art for linear actuator technologies is reviewed, and lastly some typical semi-active control devices are described.

7.2.2 Force Application Schemes

The schematic drawing contained in Fig. 7.8 shows the typical makeup of hydraulic, electromechanical, and electromagnetic

CHAPTER 7. APPLICATIONS OF ACTIVE CONTROL

linear actuators. There are two basic elements, a piston and a mechanism that translates the piston linearly either by applying a force to one end or by moving the end with a gear mechanism. The interaction of the piston with an adjacent body produces a pair of contact forces F at the contact point and a corresponding reaction force at the actuator support. If the body moves under the action of F , the mechanism usually compensates for this motion such that the force remains constant until instructed by the controller to change the force magnitude.

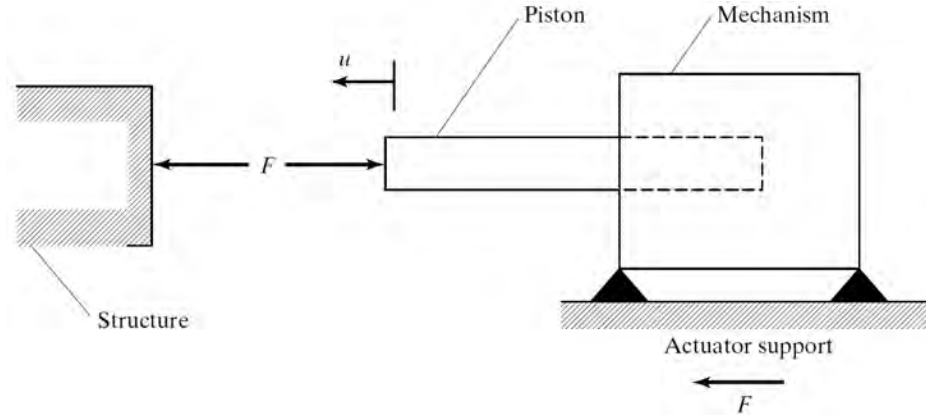


Figure 7.8: Linear actuator.

Consider the structural frame shown in Fig. 7.9(a). Suppose the objective is to apply a horizontal force at point A and there is no adjacent structure that could support the actuator. One option (Fig. 7.9(b)) is to fasten a tendon to point A , pass it over a pulley attached to the base, and then connect it to a linear actuator, which can generate a tensile force in the tendon. In this scheme, the actuator reaction force is transmitted directly to the base. A second option would be to place the actuator directly on the structure. The actuator reaction force is now transmitted to the structure; however, the other end of the piston

7.2. ACTIVE AND SEMI-ACTIVE DEVICE TECHNOLOGIES

needs to be restrained in order to generate a control force. If the restraining body is rigidly connected to the structure, as shown in Fig. 7.9(c), the force system is self-equilibrating and the structure “feels” no lateral force. Member AC is in tension. In order to have a “nonzero” lateral force acting on the structure, the restraining body must be allowed to move laterally. This objective can be achieved by attaching an auxiliary mass, m_a , to the piston and supporting the mass on rollers (Fig. 7.9(d)). The mass moves with respect to the structure with an absolute acceleration equal to F/m_a . We specify the peak force and magnitude of the auxiliary mass and design the actuator so that it can provide the required force at that level of acceleration. Since the force is generated by driving the mass, this scheme is referred to as an *active mass driver*.

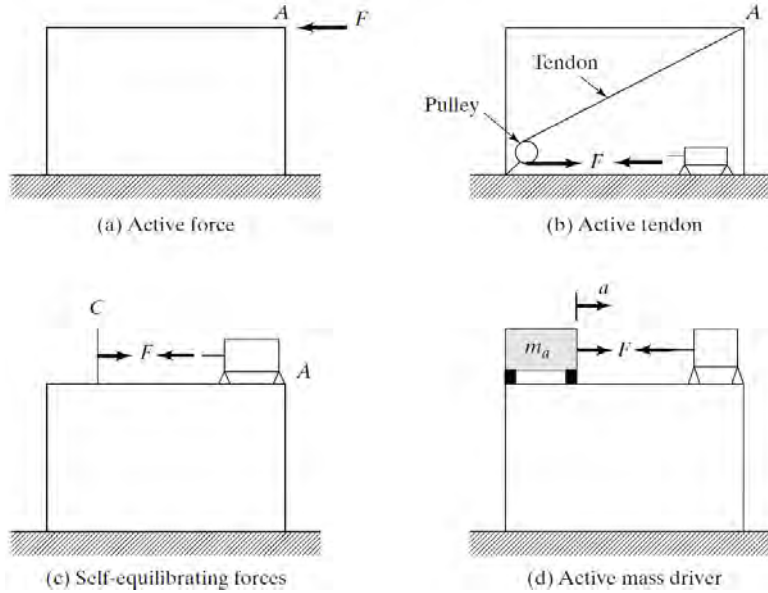


Figure 7.9: Control force schemes.

The extension of these schemes to a multistory structure is shown in Fig. 7.10. A linear actuator placed on a diagonal

CHAPTER 7. APPLICATIONS OF ACTIVE CONTROL

produces a set of self-equilibrating forces that impose a shearing action on the particular story to which it is attached. The other stories experience no deformation since the story shear due to this actuator is zero. It follows that we need to incorporate active braces throughout the structure in order to achieve global displacement control. Forces generated with active mass drivers are not self-equilibrating and consequently have more influence on the global displacement response.

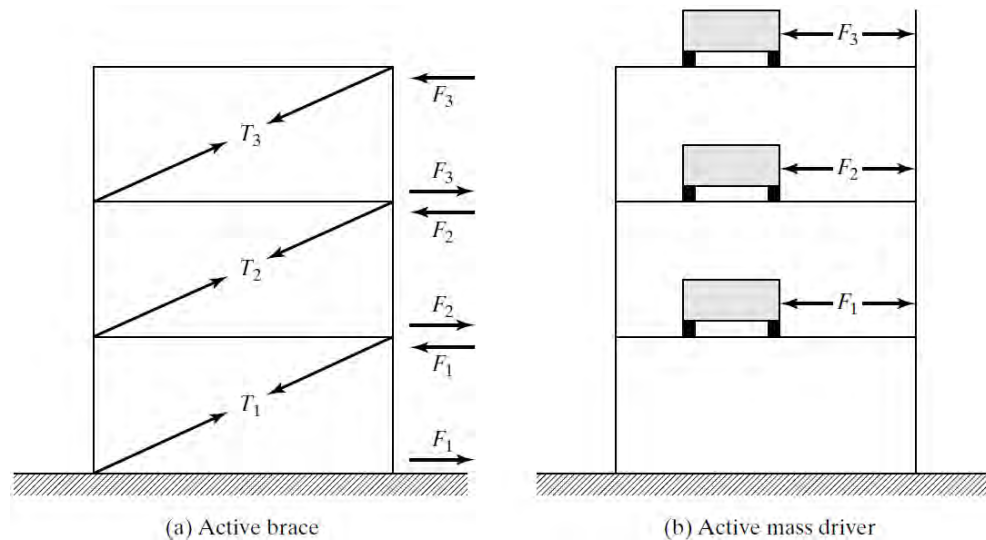


Figure 7.10: Control force schemes for a multistory structure.

The previous examples relate to shear beam structures that require forces that act in the transverse direction. For bending beam problems, control force systems that produce bending moments are required. This action can be obtained with linear actuators placed on the upper and lower surfaces, as illustrated in Fig. 7.11. The region between A and B is subjected to a constant moment equal to F_d . Another scheme is shown in Fig. 7.12. The actuator is attached to the beam with rods

7.2. ACTIVE AND SEMI-ACTIVE DEVICE TECHNOLOGIES

that provide the resistance to the piston motion, resulting in the self-equilibrating system that produces a triangular moment distribution over the region $A - B - C$. By combining a number of these actuator-rod configurations, we can generate a piecewise linear bending moment distribution.

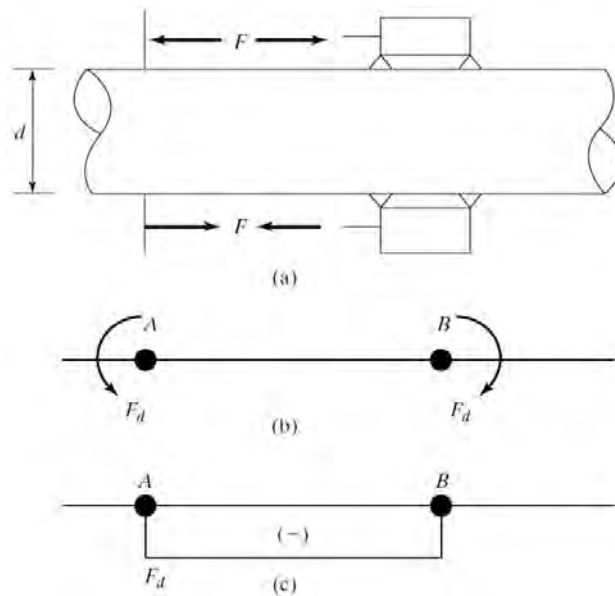


Figure 7.11: Constant moment field.

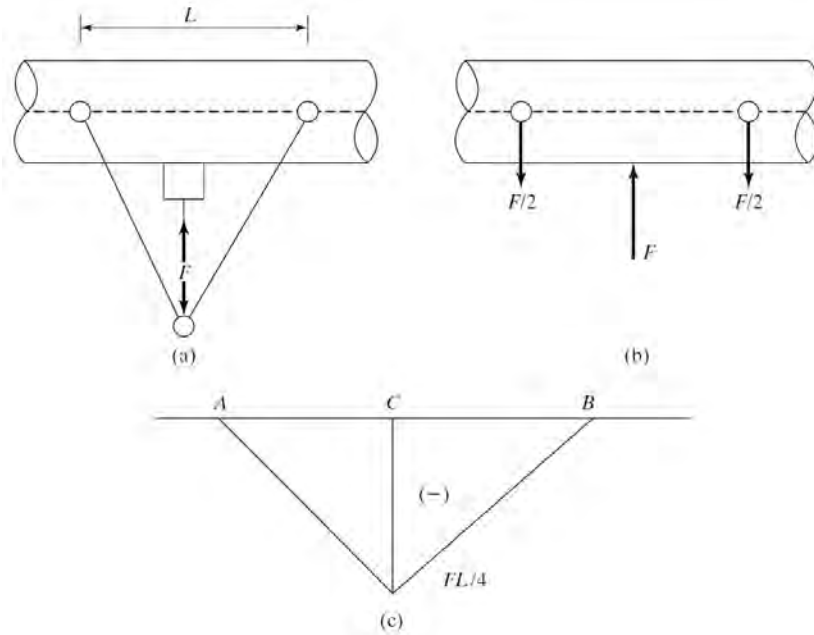


Figure 7.12: Triangular moment field.

Linear actuators generate control force systems composed of concentrated forces. For discrete structures such as frames, this type of force distribution is appropriate. However, for continuous structures such as beams and plates, a continuous force distribution is more desirable. One strategy that has been examined is based on using an adaptive material in the form of a thin plate. Fig. 7.13 illustrates this approach for a continuous beam. Plates are attached by epoxy to the upper and lower surfaces. Applying a voltage to the plate generates a longitudinal strain. Since the plate is attached to the surface, the motion of the plate is restrained and an interfacial shear stress $\tau(t)$ is generated. This stress produces a distributed control moment $m_c(x, t)$ equal to

$$m_c(x, t) = \tau b_f d \quad (7.24)$$

7.2. ACTIVE AND SEMI-ACTIVE DEVICE TECHNOLOGIES

where b_f is the width of the plate. Spatial and temporal variation of the control force system is achieved by varying the voltage applied to the plate.

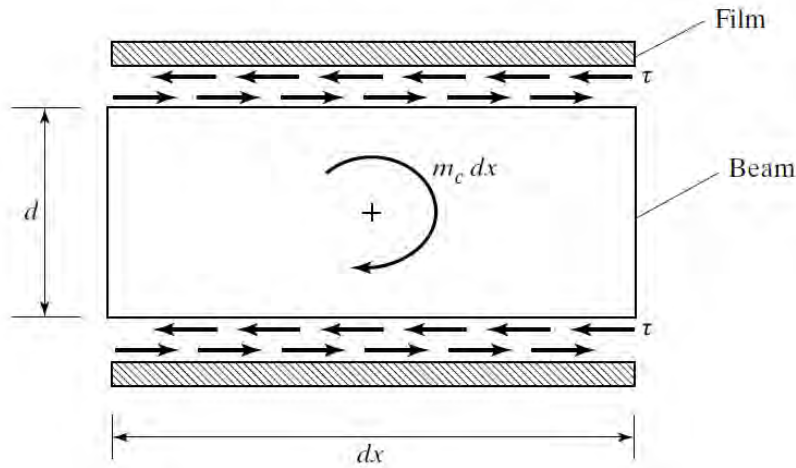


Figure 7.13: Moment generated by strain actuators.

7.2.3 Large-Scale Linear Actuators

Referring back to Fig. 7.8, a linear actuator can be considered to consist of a piston and a mechanism that applies a force to the piston and also controls the motion of the piston. This actuator type is the most widely available and extensively used, particularly for applications requiring a large force and short response time. The descriptors *hydraulic*, *electromechanical*, and *electromagnetic* refer to the nature of the force generation mechanisms. These devices generally have a high energy demand.

Hydraulic systems generate the force by applying a pressure on the face of a piston head contained within a cylinder. Fluid is forced in or out of the cylinder through an orifice to compensate for the piston displacement and maintain a certain pressure. These systems have the highest force capacity of the linear actu-

CHAPTER 7. APPLICATIONS OF ACTIVE CONTROL

ator group, on the order of meganewtons [74]. Precise control movement and force can be achieved with a suitable control system. Protection against overload is provided by a pressure relief valve. The disadvantages of this type of system are the requirements for fluid storage systems, complex valves and pumps to regulate the flow and pressure, seals, and continuous maintenance. Durability of the seals and the potential for fluid spills are critical issues.

Electromechanical linear actuators generate the force by moving the piston with a gear mechanism that is driven by an electric motor. The motion, and therefore the force, is controlled by adjusting the power input to the motor. These devices are compact in size, environmentally safe, and economical. Fig. 7.14 illustrates the various components of a linear electric actuator system (Raco, www.raco.de). The largest electric actuator that can be ordered off the shelf is rated for 600 kN force.

Hydraulic and electromechanical actuators are composed of many parts that are in contact with each other, and therefore have a high risk of breakdown. Since electromagnetic actuators are driven by magnetic forces which do not require mechanical contact, they are theoretically more reliable. Small-scale electromagnetic actuators with a force capacity ranging from tens of newtons to several kilonewtons are commercially available. In addition to their compact nature and low voltage and amperage requirements, their response time is low, on the order of milliseconds. These features are ideal for active force generation, and electromagnetic actuators are a popular choice for small scale structures.

7.2. ACTIVE AND SEMI-ACTIVE DEVICE TECHNOLOGIES

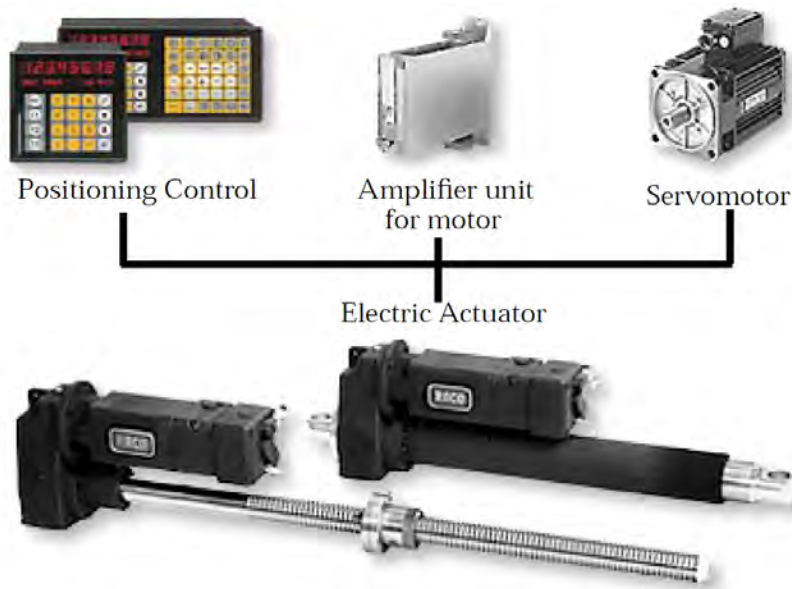


Figure 7.14: Components of linear electric actuator systems (Courtesy of Raco, Inc.).

Fig. 7.15 shows a schematic cross-sectional view of a design concept for a large-scale electromagnetic actuator developed by Chaniotakis [18] at the Plasma Science and Fusion Center, Massachusetts Institute of Technology. The unit consists of a cylindrical shell housing and a piston. Two sets of axisymmetric electromagnets are used. The field coil is embedded in the cylinder and generates a stationary magnetic field. A driving coil is attached to the piston, which translates with respect to the housing. The force mechanism is based on the interaction between the magnetic field generated by the stationary field magnet and the current in the driving coil. For this particular design, the electromagnetic force is a linear function of the coil currents and is independent of the position of the piston:

$$F_{cm} = cI_f I_d$$

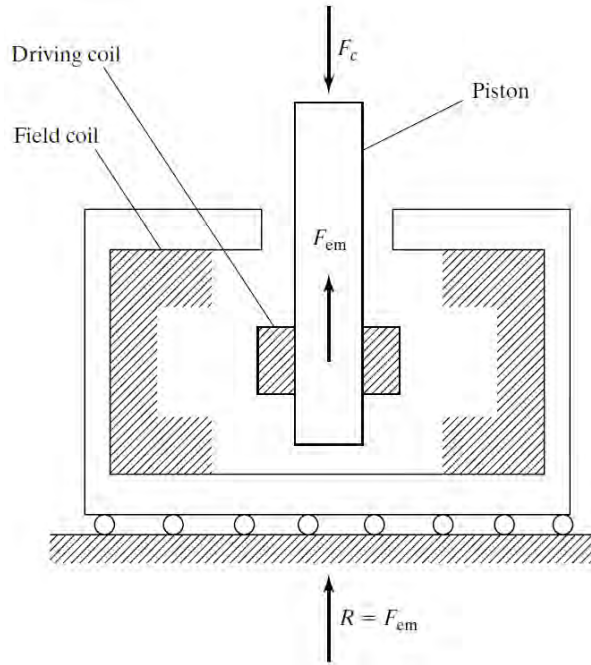


Figure 7.15: Schematic view - MIT electromagnetic actuator design.

where I_f , I_d are the currents in the field and driving coils, and c is a design parameter. The equation of motion for the piston relates the electromagnetic force, the inertia force for the piston mass, and the external contact force, F_c .

$$m_p \ddot{u} = F_{em} - F_c$$

When the device is used as an active mass driver, an auxiliary mass, m_a , is attached to the end of the piston, and F_c is set equal to $m_a \ddot{u}$. The reaction at the base of the housing is equal to the electromagnetic force, which acts on the field coil and is transmitted to the housing.

There are several advantages to this concept: (1) The response time is on the order of milliseconds, (2) there is minimal mechanical contact, and (3) the technology for controlling the

7.2. ACTIVE AND SEMI-ACTIVE DEVICE TECHNOLOGIES

current is mature. The disadvantages are that (1) the current and voltage requirements for a force on the order of meganewton cannot be satisfied with conventional electrical power supply technology, and (2) there is minimal experience related to the design, fabrication, and operating performance of large-scale electromagnetic actuators.

7.2.4 Semi-Active Device Technologies

The category of semi-active devices includes mechanical devices such as dampers, friction elements, and stiffness elements that have the ability to generate a resisting force *by changing their physical makeup*. Their distinguishing features are their low ratio of energy demand to force output. This feature is very desirable for applications to large-scale civil structures. Their name *semi-active* arises from their passive devices-like behavior, in the sense that they dissipate energy and require minimal external energy. The key point is stability. A semiactive actuator will never destabilize a system whereas an active actuator may destabilize a system even though it has a low energy demand. These devices are generally divided into four main classes:

- variable orifices
- variable stiffnesses
- controllable fluids
- variable frictions

Variable Orifices

The use of a variable orifice damper as a force actuator was suggested by Feng & Shinozuka [31] and developed further by

CHAPTER 7. APPLICATIONS OF ACTIVE CONTROL

Shinozuka *et al.* [92]. Kurata *et al.* [57] implemented variable dampers in a large-scale three-story frame structure and Patten & Sack [84] installed a hydraulic actuator with a controllable orifice on a bridge on interstate highway I-35 in Oklahoma. The force required to adjust the valve position is small, and therefore the energy demand is low. An actual application in a chevron brace scheme is shown in Fig. 7.16. Kurata's experiment required only 30 watts to operate a valve. Variable orifice dampers are capable of large resisting forces (e.g. 1-2 MN) and dynamic ranges (e.g. $c_{\max}/c_{\min} = 200$).



Figure 7.16: Variable damping mechanism (Courtesy of J. Connor.)

7.2. ACTIVE AND SEMI-ACTIVE DEVICE TECHNOLOGIES

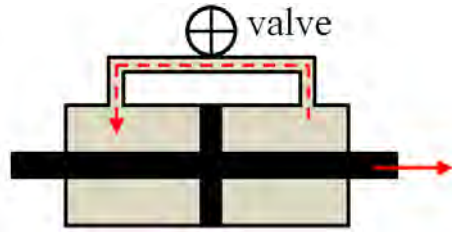


Figure 7.17: Schematic of a variable orifice damper.

Fig. 7.17 shows a variable orifice damper; it consists of a cylinder-piston with a by-pass valve connected on each side of the piston head. By adjusting the valve using a servo-controller, the damping coefficient $c(t)$ can be modified in real time. Letting v denote the velocity of the piston, the damping force, F , can thus be expressed as

$$F = c(t)v \quad (7.25)$$

In the case of a passive damper, c is a prescribed function of v , and F is determined uniquely by specifying v . In the case of a variable damper, c is a function of the valve position as well as v . When used as an actuator, F is specified, v is observed, c is calculated with Eq. (7.25), and the valve position is determined using the values of c and v . The limitation of this device is the dependency of the direction of F on the direction of v ; F is always opposite in direction to v . *Therefore, if the force required by the control algorithm at a particular time has the same sense as the observed velocity, the force demand cannot be met, and the actuator needs to be inactivated until a later time when the phase is reversed.* Such control algorithm is a type of *bang-bang controller* because it switches between control states abruptly. This may lead to high discontinuities in acceleration. Control algorithms for semi-active devices are further discussed

in Chapter 10.

Variable Stiffness

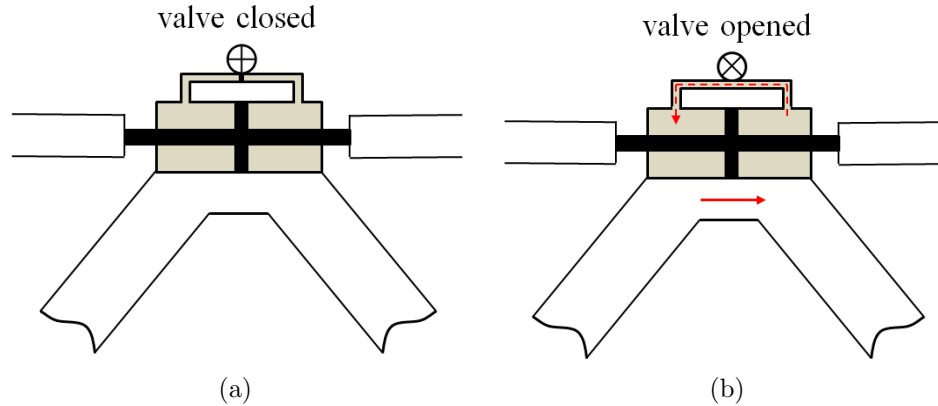


Figure 7.18: Illustration of the variable stiffness mechanism. Locked (left) and unlocked (right).

Variable stiffness devices are conceptualized as stiffness elements that can be switched *on* and *off*, allowing the controlled structure to adapt its resonant frequencies. They were first introduced in combination with variable orifice dampers. In this setup, the variable orifice damper can be switched on/off to lock/unlock the stiffness mechanism, offering a binary control over the stiffness. Figs. 7.18a and 7.18b illustrate the lock/unlock position of the mechanism. These dampers are also known as *active variable stiffness* (AVS) systems. Civil structures equipped with AVS systems can be modeled with two independent stiffness systems; one is fixed, it cannot be varied, and the other is variable, it can be switched on or off. Fig. 7.19 illustrates the concept. The structure's stiffness (left) can be modeled as two independent stiffness systems in parallel (right), a fixed stiffness system k_f and a variable stiffness system k_v .

7.2. ACTIVE AND SEMI-ACTIVE DEVICE TECHNOLOGIES

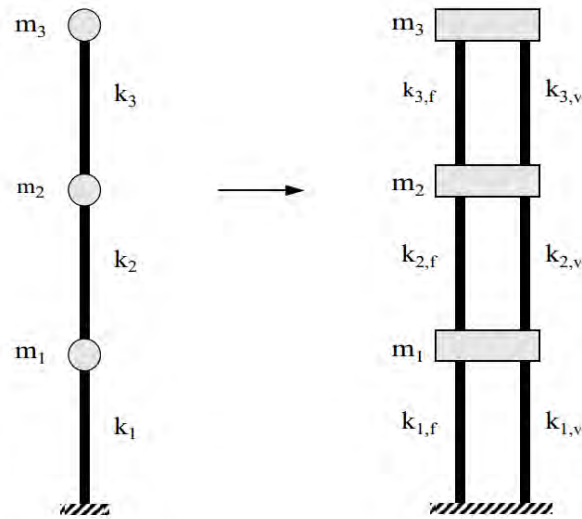


Figure 7.19: 3DOF structure represented with two independent stiffness systems in parallel.

Example of Application: Kajima Technical Research Institute

An AVS system was implemented in a steel structure, three stories high, weighing about 400 metric tons, located at the Kajima Technical Research Institute (see Fig. 7.20a). The lateral bracing system consists of steel braces placed in the transverse direction (gable side), and variable stiffness devices (VSD) installed between the brace tops and the lateral beams. These devices alter the buildings stiffness by shifting from the locked mode (switched *on*: brace is effective) to the unlocked mode (switched *off*: brace is ineffective). The variable stiffness range of the building was designed such that the natural resonant frequency is about 2.5 Hz for the locked condition and about 1 Hz for the unlocked condition. Auxiliary reinforcing braces are installed in the longitudinal direction to increase the buildings stiffness so that the control for the transverse direction is executed

CHAPTER 7. APPLICATIONS OF ACTIVE CONTROL

with minimum torsion. Fig. 7.20a shows the structure quipped with the AVS system. Fig. 7.20b is a close-up on the actual AVS system.



Figure 7.20: Kajima Technical Research Institute AVS system. Structure with braces (left), and close-up on the AVS system (right) (courtesy of Kajima Technical Research Institute).

Kajima's AVS system consists of the following:

- A measurement and control device consisting of an accelerometer placed on the first floor of the building that feeds the earthquake input into a motion analyzer. The analyzer consists of several special bandpass filters that approximate the response transfer characteristics to each stiffness type. Three stiffness types (eight stiffness types are possible) with mutually different resonant frequencies were selected for the building: All braces locked, all braces unlocked, and only the braces in the bottom floor locked. Based on the filtered output, the control computer selects the instantaneous stiffness that yields the minimum building response. The control interval required to judge stiffness selection is 0.004 s. To maximize the reliability and redundancy of the system,

7.2. ACTIVE AND SEMI-ACTIVE DEVICE TECHNOLOGIES

the control computer system is made up of a host computer, which determines the operation of the entire system, and three controllers. As the host computer requires extremely fast data acquisition and processing, the real-time UNIX operating system was used. Personal computers utilizing MS-DOS were selected for the controllers which are placed between the host computer and each variable stiffness device (VSD).

- The VSD switches over the connection condition between the brace and the beam in accordance with the signals from the control computer. A VSD consists of a two-ended-type enclosed hydraulic cylinder with a regulator valve inserted in the tube connecting the two cylinder chambers. The open/ close function is controlled by oil movements, thus locking or unlocking the connection between the beam and the braces. Twenty watts of electric power per device is required for the valve function. The time needed to alter the lock/unlock condition is about 0.03 s.
- The emergency power source counteracts power blackout and enables the entire control system to continue to operate for at least 30 minutes even after sudden termination of the regular power supply. Moreover, in case of sudden power termination, the mechanism will cause the devices to automatically adopt a locked condition, thus increasing the buildings strength capacity. Under normal conditions, all the braces are kept in the locked condition.

Similar to the vast majority of AVS applications, the AVS implemented in the Kajima Technical Research Institute is a binary on/off mode. Recently, researchers have suggested modified meth-

CHAPTER 7. APPLICATIONS OF ACTIVE CONTROL

ods to reach higher controllability. For instance, Narasimhan and Nagarajaiah [78] proposed a semi-active variable stiffness system (SAIVS), enabling continuous variation of the stiffness.

Controllable Fluids

As their name suggests, controllable fluid devices are capable of modifying their damping characteristics by adapting their fluid properties. These *smart fluids* are often called *rheological fluids*, which typically consist of silicon or oil mixed with ferric ion particles. These particles can be polarized using an electric or magnetic field, aligning the suspended ion particles which alters the liquid flow. Electric-based activated fluids are termed *electrorheological* (ER), while magnetic-based activated fluids are termed *magnetorheological* (MR). In the form of shock absorbers, they are termed semi-active ER and MR dampers. Fig. 7.21 shows the cross-section of an MR damper: the main cylinder houses the piston, the MR fluid, and the magnetic circuit. A small electromagnet is embedded in the piston head and supplied with current that generates the magnetic field across the annular orifice.

Applications of controllable fluid dampers began with the ER damping technology. Later, as the technology developed, MR dampers replaced the ER technology which is sensitive to temperature effects and fluid impurities and also requires a large amount of power to operate. The most recent MR dampers can generate large resistive forces, while operating under battery power. For instance, MR dampers capable of reaching 200 kN resisting forces in 60 msec on a 50 W power input have been reported [98, 127]. Fig. 7.22 shows a schematic of a 200 kN capacity MR damper. Recently, a 500 kN capacity has been

7.2. ACTIVE AND SEMI-ACTIVE DEVICE TECHNOLOGIES

designed and fabricated [70]. Also, it has been suggested that a MR damper of 1000 kN capacity could be theoretically fabricated [48].

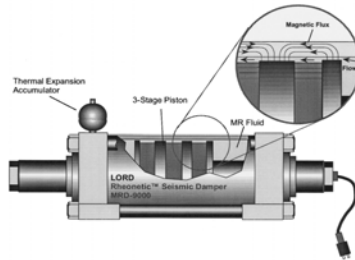


Figure 7.21: Cross-section of an MR damper [127], reprinted with permission of Elsevier.



Figure 7.22: 200 kN MR damper (courtesy of Simon Laflamme).

The idealized force-displacement and force-velocity plots of a 200 kN MR damper for a periodic excitation under different voltages are represented in Fig. 7.23. Long-term performance of MR dampers may be affected by sedimentation of the ferric ion particles if the damper is not used for a long period of time [11], and may exhibit fluid leakage around the seal.

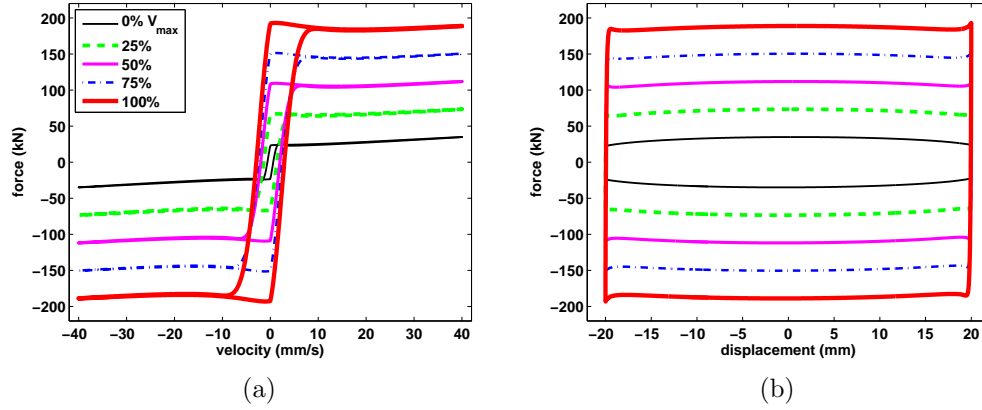


Figure 7.23: Dynamic behavior of an MR damper. (a) Force-velocity plot; and (b) force-displacement plot [58].

Because of their high resistance force capabilities and low power requirement, MR dampers for structural control have attracted the attention of the research community since the 1990's. In civil engineering, the first MR dampers full-scale application was to mitigate stay cables vibrations on the Dongting Lake Bridge in China [124]. Other applications have followed, including building braces [97], semi-active TMDs [129], ship lift towers [106], and offshore platforms [121].

The controllable fluid-type device is more effective than a variable orifice damper since the yield force is the primary component, and this force is independent of velocity. However, unlike variable orifice devices, controllable fluids exhibit a high degree of nonlinearity, which makes mapping the voltage-to-force relationship difficult for control applications [62]. For this reason, several mathematical [99, 96] and non-mathematical [103] models have been proposed. Popular mathematical models include the Bingham and the Bouc-Wen models, shown in Fig. 7.24. The Bingham model is perhaps the simplest, reasonably accurate

7.2. ACTIVE AND SEMI-ACTIVE DEVICE TECHNOLOGIES

model. It consists of a Coulomb friction element in parallel with a viscous element. The MR force output f_{MR} is written as:

$$f_{\text{MR}} = f_c(v) \cdot \text{sign}(\dot{x}) + c_0 \dot{x} \quad (7.26)$$

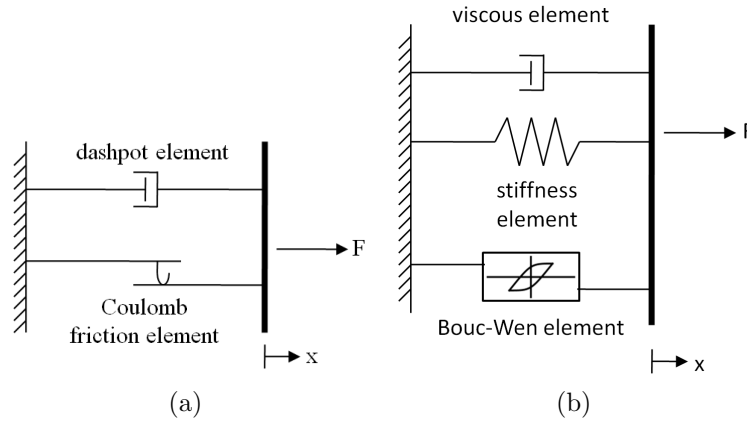


Figure 7.24: Dynamic behavior of an MR damper. (a) Bingham model [99], reprinted with permission of Elsevier; and (b) Bouc-Wen model.

where f_c is the Coulomb friction force and depends on the voltage input v ; \dot{x} is the device velocity; and c_0 is the viscous damping coefficient. The voltage can be computed using (7.26) assuming \dot{x} is measurable.

Variable Friction

Variable friction devices dissipate energy due to the relative motion between two structural components in direct contact, clamped by a varying normal normal force $N(t)$. In general, the frictional force $F_{\text{friction}}(t)$ is given by:

$$F_{\text{friction}}(t) = \mu N(t) \quad (7.27)$$

CHAPTER 7. APPLICATIONS OF ACTIVE CONTROL

where μ is the friction coefficient. The normal force is varied using actuators, such as hydraulic [49], electromagnetic [128], and piezoelectric [37] actuators. Fig. 7.25a shows the variable friction damper proposed in [128]; Fig. 7.25b shows a typical piezoelectric friction damper.

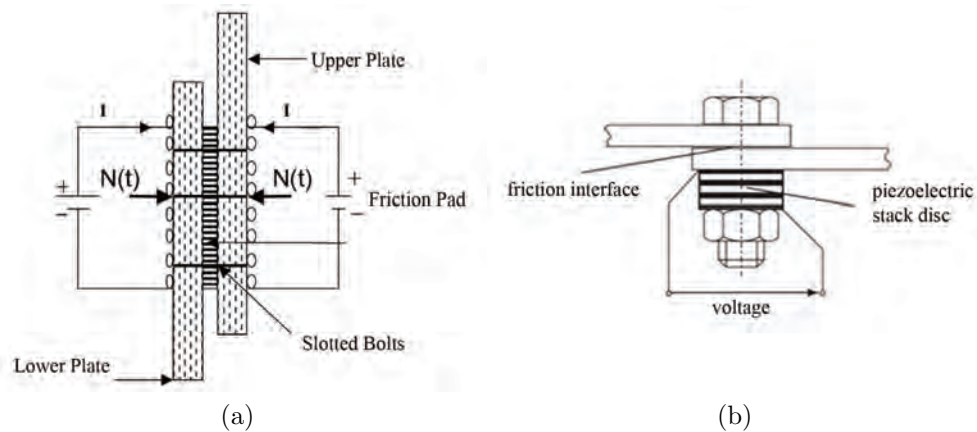


Figure 7.25: (a) Semi-active electromagnetic friction damper [128], reprinted with permission of Elsevier; and (b) piezoelectric friction damper [79], reprinted with permission of IOP Science.

In large-scale applications, Gu & Oyadiji [86] investigated the performance of variable friction dampers on a wind-excited truss tower. Chen & Chen [19] experimentally studied a variable friction damper made from piezoelectric actuators. The damper had a capacity of 800 N and operated in the range of 0 to 1000 V. Xu [125] also studied a similar friction damper, but with a capacity in the range of 5 to 340 N for an input voltage from 0 to 150 V. Durmaz et al. [28] developed a high-capacity friction damper with a force range of 0.890 kN to 11 kN. Laflamme *et al.* [60] proposed a design based on drum brake technology capable of very high damping forces, in the ranges of 0 to 200 kN. This

7.2. ACTIVE AND SEMI-ACTIVE DEVICE TECHNOLOGIES

novel damper, termed the *Modified Friction Device* (MFD), is presented it what follows.

- The Modified Friction Device

The MFD is inspired by the dynamic behavior of MR dampers and consists of a friction mechanism installed in parallel with a viscous and a stiffness element. The friction device is a rotating drum on which a variable friction can be smoothly applied. The MFD is novel because of its capability of generating very large damping forces, on the order of 200 kN, while requiring only 12-volt batteries. This is a major improvement compared to existing variable friction schemes proposed in the literature. The significant difference in the theoretical high operating range arises from the self-energizing capacity of the braking mechanism, which greatly amplifies the frictional force. A MFD is based on current reliable and robust mechanical technologies, and thus is a mechanically reliable and robust semi-active device.

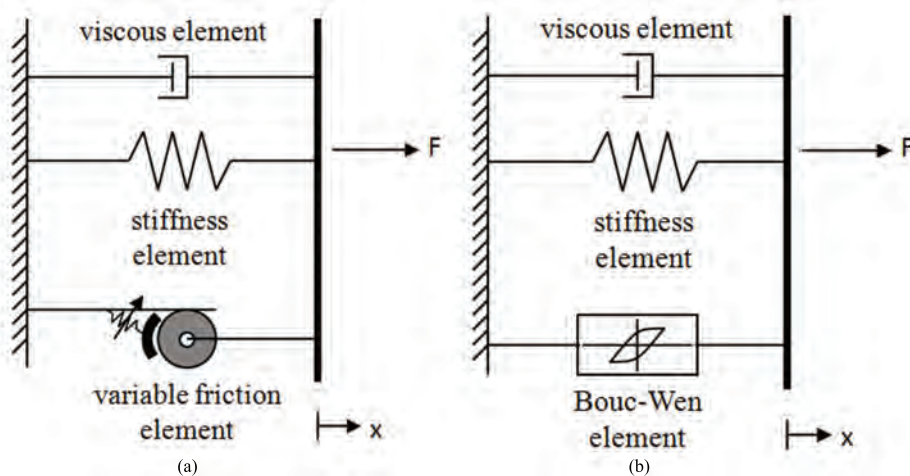


Figure 7.26: Schematic representation of the dynamics of (a) the MFD; and (b) the MR damper

CHAPTER 7. APPLICATIONS OF ACTIVE CONTROL

The MFD consists of a stiffness, a viscous, and a controllable friction element installed in parallel, as schematized in Fig. 7.26(a), where x represents the device displacement and F the reaction force. The variable spring in the variable friction element depicts a variable braking force. The controllable friction element differs from the other variable friction types by using a reliable mechanical system analogous to the braking system of a vehicle. It is also novel by the incorporation of both a stiffness and a viscous element, which provides a nominal damping when the current is switched off or in the unfortunate failure of the friction element. This mechanism is termed *fail-safe* mechanism. Fig. 7.26(b) shows the dynamics of the MR damper based under the Bouc-Wen model representation. Since the MFD has a friction element in lieu of a Bouc-Wen element, the main difference in the dynamics of these devices is in their hystereses. The MR damper hysteresis loop in the force-velocity plot is typically larger, but is also frequency-dependant.

The resisting force F of the MFD can be written:

$$F = F_{\text{friction}} + k_{\text{mfd}}x + c_{\text{mfd}}\dot{x}^\beta \quad (7.28)$$

7.2. ACTIVE AND SEMI-ACTIVE DEVICE TECHNOLOGIES

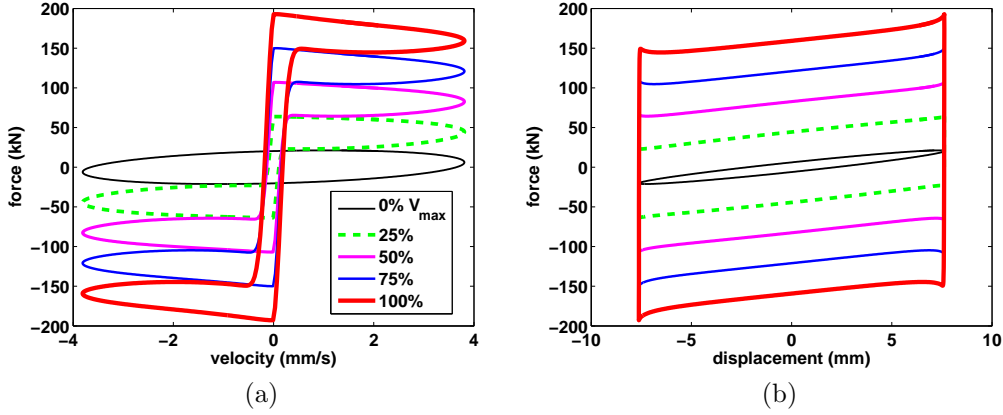


Figure 7.27: Dynamic behavior of a MFD. (a) Force-velocity plot; and (b) force-displacement plot [58].

where k_{mfd} and c_{mfd} are the stiffness and viscous coefficients of the MFD respectively, and β is a constant, taken as $\beta = 1$ for a linear viscous damper. While k_{mfd} can be designed based on the required stroke and dynamic range, c_{mfd} can be selected based on the fail-safe requirements or enhanced performance of the MFD. The force-displacement plot and the force-velocity plot under an harmonic excitation of 0.5 Hz with an amplitude of 7.62 mm (0.3 in) for different levels of voltage are shown in Fig. 7.27a and Fig. 7.27b respectively. The performance of the MFD at mitigating earthquake and wind-induced vibrations has been numerically studied in [58, 60, 59].

7.2.5 Smart Materials

Low force capacity electromechanical and electromagnetic linear actuators are standard “off-the-shelf” products offered by a number of suppliers. Our interest here is not with these devices but rather with a new generation of small-scale force actuators that

CHAPTER 7. APPLICATIONS OF ACTIVE CONTROL

utilize the unique properties of adaptive materials to generate the force. Research and development in this area was initiated by the aerospace industry as a potential solution for shape control of satellite arms and airplane control surfaces. As the technology evolved, other applications related to motion control of small-scale structures such as robot arms and biomedical devices have occurred. Although the technology continues to evolve, and reliability is still a major concern, these devices are being seriously considered as candidates for force control where the required force level is on the order of a kilonewton. Brief descriptions of the various adaptive material based actuators are presented next. Note that smart fluids, discussed under *controllable fluids*, are also considered as smart materials.

Piezoelectric actuators

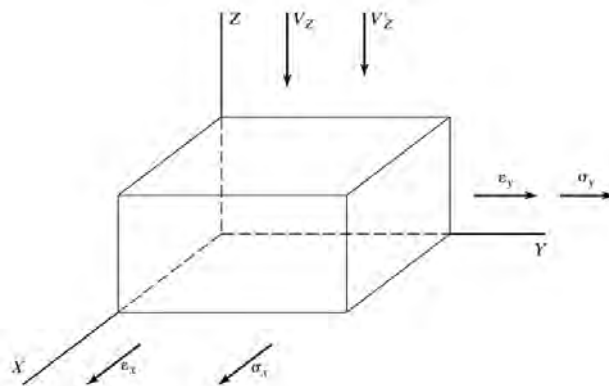


Figure 7.28: Piezoelectric electrical-mechanical interaction.

Piezoelectric materials belong to the electrostrictive material category. When subjected to a voltage, they undergo a molecular transformation that results in the material extending (or contracting) in a manner similar to the Poisson effect for applied

7.2. ACTIVE AND SEMI-ACTIVE DEVICE TECHNOLOGIES

stress [44]. Fig. 7.28 illustrates this behavioral mode; a voltage V_z in the Z direction produces extensional strains ϵ_x and ϵ_y in the X and Y directions. The opposite behavioral mode occurs when the material is stressed in the $X - Y$ plane; a voltage V'_z in the Z direction is generated by σ_x and σ_y . This behavior was first reported by Pierre and Jacques Curie in 1880. Pierre later won a Nobel prize in physics with his wife Marie for their work on radioactivity. Historically, piezoelectric materials have been used as strain sensors. Their use as actuators is more recent and stimulated primarily by the aerospace industry [24].

Piezoelectric actuators are fabricated with piezoceramic block-type elements or piezopolymer films. Lead zirconate titanate (PZT) is the dominant piezoceramic composite used for sensors and actuators in the frequency range up to 10^6 Hz. Polyvinylidene fluoride (PVDF) is the most common piezoelectric film. Since it has a relatively low strength, PVDF is used mainly as a sensor, particularly for the high frequency range up to 10^9 Hz. The underlying principle is the same for both materials. The piezoelectric object is attached to a surface which restrains its motion. When a voltage is applied, the object tends to expand immediately, and contact forces between the object and the restraining medium are produced. Two actuator configurations have been developed. The first model is a conventional linear actuator, such as shown in Fig. 7.29. Piezoceramic wafers are stacked vertically, bonded, enclosed in a protective housing, and fitted with electrical connectors. These devices can deliver large forces, on the order of 20 kN, with a response time of several milliseconds (Kinetic Ceramics Inc., www.kineticceramics.com).

The second configuration has the form of a thin plate, as illustrated in Fig. 7.30. Piezoceramic wafers are distributed

CHAPTER 7. APPLICATIONS OF ACTIVE CONTROL

over the area in a regular pattern. They may also be stacked through the thickness. This type of device is bonded to a surface and applies a pair of self-equilibrating tangential forces to the surface. The peak force depends on the applied voltage and degree of restraint. A force level of 500 N at 200 volts, and millisecond response, are typical upper limits for off-the-shelf plate-type piezoceramic actuators. Current developments are concerned with lowering the voltage requirement.

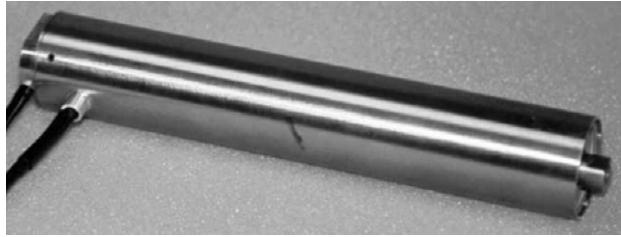


Figure 7.29: Cylindrical piezoceramic linear actuator (courtesy of Kinetic Ceramics, Inc.).

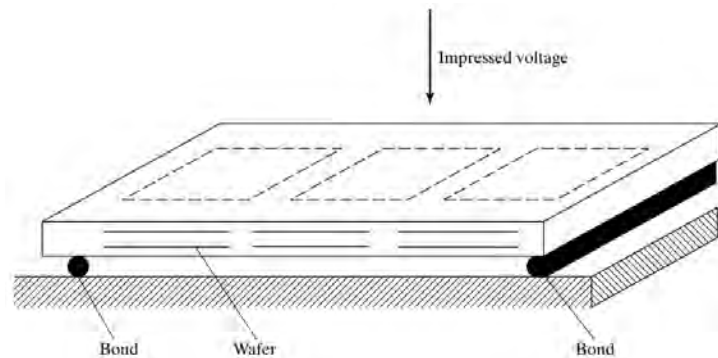


Figure 7.30: Plate-type piezoelectric actuator.

Shape Memory Alloys

Shape memory alloys are metal alloys that, if deformed inelastically at room temperature, return to their original shape when

7.2. ACTIVE AND SEMI-ACTIVE DEVICE TECHNOLOGIES

heated above a certain temperature. Fig. 7.31 illustrates this behavior. The initial straight form is deformed inelastically at room temperature to the curved form. When the temperature is elevated, the curved form shifts back to the straight form and remains in that form when the temperature is lowered to room temperature. If no further deformation is introduced, the straight form remains invariant during any subsequent thermal cycling.

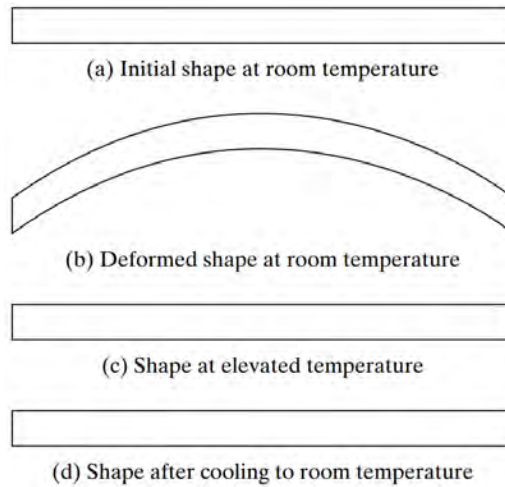


Figure 7.31: Plate-type piezoelectric actuator.

The ability to return to its initial shape when heated is due to a phase transformation from martensite at room temperature to austenite at elevated temperature [113, 83]. Inelastic deformation introduced during the martensite phase is eliminated when the state passes over to the austenite phase. The phase transitions are illustrated in Fig. 7.32: A_s and A_f define the temperatures for the start and finish of the transition from martensite to austenite for the case when the material is being heated; the corresponding temperatures for the cooling case are M_s and M_f .

CHAPTER 7. APPLICATIONS OF ACTIVE CONTROL

When T is greater than A_f , the phase is austenite but it is possible to convert it back to martensite by applying stress. The quantity M_d is the temperature beyond which austenite cannot be converted to martensite by stress (i.e., the phase remains austenite for arbitrary applied stress).

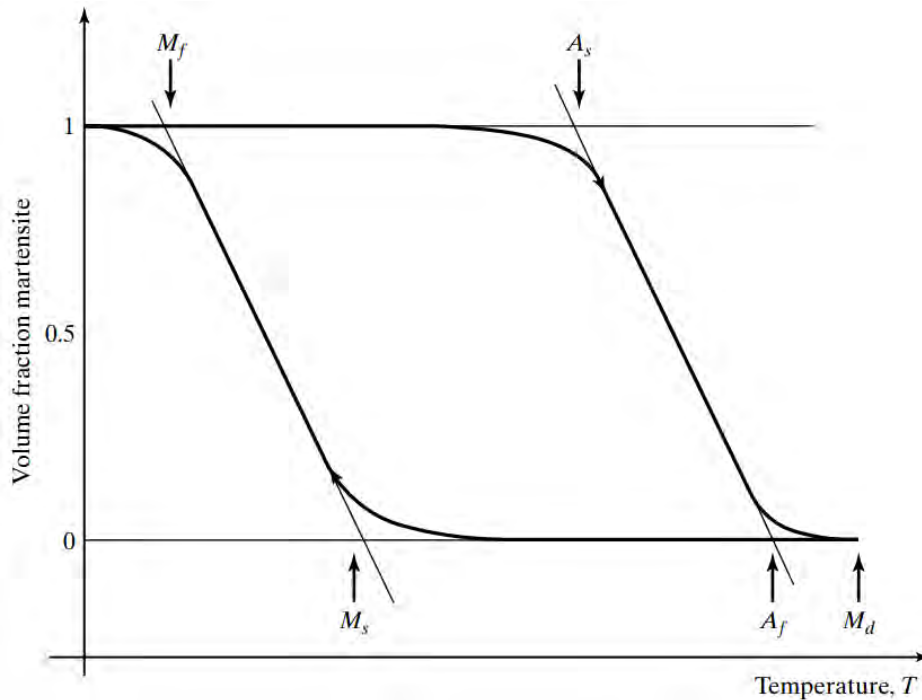


Figure 7.32: Martensitic transformation on cooling and heating.

The stress-strain behavior is strongly dependent on temperature. Fig. 7.33 shows the limiting stress-strain curves for Nitinol, a nickel-titanium alloy [47]. For $T < M_f$, the lowest temperature for the fully martensitic phase, the material behaves like a typical ductile metal. Yielding occurs at about 150 MPa, and inelastic deformation is introduced. The behavior for $T > M_d$ is elastic up to 650 MPa, and the modulus, E_1 , is about four times larger than the initial value, E_0 . Between these limiting temperatures,

7.2. ACTIVE AND SEMI-ACTIVE DEVICE TECHNOLOGIES

there is a gradation in behavior between fully ductile to fully elastic.

Referring to Fig. 7.33, the one-way effect can be explained by tracking the response as a stress, σ^* , is applied and then removed at $T < M_f$. This action produces the path $a - b - c$. Increasing the temperature at this time to $T > M_d$ shifts c back to a since the behavior for $T > M_d$ is elastic. Further cycling of the temperature with no stress applied will not cause the point to shift from a .

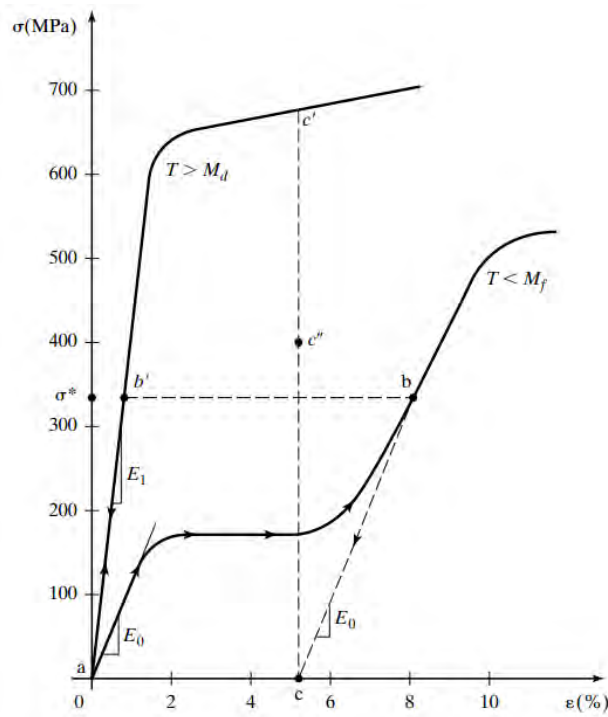


Figure 7.33: Effect of temperature on stress strain behavior of Nitinol [47].

A different type of response is obtained when the stress is held constant and the temperature is cycled a number of times between M_f and M_d . In this case, the path is $b - b' - b$. The effect of thermal cycling is to introduce two-way shape memory.

CHAPTER 7. APPLICATIONS OF ACTIVE CONTROL

Repeating the scenario described previously, starting at b and removing the stress shifts the b position to c . Then, increasing the temperature causes the position to shift to a . However, when the temperature is now lowered to M_f , the position shifts back to point c instead of remaining at a . Further thermal cycling at no stress results in the deformation switching between a and c . At high temperature, the material remembers the initial state; at low temperature it remembers the deformed state. Fig. 7.34 is a modified version of Fig. 7.31 that shows this behavioral mode. Applying the stress and subsequent thermal cycling trains the material to remember two shapes [33].

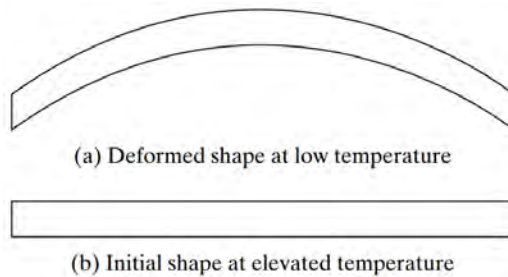


Figure 7.34: Two-way shape memory behavior.

The two-way shape memory behavior provides the basis for force actuation. If a trained shape memory alloy is restrained at low temperature so that it cannot deform, a force is generated when the alloy is heated since it wants to return to its initial undeformed shape. Referring back to the stress-strain plots in Fig. 7.33, suppose the position at low temperature is point c . When heat is applied, the behavior is governed by the curve for $T > M_d$. The material reacts as if it were subjected to the positive strain $a - c$, and the position jumps to c' . This behavior is “ideal”; the actual position is lower, such as point c'' , but the induced stress is still a significant value, on the order of 300 to

7.2. ACTIVE AND SEMI-ACTIVE DEVICE TECHNOLOGIES

400 MPa.

Nitinol alloys in the form of small diameter wires (≈ 0.4 mm) are used to assemble a force actuator. Heating is applied by passing an electric current through the wire. This process limits the response time to seconds versus milliseconds for piezoelectric materials. Another limitation is the material cost; a typical price is on the order of \$250/kg. Most of the applications of shape memory actuators are for small scale products requiring low capacity, and where cost and response time are not critical issues.

7.2.6 Hybrid Systems

Like semi-active devices, hybrid systems are used for an enhanced controllability using minimum voltage. Several hybrid control schemes have been proposed in the literature. They are typically composed of passive dissipation systems coupled with active or semi-active devices. The most popular ones are described in this section.

Hybrid Tuned-Mass Dampers

Active tuned-mass dampers (ATMDs) and active mass-drivers (AMD) are the most widely accepted active control systems for civil structures [9]. ATMDs have been proposed by Lund [68], and since widely studied [69, 16, 7]. They can be found in a variety of applications [21]. They consist of a tuned-mass damper (TMD) or a mass on rollers installed in series with an actuator. Their first large-scale application was conducted on the Kyobashi Seiwa Building [45]. The structure, shown in Fig. 7.35a, is a very slender building with a width of only 4 m, a length of 12 m, and a height of 33 m (11 floors). It is constructed of rigidly connected

CHAPTER 7. APPLICATIONS OF ACTIVE CONTROL

steel frames consisting of box columns and H-shaped beams. The total structural weight is about 400 metric tons (1 metric ton equals 10^4 newtons). The AMD system, illustrated in Figs. 7.35b and 7.35c, is installed on the top floor. The objective of this AMD is to reduce the maximum lateral response associated with frequent earthquakes (i.e., peak ground acceleration of 10 cm/s^2) and strong winds (i.e., maximum speed of 20 m/s) to about one-third of the *uncontrolled* value. The basic components of the control system are as follows:

- Sensors installed at several locations including: ground level, midheight, and the roof level to detect seismic motions and tremors at the ground level and in the building.
- The control computer, which analyzes each signal and issues a drive order. The control algorithm of the system is of the closed-loop control type, where the active control force is determined through linear velocity feed-back of the structures response.
- Actuators, which execute the control order and drive the masses. The hydraulic pressure source for the actuator consists of two pumps and an accumulator. One pump is small in comparison to the other; its function is to provide a minimum level of pressure continuously. The larger pump is activated when the earthquake occurs.
- Two added masses driven by the actuators. Lateral vibration in the width direction is controlled with one mass (weighing about 4 metric tons, about 1% of the building weight) located at the center of the building. Torsional vibration is reduced with a second mass, weighing about 1 metric

7.2. ACTIVE AND SEMI-ACTIVE DEVICE TECHNOLOGIES

ton, located at one end of the structure. These masses are suspended by steel cables to reduce the frictional effects. The lag in the response is about 0.01 s.

Another hybrid application is the DUOX Active-Passive TMD in the Ando Nishikicho Building, in which an AMD is installed in combination with a TMD. This structure, shown in Fig. 7.36 consists of four main steel columns located at the corners, 14 stories above ground, and two basements. The building is located in an area of Tokyo that has mainly small, low-rise buildings, and consequently is susceptible to strong winds. The DUOX system was installed near the center of the top floor (i.e., at the building's center of gravity) to control vibration in both horizontal directions.

The DUOX system consists of the following:

- Sensors installed in the basement and on the top floor of the building to monitor the ground acceleration and building motion. Sensors are also installed on the AMD and TMD to measure the motion of these devices.
- A digital control computer, which receives the feedback signals from the sensors, analyzes them, and determines the optimal control forces that will achieve the required control effect and also maintain the stroke of the AMD within the allowable range.
- A passive TMD weighing 18 metric tons, about 0.8% of the weight of the above ground portion of the building (about 2600 metric tons). The TMD is supported by laminated rubber bearings that provide the required stiffness. Oil dampers provide additional viscous damping in the system.

- Two AMD units, driven by alternating current (AC) servo motors and ball screws and weighing about 10% of the weight of the TMD (about 0.08% of the buildings weight). The units are mounted one on top of the other in a criss-cross manner to provide control in the two horizontal directions. The mass of the TMD moves out of phase with the building so that the building motion is always being retarded. The active mass is driven in the direction opposite to that of the TMD so as to magnify the motion of the TMD. When the building response falls within the allowable zone, the AMD operates to dampen out the motion of the TMD.

Semi-active TMDs (STMDs) have also been proposed, but their physical applications are very recent. The first type of STMD to have been studied is the ER-TMD system [4, 41]. More recently, MR-TMD schemes have been researched [56, 55, 15, 64], and the first application of an MR-TMD has been documented in [129]. It is installed in a tall building located in Santiago, Chile. Fig. 7.37 shows the building along with its two TMDs (the MR damper is not shown). In addition to ER- and MR-TMD, semi-active tuned-liquid column dampers have been studied [53], as well as SAIVS-TMD systems [76]. Lin *et al.* [63] and Lindh *et al.* [65] studied STMDs equipped with a variable friction damper.

Hybrid Base Isolation

Hybrid base-isolated systems mainly consist of a passive base isolation coupled with an active or semi-active device. The main purpose of such a system is to decrease the displacement between the ground and the structure. However, this result comes at the expense of larger inter-story displacements. Examples of hybrid systems include variable-orifice base isolation systems [120], and

7.2. ACTIVE AND SEMI-ACTIVE DEVICE TECHNOLOGIES

MR base-isolated structures [61, 93, 66]. The first large-scale application of an MR-base isolation was achieved in Japan using a 400 kN MR damper [34]. Lu *et al.* [67] proposed a base isolated system with a controllable stiffness device. The hybrid system, termed the stiffness controllable isolation system (SCIS), consists of a passive base-isolated system coupled with a variable friction device. Fig. 7.38 illustrates the mechanism.

CHAPTER 7. APPLICATIONS OF ACTIVE CONTROL

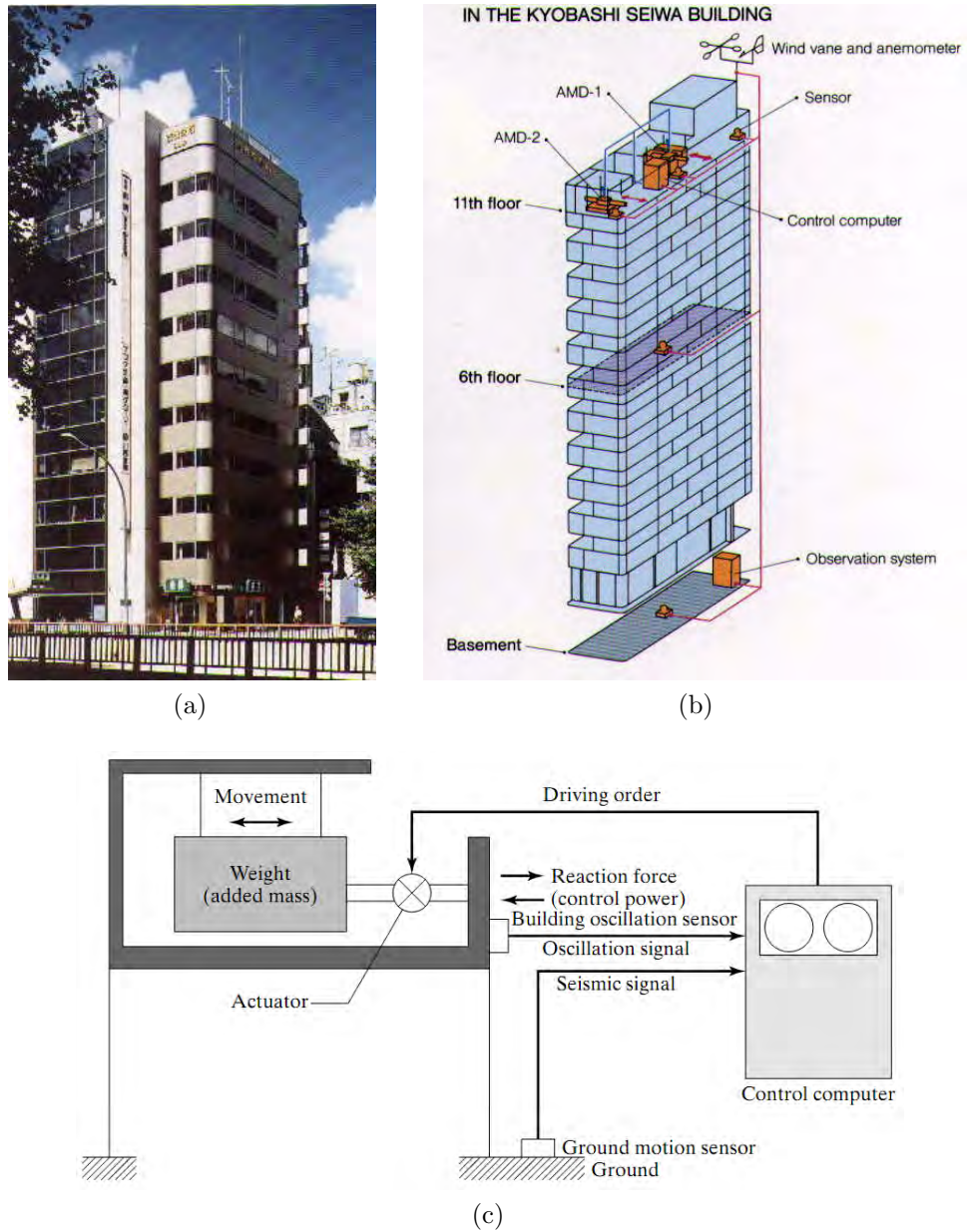


Figure 7.35: Large-scale application of an AMD to the Kyobashi Seiwa Building. a) Picture of the structure; b) schematic of the installation; and c) control diagram (courtesy of Kajima Technical Research Institute).

7.2. ACTIVE AND SEMI-ACTIVE DEVICE TECHNOLOGIES

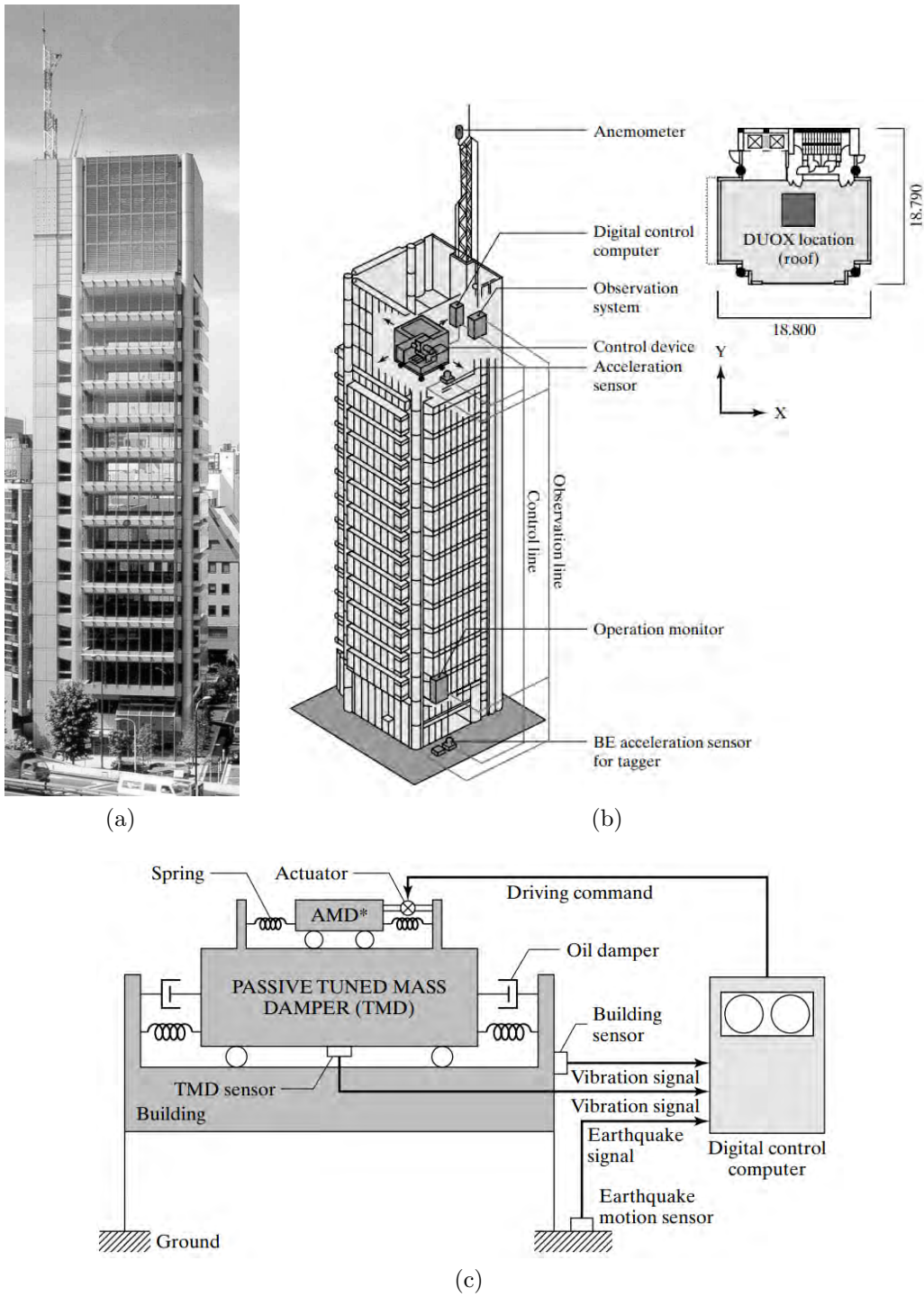


Figure 7.36: Nishikicho building motion control system.

CHAPTER 7. APPLICATIONS OF ACTIVE CONTROL

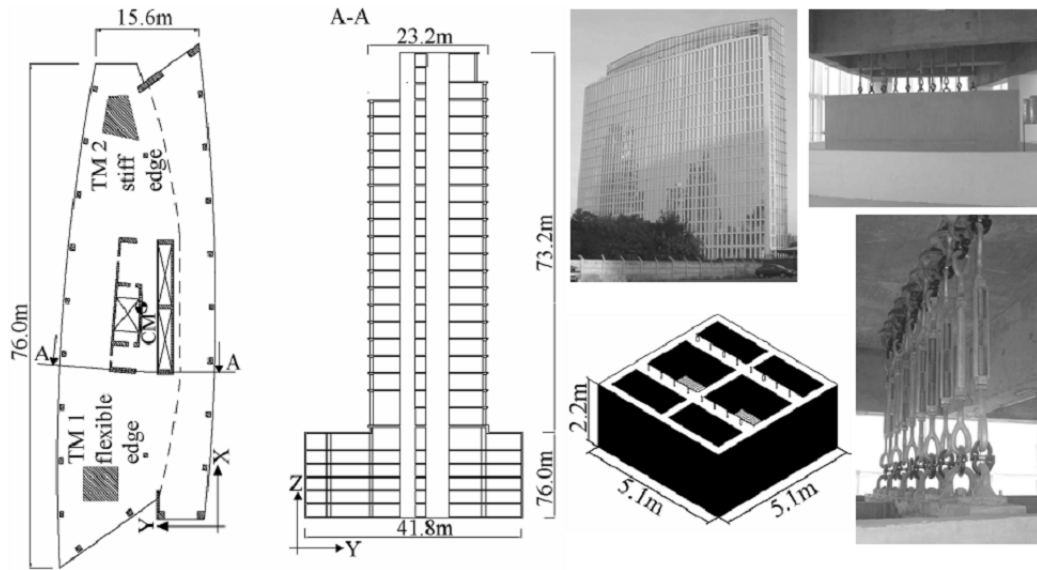


Figure 7.37: Structure equipped with the MR-TMD (MR damper not shown) [129], reprinted with permission of Wiley.

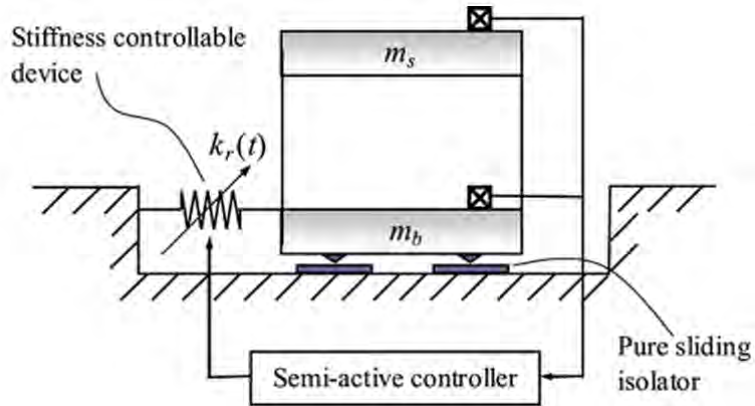


Figure 7.38: SCIS system [67], reprinted with permission of Elsevier.

8

Structural Control Dynamics

8.1 Introduction

This chapter introduces key mathematical formulations associated with structural control dynamics. These formulations are used to derive linear and nonlinear control algorithms presented in Chapters 9 and 10 respectively.

The material presented here is organized as follows. First, the state-space formulation for a linear time-invariant SDOF system (i.e., the case where the system properties and force feedback algorithm are constant over the duration of the time response) is developed and used to generate the free vibration response. This solution provides the basis for establishing a criterion for dynamic stability of a linear SDOF system. Second, the linear SDOF state-space formulation is specialized to deal with discrete time control, where the feedback forces are computed at discrete time points and held constant over time intervals. Stability for discrete time feedback with time delay is examined in detail, and a numerical procedure for determining the time increment corresponding to a stability transition is presented and illustrated with examples. Finally, the state-space formulation is extended to linear MDOF systems. The modal properties for an arbitrary damping scheme are derived and used to generate the governing equations expressed in terms of the modal coordinates.

8.2 State-Space Formulation: Linear Time-Invariant SDOF Systems

8.2.1 Governing Equations

The dynamic response of the SDOF linear system shown in Fig. 8.1 is governed by the second-order equation

8.2. STATE-SPACE FORMULATION: LINEAR TIME-INVARIANT SDOF SYSTEMS

$$m\ddot{u} + c\dot{u} + ku = -ma_g + p + F \quad (8.1)$$

where p is the applied external loading, F is the active force, and m , k , c are constant system parameters. Integrating Eq. (8.1) in time and enforcing the initial conditions on u and \dot{u} at $t = 0$, we obtain the velocity and displacement as functions of time. These quantities characterize the state of the system in the sense that once u and \dot{u} are specified, the acceleration and internal forces can be determined by back-substitution.

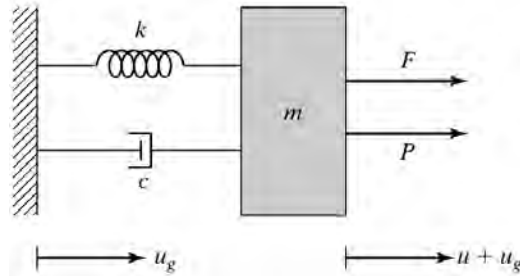


Figure 8.1: SDOF system.

Rather than working with a second-order equation, it is more convenient to transform Eq. (8.1) to a set of first-order equations involving the *state variables* u and \dot{u} . The new form is

$$\begin{aligned} \frac{du}{dt} &= \dot{u} \\ \frac{d\dot{u}}{dt} &= \left(-\frac{c}{m}\right)\dot{u} + \left(-\frac{k}{m}\right)u + (-1)a_g + \left(\frac{1}{m}\right)p + \left(\frac{1}{m}\right)F \end{aligned} \quad (8.2)$$

This form is called the *state-space* representation. The motivation for the state-space representation is mainly the reduced complexity in generating both analytical and numerical solutions.

CHAPTER 8. STRUCTURAL CONTROL DYNAMICS

Matrix notation is convenient for expressing the state-space equations in a compact form. Defining \mathbf{X} as the state vector,

$$\mathbf{X} = \begin{bmatrix} u \\ \dot{u} \end{bmatrix} = \mathbf{X}(t) \quad (8.3)$$

the matrix equilibrium equation is written as

$$\frac{d\mathbf{X}}{dt} = \dot{\mathbf{X}} = \mathbf{A}\mathbf{X} + \mathbf{B}_f F + \mathbf{B}_g a_g + \mathbf{B}_p p \quad (8.4)$$

where the various constant coefficient matrices are defined as follows:

$$\mathbf{A} = \begin{bmatrix} 0 & 1 \\ -\frac{k}{m} & -\frac{c}{m} \end{bmatrix} \quad (8.5)$$

$$\mathbf{B}_f = \mathbf{B}_p = \begin{bmatrix} 0 \\ \frac{1}{m} \end{bmatrix} \quad (8.6)$$

$$\mathbf{B}_g = \begin{bmatrix} 0 \\ -1 \end{bmatrix} \quad (8.7)$$

The initial conditions at $t = 0$ are denoted by \mathbf{X}_0 .

$$\mathbf{X}(0) = \begin{bmatrix} u(0) \\ \dot{u}(0) \end{bmatrix} \equiv \mathbf{X}_0 \quad (8.8)$$

With this representation, the problem is reduced to solving a first order equation involving \mathbf{X} .

8.2.2 Free Vibration Uncontrolled Response

The free vibration uncontrolled response is governed by a reduced form of Eq. (8.4)

8.2. STATE-SPACE FORMULATION: LINEAR TIME-INVARIANT SDOF SYSTEMS

$$\dot{\mathbf{X}} = \mathbf{A}\mathbf{X} \quad (8.9)$$

When \mathbf{A} is constant, the general solution has the form

$$\mathbf{X} = \mathbf{V}e^{\lambda t} \quad (8.10)$$

where \mathbf{V} is an unspecified vector of order 2 and λ is a scalar. Substituting for \mathbf{X} results in

$$(\mathbf{A} - \lambda\mathbf{I})\mathbf{V} = \mathbf{0} \quad (8.11)$$

where I is the identity matrix. According to Eq. (8.11), the eigenvalues of \mathbf{A} define the frequency and damping characteristics of the free vibration response.

Expanding $|\mathbf{A} - \lambda\mathbf{I}| = 0$,

$$\begin{vmatrix} -\lambda & 1 \\ -\frac{k}{m} & -\frac{c}{m} - \lambda \end{vmatrix} = 0 \quad (8.12)$$

leads to the characteristic equation

$$\lambda^2 + \frac{c}{m}\lambda + \frac{k}{m} = 0 \quad (8.13)$$

and two eigenvalues

$$\lambda_{1,2} = \frac{1}{2} \left[-\frac{c}{m} \pm i\sqrt{4\left(\frac{k}{m}\right) - \left(\frac{c}{m}\right)^2} \right] = \lambda_R \pm i\lambda_I \quad (8.14)$$

Noting that $k/m = \omega^2$ and $c/m = 2\xi\omega$, Eq. (8.14) is identical to Eq. (7.11), which was obtained from the second-order equation. Given λ , Eq. (8.11) can be solved for the eigenvectors that define the state-space modes. Since λ is complex, the eigenvectors occur as complex conjugates.

$$\mathbf{V}_{1,2} = \begin{bmatrix} 1 \\ \lambda_R \end{bmatrix} \pm i \begin{bmatrix} 1 \\ \lambda_I \end{bmatrix} = \mathbf{V}_R \pm i\mathbf{V}_I = \mathbf{V}_1, \tilde{\mathbf{V}}_1 \quad (8.15)$$

The total free vibration response is obtained by combining the two complex solutions such that the resulting expression is real. Starting with

$$\mathbf{X} = A_1 e^{\lambda_1 t} \mathbf{V}_1 + A_2 e^{\tilde{\lambda}_1 t} \tilde{\mathbf{V}}_1 \quad (8.16)$$

and taking

$$\begin{aligned} A_1 &= \frac{1}{2}(A_R + iA_I) \\ A_2 &= \tilde{A}_1 \end{aligned} \quad (8.17)$$

where A_R and A_I are real scalars, results in

$$\mathbf{X}(t) = e^{\lambda_R t} [(A_R \mathbf{V}_R - A_I \mathbf{V}_I) \cos \lambda_1 t + (-A_R \mathbf{V}_I - A_I \mathbf{V}_R) \sin \lambda_1 t] \quad (8.18)$$

The constants A_R and A_I are determined by enforcing the initial conditions on \mathbf{X} at $t = 0$.

$$\begin{aligned} \mathbf{X}(0) &= A_1 \mathbf{V}_1 + \tilde{A}_1 \tilde{\mathbf{V}}_1 = A_R \mathbf{V}_R - A_I \mathbf{V}_I \\ &\Downarrow \\ \begin{bmatrix} u_0 \\ \dot{u}_0 \end{bmatrix} &= \begin{bmatrix} A_R \\ A_R \lambda_R - A_I \lambda_I \end{bmatrix} \\ &\Downarrow \\ A_R &= u_0 \\ A_I &= -\frac{1}{\lambda_I}(\dot{u}_0 + \lambda_R u_0) \end{aligned} \quad (8.19)$$

8.2. STATE-SPACE FORMULATION: LINEAR TIME-INVARIANT SDOF SYSTEMS

Lastly, the solution for $u(t)$ is given by the first scalar equation in Eq. (8.18).

$$u(t) = e^{\lambda_R t} (A_R \cos \lambda_I t - A_I \sin \lambda_I t) \quad (8.20)$$

8.2.3 General Solution: Linear Time-Invariant Systems

The general solution for an arbitrary loading can be expressed as a Duhamel integral involving a specialized form of the free vibration response. Considering first a first-order scalar equation,

$$\dot{y} = ay + g \quad (8.21)$$

where a is constant and g is a function of t , the complete solution has the form

$$y(t) = e^{a(t-t_0)} y_0 + \int_{t_0}^t e^{a(t-\tau)} g(\tau) d\tau \quad (8.22)$$

A similar form can be generated for the first-order matrix equation,

$$\dot{\mathbf{X}}(t) = \mathbf{A}\mathbf{X} + \mathbf{G} \quad (8.23)$$

The free vibration solution defined by Eq. (8.18) can be expressed as

$$\mathbf{X}(t) = \mathbf{e}^{\mathbf{A}t} \mathbf{X}_0 \quad (8.24)$$

where $\mathbf{e}^{\mathbf{A}t}$ is defined by the following series:

$$\mathbf{e}^{\mathbf{A}t} = \mathbf{I} + \mathbf{A}t + \frac{1}{2} \mathbf{A}\mathbf{A}t^2 + \dots + \frac{1}{n!} \mathbf{A}^n t^n + \dots \quad (8.25)$$

This matrix exponential function has the same property as the corresponding scalar function.

$$\frac{d}{dt}(\mathbf{e}^{\mathbf{A}t}) = \mathbf{A}\mathbf{e}^{\mathbf{A}t} \quad (8.26)$$

Using Eq. (8.24), the Duhamel integral matrix form of the total solution for Eq. (8.4) is

$$\mathbf{X}(t) = \mathbf{e}^{\mathbf{A}(t-t_0)}\mathbf{X}_0 + \int_{t_0}^t \mathbf{e}^{\mathbf{A}(t-\tau)}\mathbf{G}(\tau)d\tau \quad (8.27)$$

where

$$\mathbf{G}(t) = \mathbf{B}_f F + \mathbf{B}_g a_g + \mathbf{B}_p p \quad (8.28)$$

The corresponding scalar form of the solution for $u(t)$ is

$$u(t) = e^{\lambda_R t} \left(u_0 \cos \lambda_I t + \frac{1}{\lambda_I} (\dot{u}_0 + \lambda_R u_0) \sin \lambda_I t \right) + \int_{t_0}^t \frac{1}{\lambda_I} e^{\lambda_R(t-\tau)} \sin \lambda_I(t-\tau) \left(-a_g(\tau) + \frac{p(\tau)}{m} + \frac{F(\tau)}{m} \right) d\tau \quad (8.29)$$

Equation (8.27) applies for an arbitrary linear time-invariant system. It is convenient for establishing a discrete formulation of the governing equations. This topic is addressed in the next section.

Example 8.1 - Equivalence of Equations (8.18) and (8.24)

Consider Eq. (8.16). The total free vibration response is given by

$$\begin{aligned} \mathbf{X}(t) &= A_1 e^{\lambda t} \mathbf{V}_1 + \tilde{A}_1 e^{\tilde{\lambda} t} \tilde{\mathbf{V}}_1 \\ \mathbf{X}(0) &= A_1 \mathbf{V}_1 + \tilde{A}_1 \tilde{\mathbf{V}}_1 \end{aligned} \quad (8.30)$$

8.2. STATE-SPACE FORMULATION: LINEAR TIME-INVARIANT SDOF SYSTEMS

Noting Eq. (8.11), the λ and \mathbf{V} terms are related by

$$\begin{aligned} \mathbf{A}\mathbf{V}_1 &= \lambda\mathbf{V}_1 \\ \mathbf{A}\tilde{\mathbf{V}}_1 &= \tilde{\lambda}\tilde{\mathbf{V}}_1 \end{aligned} \quad (8.31)$$

Expanding the product, $e^{\lambda t}\mathbf{V}_1$, and using Eq. (8.31) leads to

$$\begin{aligned} e^{\lambda t}\mathbf{V}_1 &= \mathbf{V}_1 + (\lambda\mathbf{V}_1)t + \lambda(\lambda\mathbf{V}_1)\frac{t^2}{2} + \dots \\ &= \left(\mathbf{I} + \mathbf{A}t + \mathbf{A}\mathbf{A}\frac{t^2}{2} + \dots \right) \mathbf{V}_1 \\ &= \mathbf{e}^{\mathbf{A}t}\mathbf{V}_1 \end{aligned} \quad (8.32)$$

It follows that Eq. (8.30) can be written as

$$\mathbf{X}(t) = \mathbf{e}^{\mathbf{A}t}(\mathbf{A}_1\mathbf{V}_1 + \tilde{\mathbf{A}}_1\tilde{\mathbf{V}}_1) = \mathbf{e}^{\mathbf{A}t}\mathbf{X}_0 \quad (8.33)$$

8.2.4 Stability Criterion

Another advantage of the state-space representation is the ability to relate the stability of the physical system to the eigenvalues of \mathbf{A} . A system is said to be stable when the motion resulting from some initial disturbance is bounded. Assuming the system state is \mathbf{X}_0 at time $t = 0$, stability requires

$$|\mathbf{X}(t) - \mathbf{X}_0| \leq \epsilon \quad \forall t \quad (8.34)$$

where ϵ defines the bound on the perturbation from \mathbf{X}_0 .

Equation (8.18) defines the general homogeneous solution for a SDOF time-invariant system. The terms contained inside the brackets depend on the initial conditions and are bounded since

the time dependency is harmonic. Therefore, it follows that the exponential term must be bounded. This requirement is satisfied when the exponent is negative,

$$\lambda_R \leq 0 \quad (8.35)$$

In words, the *real* part of the eigenvalues of \mathbf{A} must be equal to or less than zero. When $\lambda_R = 0$, the response is pure harmonic oscillation. A negative λ_R produces a damped harmonic response.

Plotting λ in the complex plane provides a geometric interpretation of the stability. For the SDOF case, there are two eigenvalues,

$$\begin{aligned} \lambda &= \lambda_R \pm i\lambda_I \\ \lambda_R &= -\frac{c}{2m} = -\xi\omega \\ \lambda_I &= \sqrt{\frac{k}{m} - \left(\frac{c}{2m}\right)^2} = \omega\sqrt{1 - \xi^2} \end{aligned} \quad (8.36)$$

Figure 8.2 shows the corresponding points in the complex plane. These points are referred to as *poles*. Undamped motion has poles on the imaginary axis. Holding stiffness constant and increasing c causes the poles to move along the circle of radius ω toward the critical damping point, $\xi = 1$. With further increase in damping, the curves bifurcate with one branch heading in the negative (real axis) direction, and the other toward the origin. Increasing the stiffness with c held constant moves the poles in the imaginary direction.

With this terminology, the stability criterion requires all the poles corresponding to the eigenvalues of \mathbf{A} to be on or to the left of the imaginary axis, as shown in Fig. 8.3. The uncontrolled

8.2. STATE-SPACE FORMULATION: LINEAR TIME-INVARIANT SDOF SYSTEMS

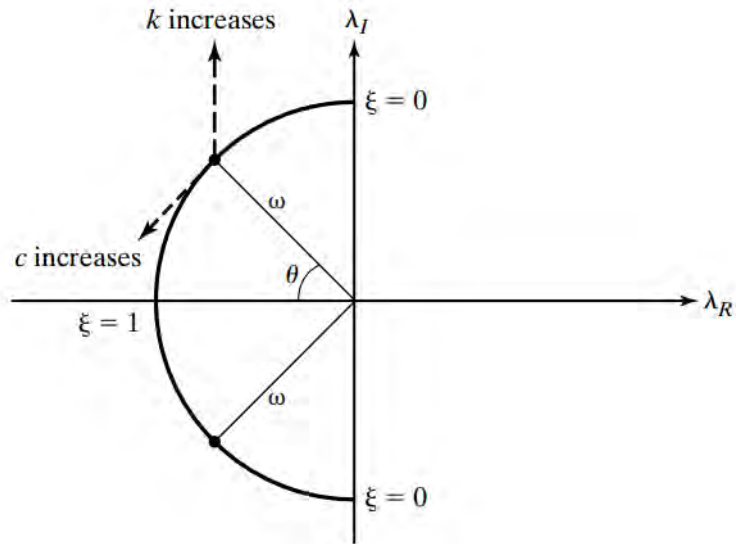


Figure 8.2: Poles for SDOF system.

SDOF system is, according to this definition, always stable since $\xi \leq 0$.

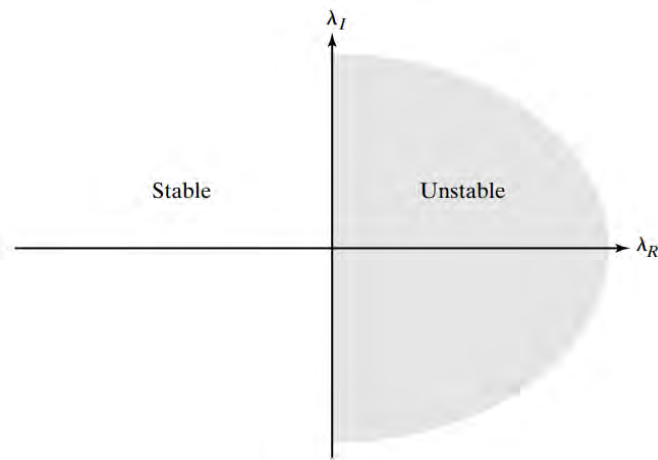


Figure 8.3: Stability condition for SDOF system.

8.2.5 Linear Negative Feedback

The response of a SDOF time-invariant system with negative linear feedback is governed by Eq. (8.4) with F taken as a linear function of the state variables and the acceleration

$$F = -k_m \ddot{u} - k_v \dot{u} - k_d u \quad (8.37)$$

Substituting for F , the governing equation is transformed to

$$\dot{\mathbf{X}} = \mathbf{A}_c \mathbf{X} + \mathbf{B}_g a_g + \mathbf{B}_p p \quad (8.38)$$

where

$$\mathbf{A}_c = \begin{bmatrix} 0 & 1 \\ -\frac{k+k_d}{m+k_m} & -\frac{c+k_v}{m+k_m} \end{bmatrix} \quad (8.39)$$

The general form of the free vibration solution of Eq. (8.38) is

$$\mathbf{X} = \mathbf{V} e^{\lambda t} \quad (8.40)$$

where λ and \mathbf{V} are the eigenvalues and eigenvectors of \mathbf{A}_c , the modified coefficient matrix. They are related by

$$[\mathbf{A}_c - \lambda \mathbf{I}] \mathbf{V} = \mathbf{0} \quad (8.41)$$

The eigenvalues of \mathbf{A}_c are written as

8.2. STATE-SPACE FORMULATION: LINEAR TIME-INVARIANT SDOF SYSTEMS

$$\begin{aligned}
 \lambda &= \lambda_R \pm i\lambda_I \\
 \lambda_R &= -\xi_{eq}\omega_{eq} \\
 \lambda_I &= \omega_{eq}\sqrt{1 - \xi_{eq}^2} \\
 \omega_{eq} &= \left(\frac{k + k_d}{m + k_m} \right)^{1/2} \\
 \omega_{eq}\xi_{eq} &= \frac{c + k_v}{2(m + k_m)}
 \end{aligned} \tag{8.42}$$

Since k_v is *positive* for negative feedback (note that the minus sign is incorporated in the definition equation, Eq. (8.37)), the system is stable for arbitrary k_v . Velocity feedback increases the effective damping. Displacement feedback moves the poles in the imaginary direction and increases the effective frequency. Acceleration-based feedback decreases both the effective damping and frequency and moves the poles toward the origin. It follows that increasing the negative velocity feedback is a more appropriate mechanism for improving the stability of a SDOF system versus either displacement or acceleration feedback. Therefore, only velocity and displacement feedback will be considered in the following stability analysis.

Noting Eqs. (8.23) and (8.27), the total solution for time-invariant linear feedback can be expressed in a form similar to Eq. (8.27).

$$\mathbf{X}(t) = \mathbf{e}^{\mathbf{A}_c(t-t_0)}\mathbf{X}_0 + \int_{t_0}^t \mathbf{e}^{\mathbf{A}_c(t-\tau)}(\mathbf{B}_g a_g(\tau) + \mathbf{B}_p p(\tau))d\tau \tag{8.43}$$

The identity established in Ex. 8.1 is also applicable here.

$$\mathbf{e}^{\mathbf{A}_c(t-t_0)}\mathbf{X}_0 \equiv A e^{\lambda(t-t_0)}\mathbf{V} + \tilde{A} e^{\tilde{\lambda}(t-t_0)}\tilde{\mathbf{V}} \quad (8.44)$$

where A is a complex scalar, and (λ, \mathbf{V}) are the solution of Eq. (8.41). Requiring $\lambda_R \leq 0$ ensures that $\mathbf{e}^{\mathbf{A}_c(t-t_0)}$ is bounded.

The preceding discussion assumes there is no delay between observing the state and generating the force. In general, there is some delay and the force at time t is computed using data observed at an earlier time, $t - t_d$. The force for linear negative feedback is expressed as

$$\begin{aligned} F(t) &= -\mathbf{K}_f \mathbf{X}(t - t_d) \\ \mathbf{K}_f &= \begin{bmatrix} k_d & k_v \end{bmatrix} \end{aligned} \quad (8.45)$$

where t_d represents the delay time. Delay introduces additional terms in λ_R and, under certain conditions, can cause λ_R to become positive and, consequently, the system becomes unstable. Therefore, although ideal linear negative feedback is unconditionally stable, we need to examine the potential destabilizing effect of delay for the actual control system. One procedure for investigating the effect of time delay on the stability of a controlled time-invariant SDOF system is described in the following section. Additional approaches are discussed in later sections.

8.2.6 Effect of Time Delay on Feedback Control

Time delay in feedback control systems is the sum of the times required to execute the following actions:

- acquire the data from sensors placed at different locations in the structure;
- process the sensor data and calculate the control force;

8.2. STATE-SPACE FORMULATION: LINEAR TIME-INVARIANT SDOF SYSTEMS

- transmit the control force signal to the actuator;
- ramp up the actuator to the desired force level.

The resultant time delay affects the synchronization between the control force and the response of the system and may, under certain conditions, cause a significant degradation in the performance of the control system that could result in instability.

In what follows, an analytical procedure for assessing the stability of a SDOF system with time delay is presented. This approach follows the method proposed in [6]. Results based on numerical simulations are included here to illustrate the effect of time delay on the response.

Assuming the feedback control algorithm consists of a linear combination of displacement and velocity terms and using data associated with the time, $t - t_d$, the feedback force at time t is written as

$$\frac{1}{m}F(t) = -\frac{k_d}{m}u(t - t_d) - \frac{k_v}{m}\dot{u}(t - t_d) = -g_d u(t - t_d) - g_v \dot{u}(t - t_d) \quad (8.46)$$

Substituting for F in Eq. (8.1), the governing equation for this case is

$$\ddot{u}(t) + 2\xi\omega\dot{u}(t) + \omega^2u(t) + g_d u(t - t_d) + g_v \dot{u}(t - t_d) = \frac{p(t)}{m} \quad (8.47)$$

The general form of the homogeneous solution of Eq. (8.47) is

$$u = Ae^{\lambda t} \quad (8.48)$$

where A is an arbitrary constant and λ satisfies

$$\lambda^2 + (2\xi\omega + g_v e^{-\lambda t_d})\lambda + (\omega^2 + g_d e^{-\lambda t_d}) = 0 \quad (8.49)$$

Letting $\lambda = \lambda_R \pm i\lambda_I$ represent the roots, the stability requirement is $\lambda_R \leq 0$.

Expressing λ_R and λ_I in a convenient form is complicated by the presence of the exponential terms. A first-order approximation can be obtained by introducing the following expansion:

$$e^{-\lambda t_d} = 1 - \lambda t_d + \frac{1}{2}(\lambda t_d)^2 - \frac{1}{6}(\lambda t_d)^3 + \dots \quad (8.50)$$

and retaining only the first two terms. The result is expressed in the same form as Eq. (8.42) with ξ_{eq} and ω_{eq} replaced with modified terms.

$$\begin{aligned} \lambda_R &= -\xi'_{eq} \omega'_{eq} \\ \lambda_I &= \omega'_{eq} \sqrt{1 - \xi'^2_{eq}} \end{aligned} \quad (8.51)$$

The modified equivalent frequency and damping are related to the time delay by

$$\omega'_{eq} = \omega \sqrt{\frac{1 + g_d/\omega^2}{1 - g_v t_d}} \quad (8.52)$$

$$\xi' = \frac{\xi + \frac{1}{2\omega}(g_v - g_d t_d)}{\sqrt{(1 - g_v t_d) \left(1 + \frac{g_d}{\omega^2}\right)}} \quad (8.53)$$

Eq. (8.51) is convenient for identifying behavioral trends.

For no initial damping and no velocity feedback ($g_v = 0$), the approximation for λ_R reduces to

$$\lambda_R = \frac{g_d t_d}{2\omega} = \frac{k_d t_d}{2\omega m} \quad (8.54)$$

8.2. STATE-SPACE FORMULATION: LINEAR TIME-INVARIANT SDOF SYSTEMS

Since λ_R is positive, it follows that according to this first-order approximation, displacement feedback with time delay produces *unstable* behavior for an initially undamped system ($\xi = 0$). The real part of λ corresponding to pure velocity feedback ($g_d = 0$) is estimated as

$$\lambda_R = -\omega \frac{\xi + \frac{g_v}{2\omega}}{1 - g_v t_d} = -\omega \frac{\xi + \frac{k_v}{2\omega m}}{1 - \frac{k_v t_d}{m}} \quad (8.55)$$

This result suggests that the response is *stable* when $(k_v t_d / m) < 1$.

An improved approximation can be obtained by substituting the Pade expansion

$$e^{-\lambda t_d} \approx \frac{1 - \lambda t_d / 2}{1 + \lambda t_d / 2} + O[(\lambda t_d)^3] \quad (8.56)$$

in Eq. (8.49). The resulting expression is now a third-degree polynomial in λ :

$$\frac{t_d}{2} \lambda^3 + \left[1 + t_d \left(\xi \omega - \frac{g_v}{2} \right) \right] \lambda^2 + \left[2\xi \omega + g_v + \frac{t_d}{2} (\omega^2 - g_d) \right] \lambda + \omega^2 + g_d = 0 \quad (8.57)$$

Introducing the notation for the equivalent frequency and damping defined earlier for the instantaneous feedback case (see Eq. (8.42)),

$$\begin{aligned} \omega_{eq}^2 &= \omega^2 + g_d \\ \xi_{eq} \omega_{eq} &= \xi \omega + \frac{1}{2} g_v \\ \xi_{eq} &= \xi + \xi_a \end{aligned} \quad (8.58)$$

transforms Eq. (8.57) to

$$\left[\frac{t_d}{2}\right] \lambda^3 + [1 + (2\xi\omega - \xi_{eq}\omega_{eq})t_d]\lambda^2 + \left[2\xi_{eq}\omega_{eq} + t_d \left(\omega^2 - \frac{\omega_{eq}^2}{2}\right)\right] \lambda + \omega_{eq}^2 = 0 \quad (8.59)$$

For pure displacement feedback, $\xi_{eq}\omega_{eq} = \xi\omega$. For pure velocity feedback, $\omega_{eq} = \omega$ and $\xi_a = k_v/(2\omega m)$.

Eq. (8.59) is solved numerically for a specific SDOF system with a period of 5 s, and the two limiting cases of pure displacement and pure velocity feedback with no initial damping. Fig. 8.4 shows the movement of the poles for pure displacement feedback as a function of ω_{eq} and t_d . When $t_d = 0$, the poles move on the imaginary axis with increasing ω_{eq} . As t_d increases, the path shifts to the right, and when t_d is about 1 s, the direction is essentially along the positive real axis.

The effect of time delay for pure velocity feedback is illustrated by Fig. 8.5. For no time delay, increasing k_v moves the poles further back in the negative real half-plane until the state of critical damping is reached. As t_d increases, the paths tend to bend toward the positive real half-plane and eventually intersect the imaginary axis. For a given value of k_v , there may be a limiting time delay beyond which the system is unstable. These observations are based on an approximation and apply for a particular system (i.e., specific values of ω and ξ). An exact analysis of the instability problem is presented in the next section.

8.2.7 Stability Analysis for Time Delay

Fig. 8.5 shows that, for a given system, there is a particular value of t_d that corresponds to a transition in the behavior of λ_R . For

8.2. STATE-SPACE FORMULATION: LINEAR TIME-INVARIANT SDOF SYSTEMS

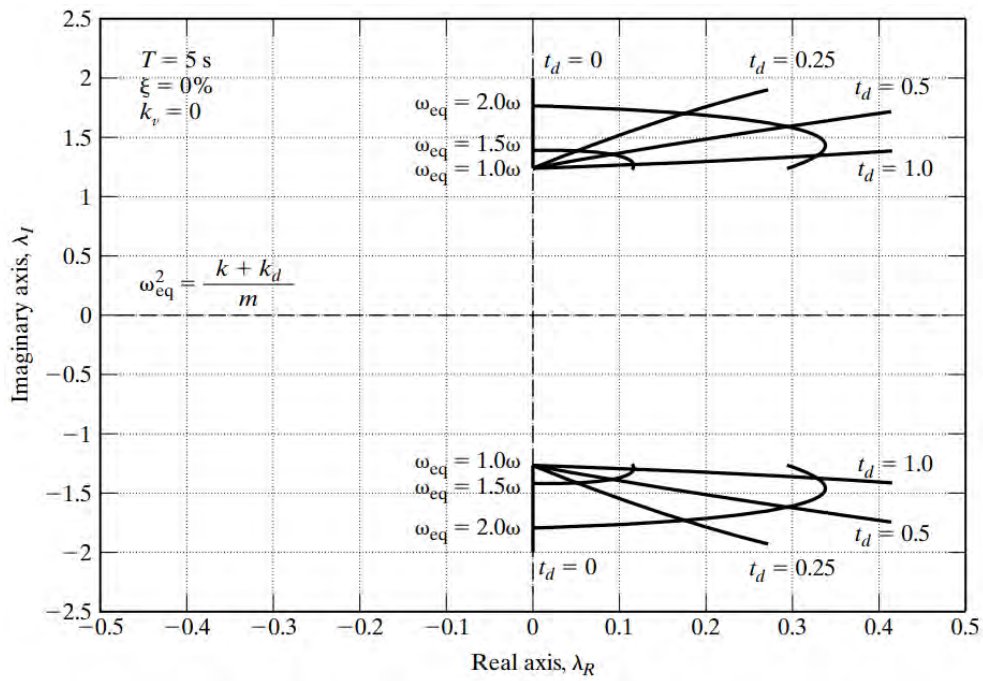


Figure 8.4: Variation of pole profile with t_d under pure displacement feedback.

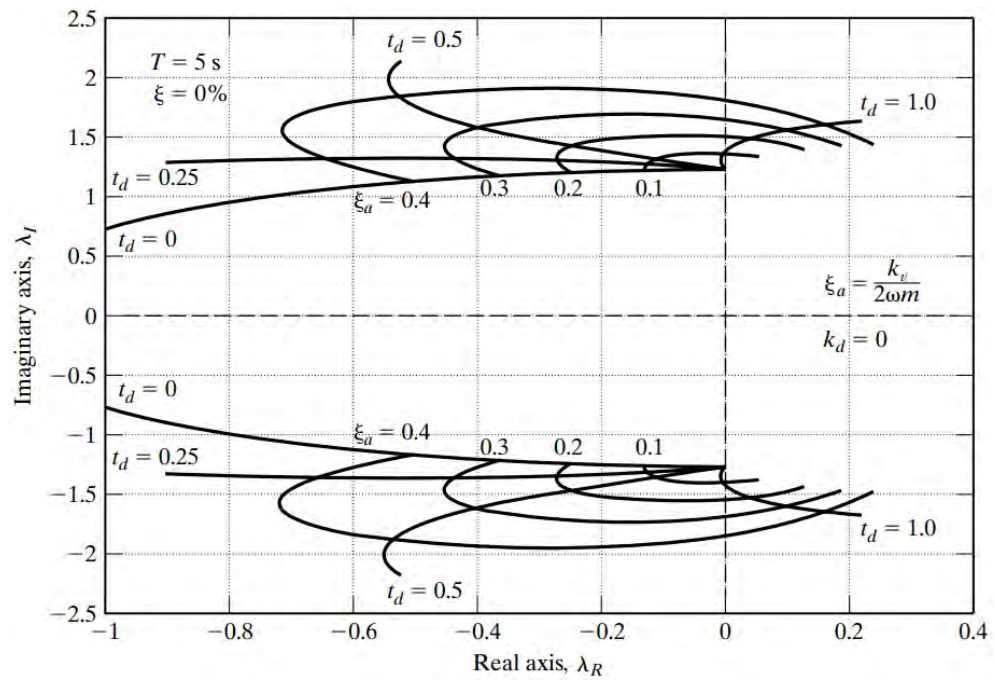


Figure 8.5: Variation of pole profile with t_d under pure velocity feedback.

8.2. STATE-SPACE FORMULATION: LINEAR TIME-INVARIANT SDOF SYSTEMS

t_d greater than this value, λ_R increases and eventually becomes positive. When $\lambda_R = 0$, there is a transition from stable to unstable behavior, and the corresponding value of t_d defines the stability limit for the system (i.e., for the particular combination of k , c , k_v , and k_d). Eq. (8.49) is the definition equation for λ . Noting that the critical time delay corresponds to $\lambda_R = 0$, by expressing λ as

$$\lambda = i\Omega \quad (8.60)$$

where Ω is a real scalar, we can specialize Eq. (8.49) for this case and determine the critical value of t_d . Substituting for λ leads to

$$-\Omega^2 + i2\xi\omega\Omega + \omega^2 + g_d e^{-it_d\Omega} + ig_v\Omega e^{-it_d\Omega} = 0 \quad (8.61)$$

Replacing the exponential term by

$$e^{-it_d\Omega} = \cos(t_d\Omega) - i \sin(t_d\Omega) \quad (8.62)$$

yields

$$\begin{aligned} -\Omega^2 + \omega^2 + g_d \cos(t_d\Omega) + g_v\Omega \sin(t_d\Omega) \\ + i[2\xi\omega\Omega - g_d \sin(t_d\Omega) + g_v\Omega \cos(t_d\Omega)] = 0 \end{aligned} \quad (8.63)$$

Eq. (8.63) is satisfied when the real and imaginary terms vanish. Then

$$g_d \sin(t_d\Omega) + g_v\Omega \cos(t_d\Omega) = 2\xi\omega\Omega \quad (8.64)$$

$$g_d \cos(t_d\Omega) + g_v\Omega \sin(t_d\Omega) = \Omega^2 - \omega^2 \quad (8.65)$$

It remains to solve these equations for t_d in terms of g_d , g_v , ω , and ξ .

CHAPTER 8. STRUCTURAL CONTROL DYNAMICS

Squaring both sides and adding the equations eliminates the trigonometric terms and results in a quartic equation for Ω .

$$\Omega^4 + (4\xi^2\omega^2 - 2\omega^2 - g_v^2)\Omega^2 + \omega^4 - g_d^2 = 0 \quad (8.66)$$

The roots of Eq. (8.66) are given by

$$\Omega_{1,2} = \pm \sqrt{-\frac{(4\xi^2\omega^2 - 2\omega^2 - g_v^2)}{2} \pm \sqrt{\frac{(4\xi^2\omega^2 - 2\omega^2 - g_v^2)^2}{4} - (\omega^4 - g_d^2)}} \quad (8.67)$$

Since the poles correspond to $\pm i\Omega$, only the positive value of Ω needs to be considered, resulting in two values of Ω .

The next step is to determine $t_d\Omega$. Noting the trigonometric identities,

$$\sin(t_d\Omega) = \frac{2 \tan\left(\frac{t_d\Omega}{2}\right)}{1 + \tan^2\left(\frac{t_d\Omega}{2}\right)} \quad (8.68)$$

$$\cos(t_d\Omega) = \frac{1 - \tan^2\left(\frac{t_d\Omega}{2}\right)}{1 + \tan^2\left(\frac{t_d\Omega}{2}\right)} \quad (8.69)$$

Eq. (8.64) can be expressed as

$$(g_v\Omega - 2\xi\omega\Omega) \tan^2\left(\frac{t_d\Omega}{2}\right) + 2g_d \tan\left(\frac{t_d\Omega}{2}\right) - (g_v\Omega + 2\xi\omega\Omega) = 0 \quad (8.70)$$

The two roots of Eq. (8.70) are

$$\tan\left(\frac{t_d\Omega}{2}\right) = \frac{-g_d \pm \sqrt{g_d^2 + g_v^2\Omega^2 - 4\xi^2\omega^2\Omega^2}}{g_v\Omega - 2\xi\omega\Omega} \quad (8.71)$$

8.2. STATE-SPACE FORMULATION: LINEAR TIME-INVARIANT SDOF SYSTEMS

Finally, the maximum time delay $t_d|_{\max}$ can be determined from

$$t_d|_{\max} = \frac{2}{\Omega} \tan^{-1} \left(\frac{-g_d \pm \sqrt{g_d^2 + g_v^2 \Omega^2 - 4\xi^2 \omega^2 \Omega^2}}{g_v \Omega - 2\xi \omega \Omega} \right) \quad (8.72)$$

The minimum positive value of $t_d|_{\max}$ is the maximum allowable time delay.

For the limiting case of pure velocity feedback control of an undamped system (i.e., $g_d = 0$ and $\xi = 0$), Eq. (8.64) reduces to

$$g_v \cos(t_d \Omega) = 0 \quad (8.73)$$

and it follows that

$$t_d|_{\max} = \frac{\pi}{2\Omega} \quad (8.74)$$

The expression for Ω can be obtained from either Eq. (8.65) or Eq. (8.67):

$$\frac{\Omega}{\omega} = \xi_a + \sqrt{1 + \xi_a^2} \quad (8.75)$$

where

$$\xi_a = \frac{g_v}{2\omega} = \frac{k_v}{2\omega m} \quad (8.76)$$

Finally, the maximum delay can be expressed in terms of the fundamental period of the uncontrolled system.

$$\frac{t_d|_{\max}}{T} = \frac{1}{4 \left(\xi_a + \sqrt{1 + \xi_a^2} \right)} \quad (8.77)$$

Fig. 8.6 through 8.8 illustrate the effect of varying the displacement feedback, velocity feedback, system damping, and system period on the maximum allowable time delay. Fig. 8.6 shows plots of the maximum allowable time delay for an undamped SDOF ($T = 0.5$ s) system as a function of the active damping ratio ξ_a (i.e., velocity feedback) for three values of displacement feedback k_d . The central curve corresponds to $k_d = 0$. The lower curve corresponds to $k_d > 0$ (i.e., leading to an increase in the frequency of the controlled system) and shows that $t_d = 0$ for no active damping. Furthermore, Fig. 8.6 illustrates the effect of underestimating/overestimating the stiffness of the system on the maximum allowable time delay. If the model used to establish the system properties underestimates the stiffness, the actual limit on the time delay will be less than the predicted limit and stability may be a problem.

Fig. 8.7 shows the effect of the damping in the system on the maximum allowable time delay. In general, damping increases the allowable time delay. The effect of the fundamental period of the system on the maximum allowable time delay is illustrated by Fig. 8.8. As expected from Eq. (8.77), the maximum allowable time delay increases with period and decreases with active damping. Finally, Fig 8.9 illustrates the degradation in performance, with increasing time delay, of the SDOF system subjected to seismic excitation. Instability occurs beyond a time delay of 1.1 s, which, according to Fig. 8.7, corresponds to the maximum allowable time delay for this level of damping. The instability is due to the unbounded growth of the homogeneous solution and will occur for any arbitrary external excitation.

8.2. STATE-SPACE FORMULATION: LINEAR TIME-INVARIANT SDOF SYSTEMS

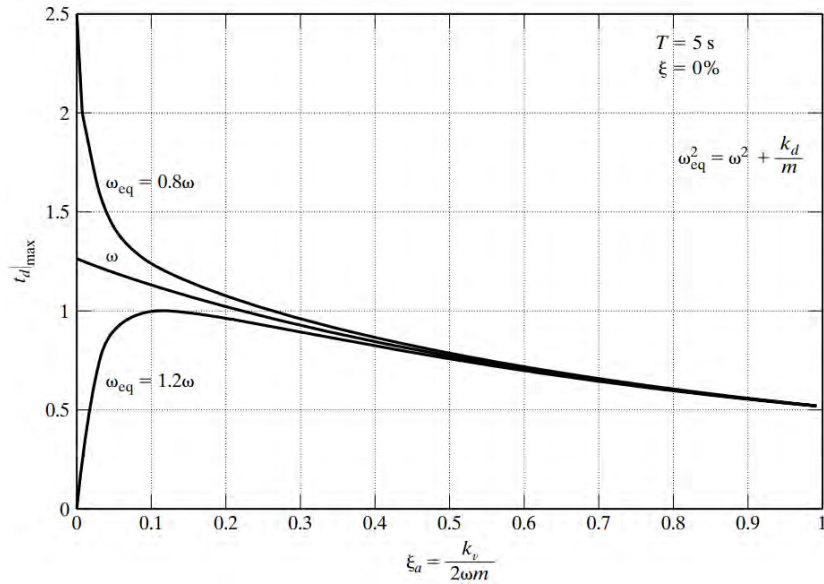


Figure 8.6: Maximum allowable time delay $t_d|_{\max}$ as a function of k_d and k_v .

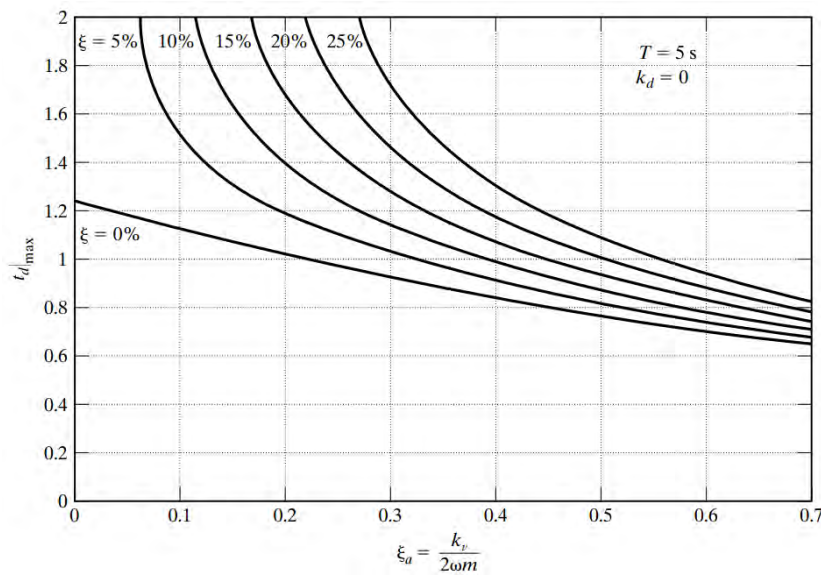


Figure 8.7: Maximum allowable time delay $t_d|_{\max}$ as a function of k_v and ξ .

CHAPTER 8. STRUCTURAL CONTROL DYNAMICS

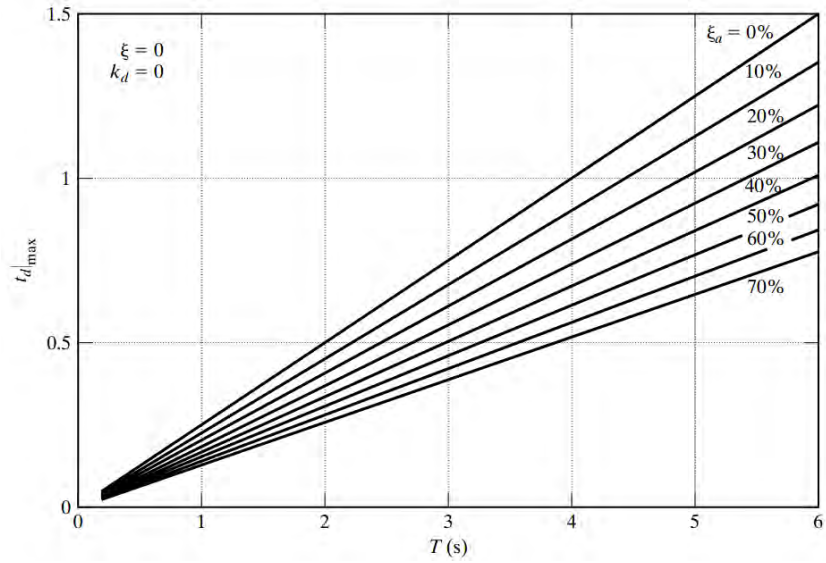


Figure 8.8: Maximum allowable time delay $t_d|_{\max}$ as a function of k_v and T .

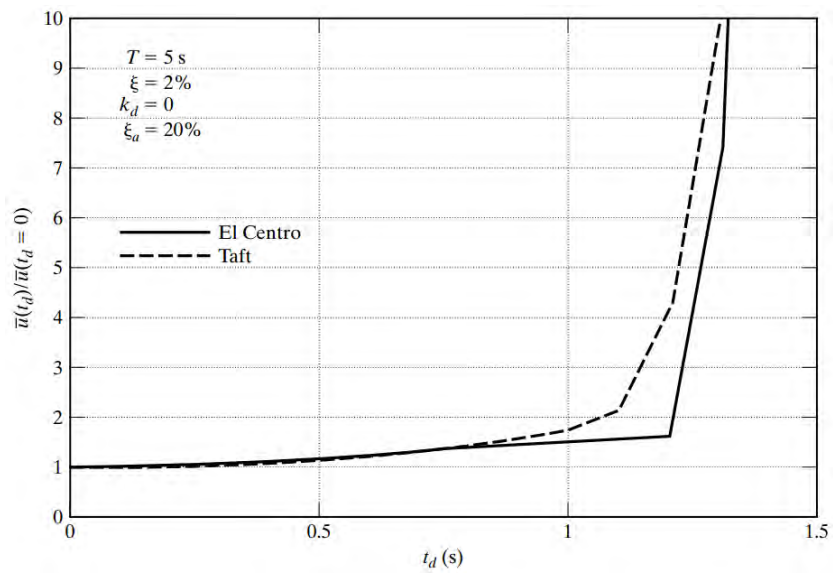


Figure 8.9: Degradation in performance of a SDOF system with time delay.

8.3 Discrete Time Formulation: SDOF Systems

8.3.1 Governing Equation

The continuous state-space linear formulation considers \mathbf{X} and F to be continuous functions of time that satisfy the following ordinary linear differential equation and initial conditions:

$$\begin{aligned}\dot{\mathbf{X}} &= \mathbf{A}\mathbf{X} + \mathbf{B}_f F + \mathbf{B}_g a_g + \mathbf{B}_p p \\ \mathbf{X}(t = 0) &= \mathbf{X}_0^*\end{aligned}\tag{8.78}$$

In the case of a SDOF system, the coefficients are second-order matrices involving the system properties

$$\begin{aligned}\mathbf{A} &= \begin{bmatrix} 0 & 1 \\ -\frac{k}{m} & -\frac{c}{m} \end{bmatrix} \\ \mathbf{B}_f = \mathbf{B}_p &= \begin{bmatrix} 0 \\ \frac{1}{m} \end{bmatrix} \\ \mathbf{B}_g &= \begin{bmatrix} 0 \\ -1 \end{bmatrix}\end{aligned}\tag{8.79}$$

The formulation presented in the previous section was based on the assumption that m , k , and c are constant. This restriction allows us to obtain Eq. (8.27), the exact analytical solution expressed in terms of a convolution integral. A numerical integration procedure is required to evaluate the convolution integral when the loading is a complex function such as a ground acceleration time history. If the system parameters and/or the feedback parameters are time dependent, an exact analytic solution of the equilibrium equation cannot be established, and we must resort to generating an approximate solution with a numerical

CHAPTER 8. STRUCTURAL CONTROL DYNAMICS

procedure, such as a finite difference method that works with values of the variables at discrete points in time. A discrete time approach is also necessary for real-time feedback control, since the control force is computed using observed values for the response at discrete time points.

We generate a discrete time formulation by subdividing the time domain into intervals, say $t_0 - t_1$, $t_1 - t_2$, ..., $t_n - t_f$, and taking as unknowns the values of $\mathbf{X}(t)$ and $F(t)$ at the discrete time points. The notation

$$\begin{aligned}\mathbf{X}(t_j) &\equiv \mathbf{X}_j \\ F(t_j) &\equiv F_j\end{aligned}\tag{8.80}$$

is convenient for representing these discrete variables. Eq. (8.79) is approximated at each time point by an algebraic equation relating the values of \mathbf{X} and F at that point and neighboring points and is used to estimate the value of at a later time. In what follows, the procedure is illustrated using a simple approximation for Eq. (8.79).

When the system parameters are constant, the solution is given by Eq. (8.27), which is provided here for convenience.

$$\mathbf{X}(t) = \mathbf{e}^{\mathbf{A}(t-t_0)}\mathbf{X}(t_0) + \int_{t_0}^t \mathbf{e}^{\mathbf{A}(t-\tau)}\mathbf{B}_f F(\tau)d\tau + \int_{t_0}^t \mathbf{e}^{\mathbf{A}(t-\tau)} (\mathbf{B}_p p + \mathbf{B}_g a_g(\tau)) d\tau$$

We can use this result to obtain an approximate solution between two time points, say t_j and $t_{j+1} = t_j + \Delta t$, by introducing assumptions for the variation of the force terms during the interval Δt . The simplest model is based on using the values at the initial time t_j .

8.3. DISCRETE TIME FORMULATION: SDOF SYSTEMS

Taking the time limits as $t = t_{j+1}$ and $t_0 = t_j$, assuming the force terms are equal to their value for $t = t_j$,

$$\begin{aligned} F(\tau) &= F(t_j) = F_j \\ p(\tau) &= p(t_j) = p_j \\ a_g(\tau) &= a_g(t_j) = a_{g,j} \end{aligned} \tag{8.81}$$

and noting the expansion for $\mathbf{e}^{\mathbf{A}t}$ transforms the convolution integrals contained in Eq. (8.27) to the following algebraic form:

$$\mathbf{X}_{j+1} = \mathbf{e}^{\mathbf{A}\Delta t} \mathbf{X}_j + \mathbf{A}^{-1}(\mathbf{e}^{\mathbf{A}\Delta t} - \mathbf{I})[\mathbf{B}_g a_{g,j} + \mathbf{B}_f \mathbf{F}_j + \mathbf{B}_p p_j] \tag{8.82}$$

Equation (8.82) provides an estimate for \mathbf{X}_{j+1} based on data associated with the time point, t_j . The first term on the right-hand side is the exact free vibration response at t_{j+1} , considering \mathbf{X}_j to be the initial state at t_j . The remaining terms represent the contribution of the constant loading terms over the time interval, Δt . Starting at $t = 0$, which corresponds to $j = 0$, we specify \mathbf{X}_0 and compute \mathbf{X}_1 . This process is repeated until the desired time is reached. The computation will be bounded when Eq. (8.82) is numerically stable. Stability is discussed in more detail later in this section.

This approach can also be applied to an adaptive system. The mass is considered to be constant, and therefore \mathbf{B}_f and \mathbf{B}_g are constant. Stiffness and damping are assumed to be constant over a time interval and to vary from one interval to another. Discrete values of stiffness and damping are defined for the time interval, $t_j \leq t < t_{j+1}$, as follows:

$$\begin{aligned}
 k(t) &= k(t_j) \equiv k_j \\
 c(t) &= c(t_j) \equiv c_j \\
 \mathbf{A}(t) &= \mathbf{A}(t_j) \equiv \mathbf{A}_j
 \end{aligned}
 \tag{8.83}$$

Since \mathbf{A} is considered constant over an interval, Eq. (8.27) is still applicable for the interval. The resulting form of the discrete equilibrium equation is obtained by replacing \mathbf{A} with \mathbf{A}_j in Eq. (8.82).

$$\mathbf{X}_{j+1} = \mathbf{e}^{\mathbf{A}_j \Delta t} \mathbf{X}_j + \mathbf{A}_j^{-1} (\mathbf{e}^{\mathbf{A}_j \Delta t} - \mathbf{I}) [\mathbf{B}_g a_{g,j} + \mathbf{B}_f \mathbf{F}_j + \mathbf{B}_p p_j]
 \tag{8.84}$$

Starting at $j = 0$, we form \mathbf{A}_0 and determine \mathbf{X}_1 . Then \mathbf{A} is updated to \mathbf{A}_1 and used to compute \mathbf{X}_2 . This process is continued for successive time points.

8.3.2 Linear Negative Feedback Control

The discrete formulation represented by Eq. (8.84) assumes that properties and forces are constant over a time interval and are updated at the starting point of the interval. A feedback law consistent with this assumption is

$$\begin{aligned}
 t_j &\leq t < t_{j+1} \\
 F_j &= -\mathbf{K}_{f,j} \mathbf{X}_j
 \end{aligned}
 \tag{8.85}$$

where $\mathbf{K}_{f,j}$ is the feedback gain matrix at $t = t_j$.

$$\mathbf{K}_{f,j} = [k_d(t_j) \quad k_v(t_j)]
 \tag{8.86}$$

Substituting for F transforms Eq. (8.84) to

8.3. DISCRETE TIME FORMULATION: SDOF SYSTEMS

$$\begin{aligned} \mathbf{X}_{j+1} = & [\mathbf{e}^{\mathbf{A}_j \Delta t} - \mathbf{A}_j^{-1}(\mathbf{e}^{\mathbf{A}_j \Delta t} - \mathbf{I})\mathbf{B}_f \mathbf{K}_f] \mathbf{X}_j \\ & + \mathbf{A}_j^{-1}(\mathbf{e}^{\mathbf{A}_j \Delta t} - \mathbf{I})[\mathbf{B}_g a_{g,j} + \mathbf{B}_p p_j] \end{aligned} \quad (8.87)$$

We can also derive this expression by specializing Eq. (8.43). The time history response is generated by starting with \mathbf{X}_0 and computing $\mathbf{X}_1, \mathbf{X}_2, \dots$, and so on. Key issues here are the specification of the time interval; the magnitude and temporal distribution of the system stiffness and damping; and the feedback parameters, k_d and k_v .

8.3.3 Stability Analysis for Time-Invariant Linear Feedback Control

The numerical stability of the discrete feedback control algorithm is determined by examining the nature of the homogeneous solution. The analysis presented here assumes the coefficient matrices are constant (i.e., the system is time invariant). Specializing Eq. (8.84) for this case and considering no external loading other than feedback leads to the governing equation

$$\mathbf{X}_{j+1} = \mathbf{e}^{\mathbf{A} \Delta t} \mathbf{X}_j + \mathbf{A}^{-1}(\mathbf{e}^{\mathbf{A} \Delta t} - \mathbf{I})\mathbf{B}_f F_j \quad (8.88)$$

For no time delay, F_j is taken as a linear function of \mathbf{X}_j . The effect of time delay is to shift the value of \mathbf{X} used to compute F_j back to $\mathbf{X}(t_j - \nu \Delta t) \equiv \mathbf{X}_{j-\nu}$. For $j < \nu$, the control force is taken as 0.

$$\begin{aligned} F_j &= 0 & j < \nu \\ F_j &= -\mathbf{K}_f \mathbf{X}_{j-\nu} & j \geq \nu \end{aligned} \quad (8.89)$$

Substituting for F_j , the discrete equilibrium equation allowing for time delay takes the following form:

CHAPTER 8. STRUCTURAL CONTROL DYNAMICS

$$\begin{aligned}\mathbf{X}_{j+1} &= \mathbf{e}^{\mathbf{A}\Delta t}\mathbf{X}_j & 0 \leq j < \nu \\ \mathbf{X}_{j+1} &= \mathbf{e}^{\mathbf{A}\Delta t}\mathbf{X}_j - \mathbf{A}^{-1}(\mathbf{e}^{\mathbf{A}\Delta t} - \mathbf{I})\mathbf{B}_f\mathbf{K}_f\mathbf{X}_{j-\nu} & \nu \leq j\end{aligned}\quad (8.90)$$

Considering first the case of no time delay, the free vibration response is determined with

$$\mathbf{X}_{j+1} = (\mathbf{e}^{\mathbf{A}\Delta t} - \mathbf{A}^{-1}(\mathbf{e}^{\mathbf{A}\Delta t} - \mathbf{I})\mathbf{B}_f\mathbf{K}_f)\mathbf{X}_j \quad j = 0, 1, 2, \dots \quad (8.91)$$

This equation applies when the control force is updated at the discrete time points and assumed constant during the time intervals. The corresponding form for the case where the force is assumed to be continuously updated can be obtained by specializing Eq. (8.43).

$$\mathbf{X}_{j+1} = \mathbf{e}^{(\mathbf{A} - \mathbf{B}_f\mathbf{K}_f)\Delta t}\mathbf{X}_j \quad (8.92)$$

The solution generated with Eq. (8.92) is the exact damped solution. According to Eq. (8.44), this solution is bounded for negative feedback applied to an initially stable system. The error introduced by approximating the control force is represented by the difference between the coefficient matrices. It remains to determine whether this “error” causes Eq. (8.91) to become numerically unstable for particular combinations of \mathbf{K}_f and Δt , and therefore to generate homogeneous solutions that increase rather than decrease with time. In what follows, a strategy for determining the numerical stability of first-order matrix difference equations such as Eqs. (8.91) and (8.92) is presented. The approach is introduced using a simple scalar equation and is then generalized to handle an n^{th} -order equation.

Consider the first-order differential equation,

8.3. DISCRETE TIME FORMULATION: SDOF SYSTEMS

$$\dot{x} = ax + bf \quad (8.93)$$

where a and b are constants and $f = f(t)$. The exact solution is determined using Eq. (8.22):

$$x(t) = e^{a(t-t_0)}x(t_0) + \int_{t_0}^t e^{a(t-\tau)}bf(\tau)d\tau \quad (8.94)$$

This solution is bounded when $a < 0$. Specializing the limits for t leads to the difference form of Eq. (8.94):

$$x_{j+1} = e^{a\Delta t}x_j + \int_{t_j}^{t_{j+1}} e^{a(t_{j+1}-\tau)}bf(\tau)d\tau \quad (8.95)$$

The homogeneous solution is exact and therefore is bounded when the system is stable (i.e., when $a < 0$).

A similar solution procedure can be followed for the case where the forcing term, f , is a continuous function of x . Assuming linear negative feedback,

$$f(t) = -kx(t) \quad (8.96)$$

transforms Eq. (8.93) to

$$\dot{x} = (a - bk)x \quad (8.97)$$

The exact solution has the form

$$x_{j+1} = e^{(a-bk)\Delta t}x_j \quad (8.98)$$

This solution is bounded when $bk > a$. Normally we start with an initially stable system, ($a < 0$), and add negative feedback so that boundness is always ensured.

CHAPTER 8. STRUCTURAL CONTROL DYNAMICS

Eq. (8.98) is based on continuous feedback. The solution corresponding to the following discrete feedback

$$\begin{aligned} f(\tau) &= -kx_j \\ t_j \leq \tau \leq t_{j+1} \end{aligned} \tag{8.99}$$

is given by

$$x_{j+1} = cx_j \tag{8.100}$$

where

$$c = e^{a\Delta t} + \frac{bk}{a}(1 - e^{a\Delta t}) \tag{8.101}$$

Taking $j = 0, 1, 2, \dots$ leads to

$$x_j = (c)^j x_0 \tag{8.102}$$

For x_j to be bounded, the absolute magnitude of c must be less than 1.

$$\begin{aligned} |c| &< 1 \\ \Downarrow \\ \left| e^{a\Delta t} + \frac{bk}{a}(1 - e^{a\Delta t}) \right| &< 1 \end{aligned} \tag{8.103}$$

Eq. (8.103) represents a constraint on k and Δt . When the system is initially stable, a is negative,

$$a = -|a| \tag{8.104}$$

Specializing Eq. (8.103) for this case and noting that the negative value controls results in

8.3. DISCRETE TIME FORMULATION: SDOF SYSTEMS

$$\frac{kb}{|a|}(1 - e^{-|a|\Delta t}) - e^{-|a|\Delta t} < 1 \quad (8.105)$$

which is written as

$$\frac{kb}{|a|} < \frac{1 + e^{-|a|\Delta t}}{1 - e^{-|a|\Delta t}} \equiv \frac{k_{\max}b}{|a|} \quad (8.106)$$

Eq. (8.106) defines the maximum value of k for a particular value of Δt .

The variation of $k_{\max}b/|a|$ with $|a|\Delta t$ is shown in Fig. 8.10. For small $|a|\Delta t$, the curve tends to ∞ as $\Delta t \rightarrow 0$; for large $|a|\Delta t$, the curve is bounded by $k_{\max}b/|a| = 1$. If $kb/|a|$ is less than 1, there is no restriction on the magnitude of Δt . When $kb/|a|$ is greater than 1, the value of Δt has to satisfy Eq. (8.106). Using Fig. 8.10, we determine the limiting value of $|a|\Delta t$ corresponding to the specified value of $kb/|a|$. The range of allowable values for $|a|\Delta t$ is between zero and this limiting value. For example, suppose $kb/|a|$ is equal to 1.6. According to Fig. 8.10, the maximum allowable value of $|a|\Delta t$ is 1.4, and the range is $0 < |a|\Delta t < 1.4$.

According to the analysis just presented, the scalar equation, $x_{j+1} = cx_j$, is numerically stable when $|c| < 1$. The matrix equation, $\mathbf{X}_{j+1} = \mathbf{c}\mathbf{X}_j$, has a similar constraint involving the matrix, \mathbf{c} . Observing that \mathbf{X}_j can be expressed as

$$\mathbf{X}_j = \mathbf{c}^j \mathbf{X}_0 \quad (8.107)$$

it follows that the elements of \mathbf{c}^j must be bounded as $j \rightarrow \infty$. A measure for \mathbf{c}^j is established by noting that the expression,

$$\mathbf{X}_j = \rho^j \Psi \quad (8.108)$$

where ρ and Ψ satisfy the characteristic equation for \mathbf{c} ,

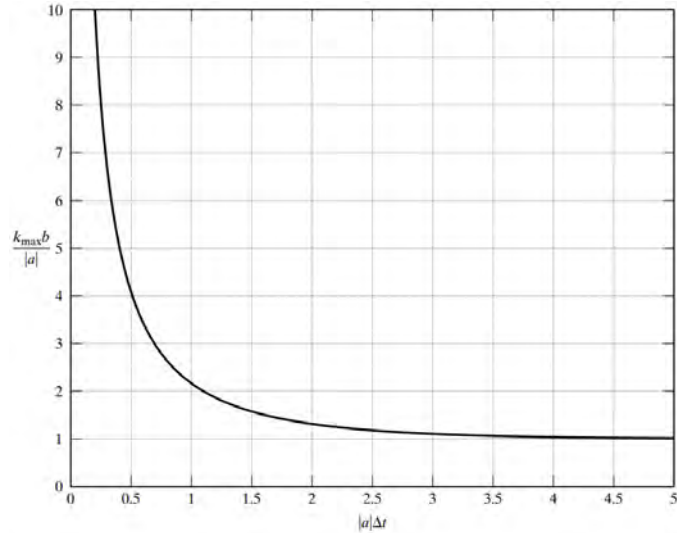


Figure 8.10: Stability limits for $x_{j+1} = cx_j$

$$(\mathbf{c} - \rho\mathbf{I})\Psi = \mathbf{0} \quad (8.109)$$

is a solution of $\mathbf{X}_{j+1} = \mathbf{c}\mathbf{X}_j$.

Suppose \mathbf{c} is of order 2. There are two eigensolutions that may be real or complex. When the solution is complex, the individual solutions are complex conjugates, and the total real solution is a linear combination of these j solutions,

$$\mathbf{X}_j = A\rho^j\Psi + \tilde{A}\tilde{\rho}^j\Psi \quad (8.110)$$

where A, \tilde{A} are complex constants. These constants are evaluated using the initial conditions for \mathbf{X}_0 .

$$\mathbf{X}_0 = A\Psi + \tilde{A}\Psi \quad (8.111)$$

Substituting for A and Ψ ,

8.3. DISCRETE TIME FORMULATION: SDOF SYSTEMS

$$\begin{aligned} A &= A_R + iA_I \\ \Psi &= \Psi_R + i\Psi_I \end{aligned} \tag{8.112}$$

results in two scalar equations for A_R and A_I .

$$2(A_R\Psi_R - A_I\Psi_I) = \mathbf{X}_0 \tag{8.113}$$

The complex eigenvalue can be expressed as

$$\rho = \rho_R + i\rho_I = \bar{\rho}e^{i\theta} \tag{8.114}$$

where $\bar{\rho}$ is the magnitude of ρ and θ is the polar angle.

$$\begin{aligned} \bar{\rho} &= (\rho_R^2 + \rho_I^2)^{1/2} \\ \tan \theta &= \frac{\rho_I}{\rho_R} \end{aligned} \tag{8.115}$$

Using the polar form for ρ , the j^{th} power is given by

$$\rho^j = (\bar{\rho})^j e^{i(j\theta)} \tag{8.116}$$

Introducing the expressions for A , Ψ , and ρ , the solution for \mathbf{X}_j expands to

$$\begin{aligned} \mathbf{X}_j &= (\bar{\rho})^j [2(A_R\Psi_R - A_I\Psi_I) \cos(j\theta) - 2(A_R\Psi_I + A_I\Psi_R) \sin(j\theta)] \\ & \qquad \qquad \qquad j = 1, 2, \dots \end{aligned} \tag{8.117}$$

Since the terms within the brackets are bounded, it follows that \mathbf{X}_j is finite as $j \rightarrow \infty$ when the modulus of ρ is less than unity,

$$\bar{\rho} < 1 \quad (8.118)$$

Extending this analysis to the case where \mathbf{c} is of order $2n$, there may be n pairs of complex conjugates solutions having the same form as Eq. (8.110), and the total solution is given by

$$\begin{aligned} \mathbf{X}_j &= \sum_{l=1}^n (A_l \rho_l^j \Psi_l + \tilde{A}_l \tilde{\rho}_l^j \tilde{\Psi}_l) \\ &= \sum_{l=1}^n (\bar{\rho}_l)^j [2(A_{R,l} \Psi_{R,l} - A_{I,l} \Psi_{I,l}) \cos(j\theta_l) \\ &\quad - 2(A_{R,l} \Psi_{I,l} + A_{I,l} \Psi_{R,l}) \sin(j\theta_l)] \end{aligned} \quad (8.119)$$

Defining $\bar{\rho}_{\max}$ as the maximum modulus for the set of eigenvalues of \mathbf{c} , the stability requirement is

$$\bar{\rho}_{\max} < 1 \quad (8.120)$$

This requirement also applies when some of the eigenvalues are real. For this case, the maximum absolute value must be less than unity.

In general, \mathbf{c} depends on the nature of the finite difference approximation, the system parameters, and the magnitude of the time step, Δt . For the case of time-invariant negative linear discrete feedback with no time delay, the form of \mathbf{c} follows from Eq. (8.87) specialized for no external loading:

$$\mathbf{x} = \mathbf{e}^{\mathbf{A}\Delta t} - \mathbf{A}^{-1}(\mathbf{e}^{\mathbf{A}\Delta t} - \mathbf{I})\mathbf{B}_f\mathbf{K}_f \quad (8.121)$$

Given \mathbf{A} , \mathbf{B}_f , and \mathbf{K}_f , we select a value for Δt , determine the corresponding eigenvalues of \mathbf{c} , and then adjust the value of Δt

8.3. DISCRETE TIME FORMULATION: SDOF SYSTEMS

if $\bar{\rho}_{\max}$ is greater than 1. The complexity of the equation for \mathbf{c} necessitates the use of a numerical eigenvalue routine such as the `eig()` function in MATLAB. The following example illustrates computational details and presents the stability limit for a SDOF system.

Example 8.2 - Stability analysis - SDOF system with no time delay

The various matrices for the SDOF case with negative velocity feedback are

$$\mathbf{A} = \begin{bmatrix} 0 & 1 \\ -\omega^2 & -2\xi\omega \end{bmatrix} \quad \mathbf{A}^{-1} = \begin{bmatrix} -\frac{2\xi}{\omega} & -\frac{1}{\omega^2} \\ 1 & 0 \end{bmatrix} \quad (8.122)$$

$$\mathbf{A}\Delta t = \begin{bmatrix} 0 & \frac{\omega\bar{\omega}}{\omega} \\ -\omega\bar{\omega} & -2\xi\bar{\omega} \end{bmatrix} \quad \mathbf{B}_f\mathbf{K}_f = \begin{bmatrix} 0 & 0 \\ 0 & \frac{k_v}{m} \end{bmatrix} \begin{bmatrix} 0 & 0 \\ 0 & 2\xi_a\omega \end{bmatrix}$$

where $\bar{\omega}$ is a dimensionless parameter.

$$\bar{\omega} = \omega\Delta t = 2\pi\frac{\Delta t}{T} \quad (8.123)$$

When $\xi = 0$, the expansion of $\mathbf{e}^{\mathbf{A}\Delta t}$ can be expressed as

$$\mathbf{e}^{\mathbf{A}\Delta t} = \cos \bar{\omega}\mathbf{I} + \left(\frac{1}{\omega} \sin \bar{\omega}\right) \mathbf{A} \quad (8.124)$$

Using Eq. (8.124), we can obtain analytical expressions for the elements of \mathbf{c} . The resulting form of \mathbf{c} is

$$\mathbf{c} = \begin{bmatrix} \cos \bar{\omega} & \frac{1}{\omega}(\sin \bar{\omega} + 2\xi_a(\cos \bar{\omega} - 1)) \\ -\omega \sin \bar{\omega} & \cos \bar{\omega} - 2\xi_a \sin \bar{\omega} \end{bmatrix} \quad (8.125)$$

Evaluating the eigenvalues of \mathbf{c} leads to

$$\begin{aligned}\rho_{1,2} &= b_1 \pm (b_1^2 - b_2)^{1/2} \\ b_1 &= \cos \bar{\omega} - \xi_a \sin \bar{\omega} \\ b_2 &= 1 - 2\xi_a \sin \bar{\omega}\end{aligned}\tag{8.126}$$

Eq. (8.126) shows that the eigenvalues depend on the dimensionless parameter, $\bar{\omega} = 2\pi(\Delta t/T)$, and the active damping ratio, ξ_a .

Fig. 8.11 contains plots of the absolute values of the eigenvalues versus $\Delta t/T$ for a representative range of ξ_a . The curves intersect at $\Delta t/T$, which corresponds to a transition in behavior. When $\Delta t/T \geq 0.5$, the eigenvalues are complex and $\bar{\rho} > 1$. For the range $0 < \Delta t/T < 0.5$, the eigenvalues start out as complex quantities and then shift over to real quantities at a particular value of $\Delta t/T$, which depends on ξ_a . The curve bifurcates at this value. When $\xi_a = 0$, the bifurcation occurs at $\Delta t/T = 0.5$. The intersection of the upper branch with $\bar{\rho} = 1$ defines the limiting value of $\Delta t/T$ for the corresponding value of ξ_a . This value corresponds to $\rho = -1$ and is related to ξ_a by $\cos \bar{\omega} - 2\xi_a \sin \bar{\omega} = -1$. Although $\bar{\rho} = 1$ for $\xi = 0$ and arbitrary $\Delta t/T$, the modulus is greater than 1 for $\xi_a > 0$ and $\Delta t/T > 0.5$. Therefore, $\Delta t/T = 0.5$ represents the limit for an undamped system.

The effect of including damping in the system is to offset the destabilizing effect of feedback. Fig. 8.12 illustrates this trend. Increasing ξ lowers $\bar{\rho}$ and decreases the range of $\bar{\omega}$ for which $\bar{\rho}$ is greater than 1. When $\xi_a \rightarrow 0$, \mathbf{c} reduces to $\mathbf{e}^{\mathbf{A}\Delta t}$. The eigenvalues of $\mathbf{e}^{\mathbf{A}\Delta t}$ are related to the eigenvalues of \mathbf{A} by

$$\rho = e^{\lambda\Delta t}\tag{8.127}$$

8.3. DISCRETE TIME FORMULATION: SDOF SYSTEMS

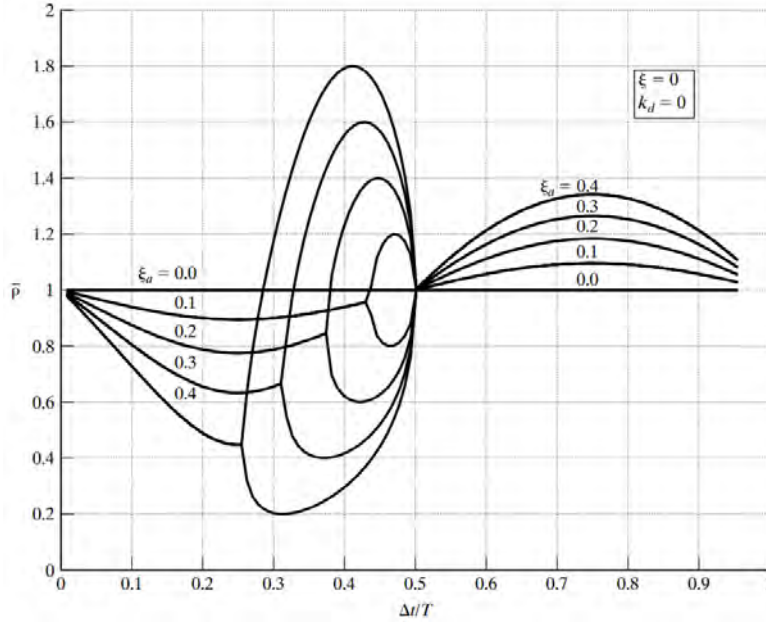


Figure 8.11

Noting that $\lambda = -\xi\omega \pm i(1 - \xi^2)\omega$, Eq. (8.127) expands to

$$\rho = e^{-\xi\bar{\omega}}(e^{\pm i(1-\xi^2)^{1/2}\bar{\omega}}) \quad (8.128)$$

and it follows that

$$\bar{\rho} = e^{-\xi\bar{\omega}} \quad (8.129)$$

Eq. (8.129) explains the trend for $\bar{\rho}$ to decrease with increasing $\bar{\omega}$. The second term in Eq. (8.128) is the source of the transition from real to complex eigenvalues. This shift occurs when $(1 - \xi^2)^{1/2}\bar{\omega} = \pi$.

The limits on $\Delta t/T$ depend on both ξ and ξ_a . As Fig. 8.12 shows, ξ has a significant effect on $\bar{\rho}$, particularly in the region $\Delta t/T > 0.5$. When $\xi = 0.1$, this region is stable even for $\xi_a = 0.4$, which represents significant active damping. A conservative

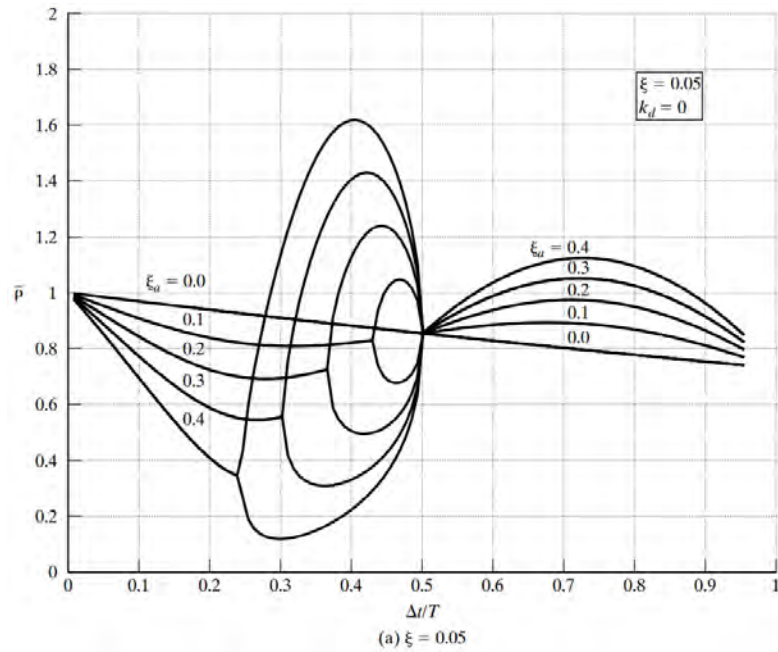


Figure 8.12

strategy would be to require $\Delta t/T$ to be less than the value for which the upper branch first intersects $\bar{\rho} = 1$. These values are listed in Table 8.1.

Table 8.1: Stability limit $\Delta t/T$

ξ	$\xi_a = 0$	$\xi_a = 0.1$	$\xi_a = 0.2$	$\xi_a = 0.3$	$\xi_a = 0.4$
0	0.50	0.44	0.38	0.33	0.29
0.05	∞	0.48	0.38	0.33	0.29
0.10	∞	∞	0.39	0.34	0.29

Fig. 8.13 illustrates the onset of instability for a SDOF system having $\mathbf{X}(0) = \{1, 0\}$. The discrete time history response is obtained by evaluating Eq. (8.91) for j ranging from 0 to 100. Increasing Δt from $0.33T$ to $0.34T$ causes the free vibration response of the initially displaced system to shift from stable to

8.3. DISCRETE TIME FORMULATION: SDOF SYSTEMS

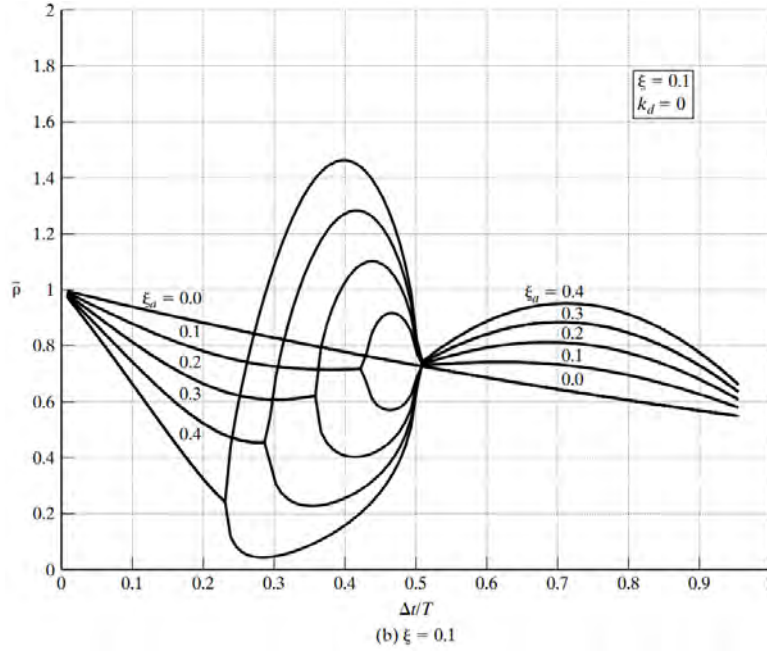


Figure 8.12

unstable behavior.

The stability analysis allowing for time delay starts with Eq. (8.91), which is written here in a simpler form:

$$\mathbf{X}_{j+1} = \mathbf{c}_1 \mathbf{X}_j + \mathbf{c}_3 \mathbf{X}_{j-\nu} \quad (8.130)$$

where

$$\mathbf{c}_1 = \mathbf{e}^{\mathbf{A}\Delta t} \quad (8.131)$$

$$\mathbf{c}_3 = -\mathbf{A}^{-1}(\mathbf{e}^{\mathbf{A}\Delta t} - \mathbf{I})\mathbf{B}_f \mathbf{K}_f \quad (8.132)$$

The previous analysis corresponds to $\nu = 0$ and $\mathbf{c}_1 + \mathbf{c}_3 = \mathbf{c}$. Given ν and the damping parameters, ξ and ξ_a , we need to establish the limiting value of the ratio of the time increment to the fundamental period, $\Delta t/T$. One option is to employ

CHAPTER 8. STRUCTURAL CONTROL DYNAMICS

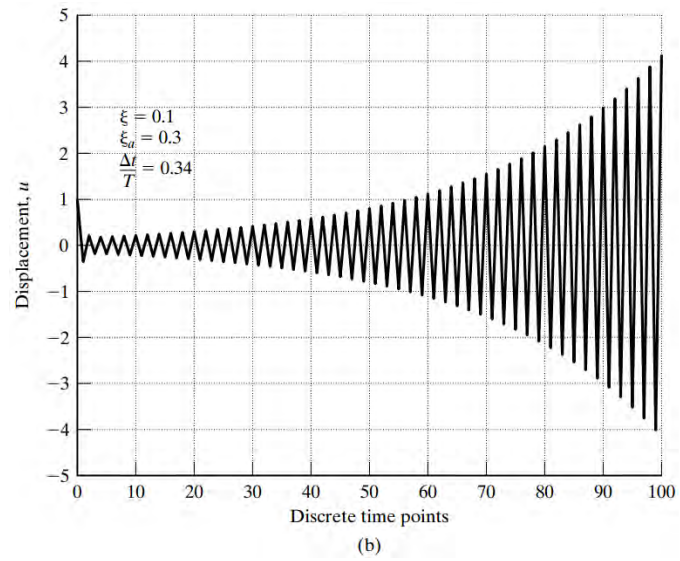
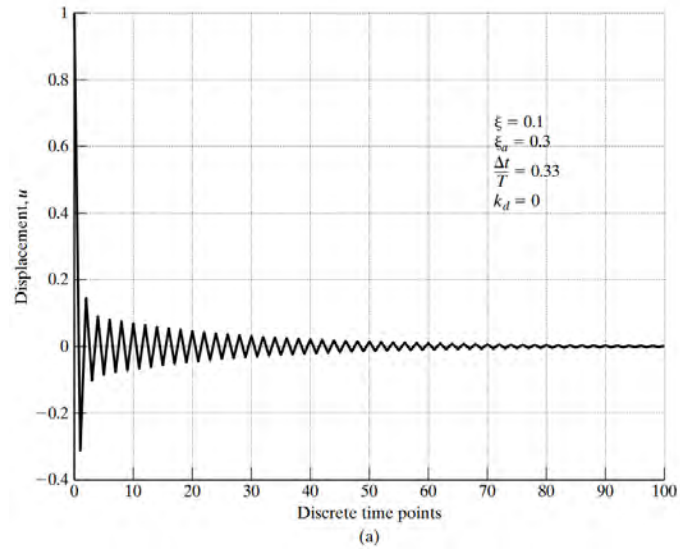


Figure 8.13

8.3. DISCRETE TIME FORMULATION: SDOF SYSTEMS

numerical simulation and solve Eq. (8.130) for a range of values of $\Delta t/T$. Fig. 8.14 illustrates the stability transition for $\nu = 1$ and a specific set of parameters. The corresponding results for $\nu = 0$ are shown in Fig. 8.13 of Ex. 8.2. In this case, the maximum time step is reduced by about 50%. The advantage of numerical simulation is that it allows arbitrary values of ξ , ξ_a , and ν to be considered. The disadvantage is that the search can be inefficient if the starting point is not reasonably close to the solution. We can start with the solution for $\nu = 0$ and decrease $\Delta t/T$. Another option is to utilize a simpler formulation based on $\xi = 0$ to generate an estimate of the starting value. The latter option is described next.

The solution of Eq. (8.130) can be expressed as

$$\mathbf{X}_j = \rho^j \Psi \quad (8.133)$$

where ρ is a complex scalar and Ψ is an unknown vector. In order for the solution to be stable, the absolute magnitude of ρ must be less than 1. Substituting for \mathbf{X}_j , Eq. (8.130) takes the following form:

$$(\mathbf{c}_3 + \rho^\nu \mathbf{c}_1 - \rho^{\nu+1} \mathbf{I}) \Psi = \mathbf{0} \quad (8.134)$$

When $\xi = 0$, the coefficient matrix reduces to (see Ex. 8.2)

$$\begin{bmatrix} \rho^\nu \cos \bar{\omega} - \rho^{\nu+1} & \rho^\nu \frac{\sin \bar{\omega}}{\omega} + 2\xi_a \frac{\cos \bar{\omega} - 1}{\omega} \\ -\rho^\nu \omega \sin \bar{\omega} & \rho^\nu \cos \bar{\omega} - 2\xi_a \sin \bar{\omega} - \rho^{\nu+1} \end{bmatrix} \quad (8.135)$$

For Ψ to have a nontrivial value, the determinant of the coefficient matrix must vanish. Enforcing this requirement leads to an equation of degree $\nu + 2$ in ρ :

CHAPTER 8. STRUCTURAL CONTROL DYNAMICS

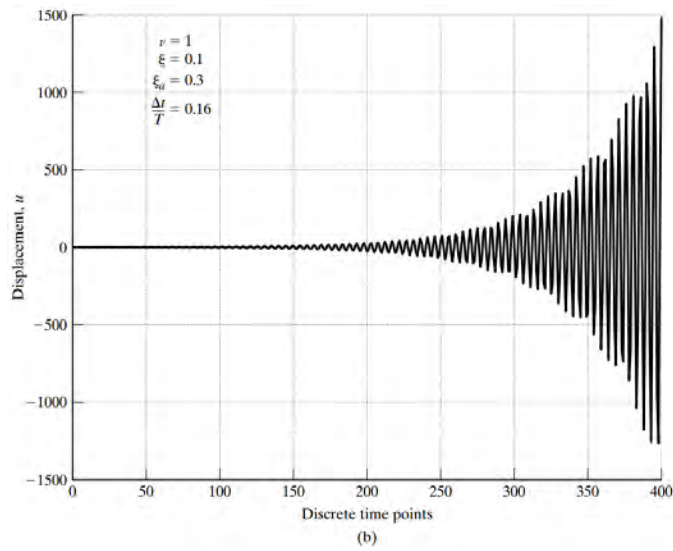
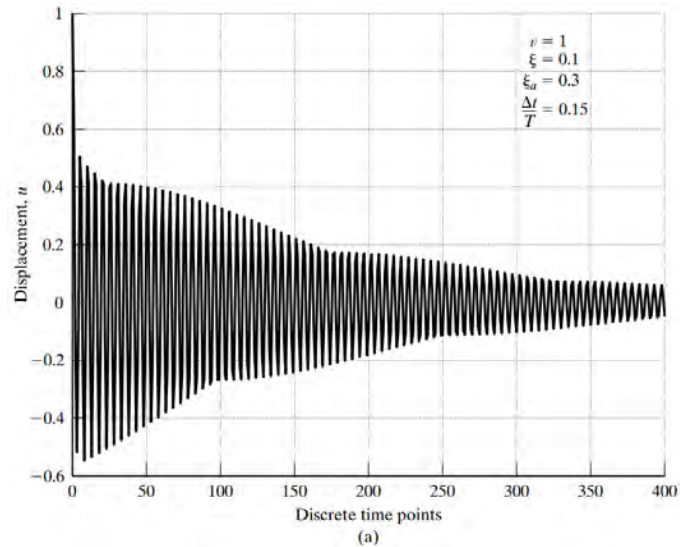


Figure 8.14: Illustration of instability due to time delay.

8.3. DISCRETE TIME FORMULATION: SDOF SYSTEMS

$$p(\rho) = \rho^{\nu+2} + a\rho^{\nu+1} + \rho^\nu + b\rho - b = 0 \quad (8.136)$$

where

$$\begin{aligned} a &= -2 \cos \bar{\omega} \\ b &= 2\xi_a \sin \bar{\omega} \end{aligned} \quad (8.137)$$

Given ν and ξ_a , we evaluate the roots of $p(\rho) = 0$ for a representative range of $\bar{\omega} = 2\pi(\Delta t/T)$. The following example illustrates this computation.

Example 8.3 - Stability analysis - SDOF system with time delay

Fig. 8.15 contains plots of $\bar{\rho}$ versus $\Delta t/T$ for a range of ξ_a and $\nu = 1, 2$. As expected, increasing the time delay lowers the magnitude of the time interval at which instability occurs. The effect of time delay becomes more significant as the active damping is increased. Table 8.2 contains the limiting values of $\Delta t/T$ for $\xi = 0$ and ξ_a ranging up to 0.4. Both active damping and time delay result in a decrease in the allowable time step. Including passive damping has the opposite effect on the time increment (i.e., it increases the allowable time increment). For example, the critical time step ratio for $\nu = 1$, $\xi_a = 0.3$ is 0.15 for $\xi = 0.1$ versus 0.124 for $\xi = 0$.

The actual time increment is governed by the responses of the monitoring and actuator systems. Given data on these response times, we can evaluate the expected ratio, $\Delta t/T$, for a particular system and determine, using Table 8.2 as a starting point for numerical simulation, whether stability will be a problem.

CHAPTER 8. STRUCTURAL CONTROL DYNAMICS

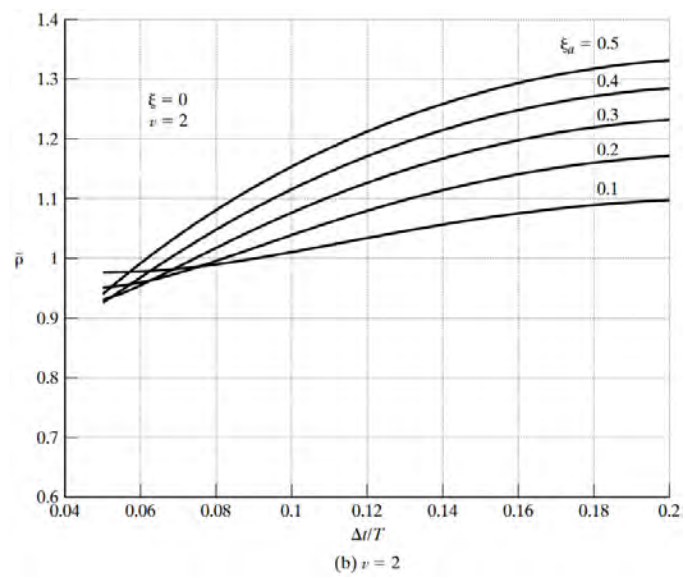
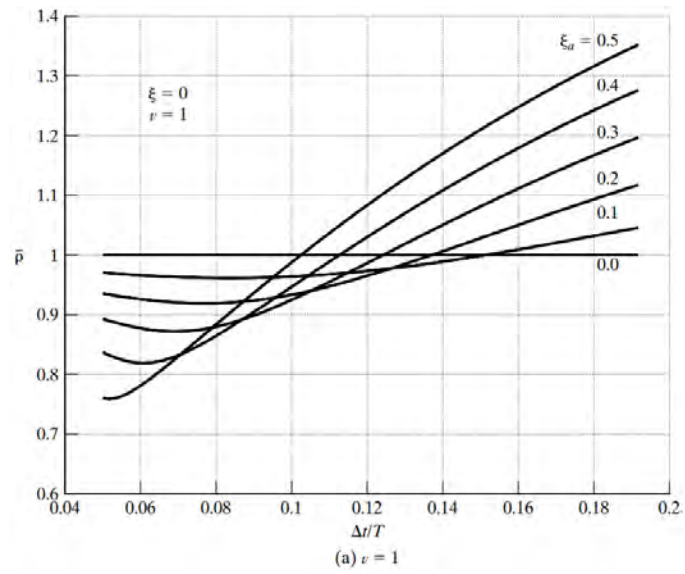


Figure 8.15

8.4. STATE-SPACE FORMULATION FOR MDOF SYSTEMS

Table 8.2: Limiting values of $\Delta t/T$ for $\xi = 0$

ξ_a	Stability limit for $\Delta t/T$		
	$\nu = 0$	$\nu = 1$	$\nu = 2$
0	0.50	0.500	0.5000
0.05		0.158	0.0955
0.10	0.44	0.151	0.0908
0.15		0.144	0.0860
0.20	0.38	0.137	0.0822
0.25		0.131	0.0780
0.30	0.33	0.124	0.0745
0.35		0.118	0.07085
0.40	0.29	0.113	0.0677

8.4 State-Space Formulation for MDOF Systems

8.4.1 Notation and Governing Equations

The material presented in the previous sections can be readily extended to the case of a multi-degree-of-freedom system. We have only to generalize the definition equations for the various matrices involved in the state-space representation. In what follows, the essential steps for an n^{th} -order linear system are discussed.

Using the notation defined in Chapter 2, the equations for an n^{th} -order linear system subjected to seismic excitation and a set of r control forces applied at various locations on the system are written as

$$\mathbf{M}\ddot{\mathbf{U}} + \mathbf{C}\dot{\mathbf{U}} + \mathbf{K}\mathbf{U} = -\mathbf{M}\mathbf{E}a_g + \mathbf{E}_f\mathbf{F} + \mathbf{P} \quad (8.138)$$

where \mathbf{E}_f is an $n \times r$ matrix that defines the location of the control forces with respect to the degrees of freedom. Fig. 8.16 illustrates the notation for the case of a lumped mass model of a

CHAPTER 8. STRUCTURAL CONTROL DYNAMICS

shear beam having four degrees of freedom and two control forces. The initial conditions involve constraints on the displacements and velocities at time $t = 0$.

$$\begin{aligned} \mathbf{U}(0) &= \mathbf{U}_0 \\ \dot{\mathbf{U}}(0) &= \dot{\mathbf{U}}_0 \end{aligned} \quad (8.139)$$

Following the approach of Sect. 8.2, the state-space form for Eq. (8.138) is taken as

$$\dot{\mathbf{X}} = \mathbf{A}\mathbf{X} + \mathbf{B}_f\mathbf{F} + \mathbf{B}_g a_g + \mathbf{B}_p \mathbf{P} \quad (8.140)$$

where \mathbf{X} is now a vector of order $2n$,

$$\mathbf{X} = \begin{bmatrix} \mathbf{U} \\ \dot{\mathbf{U}} \end{bmatrix} \quad (8.141)$$

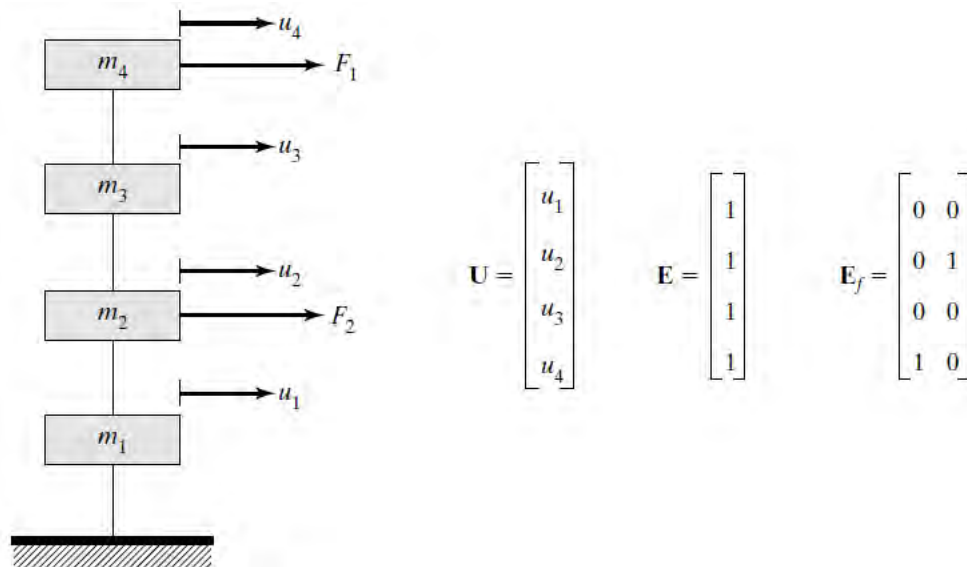


Figure 8.16: 4DOF system with two control forces.

8.4. STATE-SPACE FORMULATION FOR MDOF SYSTEMS

and the coefficient matrices are given by

$$\mathbf{A} = \begin{bmatrix} \mathbf{0} & \mathbf{I} \\ -\mathbf{M}^{-1}\mathbf{K} & -\mathbf{M}^{-1}\mathbf{C} \end{bmatrix} \quad (2n \times 2n) \quad (8.142)$$

$$\mathbf{B}_f = \begin{bmatrix} \mathbf{0} \\ \mathbf{M}^{-1}\mathbf{E}_f \end{bmatrix} \quad (2n \times r) \quad (8.143)$$

$$\mathbf{B}_g = \begin{bmatrix} \mathbf{0} \\ -\mathbf{E} \end{bmatrix} \quad (2n \times 1) \quad (8.144)$$

$$\mathbf{B}_p = \begin{bmatrix} \mathbf{0} \\ \mathbf{M}^{-1} \end{bmatrix} \quad (2n \times 1) \quad (8.145)$$

8.4.2 Free Vibration Response: Time-Invariant Uncontrolled System

Specializing Eq. (8.140) for no external forcing leads to a set of $2n$ homogeneous first-order differential equations.

$$\dot{\mathbf{X}} = \mathbf{A}\mathbf{X} \quad (8.146)$$

Considering \mathbf{A} to be constant, the general solution has the form

$$\mathbf{X} = e^{\lambda t}\mathbf{V} \quad (8.147)$$

where λ and \mathbf{V} satisfy the following set of $2n$ homogeneous algebraic equations:

$$[\mathbf{A} - \lambda\mathbf{I}]\mathbf{V} = 0 \quad (8.148)$$

Substituting for \mathbf{A} , Eq. (8.148) expands to

$$\begin{bmatrix} -\lambda \mathbf{I} & \mathbf{I} \\ -\mathbf{M}^{-1} \mathbf{K} & -\mathbf{M}^{-1} \mathbf{C} - \lambda \mathbf{I} \end{bmatrix} \mathbf{V} = 0 \quad (8.149)$$

The solution of Eq. (8.149) has the form

$$\mathbf{V} = \begin{Bmatrix} \Phi \\ \lambda \Phi \end{Bmatrix} \quad (8.150)$$

where λ and Φ are constrained by n conditions,

$$\lambda^2 \Phi + \lambda \mathbf{M}^{-1} \mathbf{C} \Phi + \mathbf{M}^{-1} \mathbf{K} \Phi = \mathbf{0} \quad (8.151)$$

For the SDOF case, the complete solution of Eq. (8.151) consists of two solutions involving a pair of complex roots for λ :

$$\begin{aligned} \lambda &= \lambda_1 & \Phi &= 1 \\ \lambda &= \tilde{\lambda}_1 & \Phi &= 1 \end{aligned} \quad (8.152)$$

There are four solutions involving two pairs of complex roots:

$$\begin{aligned} \lambda &= \lambda_1, \tilde{\lambda}_1 & \Phi &= \Phi_1, \tilde{\Phi}_1 \\ \text{and} & & & \\ \lambda &= \lambda_2, \tilde{\lambda}_2 & \Phi &= \Phi_2, \tilde{\Phi}_2 \end{aligned} \quad (8.153)$$

Then, for an n^{th} -order system, it follows that there are $2n$ complex solutions involving n pairs of complex roots.

$$\begin{aligned} \lambda &= \lambda_1, \tilde{\lambda}_1, \lambda_2, \tilde{\lambda}_2, \dots, \lambda_n, \tilde{\lambda}_n \\ \Phi &= \Phi_1, \tilde{\Phi}_1, \Phi_2, \tilde{\Phi}_2, \dots, \Phi_n, \tilde{\Phi}_n \\ \mathbf{V} &= \left\{ \begin{Bmatrix} \Phi_1 \\ \lambda_1 \Phi_1 \end{Bmatrix}, \begin{Bmatrix} \tilde{\Phi}_1 \\ \tilde{\lambda}_1 \tilde{\Phi}_1 \end{Bmatrix}, \dots, \begin{Bmatrix} \Phi_n \\ \lambda_n \Phi_n \end{Bmatrix}, \begin{Bmatrix} \tilde{\Phi}_n \\ \tilde{\lambda}_n \tilde{\Phi}_n \end{Bmatrix} \right\} \end{aligned} \quad (8.154)$$

Each term in Eq. (8.154) is complex:

8.4. STATE-SPACE FORMULATION FOR MDOF SYSTEMS

$$\begin{aligned}
 \lambda_j &= \lambda_{R,j} + i\lambda_{I,j} \\
 \Phi_j &= \Phi_{R,j} + i\Phi_{I,j} \\
 \mathbf{V}_j &= \mathbf{V}_{R,j} + i\mathbf{V}_{I,j}
 \end{aligned}
 \tag{8.155}$$

The complete solution is obtained by combining the $2n$ solutions using complex constants, A_j and \tilde{A}_j .

$$\mathbf{X} = \sum_{j=1}^n (A_j e^{\lambda_j t} \mathbf{V}_j + \tilde{A}_j e^{\bar{\lambda}_j t} \tilde{\mathbf{V}}_j)
 \tag{8.156}$$

Substituting for A_j and $e^{\lambda_j t}$,

$$\begin{aligned}
 A_j &= \frac{1}{2} (A_{R,j} + iA_{I,j}) \\
 e^{\lambda_j t} &= e^{\lambda_{R,j} t} (\cos \lambda_{I,j} t + i \sin \lambda_{I,j} t)
 \end{aligned}
 \tag{8.157}$$

transforms Eq. (8.156) to

$$\begin{aligned}
 \mathbf{X}(t) &= \sum_{j=1}^n e^{\lambda_{R,j} t} [(A_{R,j} \mathbf{V}_{R,j} - A_{I,j} \mathbf{V}_{I,j}) \cos \lambda_{I,j} t \\
 &\quad - (A_{R,j} \mathbf{V}_{I,j} + A_{I,j} \mathbf{V}_{R,j}) \sin \lambda_{I,j} t]
 \end{aligned}
 \tag{8.158}$$

We determine $A_{R,j}$ and $A_{I,j}$ using the initial conditions on \mathbf{X} at time $t = 0$. This computation is discussed in the next section. Stability requires the homogeneous solutions to be bounded. Noting Eq. (8.158), a system having n DOF is stable when

$$\lambda_{R,j} < 0 \quad j = 1, 2, \dots, n
 \tag{8.159}$$

The free vibration solution given by Eq. (8.156) can also be expressed as

$$\mathbf{X}(t) = \mathbf{e}^{\mathbf{A}t}\mathbf{X}(0) \quad (8.160)$$

where \mathbf{A} is defined by Eq. (8.142) and $\mathbf{e}^{\mathbf{A}t}$ is generated with the following series:

$$\mathbf{e}^{\mathbf{A}t} = \mathbf{I} + \mathbf{A}t + \frac{1}{2}\mathbf{A}\mathbf{A}t^2 + \dots + \frac{1}{n!}\mathbf{A}^n t^n \quad (8.161)$$

Eq. (8.160) is a generalized form of the SDOF solution. We can establish this result by specializing Eq. (8.156) for $t = 0$,

$$\mathbf{X}(0) = \sum_{j=1}^n (A_j \mathbf{V}_j + \tilde{A}_j \tilde{\mathbf{V}}_j) \quad (8.162)$$

and noting that

$$\begin{aligned} \mathbf{e}^{\mathbf{A}t}\mathbf{V}_j &= e^{\lambda_j t}\mathbf{V}_j \\ \mathbf{e}^{\mathbf{A}t}\tilde{\mathbf{V}}_j &= e^{\tilde{\lambda}_j t}\tilde{\mathbf{V}}_j \end{aligned} \quad (8.163)$$

Example 8.4 - Free vibration solution for proportional damping

Consider Eq. (8.151) pre-multiplied by \mathbf{M} .

$$\lambda^2 \mathbf{M}\Phi + \lambda \mathbf{C}\Phi + \mathbf{K}\Phi = \mathbf{0} \quad (8.164)$$

Suppose \mathbf{C} is a linear function of \mathbf{K} and \mathbf{M}

$$\mathbf{C} = \alpha \mathbf{K} + \beta \mathbf{M} \quad (8.165)$$

Substituting for \mathbf{C} results in

$$\left(\frac{\lambda^2 + \beta\lambda}{1 + \alpha\lambda} \right) \mathbf{M}\Phi + \mathbf{K}\Phi = \mathbf{0} \quad (8.166)$$

8.4. STATE-SPACE FORMULATION FOR MDOF SYSTEMS

When the coefficient of $\mathbf{M}\Phi$ is expressed as

$$\frac{\lambda^2 + \beta\lambda}{1 + \alpha\lambda} = -|\omega|^2 \quad (8.167)$$

eq. (8.166) takes the form of the classical eigenvalue equation.

$$\mathbf{K}\Phi = |\omega|^2 \mathbf{M}\Phi \quad (8.168)$$

There are n eigensolutions to Eq. (8.168):

$$\begin{array}{l} |\omega_1|^2, |\omega_2|^2, \dots, |\omega_n|^2 \\ \Phi_1, \Phi_2, \dots, \Phi_n \end{array} \quad (8.169)$$

All the eigenvectors are *real* vectors. Also, all the eigenvalues are positive real quantities.

$$|\omega_j|^2 > 0 \quad (8.170)$$

Given $|\omega_j|^2$, we solve Eq. (8.167) for λ_j . The pair of complex roots are written as

$$\lambda_j, \tilde{\lambda}_j = -\xi_j |\omega_j| \pm i |\omega_j| \{1 - \xi_j^2\}^{1/2} \quad (8.171)$$

where the damping ratio is related to α and β by

$$\xi_j = \frac{\beta + \alpha |\omega_j|^2}{2 |\omega_j|} \quad (8.172)$$

In what follows, ω_j is considered to be positive, and $|\omega_j|$ is set equal to ω_j .

The eigenvectors, Φ_j , are real and satisfy the following orthogonality relationships:

$$\Phi_j^T \mathbf{M} \Phi_k = \delta_{jk} \tilde{m}_k \quad (8.173)$$

$$\Phi_j^T \mathbf{K} \Phi_k = \delta_{jk} \omega_k^2 \tilde{m}_k \quad (8.174)$$

Since Φ is real, the state eigenvector, \mathbf{V} , has the following form:

$$\mathbf{V}_j = \begin{Bmatrix} \Phi_j \\ \lambda_j \Phi_j \end{Bmatrix} = \begin{Bmatrix} \Phi_j \\ \lambda_{R,j} \Phi_j \end{Bmatrix} + i \begin{Bmatrix} 0 \\ \lambda_{I,j} \Phi_j \end{Bmatrix} \quad (8.175)$$

Undamped free vibration response is the special case where $\alpha = \beta = 0$. The corresponding solution is

$$\lambda_j = \pm i \omega_j \quad (8.176)$$

$$\mathbf{V}_j = \begin{Bmatrix} \Phi_j \\ 0 \end{Bmatrix} + i \begin{Bmatrix} 0 \\ \omega_j \Phi_j \end{Bmatrix} \quad (8.177)$$

Example 8.5 - General uncoupled damping

The previous example dealt with the case where the damping matrix is a linear combination of the mass and stiffness matrices. This approach can be extended to deal with a more general form of \mathbf{C} . Suppose \mathbf{C} satisfies the following orthogonality conditions:

$$\Phi_j^T \mathbf{C} \Phi_k = 2 \delta_{jk} \tilde{m}_k \omega_k \xi_k \quad j = 1, 2, \dots, r \quad (8.178)$$

where ξ_k are now considered to be independent parameters. The free vibration solution is the same as presented in Ex. 8.4.

$$\begin{aligned} \lambda_j &= -\xi_j \omega_j \pm i \omega_j [1 - \xi_j^2]^{1/2} \\ \mathbf{V}_j &= \begin{Bmatrix} \Phi_j \\ \lambda_j \Phi_j \end{Bmatrix} \\ \mathbf{K} \Phi_j &= \omega_j^2 \mathbf{M} \Phi_k \end{aligned} \quad (8.179)$$

8.4. STATE-SPACE FORMULATION FOR MDOF SYSTEMS

The ability to specify independently the modal damping ratio for the first r modes by adjusting \mathbf{C} is very convenient since it allows us to deal more effectively with the problem of suppressing the response of a particular subset of modes contained within this group.

The form of \mathbf{C} that satisfies Eq. (8.178) is established by noting the following identities:

$$\begin{aligned}\Phi_j^T \mathbf{M} (\mathbf{M}^{-1} \mathbf{K})^n \Phi_k &= \omega_j^{2n} \tilde{m}_j \delta_{jk} \\ \Phi_j^T \mathbf{K} (\mathbf{M}^{-1} \mathbf{K})^n \Phi_k &= \omega_j^{2n+2} \tilde{m}_j \delta_{jk}\end{aligned}\quad (8.180)$$

A linear combination of these matrices is a candidate solution.

$$\mathbf{C} = \sum_{n=0}^s [a_n (\mathbf{M} (\mathbf{M}^{-1} \mathbf{K})^n) + b_n (\mathbf{K} (\mathbf{M}^{-1} \mathbf{K})^n)] \quad (8.181)$$

Taking $s = 0$ corresponds to Rayleigh damping. Taking $s \leq r$ allows us to specify r modal damping ratios. The coefficients for this case are determined with

$$\sum_{n=0}^s (a_n \omega_j^{2n-1} + b_n \omega_j^{2n+1}) = 2\xi_j \quad j = 1, 2, \dots, r \quad (8.182)$$

If both a and b are used, $s = r/2$.

The basic problem with this approach is the form of \mathbf{C} generated with Eq. (8.180). The coupling between the off-diagonal elements extends beyond adjacent nodes when $n \geq 1$. This pattern requires a deployment of dampers that involves connecting dampers to nodes that are not adjacent (e.g., a damper between floor 1 and floor 3). Realistically, the required pattern cannot be achieved.

8.4.3 Orthogonality Properties of the State Eigenvectors

The eigenvector \mathbf{V}_j satisfies Eq. (8.148).

$$\mathbf{A}\mathbf{V}_j = \lambda_j\mathbf{V}_j \quad (8.183)$$

Since \mathbf{A} is not symmetrical, \mathbf{V}_j is not orthogonal to \mathbf{V}_k .

$$\mathbf{V}_j^T\mathbf{V}_k \neq \delta_{jk} \quad (8.184)$$

A set of vectors that are orthogonal to \mathbf{V} can be established by considering the eigenvalue problem for the transpose of \mathbf{A} :

$$\mathbf{A}^T\mathbf{W}_j = \lambda_j^*\mathbf{W}_j \quad (8.185)$$

where λ^* , \mathbf{W} represent the eigenvalue and corresponding eigenvector for \mathbf{A}^T . Eq. (8.185) requires the determinant of the coefficient matrix to vanish.

$$|\mathbf{A}^T - \lambda^*\mathbf{I}| = 0 \quad (8.186)$$

Noting that the determinant of the transpose of a matrix is equal to the determinant of the original matrix,

$$|\mathbf{b}| \equiv |\mathbf{b}^T| \quad (8.187)$$

it follows that

$$\lambda_j^* \equiv \lambda_j \quad (8.188)$$

and Eq. (8.185) is equivalent to

$$\mathbf{A}^T\mathbf{W}_j = \lambda_j\mathbf{W}_j \quad (8.189)$$

Starting with

8.4. STATE-SPACE FORMULATION FOR MDOF SYSTEMS

$$\begin{aligned} \mathbf{A}\mathbf{V}_j &= \lambda_j \mathbf{V}_j & k \neq j \\ \mathbf{A}^T \mathbf{W}_k &= \lambda_k \mathbf{W}_k \end{aligned} \quad (8.190)$$

and pre-multiplying the first equation with \mathbf{W}_k and the second with \mathbf{V}_j , we obtain

$$\mathbf{W}_k^T \mathbf{A} \mathbf{V}_j = \lambda_j \mathbf{W}_k^T \mathbf{V}_j \quad (8.191)$$

$$\mathbf{V}_j^T \mathbf{A}^T \mathbf{W}_k = \lambda_k \mathbf{V}_j^T \mathbf{W}_k \quad (8.192)$$

Eq. (8.192) can be written as

$$\mathbf{W}_k^T \mathbf{A} \mathbf{V}_j = \lambda_k \mathbf{W}_k^T \mathbf{V}_j \quad (8.193)$$

Then subtracting Eq. (8.191) from (8.193) results in

$$0 = (\lambda_k - \lambda_j) \mathbf{W}_k^T \mathbf{V}_j \quad (8.194)$$

According to Eq. (8.194), \mathbf{W}_k and \mathbf{V}_j are orthogonal:

$$\mathbf{W}_k^T \mathbf{V}_j = 0 \quad \text{for} \quad j \neq k \quad (8.195)$$

The result for $j = k$ is written as

$$\mathbf{W}_j^T \mathbf{V}_j = f_j \quad (8.196)$$

One can show that

$$\begin{aligned} \tilde{\mathbf{W}}_k^T \mathbf{V}_j &= 0 \\ \mathbf{W}_k^T \tilde{\mathbf{V}}_j &= 0 \quad \forall j, k \end{aligned} \quad (8.197)$$

and

$$\tilde{\mathbf{W}}_j^T \tilde{\mathbf{V}}_j = \tilde{f}_j \quad (8.198)$$

Example 8.6 - Initial conditions - free vibration response

Consider the general free vibration solution defined by Eq. (8.156).

$$\mathbf{X}(t) = \sum_{j=1}^n (A_j e^{\lambda_j t} \mathbf{V}_j + \tilde{A}_j e^{\tilde{\lambda}_j t} \tilde{\mathbf{V}}_j) \quad (8.199)$$

The integration constants are determined using the initial conditions on \mathbf{X} at $t = 0$.

$$\mathbf{X}(0) = \sum_{j=1}^n (A_j \mathbf{V}_j + \tilde{A}_j \tilde{\mathbf{V}}_j) \quad (8.200)$$

Noting the orthogonality relations, the expressions for the constants are

$$\begin{aligned} A_j &= \frac{1}{f_j} \mathbf{W}_j^T \mathbf{X}(0) \\ \tilde{A}_j &= \frac{1}{\tilde{f}_j} \tilde{\mathbf{W}}_j^T \mathbf{X}(0) \end{aligned} \quad (8.201)$$

8.4.4 Determination of \mathbf{W} and f_j

We establish \mathbf{W} by solving the following eigenvalue problem:

$$\mathbf{A}^T \mathbf{W} = \lambda \mathbf{W} \quad (8.202)$$

8.4. STATE-SPACE FORMULATION FOR MDOF SYSTEMS

Substituting for \mathbf{A}^T , the coefficient matrix expands to

$$\begin{bmatrix} -\lambda\mathbf{I} & -\mathbf{KM}^{-1} \\ \mathbf{I} & -\mathbf{CM}^{-1} - \lambda\mathbf{I} \end{bmatrix} \mathbf{W} = \mathbf{0} \quad (8.203)$$

Expressing \mathbf{W} in partitioned form,

$$\mathbf{W} = \begin{Bmatrix} \mathbf{W}_1 \\ \mathbf{W}_2 \end{Bmatrix} \quad (8.204)$$

and expanding Eq. (8.203) leads to

$$\begin{aligned} -\lambda\mathbf{W}_1 - \mathbf{KM}^{-1}\mathbf{W}_2 &= \mathbf{0} \\ \mathbf{W}_1 - \mathbf{CM}^{-1}\mathbf{W}_2 - \lambda\mathbf{W}_2 &= \mathbf{0} \end{aligned} \quad (8.205)$$

Solving the first equation for \mathbf{W}_2 ,

$$\mathbf{W}_2 = -\lambda\mathbf{MK}^{-1}\mathbf{W}_1 \quad (8.206)$$

and substituting into the second equation results in

$$\mathbf{W}_1 = -\lambda\mathbf{CK}^{-1}\mathbf{W}_1 - \lambda^2\mathbf{MK}^{-1}\mathbf{W}_1 \quad (8.207)$$

This equation can be transformed to a form similar to the eigenequation for Φ by expressing \mathbf{W}_1 as

$$\mathbf{W}_1 = \mathbf{K}\bar{\mathbf{W}}_1 \quad (8.208)$$

The result is

$$\lambda^2\mathbf{M}\bar{\mathbf{W}}_1 + \lambda\mathbf{C}\bar{\mathbf{W}}_1 + \mathbf{K}\bar{\mathbf{W}}_1 = \mathbf{0} \quad (8.209)$$

Comparing this form with Eq. (8.151) shows that

$$\bar{\mathbf{W}}_1 \equiv \Phi \quad (8.210)$$

It follows that the forms of \mathbf{V}_j and \mathbf{W}_j are related by

$$\mathbf{W}_j = \left\{ \begin{array}{c} \mathbf{K}\Phi_j \\ -\lambda_j\mathbf{M}\Phi_j \end{array} \right\} \quad \mathbf{V}_j = \left\{ \begin{array}{c} \Phi_j \\ -\lambda_j\Phi_j \end{array} \right\} \quad (8.211)$$

Using these expressions, the definition equation for f expands to

$$\begin{aligned} f_j &= \mathbf{W}_j^T \mathbf{V}_j = \Phi_j^T \mathbf{K} \Phi_j - \lambda_j^2 \Phi_j^T \mathbf{M} \Phi_j \\ &= -2\lambda_j^2 \Phi_j^T \mathbf{M} \Phi_j - \lambda_j \Phi_j^T \mathbf{C} \Phi_j \end{aligned} \quad (8.212)$$

When \mathbf{C} is proportional to either \mathbf{K} or \mathbf{M} , Φ is real and f_j is given by

$$f_j = \tilde{m}_j(\omega_j^2 - \lambda_j^2) \quad (8.213)$$

The value for no damping is $f_j = 2\tilde{m}_j\omega_j^2$.

8.4.5 General Solution: Time-Invariant System

Following the approach employed for the SDOF case, the general solution for an arbitrary loading applied to a time invariant MDOF system can be expressed as a Duhamel integral involving the free vibration response. Noting Eqs. (8.140) and (8.160), the complete solution has the form

$$\mathbf{X}(t) = \mathbf{e}^{\mathbf{A}(t-t_0)} \mathbf{X}_0 + \int_{t_0}^t \mathbf{e}^{\mathbf{A}(t-\tau)} (\mathbf{B}_f \mathbf{F} + \mathbf{B}_p \mathbf{P} + \mathbf{B}_g a_g) d\tau \quad (8.214)$$

where the coefficient matrices (\mathbf{A} , \mathbf{B}_f , \mathbf{B}_p , \mathbf{B}_g) are defined by Eqs. (8.142) to (8.145). This equation is similar to the SDOF solution given by Eq. (8.27); we have only to introduce the

8.4. STATE-SPACE FORMULATION FOR MDOF SYSTEMS

appropriate forms of \mathbf{A} , \mathbf{B}_f , \mathbf{B}_p , and \mathbf{B}_g . The discrete time equilibrium equation for the MDOF case follows from Eq. (8.82).

$$\mathbf{X}_{j+1} = \mathbf{e}^{\mathbf{A}\Delta t}\mathbf{X}_j + \mathbf{A}^{-1}(\mathbf{e}^{\mathbf{A}\Delta t} - \mathbf{I})[\mathbf{B}_g a_{g,i} + \mathbf{B}_f \mathbf{F}_j + \mathbf{B}_p \mathbf{P}_j] \quad (8.215)$$

Working with the full set of equations for an n^{th} -order system requires dealing with matrices of order $2n$. As n increases, the computational costs for $\mathbf{e}^{\mathbf{A}\Delta t}$ and \mathbf{A}^{-1} become excessive, and we need to consider an alternative approach. In conventional dynamic analysis, this reduction in computational effort is achieved by expressing the state vector as a linear combination of prescribed modal vectors multiplied by unknown coordinate variables that are functions of time. The conventional modal formulation is treated in Sect. 3.2. Depending on the nature of the loading, one can obtain a reasonably accurate solution by suitably selecting the participating modes so as to minimize the required number of modal coordinate functions, and consequently reduce the computational cost. Interpreting the total response as a superposition of modal responses is also useful from the perspective of active control. A key issue of active control is the optimal location of active forces so as to minimize the response of a particular mode. In what follows, the state-space formulation of the governing equations in terms of modal coordinates is presented.

This formulation is used later to establish the form of control algorithms in terms of modal coordinates.

8.4.6 Modal State-Space Formulation: Uncoupled Damping

We start with a brief review of the conventional modal expansion approach described in Sect. 3.2. The displacement vector is expressed as a linear combination of a subset of the eigenvectors for the undamped system scaled with functions of time.

$$\mathbf{U}(t) = \sum_{j=1}^s q_j(t) \Phi_j \quad (8.216)$$

Assuming the system has n DOF, this expression will produce the exact solution when s is taken to be n . Substituting for $\mathbf{U}(t)$ in the force equilibrium equation, pre-multiplying the result with Φ_k , and noting the orthogonality conditions for Φ_k , we obtain s equations having the following form:

$$\begin{aligned} \tilde{m}_k \ddot{q}_k + \sum_{j=1}^p (\Phi_k^T \mathbf{C} \Phi_j) \dot{q}_j + \tilde{m}_k \omega_k^2 q_k \\ = -\Phi_k^T \mathbf{M} \mathbf{E} a_g + \Phi_k^T \mathbf{P} + \Phi_k^T \mathbf{E}_f \mathbf{F} \quad k = 1, 2, \dots, s \end{aligned} \quad (8.217)$$

These equations uncouple when \mathbf{C} is orthogonal to Φ_j . Assuming this condition is satisfied, and taking

$$\Phi_k^T \mathbf{C} \Phi_j = 2\delta_{jk} \tilde{m}_k \omega_k \xi_k \quad (8.218)$$

results in

$$\begin{aligned} \ddot{q}_k + 2\xi_k \omega_k \dot{q}_k + \omega_k^2 q_k \\ = -\frac{1}{\tilde{m}_k} \Phi_k^T \mathbf{M} \mathbf{E} a_g + \frac{1}{\tilde{m}_k} \Phi_k^T \mathbf{P} + \frac{1}{\tilde{m}_k} \Phi_k^T \mathbf{E}_f \mathbf{F} \end{aligned} \quad (8.219)$$

8.4. STATE-SPACE FORMULATION FOR MDOF SYSTEMS

The initial conditions for q_k are

$$\begin{aligned} q_k(0) &= \frac{1}{\tilde{m}_k} \Phi_k^T \mathbf{M} \mathbf{U}(0) \\ \dot{q}_k(0) &= \frac{1}{\tilde{m}_k} \Phi_k^T \mathbf{M} \dot{\mathbf{U}}(0) \end{aligned} \quad (8.220)$$

When $\mathbf{F} = \mathbf{0}$, these equations can be solved separately. The effect of feedback is to introduce coupling between the modal equations.

In order to deal with coupling, the equations are transformed to the standard state-space form by defining \mathbf{q} as the modal coordinate vector,

$$\mathbf{q} = \begin{Bmatrix} q_1 \\ q_2 \\ \dots \\ q_s \end{Bmatrix} \quad s \times 1 \quad (8.221)$$

and \mathbf{X}_m as the modal coordinate state vector,

$$\mathbf{X}_m = \begin{Bmatrix} \mathbf{q} \\ \dot{\mathbf{q}} \end{Bmatrix} \quad 2s \times 1 \quad (8.222)$$

Note that \mathbf{X}_m now contains only $2s$ modal coordinate terms. The equations are expressed in the same form as Eq. (8.140):

$$\dot{\mathbf{X}}_m = \mathbf{A}_m \mathbf{X}_m + \mathbf{B}_{fm} \mathbf{F} + \mathbf{B}_{pm} \mathbf{P} + \mathbf{B}_{gm} a_g \quad (8.223)$$

where the modal forms of the coefficient matrices along with their sizes are

$$\bar{\mathbf{m}} = [\tilde{m}_j \delta_{ij}] \quad (s \times s) \quad (8.224)$$

$$\Lambda = [\omega_j^2 \delta_{ij}] \quad (s \times s) \quad (8.225)$$

$$\Lambda_1 = [2\xi_j \omega_j \delta_{ij}] \quad (s \times s) \quad (8.226)$$

$$\Phi = [\Phi_1 \quad \Phi_2 \quad \dots \quad \Phi_s] \quad (n \times s) \quad (8.227)$$

$$\mathbf{A}_m = \begin{bmatrix} \mathbf{0} & \mathbf{I} \\ -\Lambda & -\Lambda_1 \end{bmatrix} \quad (2s \times 2s) \quad (8.228)$$

$$\mathbf{B}_{fm} = \begin{bmatrix} \mathbf{0} \\ \bar{\mathbf{m}}^{-1} \Phi^T \mathbf{E}_f \end{bmatrix} \quad (2s \times r) \quad (8.229)$$

$$\mathbf{B}_{pm} = \begin{bmatrix} \mathbf{0} \\ \bar{\mathbf{m}}^{-1} \Phi^T \end{bmatrix} \quad (2s \times r) \quad (8.230)$$

$$\mathbf{B}_{gm} = \begin{bmatrix} \mathbf{0} \\ -\bar{\mathbf{m}}^{-1} \Phi^T \mathbf{M} \mathbf{E} \end{bmatrix} \quad (2s \times 1) \quad (8.231)$$

Lastly, the initial conditions follow from Eq. (8.220):

$$\mathbf{X}_m(0) = \begin{Bmatrix} \mathbf{q}(0) \\ \dot{\mathbf{q}}(0) \end{Bmatrix} = \begin{bmatrix} \bar{\mathbf{m}}^{-1} \Phi^T \mathbf{M} \mathbf{U}(0) \\ \bar{\mathbf{m}}^{-1} \Phi^T \mathbf{M} \dot{\mathbf{U}}(0) \end{bmatrix} \quad (2s \times 1) \quad (8.232)$$

Feedback is introduced by expressing \mathbf{F} as a linear function of the modal state vector

$$\mathbf{F} = -\mathbf{K}_{fm} \mathbf{X}_m = -\mathbf{k}_d \mathbf{q} - \mathbf{k}_v \dot{\mathbf{q}} \quad (8.233)$$

The individual feedback matrices are of order $r \times s$. For pure velocity feedback, \mathbf{k}_d is set equal to $\mathbf{0}$.

Substituting for \mathbf{F} in Eq. (8.223) leads to the state equation specialized for continuous negative linear feedback.

$$\dot{\mathbf{X}}_m = (\mathbf{A}_m - \mathbf{B}_{fm} \mathbf{K}_{fm}) \mathbf{X}_m + \mathbf{B}_{pm} \mathbf{P} + \mathbf{B}_{gm} a_g \quad (8.234)$$

8.4. STATE-SPACE FORMULATION FOR MDOF SYSTEMS

where

$$\mathbf{A}_m - \mathbf{B}_{fm}\mathbf{K}_{fm} = \begin{bmatrix} \mathbf{0} & \mathbf{I} \\ -\Lambda - \bar{\mathbf{m}}^{-1}\Phi^T\mathbf{E}_f\mathbf{k}_d & -\Lambda_1 - \bar{\mathbf{m}}^{-1}\Phi^T\mathbf{E}_f\mathbf{k}_v \end{bmatrix} \quad (8.235)$$

The discrete form is similar to Eq. (8.215).

$$\begin{aligned} \mathbf{X}_{m,j+1} &= \mathbf{e}^{\mathbf{A}_m\Delta t}\mathbf{X}_{m,j} + \mathbf{A}_m^{-1}(\mathbf{e}^{\mathbf{A}_m\Delta t} - \mathbf{I})[\mathbf{B}_{fm}\mathbf{F}_j + \mathbf{B}_{pm}\mathbf{P}_j + \mathbf{B}_{gm}a_g] \\ \mathbf{F}_j &= -\mathbf{K}_{fm}\mathbf{X}_{m,j} \end{aligned} \quad (8.236)$$

For the continuous case, the free vibration solution with feedback is stable when \mathbf{A}_m is stable and \mathbf{k}_v is positive. This condition is always satisfied. The discrete solution is stable provided that the modulus of the largest eigenvalue of \mathbf{c}_m is less than unity.

$$\bar{\rho}_{\max}(\mathbf{c}_m) < 1 \quad (8.237)$$

$$\mathbf{c}_m = \mathbf{e}^{\mathbf{A}_m\Delta t} - \mathbf{A}_m^{-1}(\mathbf{e}^{\mathbf{A}_m\Delta t} - \mathbf{I})\mathbf{B}_{fm}\mathbf{K}_{fm} \quad (8.238)$$

Given the selection of the modes and the feedback matrix, \mathbf{K}_{fm} , one can establish the limit on Δt by computing the eigenvalues of \mathbf{c}_m for a range of values of Δt . This computation is illustrated in Ex. 8.12.

8.4.7 Modal State-Space Formulation: Arbitrary Damping

When \mathbf{C} is an arbitrary symmetric positive definite matrix, the expansion in terms of the eigenvectors for the undamped system and real modal coordinates does not lead to uncoupled modal

CHAPTER 8. STRUCTURAL CONTROL DYNAMICS

equations. In this case, we have to work with an expansion involving complex modal coordinates and complex state eigenvectors. The state-space vector is approximated as a linear combination of s modal vectors and coordinates,

$$\mathbf{X}(t) = \begin{bmatrix} \mathbf{U}(t) \\ \dot{\mathbf{U}}(t) \end{bmatrix} = \frac{1}{2} \sum_{j=1}^s (q_j \mathbf{V}_j + \tilde{q}_j \tilde{\mathbf{V}}_j) \quad (8.239)$$

where q and \mathbf{V} are complex quantities defined by

$$q_j(t) = q_{R,j}(t) + iq_{I,j}(t) \quad (8.240)$$

$$\mathbf{V}_j = \begin{bmatrix} \Phi_j \\ \lambda_j \Phi_j \end{bmatrix} \quad (8.241)$$

The expanded real forms for $\mathbf{U}(t)$ and $\dot{\mathbf{U}}(t)$ are

$$\mathbf{U}(t) = \sum_{j=1}^s (q_{R,j} \Phi_{R,j} - q_{I,j} \Phi_{I,j}) \quad (8.242)$$

$$\dot{\mathbf{U}}(t) \sum_{j=1}^s [q_{R,j} (\lambda_{R,j} \Phi_{R,j} - \lambda_{I,j} \Phi_{I,j}) - q_{I,j} (\lambda_{R,j} \Phi_{I,j} + \lambda_{I,j} \Phi_{R,j})] \quad (8.243)$$

When damping is uncoupled, $\Phi_{I,j} = \mathbf{0}$. The fully undamped case has $\lambda_{R,j} = 0$, $\lambda_{I,j} = \omega_j$, and $\Phi_{I,j} = \mathbf{0}$.

The initial conditions for the modal coordinates are determined by specializing $\mathbf{X}(t)$ for $t = 0$.

$$\mathbf{X}(0) = \frac{1}{2} \sum_{j=1}^s (q_j(0) \mathbf{V}_j + \tilde{q}_j(0) \tilde{\mathbf{V}}_j) \quad (8.244)$$

8.4. STATE-SPACE FORMULATION FOR MDOF SYSTEMS

Pre-multiplying by \mathbf{W}_k and noting the orthogonality relation between \mathbf{W}_k and \mathbf{V}_j , we obtain

$$q_k(0) = \frac{2}{f_k} \mathbf{W}_k^T \mathbf{X}(0) \quad (8.245)$$

Substituting for \mathbf{W}_k , the expression for $q_k(0)$ expands to

$$q_k(0) = \left(\frac{2}{f_k} \Phi_k^T \mathbf{K} \right) \mathbf{U}(0) - \left(\frac{2\lambda_k}{f_k} \Phi_k^T \mathbf{M} \right) \dot{\mathbf{U}}(0) \quad k = 1, 2, \dots, s \quad (8.246)$$

Introducing the expression for $\mathbf{X}(t)$ in the state equilibrium equation Eq. (8.240), pre-multiplying for \mathbf{W}_k and noting the orthogonality relation between \mathbf{W}_k and \mathbf{V}_j results in a set of s complex scalar equations:

$$\dot{q}_k = \lambda_k q_k + \left(\frac{2}{f_k} \mathbf{W}_k^T \mathbf{B}_f \right) \mathbf{F} + \left(\frac{2}{f_k} \mathbf{W}_k^T \mathbf{B}_g \right) a_g + \left(\frac{2}{f_k} \mathbf{W}_k^T \mathbf{B}_p \right) \mathbf{P} \quad k = 1, 2, \dots, s \quad (8.247)$$

The terms involving \mathbf{F} , a_g , and \mathbf{P} can be interpreted as complex modal forces associated with the k^{th} mode. Expanding the matrix products and substituting the notation

$$\begin{aligned} \mathbf{b}_{f,k} &= \frac{2}{f_k} \mathbf{W}_k^T \mathbf{B}_f = -\frac{2\lambda_k}{f_k} \Phi_k^T \mathbf{E}_f \\ \mathbf{b}_{g,k} &= \frac{2}{f_k} \mathbf{W}_k^T \mathbf{B}_g = -\frac{2\lambda_k}{f_k} \Phi_k^T \mathbf{M} \mathbf{E} \\ \mathbf{b}_{p,k} &= \frac{2}{f_k} \mathbf{W}_k^T \mathbf{B}_p = -\frac{2\lambda_k}{f_k} \Phi_k^T \end{aligned} \quad (8.248)$$

reduces the governing modal equations to a simpler form,

$$\dot{q}_k = \lambda_k q_k + \mathbf{b}_{f,k} \mathbf{F} + \mathbf{b}_{p,k} \mathbf{P} + b_{g,k} a_g \quad k = 1, 2, \dots, s \quad (8.249)$$

Since q_k is complex, there are a total of $2s$ equations. The corresponding set of “real” equations for the k^{th} mode are

$$\begin{aligned} \dot{q}_{R,k} &= \lambda_{R,k} q_{R,k} - \lambda_{I,k} q_{I,k} + \mathbf{b}_{fR,k} \mathbf{F} + \mathbf{b}_{pR,k} \mathbf{P} + b_{gR,k} a_g \\ \dot{q}_{I,k} &= \lambda_{I,k} q_{R,k} + \lambda_{R,k} q_{I,k} + \mathbf{b}_{fI,k} \mathbf{F} + \mathbf{b}_{pI,k} \mathbf{P} + b_{gI,k} a_g \end{aligned} \quad (8.250)$$

$$k = 1, 2, \dots, s$$

We establish the initial conditions for q_R and q_I by expanding Eq. (8.246). The resulting expressions are

$$\begin{aligned} q_{R,k}(0) &= \frac{2}{f_{R,k}^2 + f_{I,k}^2} [(f_{R,k} \Phi_{R,k}^T + f_{I,k} \Phi_{I,k}^T) \mathbf{K} \mathbf{U}(0) \\ &\quad - \{f_{R,k} (\lambda_{R,k} \Phi_{R,k}^T - \lambda_{I,k} \Phi_{I,k}^T) + f_{I,k} (\lambda_{R,k} \Phi_{I,k}^T + \lambda_{I,k} \Phi_{R,k}^T)\} \mathbf{M} \dot{\mathbf{U}}(0)] \end{aligned} \quad (8.251)$$

$$\begin{aligned} q_{I,k}(0) &= -\frac{f_{I,k}}{f_{R,k}} q_{R,k} + 2 \Phi_{I,k}^T \mathbf{K} \mathbf{U}(0) \\ &\quad - \frac{2}{f_{R,k}} (\lambda_{R,k} \Phi_{I,k}^T + \lambda_{I,k} \Phi_{R,k}^T) \mathbf{M} \dot{\mathbf{U}}(0) \end{aligned} \quad (8.252)$$

Various specialized forms of these equations are presented in the following examples.

Example 8.7 - Modal formulation - undamped case

It is of interest to specialize the general formulation presented in this section for the case of no damping and compare this result with the solution obtained with the conventional formulation

8.4. STATE-SPACE FORMULATION FOR MDOF SYSTEMS

derived in the previous section. Setting $\mathbf{C} = \mathbf{0}$ reduces the various terms to

$$\begin{aligned}
 \Phi_{I,k} &= 0 \\
 \lambda_{R,k} &= 0 \\
 \lambda_{I,k} &= \omega_k \\
 f_k &= 2\tilde{m}_k\omega_k^2 \\
 \mathbf{b}_{f,k} &= -\frac{i}{\tilde{m}_k\omega_k}\Phi_k^T\mathbf{E}_f \\
 \mathbf{b}_{p,k} &= -\frac{i}{\tilde{m}_k\omega_k}\Phi_k^T \\
 b_{g,k} &= \frac{i}{\tilde{m}_k\omega_k}\Phi_k^T\mathbf{M}\mathbf{E}
 \end{aligned} \tag{8.253}$$

Substituting in Eqs. (8.250) leads to

$$\dot{q}_{R,k} = -\omega_k q_{I,k} \tag{8.254}$$

$$\dot{q}_{I,k} = \omega_k q_{R,k} - \frac{1}{\tilde{m}\omega_k}\Phi_k^T(\mathbf{E}_f\mathbf{F} + \mathbf{P} - \mathbf{M}\mathbf{E}a_g) \tag{8.255}$$

Eq. (8.254) shows that

$$q_{I,k} = -\frac{1}{\omega_k}\dot{q}_{R,k} \tag{8.256}$$

Then Eq. (8.255) can be written as

$$\ddot{q}_{R,k} + \omega_k^2 q_{R,k} = \frac{1}{\tilde{m}}\Phi_k^T(\mathbf{E}_f\mathbf{F} + \mathbf{P} - \mathbf{M}\mathbf{E}a_g) \tag{8.257}$$

This result is identical to Eq. (8.4.6).

Example 8.8 - Modal formulation - uncoupled damping

CHAPTER 8. STRUCTURAL CONTROL DYNAMICS

When the damping matrix is proportional to \mathbf{K} and \mathbf{M} , the eigenvector, Φ , is real. However, the eigenvalue is complex. The various terms specialized for this case are as follows:

$$\begin{aligned}
 \Phi_{I,j} &= 0 \\
 \lambda_{R,k} &= -\xi_k \omega_k \\
 \lambda_{I,k} &= \omega_k [1 - \xi_k^2]^{1/2} \\
 f_k &= 2\tilde{m}_k \lambda_{I,k} (\lambda_{I,k} - i\lambda_{R,k}) = -(2\tilde{m}_k \lambda_I \lambda) i \\
 \frac{\lambda_k}{f_k} &= \frac{i}{2\tilde{m}_k \lambda_{I,k}} \\
 \mathbf{b}_{f,k} &= -\frac{i}{\tilde{m}_k \lambda_{I,k}} \Phi_k^T \mathbf{E}_f \\
 b_{g,k} &= -\frac{i}{\tilde{m}_k \lambda_{I,k}} \Phi_k^T \mathbf{M} \mathbf{E} \\
 \mathbf{b}_{p,k} &= -\frac{i}{\tilde{m}_k \lambda_{I,k}} \Phi_k^T
 \end{aligned} \tag{8.258}$$

Since the forcing terms are pure imaginary, the equations simplify to

$$\begin{aligned}
 \dot{q}_{R,k} &= \lambda_{R,k} q_{R,k} - \lambda_{I,k} q_{I,k} \\
 \dot{q}_{I,k} &= \lambda_{I,k} q_{R,k} + \lambda_{R,k} q_{I,k} - \frac{1}{\tilde{m}_k \lambda_{I,k}} \Phi_k^T (\mathbf{E}_f \mathbf{F} + \mathbf{P} - \mathbf{M} \mathbf{E} a_g)
 \end{aligned} \tag{8.259}$$

The initial conditions are

$$\begin{aligned}
 q_{R,k}(0) &= \frac{1}{\tilde{m}_k} \Phi_k^T \mathbf{M} \mathbf{U}(0) \\
 q_{I,k}(0) &= \frac{1}{\lambda_{I,R}} \left[\lambda_{R,k} q_{R,k}(0) - \frac{1}{\tilde{m}_k} \Phi_k^T \mathbf{M} \dot{\mathbf{U}}(0) \right]
 \end{aligned} \tag{8.260}$$

8.4. STATE-SPACE FORMULATION FOR MDOF SYSTEMS

This example shows that $q_{I,k}$ involves a combination of $q_{R,k}$ and $\dot{q}_{R,k}$. The actual displacements are given by

$$\begin{aligned} \mathbf{U}(t) &= \sum_{j=1}^s q_{R,j} \Phi_j \\ \dot{\mathbf{U}} &= \sum_{j=1}^s (\lambda_{R,j} q_{R,j} - \lambda_{I,j} q_{I,j}) \Phi_j = \sum_{j=1}^s \dot{q}_{R,j} \Phi_j \end{aligned} \quad (8.261)$$

Example 8.9 - Modal parameters - 4DOF system

This example presents modal data for the 4DOF system shown in Fig. 8.17. The element stiffness and damping values are listed in Table 8.3. The element stiffness factors are selected so that the displacement profile for the first mode is essentially linear. Two damping distributions are considered. Case 1 represents a low damping level for the first mode. The damping coefficients for case 2 are adjusted so that the sum, $\sum c_j$, is 3 times the corresponding sum for the first case. Since the internodal displacement for the first mode is essentially constant, this adjustment increases the modal damping ratio for the first mode by a factor of 3. More emphasis is placed on element 1 to exaggerate the nonproportional distribution and therefore increase the magnitude of the imaginary part of the modal vector.

Scaled versions of the modal displacement profiles for the two damping distributions are plotted in Figs. 8.18 and 8.19. The real parts are essentially identical. Since Case 1 represents a low level of damping, the amplitude of the corresponding imaginary part is negligible in comparison to the real part, which is of order 1. Case 2 results show a significant increase in the amplitude for

CHAPTER 8. STRUCTURAL CONTROL DYNAMICS

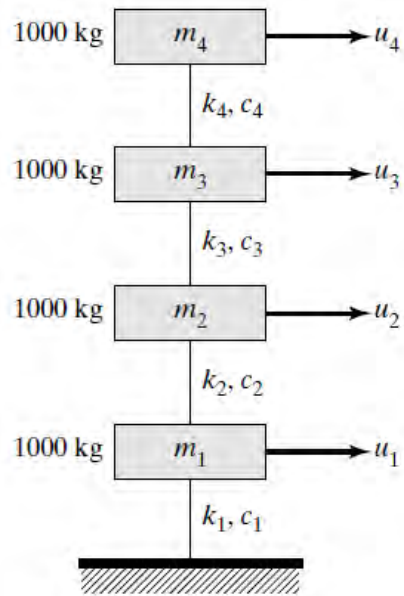


Figure 8.17

Table 8.3

Element number	Element stiffness (kN/m)	Element damping c (kN·s/m)	
		Case 1	Case 1
1	1700	4	20
2	1400	3	7
3	1000	2	2
4	700	1	1
		$\Sigma = 10$	$\Sigma = 30$

8.4. STATE-SPACE FORMULATION FOR MDOF SYSTEMS

the imaginary part. This shift is due to the large increment in c assigned to element 1. The modal periods and damping ratios are shown in Fig. 8.20 and 8.21. There is essentially no change in the periods. As expected, all the modal damping ratios are higher for Case 2. Lastly, to illustrate the effect of damping, time history responses were generated for the El Centro ground excitation. The maximum values of the internodal displacements for the elements are plotted in Fig. 8.22. Increasing the damping reduces the absolute maximum value from 0.0258 to 0.0217 and decreases the average value.

Referring back to Eq. (8.250), when $\mathbf{F} = \mathbf{0}$, the problem reduces to solving a set of two equations for each mode. Including \mathbf{F} couples the modal equations, and now we have to solve $2s$ simultaneous equations. In this case, it is convenient to shift over to a state-space type of formulation.

The state vector is defined in a similar way as for the previous formulations. Firstly, the real and imaginary modal coordinates are grouped separately,

$$\mathbf{q}_R = \begin{Bmatrix} q_{R1} \\ q_{R2} \\ \dots \\ q_{Rs} \end{Bmatrix} \quad \mathbf{q}_I = \begin{Bmatrix} q_{I1} \\ q_{I2} \\ \dots \\ q_{Is} \end{Bmatrix} \quad (8.262)$$

Secondly, the modal state vector is taken as

$$\mathbf{X}_m = \begin{Bmatrix} \mathbf{q}_R \\ \mathbf{q}_I \end{Bmatrix} \quad (8.263)$$

Lastly, the state equilibrium equation is expressed in the same form as for uncoupled damping

CHAPTER 8. STRUCTURAL CONTROL DYNAMICS

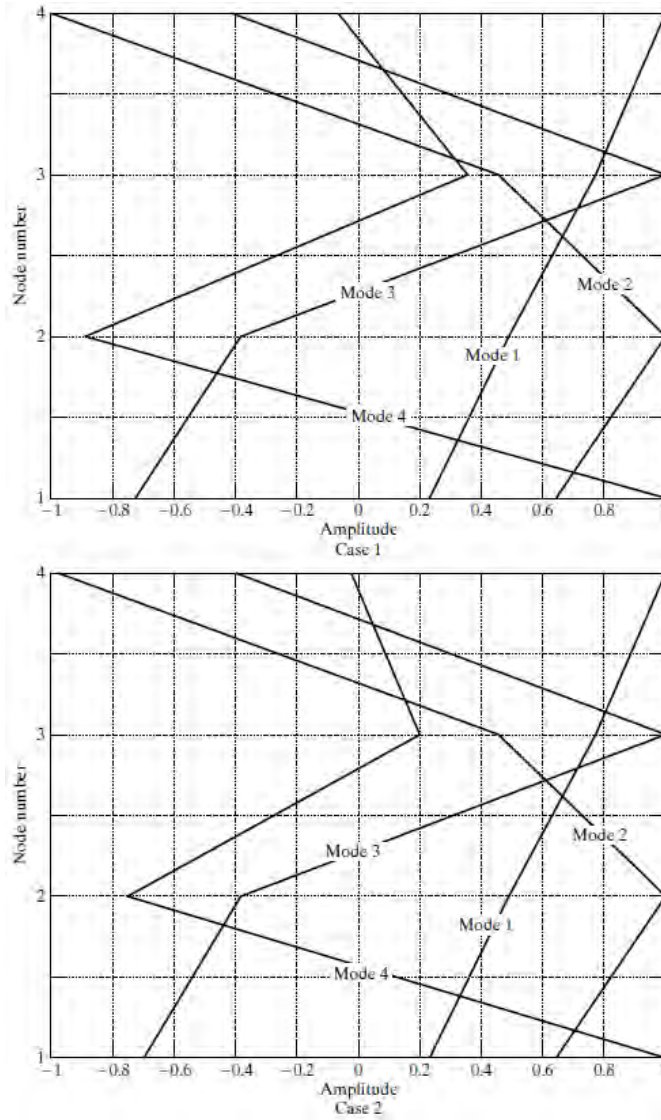


Figure 8.18: Modal displacement profile - real part.

8.4. STATE-SPACE FORMULATION FOR MDOF SYSTEMS

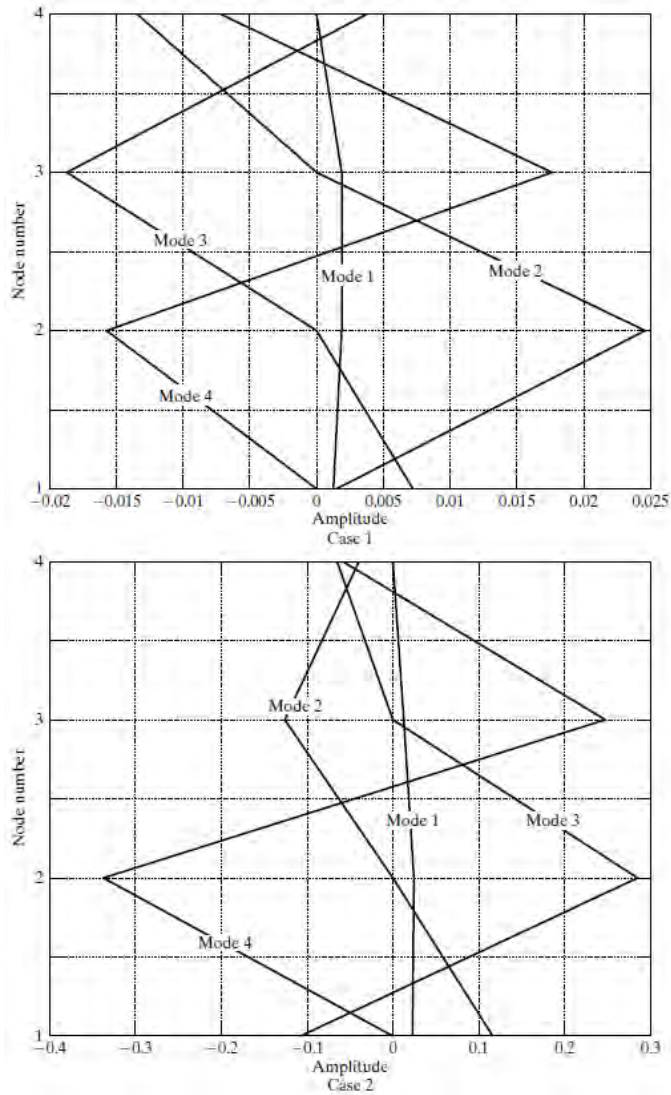


Figure 8.19: Modal displacement profile - imaginary part.

CHAPTER 8. STRUCTURAL CONTROL DYNAMICS

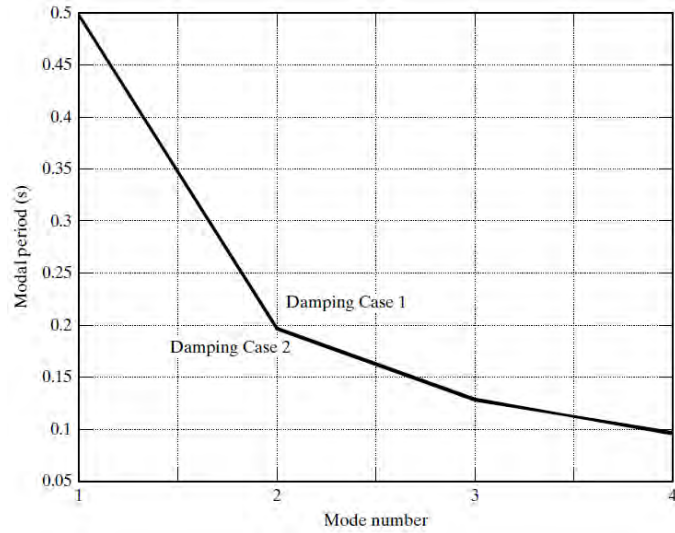


Figure 8.20: Modal period - no feedback.

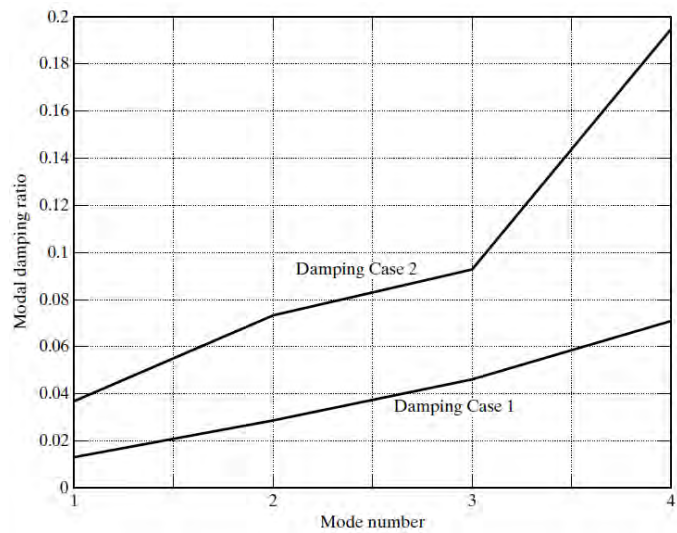


Figure 8.21: Modal damping ratio - no feedback.

8.4. STATE-SPACE FORMULATION FOR MDOF SYSTEMS

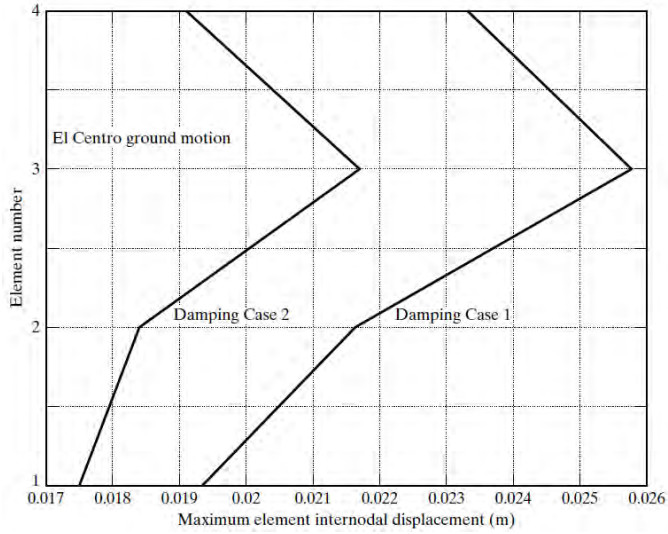


Figure 8.22: Element intermodal displacement profile - no feedback.

$$\dot{\mathbf{X}}_m = \mathbf{A}_m \mathbf{X}_m + \mathbf{B}_{fm} \mathbf{F} + \mathbf{B}_{pm} \mathbf{P} + \mathbf{B}_{gm} a_g \quad (8.264)$$

where the corresponding form of the coefficient matrices follow from Eq. (8.250)

$$\lambda_R = [\lambda_{R,k} \delta_{jk}] \quad \lambda_I = [\lambda_{I,k} \delta_{jk}] \quad (8.265)$$

$$\mathbf{b}_{fR} = \begin{bmatrix} \mathbf{b}_{fR,1} \\ \mathbf{b}_{fR,2} \\ \dots \\ \mathbf{b}_{fR,s} \end{bmatrix} \quad \mathbf{b}_{fI} = \begin{bmatrix} \mathbf{b}_{fI,1} \\ \mathbf{b}_{fI,2} \\ \dots \\ \mathbf{b}_{fI,s} \end{bmatrix} \quad (8.266)$$

$$\mathbf{b}_{pR} = \begin{bmatrix} \mathbf{b}_{pR,1} \\ \mathbf{b}_{pR,2} \\ \dots \\ \mathbf{b}_{pR,s} \end{bmatrix} \quad \mathbf{b}_{pI} = \begin{bmatrix} \mathbf{b}_{pI,1} \\ \mathbf{b}_{pI,2} \\ \dots \\ \mathbf{b}_{pI,s} \end{bmatrix} \quad (8.267)$$

$$\mathbf{b}_{gR} = \begin{bmatrix} b_{gR,1} \\ b_{gR,2} \\ \dots \\ b_{gR,s} \end{bmatrix} \quad \mathbf{b}_{gI} = \begin{bmatrix} b_{gI,1} \\ b_{gI,2} \\ \dots \\ b_{gI,s} \end{bmatrix} \quad (8.268)$$

$$\mathbf{A}_m = \begin{bmatrix} \lambda_R & -\lambda_I \\ \lambda_I & \lambda_R \end{bmatrix} \quad (8.269)$$

$$\mathbf{B}_{fm} = \begin{bmatrix} \mathbf{b}_{fR} \\ \mathbf{b}_{fI} \end{bmatrix} \quad \mathbf{B}_{pm} = \begin{bmatrix} \mathbf{b}_{pR} \\ \mathbf{b}_{pI} \end{bmatrix} \quad \mathbf{B}_{gm} = \begin{bmatrix} \mathbf{b}_{gR} \\ \mathbf{b}_{gI} \end{bmatrix} \quad (8.270)$$

The initial conditions for \mathbf{X}_m are obtained with Eqs. (8.251) and (8.252).

Negative linear feedback is taken as

$$\mathbf{F} = -\mathbf{K}_{fm}\mathbf{X}_m = -[\mathbf{k}_d \quad \mathbf{k}_v] \begin{bmatrix} \mathbf{q}_R \\ \mathbf{q}_I \end{bmatrix} \quad (8.271)$$

Ex. 8.7 showed that \mathbf{q}_I is a linear function of $\dot{\mathbf{q}}_R$ for no damping. Including damping results in \mathbf{q}_I being a function of both $\dot{\mathbf{q}}_R$ and \mathbf{q}_R . For a lightly damped system, it is reasonable to assume \mathbf{q}_I depends only on $\dot{\mathbf{q}}_R$, and therefore to approximate pure velocity feedback by setting $\mathbf{k}_d = \mathbf{0}$. The feedback term for this case reduces to

$$\mathbf{B}_{fm}\mathbf{F} = \begin{bmatrix} \mathbf{0} & -\mathbf{b}_{fR}\mathbf{k}_v \\ \mathbf{0} & -\mathbf{b}_{fI}\mathbf{k}_v \end{bmatrix} \begin{Bmatrix} \mathbf{q}_R \\ \mathbf{q}_I \end{Bmatrix} \quad (8.272)$$

Example 8.10 - Modal response for Example 8.9

The state-space modal formulation is applied to the 4DOF system with Case 1 damping defined in Ex. 8.9. Results for the

8.4. STATE-SPACE FORMULATION FOR MDOF SYSTEMS

real and imaginary parts of the modal coordinates for the first two modes are plotted in Fig. 8.23 and 8.24. Comparison of the plots in Fig. 8.23 shows that the response is dominated by the first mode. The ratio of the amplitudes for the first and second modes is approximately 30, which indicates that the second mode contributes about 3% to the total response for this combination of structure and excitation.

Example 8.11 - Modal response with feedback for Example 8.9

This example illustrates the effect of linear negative velocity feedback on the modal damping ratios. The modal state space formulation defined by Eqs. (8.262) through (8.272) is applied to the 4DOF system with Case 1 damping described in Ex. 8.9. Two control force systems are considered. The first system is a single force applied at node 4; the second system consists of self-equilibrating sets of nodal forces applied on each element. Fig. 8.25 shows the spatial distribution of the control forces.

Given the feedback matrix, \mathbf{K}_{fm} , we determine \mathbf{F} using Eq. (8.271):

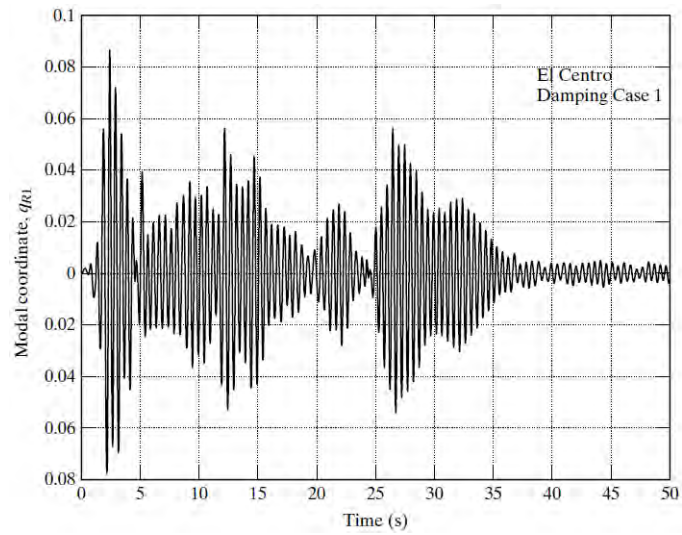
$$\mathbf{F} = -\mathbf{K}_{fm}\mathbf{X}_m \quad (8.273)$$

and then solve for \mathbf{X}_m with Eq. (8.311).

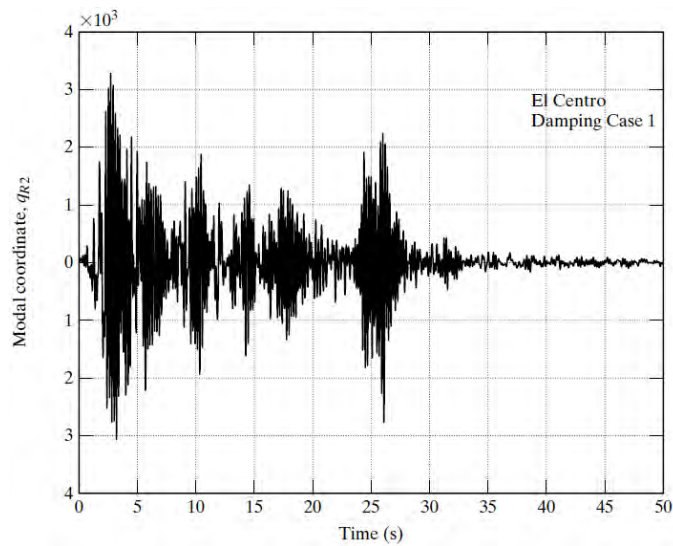
$$\dot{\mathbf{X}}_m = (\mathbf{A}_m - \mathbf{B}_{fm}\mathbf{K}_{fm})\mathbf{X}_m + \mathbf{B}_{pm}\mathbf{P} + \mathbf{B}_{gm}a_g \quad (8.274)$$

The frequency and damping parameters for the system with feedback are related to the eigenvalues of $\mathbf{A}_m - \mathbf{B}_{fm}\mathbf{K}_{fm}$ and depend on the control force scheme as well as \mathbf{K}_{fm} . Particular forms of \mathbf{K}_{fm} obtained with the algebraic Riccati equation and

CHAPTER 8. STRUCTURAL CONTROL DYNAMICS



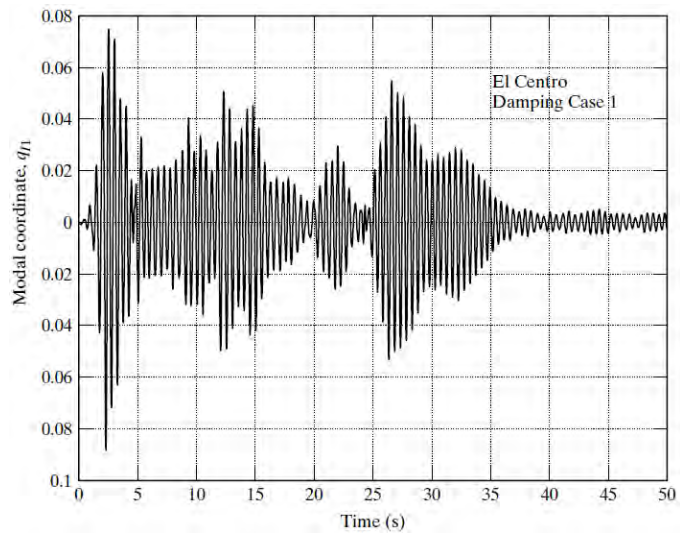
(a)



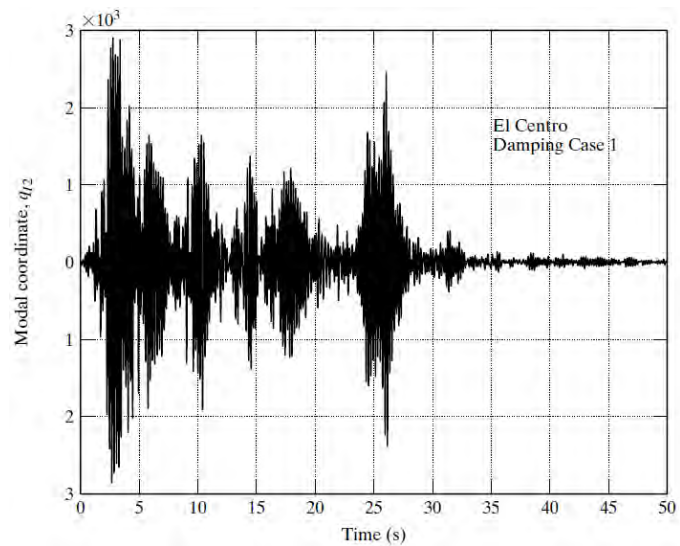
(b)

Figure 8.23: Time history response of the real part of the modal coordinate. (a) Mode 1; and (b) Mode 2.

8.4. STATE-SPACE FORMULATION FOR MDOF SYSTEMS



(a)



(b)

Figure 8.24: Time history response of the imaginary part of the modal coordinate. (a) Mode 1; and (b) Mode 2.

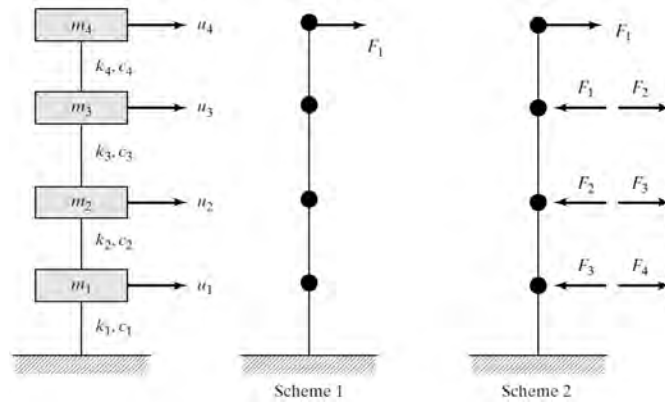


Figure 8.25

specialized for pure velocity feedback [see Eq. (8.272)] are used here to generate results for the two force schemes. This formulation is discussed in detail in the next chapter. Our objective here is to illustrate the variation in behavior associated with feedback systems.

Fig. 8.26 shows the modal damping ratios for the 4DOF model with Case 1 damping, force scheme 1, and a particular choice for \mathbf{K}_{fm} . Feedback results in a significant increase (a factor of 10) in the damping ratio for the first mode. Since this response is dominated by the first mode, there also is a reduction in the displacement response. The relevant displacement quantities are plotted in Fig. 8.26, parts(b) and (c). The last plot shows the variation of the control force magnitude with time.

Results for the control force scheme 2 are plotted in Fig. 8.27. This combination of control forces and weighting produces essentially equal nodal damping ratios, whereas scheme 1 places the priority on the first mode. Since the damping ratio is less, the displacement response is greater. There also is a reduction in the peak magnitudes of the four control forces.

8.4. STATE-SPACE FORMULATION FOR MDOF SYSTEMS

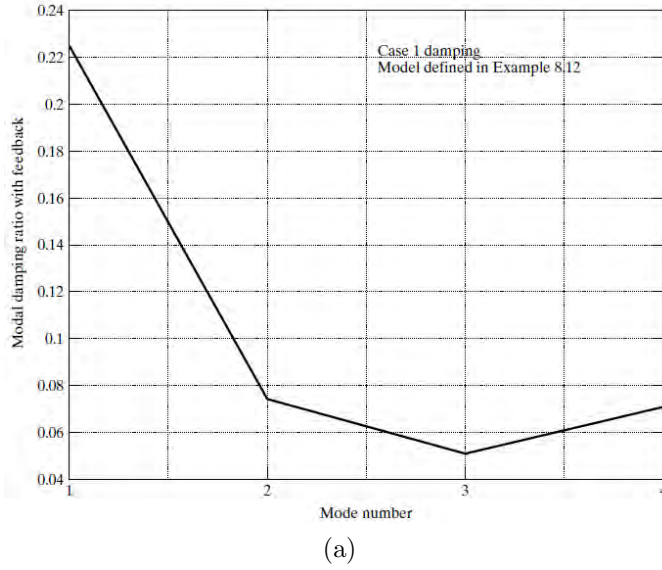


Figure 8.26: Modal response for control force scheme 1. (a) Modal damping ratio with continuous feedback - no saturation limit.

8.4.8 Stability Analysis: Discrete Modal Formulation

The discrete form of the state equilibrium equation expressed in terms of modal coordinates is used here to evaluate the effect of the time interval and the delay time on the stability. Allowing for linear feedback, the governing equation for free vibration response is

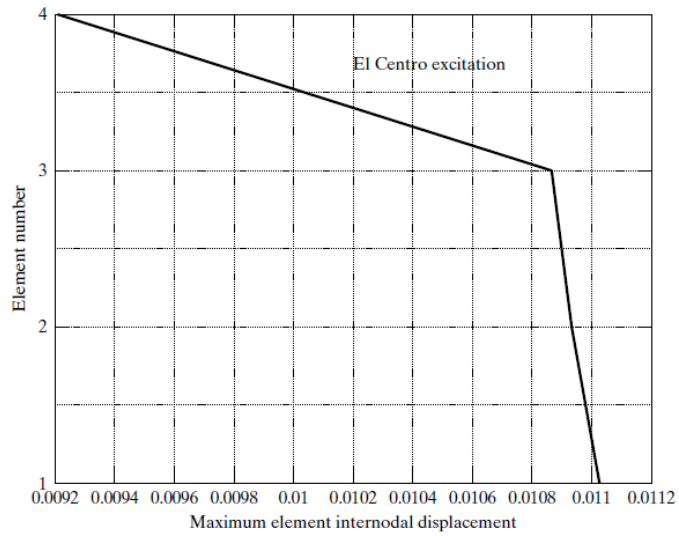
$$\mathbf{X}_{m,j+1} = \mathbf{e}^{\mathbf{A}_m \Delta t} \mathbf{X}_{m,j} + \mathbf{A}_m^{-1} (\mathbf{e}^{\mathbf{A}_m \Delta t} - \mathbf{I}) \mathbf{B}_{fm} \mathbf{F}_j \quad (8.275)$$

Time delay is introduced by taking \mathbf{F}_j as

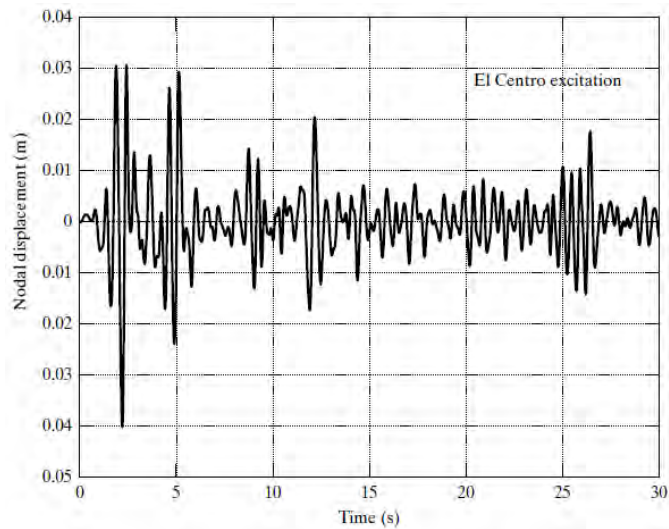
$$\begin{aligned} \mathbf{F}_j &= \mathbf{0} & 0 \leq j < v \\ \mathbf{F}_j &= -\mathbf{K}_{fm} \mathbf{X}_{m,j-v} & j \geq v \end{aligned} \quad (8.276)$$

With this specification for \mathbf{F}_j , the response equations take the following form:

CHAPTER 8. STRUCTURAL CONTROL DYNAMICS



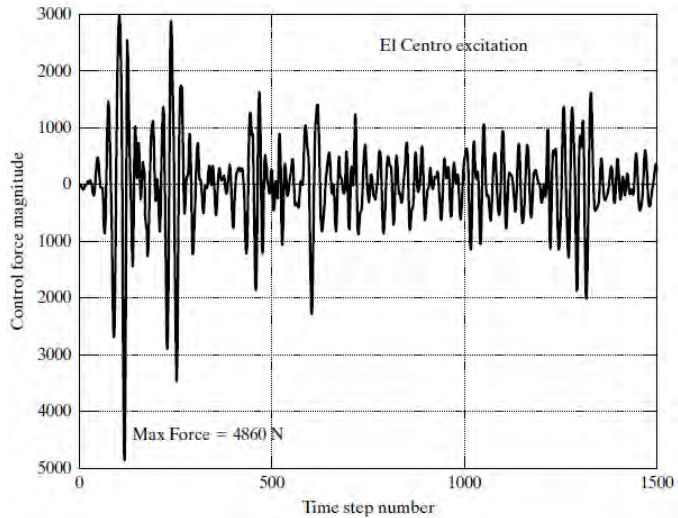
(b)



(c)

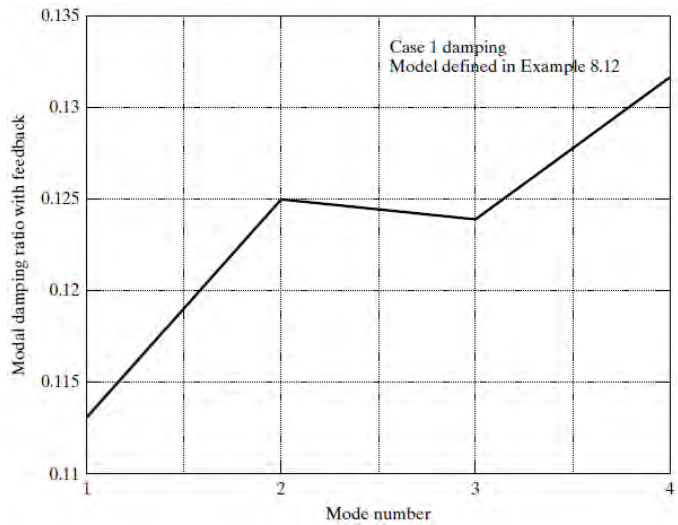
Figure 8.26: Modal response for control force scheme 1. (b) Element internodal displacement profile; and (c) Displacement of node 4.

8.4. STATE-SPACE FORMULATION FOR MDOF SYSTEMS



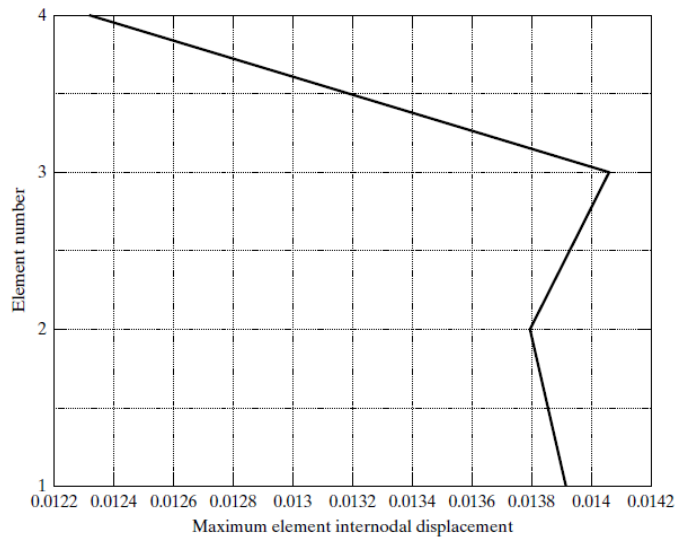
(d)

Figure 8.26: Modal response for control force scheme 1. (d) Control force time history.

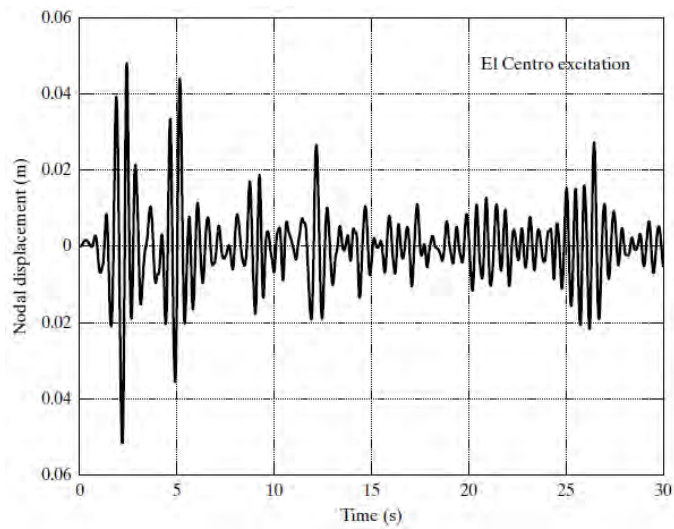


(a)

Figure 8.27: Modal response for control force scheme 2. (a) Modal damping ratio with continuous feedback - no saturation limit.



(b)



(c)

Figure 8.27: Modal response for control force scheme 2. (b) Element internodal displacement profile; and (c) Displacement of node 4.

8.4. STATE-SPACE FORMULATION FOR MDOF SYSTEMS

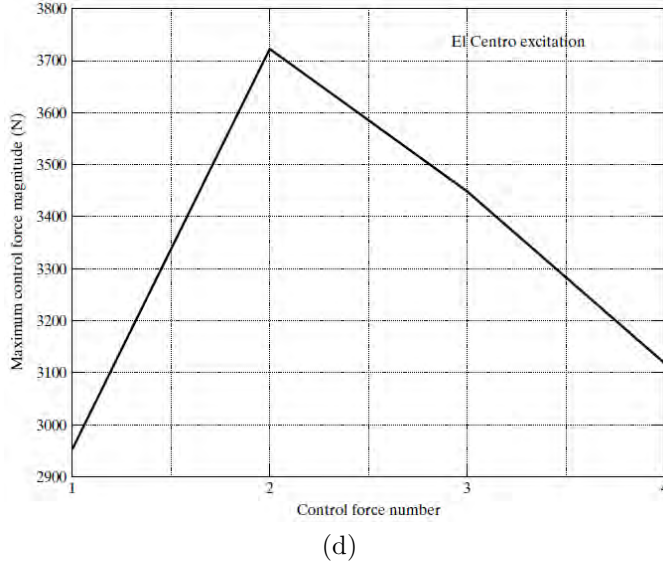


Figure 8.27: Modal response for control force scheme 2. (d) Control force time history.

$$\begin{aligned} \mathbf{X}_{m,j+1} &= \mathbf{c}_{m1} \mathbf{X}_{m,j} & 0 \leq j \leq \nu \\ \mathbf{X}_{m,j+1} &= \mathbf{c}_{m1} \mathbf{X}_{m,j} + \mathbf{c}_{m3} \mathbf{X}_{m,j-\nu} & j \geq \nu \end{aligned} \quad (8.277)$$

where

$$\begin{aligned} \mathbf{c}_{m1} &= \mathbf{e}^{\mathbf{A}_m \Delta t} \\ \mathbf{c}_{m3} &= -\mathbf{A}_m^{-1} (\mathbf{e}^{\mathbf{A}_m \Delta t} - \mathbf{I}) \mathbf{B}_{fm} \mathbf{K}_{fm} \end{aligned} \quad (8.278)$$

The stability analysis for the SDOF system showed that time delay lowered the limiting value of the time interval. Therefore, we can obtain an upper bound estimate for Δt by considering no time delay. For this case, Eq. (8.277) simplifies to

$$\mathbf{X}_{m,j+1} = (\mathbf{c}_{m1} + \mathbf{c}_{m3}) \mathbf{X}_{m,j} = \mathbf{c}_m \mathbf{X}_{m,j} \quad (8.279)$$

CHAPTER 8. STRUCTURAL CONTROL DYNAMICS

Stability requires the modulus of the largest eigenvalue of \mathbf{c}_m to be less than 1.

$$\rho_{\max}(\mathbf{c}_m) < 1 \quad (8.280)$$

The complexity of \mathbf{c}_m necessitates the use of a numerical computational procedure. Ex. 8.2 illustrates the computational details for a SDOF system with negative velocity feedback. In general, we range over Δt to determine the value corresponding to $\rho_{\max}(\mathbf{c}_m) = 1$.

When there is time delay, the eigenvalue problem is of order $v + 1$,

$$(\mathbf{c}_{m3} + \rho^v \mathbf{c}_{m1} - \rho^{v+1} \mathbf{I}) \Psi = \mathbf{0} \quad (8.281)$$

For the SDOF case, it was possible to expand the determinant of the coefficient matrix and obtain a polynomial expansion for ρ . However, a numerical procedure is still required to evaluate the roots. For MDOF systems, this hybrid approach is not feasible and we must resort to a fully numerical approach. Given Δt and ν , Eq. (8.277) can be used to generate the corresponding free vibration response. By decreasing Δt in increments from the critical value for no time delay, we can converge on the limiting value for the specified time delay. This solution strategy is efficient when the number of modal DOF is small, on the order of 5. The computational cost for the exponential matrix increases nonlinearly with the number of modes and eventually becomes excessive. In this case, we can resort to an approximate formulation that assumes the modal equations are fully uncoupled. This assumption reduces the stability analysis for a problem involving s modes to s individual SDOF stability analyses.

8.4. STATE-SPACE FORMULATION FOR MDOF SYSTEMS

The approximate stability formulation proceeds as follows. First the feedback force is considered to involve only q_I .

$$\mathbf{F} = - \sum_{j=1}^s \mathbf{k}_{v,j} q_{I,j} \quad (8.282)$$

Second, $\mathbf{b}_{fR,k}$ is taken as a null matrix in Eq. (8.250). These conditions correspond to pure velocity feedback for a system with uncoupled damping. Lastly, the feed-back terms in the k^{th} equation are assumed to involve only $\mathbf{q}_{I,k}$. With these assumptions, Eq. (8.250) takes the form

$$\begin{aligned} \dot{q}_{R,k} &= \lambda_{R,k} q_{R,k} - \lambda_{I,k} q_{I,k} \\ \dot{q}_{I,k} &= \lambda_{I,k} q_{R,k} + \lambda_{R,k} q_{I,k} - \bar{b}_k q_{I,k} \end{aligned} \quad (8.283)$$

where

$$\bar{\mathbf{b}}_k = \mathbf{b}_{fI,k} \mathbf{k}_{v,k} \quad (8.284)$$

The remaining steps are the same as for the SDOF formulation presented in Sect. 8.3.

Introducing matrix notation, Eq. (8.283) is expressed as

$$\dot{\mathbf{q}}_k = \mathbf{A}_k \mathbf{q}_k - \bar{\mathbf{B}}_k \mathbf{q}_k \quad (8.285)$$

where

$$\mathbf{q}_k = \begin{Bmatrix} q_{R,k} \\ q_{I,k} \end{Bmatrix} \quad (8.286)$$

$$\mathbf{A}_k = \begin{bmatrix} \lambda_{R,k} & -\lambda_{I,k} \\ \lambda_{I,k} & \lambda_{R,k} \end{bmatrix} \quad (8.287)$$

$$\bar{\mathbf{B}}_k = \begin{bmatrix} \mathbf{0} \\ \bar{\mathbf{b}}_k \end{bmatrix} \quad (8.288)$$

The discrete form allowing for time delay is written as

$$\mathbf{q}_{k,j+1} = \mathbf{c}_{k1}\mathbf{q}_{k,j} + \mathbf{c}_{k3}\mathbf{q}_{k,j-\nu} \quad (8.289)$$

where the \mathbf{c} matrices are now 2×2 .

$$\mathbf{c}_{k1} = \mathbf{e}^{\mathbf{A}_k\Delta t} \quad (8.290)$$

$$\mathbf{c}_{k3} = -\mathbf{A}_k^{-1}(\mathbf{e}^{\mathbf{A}_k\Delta t} - \mathbf{I})\bar{\mathbf{B}}_k \quad (8.291)$$

We determine the limiting value of Δt for each k ranging from 1 to s , the total number of modes selected to represent the solution. The lowest value controls the change of the time interval.

Example 8.12 - Stability analysis for Example 8.12

This example examines the effect of time delay on the response of the 4DOF system considered in Ex. 8.12. Modal properties corresponding to the two control force schemes are listed in Table 8.4. The time increment is considered to be equal to 0.02 s. An estimate of the limiting value of ν for each force scheme can be obtained using the data contained in Table 8.2 of Ex. 8.3. These results are for $\xi = 0$ and provide a lower bound estimate, ν_0 . The limiting value of ν for $\xi > 0$ is higher than ν_0 . For convenience, the table is listed here as Table 8.5.

For force scheme 1, the first and second modes have the larger values of and therefore control the delay. Assuming $\xi = 0$, Table 8.5 indicates that mode 2 is close to instability for $\nu = 2$ ($\Delta t/T = 0.102$ versus 0.096). The value for mode 1 is closer to

8.4. STATE-SPACE FORMULATION FOR MDOF SYSTEMS

Table 8.4

Mode	T	$\Delta t/T$	ξ	Force scheme 1	Force scheme 2
				ξ_a	ξ_a
1	0.498	0.040	0.013	0.212	0.100
2	0.197	0.102	0.029	0.045	0.096
3	0.129	0.155	0.046	0.005	0.078
4	0.095	0.211	0.071	0.000	0.060

Table 8.5: Limiting values of $\Delta t/T$ for $\xi = 0$ (Ex. 8.3, Table 8.2)

ξ_a	Stability limit for $\Delta t/T$		
	$\nu = 0$	$\nu = 1$	$\nu = 2$
0	0.50	0.500	0.5000
0.05		0.158	0.0955
0.10	0.44	0.151	0.0908
0.15		0.144	0.0860
0.20	0.38	0.137	0.0822
0.25		0.131	0.0780
0.30	0.33	0.124	0.0745
0.35		0.118	0.0709
0.40	0.29	0.113	0.0677

3. Since ξ_a is ≈ 0 for modes 3 and 4, they are not critical even though the corresponding time ratios are higher.

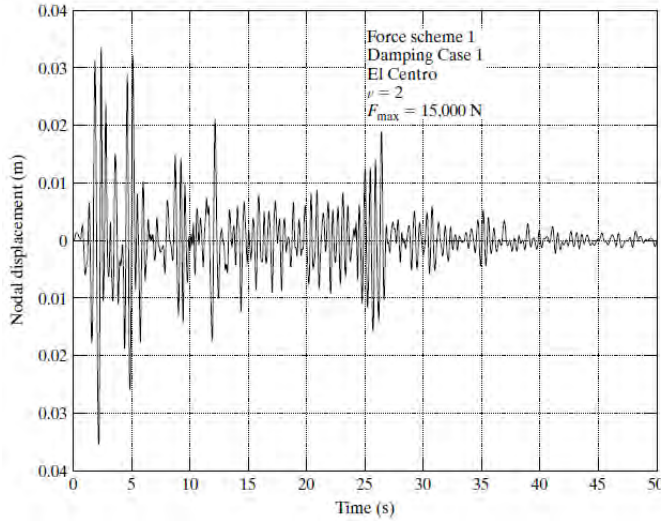
Force scheme 2 produces some damping for modes 3 and 4, and since these time ratios are the highest, they control the stability limit. Allowing for some increase due to initial damping, the critical value for ν is between 1 and 2 for modes 3, 4, and > 2 for modes 1, 2. The least critical mode is mode 1 since it has the lowest time ratio.

Fig. 8.28 contains results generated for control force scheme 1, with ν taken equal to 2. They are in close agreement with the solution for $\nu = 0$ presented in Ex. 8.12. Increasing ν to 3 produces the responses plotted in Fig. 8.29. Mode 2 has gone critical and dominates the response, whereas mode 1 remains at essentially the same peak level as for $\nu = 2$. These results are based on limiting the peak magnitude of the control force to 15,000 N, which is 3 times the peak value for $\nu = 2$. Limiting F simulates saturation of the force actuators. Comparison of the power input plots shows that shifting ν from 2 to 3 transforms the energy dissipation process, resulting in energy being supplied to the system and a periodic forced vibration response following the seismic induced response. Reducing the peak magnitude down to 5000 N, the value required for $\nu = 0$ (and also $\nu = 2$), leads to the responses plotted in Fig. 8.30. The magnitudes have been reduced, but the system is still responding as if it were subjected to a periodic forced vibration as well as a seismic excitation. Decreasing F_{\max} further will not eliminate this additional motion, as illustrated by the plot for $F = 2500$ and 1000 N contained in Fig. 8.31.

Results for force scheme 2 are plotted in Figs. 8.32 and 8.33. Mode 4 controls the allowable delay. For $\nu = 1$, there is a

8.4. STATE-SPACE FORMULATION FOR MDOF SYSTEMS

negligible effect on the response. For $\nu = 2$, mode 1 is essentially unchanged, while mode 2 shows some additional motion due to delay. Two out of four of the control forces reach the prescribed peak value of 15,000 N. The response corresponding to $F_{\max} = 4000$ N shown in Fig. 8.34 exhibits similar features.



(a)

Figure 8.28: (a) Displacement of node 4;

8.4.9 Controllability of a Particular Modal Response

The governing equation for the response of the k^{th} mode is given by Eq. (8.249).

$$\dot{q}_k = \lambda_k q_k + \mathbf{b}_{f,k} \mathbf{F} = \lambda_k q_k - \frac{2\lambda_k}{f_k} \Phi_k^T \mathbf{E}_f \mathbf{F} \quad (8.292)$$

By definition, the j^{th} column of \mathbf{E}_f defines the nodal force pattern corresponding to F_j . Pre-multiplication by Φ_k^T generates the equivalent modal force for mode k . If Φ_k^T is orthogonal to the

CHAPTER 8. STRUCTURAL CONTROL DYNAMICS

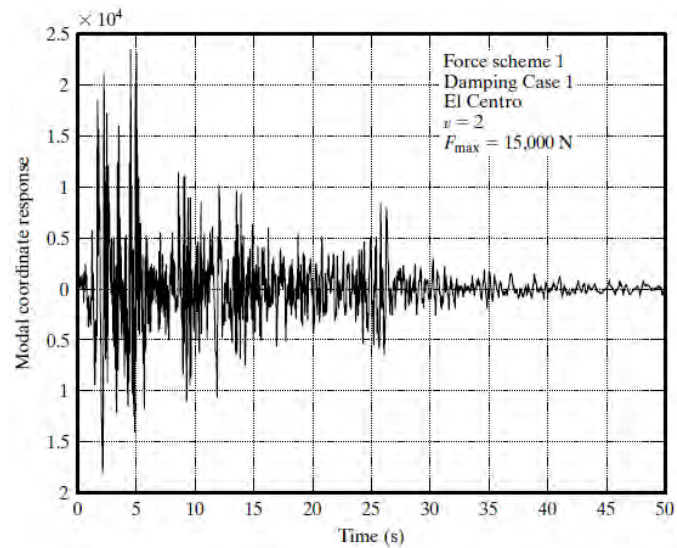
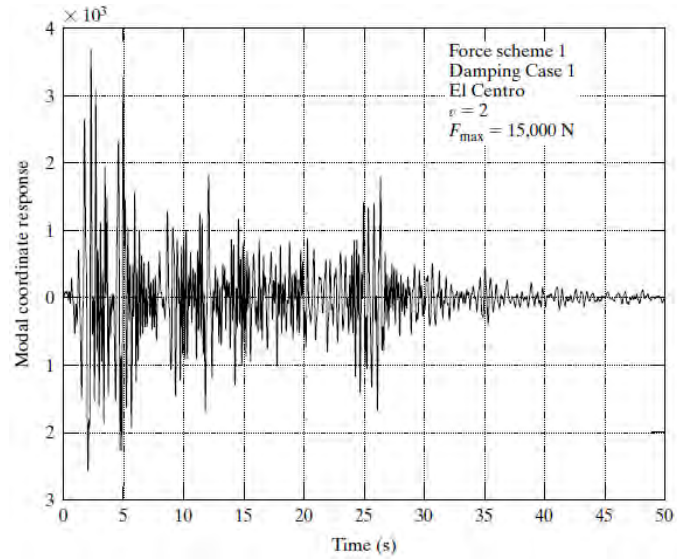
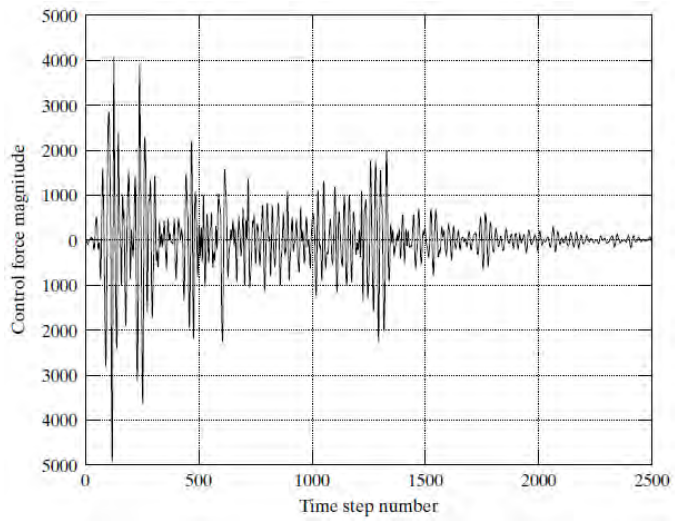
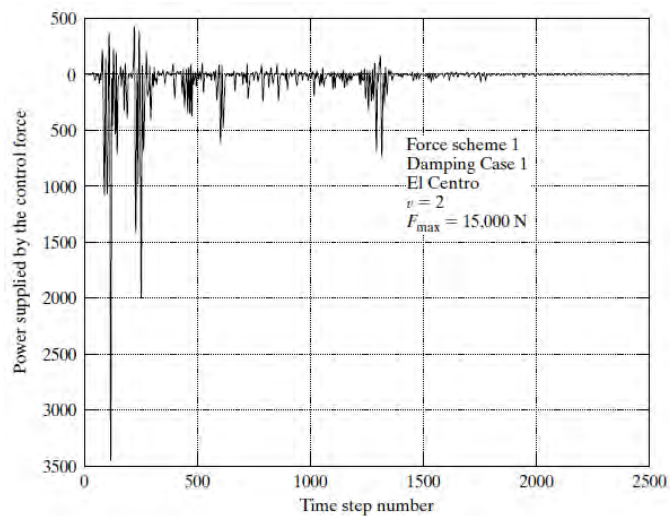


Figure 8.28: (b) time history response of the real part of the coordinate for mode 2; (c) time history response of the real part of the coordinate for mode 4;

8.4. STATE-SPACE FORMULATION FOR MDOF SYSTEMS



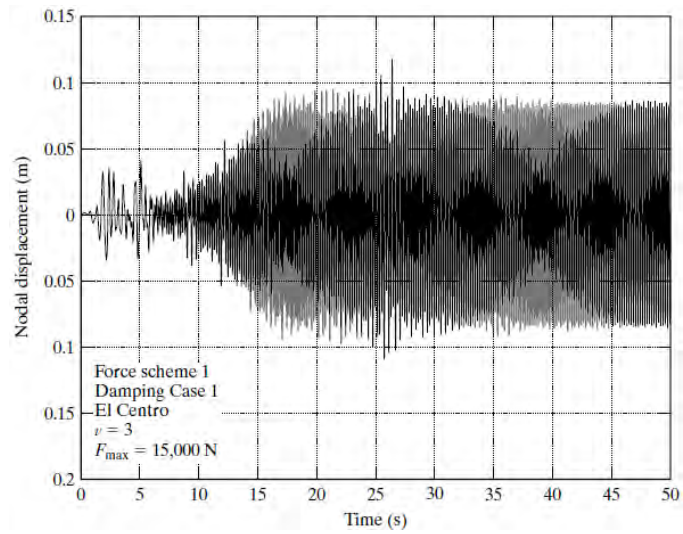
(d)



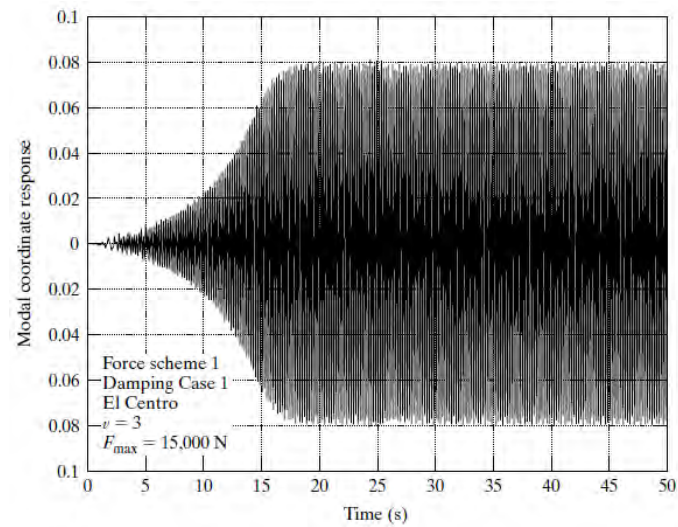
(e)

Figure 8.28: (d) time history response of the magnitude of the control force; (e) time history response of the input power.

CHAPTER 8. STRUCTURAL CONTROL DYNAMICS



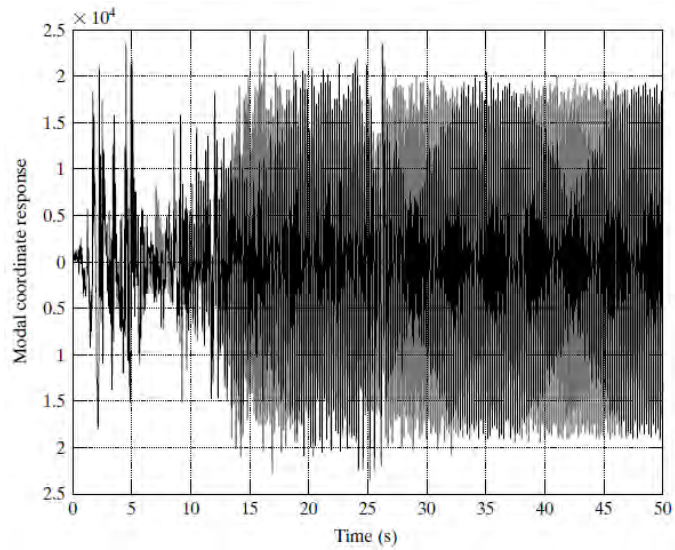
(a)



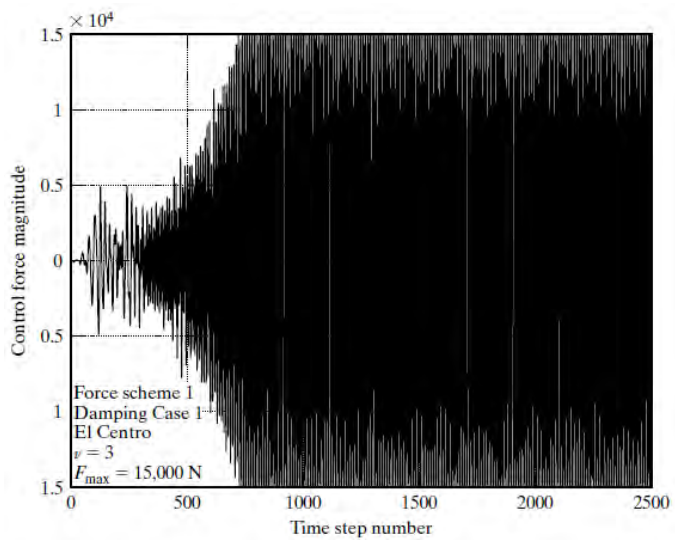
(b)

Figure 8.29: (a) Displacement of node 4; (b) time history response of the real part of the coordinate for mode 2;

8.4. STATE-SPACE FORMULATION FOR MDOF SYSTEMS



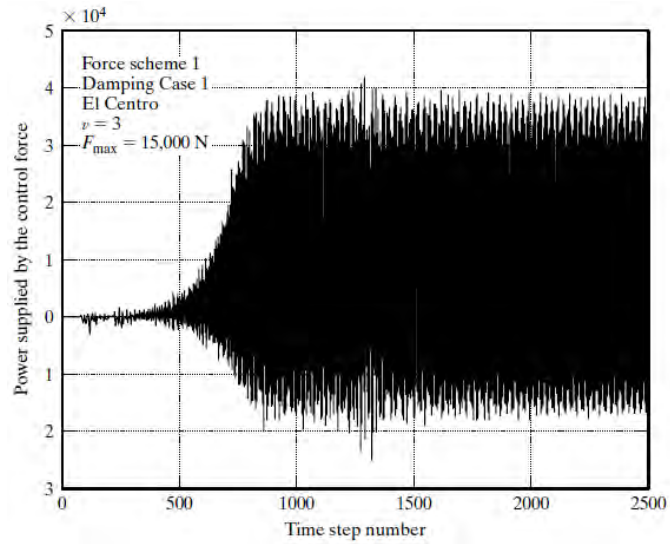
(c)



(d)

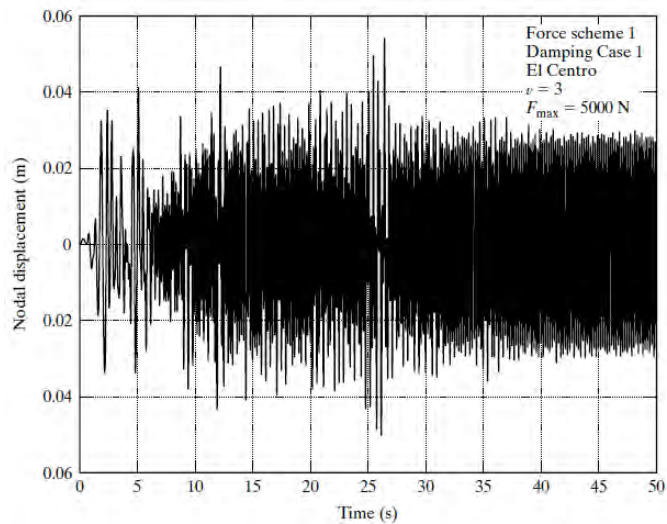
Figure 8.29: (c) time history response of the real part of the coordinate for mode 4; (d) control force magnitude;

CHAPTER 8. STRUCTURAL CONTROL DYNAMICS



(e)

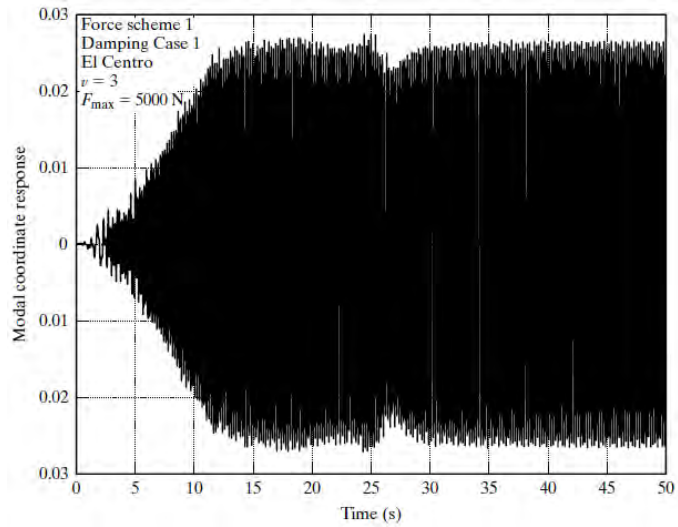
Figure 8.29: (e) Input power.



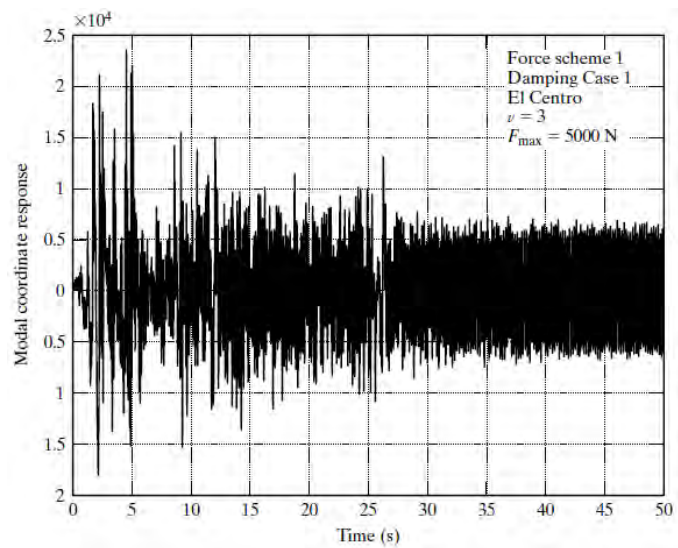
(a)

Figure 8.30: (a) Displacement of node 4;

8.4. STATE-SPACE FORMULATION FOR MDOF SYSTEMS

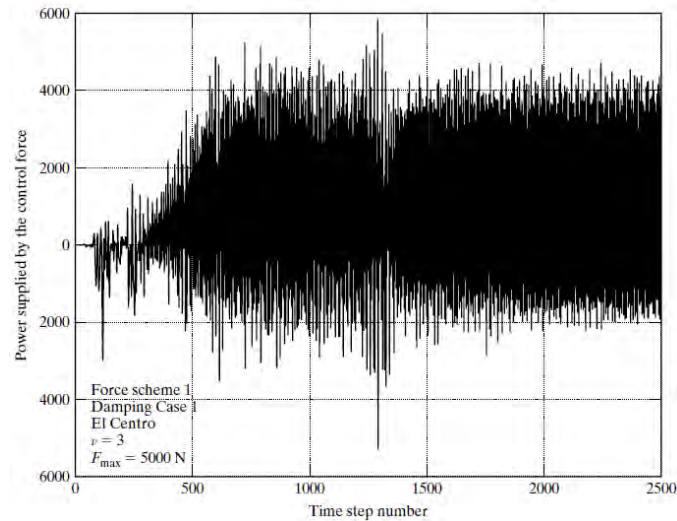


(b)



(c)

Figure 8.30: (b) time history response of the real part of the coordinate for mode 2; (c) time history response of the real part of the coordinate for mode 4;



(d)

Figure 8.30: (d) time history response of the input power.

j^{th} column of \mathbf{E}_f , F_j will have no effect on the response of the k^{th} mode. Therefore, for mode k to be controllable, the nodal location of the active control forces must satisfy the following constraint:

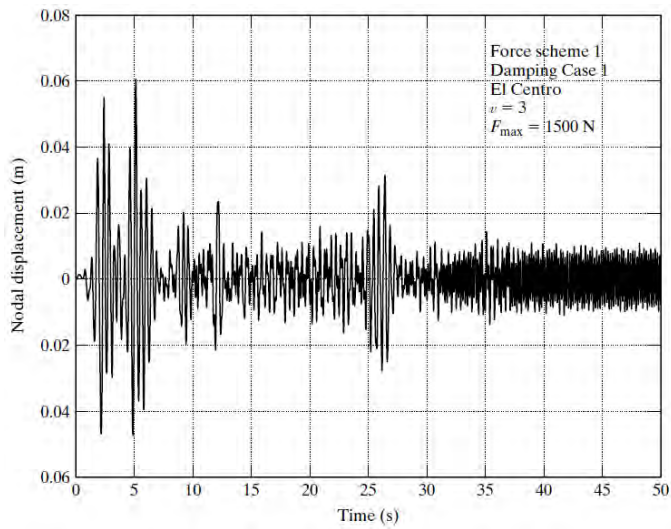
$$\Phi_k^T \mathbf{E}_f \neq 0 \quad (8.293)$$

When damping is uncoupled, Φ_k is real, and this constraint is obvious. We cannot apply a control force at a null point of a mode.

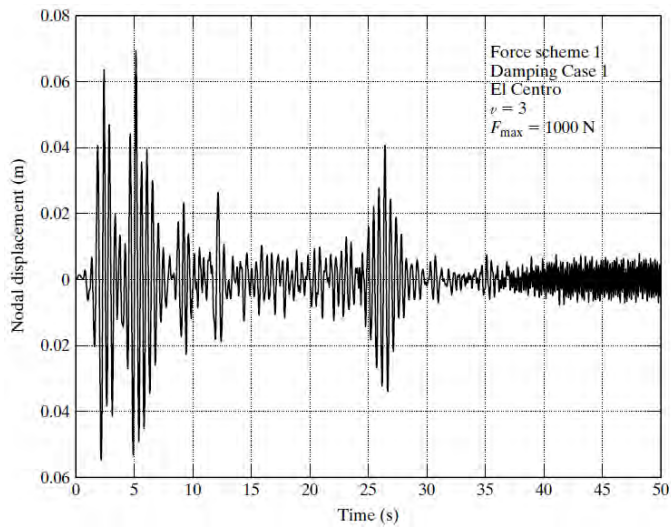
Example 8.13 - Controllability analysis for a 20DOF Model

Controllability is illustrated using a 20DOF shear beam model having constant mass and stiffness. Fig. 8.35 shows the first four modal displacement profiles, which are real in this case since there is no damping. The corresponding internodal displacement

8.4. STATE-SPACE FORMULATION FOR MDOF SYSTEMS



(a)



(b)

Figure 8.31: (a) Displacement of node 4; and (b) displacement of node 4.

CHAPTER 8. STRUCTURAL CONTROL DYNAMICS

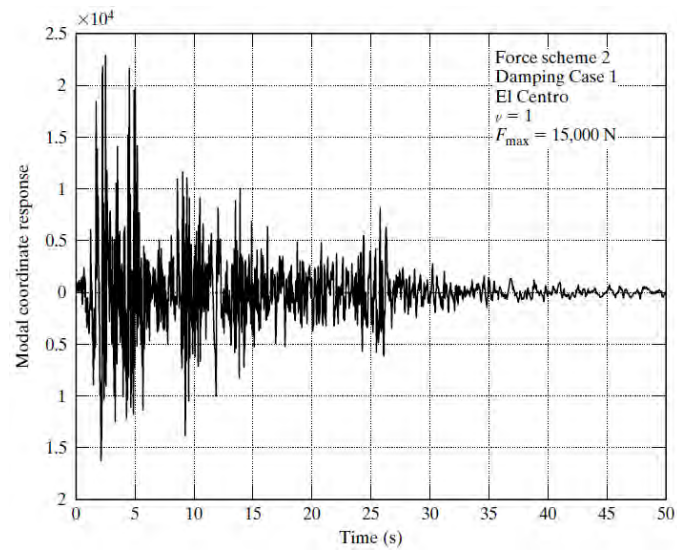
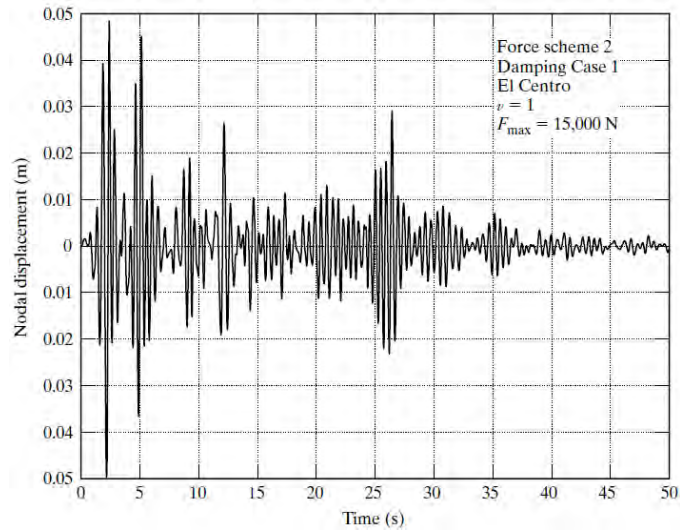


Figure 8.32: (a) Displacement of node 4; (b) time history response of the real part of the coordinate for mode 4;

8.4. STATE-SPACE FORMULATION FOR MDOF SYSTEMS

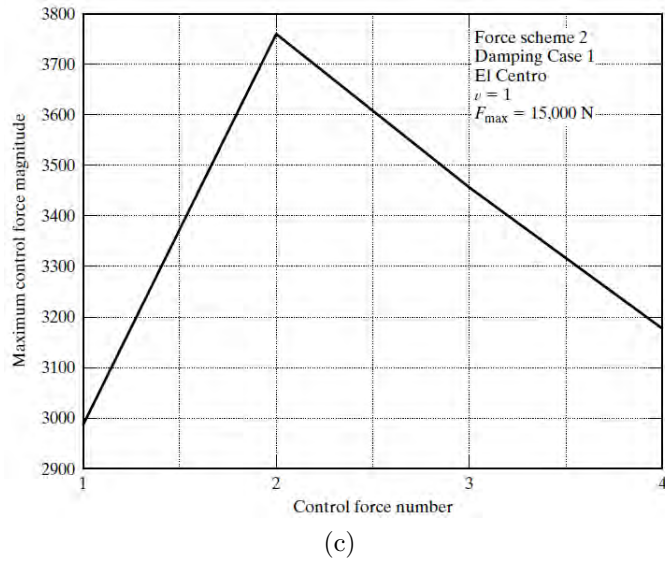


Figure 8.32: (c) peak values of the control forces.

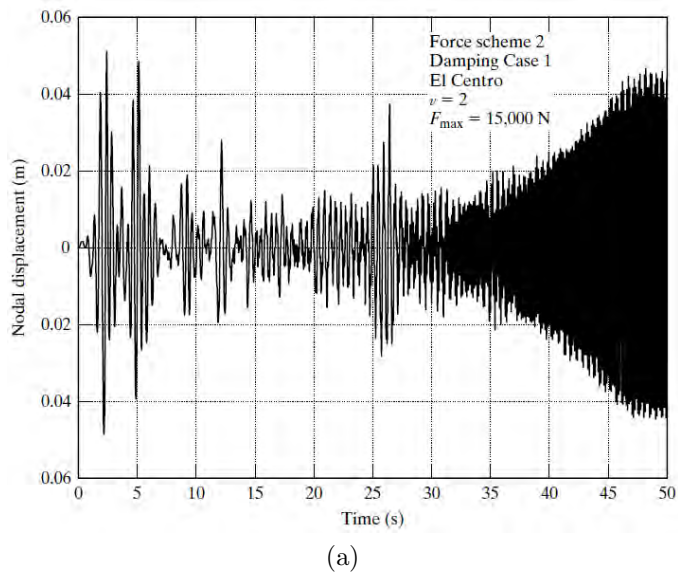
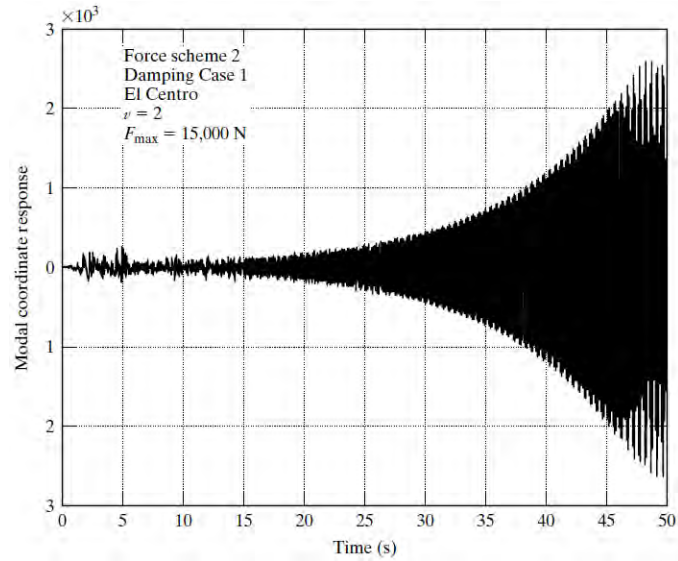
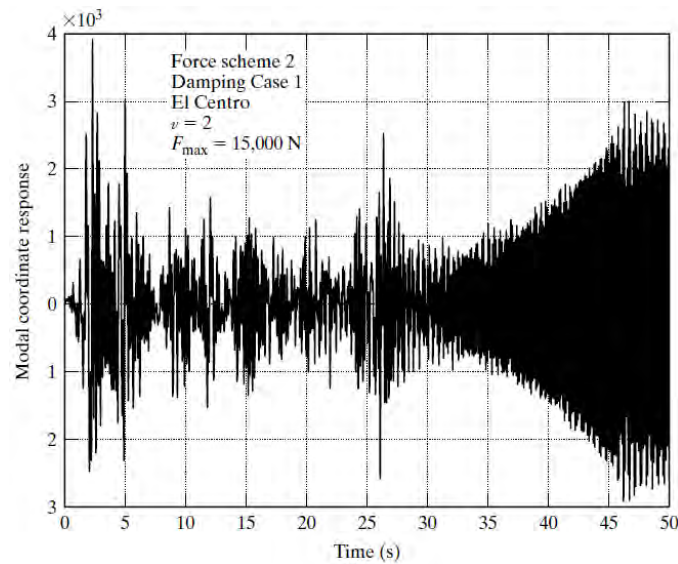


Figure 8.33: (a) Displacement of node 4;

CHAPTER 8. STRUCTURAL CONTROL DYNAMICS



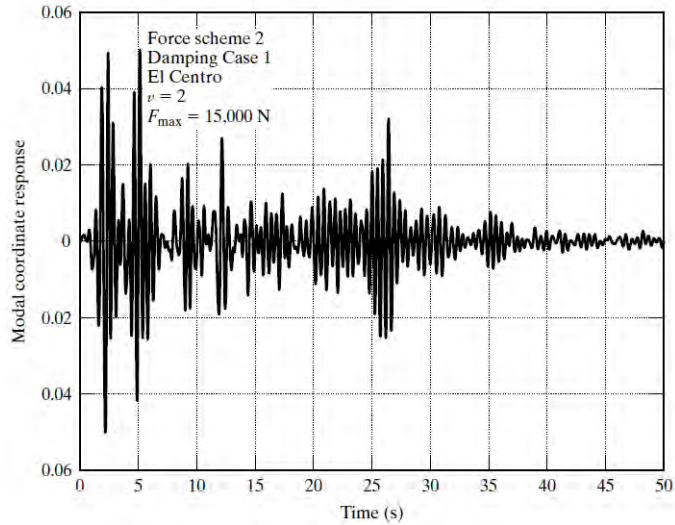
(b)



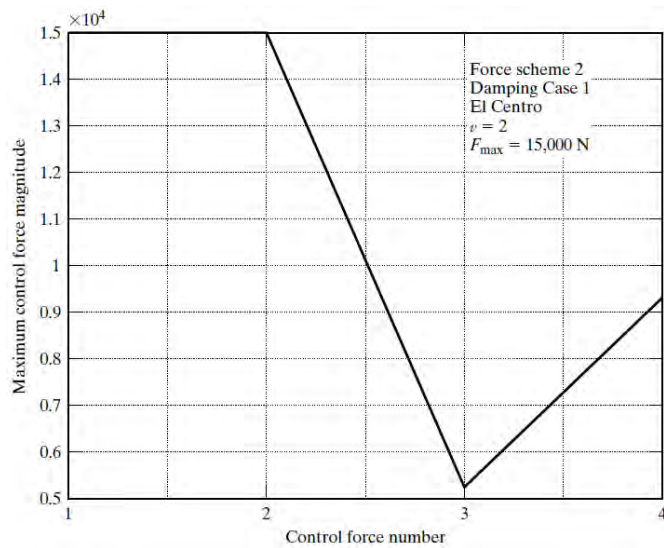
(c)

Figure 8.33: (b) time history response of the real part of the coordinate for mode 4; (c) time history response of the real part of the coordinate for mode 2;

8.4. STATE-SPACE FORMULATION FOR MDOF SYSTEMS



(d)



(e)

Figure 8.33: (d) time history response of the real part of the coordinate for mode 1; and (e) peak values of the control forces.

CHAPTER 8. STRUCTURAL CONTROL DYNAMICS

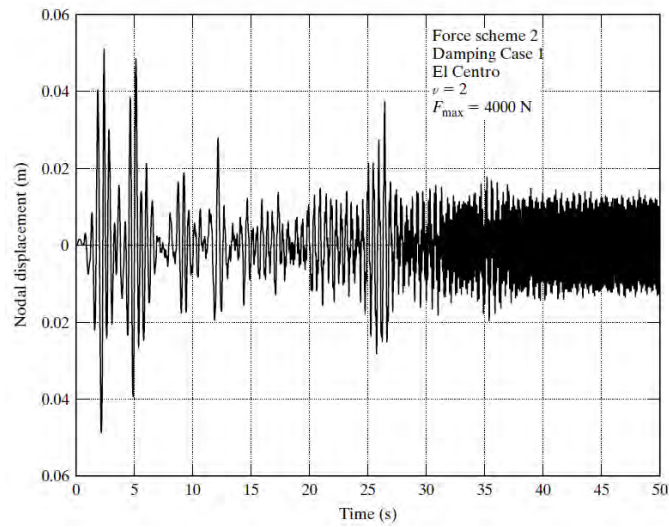


Figure 8.34: Displacement of node 4.

profiles are plotted in Fig. 8.36. The latter curves are scaled versions of the element shear deformation profiles.

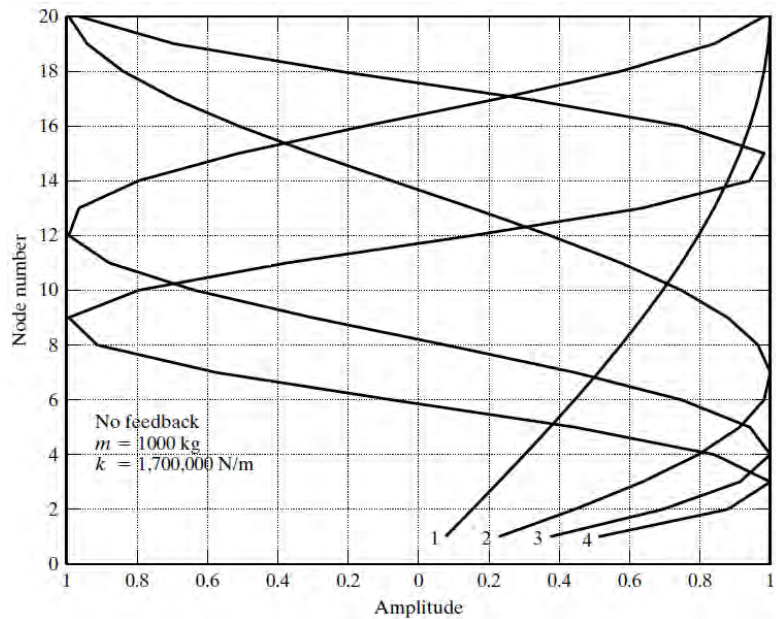


Figure 8.35: Modal displacement profiles.

8.4. STATE-SPACE FORMULATION FOR MDOF SYSTEMS

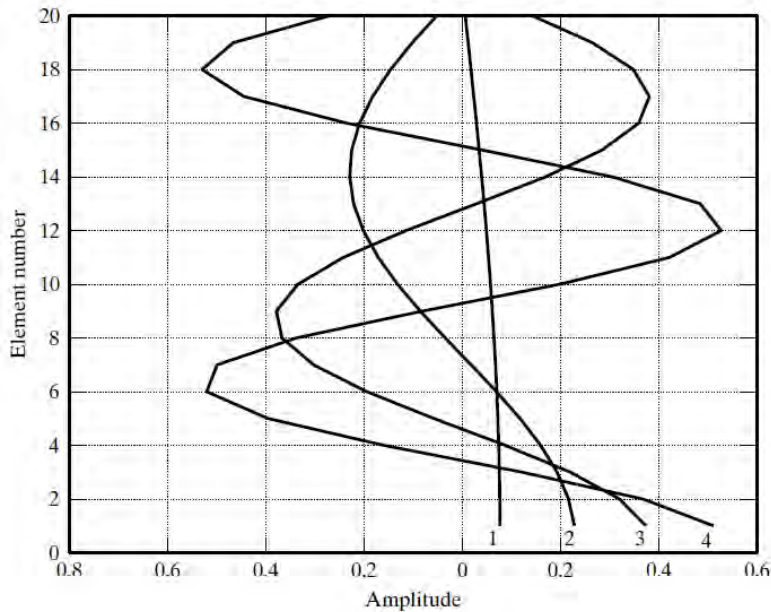


Figure 8.36: Scaled modal element shear deformation profiles.

Suppose the j^{th} control force system consists of a single force applied at one of the 20 nodes, say node l . If node l is a null point for a particular mode, the j^{th} force has no effect on the response of that mode. Considering Fig. 8.35, the first mode has no null points, and it follows that this mode can be controlled by applying the force at any of the 20 nodes. The second mode has a null point between nodes 13 and 14. Therefore, these nodes are ineffective. The optimum locations for controlling mode 2 are nodes 7 and 20, which correspond to the maximum amplitudes. Mode 3 has null points adjacent to nodes 8 and 16. Nodes 4, 12, and 20 are the optimal force locations. Lastly, mode 4 has null points adjacent to nodes 6, 12, and 18. The corresponding optimal locations are nodes 3, 9, 15, and 20. These results are summarized below in Table 8.6.

Another option is for the j^{th} control force system to consist of

CHAPTER 8. STRUCTURAL CONTROL DYNAMICS

Table 8.6

Mode	Nodal location - single control force	
	Optimal	Not allowed
1	20	1
2	7, 20	13, 14
3	4, 12, 20	8, 16
4	3, 9, 15, 20	6, 12, 18

a set of self-equilibrating forces applied at adjacent nodes, say l and $l + 1$. The product of the k^{th} modal vector, Φ_k , and the j^{th} column of \mathbf{E}_f is proportional to the shear deformation for the element located between nodes l and $l + 1$. Therefore, if this element corresponds to a null point for the modal element shear deformation profile, control force system j has no effect on the response of mode k . It follows that null points are to be avoided, and the elements corresponding to the peak values are the optimal locations for the pair of self-equilibrating control forces. Considering element j to be between nodes j and $j - 1$ and the forces to be applied at the ends of an element, the constraints and optimal locations for this case follow from Fig. 8.36, and are listed in Table 8.7.

Table 8.7

Mode	Element location - self-equilibrating force	
	Optimal	Not allowed
1	1	20
2	1, 14	7
3	1, 9, 17	5, 13
4	1, 6, 12, 18	3, 4, 9, 10, 15

8.4.10 Observability of a Particular Modal Response

Feedback is implemented by observing the response, computing the control forces with an algorithm, and then applying these forces with actuators. When the general modal formulation is used, \mathbf{F} is taken as a linear function of the modal coordinates:

$$\mathbf{F} = -\mathbf{k}_d \mathbf{q}_R - \mathbf{k}_v \mathbf{q}_I \quad (8.294)$$

Assuming s modes are considered, each q is of order $s \times 1$. If both terms are retained, $2s$ observations are required to uniquely define the modal response.

Let y_1, y_2, \dots, y_N denote the observations. These observations may be displacements, velocities, strains, strain rates, or some other measures that are linearly related to the state variables. The k^{th} observation is expressed as

$$y_k = \mathbf{D}_k \begin{bmatrix} \mathbf{U} \\ \dot{\mathbf{U}} \end{bmatrix} = \mathbf{D}_k \mathbf{X} \quad (8.295)$$

where \mathbf{D}_k depends on the nature and location of the observation represented by y_k . We can interpret \mathbf{D}_k as defining the nodal variables that y_k is monitoring. Substituting for the state vector in terms of the full set of n coordinates leads to the following exact expression for y_k :

$$y_k = \frac{1}{2} \sum_{j=1}^n \mathbf{D}_k (q_j \mathbf{V}_j + \tilde{q}_j \tilde{\mathbf{V}}_j) = \sum_{j=1}^n \mathbf{D}_k (\mathbf{V}_{R,j} q_{R,j} - \mathbf{V}_{I,j} q_{I,j}) \quad (8.296)$$

If \mathbf{D}_k is orthogonal to $\mathbf{V}_{R,j}$, $q_{R,j}$ does not contribute to y_k and it follows that y_k does not observe $q_{R,j}$. A similar statement applies for $q_{I,j}$. Therefore, for the j^{th} mode to be observable,

CHAPTER 8. STRUCTURAL CONTROL DYNAMICS

at least one of the set of \mathbf{D}_k 's cannot be orthogonal to the modal vectors for those modes that are included in the modal approximation for the solution.

Assuming s modes are retained and N observations are made at a particular instant in time, Eq. (8.296) is approximated by

$$\mathbf{y} \approx \mathbf{D}\mathbf{V}_R\mathbf{q}_R - \mathbf{D}\mathbf{V}_I\mathbf{q}_I \quad (8.297)$$

where \mathbf{y} is of order $N \times 1$; $\mathbf{q}_R, \mathbf{q}_I$ are of order $s \times 1$; the j^{th} row of \mathbf{D} contains \mathbf{D}_j ; and the k^{th} column of \mathbf{V} contains \mathbf{V}_k . Observability for the modal coordinates selected to approximate the solution requires each column of the products, $\mathbf{D}\mathbf{V}_R$ and $\mathbf{D}\mathbf{V}_I$, to have at least one nonzero term. This constraint can be expressed in terms of the rank of the products.

$$\begin{aligned} \text{rank}(\mathbf{D}\mathbf{V}_R) &= s \\ \text{rank}(\mathbf{D}\mathbf{V}_I) &= s \end{aligned} \quad (8.298)$$

Since $\mathbf{D}\mathbf{V}$ is of order $N \times s$, it follows that $N \geq s$. If $N = 2s$ and the rank constraint is satisfied, the solution for \mathbf{q}_R and \mathbf{q}_I is unique. Otherwise, a least squares type of solution has to be generated.

When damping is uncoupled, the linear velocity feedback law expressed in terms of modal coordinates simplifies to

$$\mathbf{F} = -\mathbf{k}_v\dot{\mathbf{q}} \quad (8.299)$$

where $\dot{\mathbf{q}}$ and $\dot{\mathbf{U}}$ are related by

$$\dot{\mathbf{U}} \approx \Phi\dot{\mathbf{q}} \quad (8.300)$$

Suppose the observations involve nodal velocities. Expressing \mathbf{y} as

$$\mathbf{y} = \mathbf{D}^T \dot{\mathbf{U}} \quad (8.301)$$

and substituting for $\dot{\mathbf{U}}$ results in

$$\mathbf{y} = (\mathbf{D}^T \Phi) \dot{\mathbf{q}} \quad (8.302)$$

Assuming s modes are retained, observability requires $\mathbf{D}^T \Phi_j \neq \mathbf{0}$ for $j = 1, 2, \dots, s$. This constraint is equivalent to the condition that the observation points are not located at null points for the j^{th} modal vector. Requiring that rank of $\mathbf{D}^T \Phi$ to be equal to s satisfies the observability condition. Since it also requires $N \geq s$, the solution is either unique ($N = s$), or over-determined.

Example 8.14 - Observability analysis for a 20DOF model

Suppose four modes are retained, and the observed variables are nodal velocities. At least four observations are necessary when damping is uncoupled. For arbitrary damping, eight observations are required. If damping is uncoupled, the constraint on the location of the observation points is that they do not coincide with null points of the modal displacement profiles. The most desirable locations are those that coincide with the maximum modal amplitudes. This choice eliminates the possibility of an ill-conditioned set of equations for the modal velocities defined by Eq. (8.302). The unacceptable and optimal locations for the velocity observations are listed in Table 8.8.

We need to select at least four observation nodes. Taking 7, 9, 12, and 20, and applying Eq. (8.302) leads to the following set of equations for the first four modal velocities:

CHAPTER 8. STRUCTURAL CONTROL DYNAMICS

Table 8.8

Modal response quantity	Nodal Location - Optimal	Velocity Observation - Not allowed
\dot{q}_1	20	1
\dot{q}_2	7, 20	13, 14
\dot{q}_3	4, 12, 20	8, 16
\dot{q}_4	3, 9, 15, 20	6, 12, 18

$$\begin{bmatrix} \dot{u}_7 \\ \dot{u}_9 \\ \dot{u}_{12} \\ \dot{u}_{20} \end{bmatrix} = \begin{bmatrix} 0.5114 & 1.0000 & 0.4440 & -0.5757 \\ 0.6367 & 0.8792 & -0.3019 & 0.9941 \\ 0.7959 & 0.3741 & -0.9941 & 0.1528 \\ 1.0000 & -0.9941 & 0.9824 & -0.9650 \end{bmatrix} \begin{bmatrix} \dot{q}_1 \\ \dot{q}_2 \\ \dot{q}_3 \\ \dot{q}_4 \end{bmatrix} \quad (8.303)$$

Inverting Eq. (8.304) results in

$$\begin{bmatrix} \dot{q}_1 \\ \dot{q}_2 \\ \dot{q}_3 \\ \dot{q}_4 \end{bmatrix} = \begin{bmatrix} 0.6124 & -0.6095 & 0.8513 & 0.3973 \\ 0.7397 & -0.0967 & 0.0262 & -0.3375 \\ 0.8881 & -0.7186 & -0.2170 & 0.1761 \\ 0.7767 & -1.2636 & 0.6343 & -0.0975 \end{bmatrix} \begin{bmatrix} \dot{u}_7 \\ \dot{u}_9 \\ \dot{u}_{12} \\ \dot{u}_{20} \end{bmatrix} \quad (8.304)$$

Problems

Problem 8.1

Refer to Eq. (8.29). Consider a SDOF system that is initially at rest ($u_0 = \dot{u}_0 = 0$).

1. Determine $u(t)$ for the case of a sinusoidal ground acceleration, $a_g = \hat{a}_g \sin \Omega t$.
2. Discuss how you would develop a numerical procedure for evaluating u at various times such as t_1, t_2, \dots and so on.

Problem 8.2

Show that the error in the Pade approximation, Eq. (8.56), is of order $(\lambda t_d)^3$.

$$e^{-\lambda t_d} = \frac{1 - \frac{1}{2}(\lambda t_d)}{1 + \frac{1}{2}(\lambda t_d)} + \text{error}$$

Problem 8.3

Consider a single-degree-of-freedom system with continuous pure velocity feedback. Suppose the natural period is 1 second. Use Eq. (8.59) to determine the maximum allowable time delay corresponding to the following values for ξ and ξ_a :

$$\begin{aligned}\xi &= 0.05 \\ \xi_a &= 0.05, 0.10, 0.20, 0.30\end{aligned}$$

Problem 8.4

Verify Eq. (8.82).

Problem 8.5

CHAPTER 8. STRUCTURAL CONTROL DYNAMICS

A SDOF system has the following properties:

$$m = 1,000 \text{ kg}$$

$$k = 70,000 \text{ N/m}$$

$$c = 320 \text{ N} \cdot \text{s/m}$$

Using the data contained in Ex. 8.2, estimate the limiting time step for each of the following values of the feedback parameters:

$$k_d = 0$$

$$k_v = 0, 800, 1600, 3200, 6400 \text{ N} \cdot \text{s/m}$$

Problem 8.6

Refer to Ex. 8.3. Extend Table 8.2 to include $\xi = 0.05$. Consider $\nu = 0, 1, 2$ and $\xi_a = 0, 0.1, 0.2, 0.3$.

Problem 8.7

Refer to Eq. (8.168) of Ex. 8.4. Show that the eigenvectors are real when \mathbf{K} and \mathbf{M} are symmetric and the eigenvalues are positive real quantities when \mathbf{K} and \mathbf{M} are positive definite.

Problem 8.8

Show that $\mathbf{W}_j^T \mathbf{V}_k = 0$ for $j \neq k$ by substituting for \mathbf{W} and \mathbf{V} using Eq. (8.211) and noting the definition equation for ϕ_j, λ_j .

$$\lambda_j^2 \mathbf{M} \phi_j + \lambda_j \mathbf{C} \phi_j + \mathbf{K} \phi_j = \mathbf{0}$$

Problem 8.9

Refer to Eq. (8.259) of Ex. 8.8. Reduce these equations to a single equation in terms of q_R and compare with the equation

8.4. STATE-SPACE FORMULATION FOR MDOF SYSTEMS

obtained with the conventional modal formulation [e.g., see Eq. (8.4.6)]. Is there any advantage to working with the state-space formulation versus the conventional modal formulation?

Problem 8.10

Consider a 20DOF system having the following constant properties:

$$\text{mass} = 1,000 \text{ kg}$$

$$\text{element stiffness} = 1,800 \text{ kN/m}$$

$$\text{element damping} = 25 \text{ kN} \cdot \text{s/m}$$

1. Determine the modal properties (period, damping, modal displacement profile, modal intermodal displacement profile) for the first four modes.
2. Determine the response for node 20 due to the Kobe ground excitation using the complete state-space formulation. Take $\Delta t = 0.02 \text{ s}$.
3. Repeat part 2. using the modal state-space formulation and only the first four modes. Compare the time history and Fourier components for node 20 with the corresponding results obtained in 2. Also compare the peak values of the modal coordinates.

9

Linear Control

9.1 Introduction

In this chapter, the concept of linear negative feedback is introduced, and the topic of stability is revisited. The primary focus is on assessing the effect of time delay in applying the control force on the stability. Subsequently, the choice of the optimal magnitudes of the feedback parameters is considered. Optimality is related to the magnitude of a quadratic performance index (LQR), which is taken as a time integral involving weighted response and control force terms. This approach is referred to as the linear quadratic regulator problem and leads to a time-invariant linear relationship between the control forces and state variables. Finally, we discuss optimal feedback based on the LQR performance index generalized for MDOF systems. Examples that illustrate the sensitivity of the response and cost parameters to variations in the location and nature of the control forces and weighting coefficients are presented. We end the chapter with a brief discussion of advanced topics for time-invariant control

9.2 Optimal Linear Feedback: Time-Invariant SDOF Systems

9.2.1 Quadratic Performance Index

The previous Chapter was concerned with presenting the state-space formulation and numerical procedures for evaluating the time history response of SDOF systems having linear time-invariant feedback. Negative velocity feedback was shown to be equivalent to damping and to result in stable behavior when it is applied in a continuous manner with no time delay. The effect of time delay can be destabilizing under certain condi-

9.2. OPTIMAL LINEAR FEEDBACK: TIME-INVARIANT SDOF SYSTEMS

tions that depend on the magnitude of the feedback force and the delay time. Discrete time control works with response data at discrete time points and considers the feedback force to be constant over a time interval. Instability can also occur if the time interval exceeds a critical value that depends on the level of feedback-induced damping and the time delay. Given the feedback parameters, k_d and k_v , and the delay time, we can determine the limiting time interval using the procedure described in the previous section. The remaining issue that needs to be addressed here is the selection of the magnitude of the feedback parameters. A strategy similar to the approach followed for quasi-static control is introduced in this section. The key step is the formulation of a performance measure that provides a rational basis for comparing different choices for the feedback parameters and establishing the optimal solution.

Dynamic control is concerned with controlling the response of the system over a specified time period. Starting at some initial state, $\mathbf{X}(0)$, the objective is to minimize the deviation between the actual response, $\mathbf{X}(t)$, and the desired response, $\mathbf{X}^*(t)$, by applying a control force $F(t)$ over the time interval. Considering the integral of the square of the difference between the actual and desired responses to be the measure of the closeness of the solution and including a cost associated with the control force leads to the following quadratic performance index for a SDOF system:

$$J = \frac{1}{2} \int_0^{t^*} [q_d(u - u^*)^2 + q_v(\dot{u} - \dot{u}^*)^2 + rF^2] dt \quad (9.1)$$

where t^* is the time period over which the performance is being measured, and q_d , q_v , are r the weighting functions for the

CHAPTER 9. LINEAR CONTROL

displacement, velocity, and force terms. Specializing F for linear time-invariant feedback transforms J to

$$J = \frac{1}{2} \int_0^{t^*} [q_d(u - u^*)^2 + q_v(\dot{u} - \dot{u}^*)^2 + r(k_d u + k_v \dot{u})^2] dt \quad (9.2)$$

where k_d and k_v are constants.

When the system and weighting parameters are specified, J reduces to a function of the feedback parameters, the external excitation, the desired response, and the time period. The optimal feedback for a specific combination of excitation, desired response, and time interval is defined as the set of values for k_d and k_v that correspond to a stationary value of J specialized for these conditions. They are determined with the following equations:

$$\frac{\delta}{\delta k_d} J^* = 0 \quad \frac{\delta}{\delta k_v} J^* = 0 \quad (9.3)$$

In general, the response depends on k_d and k_v , as well as the system parameters and external excitation. One option is to evaluate J^* numerically and use simulation to locate the optimal values for k_d and k_v . This approach is not very efficient since it requires ranging over both k_d and k_v . Another option is to apply variational calculus methodology and transform the stationary requirement to a differential equation.

In the following section, an example illustrating the first option is presented. This example deals with the special case where u^* is taken as 0, the response is due to an initial velocity at $t = 0$, and the time interval extends out to infinity. These conditions are typical for the regulator problem, which is concerned with applying control forces to take a system from an arbitrary

9.2. OPTIMAL LINEAR FEEDBACK: TIME-INVARIANT SDOF SYSTEMS

nonzero initial state \mathbf{X}_0 , to a final state \mathbf{X}_f at time t_f . The regulator problem is encountered when a system is perturbed from its steady-state equilibrium position and there is a need to eliminate the unwanted perturbation as quickly as possible. Since the required force increases as the time interval decreases, it is necessary to include the force cost as well as the response magnitude in the performance index in order to obtain a realistic solution.

Subsequent sections describe the variational calculus formulation of the stationary requirement for J as a differential equation and illustrate its application. This derivation is extended to deal with multi-degree-of-freedom systems later in this chapter.

9.2.2 An Example: Linear Quadratic Regulator Control Algorithm

Suppose a single-degree-of-freedom system is subjected to an impulse at $t = 0$. Considering only velocity feedback, the response is given by

$$u = \frac{\dot{u}_0}{\lambda_I} e^{\lambda_R t} \sin \lambda_I t \quad (9.4)$$

where \dot{u}_0 is the initial velocity, and the lambda terms depend on the system properties and the velocity feedback parameter.

$$\begin{aligned} \lambda_R &= -\xi_{eq}\omega \\ \lambda_I &= \omega(1 - \xi_{eq}^2)^{1/2} \\ \xi_{eq} &= \xi + \frac{k_v}{2\omega m} = \xi + \xi_a \end{aligned} \quad (9.5)$$

Interpreting u as a disturbance from the steady-state position, $\dot{u}^* = 0$, the objective is to reduce u to a small quantity (i.e., to

CHAPTER 9. LINEAR CONTROL

regulate the response, in a specified time interval). The linear quadratic regulator control algorithm specialized for only velocity feedback is based on the following form of J :

$$J = \frac{1}{2} \int_0^{\infty} [q_d u^2 + q_v \dot{u}^2 + r(k_v \dot{u})^2] dt \quad (9.6)$$

and determines the optimal value of k_v by enforcing the stationary requirement with respect to k_v :

$$\frac{\delta J}{\delta k_v} = 0 \quad (9.7)$$

Substituting for u in Eq. (9.6), considering the weighting functions to be constant, and expressing k_v in terms of ξ_a leads to

$$\left(\frac{8\omega}{\dot{u}_0^2}\right) J = \frac{1}{\xi + \xi_a} \left(\frac{q_d}{\omega^2} + q_v + 4m^2\omega^2 r \xi_d^2\right) \quad (9.8)$$

The form of the terms within the square bracket suggest the following scale factors for the weights:

$$\begin{aligned} q_d &= \omega^2 \bar{q}_d \\ q_v &= \bar{q}_v \\ r &= \frac{\bar{r}}{4m^2\omega^2} \end{aligned} \quad (9.9)$$

With these definitions, all the superscripted weights have the units of $(1/\text{velocity})^2$ and the performance index simplifies to

$$\left(\frac{8\omega}{\dot{u}_0^2}\right) J = \frac{\bar{q}_d + \bar{q}_v}{\xi + \xi_a} + \bar{r} \frac{\xi_a^2}{\xi + \xi_a} \quad (9.10)$$

9.2. OPTIMAL LINEAR FEEDBACK: TIME-INVARIANT SDOF SYSTEMS

Finally, enforcing the stationary requirement on J with respect to ξ_a results in the following equation for the optimal active damping ratio:

$$\xi_a|_{\text{optimal}} = \left(\xi^2 + \frac{\bar{q}_d + \bar{q}_v}{\bar{r}} \right)^{1/2} - \xi \quad (9.11)$$

Fig. 9.1 shows the variation of ξ_a with the weighting parameters. Increasing \bar{r} places more emphasis on minimizing the control force, and ξ_a decreases. Increasing the displacement and velocity weights places more emphasis on decreasing the response, and the result is an increase in ξ_a .

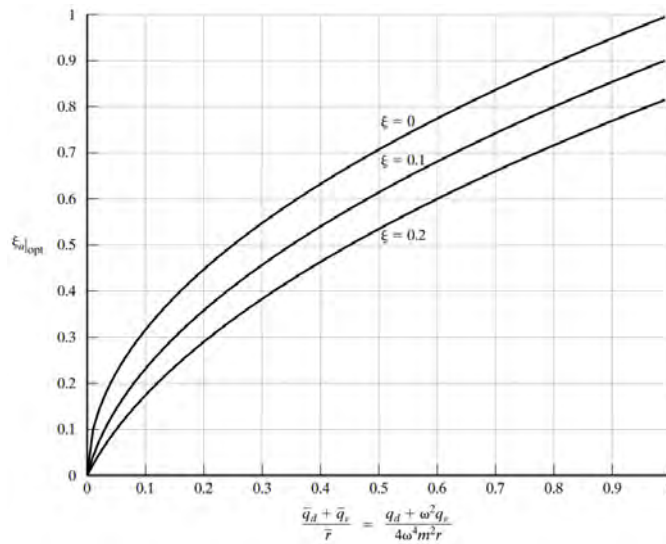


Figure 9.1: Variation of the optimal velocity feedback with the weighting parameters.

The previous analysis considered the weighting functions to be constant over the time period during which the performance index is being evaluated. This restriction fixes the relative priorities on the various terms that contribute to the index. If the weights

CHAPTER 9. LINEAR CONTROL

are allowed to vary with time, the priorities can be adjusted as to place more emphasis on a certain term at a particular point in time.

For example, we may want to suppress the response more aggressively later in the period. This shift in emphasis can be achieved by taking the weights as

$$\begin{aligned} q_d &= \omega^2 \frac{t}{T^*} \bar{q}_d \\ q_v &= \frac{t}{T^*} \bar{q}_v \\ r &= \frac{\bar{r}}{4m^2\omega^2} \end{aligned} \quad (9.12)$$

where T^* is a time constant that defines the transition for the priority shift. It is convenient to express T^* in terms of the fundamental period for the system and a scaling factor, α .

$$T^* = \alpha T = \frac{2\pi\alpha}{\omega} \quad (9.13)$$

The performance index for this case has the following form:

$$\left(\frac{8\omega}{\dot{u}_0^2}\right) J = \frac{1}{4\pi\alpha} \left[2\bar{q}_d + \frac{\bar{q}_d + \bar{q}_v}{(\xi + \xi_a)^2} \right] + \bar{r} \frac{\xi_a^2}{\xi + \xi_a} \quad (9.14)$$

Requiring J to be stationary with respect to ξ_a results in a cubic polynomial for the optimal value of ξ_a .

$$\xi_a(\xi_a + \xi)(\xi_a + 2\xi) - \frac{1}{2\pi\alpha} \frac{\bar{q}_d + \bar{q}_v}{\bar{r}} = 0 \quad (9.15)$$

Fig. 9.2 contains plots corresponding to $\xi = 0$ and various values of α . Also shown is the plot for the uniform (time)

9.2. OPTIMAL LINEAR FEEDBACK: TIME-INVARIANT SDOF SYSTEMS

weighting case defined by Eq. (9.11). Assuming that q_d , q_v , and r are fixed, the effect of increasing α is to reduce the optimal value of ξ_a . This trend is due to the decrease in magnitude of the weighted response during the initial phase of the response, where the actual response magnitude is a maximum. Lowering this term decreases the demand on the control force, and consequently the required value of ξ_a decreases.

CHAPTER 9. LINEAR CONTROL

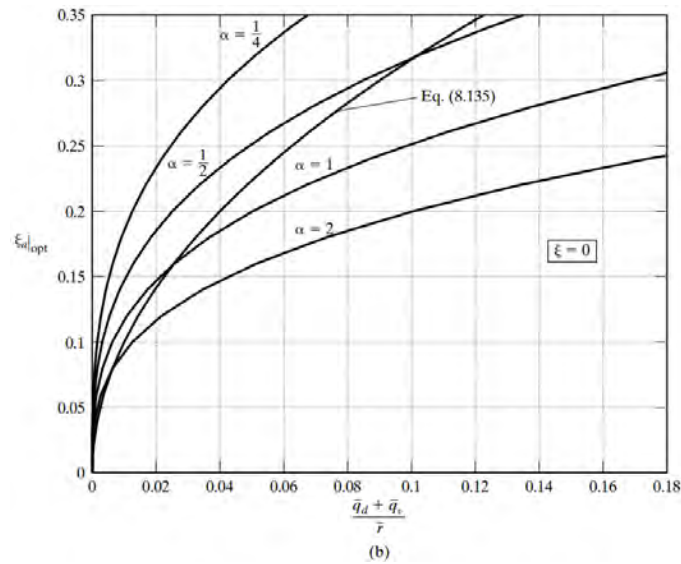
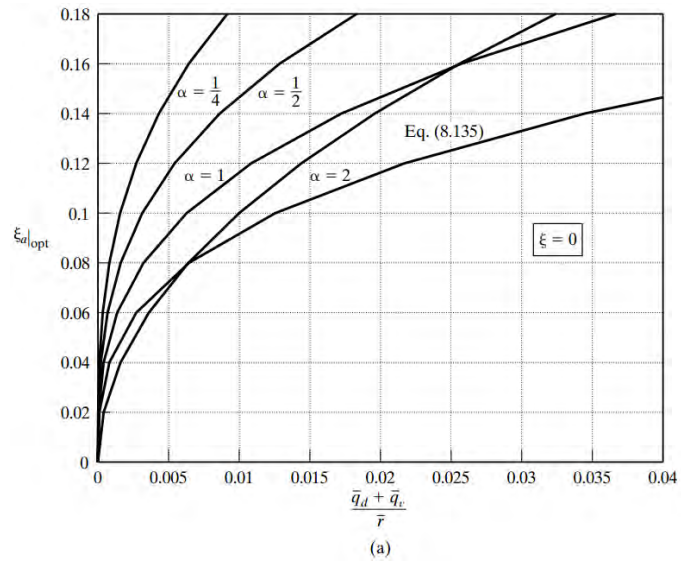


Figure 9.2: Variation of the optimal velocity feedback with the time scale factor, α .

9.2. OPTIMAL LINEAR FEEDBACK: TIME-INVARIANT SDOF SYSTEMS

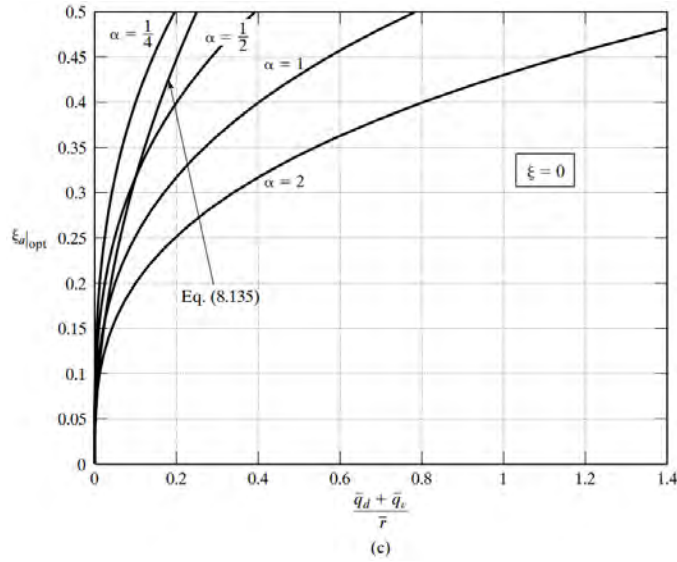


Figure 9.2: Variation of the optimal velocity feedback with the time scale factor, α (continued).

9.2.3 The Continuous Time Algebraic Riccati Equation

The previous example illustrated the application of the linear quadratic regulator algorithm for a particular initial state and velocity feedback. In what follows, the performance index is expressed in matrix form, and the analysis is extended to be applicable for both displacement and velocity feedback and arbitrary initial conditions.

The scalar form of the performance index for the linear quadratic regular problem is obtained by setting $u^* = \dot{u}^* = 0$ in Eq. (9.2) and taking $t^* = \infty$.

$$J = \frac{1}{2} \int_0^\infty [q_d u^2 + q_v \dot{u}^2 + r(k_d u + k_v \dot{u})^2] dt \quad (9.16)$$

Introducing the state vector notation, J is expressed as

$$J = \frac{1}{2} \int_0^{\infty} \mathbf{X}^T (\mathbf{Q} + \mathbf{K}_f^T \mathbf{R} \mathbf{K}_f) \mathbf{X}^T dt \quad (9.17)$$

where \mathbf{Q} and \mathbf{R} are diagonal weighting matrices, and \mathbf{K}_f is the linear state feedback matrix.

$$\begin{aligned} \mathbf{Q} &= \begin{bmatrix} q_d & \\ & q_v \end{bmatrix} \\ \mathbf{R} &= r [1] \\ \mathbf{K}_f &= [k_d \quad k_v] \end{aligned} \quad (9.18)$$

The governing differential equation for free vibration response follows from Eq. (8.38):

$$\dot{\mathbf{X}} = \mathbf{A}_c \mathbf{X} = (\mathbf{A} - \mathbf{B}_f \mathbf{K}_f) \mathbf{X} \quad (9.19)$$

Solutions of Eq. (9.19) satisfy

$$X(t) \rightarrow 0 \quad \text{as} \quad t \rightarrow \infty \quad (9.20)$$

when the feedback parameters (k_v , k_d) are selected such that the eigenvalues of \mathbf{A}_c have a negative real part.

When the weighting matrices are taken to be constant, an explicit expression for J can be obtained by expressing the integrand as a Liapunov function [80]:

$$\mathbf{X}^T (\mathbf{Q} + \mathbf{K}_f^T \mathbf{R} \mathbf{K}_f) \mathbf{X} = -\frac{d}{dt} (\mathbf{X}^T \mathbf{H} \mathbf{X}) \quad (9.21)$$

where \mathbf{H} is a symmetric positive-definite second-order matrix. Noting Eq. (9.19), the right-hand side expands to

9.2. OPTIMAL LINEAR FEEDBACK: TIME-INVARIANT SDOF SYSTEMS

$$-\frac{d}{dt}(\mathbf{X}^T \mathbf{H} \mathbf{X}) = \dot{\mathbf{X}}^T \mathbf{H} \mathbf{X} + \mathbf{X}^T \mathbf{H} \dot{\mathbf{X}} = \mathbf{X}^T (\mathbf{A}_c^T \mathbf{H} + \mathbf{H} \mathbf{A}_c) \mathbf{X} \quad (9.22)$$

and it follows that

$$\mathbf{A}_c^T \mathbf{H} + \mathbf{H} \mathbf{A}_c = -(\mathbf{Q} + \mathbf{K}_f^T \mathbf{R} \mathbf{K}_f) \quad (9.23)$$

With this change in variables, the integral reduces to

$$J = \frac{1}{2} \mathbf{X}^T(0) \mathbf{H} \mathbf{X}(0) \quad (9.24)$$

Requiring J to be stationary with respect to \mathbf{K}_f and noting that $\mathbf{X}(0)$ is independent of \mathbf{K}_f leads to $\delta \mathbf{H} = 0$. The differential of \mathbf{H} is generated by operating on Eq. (9.23).

$$\mathbf{A}_c^T \delta \mathbf{H} + \delta \mathbf{H} \mathbf{A}_c + \delta \mathbf{A}_c^T \mathbf{H} + \mathbf{H} \delta \mathbf{A}_c = -\delta \mathbf{K}_f^T \mathbf{R} \mathbf{K}_f - \mathbf{K}_f^T \mathbf{R} \delta \mathbf{K}_f \quad (9.25)$$

Substituting for \mathbf{A}_c ,

$$\delta \mathbf{A}_c = -\mathbf{B}_f \delta \mathbf{K}_f \quad (9.26)$$

and setting $\delta \mathbf{H} = 0$, the stationary condition takes the form

$$\delta \mathbf{K}_f^T (\mathbf{B}_f^T \mathbf{H} - \mathbf{R} \mathbf{K}_f) + (\mathbf{H} \mathbf{B}_f - \mathbf{K}_f^T \mathbf{R}) \delta \mathbf{K}_f = \mathbf{0} \quad (9.27)$$

For Eq. (9.27) to be satisfied for arbitrary $\delta \mathbf{K}_f$, the coefficients must vanish. Then the optimal feedback is related to \mathbf{H} by

$$\mathbf{R}^{-1} \mathbf{B}_f^T \mathbf{H} = \mathbf{K}_f|_{\text{optimal}} \quad (9.28)$$

CHAPTER 9. LINEAR CONTROL

The last step involves substituting for \mathbf{K}_f in Eq. (9.23). This operation leads to the following definition equation for \mathbf{H} , which is called the continuous time algebraic Riccati equation:

$$\mathbf{A}^T \mathbf{H} + \mathbf{H} \mathbf{A} - \mathbf{H} \mathbf{B}_f \mathbf{R}^{-1} \mathbf{B}_f^T \mathbf{H} = -\mathbf{Q} \quad (9.29)$$

Given the system parameters (\mathbf{A} , \mathbf{B}_f), we specify the weights (\mathbf{Q} and \mathbf{R}) and solve for the elements of \mathbf{H} . Note that by definition, \mathbf{H} is symmetric and positive definite. With \mathbf{H} known, the feedback matrix is determined with Eq. (9.28). Substituting for \mathbf{A} and \mathbf{B}_f ,

$$\begin{aligned} \mathbf{A} &= \begin{bmatrix} 0 & 1 \\ -\omega^2 & -2\xi\omega \end{bmatrix} \\ \mathbf{B}_f &= \begin{bmatrix} 0 \\ \frac{1}{m} \end{bmatrix} \end{aligned} \quad (9.30)$$

and expressing \mathbf{H} as

$$\mathbf{H} = \begin{bmatrix} H_{11} & H_{12} \\ H_{12} & H_{22} \end{bmatrix} \quad (9.31)$$

in Eq. (9.29) yields the following three equations for the elements of \mathbf{H} :

$$\begin{aligned} \left(\frac{1}{rm^2}\right) H_{12}^2 + 2\omega^2 H_{12} - q_d &= 0 \\ \left(\frac{1}{rm^2}\right) H_{12} H_{22} - H_{11} + 2\xi\omega H_{12} + \omega^2 H_{22} &= 0 \\ \left(\frac{1}{rm^2}\right) H_{22}^2 + 4\xi\omega H_{22} - 2H_{12} - q_v &= 0 \end{aligned} \quad (9.32)$$

9.2. OPTIMAL LINEAR FEEDBACK: TIME-INVARIANT SDOF SYSTEMS

The elements of \mathbf{H} are also constrained by the requirement that \mathbf{H} must be positive definite.

$$H_{11} > 0 \quad H_{22} > 0 \quad H_{11}H_{22} - H_{12}^2 > 0 \quad (9.33)$$

Given \mathbf{H} , the elements of \mathbf{K}_f are determined with Eq. (9.28).

$$\begin{aligned} k_d &= \frac{H_{12}}{rm} \\ k_v &= \frac{H_{22}}{rm} \end{aligned} \quad (9.34)$$

Solving for H_{12} and H_{22} enforcing the positive-definite requirement leads to

$$\begin{aligned} H_{12} &= r\omega^2 m^2 \left[-1 + \left(1 + \frac{q+d}{r\omega^4 m^2} \right)^{1/2} \right] \\ H_{22} &= 2r\omega m^2 \left[-\xi + \left(\xi^2 + \frac{q_v}{4r\omega^2 m^2} + \frac{H_{12}}{2r\omega^2 m^2} \right)^{1/2} \right] \end{aligned} \quad (9.35)$$

The equivalent frequency and damping for the SDOF system with feedback corresponding to Eq. (9.34) are determined with Eq. (8.42) and (9.34).

$$\begin{aligned} \omega_{\text{eq}} &= \omega \left(1 + \frac{k_d}{\omega^2 m} \right)^{1/2} \Rightarrow \omega \left(1 + \frac{q_d}{r\omega^4 m^2} \right)^{1/4} \\ \xi_{\text{eq}} &= \xi \frac{\omega}{\omega_{\text{eq}}} + \frac{k}{2m\omega_{\text{eq}}} \Rightarrow \frac{\omega}{\omega_{\text{eq}}} \left\{ \xi^2 + \frac{q_v}{4r\omega^2 m^2} + \frac{1}{2} \left[-1 + \left(1 + \frac{q_d}{r\omega^4 m^2} \right)^{1/2} \right] \right\}^{1/2} \end{aligned} \quad (9.36)$$

CHAPTER 9. LINEAR CONTROL

Weighting the displacement introduces additional stiffness and increases the frequency. Weighting the velocity generates additional damping but has no effect on the frequency. It follows that pure velocity feedback corresponds to $q_d = 0, q_v \neq 0$. The active damping ratio for this case is given by

$$\xi_a = \frac{H_{22}}{2rm^2\omega} = -\xi + \left(\xi^2 + \frac{q_v}{4r\omega^2m^2} \right)^{1/2} \quad (9.37)$$

This result coincides with Eq. (9.11), which was generated by integrating the analytic solution for the impulse generated response. These solutions must coincide since the approach followed earlier is a simplified version of this procedure.

The matrix formulation just presented is also applicable to multi-degree-of-freedom systems. **MATLAB** has a function called **care** (Continuous-time Algebraic Riccati Equation) that generates **H**, **K_f**, and the eigenvalues of **A** – **B_fK_f** for specified values of **A**, **B_f**, **Q**, and **R**. One option for scaling **Q** and **R** is to use the factors defined by Eq. (9.9). The corresponding forms are

$$\begin{aligned} \mathbf{Q} &= \begin{bmatrix} q_d & \\ & q_v \end{bmatrix} = \begin{bmatrix} \omega^2 \bar{q}_d & 0 \\ 0 & \bar{q}_v \end{bmatrix} \\ \mathbf{R} &= [r] = \left[\frac{\bar{r}}{4m^2\omega^2} \right] \end{aligned} \quad (9.38)$$

where \bar{q}_d , \bar{q}_v , and \bar{r} range from 0 to ≈ 1 . **MATLAB**'s default option is to assume $\mathbf{R} \equiv \mathbf{I}$. In this case, taking **Q** as

$$\mathbf{Q}|_{\mathbf{R}=\mathbf{I}} = \begin{bmatrix} 4\omega^4 m^2 \bar{q}_d & 0 \\ 0 & 4m^2 \omega^2 \bar{q}_v \end{bmatrix} \quad (9.39)$$

maintains the same range ($0 \rightarrow 1$) for \bar{q}_d and \bar{q}_v .

9.2. OPTIMAL LINEAR FEEDBACK: TIME-INVARIANT SDOF SYSTEMS

The form of the continuous algebraic Riccati solution corresponding to $r = 1$ and q_d, q_v defined by Eq. (9.39) is

$$\begin{aligned} \frac{k_d}{k} &= -1 + (1 + 4\bar{q}_d)^{1/2} \\ \frac{k_v}{2\omega m} &= \xi_a = -\xi + \left(\xi^2 + \bar{q}_v + \frac{k_d}{2k} \right)^{1/2} \end{aligned} \quad (9.40)$$

A similar scaling strategy can be employed for a multi-degree-of-freedom system. In this case the magnitude of the weighting factor for each of the displacement and velocity variables can be independently assigned.

9.2.4 The Discrete Time Algebraic Riccati Equation

The discrete time formulation of the algebraic Riccati equation is based on a performance index that involves a summation of weighted response terms evaluated at discrete times. The discrete form of the performance index corresponding to the same assumptions introduced for the continuous time formulation is

$$J = \frac{1}{2} \sum_{j=0}^{\infty} \mathbf{X}_j^T (\mathbf{Q} + \mathbf{K}_f^T \mathbf{R} \mathbf{K}_f) \mathbf{X}_j \quad (9.41)$$

where \mathbf{X}_j is determined with Eq. (8.88), which is written here as

$$\begin{aligned} \mathbf{X}_{j+1} &= \mathbf{c}_1 \mathbf{X}_j + \mathbf{c}_2 \mathbf{F}_f \\ \mathbf{c}_1 &= \mathbf{e}^{\mathbf{A}\Delta t} \\ \mathbf{c}_2 &= \mathbf{A}^{-1} (\mathbf{e}^{\mathbf{A}\Delta t} - \mathbf{I}) \mathbf{B}_f \end{aligned} \quad (9.42)$$

Taking $\mathbf{F}_j = -\mathbf{K}_f \mathbf{X}_j$, Eq. (9.42) reduces to

$$\mathbf{X}_{j+1} = (\mathbf{c}_1 - \mathbf{c}_2 \mathbf{K}_f) \mathbf{X}_j = \mathbf{c} \mathbf{X}_j \quad (9.43)$$

Finally, Eq. (9.41) is expressed as

$$J = \frac{1}{2} \mathbf{X}_0^T \left[\sum_{j=0}^{\infty} (\mathbf{c}^j)^T (\mathbf{Q} + \mathbf{K}_f^T \mathbf{R} \mathbf{K}_f) \mathbf{c}^j \right] \mathbf{X}_0 = \frac{1}{2} \mathbf{X}_0^T \mathbf{H} \mathbf{X}_0 \quad (9.44)$$

where \mathbf{H} is a symmetrical positive-definite matrix. Stability requires that \mathbf{c}^j approach $\mathbf{0}$ as $j \rightarrow \infty$. Noting this constraint, the expression for \mathbf{H} reduces to

$$\mathbf{H} - \mathbf{c}^T \mathbf{H} \mathbf{c} = \mathbf{Q} + \mathbf{K}_f^T \mathbf{R} \mathbf{K}_f \quad (9.45)$$

Imposing the stationary requirement on J leads to

$$\begin{aligned} \delta J &= \frac{1}{2} \mathbf{X}_0^T \delta \mathbf{H} \mathbf{X}_0 = 0 \quad \text{for arbitrary } \delta \mathbf{K}_f \\ &\Downarrow \\ \delta \mathbf{H} &= 0 \end{aligned} \quad (9.46)$$

Operating on Eqs. (9.45) and (9.42),

$$\delta \mathbf{H} - \mathbf{c}^T \delta \mathbf{H} \mathbf{c} - \delta \mathbf{c}^T \mathbf{H} \mathbf{c} - \mathbf{c}^T \mathbf{H} \delta \mathbf{c} = \delta \mathbf{K}_f^T \mathbf{R} \mathbf{K}_f + \mathbf{K}_f^T \mathbf{R} \delta \mathbf{K}_f \quad (9.47)$$

$$\delta \mathbf{c} = -\mathbf{c}_2 \delta \mathbf{K}_f \quad (9.48)$$

and setting $\delta \mathbf{H} = \mathbf{0}$ results in the following expression for the optimal feedback matrix:

$$\mathbf{K}_f|_{\text{optimal}} = (\mathbf{R} + \mathbf{c}_2^T \mathbf{H} \mathbf{c}_2)^{-1} \mathbf{c}_2^T \mathbf{H} \mathbf{c}_1 \quad (9.49)$$

9.2. OPTIMAL LINEAR FEEDBACK: TIME-INVARIANT SDOF SYSTEMS

The final form of the discrete algebraic Riccati equation is

$$\mathbf{H} - \mathbf{c}_1^T \mathbf{H} \mathbf{c}_1 + (\mathbf{c}_1^T \mathbf{H} \mathbf{c}_2)(\mathbf{R} + \mathbf{c}_2^T \mathbf{H} \mathbf{c}_2)^{-1} (\mathbf{c}_1^T \mathbf{H} \mathbf{c}_2)^T = \mathbf{Q} \quad (9.50)$$

Given m , k , c , and Δt , \mathbf{c}_1 and \mathbf{c}_2 can be evaluated. We specify the weighting matrices \mathbf{R} and \mathbf{Q} and then determine \mathbf{H} . MATLAB has a function called `dare` that computes \mathbf{H} , $\mathbf{K}_f|_{\text{opt}}$ and the eigenvalues of \mathbf{c} specialized for \mathbf{K}_f set equal to the optimal value. The scaling strategies discussed earlier for the continuous time case are also applicable for the discrete time formulation. The function `dare` assumes the default value $\mathbf{R} \equiv \mathbf{I}$, and therefore Eq. (9.39) can be used to determine the corresponding value of \mathbf{Q} . The following example describes the solution procedure in considerable detail.

Example 9.1 - Solution of the discrete time algebraic Riccati equation for a SDOF system

The undamped case is considered first. Noting the results presented in Ex. 8.2, the various coefficient matrices are

$$\mathbf{c}_1 = \begin{bmatrix} \cos \bar{\omega} & \frac{\sin \bar{\omega}}{\omega} \\ -\omega \sin \bar{\omega} & \cos \bar{\omega} \end{bmatrix} \quad (9.51)$$

$$\mathbf{c}_2 = \frac{1}{m\omega^2} \begin{bmatrix} 1 - \cos \bar{\omega} \\ \omega \sin \bar{\omega} \end{bmatrix} \quad (9.52)$$

$$\mathbf{c}_1^T \mathbf{H} \mathbf{c}_2 = \frac{1}{m\omega^2} \begin{bmatrix} f_1 \\ f_2 \end{bmatrix} \quad (9.53)$$

$$\mathbf{c}_2^T \mathbf{H} \mathbf{c}_2 = \frac{1}{m^2\omega^4} f_3 \quad (9.54)$$

where

$$\bar{\omega} = \omega \Delta t = 2\pi \frac{\Delta t}{T} \quad (9.55)$$

$$f_1 = H_{11}(\cos \bar{\omega})(1 - \cos \bar{\omega}) + H_{12}(\omega \sin \bar{\omega})(2 \cos \bar{\omega} - 1) - H_{22}(\omega \sin \bar{\omega})^2 \quad (9.56)$$

$$f_2 = H_{11} \frac{\sin \bar{\omega}(1 - \cos \bar{\omega})}{\omega} + H_{12}[2(\sin \bar{\omega})^2 - 1 + \cos \bar{\omega}] + H_{22}(\omega \cos \bar{\omega} \sin \bar{\omega}) \quad (9.57)$$

$$f_3 = H_{11}(1 - \cos \bar{\omega})^2 + H_{12}[2\omega \sin \bar{\omega}(1 - \cos \bar{\omega})] + H_{22}(\omega \sin \bar{\omega})^2 \quad (9.58)$$

The optimal feedback matrix is determined using Eq. (9.49),

$$\mathbf{K} = [k_d \quad k_v] = \frac{1}{m\omega^2 \left(r + \frac{f_3}{m^2\omega^4} \right)} [f_1 \quad f_2] \quad (9.59)$$

Finally, the elements of \mathbf{H} are obtained by expanding Eq. (9.50). This step leads to the following three scalar equations:

$$\begin{aligned} & (\sin \bar{\omega})^2 H_{11} + (2\omega \sin \bar{\omega} \cos \bar{\omega}) H_{12} - (\omega^2 \sin^2 \bar{\omega}) H_{22} \\ & \quad = q_d - \frac{f_1^2}{f_3 + \omega^4 m^2 r} \\ & \left(-\frac{\sin \bar{\omega} \cos \bar{\omega}}{\omega} \right) H_{11} + (2 \sin^2 \bar{\omega}) H_{12} + (\omega \sin \bar{\omega} \cos \bar{\omega}) H_{22} \\ & \quad = \frac{-f_1 f_2}{f_3 + 3 + \omega^4 m^2 r} \quad (9.60) \\ & \left(-\frac{\sin^2 \bar{\omega}}{\omega^2} \right) H_{11} - \left(\frac{2 \sin \bar{\omega} \cos \bar{\omega}}{\omega} \right) H_{12} + (-\cos^2 \bar{\omega}) H_{22} \\ & \quad = q_v - \frac{f_2^2}{f_3 + \omega^4 m^2 r} \end{aligned}$$

9.2. OPTIMAL LINEAR FEEDBACK: TIME-INVARIANT SDOF SYSTEMS

The preceding equations are reduced to a dimensionless form by scaling the various terms according to the following laws:

$$\begin{aligned}
 f_1 &= \omega^4 m^2 r \bar{f}_1 \\
 f_2 &= \omega^3 m^2 r \bar{f}_2 \\
 f_3 &= \omega^4 m^2 r \bar{f}_3 \\
 H_{11} &= \omega^4 m^2 r \bar{H}_{11} \\
 H_{12} &= \omega^3 m^2 r \bar{H}_{12} \\
 H_{22} &= \omega^2 m^2 r \bar{H}_{22} \\
 q_d &= \omega^4 m^2 r \bar{q}_d \\
 q_v &= \omega^2 m^2 r \bar{q}_v
 \end{aligned} \tag{9.61}$$

Using Eq. (9.61), the expression for the optimal feedback matrix takes the form

$$\mathbf{K}_f = \frac{\omega^2 m}{1 + \bar{f}_3} \begin{bmatrix} \bar{f}_1 & \frac{1}{\omega} \bar{f}_2 \end{bmatrix} \tag{9.62}$$

Eq. (9.60) reduces to

$$\begin{aligned}
 (\bar{H}_{11} - \bar{H}_{22}) \sin^2 \bar{\omega} + 2 \sin \bar{\omega} \cos \bar{\omega} \bar{H}_{12} &= 4\bar{q}_d - \frac{\bar{f}_1^2}{1 + \bar{f}_3} \\
 (\bar{H}_{11} - \bar{H}_{22}) \sin^2 \bar{\omega} + 2 \sin \bar{\omega} \cos \bar{\omega} \bar{H}_{12} &= -4\bar{q}_v + \frac{\bar{f}_2^2}{1 + \bar{f}_3} \\
 (\bar{H}_{11} - \bar{H}_{22}) \sin(\bar{\omega} \cos \bar{\omega} - 2 \sin^2 \bar{\omega} \bar{H}_{12}) &= \frac{\bar{f}_1 \bar{f}_2}{1 + \bar{f}_3}
 \end{aligned} \tag{9.63}$$

Lastly, the \bar{f} terms are determined with

$$\begin{aligned}
 \bar{f}_1 &= \bar{H}_{11} \cos \bar{\omega}(1 - \cos \bar{\omega}) + \bar{H}_{12} \sin \bar{\omega}(2 \cos \bar{\omega} - 1) - \bar{H}_{22} \sin^2 \bar{\omega} \\
 \bar{f}_2 &= \bar{H}_{11} \sin \bar{\omega}(1 - \cos \bar{\omega}) + \bar{H}_{12}(2 \sin^2 \bar{\omega} - 1 + \cos \bar{\omega}) + \bar{H}_{22} \sin \bar{\omega} \cos \bar{\omega} \\
 \bar{f}_3 &= \bar{H}_{11}(1 - \cos \bar{\omega})^2 + \bar{H}_{12}[2 \sin \bar{\omega}(1 - \cos \bar{\omega})] + \bar{H}_{22} \sin^2 \bar{\omega}
 \end{aligned} \tag{9.64}$$

We specify the relative weights (\bar{q}_d, \bar{q}_v) , and the relative time step ratio, $\omega = 2\pi(\Delta t/T)$, solve Eq. (9.63) for the elements of H , compute the optimal feedback with Eq. (9.62), and lastly check for stability by evaluating the eigenvalues of $\mathbf{c}_1 - \mathbf{c}_2 \mathbf{K}_f$.

As $\Delta t \rightarrow 0$, the solution for the discrete formulation approaches the solution for the continuous case. This can be shown by introducing second-order approximations for $\cos \bar{\omega}$, $\sin \bar{\omega}$ and letting ω approach 0. Assuming $\bar{\omega}^2 \ll 1$, the trigonometric terms are replaced with

$$\begin{aligned}
 \cos \bar{\omega} &\approx 1 \\
 \sin \bar{\omega} &\approx \bar{\omega}
 \end{aligned} \tag{9.65}$$

The corresponding equations are

$$\begin{aligned}
 \bar{f}_1 &\approx \bar{\omega} \bar{H}_{12} + O(\bar{\omega}^2) \\
 \bar{f}_2 &\approx \bar{\omega} \bar{H}_{22} + O(\bar{\omega}^2) \\
 \bar{f}_3 &\approx \bar{\omega}^2 \bar{H}_{22} + O(\bar{\omega}^3)
 \end{aligned} \tag{9.66}$$

and

$$\begin{aligned}
 \bar{\omega}^2(\bar{H}_{11} - \bar{H}_{22}) + 2\bar{\omega} \bar{H}_{12} &\approx 4\bar{q}_d - \bar{\omega}^2 \bar{H}_{12} \\
 \bar{\omega}^2(\bar{H}_{11} - \bar{H}_{22}) + 2\bar{\omega} \bar{H}_{12} &\approx -4\bar{q}_v + \bar{\omega}^2 \bar{H}_{22}^2 \\
 \bar{\omega}(\bar{H}_{11} - \bar{H}_{22}) - 2\bar{\omega}^2 \bar{H}_{12} &\approx \bar{\omega}^2 \bar{H}_{11} \bar{H}_{22}
 \end{aligned} \tag{9.67}$$

9.2. OPTIMAL LINEAR FEEDBACK: TIME-INVARIANT SDOF SYSTEMS

Based on Eq. (9.67), the limiting solution is

$$\begin{aligned} 2\bar{\omega}\bar{H}_{12} &\approx 4\bar{q}_d \\ \bar{\omega}^2\bar{H}_{22}^2 &\approx 4\bar{q}_v + 4\bar{q}_d - \bar{\omega}^2\bar{H}_{12}^2 \\ &\approx 4\bar{q}_v + 4\bar{q}_d(1 - \bar{q}_d) \end{aligned} \quad (9.68)$$

Noting Eq. (9.66), the limiting forms for \bar{f}_1 , \bar{f}_2 are

$$\begin{aligned} \bar{f}_1 &\approx 2\bar{q}_d \\ \bar{f}_2 &\approx 2[\bar{q}_v + \bar{q}_d(1 - \bar{q}_d)]^{1/2} \end{aligned} \quad (9.69)$$

Finally, the feedback terms are

$$\mathbf{K}_f = [2\omega^2 m \bar{q}_d \quad 2\omega m \{ \bar{q}_v + \bar{q}_d(1 - \bar{q}_d) \}^{1/2}] \quad (9.70)$$

Setting $\bar{q}_d = 0$ produces pure velocity feedback with

$$k_v = 2\omega m (\bar{q}_v)^{1/2} \quad (9.71)$$

The corresponding damping ratio is

$$\xi_a = \frac{k_v}{2\omega m} = (\bar{q}_v)^{1/2} = \left(\frac{q_v}{4\omega^2 m^2 r} \right)^{1/2} \quad (9.72)$$

This result coincides with Eq. (9.37).

In the discrete case, setting $q_d = 0$ does not produce pure velocity feedback for finite $\bar{\omega}$. However, when $\bar{\omega}$ is small, \bar{f}_1 is small and k_d is usually neglected. To determine the behavior of the feedback parameters, `dare` is used to solve the discrete algebraic Riccati equation for a set of damped SDOF systems, taking a range of values for q_v and $\Delta t/T$, with q_d set to 0, q_v scaled according to Eq. (9.61), and r set to 1. The results for

CHAPTER 9. LINEAR CONTROL

k_d/k are plotted in Fig. 9.3. Fig. 9.4 shows the variation of $k_v/(2\omega m)$.

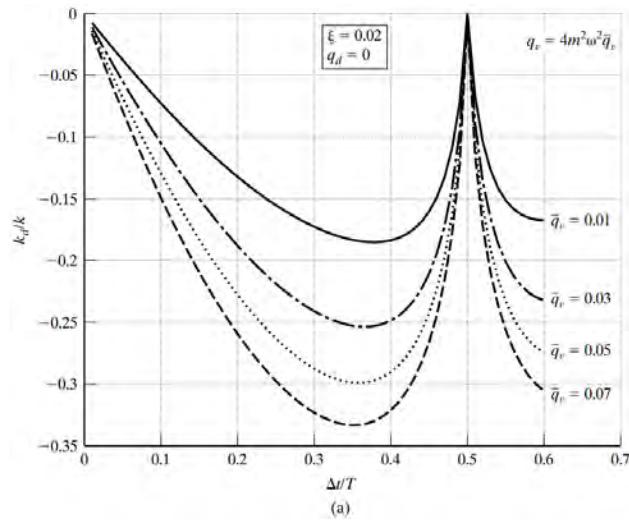


Figure 9.3: Displacement feedback predicted by the discrete algebraic Riccati equation for a SDOF system.

9.2. OPTIMAL LINEAR FEEDBACK: TIME-INVARIANT SDOF SYSTEMS

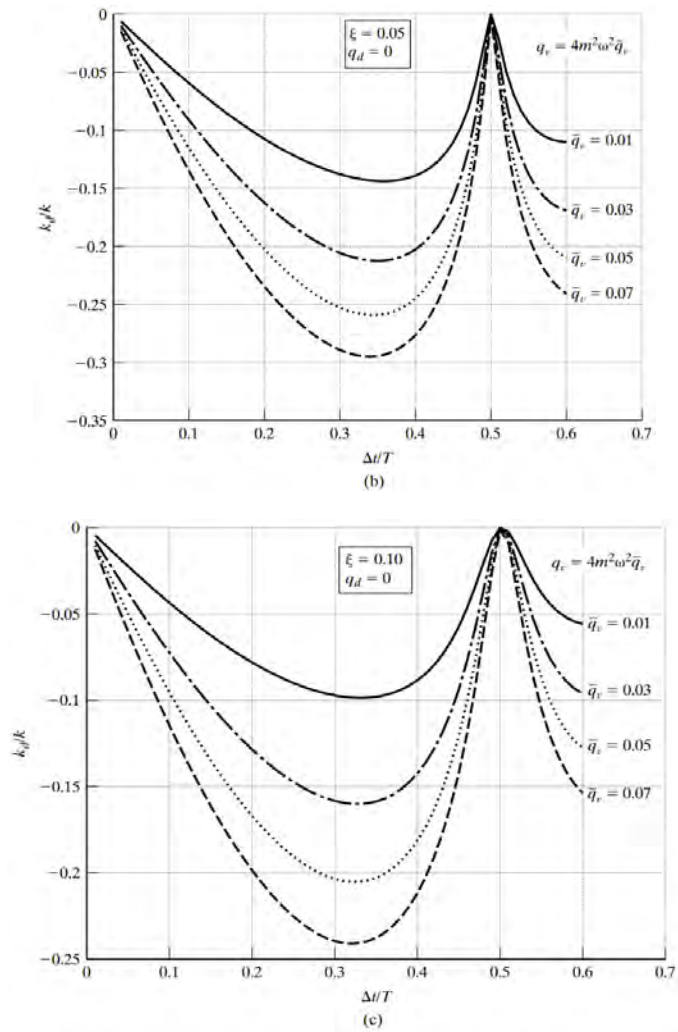


Figure 9.3: Displacement feedback predicted by the discrete algebraic Riccati equation for a SDOF system (continued).

CHAPTER 9. LINEAR CONTROL

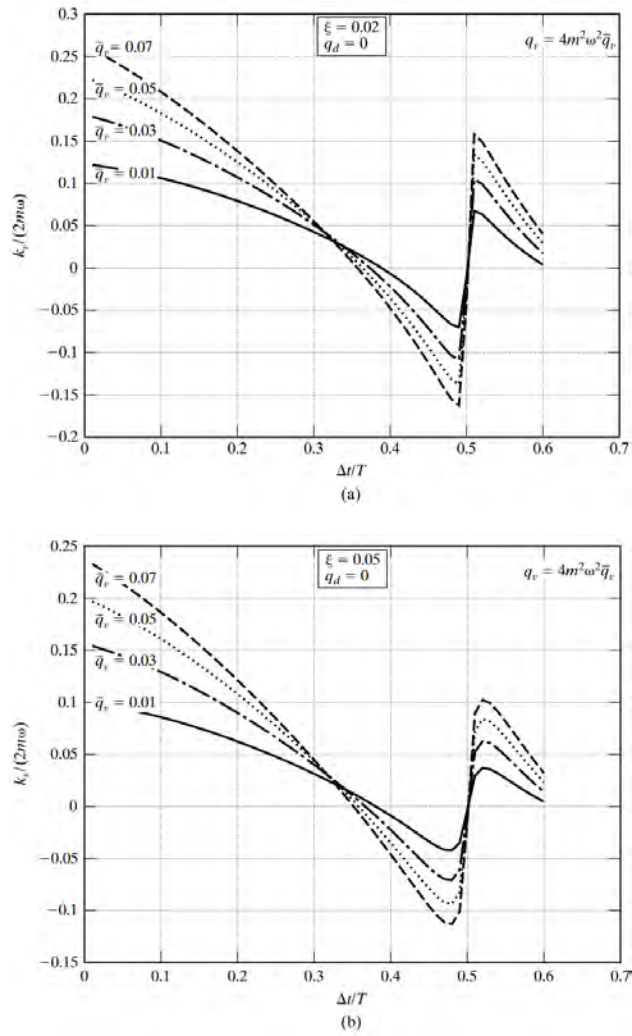


Figure 9.4: Velocity feedback predicted by the discrete algebraic Riccati equation.

9.2. OPTIMAL LINEAR FEEDBACK: TIME-INVARIANT SDOF SYSTEMS

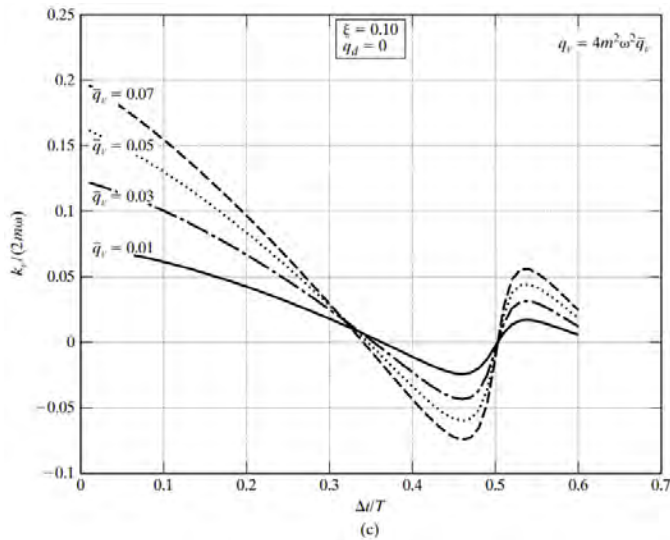


Figure 9.4: Velocity feedback predicted by the discrete algebraic Riccati equation (continued).

In general, the feedback parameters decrease with increasing damping in the uncontrolled system. As expected, increasing q_v with r held constant places more emphasis on lowering the magnitude of the response and consequently the magnitudes of the feedback terms increase. As $\Delta t/T$ approaches 0, the solution tends toward the continuous solution given by Eq. (9.36). As $\Delta t/T$ increases, k_v decreases and eventually becomes negative in the region of $\Delta t/T \approx 0.35$. The feedback stiffness term is also negative. All these solutions are stable (i.e., the maximum modulus of the eigenvalues of $\mathbf{c}_1 - \mathbf{c}_2 \mathbf{K}_f$ is less than unity). The pattern of behavior near $\Delta t/T = 0.5$ was also observed in the stability analysis for the discrete state-space formulation presented in Sect. 8.3 It should be noted that the typical value for $\Delta t/T$ is small, on the order of 0.02. For this range, it is reasonable to take $(k_d/k) \approx 0$. For seismic excitation, the minimum value of Δt is controlled by the ground motion data. The typical time

interval for acceleration time history records is 0.02 s.

9.2.5 Finite Interval Discrete Time Algebraic Riccati Equation

The algebraic Riccati equations presented in the previous sections are based on performance indices that involve integration over an infinite time interval. By considering the time interval to be finite, we can generate a spectrum of Riccati-type equations corresponding to specific values of the time interval. The minimum value is equal to the time step used to generate the discrete time solution; the maximum value is equal to infinity. Eq. (9.50) corresponds to the latter choice. An equation corresponding to the first choice is derived next. The discrete quadratic cost function associated with the time interval between t_j and t_{j+1} is a convenient choice.

$$J_{j,j+1} = \frac{1}{2}(\mathbf{X}_{j+1}^T \mathbf{Q}_j \mathbf{X}_{j+1} + \mathbf{F}_j^T \mathbf{R}_j \mathbf{F}_j) \quad (9.73)$$

It allows for updating the system properties and weighting parameters at each discrete time and consequently is applicable for adaptive as well as time invariant systems. The equilibrium equation follows from Eq. (9.42).

$$\mathbf{X}_{j+1} = \mathbf{c}_{1,j} \mathbf{X}_j + \mathbf{c}_{2,j} \mathbf{F}_j \quad (9.74)$$

Requiring $J_{j,j+1}$ to be stationary with respect to \mathbf{F}_j ,

$$\delta J_{j,j+1} = \delta \mathbf{X}_{j+1}^T \mathbf{Q}_j \mathbf{X}_{j+1} + \delta \mathbf{F}_j^T \mathbf{R}_j \mathbf{F}_j = 0 \quad (9.75)$$

and noting that

$$\delta \mathbf{X}_{j+1} = \mathbf{c}_{2,j} \delta \mathbf{F}_j \quad (9.76)$$

9.2. OPTIMAL LINEAR FEEDBACK: TIME-INVARIANT SDOF SYSTEMS

results in

$$\mathbf{R}_j \mathbf{F}_j + \mathbf{c}_{2,j}^T \mathbf{Q}_j \mathbf{X}_{j+1} = \mathbf{0} \quad (9.77)$$

Finally, substituting for \mathbf{X}_{j+1} yields the following linear feedback law for \mathbf{F}_j :

$$\mathbf{F}_j = -(\mathbf{R}_j + \mathbf{c}_{2,j}^T \mathbf{Q}_j \mathbf{c}_{2,j})^{-1} (\mathbf{c}_{2,j}^T \mathbf{Q}_j \mathbf{c}_{1,j}) \mathbf{X}_j = -\mathbf{K}_{f,j} \mathbf{X}_j \quad (9.78)$$

This expression is similar to Eq. (9.49), which is based on an infinite time interval. Replacing \mathbf{H} with \mathbf{Q} reduces Eq. (9.49) to Eq. (9.78). Working with the latter equations is more convenient since it avoids solving the nonlinear Riccati equation. The following example illustrates the expanded form of \mathbf{K}_f for the undamped case.

Example 9.2 - Example 9.1 revisited

The various matrices derived in Ex. 9.1 are applicable for this case when \mathbf{H} is replaced by \mathbf{Q} . The resulting forms are (the subscript j is dropped here to simplify the notation):

$$\mathbf{K}_f = \frac{1}{r + \frac{f_3}{m^2 \omega^4}} \begin{bmatrix} \frac{f_1}{m \omega^2} & \frac{f_2}{m \omega^2} \end{bmatrix} \quad (9.79)$$

$$q_d = \omega^4 m^2 r \bar{q}_d \quad (9.80)$$

$$q_v = \omega^2 m^2 r \bar{q}_v \quad (9.81)$$

$$\frac{f_1}{m \omega^2} = r m \omega^2 (\bar{q}_d \cos \bar{\omega} (1 - \cos \bar{\omega}) - \bar{q}_v \sin^2 \bar{\omega}) \quad (9.82)$$

$$\frac{f_2}{m\omega^2} = rm\omega(\bar{q}_d \sin \bar{\omega}(1 - \cos \bar{\omega}) + \bar{q}_v \sin \bar{\omega} \cos \bar{\omega}) \quad (9.83)$$

$$r + \frac{f_3}{m^2\omega^4} = r(1 + \bar{q}_d(1 - \cos \bar{\omega})^2 + \bar{q}_v \sin^2 \bar{\omega}) \quad (9.84)$$

Expressing \mathbf{K}_f as

$$\mathbf{K}_f = [k_d \quad k_v] \quad (9.85)$$

and using the preceding equations leads to the dimensionless form of the feedback parameters:

$$\frac{k_d}{m\omega^2} = \frac{\bar{q}_d \cos \bar{\omega}(1 - \cos \bar{\omega}) - \bar{q}_v \sin^2 \bar{\omega}}{1 + \bar{q}_d(1 - \cos \bar{\omega})^2 + \bar{q}_v \sin^2 \bar{\omega}} \quad (9.86)$$

$$\frac{k_v}{2m\omega} = \frac{\bar{q}_d \sin \bar{\omega}(1 - \cos \bar{\omega}) + \bar{q}_v \sin \bar{\omega} \cos \bar{\omega}}{2(1 + \bar{q}_d(1 - \cos \bar{\omega})^2 + \bar{q}_v \sin^2 \bar{\omega})} \quad (9.87)$$

These equations show that k_d depends mainly on \bar{q}_d , and k_v on \bar{q}_v . The limiting forms for $\bar{q}_d = 0$ are

$$\frac{k_d}{m\omega^2} = \frac{-\sin^2 \bar{\omega} \bar{q}_v}{1 + \sin^2 \bar{\omega} \bar{q}_v} \quad (9.88)$$

$$\frac{k_v}{2m\omega} = \frac{\sin \bar{\omega} \cos \bar{\omega} \bar{q}_v}{2(1 + \sin^2 \bar{\omega} \bar{q}_v)} \quad (9.89)$$

Suppose $\Delta t/T = 0.02$. The corresponding values of the feedback parameters are

$$\frac{k_d}{m\omega^2} = \frac{-0.015775 \bar{q}_v}{1 + 0.015775 \bar{q}_v} \quad (9.90)$$

9.2. OPTIMAL LINEAR FEEDBACK: TIME-INVARIANT SDOF SYSTEMS

$$\frac{k_v}{2m\omega} = \frac{0.1243\bar{q}_v}{2 + 0.03155\bar{q}_v} \quad (9.91)$$

Taking $\bar{q}_v = 1$ results in an active damping ratio of ≈ 0.06 . The change in stiffness is on the order of 1.5% and can be neglected.

9.2.6 Continuous Time Riccati Differential Equation

The algebraic Riccati equation is based on Eq. (9.17), which involves an integral extending from $t = 0$ to $t = \infty$. A more general formulation considers the time interval to be finite and allows for a nonzero final state. Suppose the initial state at $t = t_0$ is \mathbf{X}_0 . Let t_f denote the final time, and \mathbf{X}_f^* the desired final state. The generalized form of the performance index is written as

$$J = \frac{1}{2} \int_{t_0}^{t_f} (\mathbf{X}^T \mathbf{Q} \mathbf{X} + \mathbf{F}^T \mathbf{R} \mathbf{F}) dt + \frac{1}{2} (\mathbf{X}_f - \mathbf{X}_f^*)^T \mathbf{S} (\mathbf{X}_f - \mathbf{X}_f^*) \quad (9.92)$$

where \mathbf{S} is a symmetric positive semidefinite matrix that provides a measure of the error associated with the boundary conditions at t_f .

Given some initial state, the optimal control force $\mathbf{F}(t)$ is determined by requiring J to be stationary. Although the solution procedure for $t_f \neq \infty$ is more complicated than for $t_f = \infty$, the optimal feedback law has the same form:

$$\mathbf{F}(t) = -(\mathbf{R}^{-1} \mathbf{B}_f \mathbf{H}) \mathbf{X} \quad (9.93)$$

However, \mathbf{H} must now satisfy a differential equation rather than an algebraic equation:

$$\dot{\mathbf{X}} + \mathbf{A}^T \mathbf{H} + \mathbf{H} \mathbf{A}^T - \mathbf{H} \mathbf{B}_f \mathbf{R}^{-1} \mathbf{B}_f^T \mathbf{H} = -\mathbf{Q} \quad (9.94)$$

and boundary conditions at $t = t_f$.

$$\mathbf{H}(t_f) = \mathbf{S} \quad (9.95)$$

These equations are derived in the following section. In addition to Eq. (9.94), the state vector and control force are constrained by

$$\begin{aligned} \dot{\mathbf{X}} &= \mathbf{A} \mathbf{X} + \mathbf{B}_f \mathbf{F} & t_0 \leq t \leq t_f \\ \mathbf{X}(t_0) &= \mathbf{X}_0 \end{aligned} \quad (9.96)$$

Since the boundary condition on \mathbf{H} is at $t = t_f$, we have to solve for \mathbf{H} backward in time (i.e., from t_f toward t_0). Given \mathbf{H} , we solve for \mathbf{X} and \mathbf{F} by moving forward in time from t_0 . The nature of the solution near is similar to an exponential decay to a steady-state solution. Since solving Eq. (9.94) is not convenient, $\mathbf{H}(t)$ is approximated by the steady-state solution obtained with the algebraic Riccati equation. This simplification is possible only when \mathbf{A} , \mathbf{Q} , and \mathbf{R} are constant.

9.2.7 Variational Formulation of the Continuous Time Riccati Equation

For completeness, the derivation of the Riccati equation is presented here. The proof is based on the requirement that \mathbf{A} , \mathbf{B}_f , \mathbf{Q} , and \mathbf{R} are bounded and piecewise continuous in the interval $t_0 \leq t \leq t_f$. Assuming an optimal control, $\bar{\mathbf{F}}$, exists, then an optimal trajectory, $\bar{\mathbf{X}}$, that satisfies

9.2. OPTIMAL LINEAR FEEDBACK: TIME-INVARIANT SDOF SYSTEMS

$$\begin{aligned}\dot{\bar{\mathbf{X}}} &= \mathbf{A}\bar{\mathbf{X}} + \mathbf{B}_f\bar{\mathbf{F}} \\ \bar{\mathbf{X}}(t_0) &= \mathbf{X}_0\end{aligned}\tag{9.97}$$

also exists. The corresponding optimal cost functional is given by

$$J(\bar{\mathbf{F}}) = \frac{1}{2} \left([\bar{\mathbf{X}}_f - \mathbf{X}^*]^* \mathbf{S} [\bar{\mathbf{X}}_f - \mathbf{X}^*]^T + \int_{t_0}^{t_f} [\bar{\mathbf{X}}^T \mathbf{Q} \bar{\mathbf{X}} + \bar{\mathbf{F}}^T \mathbf{R} \bar{\mathbf{F}}] dt \right)\tag{9.98}$$

The proof proceeds as follows. Let

$$\mathbf{F} = \bar{\mathbf{F}} + \delta\mathbf{F} = \bar{\mathbf{F}} + \epsilon\tilde{\mathbf{F}}\tag{9.99}$$

where ϵ is an arbitrary positive or negative scalar and $\tilde{\mathbf{F}}$ is an arbitrary valued time function representing a perturbation of the control force from the optimal value. Substituting for \mathbf{F} , Eq. (9.96) expands to

$$\begin{aligned}\dot{\mathbf{X}} &= \mathbf{A}\mathbf{X} + \mathbf{B}_f\bar{\mathbf{F}} + \epsilon\mathbf{B}_f\tilde{\mathbf{F}} \\ \mathbf{X}(t_0) &= \mathbf{X}_0\end{aligned}\tag{9.100}$$

The solution for \mathbf{X} can be expressed in terms of the optimal trajectory and a perturbation due to the variation in the control force:

$$\mathbf{X} = \bar{\mathbf{X}} + \delta\mathbf{X} = \bar{\mathbf{X}} + \epsilon\tilde{\mathbf{X}}\tag{9.101}$$

where the state perturbation $\tilde{\mathbf{X}}$ is related to the control perturbation $\tilde{\mathbf{F}}$ by

$$\begin{aligned}\dot{\tilde{\mathbf{X}}} &= A\tilde{\mathbf{X}} + \mathbf{B}_f\tilde{\mathbf{F}} \\ \tilde{\mathbf{X}}(t_0) &= \mathbf{0}\end{aligned}\tag{9.102}$$

The constraint equation can be incorporated in the cost function by introducing a Lagrangian multiplier, $\beta(t)$, and treating β as a variable as well as \mathbf{X} and \mathbf{F} [100]. The modified cost function is

$$\begin{aligned}J(\mathbf{F}) &= \frac{1}{2} ([\mathbf{X} - \mathbf{X}_f]^T \mathbf{S} [\mathbf{X} - \mathbf{X}_f]) \\ &\quad + \int_{t_0}^{t_f} \left(\frac{1}{2} \mathbf{X}^T \mathbf{Q} \mathbf{X} + \frac{1}{2} \mathbf{F}^T \mathbf{R} \mathbf{F} + \beta^T [\mathbf{A} \mathbf{X} + \mathbf{B}_f \mathbf{F} - \dot{\mathbf{X}}] \right) dt\end{aligned}\tag{9.103}$$

Noting that

$$\int_{t_0}^{t_f} \beta^T \dot{\mathbf{X}} dt = \beta^T(t_f) \mathbf{X}(t_f) - \beta^T(t_0) \mathbf{X}(t_0) - \int_{t_0}^{t_f} \dot{\beta}^T \mathbf{X} dt\tag{9.104}$$

we can write Eq. (9.103) as

$$\begin{aligned}J(\mathbf{F}) &= \frac{1}{2} ([\mathbf{X}(t_f) - \mathbf{X}^*]^T \mathbf{S} [\mathbf{X}(t_f) - \mathbf{X}^*]) - \beta^T(t_f) \mathbf{X}(t_f) + \beta^T(t_0) \mathbf{X}(t_0) \\ &\quad + \int_{t_0}^{t_f} \left(\frac{1}{2} \mathbf{X}^T \mathbf{Q} \mathbf{X} + \beta^T \mathbf{A} \mathbf{X} + \dot{\beta}^T \mathbf{X} + \frac{1}{2} \mathbf{F}^T \mathbf{R} \mathbf{F} + \beta^T \mathbf{B}_f \mathbf{F} \right) dt\end{aligned}\tag{9.105}$$

The cost for optimal control is

9.2. OPTIMAL LINEAR FEEDBACK: TIME-INVARIANT SDOF SYSTEMS

$$\begin{aligned}
 J(\mathbf{F}) = & \frac{1}{2} \left([\bar{\mathbf{X}}(t_f) - \mathbf{X}^*]^T \mathbf{S} [\bar{\mathbf{X}}(t_f) - \mathbf{X}^*] - \beta^T(t_f) \bar{\mathbf{X}}(t_f) + \beta^T(t_0) \bar{\mathbf{X}}(t_0) \right. \\
 & \left. + \int_{t_0}^{t_f} \left(\frac{1}{2} \bar{\mathbf{X}}^T \mathbf{Q} \bar{\mathbf{X}} + \beta^T \mathbf{A} \bar{\mathbf{X}} + \dot{\beta}^T \bar{\mathbf{X}} + \frac{1}{2} \bar{\mathbf{F}}^T \mathbf{R} \bar{\mathbf{F}} + \beta^T \mathbf{B}_f \bar{\mathbf{F}} \right) dt \right)
 \end{aligned} \tag{9.106}$$

Since by definition $\bar{\mathbf{F}}$ and $\bar{\mathbf{X}}$ are optimal, the cost difference must be positive,

$$J(\mathbf{F}) - J(\bar{\mathbf{F}}) \geq 0 \tag{9.107}$$

for all \mathbf{F} , $t_0 \leq t \leq t_f$. Substituting for \mathbf{F} and \mathbf{X} in terms of the perturbations, we obtain an expansion for the cost difference in terms of ϵ .

$$\begin{aligned}
 J(\mathbf{F}) - J(\bar{\mathbf{F}}) = & \epsilon \left([\bar{\mathbf{X}}(t_f) - \mathbf{X}^*]^T \mathbf{S} - \beta^T(t_f) \right) \tilde{\mathbf{X}}(t_f) + \frac{\epsilon^2}{2} \tilde{\mathbf{X}}^T(t_f) \mathbf{S} \tilde{\mathbf{X}}(t_f) \\
 & + \epsilon \int_{t_0}^{t_f} \left([\bar{\mathbf{X}}^T \mathbf{Q} + \beta^T \mathbf{A} + \dot{\beta}^T] \tilde{\mathbf{X}} + [\bar{\mathbf{F}}^T \mathbf{R} + \beta^T \mathbf{B}_f] \tilde{\mathbf{F}} \right) dt \\
 & + \frac{\epsilon^2}{2} \int_{t_0}^{t_f} [\tilde{\mathbf{F}}^T \mathbf{R} \tilde{\mathbf{F}} + \tilde{\mathbf{X}}^T \mathbf{Q} \tilde{\mathbf{X}}] dt
 \end{aligned} \tag{9.108}$$

A necessary condition for Eq. (9.107) to be satisfied is that the first-order terms in ϵ vanish for all ϵ , $\tilde{\mathbf{X}}$, and $\tilde{\mathbf{F}}$. This requirement leads to a first-order differential equation for β :

$$\begin{aligned}
 \bar{\mathbf{X}}^T \mathbf{Q} + \beta^T \mathbf{A} + \dot{\beta}^T &= \mathbf{0} \\
 [\bar{\mathbf{X}}(t_f) - \mathbf{X}^*]^T \mathbf{S} - \beta^T(t_f) &= \mathbf{0}
 \end{aligned} \tag{9.109}$$

and the control law

$$\begin{aligned}\bar{\mathbf{F}}^T \mathbf{R} + \beta^T \mathbf{B}_f &= \mathbf{0} \\ \Downarrow \\ \bar{\mathbf{F}} &= -\mathbf{R}^{-1} \mathbf{B}_f^T \beta\end{aligned}\tag{9.110}$$

The sufficient condition for Eq. (9.107) is related to the second-order terms.

$$J(\mathbf{F}) - J(\bar{\mathbf{F}}) = \frac{\epsilon^2}{2} \left(\tilde{\mathbf{X}}^T(t_f) \mathbf{S} \tilde{\mathbf{X}}(t_f) + \int_{t_0}^{t_f} \left[\tilde{\mathbf{F}}^T \mathbf{R} \tilde{\mathbf{F}} + \tilde{\mathbf{X}}^T \mathbf{Q} \tilde{\mathbf{X}} \right] dt \right)\tag{9.111}$$

Since \mathbf{S} and \mathbf{Q} are positive semi-definite and \mathbf{R} is positive definite, this term is always positive, and it follows that $\bar{\mathbf{X}}$ and $\bar{\mathbf{F}}$ represent the solution that corresponds to the minimum value of $J(\mathbf{F})$.

Eqs. (9.97) and (9.109) can be combined into a set of coupled linear vector differential equations involving \mathbf{X} and β .

$$\begin{bmatrix} \dot{\bar{\mathbf{X}}} \\ \dot{\beta} \end{bmatrix} = \begin{bmatrix} \mathbf{A} & -\mathbf{B}_f \mathbf{R}^{-1} \mathbf{B}_f^T \\ -\mathbf{Q} & -\mathbf{A}^T \end{bmatrix} \begin{bmatrix} \bar{\mathbf{X}} \\ \beta \end{bmatrix}\tag{9.112}$$

The solution can be expressed as

$$\begin{bmatrix} \bar{\mathbf{X}}(t_2) \\ \beta(t_2) \end{bmatrix} = \Phi(t_2, t_1) \begin{bmatrix} \bar{\mathbf{X}}(t_1) \\ \beta(t_1) \end{bmatrix}\tag{9.113}$$

where t_1 and t_2 are arbitrary times, and Φ is a $2n \times 2n$ state transition matrix of the form

$$\Phi(t_2, t_1) = \begin{bmatrix} \Phi_{11}(t_2, t_1) & \Phi_{12}(t_2, t_1) \\ \Phi_{21}(t_2, t_1) & \Phi_{22}(t_2, t_1) \end{bmatrix}\tag{9.114}$$

9.2. OPTIMAL LINEAR FEEDBACK: TIME-INVARIANT SDOF SYSTEMS

Taking $t_1 = t$ and $t_2 = t_f$, we obtain

$$\begin{aligned}\bar{\mathbf{X}}(t_f) &= \Phi_{11}(t_f, t)\bar{\mathbf{X}}(t) + \Phi_{12}(t_f, t)\beta(t) \\ \beta(t_f) &= \Phi_{21}(t_f, t)\bar{\mathbf{X}}(t) + \Phi_{22}(t_f, t)\beta(t)\end{aligned}\quad (9.115)$$

Using the boundary condition,

$$\beta(t_f) = \mathbf{S}[\bar{\mathbf{X}}(t_f) - \mathbf{X}^*] \quad (9.116)$$

we can solve for $\beta(t)$ in terms of $\bar{\mathbf{X}}(t)$:

$$[\mathbf{S}\Phi_{12}(t_f, t) - \Phi_{22}(t_f, t)]\beta(t) = [\Phi_{21}(t_f, t) - \mathbf{S}\Phi_{11}(t_f, t)]\bar{\mathbf{X}}(t) + \mathbf{S}\mathbf{X}^* \quad (9.117)$$

The preceding relation is expressed as

$$\beta(t) = \mathbf{H}(t)\bar{\mathbf{X}}(t) + \mathbf{G}(t) \quad (9.118)$$

Finally, substituting for $\beta(t)$ in Eq. (9.110) results in a linear state feedback control law:

$$\bar{\mathbf{F}}(t) = -\mathbf{R}^{-1}\mathbf{B}_f^T[\mathbf{H}\bar{\mathbf{X}} + \mathbf{G}] \quad (9.119)$$

The equation for \mathbf{H} is derived by operating on the governing equations. Differentiating Eq. (9.118), we obtain

$$\dot{\beta} = \mathbf{H}\dot{\bar{\mathbf{X}}} + \dot{\mathbf{H}}\bar{\mathbf{X}} + \dot{\mathbf{G}} \quad (9.120)$$

Substituting for $\dot{\bar{\mathbf{X}}}$, $\dot{\beta}$ expands to

$$\dot{\beta} \left[\dot{\mathbf{H}} + \mathbf{H}\mathbf{A} - \mathbf{H}\mathbf{B}_f\mathbf{R}^{-1}\mathbf{B}_f^T\mathbf{H} \right] \bar{\mathbf{X}} + \dot{\mathbf{G}} - \mathbf{H}\mathbf{B}_f\mathbf{R}^{-1}\mathbf{B}_f^T\mathbf{G} \quad (9.121)$$

Finally, introducing β and $\dot{\beta}$ in Eq. (9.109),

$$\begin{aligned} & [\dot{\mathbf{H}} + \mathbf{H}\mathbf{A} + \mathbf{A}^T\mathbf{H} - \mathbf{H}\mathbf{B}_f\mathbf{R}^{-1}\mathbf{B}_f^T\mathbf{H} + \mathbf{Q}]\mathbf{X} \\ & + [\mathbf{A}^T - \mathbf{H}\mathbf{B}_f\mathbf{R}^{-1}\mathbf{B}_f^T]\mathbf{G} + \dot{\mathbf{G}} = \mathbf{0} \end{aligned} \quad (9.122)$$

and setting the coefficient of \mathbf{X} to zero results in equations for \mathbf{H} and \mathbf{G} :

$$\dot{\mathbf{H}} + \mathbf{H}\mathbf{A} + \mathbf{A}^T\mathbf{H} - \mathbf{H}\mathbf{B}_f\mathbf{R}^{-1}\mathbf{B}_f^T\mathbf{H} + \mathbf{Q} = \mathbf{0} \quad (9.123)$$

$$\dot{\mathbf{G}} + [\mathbf{A}^T - \mathbf{H}\mathbf{B}_f\mathbf{R}^{-1}\mathbf{B}_f^T]\mathbf{G} = \mathbf{0} \quad (9.124)$$

The boundary conditions follow from the condition on β at t_f and have the form

$$\begin{aligned} \mathbf{H}(t_f) &= \mathbf{S} \\ \mathbf{G}(t_f) &= -\mathbf{S}\mathbf{X}^* \end{aligned} \quad (9.125)$$

For the regulator problem, \mathbf{X}^* is taken as zero. Then $\mathbf{G} = \mathbf{0}$ and $\beta = \mathbf{H}\mathbf{X}$.

As a final point, we can show that the minimum remaining cost at time t is equal to

$$\bar{J}(\mathbf{F}) = \frac{1}{2}[\mathbf{X}^T(t)\mathbf{H}\mathbf{X}(t)] \quad (9.126)$$

Example 9.3 - Application to scalar case

To illustrate the solution procedure, the scalar form of the LQR formulation is considered here. The equations for $t_0 < t < t_f$ are

$$\dot{X} - AX - B_f F = 0 \quad (9.127)$$

9.2. OPTIMAL LINEAR FEEDBACK: TIME-INVARIANT SDOF SYSTEMS

$$\dot{\beta} + A\beta + QX = 0 \quad (9.128)$$

$$F = - \left[\frac{1}{R} \right] B_f \beta \quad (9.129)$$

At $t = t_0$,

$$X(t_0) = X_0 \quad (9.130)$$

At $t = t_f$,

$$\beta(t_f) = S[X(t_f) - X^*] \quad (9.131)$$

Substituting for F transforms Eq. (9.127) to

$$\dot{X} - AX + \left[\frac{B_f^2}{R} \right] \beta = 0 \quad (9.132)$$

For stability, $A < 0$.

The homogeneous solution has the form

$$X = Ce^{\lambda t} \quad (9.133)$$

$$\beta = De^{\lambda t} \quad (9.134)$$

where λ satisfies

$$\lambda^2 = A^2 + \frac{QB_f^2}{R} \quad (9.135)$$

and the constants are related by

$$C = - \left[\frac{\lambda + A}{Q} \right] F \quad (9.136)$$

Then

$$\lambda_{1,2} = \pm \bar{\lambda} \quad (9.137)$$

$$\bar{\lambda} = \sqrt{\left| A^2 + \frac{QB_f^2}{R} \right|} \quad (9.138)$$

$$C_i = - \left[\frac{A + \lambda_i}{Q} \right] D_i = v_i D_i \quad (9.139)$$

and the full solution is

$$\beta = D_1 e^{\bar{\lambda}t} + D_2 e^{-\bar{\lambda}t} \quad (9.140)$$

$$X = v_1 D_1 e^{\bar{\lambda}t} + v_2 D_2 e^{-\bar{\lambda}t} \quad (9.141)$$

Imposing the end conditions results in two equations for D_1 and D_2 .

$$v_1 D_1 + v_2 D_2 = X_0 \quad (9.142)$$

$$[1 - Sv_1] D_1 + [1 - Sv_2] D_2 e^{-2\bar{\lambda}t_f} = -e^{-\bar{\lambda}t_f} S X^* \quad (9.143)$$

The case of finite t_f is handled by expressing D_1 as

$$D_1 = \bar{D}_1 e^{-\bar{\lambda}t_f} \quad (9.144)$$

This substitution transforms the solution to

$$\beta = \bar{D}_1 e^{-\bar{\lambda}(t_f-t)} + D_2 e^{-\bar{\lambda}t} \quad (9.145)$$

9.2. OPTIMAL LINEAR FEEDBACK: TIME-INVARIANT SDOF SYSTEMS

$$X = v_1 \bar{D}_1 e^{-\bar{\lambda}(t_f-t)} + v_2 D_2 e^{-\bar{\lambda}t} \quad (9.146)$$

The first term applies near t_f and the second term near t_0 . Enforcing the boundary conditions leads to

$$D_2 = \frac{1}{v_2} \left[X_0 - v_1 \bar{D}_1 e^{-\bar{\lambda}t_f} \right] \quad (9.147)$$

$$\bar{D}_1 = \frac{-SX^* - \frac{X_0}{v_2} [1 - Sv_2] e^{-\bar{\lambda}t_f}}{\left([1 - v_1 S] - \frac{v_1}{v_2} [1 - v_2 S] e^{-2\bar{\lambda}t_f} \right)} \quad (9.148)$$

When $\bar{\lambda} > 3$, the solutions uncouple as follows:
For $0 < t \leq \frac{3}{\bar{\lambda}}$

$$\begin{aligned} \beta &= D_2 e^{-\bar{\lambda}t} \\ X &= v_2 \beta \\ F &= - \left[\frac{B_f}{R} \right] \beta = \left[\frac{B_f}{v_2 R} \right] X \\ D_2 &\approx \frac{X_0}{v_2} \end{aligned} \quad (9.149)$$

$$v_2 = - \left[\frac{A - \lambda}{Q} \right] = -\frac{A}{Q} + \frac{|A|}{Q} \sqrt{1 + \frac{QB_f^2}{A^2 R}}$$

For $\frac{3}{\bar{\lambda}} < t < t_f - \frac{3}{\bar{\lambda}}$

$$\begin{aligned} \beta &= 0 \\ X &= 0 \\ F &= 0 \end{aligned} \quad (9.150)$$

For $t_f - \frac{3}{\bar{\lambda}} < t \leq t_f$

$$\begin{aligned}
 \beta &= \bar{D}_1 e^{-\bar{\lambda}(t_f-t)} \\
 X &= v_1 \beta \\
 F &= - \left[\frac{B_f}{R} \right] \beta = - \left[\frac{B_f}{v_1 R} \right] X \\
 \bar{D}_1 &= \frac{-S X^*}{1 - v_1 S} \\
 v_1 &= - \left[\frac{A + \bar{\lambda}}{Q} \right] = - \frac{A}{Q} - \frac{|A|}{Q} \sqrt{1 + \frac{Q B_f^2}{A^2 R}}
 \end{aligned} \tag{9.151}$$

Stability of the controlled system requires $A < 0$. Then, for the *stable* case

$$\begin{aligned}
 v_2 &> 0 \\
 v_1 &< 0
 \end{aligned} \tag{9.152}$$

The feedback is negative near $t = 0$ and positive near $t = t_f$. Letting $X^* \rightarrow 0$ eliminates the solution in the region of t_f .

The algebraic Riccati equation approach for this set of equations starts with the scalar form of Eq. (9.123):

$$-H^2 \left[\frac{B_f^2}{R} \right] + 2AH + Q = 0 \tag{9.153}$$

The roots are

$$H_{1,2} = \frac{R}{B_f^2} \left[A \pm |A| \sqrt{1 + \frac{Q B_f^2}{R A^2}} \right] \tag{9.154}$$

Enforcing the requirement that the uncontrolled system be stable,

9.2. OPTIMAL LINEAR FEEDBACK: TIME-INVARIANT SDOF SYSTEMS

$$A < 0 \quad (9.155)$$

transforms Eq. (9.154) to

$$H_{1,2} = \frac{R|A|}{B_f^2} \left[-1 \pm \sqrt{1 + \frac{QB_f^2}{RA^2}} \right] \quad (9.156)$$

Finally, the requirement that $H > 0$ eliminates the negative root, and we obtain

$$H_{\text{opt}} = \frac{R|A|}{B_f^2} \left[\sqrt{1 + \frac{QB_f^2}{RA^2}} - 1 \right] \quad (9.157)$$

Referring back to Eq. (9.149), the solution near $t = 0$ for the case where t_f is large has the form

$$\begin{aligned} X &= X_0 e^{-\bar{\lambda}t} \\ \beta &= \frac{X_0}{v_2} e^{-\bar{\lambda}t} \\ v_2 &= -\frac{A}{Q} + \frac{|A|}{Q} \sqrt{1 + \frac{QB_f^2}{RA^2}} \end{aligned} \quad (9.158)$$

Taking $A < 0$, the expression for v_2 becomes

$$v_2 = \frac{|A|}{Q} \left[1 + \sqrt{1 + \frac{QB_f^2}{RA^2}} \right] \quad (9.159)$$

Forming the ratio β of to X ,

$$\frac{\beta}{X} = \frac{1}{v_2} \quad (9.160)$$

and substituting for v_2 leads to

$$\frac{1}{v_2} = \frac{Q}{|A| \left[1 + \sqrt{1 + \frac{QB_f^2}{RA^2}} \right]} = \frac{R|A|}{B_f^2} \left[\sqrt{1 + \frac{QB_f^2}{RA^2}} - 1 \right] \quad (9.161)$$

Comparing Eq. (9.161) with Eq. (9.157) shows that $H_{\text{opt}} = 1/v_2$. The negative root of Eq. (9.156) is equal to $1/v_1$ and corresponds to positive feedback in the region of t_f .

9.3 LQR Control Algorithm: MDOF Time-Invariant Systems

The formulation of the linear quadratic regulator problem developed for a time-invariant SDOF system in Sect. 9.2 is extended here to MDOF systems. Since matrix notation was used for the SDOF case, the only difference between the SDOF and MDOF formulations is the form of the weighting matrices, \mathbf{Q} and \mathbf{R} , contained in the quadratic performance index. In what follows, the LQR control algorithm corresponding to the modal state-space formulation is derived for both the continuous and discrete time feedback scenarios. The role of \mathbf{Q} in this case is to assign relative weights to the different modal responses. Weighting the different control forces is achieved by adjusting the elements of \mathbf{R} . Examples illustrating the sensitivity of the modal damping due to feedback as a function of \mathbf{Q} and \mathbf{R} are presented. Lastly, various issues involved in “selecting” a control force scheme are also discussed.

9.3. LQR CONTROL ALGORITHM: MDOF TIME-INVARIANT SYSTEMS

9.3.1 Continuous Time Modal Formulation

The governing equation for this formulation is Eq. (8.264). For convenience, the relevant equations are listed here.

$$\dot{\mathbf{X}}_m = \mathbf{A}_m \mathbf{X}_m + \mathbf{B}_{fm} \mathbf{F} + \mathbf{B}_{pm} \mathbf{P} + \mathbf{B}_{gm} a_g \quad (9.162)$$

where \mathbf{X}_m contains the real and imaginary parts of the modal coordinates,

$$\mathbf{X}_m = \begin{Bmatrix} \mathbf{q}_R \\ \mathbf{q}_I \end{Bmatrix} \quad (9.163)$$

and the coefficient matrices depend on the modal properties of the MDOF system and the nodal distribution of the control forces defined by \mathbf{E}_f . Negative linear feedback is taken as

$$\mathbf{F} = -\mathbf{K}_{fm} \mathbf{X}_m = -\begin{bmatrix} \mathbf{k}_d & \mathbf{k}_v \end{bmatrix} \begin{bmatrix} \mathbf{q}_R \\ \mathbf{q}_I \end{bmatrix} \quad (9.164)$$

An expression for \mathbf{K}_{fm} is established by requiring the following performance index to be stationary:

$$\mathbf{J} = \frac{1}{2} \int_0^\infty (\mathbf{X}_m^T \mathbf{Q} \mathbf{X}_m + \mathbf{F}^T \mathbf{Q} \mathbf{F}) dt \quad (9.165)$$

where \mathbf{Q} and \mathbf{R} are taken as diagonal weighting matrices,

$$\mathbf{Q} = \begin{bmatrix} \mathbf{Q}_d & \mathbf{0} \\ \mathbf{0} & \mathbf{Q}_v \end{bmatrix} \quad (9.166)$$

$$\mathbf{R} = [r_i \delta_{ij}]$$

When \mathbf{Q} and \mathbf{R} are constant, the solution is

$$\mathbf{K}_{fm} = \mathbf{R}^{-1} \mathbf{B}_{fm}^T \mathbf{H} = -\begin{bmatrix} \mathbf{k}_d & \mathbf{k}_v \end{bmatrix} \quad (9.167)$$

where \mathbf{H} is determined by

$$\mathbf{A}_m^T \mathbf{H} + \mathbf{H} \mathbf{A}_m - \mathbf{H} \mathbf{B}_{fm} \mathbf{R}^{-1} \mathbf{B}_{fm}^T \mathbf{H} = \mathbf{Q} \quad (9.168)$$

Just as for the SDOF case, $\mathbf{k}_d \equiv \mathbf{0}$ when \mathbf{Q}_d is taken as a null matrix. This choice avoids the potential instability associated with displacement feedback.

Given \mathbf{A}_m , \mathbf{B}_{fm} , \mathbf{R} , and \mathbf{Q} , we can determine \mathbf{K}_{fm} and the eigenvalues of $\mathbf{A}_m - \mathbf{B}_{fm} \mathbf{K}_{fm}$ with the MATLAB function `care`. These eigenvalues define the modal damping ratios and frequencies for the system corresponding to the particular choice of control force locations, (\mathbf{E}_f), and weighting matrices. Given \mathbf{E}_f , we can generate a range of modal damping ratio distributions by varying the individual weighting factors contained in \mathbf{Q} and \mathbf{R} .

To avoid a potential instability due to displacement feedback, \mathbf{Q}_d is taken as a null matrix. The form of \mathbf{Q}_v is a generalized version of Eq. (9.39) that applies for the SDOF case.

$$\mathbf{Q}_v = [4\bar{m}_i^2 \omega_i^2 w_i \delta_{ij}] \quad (9.169)$$

where \bar{m}_i is the modal mass, ω_i is the modal frequency, and w_i is the relative weighting for the i^{th} mode. With this scaling law, w_i and r_i are of $O(1)$. Increasing w_n places more emphasis on reducing the response of mode n . Increasing r_m places more emphasis on reducing the “cost” for the m^{th} control force. Both of these perturbations result in changes in the magnitudes of the modal damping ratios.

In addition to these parameters, the modal damping distribution is also influenced by the nature of the control force scheme. A pair of self-equilibrating control forces is equivalent to “material” damping, which tends to produce damping that increases with the modal frequency. A single control force applied at a node

9.3. LQR CONTROL ALGORITHM: MDOF TIME-INVARIANT SYSTEMS

is similar to mass proportional damping and results in damping that decreases with the modal frequency. The force schemes considered in Ex. 8.12 exhibited these behavioral trends.

Continuous time LQR control is useful for establishing an initial estimate of the control force system properties required to achieve certain performance objectives, such as limiting the peak deformations and accelerations in a structure subject to constraints on the external power requirement and the peak value of the control forces. This estimate is then evaluated using the discrete time formulation specialized for the particular time step selected, and the design is modified if necessary. The effect of time delay is also considered at this stage.

9.3.2 Discrete Time Modal Formulation

The discrete time free vibration formulation allowing for feedback is based on Eq. (8.275), which is expressed here as

$$\mathbf{X}_{m,j+1} = \mathbf{c}_{m1}\mathbf{X}_{m,j} + \mathbf{c}_{m2}\mathbf{F}_j \quad (9.170)$$

where

$$\begin{aligned} \mathbf{c}_{m1} &= \mathbf{e}^{\mathbf{A}_m\Delta t} \\ \mathbf{c}_{m2} &= \mathbf{A}_m^{-1}(\mathbf{e}^{\mathbf{A}_m\Delta t} - \mathbf{I})\mathbf{B}_{fm} \end{aligned} \quad (9.171)$$

For the discrete time case, the quadratic performance index is taken as

$$\mathbf{J} = \frac{1}{2} \sum_{j=0}^{\infty} (\mathbf{X}_{m,j}^T \mathbf{Q} \mathbf{X}_{m,j} + \mathbf{F}_j^T \mathbf{R} \mathbf{F}_j) \quad (9.172)$$

with \mathbf{Q} , \mathbf{R} defined by Eq. (9.166). Expressing \mathbf{F}_j as

$$\mathbf{F}_j = -\mathbf{K}_{fm}\mathbf{X}_{m,j} \quad (9.173)$$

and requiring \mathbf{J} to be stationary with respect to \mathbf{K}_{fm} leads to the discrete algebraic Riccati equation,

$$\mathbf{H} - \mathbf{c}_{m1}^T \mathbf{H} \mathbf{c}_{m1} + (\mathbf{c}_{m1}^T \mathbf{H} \mathbf{c}_{m2})(\mathbf{R} + \mathbf{c}_{m2}^T \mathbf{H} \mathbf{c}_{m2})^{-1} (\mathbf{c}_{m1}^T \mathbf{H} \mathbf{c}_{m2})^T = \mathbf{Q} \quad (9.174)$$

and the following expression for the optimal feedback:

$$\mathbf{K}_{fm}|_{\text{optimal}} = (\mathbf{R} + \mathbf{c}_{m2}^T \mathbf{H} \mathbf{c}_{m2})^{-1} (\mathbf{c}_{m1}^T \mathbf{H} \mathbf{c}_{m2})^T \quad (9.175)$$

This solution can be generated with the MATLAB function `dare`.

Substituting for \mathbf{F}_j , the free vibration response with optimal feedback is governed by

$$\mathbf{X}_{m,j+1} = (\mathbf{c}_{m1} - \mathbf{c}_{m2} \mathbf{K}_{fm}|_{\text{opt}}) \mathbf{X}_j = \mathbf{c}_m \mathbf{X}_j \quad (9.176)$$

The frequency and damping properties of the discrete model with feedback are related to the eigenvalues of \mathbf{c}_m . Suppose s modes are considered. There are s pairs of complex conjugates,

$$\rho = \rho_1, \tilde{\rho}_1, \rho_2, \tilde{\rho}_2, \dots, \rho_s, \tilde{\rho}_s \quad (9.177)$$

The j^{th} pair is expressed in polar form.

$$\rho_j, \tilde{\rho}_j = \bar{\rho}_j e^{\pm i\theta_j} \quad (9.178)$$

With this notation, the modal periods and corresponding damping ratios are given by

9.3. LQR CONTROL ALGORITHM: MDOF TIME-INVARIANT SYSTEMS

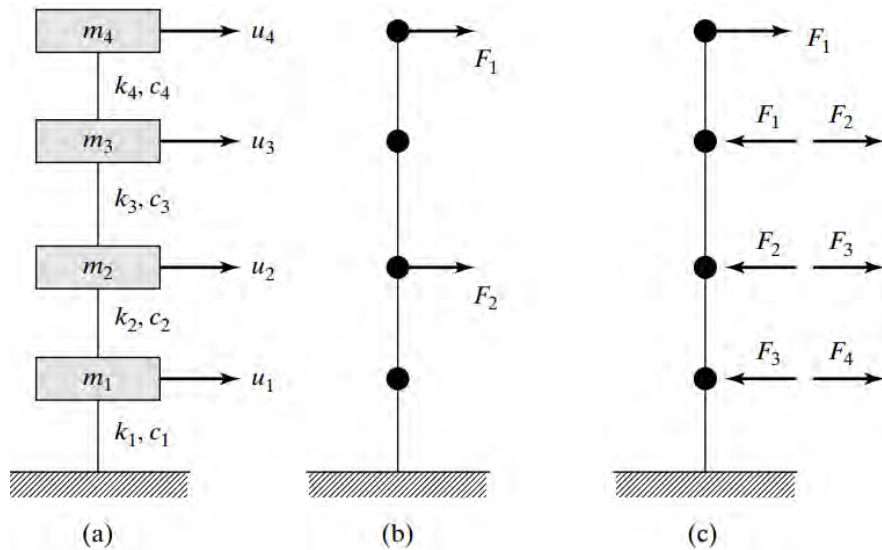
$$\begin{aligned}\xi_j &= \frac{\delta_j}{[\delta_j^2 + \theta_j^2]^{1/2}} \\ T_j &= \frac{2\pi\Delta t}{\theta_j} \\ \delta_j &= -\ln(\bar{\rho}_j)\end{aligned}\tag{9.179}$$

These equations are useful for comparing discrete versus continuous feedback.

Although the actual control system is based on discrete time feedback, it is convenient to work with the continuous time formulation during the preliminary design phase, which is concerned with selecting the location and nature of the control forces and estimating the relative weighting factors in order to satisfy the specified performance requirements. Shifting from continuous to discrete time feedback with time delay changes the response characteristics, such as the modal damping, and can be potentially destabilizing. For this formulation, the free vibration response becomes unstable when $\bar{\rho} > 1$, which corresponds to a negative value for ξ . Examples illustrating various behavioral aspects of MDOF systems controlled with the LQR algorithm are presented in the following section.

9.3.3 Application Studies: LQR Control

The 4DOF model defined in Fig. 9.5 is utilized to illustrate the design of LQR-based control force systems. Versions of this model were used in the preceding examples to demonstrate instability. The focus here is on modal damping introduced by feedback. Both global and self-equilibrating force schemes (Figs. 9.5(b) and 9.5(c) are considered).



Node/Element	m (kg)	k (kN/m)	c (kN·s/m)
1	1000	1700	4
2	1000	1400	3
3	1000	1000	2
4	1000	700	1

Figure 9.5: Definition of model and control force schemes.

Case 1 Global forcing

The scheme shown in Fig. 9.5(b) involves specifying two force weighting parameters (r_1 and r_2) in \mathbf{R} and four modal velocity weighting parameters ($w_1 \rightarrow w_4$) in \mathbf{Q}_v . Suppose the design objective is a uniform distribution of the peak internodal displacements for a specified dynamic excitation, such as an earthquake. Starting with uniform weighting, we can adjust the r 's and w 's separately until the desired uniform displacement profile is obtained. The strategy followed here is based on first perturbing the force weights to obtain a reasonable level of damping, then adjusting the modal weights to obtain essentially

9.3. LQR CONTROL ALGORITHM: MDOF TIME-INVARIANT SYSTEMS

uniform modal damping, and finally scaling the r 's to shift the average value of the peak internodal displacement to the desired value.

Results for the first step are shown in Fig. 9.6a. Starting with w and r set to unity, the r 's are reduced to 0.5 and 0.25. The modal damping for the first mode (period ≈ 0.5 s) is essentially doubled, while the change in the corresponding damping ratios for the third and fourth modes is small. There is close agreement between the continuous and discrete feedback results for all but the second mode.

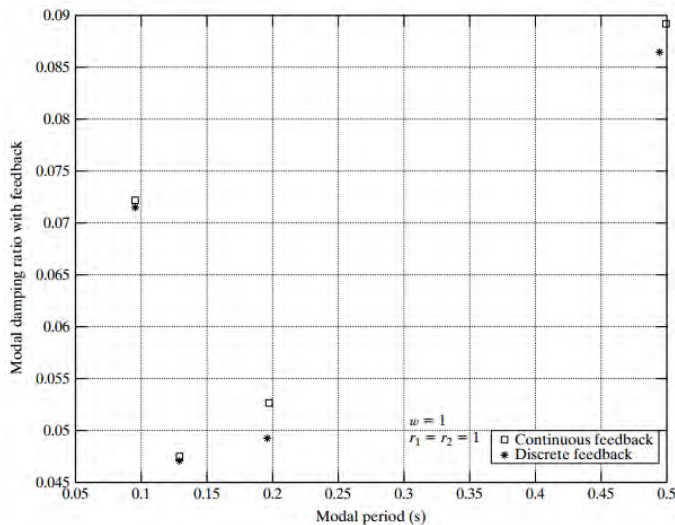


Figure 9.6: Sensitivity of the modal damping ratio to the control force weighting factor, r .

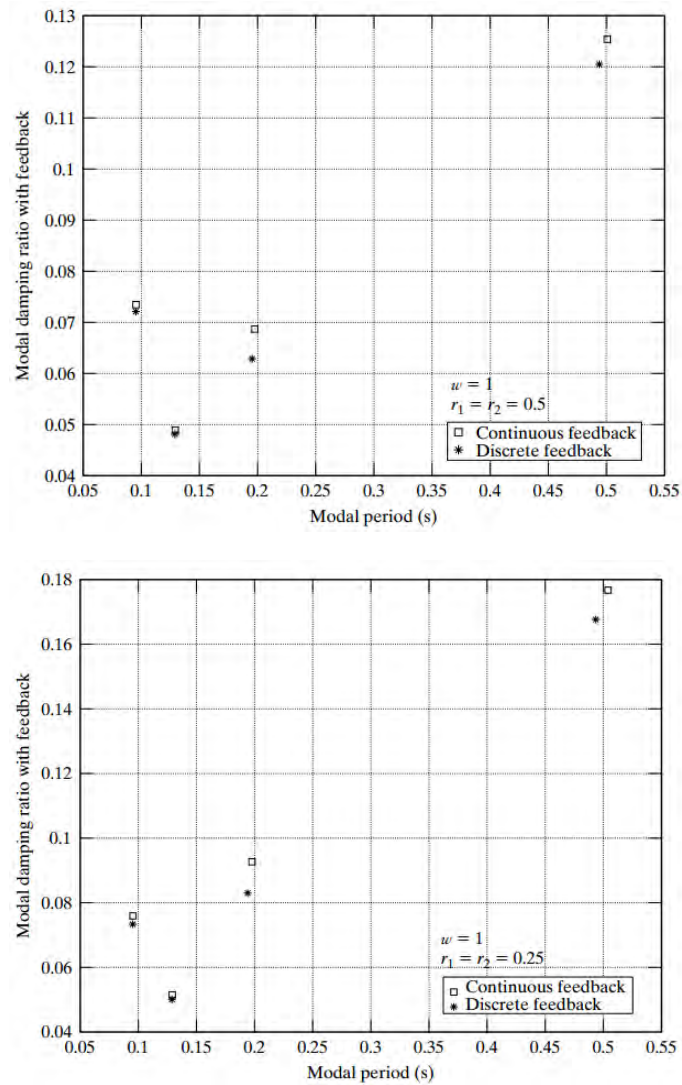


Figure 9.6: Sensitivity of the modal damping ratio to the control force weighting factor, r (continued).

Taking $r = 0.25$ as a first trial value for r , the modal weightings are adjusted to increase the damping ratios for the higher modes. Fig. 9.7 shows results for a particular w distribution that places the primary emphasis on modes 3 and 4. The modal damping is nearly uniform, but note that there is a significant

9.3. LQR CONTROL ALGORITHM: MDOF TIME-INVARIANT SYSTEMS

difference between the continuous and discrete damping ratios. This weighting scheme produces the peak internodal displacement profile plotted in Fig. 9.7(b).

Holding the w values constant and decreasing r generates the results shown in Fig. 9.8. The average damping is increased, and the average peak displacement is decreased. We continue this process until the design displacement value is obtained. In addition to motion-based design requirements, there are also constraints on the peak values of the control forces and the peak power required. For this design the peak quantities are

$$F_{1,\max} = 4.234 \text{ kN}$$

$$F_{2,\max} = 1.783 \text{ kN}$$

$$\text{Peak power} = 3.772 \text{ kN}\cdot\text{m/s}$$

$$\text{Average internodal displacement} = 0.011 \text{ m}$$

Optimal design involves considering all of these requirements and assigning priorities for the multiple objectives.

CHAPTER 9. LINEAR CONTROL

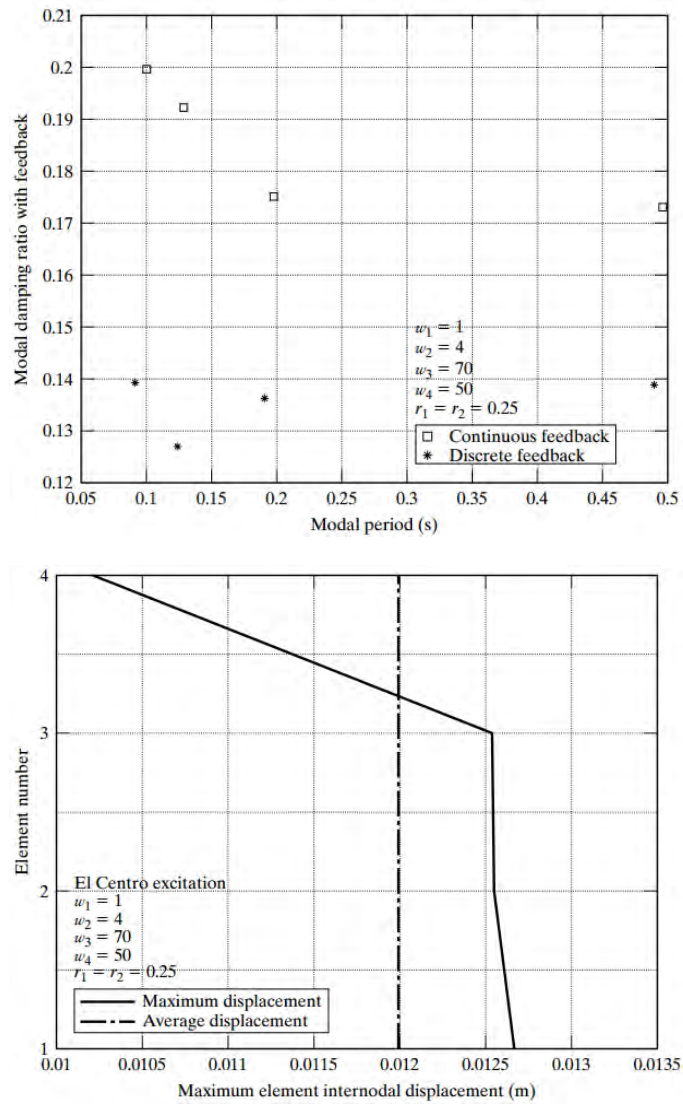


Figure 9.7: Modal damping and peak response for initial weighting scheme. (a) Modal damping ratio with continuous and discrete feedback - no saturation limit; and (b) element internodal displacement profile.

9.3. LQR CONTROL ALGORITHM: MDOF TIME-INVARIANT SYSTEMS

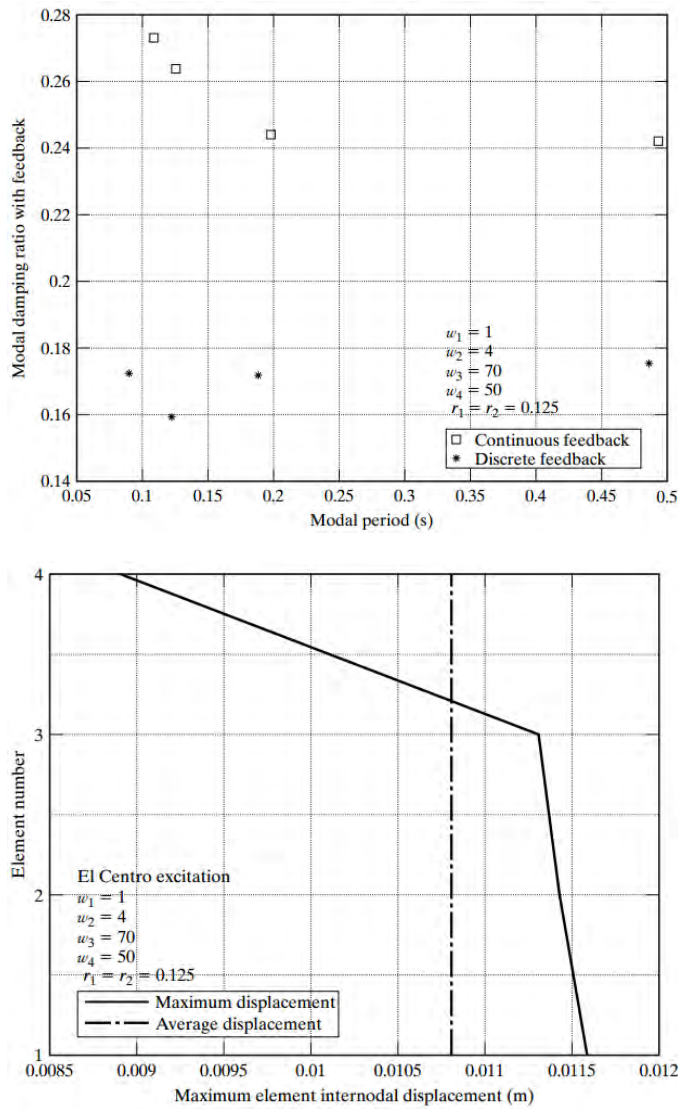


Figure 9.8: (a) Modal damping ratio with continuous and discrete feedback - no saturation limit; and (b) element internodal displacement profile.

Case 2 Self-equilibrating control force

The force scheme defined by Figure 8.15(c) involves four control forces. Starting with uniform weightings, the scale factors are adjusted until the modal damping ratio distribution is essen-

CHAPTER 9. LINEAR CONTROL

tially the same as obtained with the final weighting scheme of Case 1. Fig. 9.9 contains the final results for Case 2. Since the modal damping distributions are nearly identical, internodal displacement profiles are also in close agreement. The peak values of the control forces and power for this control force scheme are

$$\begin{aligned}F_{1,\max} &= 3.818 \text{ kN} \\F_{2,\max} &= 5.074 \text{ kN} \\F_{3,\max} &= 4.849 \text{ kN} \\F_{4,\max} &= 4.449 \text{ kN} \\ \text{Peak power} &= 3.599 \text{ kN}\cdot\text{m/s} \\ \text{Average internodal displacement} &= 0.0108 \text{ m}\end{aligned}$$

This scheme requires a larger force, 5.074 kN versus 4.234 kN. The peak power required depends on the equivalent damping, and since this quantity is essentially the same, it follows that the power requirements will also be close.

9.3. LQR CONTROL ALGORITHM: MDOF TIME-INVARIANT SYSTEMS

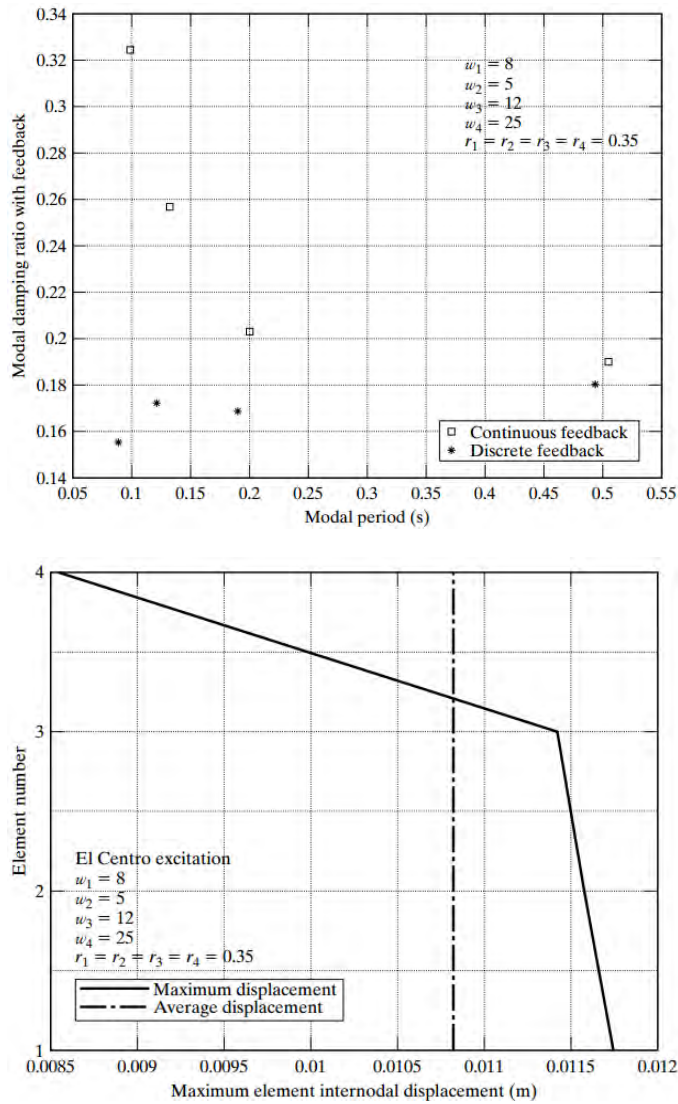


Figure 9.9: Modal damping and peak response - self-equilibrating control force system. (a) Modal damping ratio with continuous and discrete feedback - no saturation limit; and (b) element internodal profile.

Example 9.4 - Control force design studies for a 20DOF shear beam

A 20DOF shear beam with constant mass (1000 kg) and

CHAPTER 9. LINEAR CONTROL

constant element damping (10,000 N·s/m) is considered. An estimate for the element stiffness distribution is selected such that the element shear deformation profile for the first mode is essentially uniform, and the average element relative displacement response due to the El Centro seismic excitation is approximately 0.0125 m. Fig. 9.10 shows the modal properties and response for this choice of stiffness and no feedback control. There is close agreement between the actual and desired deformation for nodes 1 through 13. Beyond this point, the difference increases rapidly and exhibits an exponential type growth pattern, similar to the internodal displacement profiles for modes 3 and 4. This result indicates that the contribution of the higher modes is dominating the response in the upper region.

9.3. LQR CONTROL ALGORITHM: MDOF TIME-INVARIANT SYSTEMS

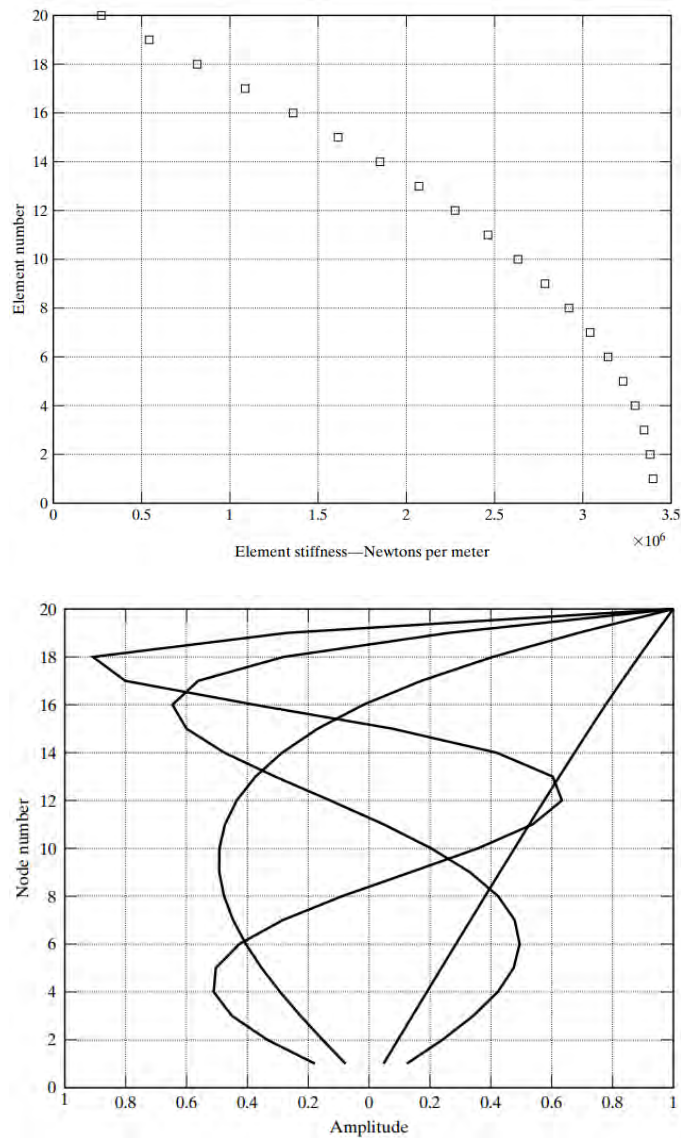


Figure 9.10: Properties for no iteration and no feedback. (a) Element shear stiffness distribution; (b) modal displacement profile - real part;

CHAPTER 9. LINEAR CONTROL

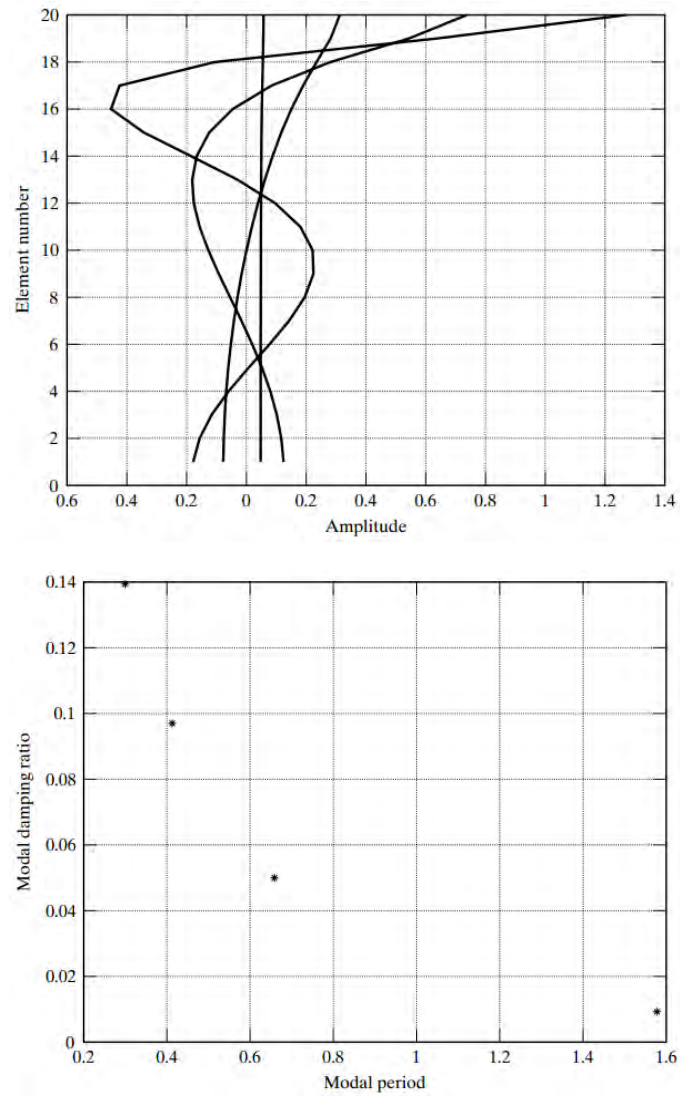


Figure 9.10: Properties for no iteration and no feedback. (c) Element internal modal displacement profile real part; (d) modal damping ratio without feedback;

9.3. LQR CONTROL ALGORITHM: MDOF TIME-INVARIANT SYSTEMS

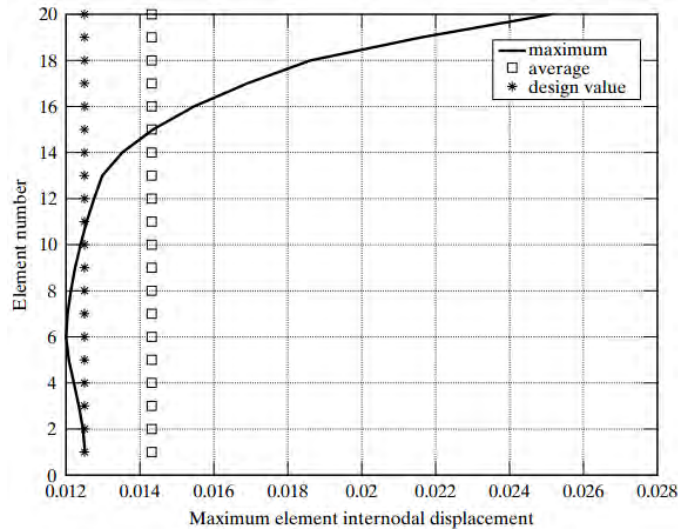


Figure 9.10: Properties for no iteration and no feedback. (e) Element internodal displacement profile.

Various options are possible. We can alter the deformation profiles for modes 3 and 4 by modifying the stiffness in the upper region so that the gradients are decreased. Another option is to work with the initial stiffness and incorporate additional damping with feedback control. These approaches generate the maximum values for stiffness (option 1) and damping (option 2). Combining these approaches results in intermediate values for these parameters.

Fig. 9.11 contains the results generated by iterating on the element stiffness according to the following algorithm:

$$k_{\text{new}} = k_{\text{old}} \left(\frac{\text{maximum element displacement}}{\text{desired element displacement}} \right) \quad (9.180)$$

CHAPTER 9. LINEAR CONTROL

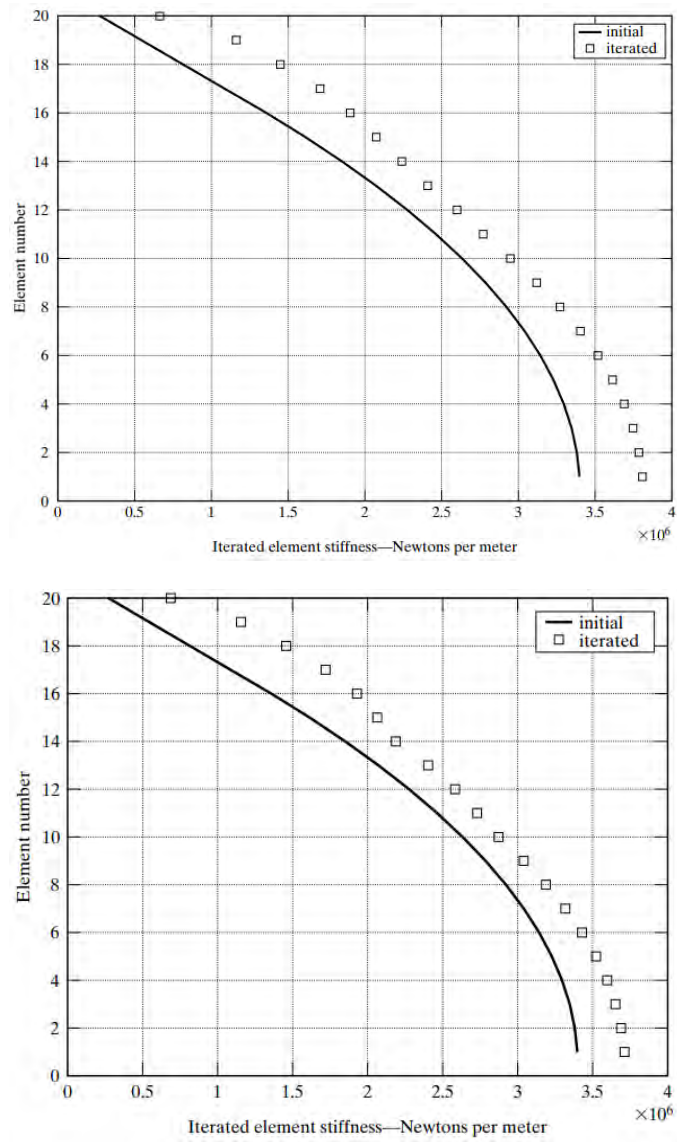


Figure 9.11: Iterated stiffness with no feedback. (a) Two iterations; (b) four iterations;

9.3. LQR CONTROL ALGORITHM: MDOF TIME-INVARIANT SYSTEMS

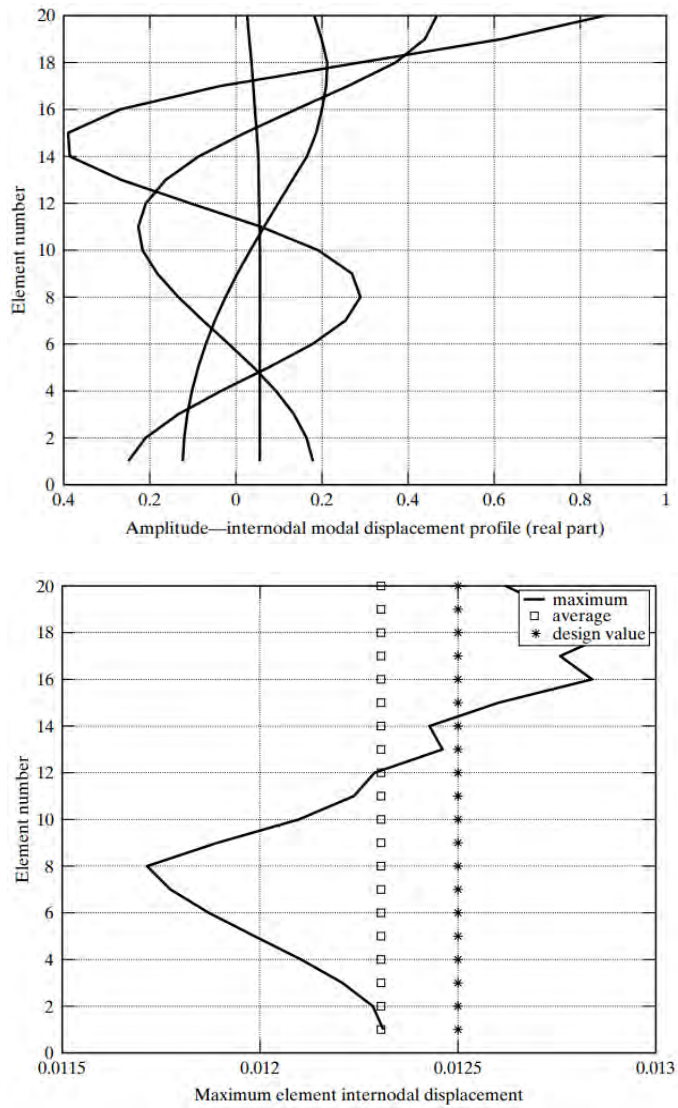


Figure 9.11: Iterated stiffness with no feedback. (c) Two iterations; (d) two iterations;

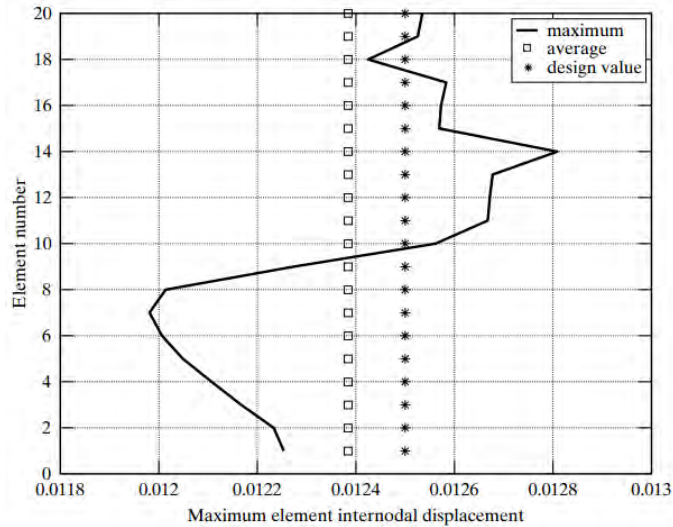


Figure 9.11: Iterated stiffness with no feedback. (e) Four iterations.

The computation proceeds as follows. Using the initial stiffness, the time history response due to El Centro is generated, and the peak value of internodal displacement is determined for each element. Eq. (9.180) is applied to update each element stiffness, and the complete analysis is then repeated. Convergence is quite rapid for this example. After two cycles, the correction process has essentially reached the final state. Fig. 9.11(c) shows the modified element displacement profiles after two iterations. The peak value for element 20, the most critical location, has been reduced by approximately 33%. This correction results in a significant improvement in the element response profiles plotted in Fig. 9.11(d). The “bulge” in the upper region has been eliminated.

Following the second approach, four self-equilibrating pairs of nodal forces are applied on elements 17, 18, 19, and 20. Fig. 9.12 defines the notation for these forces. Results based on the initial stiffness and the following set of weighting coefficients are

9.3. LQR CONTROL ALGORITHM: MDOF TIME-INVARIANT SYSTEMS

plotted in Fig. 9.13.

$$\begin{aligned} w_1 = 0 \quad w_2 = 1 \quad w_3 = 3 \quad w_4 = 5 \\ r_1 = r_2 = r_3 = r_4 = 0.125 \end{aligned} \quad (9.181)$$

These coefficients were selected to focus the control mainly on modes 3 and 4. Even though the modal damping for these modes is increased significantly, there is still a substantial difference between the actual and desired response in the upper zone.

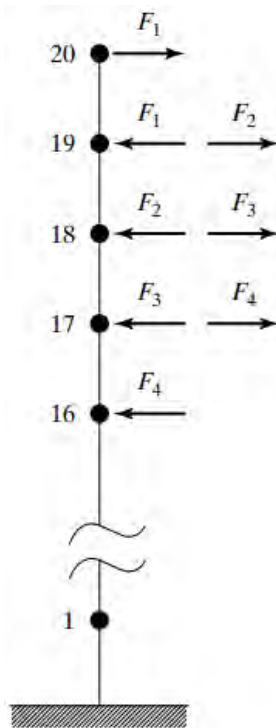


Figure 9.12: Position of nodal force pairs.

CHAPTER 9. LINEAR CONTROL

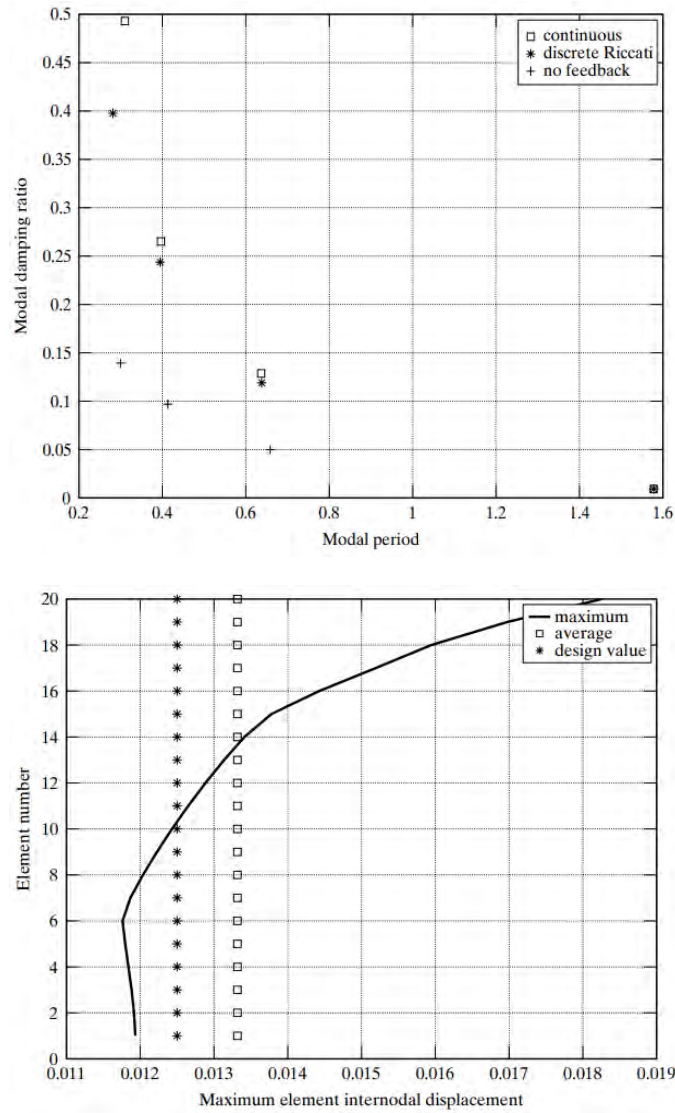


Figure 9.13: Initial stiffness and feedback. (a) Modal damping ratio with and without continuous or discrete feedback - no saturation limit; (b) Element internodal displacement profile;

9.3. LQR CONTROL ALGORITHM: MDOF TIME-INVARIANT SYSTEMS

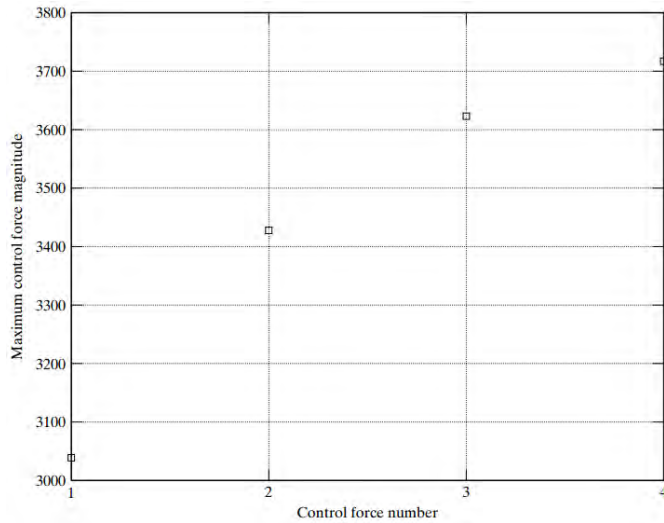


Figure 9.13: Initial stiffness and feedback. (c) Maximum value of the control force.

Results based on iterating once on the stiffness, and then applying feedback to the “modified” system are plotted in Fig. 9.14. The weighting coefficients for this case are

$$\begin{aligned} w_1 &= 0 & w_2 &= 1 & w_3 &= 3 & w_4 &= 5 \\ r_1 &= r_2 = r_3 = r_4 &= 1.0 \end{aligned} \quad (9.182)$$

Increasing the r values reduces the equivalent damping, as shown in Fig. 9.14(a). However, since the stiffness was corrected, the net effect is a significantly improved element displacement profile and lower magnitudes for the control forces.

CHAPTER 9. LINEAR CONTROL

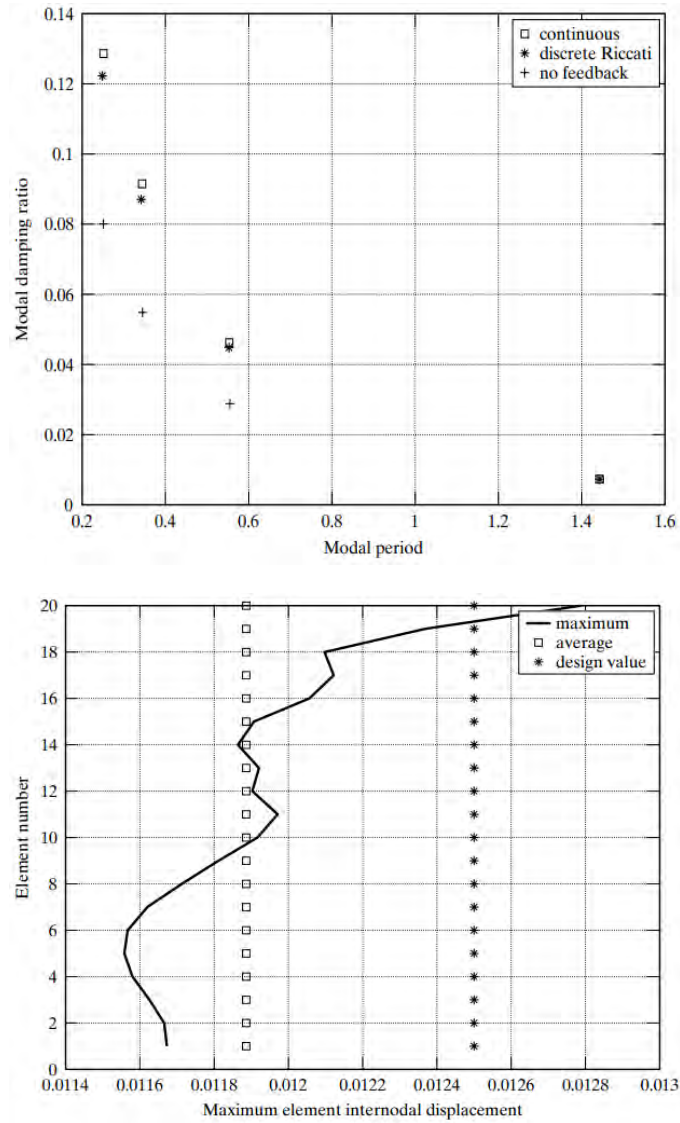


Figure 9.14: Single iteration on stiffness and then feedback. (a) Modal damping ratio with and without continuous or discrete feedback - no saturation limit; (b) element internodal displacement profile;

9.3. LQR CONTROL ALGORITHM: MDOF TIME-INVARIANT SYSTEMS

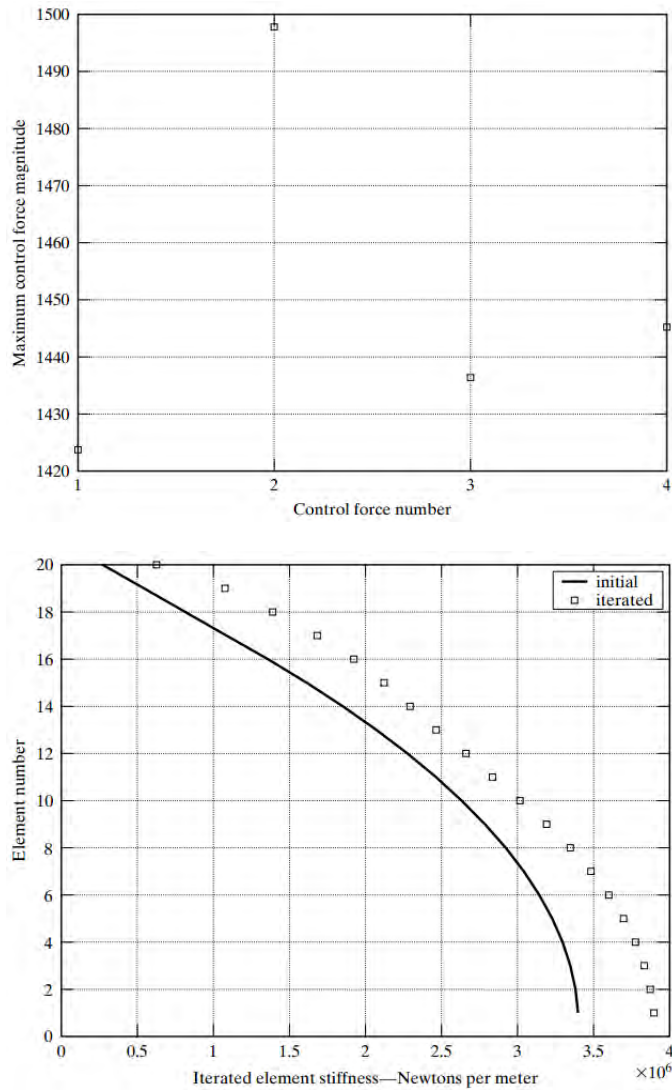


Figure 9.14: Single iteration on stiffness and then feedback. (c) Maximum value of the control forces; and (d) iterated element shear stiffness distribution.

Applying a single control force at node 20 produces the results shown in Fig. 9.15. The corresponding weights and peak value of the control force are

$$w_1 = 0 \quad w_2 = 1 \quad w_3 = 3 \quad w_4 = 5$$

$$r_1 = 3$$

$$F_1|_{\max} = 1719N$$

9.183

9.3. LQR CONTROL ALGORITHM: MDOF TIME-INVARIANT SYSTEMS

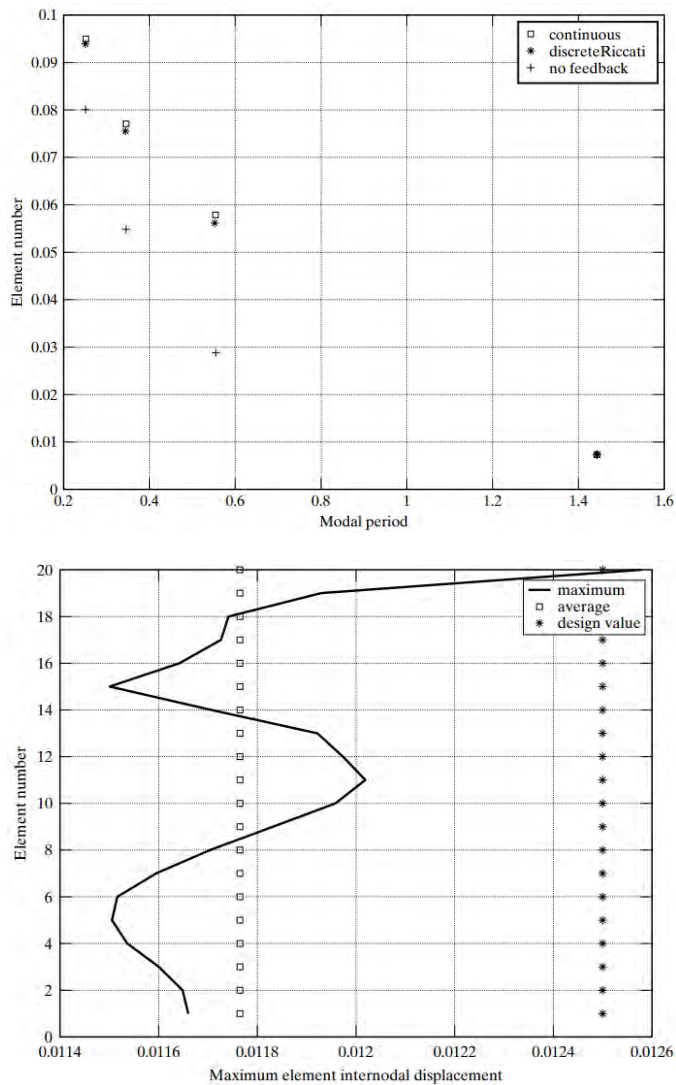


Figure 9.15: Single iteration on stiffness and a single control force. (a) Modal damping ratio with and without continuous or discrete feedback no saturation limit; and (b) element internodal displacement profile.

This example illustrates that there is no unique solution. We can vary the stiffness, damping, and active feedback control scheme to adjust the response. In order to determine the optimal solution, cost measures need to be assigned to each of the

CHAPTER 9. LINEAR CONTROL

parameters. Simulation studies, as illustrated here, provide the data on sensitivities which allows for a more informed decision as to the final design.

Example 9.5 - Alternate choice of response measures

The previous examples are based on the specification of either nodal velocities or the first derivative of the modal coordinates as the response measures included in the performance index for the LQR control algorithm. Other response measures, such as element shear deformation rate, can also be selected. We need only to specify the relationship between the alternate measures and the state vector, and specify weights for the alternate measures. Defining \mathbf{Y} as the vector containing the alternate measures, the relationship is expressed as either $\mathbf{Y} = \mathbf{DX}$ or $\mathbf{Y} = \mathbf{DX}_m$ depending on whether the nodal or modal formulation is used. Taking the index as $\mathbf{Y}^T \mathbf{Q}_0 \mathbf{Y}$ and substituting for \mathbf{Y} leads to $\mathbf{Q} = \mathbf{D}^T \mathbf{Q}_0 \mathbf{D}$. The remaining steps are the same as for the standard formulation.

This formulation is applied to the system considered in Ex. 9.4. The response measures are taken as the shear deformation rates for elements 18, 19, and 20. Uniform weighting ($w_1 = w_2 = w_3 = 1$) is used for the element deformations. The location of the control force is the same as for Ex. 9.4. Fig. 9.16 shows some of the results for this case. These plots correspond to Fig. 9.15 of Ex. 9.4. The peak value of the control force is 1200 N for Fig. 9.16(b), and 1719 N for Fig. 9.15.

9.3. LQR CONTROL ALGORITHM: MDOF TIME-INVARIANT SYSTEMS

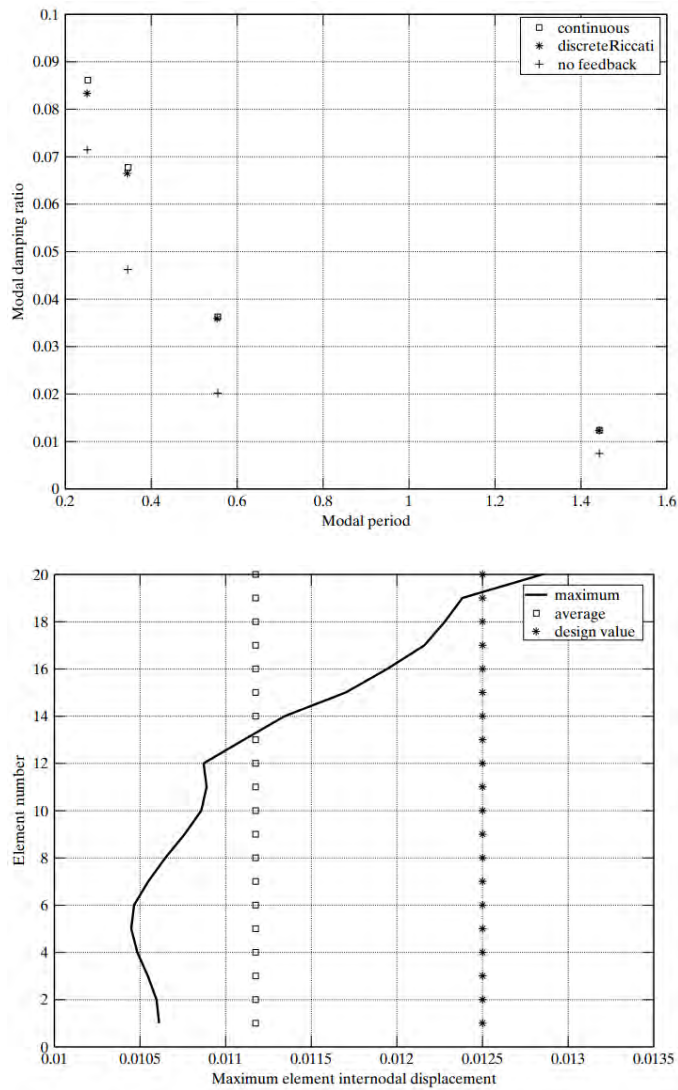


Figure 9.16: Solution based on using deformation rates for elements 18, 19, 20 and a single control force at node 20. (a) Modal damping ratio with and without continuous or discrete feedback - no saturation limit; and (b) element internodal displacement profile.

Problems

Problem 9.1

Consider Eq. (8.79). Integrating this equation between t_j and t_{j+1} leads to

$$\mathbf{X}_{j+1} - \mathbf{X}_j = \int_{t_j}^{t_{j+1}} (\mathbf{A}\mathbf{X} + \mathbf{B}_f\mathbf{F} + \mathbf{B}_g a_g + \mathbf{B}_p p) dt$$

Suppose the integrand is assumed to vary linearly over the time interval, and the coefficient matrices \mathbf{A} , \mathbf{B}_f , ..., are constant.

1. Derive the expression for corresponding to these conditions. Compare this result with Eq. (8.82). Comment on the nature of the error.
2. Specialize 1. for negative linear feedback, and compare with Eq. (8.87).
3. Specialize 2. for no time delay and free vibration response. Compare with Eq. (8.91). Define the stability requirement for this approximation.

Problem 9.2

Verify Eq. (9.34) using the CARE function of MATLAB. Take

$$\begin{aligned} m &= 1,000 \text{ kg} & k &= 60,000 \text{ N/m} & c &= 750 \text{ N} \cdot \text{s/m} \\ c &= 1 & q_d &= 0 & q_v &= 4\omega^2 m^2 \bar{q}_v \end{aligned}$$

and consider \bar{q}_v to have the following values: 0, 0.5, 1.0.

Problem 9.3

9.3. LQR CONTROL ALGORITHM: MDOF TIME-INVARIANT SYSTEMS

Refer to Eq. (9.36). Will the LQR algorithm ever produce an unstable system?

Problem 9.4

Consider Eq. (9.44). Let

$$\mathbf{D} = \mathbf{Q} + \mathbf{K}_f^T \mathbf{R} \mathbf{K}_f$$
$$\mathbf{S}_n = \sum_{j=0}^n \mathbf{C}^{j,T} \mathbf{D} \mathbf{C}^j$$

Noting the identity,

$$\mathbf{C}^T \mathbf{S}_n \mathbf{C} - \mathbf{S}_n = -\mathbf{S} + \mathbf{C}^{n+1,T} \mathbf{D} \mathbf{C}^{n+1}$$

and the limit condition,

$$\mathbf{C}^j \rightarrow \mathbf{0} \quad \text{as} \quad j \rightarrow \infty \quad (9.184)$$

derive Eq. (9.45).

Problem 9.5

Refer to Figs. 9.3 and 9.4 of Ex. 9.1. Suppose the time ratio $\Delta t/T$ is determined by the external loading, and is equal to 0.1. Suggest a value for \bar{q}_v such that ξ_a is close to 0.2 when $\xi = 0.05$.

Problem 9.6

Consider the following system:

$$m = 1,000 \text{ kg}$$
$$k = 60,000 \text{ N/m}$$
$$c = 1,000 \text{ N} \cdot \text{s/m}$$

CHAPTER 9. LINEAR CONTROL

Suppose $\Delta t = 0.02$ s. Select the parameters for discrete time feedback control such that the effective damping ratio is equal to 0.2. Use Figs. 9.3 and 9.4 of Ex. 9.1 to obtain an initial estimate, and the function `dare` in MATLAB to refine the estimate. Note that the solution tends toward the continuous time feedback case as $\Delta t/T$ approaches 0.

Problem 9.7

Refer to Ex. 9.2. Compare the expressions for k_d and k_v corresponding to $q_d = 0$ with the continuous time Riccati solution defined by Eq. (9.37). Use the discrete time Riccati solution for $\xi = 0.02$ listed in Ex. 9.1 to compare the values of q_v required to produce $(k_v/2\omega m) = 0.2$ for two time increments, $\Delta t/T = 0.02$ and 0.1.

Problem 9.8

Rework Problem 9.12 using the finite interval discrete time algebraic Riccati equation. Note that the weighting factors for the finite interval formulation are different from the corresponding weighting factors for the discrete time algebraic Riccati equation.

Problem 9.9

Verify Eq. (8.158)

Problem 9.10

Consider a SDOF system having the following properties:

$$\begin{aligned}m &= 10,000 \text{ kg} \\k &= 400,000 \text{ kN/m} \\c &= 2500 \text{ kN} \cdot \text{s/m}\end{aligned}$$

9.3. LQR CONTROL ALGORITHM: MDOF TIME-INVARIANT SYSTEMS

1. Using the LQR control algorithm, establish values for the weighting parameters such that the effective damping for continuous velocity feedback has the following values: $\xi_{\text{eq}} = 0.05, 0.1, 0.2$.
2. Take $\Delta t = 0.02$ s. Evaluate the discrete time damping ratios for 1.
3. Using the finite time interval control algorithm, establish values for the weighting parameters such that the discrete time damping ratios are the same as found in 2.
4. Using the model properties corresponding to ξ_{eq} established in 1., determine the maximum values of the displacement, control force, and power associated with the El Centro accelerogram. Use $\Delta t = 0.02$.
5. Repeat 4. for the Kobe accelerogram.
6. Repeat 4. for the Mexico City 1 accelerogram.

Problem 9.11

Consider a 4DOF system having the properties shown in Table P9.11a.

Table P9.11a

Node/Element	m (kg)	k (kN/m)	c (kN·s/m)
1	1,000	1,700	4
2	1,000	1,400	3
3	1,000	1,000	2
4	1,000	700	1

Suppose a single control force is applied at the top node. Using the LQR algorithm, select the weighting parameters which result

CHAPTER 9. LINEAR CONTROL

in a value of the damping ratio for discrete feedback equal to 0.2 for the first mode. Take $\Delta t = 0.02$ s, and apply the following strategies:

1. Use the conventional state-space formulation and weight the nodal velocities uniformly.
2. Use the modal state-space formulation and weight the first derivative of the modal coordinates uniformly.
3. Use the conventional state-space formulation and weight the element deformation rates uniformly.
4. Repeat 3. using the modal state-space formulation.

Problem 9.12

Consider a 5DOF shear beam with the following constant mass and stiffness properties:

$$m = 10,000 \text{ kg}$$

$$k = 350,000 \text{ N/m}$$

1. Assuming uniform element viscous damping, determine the magnitude of element damping such that the first mode damping ratio is 0.02.
2. Apply a single control force at mode 5. Assuming all five modes are retained, and they are weighted equally, determine the weighting parameters such that the equivalent damping for continuous feedback is 0.15 for the first mode.
3. Determine the corresponding damping ratio for discrete time feedback. Take $\Delta t = 0.02$ s.

9.3. LQR CONTROL ALGORITHM: MDOF TIME-INVARIANT SYSTEMS

- Investigate the effect of delay on the free vibration response of the modal coordinates due to an initial displacement. Use $\Delta t = 0.02$ s and the parameters established in part 2.

Problem 9.13

Consider the 5DOF systems shown in Table P9.13a.

Table P9.13a

Node/Element	m (kg)	k (kN/m)	c (kN·s/m)
1	1,000	2,000	5
2	1,000	1,700	5
3	1,000	1,400	5
4	1,000	1,000	5
5	1,000	700	5

- Suppose control forces are applied at all five nodes. Determine the modal coordinate weighting parameters such that the equivalent damping ratio corresponding to continuous feedback is equal to 0.15 for the first mode. Assume uniform weighting.
- Suppose self-equilibrating sets of control forces are applied on all five elements and the weighting is applied to the element deformation time rates. Determine the weights such that the first mode damping ratio is 0.15. Assume uniform weighting.
- Apply the Northridge earthquake to the models obtained in 1. and 2. Compare
 - the internode displacement profiles
 - the peak power

CHAPTER 9. LINEAR CONTROL

(c) the peak value of the control forces

Problem 9.14

Consider a 10DOF shear beam with constant mass, element stiffness, and element damping. Take $m = 10,000$ kg.

1. Determine the stiffness and damping constants such that the properties for the first mode are

$$\text{Period} = 1 \text{ s}$$

$$\text{Damping ratio} = 0.02$$

2. Select an active control force scheme which provides a damping ratio of 0.2 for the first mode.
3. Apply the Kobe ground acceleration to the system defined in 2. Examine the responses of the first three modes. Generate both the time histories and the Fourier components.
4. If the design objective is to have uniform peak element shear deformation throughout the system, what design modifications would you suggest? Illustrate your strategy for the case where the target value of the relative internodal displacement is 0.0125 m.

Problem 9.15

Consider a 10DOF shear beam with constant nodal mass equal to 10,000 kg.

1. Select a parabolic distribution of element stiffness and a constant element viscous damping so that the period for the first mode is 1 second, and the modal damping ratio is 0.02.

9.3. LQR CONTROL ALGORITHM: MDOF TIME-INVARIANT SYSTEMS

2. Carry out iteration on the element stiffness using the El Centro ground excitation and 0.0125 m as the desired value of internodal displacement.

3. Incorporate active control in the system obtained in part 2. Select the weighting parameters such that the modal damping ratios (for continuous feedback) for the first three modes are approximately equal to 0.15. Consider a global forcing scheme and weight the modal coordinate velocities.

4. Repeat 3. using self-equilibrating control force schemes and weight the modal coordinate velocities.

5. Repeat 4. using the internodal element displacements as the performance measures. (See Ex. 9.5.)

Problem 9.16

Consider the bending beam-outrigger system shown in Fig. P9.16a. Assume the outriggers are infinitely stiff, the beam bending rigidity is constant, and the cables are initially tensioned to a level of T_0 . Suppose the cable tensions can be continuously adjusted to counteract the effect of lateral load.

CHAPTER 9. LINEAR CONTROL

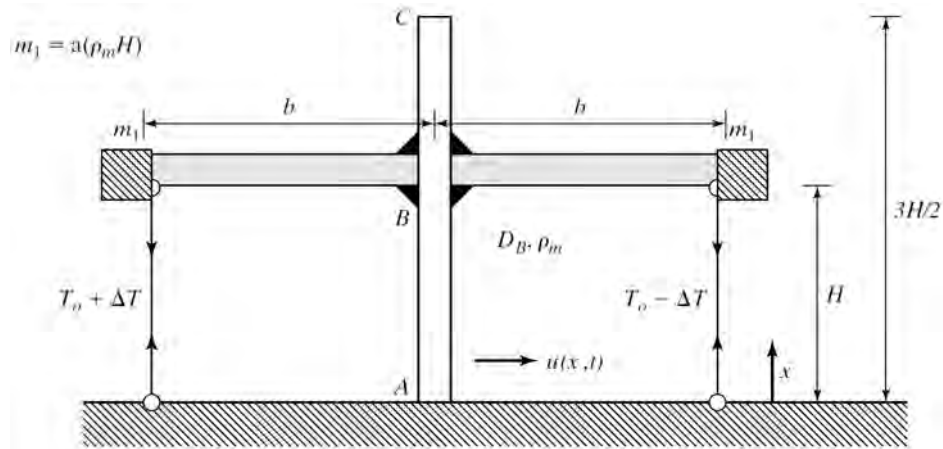


Figure P9.16a

1. Take the lateral displacement and rotation at points B , C as the degrees of freedom and establish the corresponding matrix form of the equilibrium equations. Work with “lumped” masses, rotatory inertias, and loads.
2. Develop the state-space formulation for 1.
3. Describe how you would implement linear velocity feedback control.
4. Suppose the bending rigidity is specified and the critical dynamic loading is a uniform periodic excitation. Discuss how you would “calibrate” the feedback parameters for the case where the design objective is to limit the maximum acceleration. Illustrate your strategy.

Problem 9.17

Consider an undamped SDOF system with acceleration-based negative linear feedback. The governing equation for free vibration response allowing for time delay is

9.3. LQR CONTROL ALGORITHM: MDOF TIME-INVARIANT SYSTEMS

$$m\ddot{u} + ku + k_m\ddot{u}(t - \tau) = 0$$

1. Express the homogeneous solution as $u = e^{\lambda t}$. Derive the following expression for λ .

$$\lambda^2(m + e^{-\lambda\tau}k_m) + k = 0 \quad \text{(P17.1)}$$

2. Substitute for $e^{-\lambda\tau}$ using the Pade approximation, Eq. (8.56), in (P17.1) and the following notation:

$$\begin{aligned} k_m &= \alpha m \\ \tau &= \frac{1}{\omega} \bar{\tau} = \frac{T}{2\pi} \bar{\tau} \end{aligned}$$

Show that (P17.1) expands to

$$\bar{\lambda}^3(1 - \alpha)\frac{\bar{\tau}}{2} + \bar{\lambda}^2(1 + \alpha) + \bar{\lambda}\frac{\bar{\tau}}{2} + 1 = 0 \quad \text{(P17.2)}$$

3. Take $\alpha = 0.05$. Solve (P17.2) for a set of values of $\bar{\tau}$ ranging from 0 to π . Plot λ_I vs λ_R . Discuss whether instability is possible as the delay increases.
4. Following the approach described in Sect. 8.2, express λ as

$$\lambda = i\Theta$$

and substitute for $\bar{\lambda}$ in (P17.1). Verify that the solution for Θ and the maximum allowable $\bar{\tau}$ is

$$\begin{aligned}\Theta^2 &= \frac{1}{1 - \alpha} \\ \bar{\tau}_{\max} &= \frac{\pi}{\Theta} = (1 - \alpha)^{1/2} \pi \\ \tau_{\max} &= \frac{T}{2} (1 - \alpha)^{1/2}\end{aligned}$$

Compare this result with that obtained with the Pade approximation.

10

Advanced Control Theory

10.1 Introduction

This chapter introduces advance topics in structural control theory. We chose the selection of topics and level of math rigor for the material presented in Chapters 8 and 9 to be appropriate for one who has some knowledge of structural dynamics but relatively no background in control theory. The role of feedback in providing damping to a physical system was stressed since damping is an important design variable for physical systems. We worked with a quadratic performance index (i.e., LQR) since it is a natural extension of the quasi-static formulation, which is based on the least squares error measure.

In what follows, we re-explain certain theoretical topics in a more rigorous way to provide sufficient background for discussing some of the more recent control algorithms, based on performance measures, that are different from the classical quadratic measure. Again, our intention is to provide an introduction to control theory for structural engineers so that they can, if they wish, pursue the topic in more depth. Suggested references are [80, 13]. We also introduce nonlinear control theory. The design of nonlinear controllers is deemed more appropriate for establishing control rules for semi-active devices, since they inherently introduce nonlinearities in the system. This chapter concludes with three semi-active control examples, which are intended to illustrate how linear and nonlinear control rules for semi-active and hybrid structural control systems are implemented.

10.2 State Controllability

In an earlier section, we explained the controllability of a particular modal response and showed that *a mode can be controlled*

10.2. STATE CONTROLLABILITY

provided that control forces are not placed at null points of the corresponding mode shape. In this section, we extend the analysis to deal with the full state equation rather than the reduced order modal equation.

Considering an n^{th} -order system, with control forces, the governing equation is written as

$$\dot{\mathbf{X}} = \mathbf{A}\mathbf{X} + \mathbf{B}\mathbf{F} \quad (10.1)$$

where \mathbf{A} is $(n \times n)$, \mathbf{F} is $(r \times 1)$, and \mathbf{B} is $(n \times r)$. Assuming the system is time invariant, the solution at $t = t_1$ due to initial conditions at $t = 0$ is

$$\mathbf{X}(t_1) = \int_0^{t_1} \mathbf{e}^{\mathbf{A}(t_1-\tau)} \mathbf{B}\mathbf{F}(\tau) d\tau + \mathbf{e}^{\mathbf{A}t_1} \mathbf{X}(0) \quad (10.2)$$

The general definition of controllability is as follows: A system is said to be controllable if a control force $\mathbf{F}(t)$ can be determined such that the system (when subjected to an initial disturbance) is brought to rest at a later time. Applying this definition to Eq. (10.2) leads to a constraint equation on $\mathbf{B}\mathbf{F}(\tau)$.

$$\int_0^{t_1} \mathbf{e}^{-\mathbf{A}\tau} \mathbf{B}\mathbf{F}(\tau) d\tau = -\mathbf{X}(0) \quad (10.3)$$

The integral can be expanded by introducing the following approximation, which is obtained by truncating the expansion for the exponential after n terms:

$$\begin{aligned} \mathbf{e}^{-\mathbf{A}\tau} &\approx \sum_{k=0}^{n-1} \alpha_k(\tau) \mathbf{A}^k \\ \alpha_k(\tau) &= \frac{1}{k!} \tau^k \end{aligned} \quad (10.4)$$

Then

$$\begin{aligned} \int_0^{t_1} \mathbf{e}^{-\mathbf{A}\tau} \mathbf{B} \mathbf{F}(\tau) dt &\approx \sum_{k=0}^{n-1} \mathbf{A}^k \mathbf{B} \int_0^{t_1} \alpha_k(\tau) \mathbf{F}(\tau) dt \\ &\approx \sum_{k=0}^{n-1} (\mathbf{A}^k \mathbf{B}) \beta_k \end{aligned} \quad (10.5)$$

and (10.3) takes the form

$$\left[\mathbf{B} \quad \mathbf{A}\mathbf{B} \quad \mathbf{A}^2\mathbf{B} \quad \dots \quad \mathbf{A}^{n-1}\mathbf{B} \right] \begin{bmatrix} \beta_0 \\ \beta_1 \\ \dots \\ \beta_{n-1} \end{bmatrix} = -\mathbf{X}_0 \quad (10.6)$$

Eq. (10.6) represents n equations in n unknowns, the scalars $\beta_0, \beta_1, \dots, \beta_{n-1}$. The issue of controllability reduces to whether a unique solution for β exists for arbitrary \mathbf{X}_0 . This will be true when the rank of the coefficient matrix is equal to n . Therefore, the controllability requirement can be expressed as

$$\text{rank} \left[\mathbf{B} \quad \mathbf{A}\mathbf{B} \quad \mathbf{A}^2\mathbf{B} \quad \dots \quad \mathbf{A}^{n-1}\mathbf{B} \right] = \text{rank}[\mathbf{B}_c] \equiv n \quad (10.7)$$

The coefficient matrix \mathbf{B} depends on the control force location. Given a force location, we form \mathbf{B} and the various matrix products, assemble \mathbf{B}_c , and evaluate the rank. This process is carried out for each control force location when there are multiple control forces.

If a modal expansion procedure is adopted, the coefficient matrix \mathbf{B} depends on the mode shape as well as the location

(see Eq. (8.292)), and the rank requirement specialized for the k^{th} modal response reduces to Eq. (8.293). In this case, it is easier to loop over the modes and determine whether an individual mode is controllable for a specified control force.

10.3 State Observability

Observability was discussed earlier in the context of modal response. Assuming m modes are retained in the formulation of the system matrices, it was shown that $2m$ observations are required to determine the full modal state vector, which is needed to generate the feedback force. Furthermore, these observation points cannot coincide with the null points of the mode shapes used in the modal formulation. Even when the proper number of observations is employed, there is still some error since the observations also contain contributions from the higher modes that are neglected in the model.

In what follows, observability is revisited for the full continuous state-space formulation, and we present a strategy for dealing with the case where the number of observations is less than the size of the full state vector.

The equations for an n^{th} -order system with feedback are written as

$$\begin{aligned}\dot{\mathbf{X}} &= \mathbf{A}\mathbf{X} + \mathbf{B}\mathbf{F} \\ \mathbf{F} &= -\mathbf{K}\mathbf{X} \\ \mathbf{Y} &= \mathbf{C}\mathbf{X}\end{aligned}\tag{10.8}$$

where \mathbf{X} denotes the n^{th} -order state vector and \mathbf{Y} contains the observations. We assume here that there are m observations,

CHAPTER 10. ADVANCED CONTROL THEORY

where $m \leq n$. The matrix \mathbf{C} relates the observations and the state variables and is of order $m \times n$. Lastly, \mathbf{A} and \mathbf{B} are the standard matrices introduced in Sect. 8.2. For all the numerical simulations carried out earlier in the chapter, \mathbf{Y} was taken as \mathbf{X} (i.e., the observations were assumed to be the predicted values for the full state vector, and \mathbf{C} reduced to an identity matrix of order n).

Example 10.1 - 5DOF Model

Consider a 5DOF shear beam. The corresponding state space formulation has $n = 10$. Suppose the displacement and velocity are measured at nodes 3, 4, and 5. The observation vector for this choice of measurements is of order 6×1 (i.e., $m = 6$).

$$\mathbf{Y} = \{u_3, u_4, u_5, \dot{u}_3, \dot{u}_4, \dot{u}_5\} \quad (10.9)$$

Assuming \mathbf{X} contains all the nodal displacements and velocities, the form of \mathbf{C} is

$$\mathbf{C} = \begin{bmatrix} 0 & 0 & 1 & 0 & 0 & 0 & 0 & 0 & 0 & 0 \\ 0 & 0 & 0 & 1 & 0 & 0 & 0 & 0 & 0 & 0 \\ 0 & 0 & 0 & 0 & 1 & 0 & 0 & 0 & 0 & 0 \\ 0 & 0 & 0 & 0 & 0 & 0 & 0 & 1 & 0 & 0 \\ 0 & 0 & 0 & 0 & 0 & 0 & 0 & 0 & 1 & 0 \\ 0 & 0 & 0 & 0 & 0 & 0 & 0 & 0 & 0 & 1 \end{bmatrix} \quad (10.10)$$

Example 10.2 - Example 10.1 revisited

Consider the shear beam of Ex. 10.1. Suppose a modal expansion strategy is employed and only the first three modes are retained. The state vector now involves the modal coordinates and velocities (i.e., $n = 6$):

$$\mathbf{X} = \{q_1, q_2, q_3, \dot{q}_1, \dot{q}_2, \dot{q}_3\} \quad (10.11)$$

If nodal displacements and nodal velocities are measured, we need to relate the nodal variables and modal coordinates. Assuming, for convenience, the modes are uncoupled, which is true for low damping, the relation reduces to

$$\mathbf{U} = \phi q \quad (10.12)$$

where the i^{th} column of ϕ contains the eigenvector for the i^{th} mode. There are three columns since only three modes are retained. We generate \mathbf{C} from ϕ by retaining the rows that correspond to the observed variables. The result is

$$\mathbf{C} = \begin{bmatrix} \phi_R & \mathbf{0} \\ \mathbf{0} & \phi_R \end{bmatrix} \quad (10.13)$$

$$\phi_R = \begin{bmatrix} \phi_{31} & \phi_{32} & \phi_{33} \\ \phi_{41} & \phi_{42} & \phi_{43} \\ \phi_{51} & \phi_{52} & \phi_{53} \end{bmatrix}$$

In this case, the full modal state vector is observed. However, the observations contain contributions from the higher modes that are neglected in the formulation.

The solution at $t = t^*$ due to initial conditions at $t = 0$ is

$$\mathbf{X}(t^*) = \mathbf{e}^{\mathbf{A}t^*} \mathbf{X}(0) + \int_0^{t^*} \mathbf{e}^{\mathbf{A}(t^*-\tau)} \mathbf{B}\mathbf{F}(\tau) d\tau \quad (10.14)$$

This solution produces the following observations at t :

$$\mathbf{Y}(t^*) = \mathbf{C}\mathbf{e}^{\mathbf{A}t^*} \mathbf{X}(0) + \int_0^{t^*} \mathbf{C}\mathbf{e}^{\mathbf{A}(t^*-\tau)} \mathbf{B}\mathbf{F}(\tau) d\tau \quad (10.15)$$

Observability is defined by the requirement that $\mathbf{X}(0)$ can be determined from observations on $\mathbf{Y}(t)$ over the finite time interval, $0 < t \leq t^*$. Rearranging Eq. (10.15) leads to a set of equations relating $\mathbf{X}(0)$ in terms of $\mathbf{Y}(t^*)$ and forcing terms:

$$\begin{aligned} \mathbf{C}e^{\mathbf{A}t^*}\mathbf{X}(0) &= \mathbf{Y}(t^*) - \int_0^{t^*} \mathbf{C}e^{\mathbf{A}(t^*-\tau)}\mathbf{B}\mathbf{F}(\tau)d\tau \\ &= \bar{\mathbf{Y}}(t^*) \end{aligned} \quad (10.16)$$

There are m equations and n unknowns. Additional equations can be established by selecting some time points in the interval $0 < t < t^*$. Whether $\mathbf{X}(0)$ can be determined, given a sufficient number of equations, depends on the coefficient matrix.

Noting the approximation for $e^{\mathbf{A}t}$ given by Eq. (10.4), the left-hand side can be written as

$$\mathbf{C}e^{\mathbf{A}t^*}\mathbf{X}(0) \approx \sum_{k=0}^{n-1} \alpha_k(t^*)\mathbf{C}\mathbf{A}^k\mathbf{X}(0) \quad (10.17)$$

and Eq. (10.16) takes the form

$$\alpha_0(t^*)\mathbf{C}\mathbf{X}(0) + \alpha_1(t^*)\mathbf{C}\mathbf{A}\mathbf{X}(0) + \cdots + \alpha_{n-1}(t^*)\mathbf{C}\mathbf{A}^{n-1}\mathbf{X}(0) = \bar{\mathbf{Y}}(t^*) \quad (10.18)$$

Suppose $\bar{\mathbf{Y}}(t^*) = 0$. This is possible only if $\mathbf{X}(0) = \mathbf{0}$. Therefore, we set $\bar{\mathbf{Y}}(t^*) = 0$ in Eq. (10.18) and determine the constraint on \mathbf{C} such that a nontrivial solution for $\mathbf{X}(0)$ does not exist. The individual sets of equations are

$$\begin{aligned}\mathbf{C}\mathbf{X}(0) &= \mathbf{0} \\ \mathbf{C}\mathbf{A}\mathbf{X}(0) &= \mathbf{0} \\ \mathbf{C}\mathbf{A}^2\mathbf{X}(0) &= \mathbf{0} \\ \dots & \\ \mathbf{C}\mathbf{A}^{n-1}\mathbf{X}(0) &= \mathbf{0}\end{aligned}\tag{10.19}$$

There are a total of $n \times m$ equations relating the n unknowns contained in $\mathbf{X}(0)$. For only a trivial ($\mathbf{X}(0) = \mathbf{0}$) solution to exist, n equations must be linearly independent. This condition can be expressed in terms of the rank of the “total” coefficient matrix, \mathbf{C}^* , which is of order $nm \times m$.

$$\mathbf{C}^* = \begin{bmatrix} \mathbf{C} \\ \mathbf{C}\mathbf{A} \\ \mathbf{C}\mathbf{A}^2 \\ \dots \\ \mathbf{C}\mathbf{A}^{n-1} \end{bmatrix}\tag{10.20}$$

Observability requires the rank of \mathbf{C}^* to be equal to n , the order of the system.

10.4 State Observer

When the full state-space formulation is used, if the number of observations is less than the order of the system, it is necessary to estimate the state vector since the feedback force is computed using the full state vector. This estimation process is based on a state observer and is outlined next.

Consider an n^{th} -order system with m observations. The governing equations are

$$\begin{aligned}\dot{\mathbf{X}} &= \mathbf{A}\mathbf{X} + \mathbf{B}_f\mathbf{F} + \mathbf{B}_p\mathbf{P} \\ \mathbf{Y} &= \mathbf{C}\mathbf{X}\end{aligned}\tag{10.21}$$

Assuming the observability requirement is satisfied by \mathbf{C} , and \mathbf{X} is known, \mathbf{F} is generated with

$$\mathbf{F} = -\mathbf{K}_f\mathbf{X}\tag{10.22}$$

If $m < n$, the number of equations represented by $\mathbf{Y} = \mathbf{C}\mathbf{X}$ is insufficient to uniquely determine \mathbf{X} , given \mathbf{Y} . This situation was encountered in Sect. 2.5, which is concerned with establishing the stiffness distribution for a statically indeterminate structure where a pseudoinverse solution technique was applied. The pseudoinverse solution is not unique. It corresponds to a minimum value of the quadratic norm, $\frac{1}{2}\mathbf{X}^T\mathbf{X}$. A different approach is followed here.

Let $\tilde{\mathbf{X}}$ represent an approximation for \mathbf{X} . The feedback force is computed using $\tilde{\mathbf{X}}$.

$$\mathbf{F} = -\mathbf{K}_f\tilde{\mathbf{X}}\tag{10.23}$$

In addition to allowing for a difference in the state vector, a measurement noise is included in the relationship between the observations and the state vector. Defining \mathbf{Y}_m as the “actual” observations, the expression for \mathbf{Y}_m is taken as

$$\mathbf{Y}_m = \mathbf{C}\tilde{\mathbf{X}} + \mathbf{V}\tag{10.24}$$

where \mathbf{V} represents measurement noise. The difference between \mathbf{Y}_m and $\mathbf{C}\tilde{\mathbf{X}}$ is the observation error due to the noise and the inexactness of the approximate state vector, $\tilde{\mathbf{X}}$.

An equation for $\tilde{\mathbf{X}}$ is established using the same form of state equation as the system, with a corrective term added to account for the observation error.

$$\dot{\tilde{\mathbf{X}}} = \mathbf{A}\tilde{\mathbf{X}} + \mathbf{B}_f(\mathbf{F}) + \mathbf{K}_e(\mathbf{Y}_m - \mathbf{C}\tilde{\mathbf{X}}) \quad (10.25)$$

where \mathbf{K}_e is a weighting matrix of order $n \times m$. The use of Eq. (10.25) corresponds to correcting the entire state vector even though certain values may be known.

If we associate a state equation with a system, the original equation (10.21) identifies with the physical system, and the corrective equation describes an “observational” system that is computationally coupled with the physical system. The systems are generally referred to as the “plant” and observed models. Fig. 10.1 contains block diagrams for both models. Block diagrams are a pictorial representation of the functions performed by each component of the model and the interrelationships between the components.

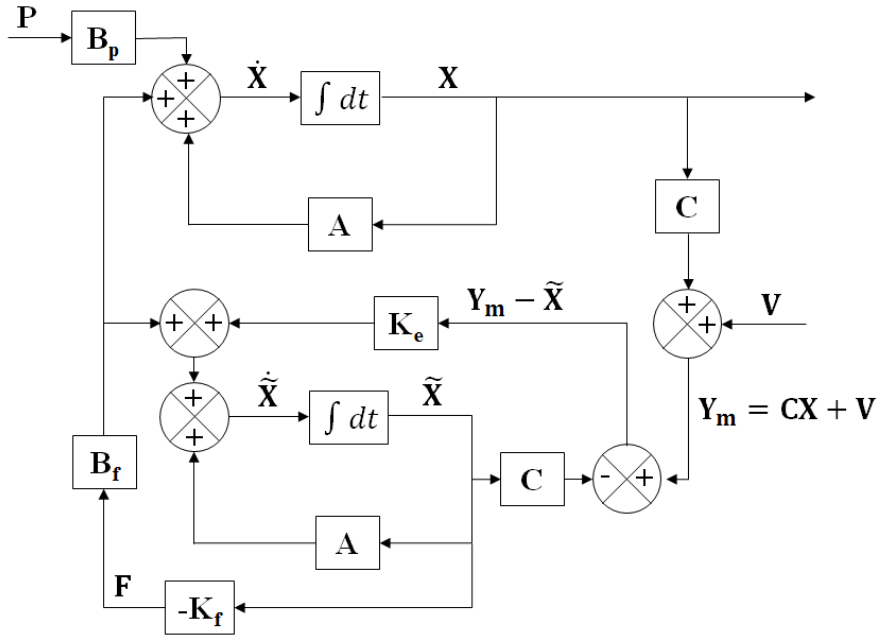


Figure 10.1: Block diagrams for plant and observer models.

Defining \mathbf{e} as the state vector error,

$$\mathbf{e} = \mathbf{X} - \tilde{\mathbf{X}} \quad (10.26)$$

and subtracting Eq. (10.25) from Eq. (10.21) leads to the following equation for \mathbf{e} :

$$\dot{\mathbf{e}} = \mathbf{A}_e \mathbf{e} + \mathbf{B}_p \mathbf{P} - \mathbf{K}_e \mathbf{V} \quad (10.27)$$

where

$$\mathbf{A}_e = \mathbf{A} - \mathbf{K}_e \mathbf{C} \quad (10.28)$$

The objective of including an observer is to reduce the error. It follows that \mathbf{A}_e must be a stable matrix (i.e., the real part of the eigenvalues of \mathbf{A}_e must be negative). High damping is desirable since the transient response decays more rapidly.

There are various strategies for selecting \mathbf{K}_e . The procedure described here is similar to the approach followed for the time-invariant LQR problem. We start by defining a performance index that involves \mathbf{K}_e and require the index to be stationary with respect to \mathbf{K}_e . The result is an equation similar to the algebraic Riccati equation for \mathbf{K}_f , the force feedback matrix derived in Sect. 9.2.

Noting Eq. (10.27), there are two forcing terms $\mathbf{p}(t)$ and $\mathbf{V}(t)$. They are taken as scaled delta functions centered at $t = 0$.

$$\begin{aligned}\mathbf{P} &= \mathbf{P}_0\delta(t) \\ \mathbf{V} &= \mathbf{V}_0\delta(t)\end{aligned}\tag{10.29}$$

The corresponding time history responses are

$$\begin{aligned}\mathbf{P} &\rightarrow \mathbf{e}_1 = \mathbf{e}^{\mathbf{A}et}\mathbf{B}_p\mathbf{P}_0 \\ \mathbf{V} &\rightarrow \mathbf{e}_2 = \mathbf{e}^{\mathbf{A}et}(-\mathbf{K}_e)\mathbf{V}_0\end{aligned}\tag{10.30}$$

These solutions are used to formulate a quadratic performance index,

$$\begin{aligned}J &= \frac{1}{2} \int_0^\infty (\mathbf{e}_1\mathbf{e}_1^T + \mathbf{e}_2\mathbf{e}_2^T)dt = J(\mathbf{K}_e) \\ &= \frac{1}{2} \int_0^\infty \mathbf{e}^{\mathbf{A}et}[\mathbf{B}_p\mathbf{P}_0\mathbf{P}_0^T\mathbf{B}_p^T + \mathbf{K}_e\mathbf{V}_0\mathbf{V}_0^T\mathbf{K}_e^T] [\mathbf{e}^{\mathbf{A}et}]^T dt\end{aligned}\tag{10.31}$$

The remaining steps are similar to those described in Sect. 9.2. We write

$$\mathbf{e}^{\mathbf{A}et}[\mathbf{B}_p\mathbf{P}_0\mathbf{P}_0^T\mathbf{B}_p^T + \mathbf{K}_e\mathbf{V}_0\mathbf{V}_0^T\mathbf{K}_e^T] [\mathbf{e}^{\mathbf{A}et}]^T = -\frac{d}{dt} \left[\mathbf{e}^{\mathbf{A}et}\mathbf{H} (\mathbf{e}^{\mathbf{A}et})^T \right]\tag{10.32}$$

CHAPTER 10. ADVANCED CONTROL THEORY

where \mathbf{H} is symmetric and time invariant. Differentiating the right-hand side, and equating corresponding terms leads to

$$-\mathbf{A}_e \mathbf{H} - \mathbf{H} \mathbf{A}_e^T = \mathbf{B}_p \mathbf{P}_0 \mathbf{P}_0^T \mathbf{B}_p^T + \mathbf{K}_e \mathbf{V}_0 \mathbf{V}_0^T \mathbf{K}_e^T \quad (10.33)$$

Also, J reduces to

$$\begin{aligned} J &= -\frac{1}{2} \int_0^\infty \frac{d}{dt} \left[\mathbf{e}^{\mathbf{A}_e t} \mathbf{H} (\mathbf{e}^{\mathbf{A}_e t})^T \right] dt \\ &= \frac{1}{2} \mathbf{H} \end{aligned} \quad (10.34)$$

since $\mathbf{e}^{\mathbf{A}_e t} \rightarrow \mathbf{0}$ as $t \rightarrow \infty$. The matrix \mathbf{H} is a function of \mathbf{K}_e . Then the stationary requirement on J requires

$$\delta J = 0 \Rightarrow \delta \mathbf{H} = \mathbf{0} \quad (10.35)$$

Finally, operating on Eq. (10.33),

$$-\delta \mathbf{A}_e \mathbf{H} - \mathbf{H} \delta (\mathbf{A}_e)^T = \delta \mathbf{K}_e \mathbf{V}_0 \mathbf{V}_0^T \mathbf{K}_e^T + \mathbf{K}_e \mathbf{V}_0 \mathbf{V}_0^T \delta (\mathbf{K}_e)^T \quad (10.36)$$

and noting that

$$\delta \mathbf{A}_e = -\delta \mathbf{K}_e \mathbf{C} \quad (10.37)$$

results in

$$\mathbf{C} \mathbf{H} = (\mathbf{V}_0 \mathbf{V}_0^T) \mathbf{K}_e^T \quad (10.38)$$

The matrix $\mathbf{V}_0 \mathbf{V}_0^T$ is singular since \mathbf{V}_0 is a vector of order $m \times 1$. However, to proceed further, it is assumed to be a diagonal matrix with positive elements. Then we can solve for \mathbf{K}_e .

$$\mathbf{K}_e = \mathbf{H}\mathbf{C}^T(\mathbf{V}_0\mathbf{V}_0^T)^{-1} \quad (10.39)$$

Lastly, substituting for \mathbf{A}_e and \mathbf{K}_e in Eq. (10.33), the expression for \mathbf{H} expands to

$$\mathbf{A}\mathbf{H} + \mathbf{H}\mathbf{A} - \mathbf{H}\mathbf{C}^T(\mathbf{V}_0\mathbf{V}_0^T)\mathbf{C}\mathbf{H} + \mathbf{B}_p\mathbf{P}_0\mathbf{P}_0^T\mathbf{B}_p^T = \mathbf{0} \quad (10.40)$$

Comparing these equations with the LQR results defined by Eqs. (9.28) and (9.29), we observe that the forms are similar and the coefficient matrices are related as shown in Table 10.1.

Table 10.1

LQR	Observer
\mathbf{A}	\mathbf{A}
\mathbf{B}_f	\mathbf{C}^T
\mathbf{H}	\mathbf{H}
\mathbf{Q}	$\mathbf{B}_p\mathbf{P}_0\mathbf{P}_0^T\mathbf{B}_p^T$
\mathbf{R}	$\mathbf{V}_0\mathbf{V}_0^T$
\mathbf{K}_f	\mathbf{K}_e^T

Using the “observer” matrices with care, we can obtain \mathbf{K}_e and the eigenvalues of \mathbf{A}_e .

The continuous time formulation just presented is useful for preliminary design of a control system. However, the actual implementation is usually done with a discrete time formulation. Using the discrete time notation introduced in Sect. 8.3 and 9.2, the state equations are expressed as

$$\mathbf{X}_{j+1} = \mathbf{C}_1\mathbf{X}_j + \mathbf{C}_2\mathbf{F}_j + \mathbf{C}_3\mathbf{P}_j \quad (10.41)$$

$$\mathbf{Y}_{m,j} = \mathbf{C}\mathbf{X}_j + \mathbf{V}_j \quad (10.42)$$

where

$$\begin{aligned} \mathbf{C}_1 &= \mathbf{e}^{\mathbf{A}\Delta t} \\ \mathbf{C}_2 &= \mathbf{A}^{-1}(\mathbf{e}^{\mathbf{A}\Delta t} - \mathbf{I})\mathbf{B}_f \\ \mathbf{C}_3 &= \mathbf{A}^{-1}(\mathbf{e}^{\mathbf{A}\Delta t} - \mathbf{I})\mathbf{B}_p \end{aligned} \quad (10.43)$$

Similarly, the observer equation is written as

$$\tilde{\mathbf{X}}_{j+1} = \mathbf{C}_1\tilde{\mathbf{X}}_j + \mathbf{C}_2\mathbf{F}_j + \mathbf{K}_e(\mathbf{Y}_{m,j} - \mathbf{C}\tilde{\mathbf{X}}_j) \quad (10.44)$$

Defining \mathbf{e}_j as the state vector error at time t_j ,

$$\mathbf{e}_j = \mathbf{X}_j - \tilde{\mathbf{X}}_j \quad (10.45)$$

and noting Eqs. (10.41) and (10.44) leads to an equation for \mathbf{e} ,

$$\mathbf{e}_{j+1} = \mathbf{A}_e\mathbf{e}_j + \mathbf{C}_3\mathbf{P}_j - \mathbf{K}_e\mathbf{V}_j \quad j = 0, 1, 2, \dots \quad (10.46)$$

where

$$\mathbf{A}_e = \mathbf{C}_1 - \mathbf{K}_e\mathbf{C} \quad (10.47)$$

For stability, the largest magnitude of the eigenvalues of \mathbf{A}_e must be less than 1.

Proceeding as for the continuous formulation, the forcing terms are taken as scaled delta functions,

$$\begin{aligned} \mathbf{P}_j &= \mathbf{P}_0\delta(j) \\ \mathbf{V}_j &= \mathbf{V}_0\delta(j) \\ \delta(j) &= 0 \quad \text{for} \quad j \neq 0 \\ \delta(j) &= 1 \quad \text{for} \quad j = 0 \end{aligned} \quad (10.48)$$

The corresponding solution is

$$\begin{aligned} \mathbf{e}_0 &= \mathbf{C}_3 \mathbf{P}_0 - \mathbf{K}_e \mathbf{V}_0 \\ \mathbf{e}_j &= \mathbf{A}_e^j \mathbf{e}_0 \quad j = 1, 2, \dots \end{aligned} \quad (10.49)$$

Forming the weighted sum,

$$\mathbf{J} = \frac{1}{2} \sum_{j=0}^{\infty} \mathbf{e}_j^T \cdot \mathbf{e}_j \quad (10.50)$$

and noting that $\mathbf{A}_e^j \rightarrow \mathbf{0}$ as $j \rightarrow \infty$ results in

$$\mathbf{J} = \frac{1}{2} \mathbf{H} \quad (10.51)$$

where

$$\mathbf{H} - \mathbf{A}_e \mathbf{H} \mathbf{A}_e^T = \mathbf{C}_3 \mathbf{P}_0 \mathbf{P}_0^T \mathbf{C}_3^T + \mathbf{K}_e \mathbf{V}_0 \mathbf{V}_0^T \mathbf{K}_e^T \quad (10.52)$$

Lastly, requiring \mathbf{J} to be stationary with respect to \mathbf{K}_e , we obtain the following equations for \mathbf{H} and \mathbf{K}_e :

$$\mathbf{K}_e = \mathbf{C}_1 \mathbf{H} \mathbf{C}^T (\mathbf{C} \mathbf{H} \mathbf{C}^T + \mathbf{V}_0 \mathbf{V}_0^T)^{-1} \quad (10.53)$$

$$\mathbf{H} - \mathbf{C}_1 \mathbf{H} \mathbf{C}_1^T + \mathbf{C}_1 \mathbf{H} \mathbf{C}^T (\mathbf{C} \mathbf{H} \mathbf{C}^T + \mathbf{V}_0 \mathbf{V}_0^T)^{-1} = \mathbf{C}_3 \mathbf{P}_0 \mathbf{P}_0^T \mathbf{C}_3^T \quad (10.54)$$

The corresponding discrete LQR equations are Eqs. (9.49) and (9.50). The coefficients are related as shown in Table 10.2.

Table 10.2

Discrete LQR	Discrete Observer
\mathbf{C}_1	\mathbf{C}_1^T
\mathbf{C}_2	\mathbf{C}_2^T
\mathbf{H}	\mathbf{H}
\mathbf{Q}	$\mathbf{C}_3 \mathbf{P}_0 \mathbf{P}_0^T \mathbf{C}_3^T$
\mathbf{R}	$\mathbf{V}_0 \mathbf{V}_0^T$
\mathbf{K}_f	\mathbf{K}_e^T

Noting the correspondence between the coefficient matrices, we can obtain \mathbf{K}_e and the eigenvalues of \mathbf{A}_e with the MATLAB function `dare`. The procedure is similar to that followed for the case of feedback where the magnitudes of \mathbf{Q} and \mathbf{R} were adjusted to reflect the priority. Increasing \mathbf{R} placed more emphasis on the magnitude of the feedback force and resulted in a decrease in \mathbf{K}_f . Increasing \mathbf{Q} placed the emphasis on this state vector, and \mathbf{K}_f increased. Here, $\mathbf{V}_0 \mathbf{V}_0^T$ plays the role of \mathbf{R} and $\mathbf{P}_0 \mathbf{P}_0^T$ corresponds to \mathbf{Q} . Increasing \mathbf{P}_0 places more emphasis on reducing the state vector error due to the external forcing applied to the plant model (i.e., the structure), and \mathbf{K}_e will increase accordingly. Noting Eq. (10.46), the measurement noise is amplified by \mathbf{K}_e and, therefore, increasing \mathbf{V}_0 produces a decrease in \mathbf{K}_e . Just as for the choice of the feedback matrix, \mathbf{K}_f , the selection of an appropriate \mathbf{K}_e is arrived at through numerical simulation using `dare` to generate the eigenvalues of \mathbf{A}_e .

Once \mathbf{K}_e is established, one solves simultaneously the 2 sets of coupled equations, the original equation associated with the physical system (Eq. (10.21)), and the corrective equation, Eq. (10.25), associated with the observer. For large systems, this additional computation cost may be excessive, and one should consider using a modal expansion approach.

10.5 Input-Output Relations: H_2 and H_∞ Control

We can interpret the problem of designing a control system as an optimization problem where we establish optimal values for system variables so as to limit the response generated by a particular loading to a specified level. For the earthquake problem, the objective is to limit the interstory drift produced by the design earthquake, a scaled version of a reference earthquake. Given a physical system, a computational model can be constructed and used to establish the relationship between the input loading and the resulting displacement response. Perturbing the system parameters provides information about the sensitivity of the response that is needed for the optimization process.

In what follows, the solution for the SDOF system is revisited and interpreted from the input-output perspective. Some background material on Fourier transforms is introduced in order to extend the analysis from the time domain to the frequency domain. Quantitative measures, called norms, are defined for functions and used to characterize the input-output relationship in terms of the norms for the input, output, and transfer function. This characterization reduces the control system design problem to selecting parameters such that the norm of the transfer function is equal to a prescribed value. In a later section, the analysis is extended to MDOF systems that involve norms of matrices and complex transfer matrices.

10.5.1 SDOF Input-Output Relations

The governing equation for a time-invariant SDOF system is given by:

$$m\ddot{u} + c\dot{u} + ku = p \quad (10.55)$$

where m , c , k are system properties which are considered constant in this discussion. Noting Eq. (8.20), the free vibration response is

$$u(t) = e^{-\xi\omega t}(C_1 \cos \omega'_n t - C_2 \sin \omega'_n t) \quad (10.56)$$

where

$$\omega^2 = \frac{k}{m} \quad \omega' = (1 - \xi^2)^{1/2}\omega \quad \xi = \frac{c}{2\omega m}$$

For small damping ratio, $\omega' \approx \omega$. A general expression for the forced vibration response follows from Eq. (8.29):

$$u(t) = \int_0^t h(t - \tau)p(\tau)d\tau \quad (10.57)$$

where $h(t)$ is the free vibration response due to a unit impulse at $t = 0$. Starting with a system at rest for $t < 0$, applying

$$p(t) = \delta(t) \quad (10.58)$$

at $t = 0$ produces the initial conditions for $t = 0^+$,

$$\begin{aligned} u(0^+) &= 0 \\ \dot{u}(0^+) &= \frac{1}{m} \end{aligned} \quad (10.59)$$

Finally, specializing the free vibration response for these conditions results in

$$u(t) \equiv h(t) = \frac{1}{m\omega'} e^{-\xi\omega t} \sin \omega' t \quad t > 0^+ \quad (10.60)$$

10.5. INPUT-OUTPUT RELATIONS: H_2 AND H_∞ CONTROL

We can interpret Eq. (10.57) as the response generated by applying a set of scaled impulses over the time interval $0 < \tau < t$. The impulse function $h(t)$ characterizes the system response to loading and is uniquely defined by the system parameters (m, ω, ξ) or, equivalently, (m, k, c) .

Given $p(t)$, we obtain $u(t)$ by integrating Eq. (10.57). Analytical solutions are possible for simple loading functions. For earthquake loading, $p = -ma_g(t)$, and numerical integration is required since p is defined as a discrete time series. This process was followed to generate response spectra for earthquakes in Chapter 2.

A quasi-algebraic relationship between p and u can be obtained by expressing these variables in terms of their Fourier transforms. The Fourier transform of $y(t)$ is denoted as $\bar{y}(\Omega)$ and defined as

$$\bar{y}(\Omega) = \int_{-\infty}^{\infty} e^{-i\Omega t} y(t) dt \quad (10.61)$$

This definition reduces to

$$\bar{y}(\Omega) = \int_0^{\infty} e^{-i\Omega t} y(t) dt \quad (10.62)$$

when $y(t)$ is a causal function (i.e., when $y = 0$ for $t < 0$). The inverse Fourier transform is determined with

$$y(t) = \frac{1}{2\pi} \int_{-\infty}^{\infty} e^{i\Omega t} \bar{y}(\Omega) d\Omega \quad (10.63)$$

Noting Eq. (10.63), the response $u(t)$ is expressed as

$$u(t) = \frac{1}{2\pi} \int_{-\infty}^{\infty} e^{i\Omega t} \bar{u}(\Omega) d\Omega \quad (10.64)$$

The derivatives with respect to time are

$$\begin{aligned} \dot{u}(t) &= i\Omega u(t) \\ \ddot{u}(t) &= (i\Omega)^2 u(t) \end{aligned} \quad (10.65)$$

Substituting in the governing equation and combining terms leads to an algebraic equation relating the transforms of u and p ,

$$\frac{1}{2\pi} \int_{-\infty}^{\infty} e^{i\Omega t} (-m\Omega^2 + i\Omega c + k) \bar{u}(\Omega) d\Omega = \frac{1}{2\pi} \int_{-\infty}^{\infty} e^{i\Omega t} \bar{p}(\Omega) d\Omega \quad (10.66)$$

Finally, equating the integrands, we obtain

$$\bar{u}(\Omega) = \frac{\bar{p}(\Omega)}{k - \Omega^2 m + i\Omega c} \equiv \bar{h}(\Omega) \bar{p}(\Omega) \quad -\infty \leq \Omega \leq \infty \quad (10.67)$$

Eq. (10.67) is a relationship between the input and output Fourier transforms. The complex function, $\bar{h}(\Omega)$, is called the transfer function for the system. We can show that $\bar{h}(\Omega)$ is the Fourier transform of the impulse function $h(t)$ defined by Eq. (10.60). Expressing the complex terms in polar form,

$$\begin{aligned} \bar{u}(\Omega) &= |\bar{u}(\Omega)| e^{i\delta} \\ \bar{p}(\Omega) &= |\bar{p}(\Omega)| e^{i\alpha} \\ \bar{h}(\Omega) &= |\bar{h}(\Omega)| e^{i\beta} \end{aligned} \quad (10.68)$$

and substituting in Eq. (8.424) results in the following real algebraic equations:

$$\begin{aligned} |\bar{u}(\Omega)| &= |\bar{h}(\Omega)| |\bar{p}(\Omega)| \\ \delta &= \alpha + \beta \\ -\infty &\leq \Omega \leq \infty \end{aligned} \quad (10.69)$$

10.5. INPUT-OUTPUT RELATIONS: H_2 AND H_∞ CONTROL

The magnitude of $\bar{h}(\Omega)$ is a function of Ω and the system parameters,

$$|\bar{h}(\Omega)| = \left[\frac{1}{(k - \Omega^2 m)^2 + (\Omega c)^2} \right]^{1/2} = \frac{1}{k} \left[\frac{1}{\left(1 - \left(\frac{\Omega}{\omega}\right)^2\right)^2 + \left(2\xi \frac{\Omega}{\omega}\right)^2} \right]^{1/2} \quad (10.70)$$

Example 10.3 - Frequency domain solution procedure

Back in Sect. 1.4, the solution for a SDOF system subjected to periodic excitation was derived using the conventional approach. Starting with

$$p = \hat{p} \sin \Omega^* t \quad (10.71)$$

and solving the differential equation of motion leads to

$$u = \hat{u} \sin(\Omega^* t - \delta) \quad (10.72)$$

where

$$\hat{u} = \frac{\hat{p}}{k} H_1 = \hat{u}(\Omega^*)$$
$$H_1(\Omega^*) = \left[\frac{1}{\left(1 - \left(\frac{\Omega^*}{\omega}\right)^2\right)^2 + \left(2\xi \frac{\Omega^*}{\omega}\right)^2} \right]^{1/2} \quad (10.73)$$

Comparing Eq. (10.73) with Eq. (10.69) specialized for $\Omega = \Omega^*$ shows that the solution for a single periodic excitation is derived from the general solution by considering $\bar{p}(\Omega)$ to be a scaled delta function at $\Omega = \Omega^*$.

CHAPTER 10. ADVANCED CONTROL THEORY

Assuming the Fourier transform of the loading is

$$\bar{p}(\Omega) = \hat{p}\delta(\Omega - \Omega^*) \quad (10.74)$$

reduces the range of Ω to just $\Omega = \Omega^*$. Then Eq. (10.69) becomes

$$|\bar{u}(\Omega^*)| = |\bar{h}(\Omega^*)|\hat{p} \quad (10.75)$$

and it follows that

$$\begin{aligned} \frac{1}{k}H_1(\Omega^*) &= |\bar{h}(\Omega^*)| \\ \hat{u}(\Omega^*) &= |\bar{u}(\Omega^*)| \end{aligned} \quad (10.76)$$

Note that (10.74) corresponds to a single periodic excitation,

$$p(t) = \hat{p}e^{i\Omega^*t} \quad (10.77)$$

Using Fourier transforms is a more general approach; however, using Eq. (10.77) as a starting point is more convenient.

Given $|\bar{h}(\Omega)|$, we can evaluate $u(t)$ by forming the product of $|\bar{h}(\Omega)|$ with the transform of the loading $|\bar{p}(\Omega)|$ and then converting from the frequency (Ω) domain to the time domain with Eq. (10.64). Plotting $|\bar{h}(\Omega)|$ versus Ω provides information about the amplification corresponding to different excitation frequencies. The plot is shown in Fig. 10.2. The critical frequency range is in the neighborhood of $\Omega = \omega$, the natural frequency for the system.

10.5. INPUT-OUTPUT RELATIONS: H_2 AND H_∞ CONTROL

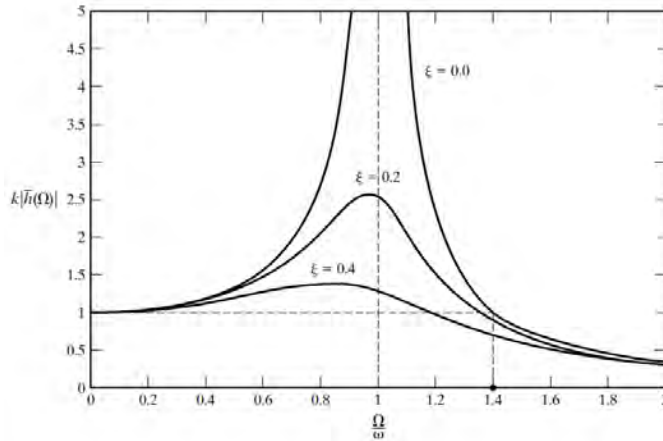


Figure 10.2: Plot of $k|\bar{h}(\Omega)|$ versus $\frac{\Omega}{\omega}$.

10.5.2 Norm of Functions

The previous section dealt with the question of what is the response produced by specific input. Given the time history of the excitation, we can obtain the time history of the response using the convolution integral. Alternatively, we can first work in the frequency domain and then transform back to the time domain. In either case, we are working with functions, and there is a need to introduce measures, called norms, that relate to the magnitude of a function and allow for a convenient interpretation of the input-output relationship.

Consider a complex function, $u(t)$, defined over the interval $-\infty \leq t \leq \infty$. The 1-norm is defined as the integral of the magnitude of $u(t)$ and denoted as $\|u\|_1$.

$$\|u\|_1 = \int_{-\infty}^{\infty} |u(t)| dt \quad (10.78)$$

The 2-norm is the square root of the integral of the square of the magnitude

$$\|u\|_2 = \left\{ \int_{-\infty}^{\infty} |u(t)|^2 dt \right\}^{1/2} \quad (10.79)$$

Generalizing, the p -norm is defined as

$$\|u\|_p = \left\{ \int_{-\infty}^{\infty} |u(t)|^p dt \right\}^{1/p} \quad (10.80)$$

Taking p to ∞ in Eq. (10.80), the integrand becomes the least upper bound of the absolute value,

$$\|u\|_{\infty} = \max \text{ all } t \text{ of } |u(t)| \quad (10.81)$$

Engineering design criteria are generally expressed in terms of the ∞ -norm (e.g., peak interstory drift, peak stress, peak acceleration). The 2-norm, when averaged over a time interval, becomes the root mean square (RMS) value, which is related to energy.

Similar norm definitions are introduced for the transform of $u(t)$. The norm is the peak value of the magnitude of $\bar{u}(\Omega)$:

$$\|\bar{u}(\Omega)\|_{\infty} = \max \text{ all } \Omega \text{ of } |\bar{u}(\Omega)| \quad (10.82)$$

Similarly, the 2-norm is defined as

$$\|\bar{u}(\Omega)\|_2 = \left\{ \frac{1}{2\pi} \int_{-\infty}^{\infty} |\bar{u}(\Omega)|^2 dt \right\}^{1/2} \quad (10.83)$$

With this definition, the 2-norms for the time and frequency domains are related by

$$\|u(t)\|_2 \equiv \|\bar{u}(\Omega)\|_2 \quad (10.84)$$

This result is known as Parseval's theorem and is useful for switching between the time domain and the frequency domain.

10.5.3 Input-Output Relationships Revisited

Eq. 10.57 expresses $u(t)$ as a convolution integral of $h(t)$ and $p(t)$. An expression in terms of ∞ norms is obtained by shifting to absolute values,

$$|u(t)| \leq \int_0^t |h(t-\tau)| |p(\tau)| d\tau \quad (10.85)$$

and taking $|p(\tau)| = \|p(t)\|_\infty$,

$$|u(t)| \leq \left\{ \int_0^t |h(t-\tau)| d\tau \right\} \|p\|_\infty \quad (10.86)$$

Letting t approach ∞ , the integral becomes the 1-norm for the transfer function and it follows that

$$\|u(t)\|_\infty \leq \|h(t)\|_1 \|p(t)\|_\infty \quad (10.87)$$

We can interpret the 1-norm for the transfer function as an upper bound for the amplification factor for the system. Given the peak value of the input, an upper bound estimate of the peak response value can be determined with Eq. (10.87).

A relationship between the 2-norms is derived using Eq. (10.67) and Parseval's theorem. The steps are

$$\begin{aligned} (\|u(t)\|_2)^2 &= (\|\bar{u}(\Omega)\|_2)^2 = \frac{1}{2\pi} \int_{-\infty}^{\infty} |\bar{h}(\Omega)|^2 |\bar{p}(\Omega)|^2 d\Omega \\ &\leq \{ \|\bar{h}(\Omega)\|_\infty \}^2 \left\{ \frac{1}{2\pi} \int_{-\infty}^{\infty} |\bar{p}(\Omega)|^2 d\Omega \right\} \end{aligned} \quad (10.88)$$

Then

$$\|u(t)\|_2 \leq \|\bar{h}(\Omega)\|_\infty \|p(t)\|_2 \quad (10.89)$$

CHAPTER 10. ADVANCED CONTROL THEORY

The ∞ -norm for is an upper bound on the gain for the 2-norm of the response.

Another relationship of interest is the 2-norm input - ∞ -norm output combination. This relation is derived by applying the Cauchy-Schwartz inequality to the convolution integral, Eq. (10.57), and has the following form [27]:

$$\|u(t)\|_{\infty} \leq \|h(t)\|_2 \|p(t)\|_2 \quad (10.90)$$

Table 10.3 summarizes the gains corresponding to the various norms. For a more rigorous derivation, see [27]. Application of this analysis to typical loadings is illustrated with the following examples

Table 10.3: System Gains

	$\ p(t)\ _{\infty}$	$\ p(t)\ _2$
$\ u(t)\ _{\infty}$	$\ h(t)\ _1$	$\ h(t)\ _2$
$\ u(t)\ _2$	∞	$\ \bar{h}(\Omega)\ _{\infty}$

Example 10.4 - Periodic excitation

Suppose the excitation is sinusoidal with frequency Ω^*

$$p = \hat{p} \sin \Omega^* t \quad (10.91)$$

The response is

$$u = \hat{u} \sin(\Omega^* t - \delta) \quad (10.92)$$

where

$$\hat{u} = |\bar{h}(\Omega^*)| \hat{p} \quad (10.93)$$

10.5. INPUT-OUTPUT RELATIONS: H_2 AND H_∞ CONTROL

$$|\bar{h}(\Omega^*)| = \left\{ \frac{1}{(k - \Omega^{*2}m) + (\Omega^*c)^2} \right\}^{1/2} \quad (10.94)$$

The input and output norms are

$$\begin{aligned} \|u(t)\|_\infty &= \hat{u} \\ \|p(t)\|_\infty &= \hat{p} \end{aligned} \quad (10.95)$$

According to Eq. (10.93), the system gain is the magnitude of the complex transfer function evaluated at the excitation frequency:

$$\text{Gain} = |\bar{h}(\Omega)| \quad (\Omega = \Omega^*) \quad (10.96)$$

Note that an upper bound for the gain is the peak value of $|\bar{h}(\Omega)|$:

$$\text{Maximum gain} = |\bar{h}(\Omega)|_\infty \quad (10.97)$$

Example 10.5 - Impulsive loading

Suppose the loading is a scaled delta function applied at $t = 0$:

$$p(t) = \delta(t)p^* \quad (10.98)$$

The corresponding solution is the impulse function,

$$\begin{aligned} u(t) &= p^* h(t) \\ h(t) &= \frac{1}{m\omega} e^{-\xi\omega t} \sin \omega t \end{aligned} \quad (10.99)$$

The Fourier transforms are

$$\begin{aligned}\bar{p}(\Omega) &= p^* \\ \bar{u}(\Omega) &= p^* \bar{h}(\Omega)\end{aligned}\tag{10.100}$$

Finally, the norms are related by

$$\begin{aligned}\|u(t)\|_\infty &= p^* \|h(t)\|_\infty \\ \|u(t)\|_2 &= p^* \|h(t)\|_2\end{aligned}\tag{10.101}$$

Example 10.6 - Seismic excitation

For seismic excitation, the input function is $p = -ma_g(t)$. The corresponding impulse function and convolution integral are

$$h(t) = \frac{-1}{\omega'} e^{-\xi\omega t} \sin \omega' t\tag{10.102}$$

$$u(t) = \int_0^t h(t - \tau) a_g(\tau) d\tau\tag{10.103}$$

Eq. (10.103) is evaluated for a particular earthquake using numerical integration. The conventional way of representing the results is to plot peak response values, such as u_{\max} and \dot{u}_{\max} as a function of period for a range of damping ratios. Introducing norm terminology, the maximum displacement is the ∞ -norm of the response.

$$S_d \equiv |u(t)|_{\max} \equiv \|u(t)\|_\infty\tag{10.104}$$

Also, the peak ground acceleration is the ∞ -norm of the input.

$$|a_g(t)|_{\max} \equiv \|a_g(t)\|_\infty\tag{10.105}$$

Then, noting Table 10.3, these norms are related by

$$S_d \leq \|h(t)\|_1 \|a_g(t)\|_\infty \quad (10.106)$$

The ratio of S_d to peak ground acceleration,

$$\frac{S_d}{\|a_g\|_\infty} \leq \|h(t)\|_1 \quad (10.107)$$

can be interpreted as a lower bound estimate for the 1 norm of the transfer function. It follows that the spectral displacement response spectrum generated with earthquakes scaled such that their peak acceleration magnitudes are equal to unity is actually the spectrum for the $\infty - \infty$ system gain. This finding provides the theoretical basis for motion based seismic design for SDOF systems.

Given an ensemble of representative scaled earthquakes, we can generate spectral displacement spectra for a specific damping ratio and apply an averaging process to construct a design spectrum for the system gain. The remaining steps are the same as followed in Chapter 3. We specify the allowable displacement, damping, and peak acceleration and determine the required system gain using Eq. (10.107). Fig. 10.3 shows a plot of displacement spectra for three earthquakes scaled to 1 m/s² peak acceleration. According to Eq. (10.107), these plots can also be interpreted as plots of $\|h(t)\|_1$ for the different earthquakes. The difference between curves is due to the difference in the frequency content of the accelerograms.

CHAPTER 10. ADVANCED CONTROL THEORY

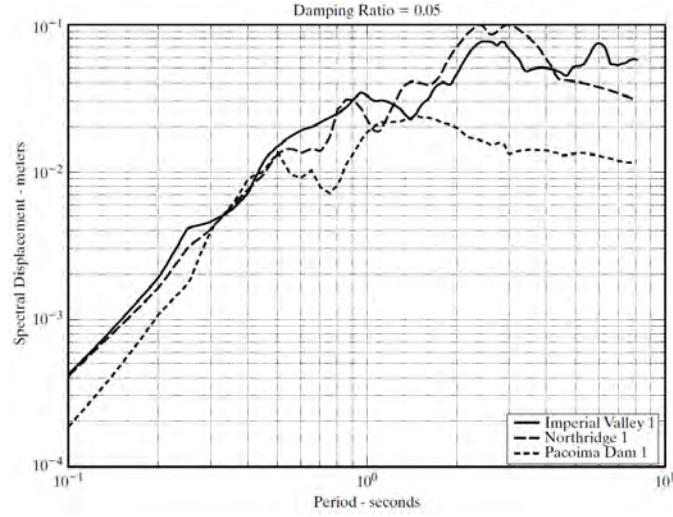


Figure 10.3: Plot of $\|h(t)\|_1$.

Example 10.7 - Estimate for $\|h(t)\|_1$, assuming $\xi^2 \ll 1$

The unit impulse response for a SDOF system simplifies to

$$h(t) = \frac{1}{m\omega} e^{-\xi\omega t} \sin \omega t \quad (10.108)$$

Substituting into the definition equation for the 1-norm,

$$\|h(t)\|_1 = \int_0^\infty |h(t)| dt \quad (10.109)$$

and integrating between $0 - \frac{\pi}{\omega}$, $\frac{\pi}{\omega} - \frac{2\pi}{\omega}$, ..., to allow for the oscillation in sign, results in the following expression:

$$\|h(t)\|_1 = \int_0^\infty |h(t)| dt = \frac{1}{m\omega^2(1 + \xi^2)} \frac{1 + e^{-\xi\pi}}{1 - e^{-\xi\pi}} \quad (10.110)$$

When $\xi = 0$, the norm is infinite. This analytical result can be used to estimate the $\infty - \infty$ gain defined by

10.5. INPUT-OUTPUT RELATIONS: H_2 AND H_∞ CONTROL

$$\|u(t)\|_\infty \leq \|h(t)\|_1 \|p(t)\|_\infty \quad (10.111)$$

Applying Eq. (10.111) for seismic excitation,

$$\begin{aligned} \|p(t)\|_\infty &= m \|a_g(t)\|_\infty \\ \|u(t)\|_\infty &\equiv S_d \end{aligned} \quad (10.112)$$

yields

$$S_d \leq \left[\frac{1}{m\omega^2(1+\xi^2)} \frac{1+e^{-\xi\pi}}{1-e^{-\xi\pi}} \right] \|a_g(t)\|_\infty \quad (10.113)$$

A similar expression can be obtained for an upper bound on the spectral velocity

$$S_v = \omega S_d \leq \left[\frac{1}{m\omega(1+\xi^2)} \frac{1+e^{-\xi\pi}}{1-e^{-\xi\pi}} \right] \|a_g(t)\|_\infty \quad (10.114)$$

Fig. 10.3 of Ex. 10.6 shows typical plots of scaled for $\|a_g(t)\|_\infty = 1$. For large T , S_d approaches a limiting value which is essentially equal to the ground displacement. Noting that $\omega = 2\pi/T$, Eq. (10.113) predicts that S_D varies as T squared. The reason for the difference can be attributed to the way in which the $\infty - \infty$ gain was derived.

Referring back to Eq. (10.85), the loading term was assumed to be constant and equal to the peak loading magnitude. This assumption is too conservative for earthquake excitation which i) is of limited duration and ii) the time history of the absolute value of the acceleration is not constant. Fig. 10.4 shows the ground acceleration time history for the El Centro earthquake. The typical duration of the earthquake signal is in the range of

CHAPTER 10. ADVANCED CONTROL THEORY

3040 seconds. For El Centro, the acceleration magnitude peaks at about 3 seconds and then decays in essentially an exponential manner. Other earthquakes peak later (e.g., Taft) and also may persist longer (e.g., Mexico City). Clearly, there is a limited time window for the excitation.

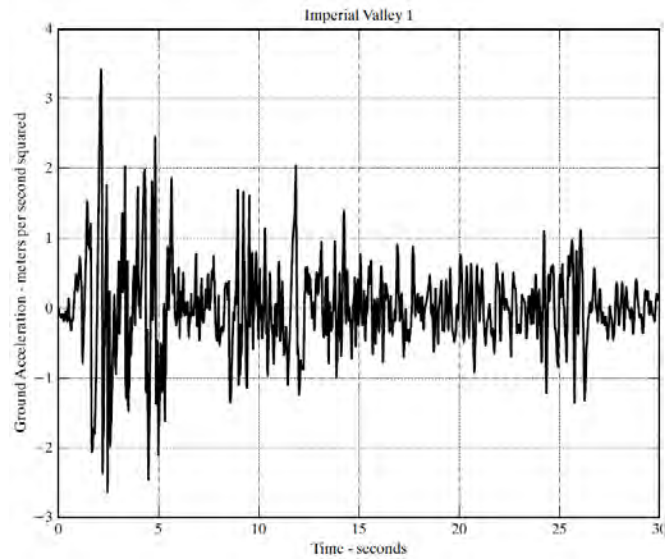


Figure 10.4: Imperial Valley Accelerogram.

Another factor which controls the response is the exponential decay nature of the impulse function defined by equation (10.108). The exponential term is essentially zero for $t > 3/3\omega = 3T/2\pi\xi$. Denoting the excitation time window as T_e and the response duration as T_d , the system response is negligible for $t > T_e + T_d$.

10.5.4 MDOF Input-Output Relations

The starting point for this discussion is the continuous state space formulation with negative linear feedback presented in Sect. 8.4. For convenience, the relevant equations are listed below.

$$\dot{\mathbf{X}} = \mathbf{A}\mathbf{X} + \mathbf{B}_f\mathbf{F} + \mathbf{B}_g a_g + \mathbf{B}_p\mathbf{P} \quad (10.115)$$

$$\mathbf{F} = -\mathbf{K}_f\mathbf{X} = - \begin{bmatrix} \mathbf{k}_d & \mathbf{k}_v \end{bmatrix} \begin{bmatrix} U \\ \dot{U} \end{bmatrix} \quad (10.116)$$

$$\mathbf{A} = \begin{bmatrix} \mathbf{0} & \mathbf{I} \\ -\mathbf{M}^{-1}\mathbf{K} & -\mathbf{M}^{-1}\mathbf{C} \end{bmatrix} \quad (10.117)$$

$$\mathbf{B}_f = \begin{bmatrix} \mathbf{0} \\ \mathbf{M}^{-1}\mathbf{E}_f \end{bmatrix} \quad \mathbf{B}_g = \begin{bmatrix} \mathbf{0} \\ -\mathbf{E} \end{bmatrix} \quad \mathbf{B}_p = \begin{bmatrix} \mathbf{0} \\ \mathbf{M}^{-1} \end{bmatrix} \quad (10.118)$$

Substituting for \mathbf{F} , and combining terms, the governing equation takes the following form:

$$\dot{\mathbf{X}} = \mathbf{A}_c\mathbf{X} + \mathbf{B}_p\mathbf{P} + \mathbf{B}_g a_g \quad (10.119)$$

where

$$\mathbf{A}_c = \mathbf{A} - \mathbf{B}_f\mathbf{K}_f = \begin{bmatrix} \mathbf{0} & \mathbf{I} \\ -\mathbf{M}^{-1}\mathbf{K}_{\text{eff}} & -\mathbf{M}^{-1}\mathbf{C}_{\text{eff}} \end{bmatrix} \quad (10.120)$$

and

$$\begin{aligned} \mathbf{K}_{\text{eff}} &= \mathbf{K} + \mathbf{E}_f\mathbf{k}_d \\ \mathbf{C}_{\text{eff}} &= \mathbf{C} + \mathbf{E}_f\mathbf{k}_v \end{aligned} \quad (10.121)$$

are the effective stiffness and damping matrices due to feedback.

There are two forcing terms, one due to external nodal forces and the other due to ground motion. In what follows, we consider here only the ground motion term. The corresponding state vector is determined by

$$\dot{\mathbf{X}} = \mathbf{A}_c \mathbf{X} + \mathbf{B}_g a_g \quad (10.122)$$

The output variables are considered to be a reduced subset, of order m , of the state variables. For example, the inter-story displacements are the response measures of primary interest for seismic excitation. They are generated by computing the difference between adjacent nodal displacements. Defining \mathbf{Y} as the output vector, the relationship is expressed as

$$\mathbf{Y} = \mathbf{C} \mathbf{X} \quad (10.123)$$

where \mathbf{Y} is of order $m \times 2n$. When \mathbf{Y} is taken as all of the inter-story displacements, $m = n$, and \mathbf{C} has the following form

$$\mathbf{C} = [\mathbf{C}_1 \quad \mathbf{0}] \quad (10.124)$$

where \mathbf{C}_1 is a first order backward difference matrix

$$\mathbf{C}_1 = \begin{bmatrix} 1 & 0 & 0 & \cdots \\ -1 & 1 & 0 & \cdots \\ 0 & -1 & 1 & \cdots \\ \cdots & \cdots & \cdots & \cdots \end{bmatrix} \quad (10.125)$$

Pre-multiplying by \mathbf{C} extracts the nodal displacement terms from \mathbf{X} and carries out the differencing.

The free vibration solution for \mathbf{X} is

$$\mathbf{X} = \mathbf{e}^{\mathbf{A}_c t} \mathbf{X}_0 \quad (10.126)$$

Taking $a_g(t)$ to be a delta function centered at $t = 0$,

$$a_g(t) = \delta(t) \quad (10.127)$$

produces the initial conditions,

10.5. INPUT-OUTPUT RELATIONS: H_2 AND H_∞ CONTROL

$$\mathbf{X}_0 = \mathbf{B}_g \quad (10.128)$$

Lastly, the corresponding unit impulse output vector is

$$\mathbf{Y}(t) = \mathbf{C}e^{\mathbf{A}_c t} \mathbf{B}_g \equiv \mathbf{H}_g(t) \quad t > 0 \quad (10.129)$$

Using this result, the output vector due to $a_g(t)$ is determined with

$$\mathbf{Y}(t)|_{\text{ground motion}} = \int_0^t \mathbf{H}_g(t - \tau) a_g(\tau) d\tau \quad (10.130)$$

Eq. (10.130) is used to establish an estimate for the $\infty - \infty$ gain of the system.

The frequency domain approach starts with the expression for the Fourier transform expansion of $\mathbf{X}(t)$

$$\mathbf{X}(t) = \frac{1}{2\pi} \int_{-\infty}^{\infty} \bar{\mathbf{X}}(\Omega) e^{i\Omega t} d\Omega \quad (10.131)$$

Substituting in Eq. (10.122)

$$(i\Omega \mathbf{I} - \mathbf{A}_c) \bar{\mathbf{X}} = \mathbf{B}_g \bar{a}_g \quad (10.132)$$

then solving for $\bar{\mathbf{X}}$ and noting Eq. (10.123) leads to a relation between the Fourier transform for \mathbf{Y} and a_g ,

$$\bar{\mathbf{Y}} = \bar{H}_g \bar{a}_g \quad (10.133)$$

where

$$\bar{H}_g(\Omega) = \mathbf{C} (i\Omega \mathbf{I} - \mathbf{A}_c)^{-1} \mathbf{B}_g \quad (10.134)$$

is the Fourier Transform of $\mathbf{H}_g(t)$. The partitioned form of $\bar{\mathbf{H}}_g$ follows by substituting for \mathbf{A}_c and \mathbf{B}_g .

$$\bar{\mathbf{H}}_g = \mathbf{C} \begin{Bmatrix} -\mathbf{G}_1 \mathbf{E} \\ -\mathbf{G}_2 \mathbf{E} \end{Bmatrix} \quad (10.135)$$

where

$$\begin{aligned} \mathbf{G}_1 &= (\mathbf{M}^{-1} \mathbf{K}_{\text{eff}} - \Omega^2 \mathbf{I} + i\Omega \mathbf{M}^{-1} \mathbf{C}_{\text{eff}})^{-1} \\ \mathbf{G}_2 &= i\Omega \mathbf{G}_1 \end{aligned} \quad (10.136)$$

The ∞ -norm of $\bar{\mathbf{H}}_g(\Omega)$ provides an estimate of the 2-2 gain for a specific choice of the system parameters (\mathbf{M} , \mathbf{K} , \mathbf{C} , \mathbf{k}_d , \mathbf{k}_v , \mathbf{E}_f) and output variables (\mathbf{Y}). When \mathbf{Y} is taken as inter-story displacements, $\bar{\mathbf{H}}_g$ reduces to an n^{th} order vector,

$$\bar{\mathbf{H}}_g = \mathbf{C}_1 \mathbf{G}_1 \mathbf{E} \quad (10.137)$$

10.6 Introduction to Nonlinear Control

In this section, we introduce the topic of nonlinear control. Nonlinear controllers are particularly useful for designing control strategies for structures equipped with semi-active or hybrid control systems due to the inherent nonlinearities introduced by these devices. Consider the equation of motion of a linear time-invariant system:

$$m\ddot{u} + c\dot{u} + ku = -ma_g + p + F \quad (10.138)$$

In linear control, the control force F is taken as a linear combination of the state variables $F = f(u, \dot{u})$. In nonlinear control, the function f is allowed to be nonlinear. For instance, take a SDOF system equipped with a variable friction damper. Modifying Eq. 7.27, we write F as:

$$\begin{aligned} F &= \mu N(t) \cdot \text{sign}(\dot{u}) \\ &= f(\dot{u}, t) \end{aligned} \tag{10.139}$$

where μ is the friction coefficient, and N is the normal force that can be varied as a function of time t . Eq. (10.139) is nonlinear because of the introduction of the signum function.

10.6.1 Lyapunov Stability Theory

Consider a physical system in equilibrium under a set of external forces. According to Lyapunov, one establishes the stability of the equilibrium position, i.e, whether it is stable, neutral, or unstable, by introducing a small perturbation to the system, and determining if the resulting motion decreases, remains constant, or increases with time. The perturbed equilibrium equations are linear in the perturbed displacement, and homogeneous, since the forces are considered to be constant during the perturbation.

For example, starting with the state equilibrium equation:

$$\dot{\mathbf{X}} = \mathbf{A}\mathbf{X} + \mathbf{B}_j\mathbf{P} \tag{10.140}$$

one introduces the perturbation,

$$\tilde{\mathbf{X}} = \mathbf{X} + \delta\mathbf{X} \tag{10.141}$$

in Eq. (10.140). This step leads to the perturbed equation:

$$\delta\dot{\mathbf{X}} = \mathbf{A}\delta\mathbf{X} \tag{10.142}$$

and the corresponding solution

$$\delta\mathbf{X} = e^{\lambda t}\Psi \tag{10.143}$$

where λ, Ψ satisfy

$$(\mathbf{A} - \lambda\mathbf{I})\Psi = \mathbf{0} \quad (10.144)$$

According to Lyapunov, the state defined by \mathbf{X} is classified as:

Stable	$\lambda_R < 0$	(10.145)
Neutral	$\lambda_R = 0$	
Unstable	$\lambda_R > 0$	

We have shown earlier that $\lambda_R < 0$ when the system has positive damping.

Lyapunov's stability criteria can also be expressed in terms of a function which involves state variables that are related to energy terms such as kinetic and strain energy. Suppose $V(t)$ is such a function. Requiring

$$\begin{aligned} V(t) &> 0 \\ \dot{V}(t) &< 0 \end{aligned} \quad (10.146)$$

is equivalent to requiring

$$V(t) \rightarrow 0 \quad \text{as} \quad t \rightarrow \infty \quad (10.147)$$

Since V involves state variables (in this case, the perturbed variables), Eq. (10.146) implies that the perturbed system returns to its initial equilibrium position, i.e., that the initial position is stable. Functions having these properties are called Lyapunov functions.

We illustrate this approach with a SDOF example. The governing equation for the perturbed position is

$$m\ddot{u} + ku = F_d \quad (10.148)$$

where F_d is an internal force associated with energy dissipation. We take V as the total energy,

$$V = \frac{1}{2}m\dot{u}^2 + \frac{1}{2}ku^2 \quad (10.149)$$

and require $\dot{V} < 0$. This leads to

$$\dot{u}(m\ddot{u} + ku) < 0 \quad (10.150)$$

Nothing Eq. (10.148), Eq. (10.150) becomes

$$\dot{u}F_d < 0 \quad (10.151)$$

Eq. (10.151) represents a constraint on F_d for stability. Various cases are:

i) Viscous damping:

$$F_d = -c\dot{u} \quad c > 0$$

ii) Coulomb friction:

$$F_d = -f \operatorname{sgn}(\dot{u}) = -f \frac{\dot{u}}{|\dot{u}|}$$

We see that linear viscous damping and Coulomb friction *never* destabilize the system.

A similar strategy applies for a MDOF system. Taking V as

$$V = \frac{1}{2}\mathbf{X}^T\mathbf{P}\mathbf{X} \quad (10.152)$$

where \mathbf{P} is a symmetric positive definite specified matrix, we form the time derivative:

$$\dot{V} = \frac{1}{2} \left(\dot{\mathbf{X}}^T \mathbf{P} \mathbf{X} + \mathbf{X}^T \mathbf{P} \dot{\mathbf{X}} \right) \quad (10.153)$$

Noting the state equilibrium equation,

$$\dot{\mathbf{X}} = \mathbf{A} \mathbf{X} + \mathbf{B}_f \mathbf{F} \quad (10.154)$$

and taking \mathbf{F} as

$$\mathbf{F} = -\mathbf{K}_f \mathbf{X} \quad (10.155)$$

Eq. (10.153) expands to

$$\dot{V} = \frac{1}{2} \left[\mathbf{X}^T (\mathbf{P} \mathbf{A} + \mathbf{A}^T \mathbf{P}) \mathbf{X} - \mathbf{X}^T (\mathbf{K}_f^T \mathbf{B}_f^T \mathbf{P} \mathbf{B}_f \mathbf{K}_f) \mathbf{X} \right] \quad (10.156)$$

For the position to be stable, one needs $\dot{V} < 0$. The first term in Eq. (10.156) is negative definite since \mathbf{A} is negative definite. It follows that the second term must be positive definite for stability

$$\mathbf{X}^T (\mathbf{K}_f \mathbf{B}_f \mathbf{P} + \mathbf{P} \mathbf{B}_f \mathbf{K}_f) \mathbf{X} > 0 \quad (10.157)$$

Eq. (10.157) represents a constraint on \mathbf{K}_f . It can be shown that any \mathbf{K}_f with all positive elements satisfies this requirement. Based on this statement, it follows that adding positive stiffness and damping always stabilizes the system.

In the approach described above, we assumed \mathbf{P} and determined the constraint in \mathbf{K}_f . A more general approach is based on treating \mathbf{P} and \mathbf{K}_f as variables, and determining these variables by optimizing a performance measure. We followed this approach to establish the LQR algorithm in Sect. 9.2.3. The performance measure is taken as

$$J = \frac{1}{2} \int_0^T (\mathbf{X}^T \mathbf{Q} \mathbf{X} + \mathbf{F}^T \mathbf{R} \mathbf{F}) dt = \frac{1}{2} \int_0^T (\mathbf{X}^T \mathbf{Q} \mathbf{X} + \mathbf{X}^T \mathbf{K}_f^T \mathbf{R} \mathbf{K}_f \mathbf{X}) dt \quad (10.158)$$

One wants to select \mathbf{K}_f so as to minimize J . The Lyapunov function is

$$V = \frac{1}{2} \mathbf{X}^T \mathbf{P} \mathbf{X} \quad (e)$$

where \mathbf{P} is not yet defined. Forming \dot{V} and noting the equilibrium equation leads to Eq. (10.156).

$$\dot{V} = \frac{1}{2} [\mathbf{X}^T (\mathbf{P} \mathbf{A} + \mathbf{A}^T \mathbf{P}) \mathbf{X} - \mathbf{X}^T (\mathbf{K}_f^T \mathbf{B}^T \mathbf{P} + \mathbf{P} \mathbf{B} \mathbf{K}_f) \mathbf{X}] \quad (f)$$

Now, we set the integrand in Eq. (10.158) equal to \dot{V} . This term is negative definite.

$$\begin{aligned} \frac{1}{2} [\mathbf{X}^T \mathbf{Q} \mathbf{X} + \mathbf{X}^T \mathbf{K}_f^T \mathbf{R} \mathbf{K}_f \mathbf{X}] &= -\dot{V} \\ &= -\frac{1}{2} [\mathbf{X}^T (\mathbf{P} \mathbf{A} + \mathbf{A}^T \mathbf{P}) \mathbf{X} - \mathbf{X}^T (\mathbf{K}_f^T \mathbf{B}^T \mathbf{P} + \mathbf{P} \mathbf{B} \mathbf{K}_f) \mathbf{X}] \end{aligned} \quad (10.159)$$

The performance measure reduces to

$$\begin{aligned} J &= -\frac{1}{2} \int_0^T \dot{V} dt \\ &= \frac{1}{2} (-V|_T + V|_0) \\ &= \frac{1}{2} \mathbf{X}_0^T \mathbf{P} \mathbf{X}_0 \end{aligned} \quad (10.160)$$

since $\mathbf{X} \rightarrow 0$ as $t \rightarrow \infty$. Differentiating J with respect to \mathbf{K}_f leads to the desired expression for \mathbf{K}_f .

$$\frac{\delta}{\delta \mathbf{K}_f} J = 0 \Rightarrow \mathbf{K}_f = \mathbf{R}^{-1} \mathbf{B}^T \mathbf{P} \quad (10.161)$$

The equation for \mathbf{P} follows from Eq. (10.159).

$$\mathbf{P} \mathbf{A} + \mathbf{A}^T \mathbf{P} - \mathbf{P} \mathbf{B} \mathbf{R}^{-1} \mathbf{B}^T \mathbf{P} = -\mathbf{Q} \quad (10.162)$$

The stability constraint defined by Eq. (10.157) evaluated for the “optimal” stiffness has the following form,

$$\mathbf{X}^T (\mathbf{P} \mathbf{B} \mathbf{R}^{-1} \mathbf{B}^T \mathbf{P}) \mathbf{X} > 0 \quad (10.163)$$

This constraint is satisfied since the coefficient matrix is positive definite.

10.6.2 Sliding Mode Control

Sliding mode control (SMC) theory is constructed around the concept of Lyapunov stability. These controllers are widely used in structural control. See Refs. [5, 124, 39] for instance. This section introduces the concept of SMC. More details and advanced discussions can be found in Ref. [94].

Conceptually, SMC aims at directing a controlled system onto a surface of known dynamics on which the error will exponentially converge to zero. Let the tracking error e of a state x be written $e = x - x_d$ where x_d denotes the desired state ($x_d \equiv 0$ for civil structures, also termed *regulatory control*). A sliding surface s is defined as:

$$s(x, t) = \left(\frac{d}{dt} + \lambda \right)^{n-1} e \quad (10.164)$$

10.6. INTRODUCTION TO NONLINEAR CONTROL

where n is the order of the controlled system dynamics, and λ represents a control weight and is a strictly positive constant. In the case of a civil structure ($n = 2$), (10.164) becomes:

$$s = \dot{e} + \lambda e = \dot{x} + \lambda x \quad (10.165)$$

The sliding surface (Eq. (10.165)) is stable for the manifold $s = 0$, and the control law can be designed based on Lyapunov stability theory. Consider the following Lyapunov function based on the surface error s

$$\begin{aligned} V &= \frac{1}{2}s^2 \\ \dot{V} &= s\dot{s} \end{aligned} \quad (10.166)$$

applied to a controlled SDOF structure

$$m\ddot{x} + c\dot{x} + kx = u + p \quad (10.167)$$

where u is the control force and p the excitation. Note that selecting the sliding surface

$$s\dot{s} \leq -\eta|s| \quad (10.168)$$

ensures that the sliding surface will converge exponentially to 0. Using Eqs. (10.166) and (10.165):

$$\dot{V} = \frac{s}{m} (u + p - c\dot{x} - kx + \lambda\dot{x} + \lambda m\dot{x}) \quad (10.169)$$

one can select u to have the form

$$u = -p + c\dot{x} - \lambda m\dot{x} + kx - \text{sgn}(s) \quad (10.170)$$

CHAPTER 10. ADVANCED CONTROL THEORY

where sgn is the sign or signum function. Eq. (10.169) reduces to

$$\dot{V} = -\frac{|s|}{m} \quad (10.171)$$

Eq. (10.171) is negative definite since the mass m is strictly positive.

The control rule Eq. (10.172) is discontinuous because of the sgn function that provokes a change in sign when the sliding surface changes sign. Such discontinuity may cause *chattering* in the the dynamics, which results in unnecessarily high control forces and a possible excitation of the high frequencies.

An alternative is to smoothen the transition around $s = 0$. A typical strategy is to define a boundary layer ϕ within which the absolute operator in (10.168) is replaced by a saturation function sat

$$u = -p + c\dot{x} - \lambda m\dot{x} + kx - \text{sat}\left(\frac{s}{\phi}\right) \quad (10.172)$$

where ϕ is selected and strictly positive, with:

$$\text{sat}(y) = \begin{cases} 1 & \text{if } y \geq 1 \\ y & \text{if } -1 < y < 1 \\ -1 & \text{if } y \leq -1 \end{cases} \quad (10.173)$$

Eq. (10.169) now reduces to

$$\begin{aligned} \dot{V} &= -\frac{|s|}{m} & \text{for } \frac{|s|}{\phi} \geq 1 \\ &= -\frac{s^2}{m\phi} & \text{for } \frac{|s|}{\phi} < 1 \end{aligned} \quad (10.174)$$

Example 10.8 - Nonlinear control of a SDOF system

Consider a SDOF system with the properties $m = 1 \text{ N}\cdot\text{s}^2/\text{m}$; $k = 2 \text{ N}\cdot\text{s}/\text{m}$, and $c = 100 \text{ N}/\text{m}$, subjected to an unmeasurable harmonic excitation $p(t) = 20 \sin(\Omega t)$, $\Omega = 10 \text{ rad/s}$, and controlled with a nonlinear force f :

$$\dot{\mathbf{X}} = \mathbf{A}\mathbf{X} + \mathbf{B}_p p + \mathbf{B}_f f \quad (10.175)$$

where $\mathbf{B}_p = \mathbf{B}_f = [0 \quad 1/m]^T \equiv \mathbf{B}$

Noting that $\mathbf{e} = \mathbf{X} - \mathbf{X}_d = \mathbf{X}$, we select the Lyapunov function based on the sliding surface $s = \mathbf{P}\mathbf{X} = 0$, where $\mathbf{P} = [\lambda \quad 1]$:

$$\begin{aligned} V &= \frac{1}{2} s^2 \\ \dot{V} &= s\dot{s} \\ &= s\mathbf{P}[\mathbf{A}\mathbf{X} + \mathbf{B}(p + f)] \\ &= \mathbf{X}^T \mathbf{P}^T \mathbf{P} \mathbf{A} \mathbf{X} + s\mathbf{P}\mathbf{B}(p + f) \end{aligned} \quad (10.176)$$

A trivial solution would be to select $f = -p$ if the force was measurable. Here, we consider p to be bounded $p \leq 10$. Noting that the first term is negative definite, a strategy is to select a control force f such that $\dot{V} \leq -\eta|s|$:

$$\begin{aligned} s\mathbf{P}\mathbf{B}(10 + f) &= -\eta|s| \\ f &= -(\mathbf{P}\mathbf{B})^{-1} \eta \cdot \text{sign}(s) - 10 \end{aligned} \quad (10.177)$$

Fig. 10.5 plots the uncontrolled versus controlled response, using $\lambda = 25$ and $\eta = 10$. The controller reduces the dynamic response.

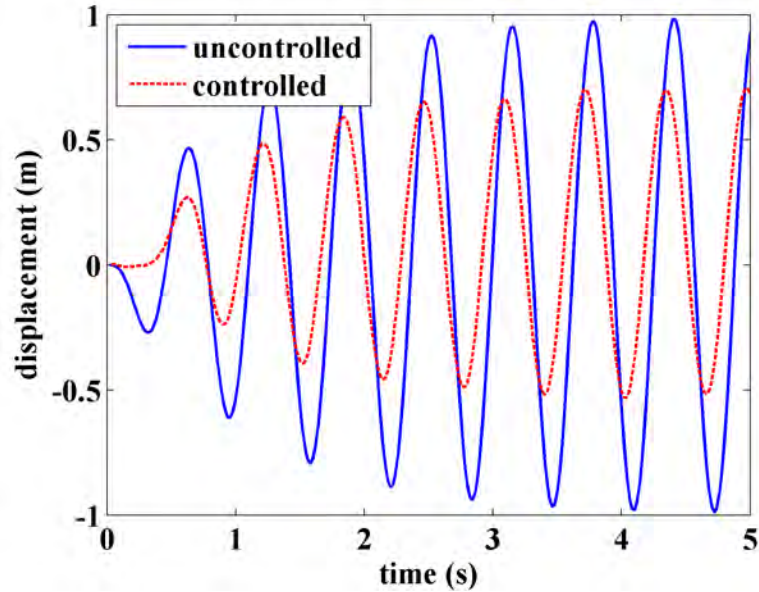
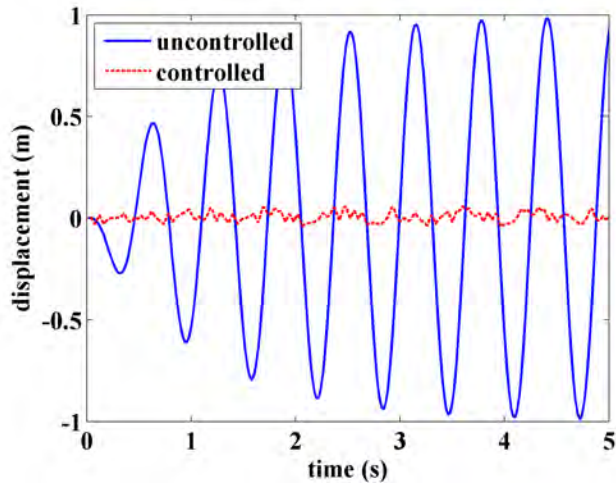


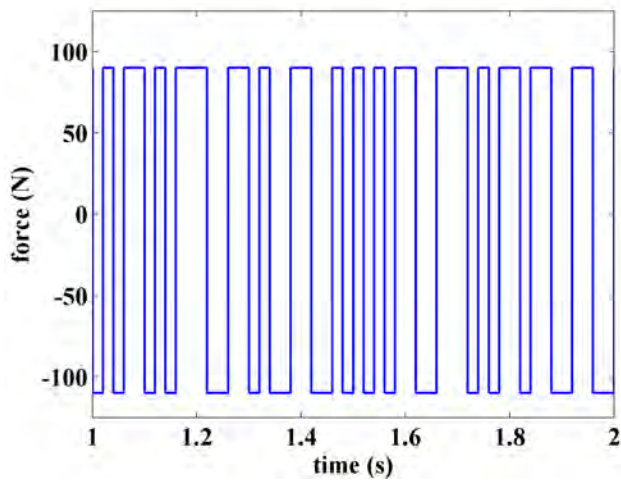
Figure 10.5: Time series response for $\lambda = 25$ and $\eta = 10$.

We now investigate a more aggressive control strategy, where $\lambda = 25$ and $\eta = 100$. Fig. 10.6(a) plots the time series response for the SDOF system, in which the control system exhibits chattering due to the switch between high magnitudes control input f around $s = 0$. The time history of the control force f for the last 1 sec of the simulation is plotted in Fig. 10.6(b).

10.6. INTRODUCTION TO NONLINEAR CONTROL



(a)



(b)

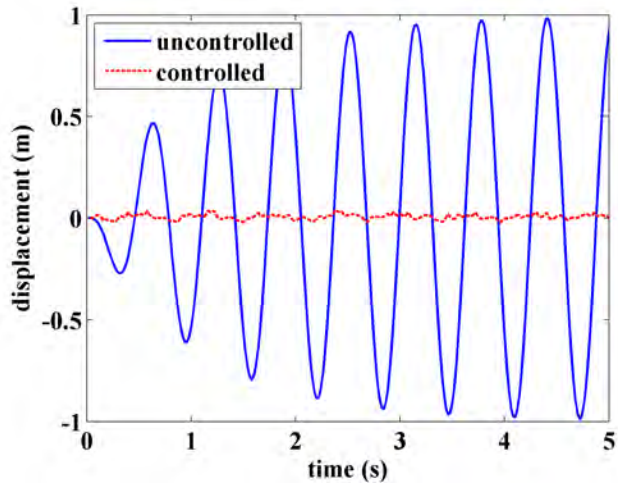
Figure 10.6: (a) Time series response for $\lambda = 25$ and $\eta = 100$; and (b) time history of the control force.

Given the chattering effect, we investigate the addition of a boundary layer around $s = 0$ to smoothen the control rule. Eq. (10.178) becomes

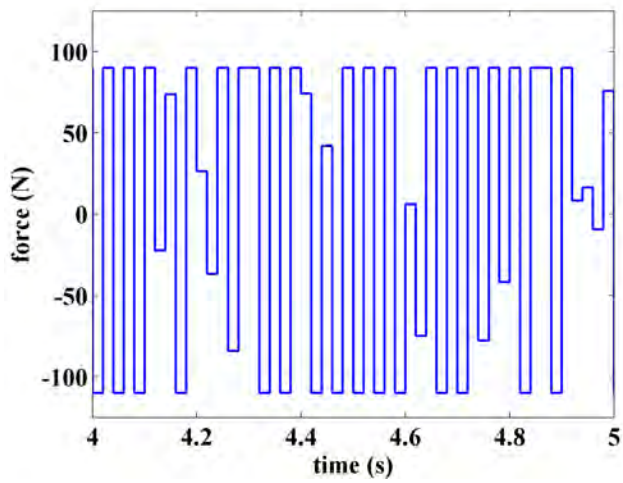
$$\begin{aligned}
 s\mathbf{PB}(10 + f) &= -\eta \cdot \text{sat} \left(\frac{s}{\phi} \right) s \\
 f &= -(\mathbf{PB})^{-1} \eta \cdot \text{sat} \left(\frac{s}{\phi} \right) - 10
 \end{aligned}
 \tag{10.178}$$

Fig. 10.7 plots the time series response after the introduction of the boundary layer using $\phi = 0.5$, along with the time series of the control input f . The chattering has reduced substantially. Fig. 10.8 shows the response with $\phi = 1.0$. In this case, chattering is eliminated. The addition of transitional control force levels between f_{\min} and f_{\max} is shown in Fig. 10.7(b), and the additional smoothness in the control force is shown in Fig. 10.8(b).

10.6. INTRODUCTION TO NONLINEAR CONTROL

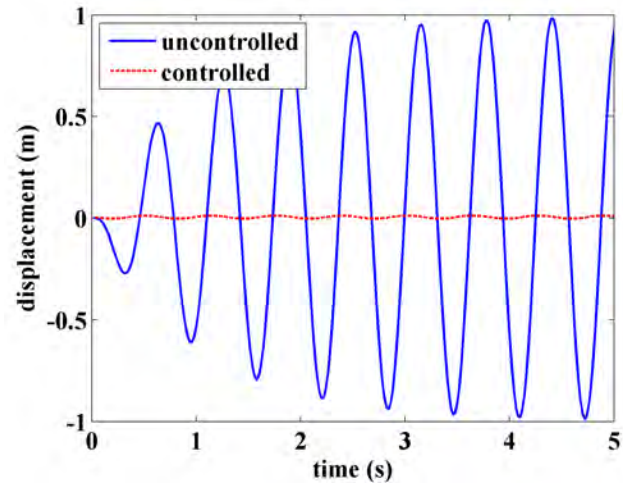


(a)

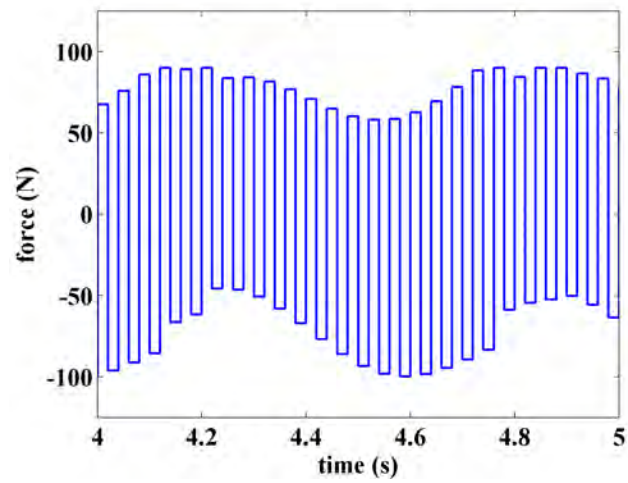


(b)

Figure 10.7: (a) Time series response for $\lambda = 25$, $\eta = 100$, and $\phi = 0.5$; and (b) time history of the control force.



(a)



(b)

Figure 10.8: (a) Time series response for $\lambda = 25$, $\eta = 100$, and $\phi = 1$; and (b) time history of the control force.

10.7 Applications to Semi-Active and Hybrid Systems

This section comprises three numerical structural control examples of structures equipped with semi-active and hybrid systems. Firstly, we investigate the integration of a simple linear controller (LQR) for a semi-active TLCD. Semi-active TLCDs are highly nonlinear mitigation devices, and this example demonstrates that a simple feedback controller may be paired with hybrid systems having complex dynamic behavior. Secondly, we look at two nonlinear control strategies to establish the stiffness switching rule on an AVS system: one in the frequency domain (H_∞), and one in the time domain (SMC). Lastly, we perform a parametric study of the control weight parameters for a linear (LQR) and a nonlinear (SMC) controller, and compare the performance between both control algorithms.

10.7.1 Linear Controller for a Semi-Active TLCD

Variable orifice damper is a tuned liquid column damper (TLCD), for which the liquid column's orifice can be varied using an external voltage. This concept referred to as a semi-active TLCD. The equations of motion are derived in Sect. 5.7, and repeated here for convenience:

$$\begin{aligned} (m + m_d)\ddot{u} + c\dot{u} + ku &= p(t) - \alpha m_d \ddot{u}_d \\ m_d \ddot{u}_d + \frac{1}{2} \rho A_d \xi |\dot{u}_d| \dot{u}_d + k_d u_d &= -\alpha m_d \ddot{u} \end{aligned} \quad (10.179)$$

The head loss ξ is now allowed to vary with time $\xi = \xi(t)$. Eq. (10.179) can be written in a state-space representation by treating the nonlinear damping term as a scalar force input:

$$\dot{\mathbf{X}}(t) = \mathbf{A}\mathbf{X} + \mathbf{B}_p p + \mathbf{B}_f f \quad (10.180)$$

where $\mathbf{X} = [u \ u_d \ \dot{u} \ \dot{u}_d]^T$. The dynamic properties matrices are:

$$\mathbf{M} = \begin{bmatrix} m + m_d & \alpha m_d \\ \alpha m_d & m_d \end{bmatrix} \quad \mathbf{M}^{-1} = \frac{1}{\tilde{m}} \begin{bmatrix} m_d & -\alpha m_d \\ -\alpha m_d & m + m_d \end{bmatrix}$$

$$\mathbf{C} = \begin{bmatrix} c & 0 \\ 0 & 0 \end{bmatrix} \quad \mathbf{K} = \begin{bmatrix} k & 0 \\ 0 & k_d \end{bmatrix}$$

with $\tilde{m} = m_d(m + m_d) - \alpha^2 m_d$ and

$$\mathbf{A} = \begin{bmatrix} \mathbf{0} & \mathbf{I} \\ -\mathbf{M}^{-1}\mathbf{K} & -\mathbf{M}^{-1}\mathbf{C} \end{bmatrix} \quad \mathbf{B}_p = \frac{1}{\tilde{m}} \begin{bmatrix} 0 \\ 0 \\ m_d \\ -\alpha m_d \end{bmatrix} \quad \mathbf{B}_f = \frac{1}{\tilde{m}} \begin{bmatrix} 0 \\ 0 \\ -\alpha m_d \\ m + m_d \end{bmatrix}$$

Note that \mathbf{M} is symmetric but no longer diagonal. The control force, f , is taken as:

$$f(t) = -\rho A_d \xi(t) |\dot{u}_d| u_d / 2 \quad (10.181)$$

Consider a SDOF system with the following properties: $m = 100 \text{ k}\cdot\text{s}^2/\text{in}$ $c = 0.1 \text{ k}\cdot\text{s}/\text{in}$; and $k = 253.3 \text{ k}/\text{in}$, and subjected to a harmonic excitation acting at the fundamental frequency $f = 10 \text{ Hz}$ with $\hat{p}/k = 0.01 \text{ in}$. The structure is equipped with a TLCD with properties $\bar{m} = 0.03$, $f|_{\text{opt}} = 0.955$, $\beta = 1$, and with the head loss allowed to vary between $\xi = 0.01$ (valve fully open) and $\xi = 10$ (valve fully closed). A linear controller is designed to control ξ using the function `care` in MATLAB with:

10.7. APPLICATIONS TO SEMI-ACTIVE AND HYBRID SYSTEMS

$$Q = \begin{bmatrix} 10 & 0 & 0 & 0 \\ 0 & 0 & 0 & 0 \\ 0 & 0 & 1 & 0 \\ 0 & 0 & 0 & 0 \end{bmatrix} \quad r = 1 \quad (10.182)$$

Note that *no* control weights in Q are assigned to the liquid column DOFs, because restricting the liquid movement would limit the controllability. Linear controllers are often used for controlling semi-active structures despite the nonlinear nature of the systems. This simplification is allowed since semi-active systems do not have the potential to destabilize the controlled structure, as discussed earlier. Using the linear controller, the control gains \mathbf{K}_f are used to determine a required force:

$$f = -\mathbf{K}_f \mathbf{X}(t) \quad (10.183)$$

This required force cannot be directly applied to the system. Instead, $\xi(t)$ needs to be modified (by varying the opening of the valve) in order to reach f_{req} . Using Eq. (10.181), the required head loss coefficient at time t is taken as:

$$\xi_{\text{req}}(t) = -f_{\text{req}}(t) \frac{2}{|\dot{u}_d(t)| u_d(t) \rho A_d} \quad (10.184)$$

Given that $\xi_{\text{req}}(t)$ is not necessarily reachable due to physical limits ($\xi_{\text{min}} \leq \xi \leq \xi_{\text{max}}$), the following saturation-type application rule is selected:

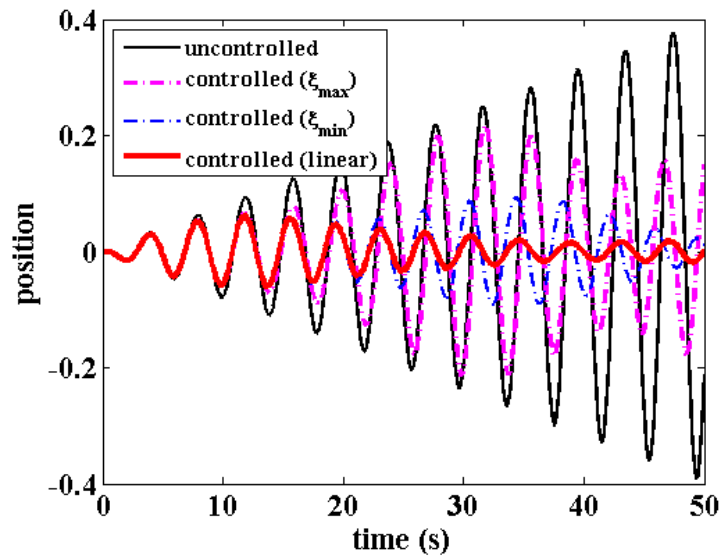
$$\xi = \begin{cases} \xi_{\text{max}} & \text{if } \xi_{\text{req}} \geq \xi_{\text{max}} \\ \xi_{\text{req}} & \text{if } \xi_{\text{min}} \leq \xi_{\text{req}} \leq \xi_{\text{max}} \\ \xi_{\text{min}} & \text{if } \xi_{\text{req}} \leq \xi_{\text{min}} \end{cases} \quad (10.185)$$

Fig. 10.9(a) compares the time series response of the uncontrolled structure (no TLCD) versus three control strategies: 1)

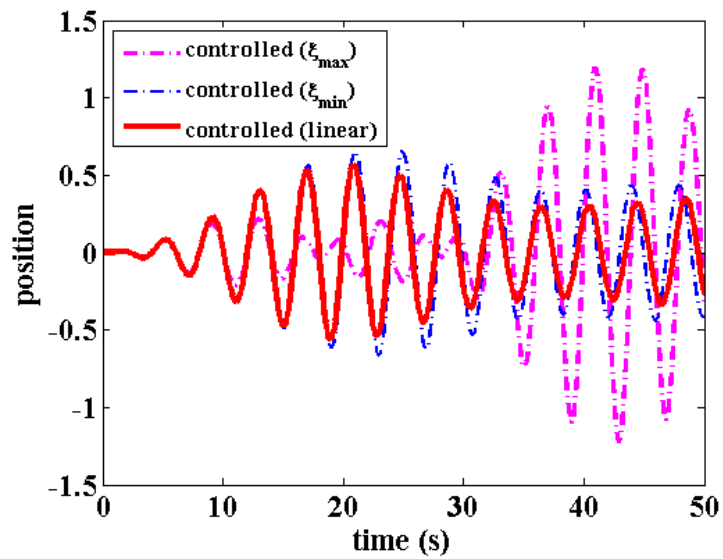
CHAPTER 10. ADVANCED CONTROL THEORY

valve fully closed (using $\xi_{\max} = 10$; 2) valve fully opened (using $\xi_{\min} = 0.01$; and 3) using the linear feedback control strategy (using $0.01 \leq \xi \leq 10$). The inclusion of the linear control rule gives the best performance at mitigating the excitation. Fig. 10.9(b) shows the time series response of the fluid. Results show that the controller is capable of mitigating the excitation based on a minimal fluid displacement, which could be interpreted as a measure of effectiveness of the control mechanism.

10.7. APPLICATIONS TO SEMI-ACTIVE AND HYBRID SYSTEMS



(a)



(b)

Figure 10.9: Time series response under various control strategies: (a) structure; and (b) TLCD.

CHAPTER 10. ADVANCED CONTROL THEORY

Fig. 10.10 plots the time history of the head loss coefficient ξ . In most cases, ξ has a binary output oscillating between ξ_{\min} and ξ_{\max} , which represents an *ideal* force application scheme. This high discontinuity in ξ might cause unnecessary acceleration in the controlled system. In reality, the head loss coefficient would be changed by operating a valve, and this operation would be continuous. For instance, assume that the valve is operated by sending a voltage v where $v = 0$ volt represents the fully opened valve state, and $v = 12$ volts represents the fully closed valve state. In addition, take the following voltage dynamics:

$$v = -\eta_v(v - v_{\text{req}}) \quad (10.186)$$

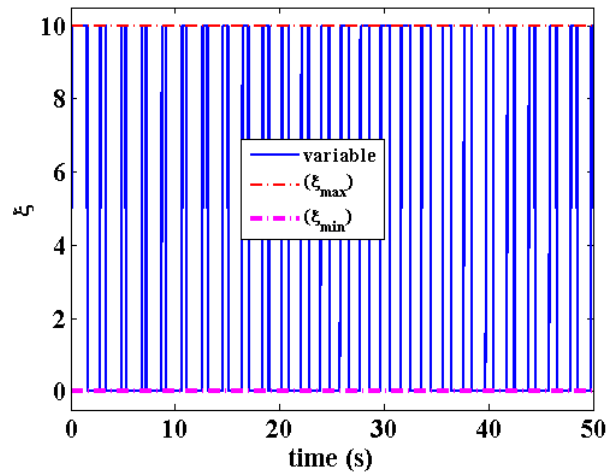
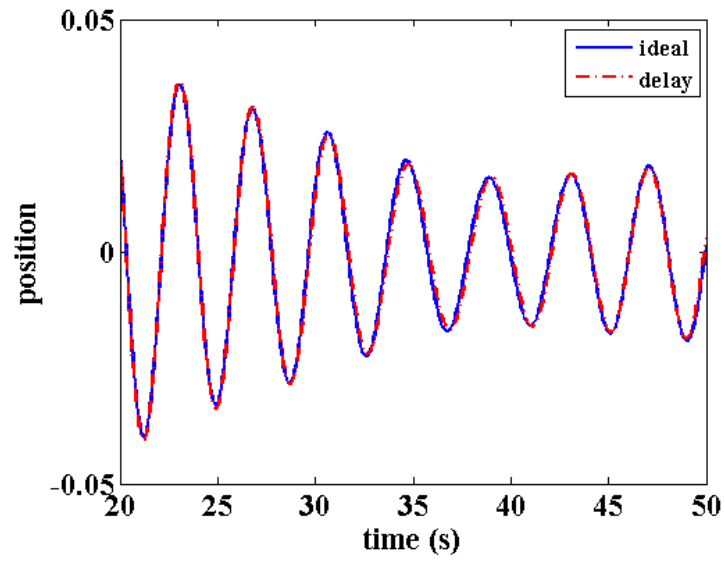


Figure 10.10: Variation of ξ in function of time.

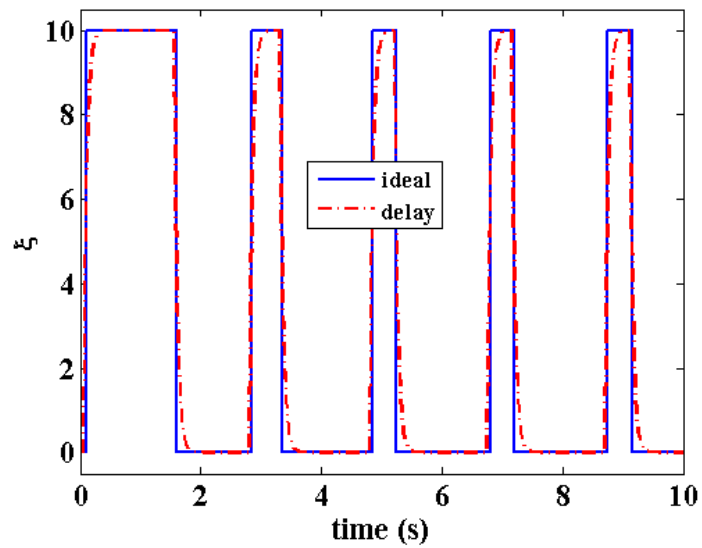
where η_v is a positive constant, taken as $\eta_v = 20$ in the simulation. This dynamic allows a smooth variation of the head loss coefficient ξ by adding a *delay* in the force application scheme. Fig. 10.11(a) shows a hardly observable difference in the time series response of the structure when a smooth force application rule is used.

10.7. APPLICATIONS TO SEMI-ACTIVE AND HYBRID SYSTEMS

Fig. 10.11(b) illustrates the delay in the head loss variation caused by the voltage dynamics.



(a)



(b)

Figure 10.11: (a) Time series response; and (b) head loss coefficient time history over the first 10 sec.

10.7. APPLICATIONS TO SEMI-ACTIVE AND HYBRID SYSTEMS

10.7.2 Variable stiffness

This example illustrates the application of two nonlinear controllers for the stiffness switching rule of an AVS system. First, an H_∞ -type controller is designed to minimize the maximum dynamic response in the frequency domain. Second, a SMC controller is designed to provide an application in the time domain.

Example 10.9 - Frequency domain controller for AVS

Take the 3DOF structure from Ex. 3.6. Arbitrarily divide \mathbf{k} into a fixed and variable system:

$$\mathbf{k}_f = \begin{bmatrix} 204 \\ 540 \\ 708 \end{bmatrix} \text{ (kN/m); } \quad \mathbf{k}_v = \begin{bmatrix} 300 \\ 300 \\ 300 \end{bmatrix} \text{ (kN/m)}$$

and consider 4 different stiffness activation strategies illustrated in Fig. 10.12. One can compute the frequency response H_2 for the first mode, and use the results to minimize the maximum response for a given excitation, constituting an H_∞ -type control strategy. Fig. 10.13 shows a plot of the 4 transfer function.

CHAPTER 10. ADVANCED CONTROL THEORY

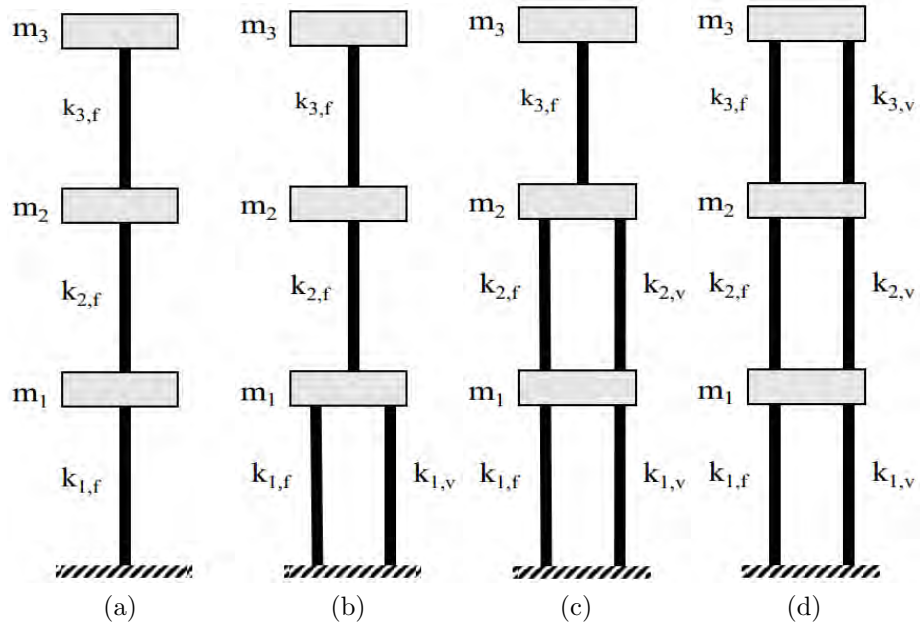


Figure 10.12: Four stiffness activation strategies. (a) case 1 - no activation; (b) case 2 - floor 1 activated; (c) case 3 - floors 1 and 2 activated; and (d) all stiffnesses activated.

10.7. APPLICATIONS TO SEMI-ACTIVE AND HYBRID SYSTEMS

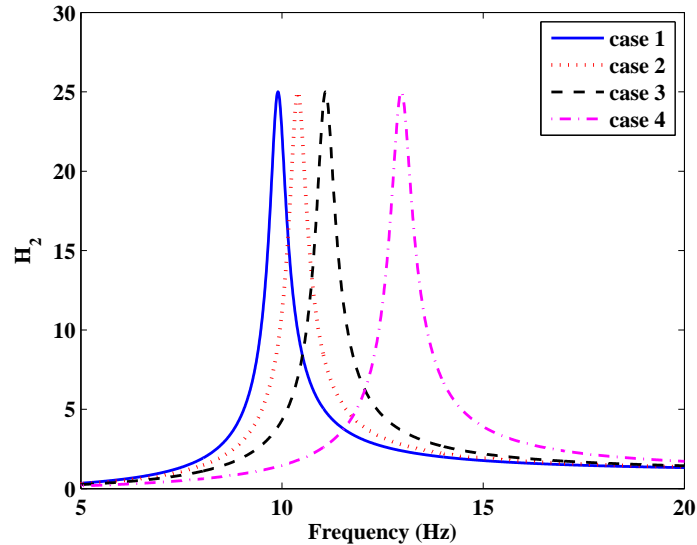


Figure 10.13: Transfer functions for 4 bracing combinations, $\xi = 2\%$.

The structure is subjected to the Imperial Valley 1940 earthquake, North-South component. At each time step, the controller selects the stiffness activation case that minimizes the dynamic response

$$\min_{\text{case}} J = \int_0^{\infty} H_2(\text{case}, \Omega) A(\Omega) d\Omega \quad (10.187)$$

where $A(\Omega)$ is the energy content of the excitation at frequency Ω . Fig. 10.14 compares the time series responses of the 3rd floor for the uncontrolled (all stiffnesses are switched *on*, equivalent to full activation strategy 4) and controlled cases, and Fig. 10.15 shows the evolution of the stiffness activation strategies over the first 10 sec of the excitation. The maximum displacements are reduced by 15.4%, 15.7%, and 5.68% for the first, second, and third floors, respectively, using the variable stiffness strategy.

CHAPTER 10. ADVANCED CONTROL THEORY

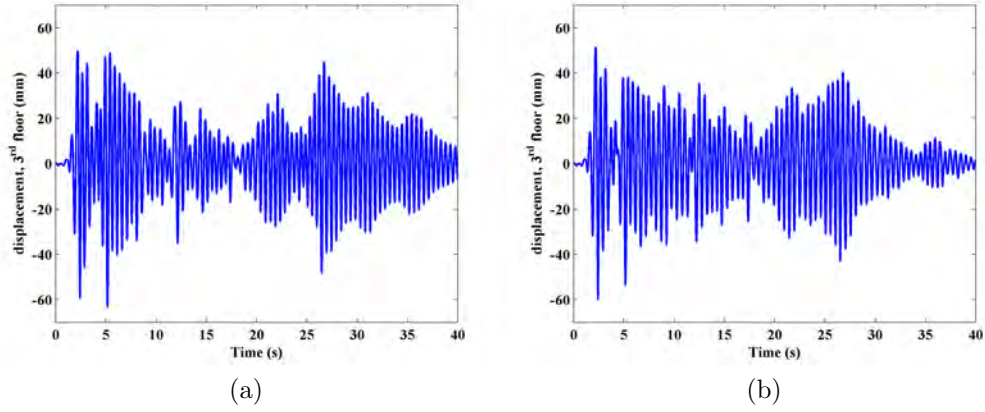


Figure 10.14: Time series response of the 3rd floor: (a) uncontrolled; and (b) controlled structure.

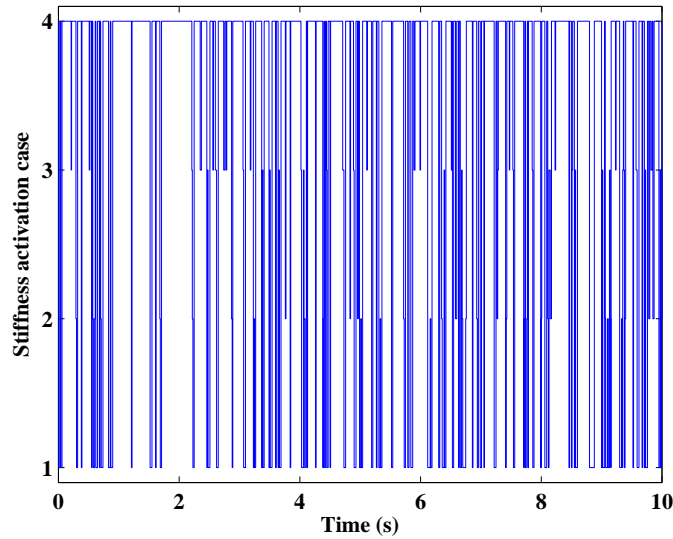


Figure 10.15: Stiffness activation cases for the first 10 sec of the excitation.

Example 10.10 - Time domain controller using AVS

We now investigate a nonlinear controller designed in the time domain. Consider the following SMC controller for the

10.7. APPLICATIONS TO SEMI-ACTIVE AND HYBRID SYSTEMS

structure from Ex. 10.12. The state-space representation for an AVS-equipped structure subjected to an earthquake is written:

$$\dot{\mathbf{X}}(t) = \mathbf{A}\mathbf{X}(t) + \mathbf{B}_{\text{avs}}\mathbf{F}(t) + \mathbf{B}_g a_g(t) \quad (10.188)$$

where \mathbf{B}_{avs} is the AVS placement matrix:

$$\mathbf{B}_{\text{avs}} = \begin{bmatrix} 0 & 0 & 0 \\ 0 & 0 & 0 \\ 0 & 0 & 0 \\ -1/m_1 & 1/m_1 & 0 \\ 0 & -1/m_2 & 1/m_2 \\ 0 & 0 & -1/m_3 \end{bmatrix}$$

and $\mathbf{F}(t) = [f_1(t) \ f_2(t) \ f_3(t)]$ is the force vector from the AVS system with:

$$f_i(t) = h_i(t)k_{v,i}z_i(t) \quad (10.189)$$

where $z_i(t)$ is the interstory displacement, $h_i(t)$ is a binary coefficient representing the *on* ($h_i(t) = 1$) or *off* ($h_i(t) = 0$) position of the AVS, and $k_{v,i}$ is the lateral variable stiffness of the i^{th} floor. We take the sliding surface as:

$$\begin{aligned} V &= \frac{1}{2}\mathbf{S}^T\mathbf{S} \\ \mathbf{S} &= \mathbf{P}\mathbf{X} = [\Lambda \quad \mathbf{I}] \begin{bmatrix} \mathbf{x} \\ \dot{\mathbf{x}} \end{bmatrix} \end{aligned} \quad (10.190)$$

The time derivative is:

$$\begin{aligned} \dot{V} &= \mathbf{S}^T\dot{\mathbf{S}} \\ &= \mathbf{S}^T\mathbf{P}(\mathbf{A}\mathbf{X}(t) + \mathbf{B}_{\text{avs}}\mathbf{F}(t) + \mathbf{B}_g a_g(t)) \end{aligned} \quad (10.191)$$

In the case of semi-active systems, it is often not possible to guarantee $\dot{V} < 0$. Instead, one tries to make Eq. (10.191) as

CHAPTER 10. ADVANCED CONTROL THEORY

negative definite as possible. Noting that only the second term in Eq. (10.191) is controllable, the control objective can be set as

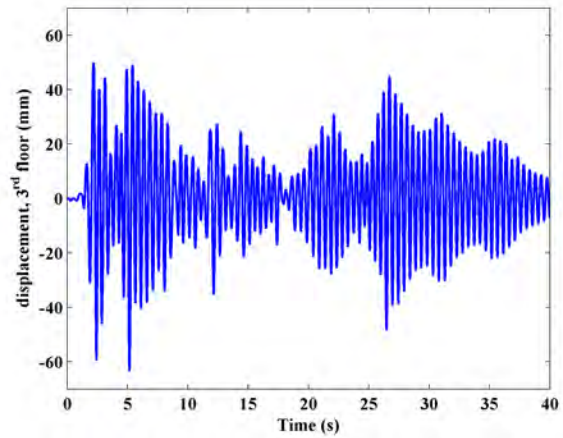
$$(\mathbf{S}^T \mathbf{P} \mathbf{B}_{\text{avs}})_i h_i(t) k_{v,i}(z_i(t)) \leq 0 \quad i = 1, 2, 3 \quad (10.192)$$

or, because $k_{v,i} \geq 0$:

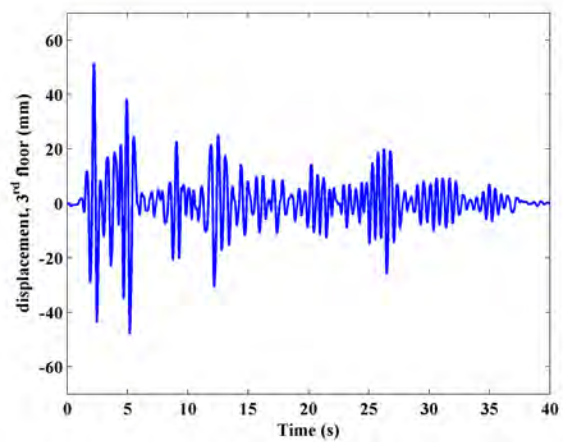
$$\begin{aligned} h_i(t) &= 0 & \text{if } (\mathbf{S}^T \mathbf{P} \mathbf{B}_{\text{avs}})_i z_i(t) \geq 0 \\ h_i(t) &= 1 & \text{if } (\mathbf{S}^T \mathbf{P} \mathbf{B}_{\text{avs}})_i z_i(t) < 0 \end{aligned} \quad (10.193)$$

Fig. 10.16 compares the time series response of the controlled structured against the uncontrolled case with full stiffness, along with the stiffness schedule for each floor. Note that the variable stiffness in this example is not restricted to only 4 strategies, as in the previous example. Results show that the time-domain controller is effective at mitigating displacements.

10.7. APPLICATIONS TO SEMI-ACTIVE AND HYBRID SYSTEMS

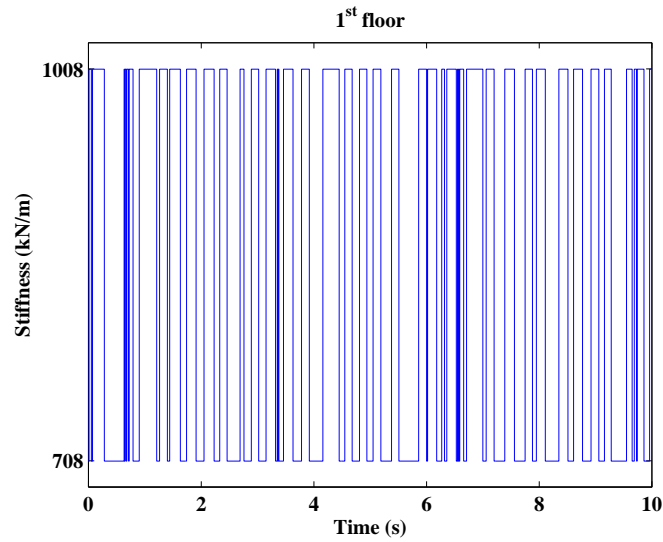


(a)



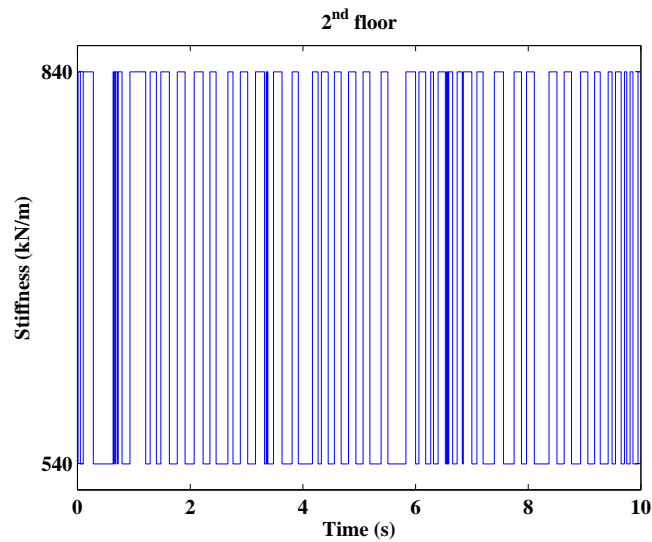
(b)

Figure 10.16: Structure subjected to Imperial Valley 1940 earthquake, North-South Component. Time series response for (a) uncontrolled; and (b) controlled cases;



(c)

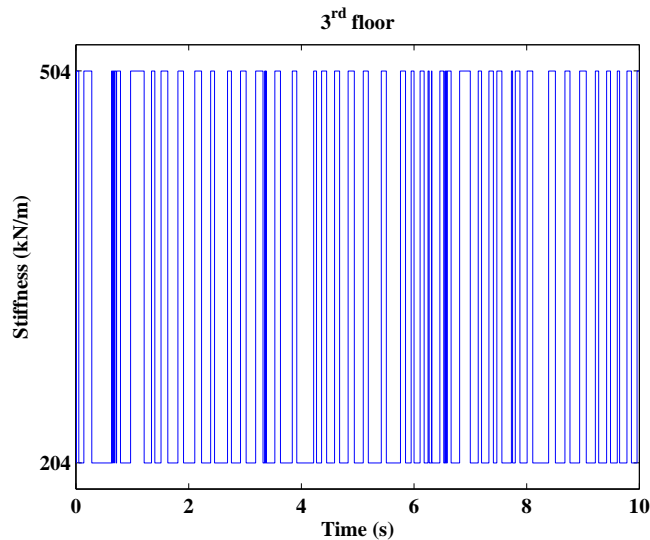
Figure 10.16: Structure subjected to Imperial Valley 1940 earthquake, North-South Component. (c) 1st floor stiffness, first 10 seconds;



(d)

Figure 10.16: Structure subjected to Imperial Valley 1940 earthquake, North-South Component. (d) 2nd floor stiffness, first 10 seconds; and

10.7. APPLICATIONS TO SEMI-ACTIVE AND HYBRID SYSTEMS



(e)

Figure 10.16: Structure subjected to Imperial Valley 1940 earthquake, North-South Component. (e) 3rd floor stiffness, first 10 seconds.

10.7.3 Variable Fluids

Here, we take the 3DOF structure from Ex. 10.12, also subjected to the Imperial Valley 1940 earthquake, North-South component, to compare the performances between a linear and a nonlinear controller. This time, the structure is equipped with three controllable fluid dampers (one per floor). Each damper is assumed to be linear, with its damping coefficient $c(t)$ varying linearly with the input voltage between 0 (c_{\min}) and 25 kN·s/m (c_{\max}). A delay in the voltage dynamic is introduced, similar to Eq. (10.186). The structural dynamics is defined by Eq. (10.188).

$$\dot{\mathbf{X}}(t) = \mathbf{A}\mathbf{X}(t) + \mathbf{B}_d\mathbf{F}(t) + \mathbf{B}_g a_g(t) \quad (10.194)$$

where \mathbf{B}_d is the damper placement matrix

$$\mathbf{B}_d = \begin{bmatrix} 0 & 0 & 0 \\ 0 & 0 & 0 \\ 0 & 0 & 0 \\ -1/m_1 & 1/m_1 & 0 \\ 0 & -1/m_2 & 1/m_2 \\ 0 & 0 & -1/m_3 \end{bmatrix}$$

The LQR gains are obtained using the function `care` in MATLAB, which is in function of the control weight matrices \mathbf{Q} and \mathbf{R} . The required control input for the i^{th} damper is

$$f_{\text{req},i} = -\mathbf{K}\mathbf{X} \quad (10.195)$$

and a saturation rule similar to Eq. 10.185 is used to select the voltage input.

The nonlinear controller is a SMC derived similarly as in Ex. 10.10. Here, the control input f_i is written

$$f_i(t) = c(t)z_i(t) \quad (10.196)$$

where $z(t)$ is the interstory velocity at the damper location. Thus, Eq. (10.193) is written:

$$\begin{aligned} c_i(t) &= c_{\min} & \text{if } (\mathbf{S}^T \mathbf{P} \mathbf{B}_d)_i z_i(t) &\geq 0 \\ c_i(t) &= c_{\max} & \text{if } (\mathbf{S}^T \mathbf{P} \mathbf{B}_d)_i z_i(t) < 0 \end{aligned} \quad (10.197)$$

It follows that the required control input for the i^{th} damper is

$$f_{\text{req},i} = c(t)z_i(t) \quad (10.198)$$

The voltage is selected as v_{\max} for $c_i(t) = c_{\max}$, and v_{\min} for $c_i(t) = c_{\min}$. The SMC control rule is a function of the sliding surface weights \mathbf{P} .

10.7. APPLICATIONS TO SEMI-ACTIVE AND HYBRID SYSTEMS

Before comparing the performance of both controllers, it is important to evaluate the individual behavior of each controller as a function of its control weights. This parametric study will allow a more fair and intuitive comparison between both controllers.

To assess performance, 10 performance indices $J_1 - J_{10}$ are established:

- J_1 to J_3 , the maximum interstory displacement reduction (%) for floor 1, 2, and 3 respectively;
- J_4 to J_6 , the total energy dissipated (kJ) for dampers 1, 2, and 3 respectively;
- J_7 , the average voltage utilization per damper (%); and
- J_8 to J_{10} , the average energy dissipated per volt (kJ/v).

Performance measures J_1 to J_3 constitute the main control objective for the earthquake mitigation (to reduce structural damage); performance measures J_4 to J_{10} are used to compare the effectiveness of the controller.

To evaluate the performance of the linear (LQR) controller as a function of its control weights \mathbf{Q} and \mathbf{R} , 10 control weight cases are studied:

$$\bullet \text{ Case 1: } \mathbf{Q} = \left[\begin{array}{ccc|ccc} 1 & 0 & 0 & 0 & 0 & 0 \\ 0 & 1 & 0 & 0 & 0 & 0 \\ 0 & 0 & 1 & 0 & 0 & 0 \\ \hline 0 & 0 & 0 & 1 & 0 & 0 \\ 0 & 0 & 0 & 0 & 1 & 0 \\ 0 & 0 & 0 & 0 & 0 & 1 \end{array} \right] \text{ and } \mathbf{R} = \begin{bmatrix} 1 & 0 & 0 \\ 0 & 1 & 0 \\ 0 & 0 & 1 \end{bmatrix};$$

CHAPTER 10. ADVANCED CONTROL THEORY

- Case 2: Case 1 with displacement weights (top-left quadrant of the matrix) increased by a factor of 100;
- Case 3: Case 1 with velocity weights (bottom-right quadrant of the matrix) increased by a factor of 100;
- Case 4: Case 1 with all weights in \mathbf{Q} increased by a factor of 100;
- Case 5: Case 1 with only displacement and velocity weights of DOF 1 increased by a factor of 100.
- Case 6: Case 1 with only displacement and velocity weights of DOF 2 increased by a factor of 100.
- Case 7: Case 1 with only displacement and velocity weights of DOF 3 increased by a factor of 100.
- Case 8: Case 1 with only displacement and velocity weights of DOF 3 increased by a factor of 1000.
- Case 9: Case 1 with the \mathbf{R} weights reduced to 1E-17 (no penalty on the control input); and
- Case 10: Voltage always set to maximum (passive-on).

Table 10.4 compares the results for the individual control weight cases. Results show that variations in \mathbf{Q} and \mathbf{R} may significantly change the system's performance. In addition, results appear to agree that controlling the velocity of the last floor, which is achieved in Cases 3, 4, and 7, leads to the best interstory mitigation performance (J_1 to J_3). This can be explained by the lower efficiency of the semi-active devices between the ground and the first floor, and between the first and the second floor, compared against the efficiency of the device installed between the second and the third floor, as shown in the total energy

10.7. APPLICATIONS TO SEMI-ACTIVE AND HYBRID SYSTEMS

mitigated (J_4 and J_5 versus J_6). Case 9 is an alternative control strategy, in which the control force is set at a very high magnitude, equivalent to dramatically increasing the weights in the \mathbf{R} matrix. This control strategy is often efficient in controlling semi-active devices, as pre-selection of the \mathbf{Q} matrix is not necessary (all weights can be set to 1). Notice that this strategy is not applicable to active devices, because active devices have the potential to destabilize a system. Another observation is that any control case is more efficient for mitigating vibration (J_8 to J_{10}) compared with Case 10. However, Case 10 (passive-on) mitigates the first and second floor interstorey displacements (J_1 and J_2) well, but offers limited performance at mitigating the interstorey displacements of the last floor (J_3).

Table 10.4: Performance measures J_1 to J_{10} for the linear (LQR) controller

	J_1 (%)	J_2 (%)	J_3 (%)	J_4 (kJ)	J_5 (kJ)	J_6 (kJ)	J_7 (%)	J_8 (kJ/v)	J_9 (kJ/v)	J_{10} (kJ/v)
Case 1	9.1	7.2	6.4	4.6	18.0	40.2	11.5	4.3	11.2	27.4
Case 2	11.0	9.2	14.9	5.0	19.8	44.2	14.1	3.7	9.9	25.8
Case 3	34.5	32.0	33.7	8.7	34.3	76.3	40.6	1.1	8.0	27.8
Case 4	34.5	32.0	33.7	8.7	34.4	76.3	40.6	1.1	8.0	27.8
Case 5	23.3	18.3	20.2	6.8	26.7	59.4	24.5	2.3	7.3	26.3
Case 6	31.9	25.8	26.3	7.8	31.0	69.0	32.4	1.6	7.3	26.0
Case 7	31.8	29.8	31.7	8.3	33.0	74.1	35.5	1.4	7.6	29.2
Case 8	35.3	34.7	34.2	8.9	35.0	77.9	46.0	1.1	6.9	24.9
Case 9	37.5	34.9	35.2	9.1	35.7	78.6	55.7	0.8	7.0	20.8
Case 10	37.7	36.0	27.5	8.2	32.9	66.5	100.0	0.7	2.7	5.50

The parametric investigation is now applied to the SMC controller. In this case, the controller is dependant on the control weights \mathbf{P} . Analogous to the LQR controller, 10 control weight cases are selected:

CHAPTER 10. ADVANCED CONTROL THEORY

- Case 1: $\mathbf{P} = \left[\begin{array}{ccc|ccc} 1 & 2 & 3 & 1 & 2 & 3 \\ 1 & 2 & 3 & 1 & 2 & 3 \\ 1 & 2 & 3 & 1 & 2 & 3 \end{array} \right]$;
- Case 2: Case 1 with displacement weights (left quadrant of the matrix) increased by a factor of 100;
- Case 3: Case 1 with velocity weights (right quadrant of the matrix) increased by a factor of 100;
- Case 4: Case 1 with all weights in \mathbf{P} increased by a factor of 100;
- Case 5: Case 1 with only displacement and velocity weights of DOF 1 increased by a factor of 100.
- Case 6: Case 1 with only displacement and velocity weights of DOF 2 increased by a factor of 100.
- Case 7: Case 1 with only displacement and velocity weights of DOF 3 increased by a factor of 100.
- Case 8: Case 1 with only displacement and velocity weights of DOF 3 increased by a factor of 1000.
- Case 9: Case 1 with all weights in \mathbf{P} increased by a factor of 1E17; and
- Case 10: Voltage always set to maximum (passive-on).

Remark that one has to be careful in selecting the control weight matrix \mathbf{P} ; the resulting \mathbf{PB}_d matrix needs to preserve full rank. Table 10.5 compares the results for each control weight cases. The same conclusion can be drawn about the control weights as for the linear case, whereas controlling for the velocity

10.7. APPLICATIONS TO SEMI-ACTIVE AND HYBRID SYSTEMS

of DOF 3 results in a more effective controller. Also, adding substantial weights to the control weight matrix is a good control strategy.

Table 10.5: Performance measures J_1 to J_{10} for the nonlinear (SMC) controller

	J_1 (%)	J_2 (%)	J_3 (%)	J_4 (kJ)	J_5 (kJ)	J_6 (kJ)	J_7 (%)	J_8 (kJ/v)	J_9 (kJ/v)	J_{10} (kJ/v)
Case 1	37.6	33.5	32.5	9.2	35.8	79.6	43.1	0.9	10.3	40.1
Case 2	25.7	16.9	19.9	6.7	26.0	56.8	35.6	1.1	6.9	18.6
Case 3	37.6	34.3	33.4	9.2	35.9	79.7	44.2	0.9	10.1	38.2
Case 4	37.6	33.5	32.5	9.2	35.8	79.6	43.1	0.9	10.3	40.1
Case 5	35.1	32.8	26.8	8.8	33.4	74.9	58.7	0.8	4.2	32.9
Case 6	38.3	35.6	29.0	8.4	32.9	67.0	69.9	0.8	6.1	7.4
Case 7	37.6	33.5	32.5	9.2	35.8	79.5	43.5	0.9	10.1	39.3
Case 8	37.6	33.5	32.5	9.2	35.8	79.5	43.5	0.9	10.1	39.2
Case 9	37.6	34.3	33.4	9.2	35.9	79.7	44.2	0.9	10.1	38.3
Case 10	37.7	36.0	27.5	8.2	32.9	66.5	100.0	0.7	2.7	5.5

We are now ready to investigate the displacement mitigation performance of both the linear and nonlinear controllers. For the comparison, we take the results from Case 9, has significantly high control weight. Table 10.6 summarizes the results for both controllers. Both control strategies perform similarly. However, there is a notable difference in the voltage required by the nonlinear controller to perform the mitigation task (J_7), resulting in an improved mitigation efficiency for J_8 to J_{10} . This difference is due to the time varying parameters being actually modeled within the nonlinear controller. Fig. 10.17 shows the variation of voltage over a window of 3 seconds (during an earthquake high impulse). The LQR controller exhibits a similar voltage behavior, but at a higher scale.

CHAPTER 10. ADVANCED CONTROL THEORY

Table 10.6: Performance comparison between the linear (LQR) and nonlinear (SMC) controllers

	J_1 (%)	J_2 (%)	J_3 (%)	J_4 (kJ)	J_5 (kJ)	J_6 (kJ)	J_7 (%)	J_8 (kJ/v)	J_9 (kJ/v)	J_{10} (kJ/v)
LQR	37.5	34.9	35.2	9.1	35.7	78.6	55.7	0.8	7.0	20.8
SMC	37.6	34.3	33.4	9.2	35.9	79.7	44.2	0.9	10.1	38.3

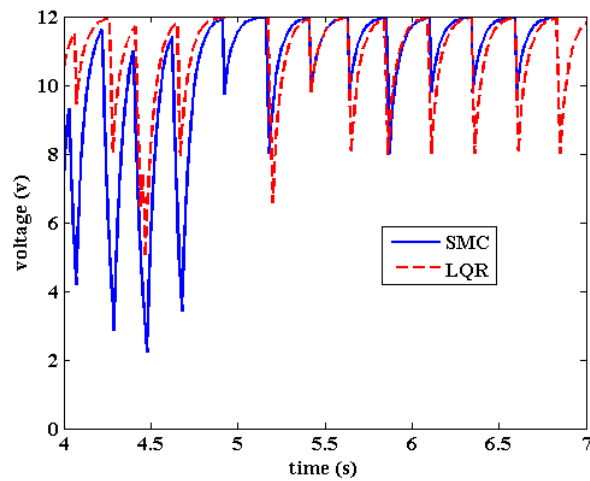


Figure 10.17: Variation of the semi-active damper voltage with time: (a) ground-floor 1 device;

10.7. APPLICATIONS TO SEMI-ACTIVE AND HYBRID SYSTEMS

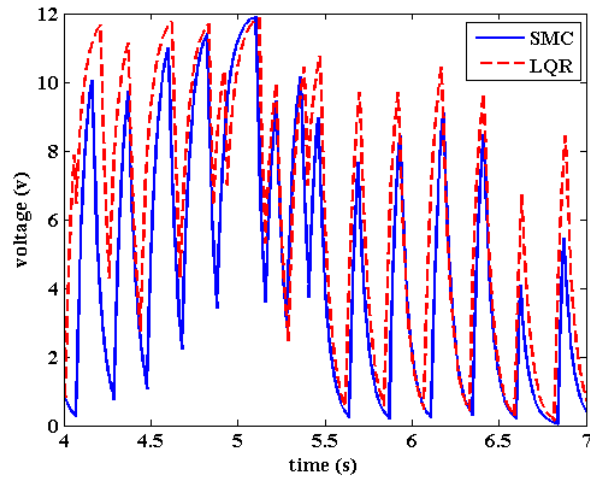


Figure 10.17: Variation of the semi-active damper voltage with time: (b) floor 1-floor 2 device; and

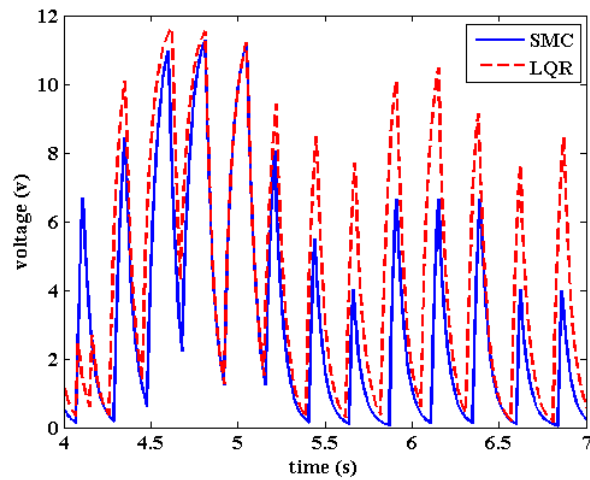


Figure 10.17: Variation of the semi-active damper voltage with time: (c) floor 2-floor 3 device.

Bibliography

- [1] Hancock tower now to get dampers. In *Engineering News Record*. October 30 1975, p. 11.
- [2] Tuned mass dampers steady sway of skyscrapers in wind. In *Engineering News Record*. August 18 1975, pp. 28–29.
- [3] Lead hula-hoops stabilize antenna. In *Engineering News Record*. July 22 1976, p. 10.
- [4] ABE, M., AND IGUSA, T. Semi-active dynamic vibration absorbers for controlling transient response. *Journal of Sound and Vibration* 198, 5 (1996), 547–569.
- [5] ADHIKARI, R., AND YAMAGUCHI, H. Sliding mode control of buildings with ATMD. *Earthquake Engineering & Structural Dynamics* 26, 4 (1997), 409–422.
- [6] AGRAWAL, A., FUJINO, Y., AND BHARTIA, B. Instability due to time delay and its compensation in active control of structures. *Earthquake engineering & structural dynamics* 22, 3 (1993), 211–224.
- [7] AHLWAT, A., AND RAMASWAMY, A. Multiobjective optimal fuzzy logic controller driven active and hybrid control systems for seismically excited nonlinear buildings. *Journal of Engineering Mechanics* 130 (2004), 416.
- [8] AMARATUNGA, K., AND WILLIAMS, J. Time integration using wavelets. In *SPIE's 1995 Symposium on OE/Aerospace Sensing and Dual Use Photonics* (1995), International Society for Optics and Photonics, pp. 894–902.

BIBLIOGRAPHY

- [9] ANKIREDDI, S., AND YANG, H. Simple ATMD control methodology for tall buildings subject to wind loads. *Journal of Structural Engineering* 122 (1996), 83.
- [10] ASHER, J. W., AND VAN VOLKINBURG, D. R. Seismic isolation of the usc university hospital. In *Seismic Engineering@ sResearch and Practice* (1989), ASCE, pp. 605–614.
- [11] AVRAAM, M. T. *MR-fluid brake design and its application to a portable muscular rehabilitation device*. PhD thesis, Université Libre de Bruxelles, Bruxelles, Belgium, 2009.
- [12] BACHMANN, H., AND AMMANN, W. *Vibrations in structures: induced by man and machines*. Iabse, 1987.
- [13] BÉLANGER, P. *Control engineering: a modern approach*. Oxford University Press, Inc., 1995.
- [14] BILLINGS, I., AND KIRKCALDIE, D. Base isolation of bridges in new zealand. In *Proceedings US-NZ Workshop on Seismic Resistance of Highway Bridges, Report* (1985), no. 12-1.
- [15] CAI, C., WU, W., AND ARAUJO, M. Cable vibration control with a TMD-MR damper system: Experimental exploration. *Journal of Structural Engineering* 133 (2007), 629.
- [16] CAO, H., AND LI, Q. New control strategies for active tuned mass damper systems. *Computers & Structures* 82, 27 (2004), 2341–2350.
- [17] CHAE, Y., SAUSE, R., AND RICLES, J. Performance-based seismic design and assessment of structures with

BIBLIOGRAPHY

- magneto-rheological dampers. Tech. Rep. 11-01, ATLSS, Lehigh University, Bethlehem, PA., 2011.
- [18] CHANIOTAKIS, E. Plasma science and fusion laboratory. *Private Communication* (1999).
- [19] CHEN, C., AND CHEN, G. Shake table tests of a quarter-scale three-storey building model with piezoelectric friction dampers. *Structural Control and Health Monitoring* 11, 4 (2004), 239–257.
- [20] CLOUGH, R. W., AND PENZIEN, J. *Dynamics of structures*, vol. 634. McGraw-Hill New York, 1993.
- [21] CONNOR, J., AND CONNOR, J. *Introduction to structural motion control*. Prentice Hall New York, 2002.
- [22] CONNOR, J. J., AND FARAJI, S. *Fundamentals of structural engineering*. Springer, 2012.
- [23] CORPORATION, K. Duoxactive-passive composite tuned mass damper. Technical Pamphlet 93-82E, Tokyo, Japan, 1993.
- [24] CRAWLEY, E., AND DE LUIS, J. Use of piezoelectric actuators as elements of intelligent structures. *AIAA journal* 25, 10 (1987).
- [25] DEIERLEIN, G., KRAWINKLER, H., MA, X., EATHERTON, M., HAJJAR, J., TAKEUCHI, T., KASAI, K., AND MIDORIKAWA, M. Earthquake resilient steel braced frames with controlled rocking and energy dissipating fuses. *Steel Construction* 4, 3 (2011), 171–175.
-

BIBLIOGRAPHY

- [26] DEN HARTOG, J. *Mechanical vibrations*. McGraw-Hill, 1940.
- [27] DOYLE, J., FRANCIS, B., AND TANNENBAUM, A. *Feedback control theory*, vol. 1. Macmillan Publishing Company New York, 1992.
- [28] DURMAZ, O., CLARK, W., BENNETT, D., PAINE, J., AND SAMUELSON, M. Experimental and analytical studies of a novel semi-active piezoelectric coulomb damper. In *Proceedings of SPIE* (2002), vol. 4697, p. 258.
- [29] (EPS), E. P. S. http://www.earthquakeprotection.com/building_mills_pe 2013.
- [30] FAJFAR, P., AND KRAWINKLER, H. *Seismic Design Methodologies for the Next Generation of Codes: Proceedings of the International Workshop on Seismic Design Methodologies for the Next Generation of Codes, Bled, Slovenia, 24-27 Jun 1997*. AA Balkema, 1997.
- [31] FENG, Q., AND SHINOZUKA, M. Use of a variable damper for hybrid control of bridge response under earthquake. In *Proa, US Nat. Workshop on Struct. Control Res., USC Pubi. No. CE-9013* (1990).
- [32] FRAHM, H. Vibrations of bodies, Apr. 18 1911. US Patent 989,958.
- [33] FRÉMOND, M. Shape memory alloys. *Phase Change in Mechanics* (2012), 67–100.
- [34] FUJITANI, H., SODEYAMA, H., TOMURA, T., HIWATASHI, T., SHIOZAKI, Y., HATA, K., SUNAKODA, K., MOR-

- ISHITA, S., AND SODA, S. Development of 400kN magnetorheological damper for a real base-isolated building. In *Proceedings of SPIE* (2003), vol. 5052, p. 265.
- [35] GALLEGOS, C. M. *Motion based design: solution algorithms to the inverse problem with applications to seismic design*. PhD thesis, Massachusetts Institute of Technology, 1998.
- [36] GAO, H., KWOK, K., AND SAMALI, B. Optimization of tuned liquid column dampers. *Engineering structures* 19, 6 (1997), 476–486.
- [37] GAUL, L., ALBRECHT, H., AND WIRNITZER, J. Damping of structural vibrations using adaptive joint connections and neural control. *CISM Courses and Lectures: Smart Structures* 429 (2001), 86–97.
- [38] GHISBAIN, P. *Seismic performance assessment for structural optimization*. PhD thesis, Massachusetts Institute of Technology, 2013.
- [39] HA, Q., KWOK, N., NGUYEN, M., LI, J., AND SAMALI, B. Mitigation of seismic responses on building structures using MR dampers with Lyapunov-based control. *Structural Control and Health Monitoring* 15, 4 (2008), 604–621.
- [40] HASKETT, T., BREUKELMAN, B., ROBINSON, J., AND KOTTELENBERG, J. Tuned mass dampers under excessive structural excitation. *Report of the Motioneering Inc* (2004).
- [41] HIDAKA, S., AHN, Y., AND MORISHITA, S. Adaptive vibration control by a variable-damping dynamic absorber
-

BIBLIOGRAPHY

- using ER fluid. *Journal of Vibration and Acoustics* 121 (1999), 373.
- [42] HROVAT, D., BARAK, P., AND RABINS, M. Semi-Active versus Passive or Active Tuned Mass Dampers for Structural Control. *Journal of Engineering Mechanics* 109 (1983), 691.
- [43] IDELCHIK, I. E., AND FRIED, E. Handbook of hydraulic resistance.
- [44] IKEDA, T. Fundamentals of piezoelectricity. 1996.
- [45] IKEDA, Y., SASAKI, K., SAKAMOTO, M., AND KOBORI, T. Active mass driver system as the first application of active structural control. *Earthquake Engineering & Structural Dynamics* 30, 11 (2001), 1575–1595.
- [46] IRWIN, P., KILPATRICK, J., ROBINSON, J., AND FRISQUE, A. Wind and tall buildings: negatives and positives. *The structural design of tall and special buildings* 17, 5 (2008), 915–928.
- [47] JACKSON, C., WAGNER, H., AND WASILEWSKI, R. 55-nitinol-the alloy with a memory: It's physical metallurgy properties, and applications. nasa sp-5110. *NASA Special Publication 5110* (1972).
- [48] JUNG, H., AND SPENCER JR, B. Control of seismically excited cable-stayed bridge employing magnetorheological fluid dampers. *Journal of Structural Engineering* 129 (2003), 873.
- [49] KANNAN, S., URAS, H., AND AKTAN, H. Active control of building seismic response by energy dissipation.
-

BIBLIOGRAPHY

- Earthquake engineering & structural dynamics* 24, 5 (1995), 747–759.
- [50] KARAVASILIS, T., SAUSE, R., AND RICLES, J. Seismic design and evaluation of steel moment-resisting frames with compressed elastomer dampers. *Earthquake Engineering & Structural Dynamics* 41, 3 (2011), 411–429.
- [51] KAYNIA, A., BIGGS, J., AND VENEZIANO, D. Seismic effectiveness of tuned mass dampers. *Journal of the Structural Division* 107, 8 (1981), 1465–1484.
- [52] KELLY, J. M., AND NAEIM, F. Design of seismic isolated structures. *From Theory to Practice, by John Wiley & Sons, Inc* (1999).
- [53] KIM, H., AND ADELI, H. Wind-induced motion control of 76-story benchmark building using the hybrid damper-TLCD system. *Journal of structural engineering* 131 (2005), 1794.
- [54] KITAMURA, H., FUJITA, T., TERAMOTO, T., AND KIHARA, H. Design and analysis of a tower structure with a tuned mass damper. In *Proceedings 9th World Conference of Earthquake Engineering, Tokyo-Kyoto, Japan* (1988), vol. 8, pp. 415–420.
- [55] KOO, J., AHMADIAN, M., AND ELAHINIA, M. Semi-active controller dynamics in a magneto-rheological tuned vibration absorber. In *Proceedings of SPIE* (2005), vol. 5760, p. 69.
- [56] KOO, J., AHMADIAN, M., SETAREH, M., AND MURRAY, T. In search of suitable control methods for semi-active
-

BIBLIOGRAPHY

- tuned vibration absorbers. *Journal of Vibration and Control* 10, 2 (2004), 163.
- [57] KURATA, N., KOBORI, T., TAKAHASHI, M., NIWA, N., AND KURINO, H. Shaking table experiments of active variable damping system. In *Proa, First World Conf. on Struct. Control, TP2* (1994), pp. 108–127.
- [58] LAFLAMME, S. *Control of large-scale structures with large uncertainties*. PhD thesis, Massachusetts Institute of Technology, 2011.
- [59] LAFLAMME, S., SLOTINE, J. E., AND CONNOR, J. Self-organizing input space for control of structures. *Smart Materials and Structures* 21, 11 (2012), 115015.
- [60] LAFLAMME, S., TAYLOR, D., ABDELLAOUI-MAANE, M., AND CONNOR, J. Modified friction device for control of large-scale systems. *Structural Control & Health Monitoring* (2011).
- [61] LEE, H., YANG, G., JUNG, H., SPENCER, B., AND LEE, I. Semi-active neurocontrol of a base-isolated benchmark structure. *Structural Control and Health Monitoring* 13, 2-3 (2006), 682–692.
- [62] LI, H., AND CHANG, Z. Semi-active control for eccentric structures with MR damper based on hybrid intelligent algorithm. *The Structural Design of Tall and Special Buildings* 17, 1 (2008), 167–180.
- [63] LIN, C., LU, L., LIN, G., AND YANG, T. Vibration control of seismic structures using semi-active friction multiple tuned mass dampers. *Engineering Structures* (2010).
-

- [64] LIN, P., AND LOH, C. Semi-active control of floor isolation system using MR-damper. In *Proceedings of SPIE* (2008), vol. 6932, p. 69320U.
- [65] LINDH, C., LAFLAMME, S., AND CONNOR, J. Effects of damping device nonlinearity on the performance of semi-active tuned mass dampers. In *5th World Conference on Structural Control and Monitoring* (2010), vol. 274, pp. 1–13.
- [66] LU, K.-C., LO, C.-H., YANG, J., AND LIN, P.-Y. Decentralized sliding model control of buildings using MR-dampers. In *Proceedings of SPIE* (2008), vol. 6932, p. 69320V.
- [67] LU, L., LIN, G., AND KUO, T. Stiffness controllable isolation system for near-fault seismic isolation. *Engineering Structures* 30, 3 (2008), 747–765.
- [68] LUND, R. Active damping of large structures in winds. In *ASCE Convention (Boston, MA, 1979)* (1979).
- [69] MACKRIELL, L., KWOK, K., AND SAMALI, B. Critical mode control of a wind-loaded tall building using an active tuned mass damper. *Engineering structures* 19, 10 (1997), 834–842.
- [70] MADHEKAR, S., AND JANGID, R. Variable dampers for earthquake protection of benchmark highway bridges. *Smart Materials and Structures* 18 (2009), 115011.
- [71] MAYES, R., KELLY, T., AND JONES, L. Seismic isolation: An economic alternative for the seismic design and
-

BIBLIOGRAPHY

- rehabilitation of buildings and bridges. *Civil Engineering Practice* 5, 1 (1990), 7–30.
- [72] MAYES, R., SVEINSSON, B., AND BUCKLE, I. Seismic isolation: An economic rehabilitation alternative. *Construction Specifier* (1987), 76–92.
- [73] MCNAMARA, R. Tuned mass dampers for buildings. *Journal of the Structural Division* 103, 9 (1977), 1785–1798.
- [74] MOORE, J. *Advances in actuators*. Taylor & Francis, 1995.
- [75] MYERS, D. Softening the jolt of the big one. *Los Angeles Times, Real Estate Section* (1989).
- [76] NAGARAJAIAH, S., AND VARADARAJAN, N. Novel semi-active variable stiffness tuned mass damper with real time tuning capability. In *Proceeding of 13th Engineering Mechanics Conference* (2000).
- [77] NAGASE, T., AND HISATOKU, T. Tuned pendulum mass damper using ice thermal storage tank installed in crystal tower. *Private Communication* (1990).
- [78] NARASIMHAN, S., AND NAGARAJAIAH, S. A STFT semi-active controller for base isolated buildings with variable stiffness isolation systems. *Engineering structures* 27, 4 (2005), 514–523.
- [79] NITSCHKE, R., AND GAUL, L. Smart friction driven systems. *Smart Materials and Structures* 14 (2005), 231–236.
- [80] OGATA, K. Modern control engineering, terza edizione, 1997.

BIBLIOGRAPHY

- [81] OHASHI, M., MOCHIZUKI, H., YAMAGUCHI, T., HAGIWARA, Y., KUWAMURA, H., OKAMURA, Y., TOMITA, Y., KOMATSU, N., AND FUNATSU, Y. Development of new steel plates for building structural use. *Nippon steel technical report. Overseas*, 44 (1990), 8–20.
- [82] ORMONDROYD, J. Theory of the dynamic vibration absorber. *Transaction of the ASME* 50 (1928), 9–22.
- [83] OTSUKA, K., AND WAYMAN, C. *Shape memory materials*. Cambridge University Press, 1999.
- [84] PATTEN, W., AND SACK, R. Semiactive control of civil engineering structures. In *American Control Conference, 1994* (1994), vol. 1, IEEE, pp. 1078–1082.
- [85] PETERSEN, N. Design of large scale tuned mass dampers. *structural control* (1980), 581–596.
- [86] QU, W., CHEN, Z., AND XU, Y. Dynamic analysis of wind-excited truss tower with friction dampers. *Computers & Structures* 79, 32 (2001), 2817–2831.
- [87] RANDALL, S., HALSTED, D., AND TAYLOR, D. Optimum vibration absorbers for linear damped systems. *Transaction of the ASME* 130 (1978), 908–913.
- [88] REAVELEY, L., MAYES, R., AND SVEINSSON, B. Seismic isolation of a computer/flight simulator research and development facility. In *Proceedings of Seismic Engineering, ASCE Structures Congress* (1989).
- [89] REITERER, M., AND ZIEGLER, F. Bi-axial seismic activation of civil engineering structures equipped with tuned

BIBLIOGRAPHY

- liquid column dampers. *Journal of Seismology and Earthquake Engineering* 7, 1 (2011).
- [90] SAKAMOTO, M., KOBORI, T., YAMADA, T., AND TAKAHASHI, M. Practical applications of active and hybrid response control systems and their verification by earthquake and strong wind observations. In *Proc, First World Conf. on Struct. Control, WP2* (1994), pp. 90–99.
- [91] SARKISIAN, M., LEE, P., LONG, E., BOSWELL, C. K., LYNN, A., REITHERMAN, R., ET AL. The materials of the cathedral of christ the light. In *AEI 2011: Building integration solutions. Proceedings of the 2011 Architectural Engineering National Conference, Oakland, California, USA, 30 March-2 April, 2011*. (2011), American Society of Civil Engineers (ASCE), pp. 327–334.
- [92] SHINOZUKA, M., CONSTANTINOU, M., AND GHANEM, R. Passive and active fluid dampers in structural applications. In *Proc, US/China/Japan Workshop on Struct. Control* (1992), pp. 507–516.
- [93] SHOOK, D., LIN, P., LIN, T., AND ROSCHKE, P. A comparative study in the semi-active control of isolated structures. *Smart Materials and Structures* 16 (2007), 1433.
- [94] SLOTINE, J., AND COETSEE, J. Adaptive sliding controller synthesis for non-linear systems. *International Journal of Control* 43, 6 (1986), 1631–1651.
- [95] SNOWDON, J. C. Vibration isolation: use and characterization. *The Journal of the Acoustical Society of America* 66 (1979), 1245.
-

BIBLIOGRAPHY

- [96] SPENCER, B., DYKE, S., SAIN, M., AND CARLSON, J. Phenomenological model for magnetorheological dampers. *Journal of engineering mechanics* 123, 3 (1997), 230–238.
- [97] SPENCER JR, B., AND NAGARAJAIAH, S. State of the art of structural control. *Journal of Structural Engineering* 129 (2003), 845.
- [98] SPENCER JR, B., YANG, G., CARLSON, J., AND SAIN, M. Smart dampers for seismic protection of structures: a full-scale study. In *Proceedings of the Second World Conference on Structural Control (2WCSC), Kyoto, Japan* (1998), vol. 1, pp. 417–426.
- [99] STANWAY, R., SPROSTON, J. L., AND STEVENS, N. G. Non-linear modeling of an electrorheological vibration damper. *Journal of Electrostatics* 20 (1987), 167–184.
- [100] STRANG, G. *Introduction to linear algebra*. Wellesley Cambridge Pr, 2003.
- [101] SYNGELLAKIS, S. *Retrofitting of Heritage Structures Against Earthquakes*. WIT Press, 2013.
- [102] TARANATH, B. *Structural analysis and design of tall buildings*, vol. 100. McGraw-Hill New York, 1988.
- [103] TERASAWA, T., SAKAI, C., OHMORI, H., AND SANO, A. Adaptive identification of MR damper for vibration control. In *43rd IEEE Conference on Decision and Control, 2004. CDC* (2004), pp. 2297–2303.
- [104] TSAI, H.-C., AND LIN, G.-C. Optimum tuned-mass dampers for minimizing steady-state response of support-

BIBLIOGRAPHY

- excited and damped systems. *Earthquake engineering & structural dynamics* 22, 11 (1993), 957–973.
- [105] TSAI, K., CHEN, H., HONG, C., AND SU, Y. Design of steel triangular plate energy absorbers for earthquake resistant construction. *Earthquake Spectra* 9, 3 (1993), 517–50.
- [106] TU, J., AND QU, W. An experimental study on semi-active seismic response control of a large-span building on top of ship lift towers. *Journal of Vibration and Control* 14, 7 (2008), 1055.
- [107] WADA, A., HUANG, Y.-H., AND IWATA, M. Passive damping technology for buildings in japan. *Progress in structural engineering and materials* 2, 3 (2000), 335–350.
- [108] WALTERS, M., AND ELSESSER, E. Base isolation of the existing city and county building in salt lake city. In *Proceedings of a Seminar on Base Isolation and Passive Energy Dissipation, Applied Technology Council, Report No. 17.* (1988).
- [109] WARBURTON, G. Optimum absorber parameters for minimizing vibration response. *Earthquake Engineering & Structural Dynamics* 9, 3 (1981), 251–262.
- [110] WARBURTON, G. Optimum absorber parameters for various combinations of response and excitation parameters. *Earthquake Engineering & Structural Dynamics* 10, 3 (1982), 381–401.
-

BIBLIOGRAPHY

- [111] WARBURTON, G., AND AYORINDE, E. Optimum absorber parameters for simple systems. *Earthquake Engineering & Structural Dynamics* 8, 3 (1980), 197–217.
- [112] WATANABE, A., HITOMI, Y., SAEKI, E., WADA, A., AND FUJIMOTO, M. Properties of brace encased in buckling-restraining concrete and steel tube. In *Proceedings of Ninth World Conference on Earthquake Engineering* (1988), vol. 4, pp. 719–724.
- [113] WAYMAN, C., AND SHIMIZU, K. The shape memory (marmem) effect in alloys. *Metal Science* 6, 1 (1972), 175–183.
- [114] WIKIPEDIA. <http://en.wikipedia.org/wiki/file:uscuh.jpg>, month = october, year = 2013, url = <http://en.wikipedia.org/wiki/File:USCUH.jpg>.
- [115] WIKIPEDIA. <http://en.wikipedia.org/wiki/file:lbva.jpg>, 2013.
- [116] WIKIPEDIA. http://en.wikipedia.org/wiki/file:salt_lake_city_county_bldg.jpg, 2013.
- [117] WIKIPEDIA. http://en.wikipedia.org/wiki/file:san_francisco_city_hall_september_2013.
- [118] WIKIPEDIA. http://en.wikipedia.org/wiki/one_wall_centre, 2013.
- [119] WIKIPEDIA. http://en.wikipedia.org/wiki/torre_mayor, 2013.
- [120] WONGPRASERT, N., AND SYMANS, M. Numerical evaluation of adaptive base-isolated structures subjected to
-

BIBLIOGRAPHY

- earthquake ground motions. *Journal of engineering mechanics* 131 (2005), 109.
- [121] WU, B., WANG, Q., SHI, P., OU, J., AND GUAN, X. Real-time substructure test of JZ 20-2 NW offshore platform with semi-active MR dampers. In *ICEE 2006: 4th International Conference on Earthquake Engineering* (2006), National Center for Research on Earthquake Engineering.
- [122] WU, J., CHANG, C., AND LIN, Y. Optimal designs for non-uniform tuned liquid column dampers in horizontal motion. *Journal of Sound and Vibration* 326, 1 (2009), 104–122.
- [123] WU, J.-C., SHIH, M.-H., LIN, Y.-Y., AND SHEN, Y.-C. Design guidelines for tuned liquid column damper for structures responding to wind. *Engineering structures* 27, 13 (2005), 1893–1905.
- [124] WU, W., CAI, C., AND CHEN, S. Experiments on reduction of cable vibration using MR dampers. In *Proceedings of 17th ASCE Engineering Mechanics Conference* (2004).
- [125] XU, Y., AND NG, C. Seismic protection of a building complex using variable friction damper: experimental investigation. *Journal of Engineering Mechanics* 134 (2008), 637.
- [126] YALLA, S., AND KAREEM, A. Optimum absorber parameters for tuned liquid column dampers. *Journal of Structural Engineering* 126, 8 (2000), 906–915.
-

BIBLIOGRAPHY

- [127] YANG, J., AND AGRAWAL, A. Semi-active hybrid control systems for nonlinear buildings against near-field earthquakes. *Engineering Structures* 24, 3 (2002), 271–280.
- [128] YANG, J. N., AND AGRAWAL, A. K. Semi-active hybrid control systems for nonlinear buildings against near-field earthquakes. vol. 24, Elsevier, pp. 271–280.
- [129] ZEMP, R., DE LA LLERA, J. C., AND ALMAZÁN, J. L. Tall building vibration control using a tm-mr damper assembly. *Earthquake Engineering & Structural Dynamics* 40, 3 (2011), 339–354.